Group 8 and 9 Bis(phosphino)silyl Pincer Complexes: Applications in Bond Activation and Catalysis

by

Helia Hollenhorst

Submitted in partial fulfillment of the requirements
for the degree of Doctor of Philosophy

at

Dalhousie University
Halifax, Nova Scotia
August 2021

"Life is a preparation for the future;

and the best preparation for the future

is to live as if there were none."

Albert Einstein

Table of Contents

List of Tables

List of Figures

List of Schemes

Abstract

Advances in homogenous transition metal catalysis are vital for the development of improved, sustainable methodologies in chemical syntheses. Tridentate pincer ligands are highly tunable and are compatible with late $3d$-, $4d$-, and $5d$-metals with applications in bond activation and catalysis. Metal-ligand cooperativity has proven integral in catalysis mediated by Earth-abundant $3d$-metals, such as iron.

Research in the Turculet group is focused on the reactivity of bis(phosphino)silyl PSiP pincer complexes. A key feature of PSiP ligation is the strongly σ-donating silyl donor, which promotes challenging bond activation by platinum group metals. Furthermore, the facile formation of η^2-(Si-H) species with $3d$-metals may play a key role in catalysis. The versatility exhibited by PSiP ligation with precious (Rh and Ir) and base (Fe) metals is highlighted in this thesis.

While (Cy-PSiP)Ir^I (Cy-PSiP = κ^3-(2-Cy$_2PC_6H_4)_2Si$Me) undergoes facile N-H oxidative addition of various amines to form complexes of the type (Cy-PSiP)IrH(NHR), subsequent insertion of unsaturated substrates (*e.g.*, alkenes, alkynes) into the Ir-NHR linkage proved challenging. To further explore this chemistry for the development of new hydroamination reactions, the synthesis of indolyl(phosphino)silyl (ᶦPr-PSiP^{Ind}) Rh and Ir complexes was targeted. While (ᶦPr-PSiP^{Ind})MH(NHR) (M = Rh, Ir) complexes could be synthesized, (ᶦPr-PSiP^{Ind})Ir^I undergoes competitive N-H and C-H oxidative addition of anilines, while the Rh analogue proved relatively unreactive. Subsequent insertion of alkenes and alkynes into the Ir-NHR linkage remained challenging, whereas the facile insertion of CO_2 afforded isolable Ir carbamato hydride complexes.

The utility of (PSiP)Fe complexes in hydrogenation catalysis was also investigated. The MgBr$_2$-bridged diiron complex [(Cy-PSiP)FeBr]$_2$(MgBr$_2$) was found to mediate diarylalkyne hydrogenation under mild conditions. Unusual selectivity for the complete hydrogenation of alkynes was observed, with no reactivity for alkene hydrogenation. The mechanism of this reaction is being investigated using DFT methods in collaboration with Dr. Erin Johnson (Dalhousie). Results suggest that metal-silyl cooperativity plays a key role in this catalysis, involving geminal transfer of H_2 to a single alkyne carbon *via* an Fe(II) carbene intermediate. Comparative studies of (ᶦPr-PSiP^{Ind})Fe coordination chemistry and reactivity are also described.

List of Abbreviations and Symbols Used

κ = hapticity (non-contiguous donors)
Anal. Calcd. = Analysis Calculated
Ad = 1-adamantyl
Ar = aryl
Å = Angstrom
COD = 1,5-cyclooctadiene
COE = cyclooctene
COSY = Homonuclear Shift
     *CO*rrelation *S*pectrsocop*Y*
Cp* = pentamethylcyclopentadienyl
(Cy-PSiP) =
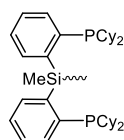
d = doublet
DMAP = 4,4-dimethylaminopyridine
δ = Chemical shift
DEPT = *D*istortionless *E*nhancement by
     *P*olarization *T*ransfer
E = main group element
equiv = equivalents
HMBC = *H*eteronuclear *M*ultiple *B*ond
     *C*orrelation
HSQC = *H*eteronuclear *S*ingle *Q*antum
     *C*orrelation
Hz = hertz
(ᶦPr-PSiPᴵⁿᵈ) =
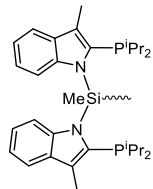
IR = infrared
ⁿ$J_{xx'}$ = n coupling constant between
atoms X and X'
M = metal, or mol/L
NMR = Nuclear Magnetic Resonance
ppm = parts per million
py = pyridine
R = alkyl or aryl
(ᵗBu-PCP) =

L = two-electron donor
m = multiplet
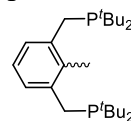
(ᵗBu-POCOP) =
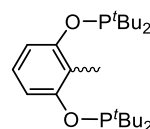
t = triplet
TBE = *tert*-butylethylene
THF = tetrahydrofuran

TOF = turnover frequency

TON = turnover number

Acknowledgements

"Time flies by so fast." That is something I have said many times throughout my degree. I started work in Dr. Laura Turculet's laboratory as an undergraduate student, curious about inorganic chemistry. Initially, I felt shy being the only girl among a group of guys, but quickly grew confident in my surroundings. Dr. Turculet's supportive and caring attitude made me feel at home. I fell in love with organometallic chemistry and decided to complete my Ph.D. I want to thank Dr. Turculet for her guidance and support in helping me grow and become a better version of myself. As I always tell myself, do not wish time away, live it.

I have really enjoyed my time in the Turculet group, and for that I thank my past and present co-workers. While I have always had a drive for chemistry, and many days were filled with frustration because of the chemistry (most often) not working as desired, the light-hearted attitude in the lab made every day enjoyable. We always found ways to support each other. We have built strong friendships, and I will hold many memories dear to my heart.

I also want to thank my family for their continuous support, whether that involved making delicious home-cooked meals or reminding me that I can get through the tough times. Family means a lot to me, and I appreciate everything they have done to help me become the person I am today.

We all know that chemistry requires a team effort. With that I want to thank Dr. Erin Johnson for conducting the DFT calculations for the iron alkyne hydrogenation mechanism. I enjoyed the process of determining a feasible catalytic cycle and to gain a new perspective. I also want to thank Dr. Mike Lumsden for help with NMR spectroscopy and his constant positive can-do attitude. I also want to thank Dr. Robert McDonald, Dr. Michael Ferguson, and Dr. Yuqiao Zhou from the University of Alberta for X-ray crystallography. Obtaining crystal structures was always exciting, especially for paramagnetic iron complexes.

While I have had many life lessons, I hope this document can give a glimpse of what these past few years have entailed. With that, I want to thank my committee members, Dr. Mark Stradiotto, Dr. Alex Speed, Dr. Mita Dasog, and Dr. Saurabh Chitnis for taking the time to review my work. I also want to thank Dr. David Herbert for taking the time to review my work as an external examiner.

I am beyond grateful for all the experiences and lessons I have learnt, especially about myself. Dalhousie Chemistry is more than a department, it is a community. Being a part of the Chemistry Graduate Student Society and participating in weekly events, as well as the connections between graduate students, undergraduate students, faculty, and staff have made this experience whole.

While time flew by, I feel beyond grateful for this experience, and I am excited to see what the future holds.

- Helia Hollenhorst

Chapter 1: Introduction

1.1 Overview: Towards Increased Sustainability in Transition Metal Catalysis

The development of homogenous metal catalysts has played a major role in the synthesis of fine chemicals and pharmaceuticals by facilitating reactions that are otherwise difficult to accomplish. Catalysts can operate at low loadings and can often facilitate reactions under mild conditions, thereby allowing chemical transformations to be more atom-economical and efficient. The significance of this field has been recognized with the awarding of the 2001, 2005, and 2010 Nobel Prizes in asymmetric catalysis,[1] olefin metathesis,[2] and Pd-catalyzed cross coupling,[3] respectively. Many notable organometallic catalysts utilize late 4d- and 5d-transition metals (aka precious metals) such as Ru, Rh, Ir, Pd, and Pt due to the highly reactive nature of such complexes in bond activation and catalysis. While major advancements have been made in the field of late transition metal catalysis, precious metals have become increasingly scarce and expensive.[4]

Given the important role of organometallic catalysis in the chemical industry, the development of increasingly sustainable catalysts is a priority. In recent years, there has been increased interest in the development of complexes with first row metals (aka base metals) such as Mn, Fe, Co, and Ni, which are more abundant and cheaper.[5] Iron in particular is an attractive substitute,[6] as it is the most abundant transition metal in the Earth's crust, and as such, it is also the metal that most often occurs in biological systems.[7] However, a major challenge in the design of such catalysts is the fine balance between reactivity and stability. In particular, while late 4d- and 5d-metals readily undergo two-electron chemistry such as oxidative addition and reductive elimination, late 3d-metals such as Fe often undergo one-electron processes that can be more challenging to predict.[8] The

resulting paramagnetic complexes are also difficult to characterize by NMR spectroscopy. Nonetheless, the investigation of first row metal complexes continues to be important for the development of improved catalysts and their applications. In this regard, ancillary ligand design has become an integral aspect in this field, given that the ligand(s) coordinated to the metal center can tune the reactivity based on steric and electronic factors.

While accessing new $3d$-metal catalysts is a topic of significant recent interest in the organometallic community and represents an important path to increasing sustainability in chemical syntheses,[8] there are also other ways to target this goal. The study of precious metal complexes that can undergo exceptionally challenging bond cleavage reactions is one such approach that can address sustainability in synthesis by developing efficient new reactions for the atom economical preparation of functionalized specialty chemicals.[9] In this regard, the metal-mediated cleavage of N-H bonds in amines by an oxidative addition pathway (*i.e.*, N-H bond activation) is a topic of relevance to this thesis. The application of such reactivity in alkene hydroamination remains relatively unknown, largely due to the fact that very few metal complexes have proven capable of N-H bond oxidative addition.[10] Yet this could constitute an important means of synthesizing new functionalized amines in a selective and atom-economical way. The prevalence of nitrogen in pharmaceuticals and fine chemicals provides motivation for the development of such new catalytic amination reactions, including reactions mediated by precious metals. Here too, ligand design plays an important role, as the steric and electronic features of ancillary ligands affect the balance between oxidative addition and reductive elimination that often plays a key role in such metal-mediated reactivity.

1.2 Ligand Design Considerations

This thesis focuses on the development of transition metal complexes supported by

tridentate pincer ancillary ligation. Pincer ligands feature an "LEL" (L = neutral donor, E = neutral or anionic donor) donor array and typically coordinate to the metal in a *meridional* fashion, such that the L-groups are *trans*-disposed (Figure 1-1), although a *facial* arrangement is also possible in some circumstances depending on the rigidity of the ligand backbone.[11] The tridentate motif is versatile, allowing for a large variety of such complexes with various combinations of donor groups and linkers, all of which can be altered systemically to tune the reactivity based on steric and electronic considerations. This ligand motif also features stabilization due to the chelate effect, thereby allowing for the development of robust homogenous catalysts.[11]
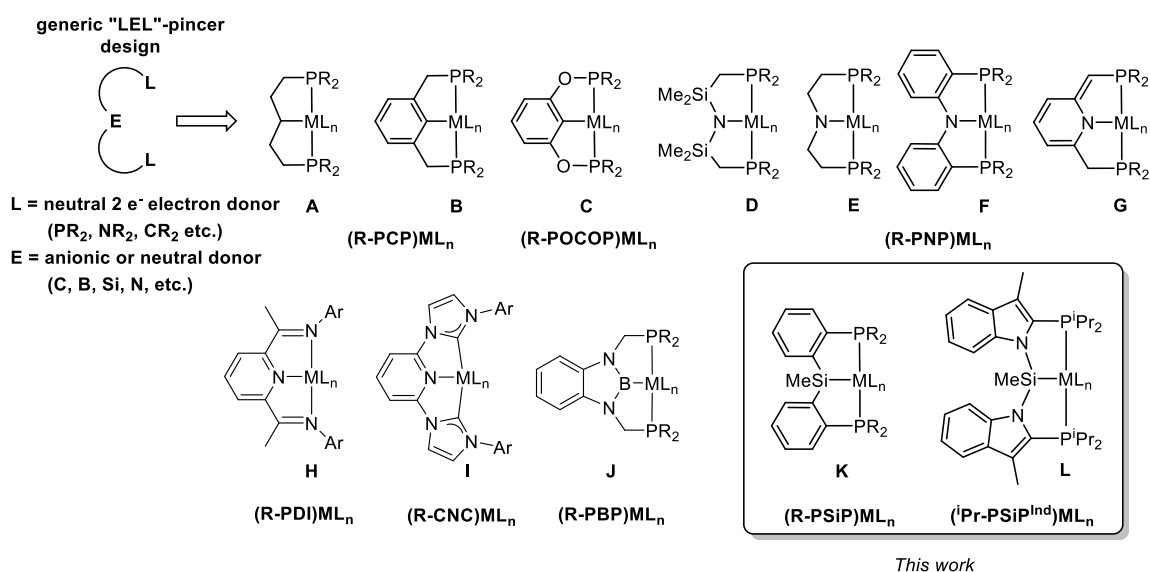
Figure 1-1. Examples of "LEL" pincer ligation.

1.2.1 Pincer Ligands for Electron Rich 4*d*- and 5*d*-Transition Metal Complexes

The first reports of pincer complexes in the literature can be traced back to the work of Shaw in the 1970's, who reported the synthesis of bis(phosphino) PCP (Figure 1-1, **A** and **B**) complexes of Rh, Ir, Pd, and Pt by chelate-assisted C-H bond oxidative addition.[12] Such bis(phosphino) pincer species have been utilized extensively since these early studies,

3

largely due to the thermodynamic stability of the chelate complexes and the well-established compatibility of platinum group metals with phosphine ligands. The implementation of bulky alkyl substituents on the phosphino donors of PCP ligands has led to the synthesis of highly reactive, electron-rich $4d$- and $5d$-metal complexes that can undergo facile oxidative addition of strong bonds, such as C-H and N-H bonds in alkanes and amines, respectively (Scheme 1-1). The utility of electron-rich (PCP)Ir complexes in alkane dehydrogenation catalysis was demonstrated by the groups of Goldman and Jensen,[13] and inspired the development of related PCP motifs, most notably the bis(phosphinite) "POCOP" family of ligands (Figure 1-1, **C**) developed by Brookhart and-coworkers,[14] which have also found application in alkane activation catalysis (Scheme 1-2). This represents a rare example of a catalytic reaction that involves alkane C-H bond oxidative addition. While such PCP and POCOP pincers have become essentially ubiquitous in organometallic chemistry, the modular nature of the pincer design also inspired the development of bis(phosphine)amido PNP variants (Figure1-1, **D-F**). Such a PNP motif was initially developed by Fryzuk and co-workers (Figure1-1, **D**),[15] and more recently by the groups of Ozerov[16] and Liang (Figure1-1, **F**).[17] These PNP variants, have also found applications in E-H bond activation chemistry and catalysis.
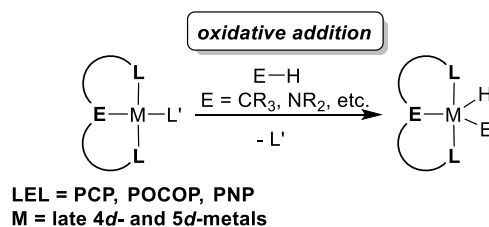
Scheme 1-1. E-H oxidative addition by pincer complexes.
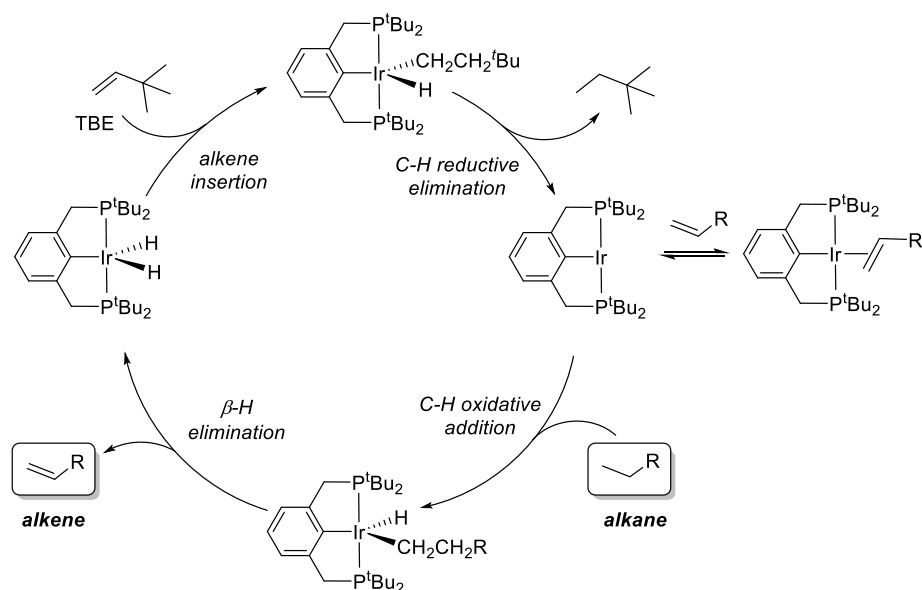
Scheme 1-2. Alkane dehydrogenation by (^{t}Bu-PCP)Ir (^{t}Bu-PCP = κ^3-2,6-(^{t}Bu$_2$$PCH_2$)$_2$$C_6H_3$) with tert-butylethylene (TBE) as a sacrificial hydrogen acceptor.

In addition to their utility in C-H bond cleavage and functionalization, electron-rich PCP- and POCOP-supported Ir complexes have also demonstrated an aptitude for N-H oxidative addition reactions that are of relevance in the search for new amine functionalization chemistry. Goldman, Hartwig and co-workers[18] demonstrated that (PCP)Ir species react with aniline as well as ammonia to afford isolable Ir(III) anilido or amido hydride complexes, respectively, resulting from N-H bond oxidative addition (Scheme 1-3, **A** and **B**). Brookhart and co-workers[19] also extended their study of (POCOP)Ir species to include the oxidative addition of N-H bonds (Scheme 1-3, **C**), finding that upon treatment with various anilines in benzene solution three products exist in equilibrium – (POCOP)Ir(H)(Ph), (POCOP)Ir(H)(NHR), and the Lewis base adduct (POCOP)Ir(NH$_2$R) (R = p-X-C$_6$H$_4$ where X = OMe, Me, H, Cl, or CF$_3$, or R = C$_6$F$_5$, 3,5-(CF$_3$)$_2$C$_6$H$_3$). These studies have highlighted that pincer ligand design can have a substantial effect on the course of C-H/N-H activation processes at Ir centres.

5

A

B

C

(^{t}Bu-POCOP)Ir

R = *p*-X-C$_6$H$_3$, C$_6$F$_5$, 3,5-(CF$_3$)$_2$C$_6$H$_3$
X = OMe, Me, H, Cl, CF$_3$
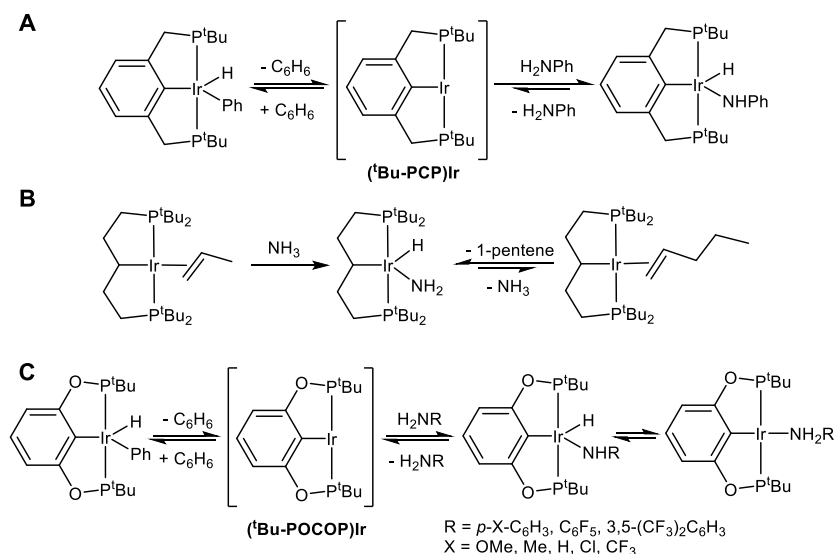
Scheme 1-3. N-H oxidative addition, and competitive reductive elimination, with (PCP)-and (POCOP)Ir complexes.

The application of N-H bond oxidative addition in catalytic reactivity has not been developed extensively, largely due to the relative scarcity of complexes that can undergo such bond activation chemistry, and the prevalence of competing reactions, such as the formation of stable amine adducts and C-H bond activation. In early studies, Milstein reported on the catalytic hydroamination of norbornene *via* a route involving N-H oxidative addition of aniline to an Ir^I center (Scheme 1-4).[20] While catalytic performance was relatively poor (TON of only 2 to 6 after 48 h in refluxing THF), this represents the first reported example of catalytic reactivity involving N-H oxidative addition processes. This reactivity also provides a relatively rare example of alkene insertion into a M-NR$_2$ linkage.[20] While subsequent studies in more recent years have led to improved catalytic performance in hydroamination reactions involving N-H oxidative addition, this remains an underdeveloped area.
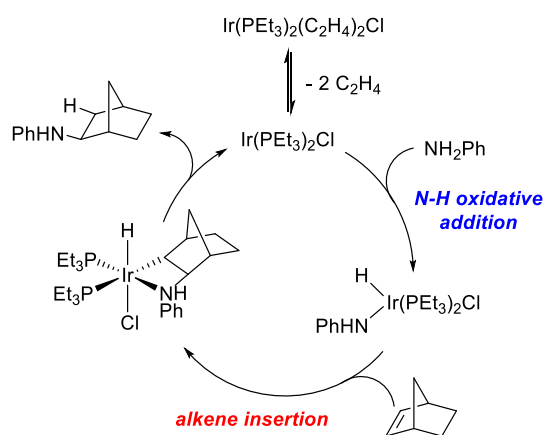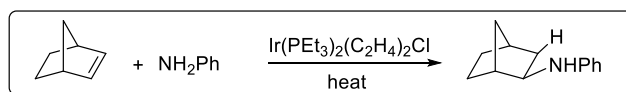
Scheme 1-4. Early example of Ir-catalyzed hydroamination involving N-H oxidative addition and insertion.

In this regard, the development of new types of electron-rich, pincer-ligated Ir complexes and the study of N-H oxidative addition chemistry involving such complexes is anticipated to play a key role in the development of improved and sustainable methods of catalysis involving the functionalization of amines. The study of the ensuing amido hydride metal complexes, their propensity for N-H reductive elimination, and the insertion of unsaturated substrates (*e.g.*, alkenes, alkynes) into metal-amido linkages is also pertinent to this goal. As such, the first part of this thesis will focus on the synthesis of new electron-rich Rh and Ir pincer complexes and their reactivity with amines to afford amido hydride complexes (Chapter 2). The reactivity of such Rh and Ir amido hydride species toward unsaturated substrates was also investigated in an effort to explore the possibility of amine functionalization subsequent to N-H oxidative addition (Chapter 3).

1.2.2 Pincer Ligands for Earth Abundant 3*d*-Metal Chemistry

Pincer ligands have also emerged as an important platform for the synthesis of Earth abundant 3*d*-metal complexes with applications in catalysis. An important ligand design

7

strategy in this regard involves the ability of an ancillary ligand to participate in and facilitate metal-mediated reactivity. Such metal-ligand cooperativity typically involves either intramolecular proton transfer or electron transfer (*i.e.*, redox non-innocence), and often provides a means for a first row metal to maintain a preferred oxidation state in the course of a catalytic reaction.

Bis(imino)pyridine (PDI) pincer ligation (Figure 1-1, **H**) has been studied extensively as a redox-active ligand platform that can undergo reversible electron transfer with a bound transition metal. In seminal studies of the electronic characteristics of PDI ligands, Wieghardt and co-workers,[21] and Budzelaar and co-workers[22] demonstrated that such ligands display a rich redox chemistry and can be coordinated in either their neutral, radical monoanion, or diradical dianion form (Scheme 1-5). While initial studies of PDI-supported Fe and Co complexes focused on olefin polymerization,[22] subsequent studies undertaken by Chirik and co-workers,[21d, 23] among others, extended the use of this ligand scaffold to catalytic applications in hydrogenation, hydrosilylation, [2+2] cycloaddition, and reductive cyclization. The bis(dinitrogen) complex (^{iPr}PDI)Fe(N$_2$)$_2$ is best described as a resonance hybrid between Fe(0) and Fe(II) and is highly active in olefin hydrogenation (Scheme 1-6). A chiral C_1-symmetric (*S*-PDI)CoMe complex, where the metal center is best described as Co^{II}, was shown to be effective for the hydrogenation of a family of substituted styrene derivatives with high enantioselectivity (Scheme 1-7).[24] Related Fe and Co complexes supported by more electron-donating CNC-pincer ligands that feature two *N*-heterocyclic carbene donors (Figure 1-1, **I**) have also been reported and display increased activity in olefin hydrogenation catalysis relative to the parent PDI catalysts.[24-25]

8

(PDI)⁰   **(PDI)⁻**   **(PDI)²⁻**
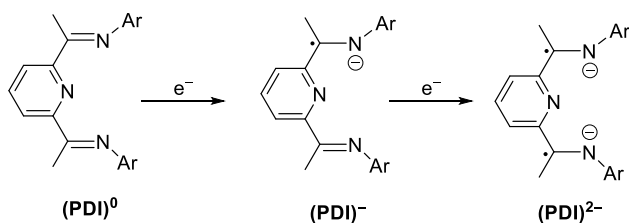
Scheme 1-5. Redox-active bis(imino)pyridine (PDI) ligands can be coordinated in either their neutral, radical monoanion, or diradical dianion form.
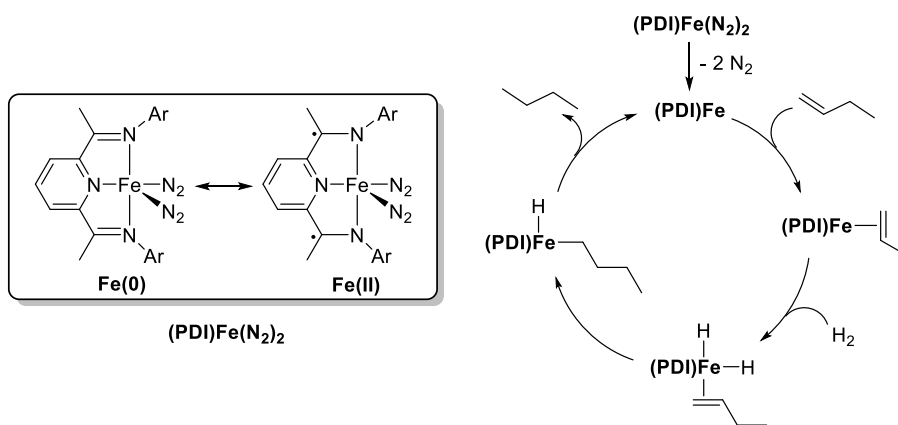
Scheme 1-6. (^{iPr}PDI)Fe(N$_2$)$_2$, a highly active olefin-hydrogenation pre-catalyst, is best described as a resonance hybrid between Fe(0) and Fe(II).
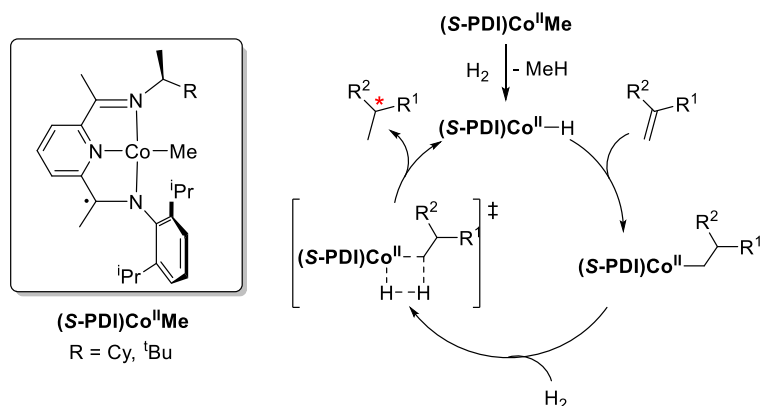
Scheme 1-7. Cobalt-catalyzed asymmetric hydrogenation of alkenes using an enantiopure C_1-symmetric PDI ligand.

Metal-ligand cooperativity involving metal-amido/metal-amine interconversion has been developed extensivley for a broad range of late transition metal complexes (Figure 1-2). Pincer PNP complexes with an aliphatic ligand backbone (Figure 1-1, **E**) have been

utilized in this regard for the catalytic hydrogenation of polar bonds, transfer hydrogenation, and dehydrogenative chemistry (*e.g.*, alcohol dehydrogenation, dehydrogenative coupling of alcohols, dehydrogenative coupling of alcohols with amines).[26] Unlike oxidative addition, which requires an increase in the oxidation state of the metal center, cooperative activation allows the metal to maintain a constant oxidation state. This same strategy has been applied in late $3d$-metal catalysis, although careful study is necessary to determine whether such cooperativity is indeed involved in the mechanism of the reaction. In an example reported by Beller and co-workers,[27] [(^{i}Pr-PNP)H]Fe(H)(HBH$_3$)(CO) was shown to be an effective catalyst for the hydrogenation of nitriles to amines. Mechanistic studies of the reaction and DFT analysis suggest that metal–ligand cooperation likely plays a role in the hydrogenation process, which features a simultaneous transfer of the Fe-*H* and the pincer N-*H* to the nitrile (Scheme 1-8). The reversible hydrogenation/dehydrogenation of [(^{i}Pr-PNP)H]Fe(H)$_2$(CO) and the amido derivative (^{i}Pr-PNP)Fe(H)(CO) is a key feature of this mechanism. By contrast to aliphatic PNP ligands, the amido nitrogen in diarylamido PNP complexes (Figure 1-1, **F**) is significantly less basic and as such metal-amido/metal-amine interconversion is far less likely.
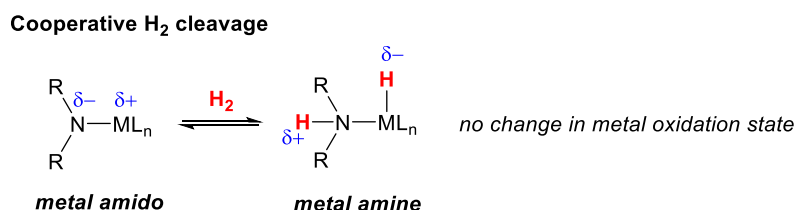
Figure 1-2. Metal-ligand cooperativity in H$_2$ activation by metal-amido/metal-amine interconversion.
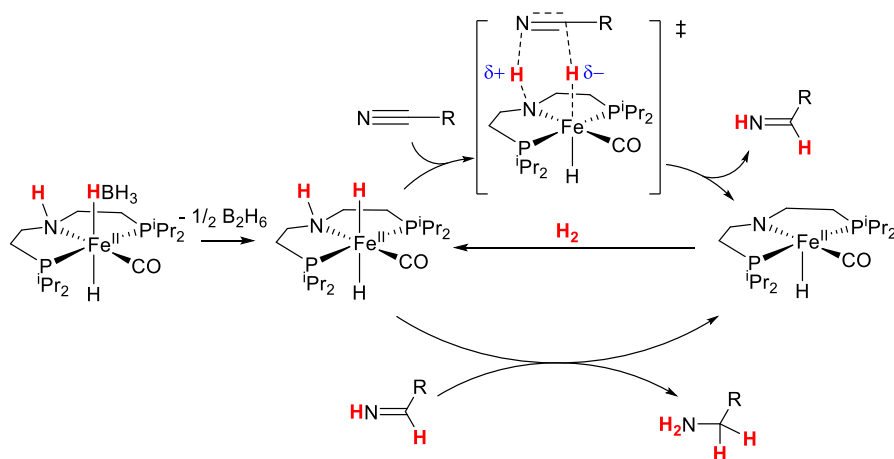
Scheme 1-8. Proposed mechanism for Fe-catalyzed nitrile hydrogenation catalysis involving metal-amido cooperativity.

Milstein and co-workers have also developed related metal-ligand cooperativity involving PNP ligands that undergo reversible aromatization/dearomatization of a central pyridine donor (Figure 1-1, **G**; Figure 1-3).[28] As in the case of aliphatic PNP ligands, the pincer ligand functions as a "proton reservoir". This design strategy has been applied across a wide range of transition metals, including late $3d$-metals. Iron PNP complexes of this type have found application in catalytic hydrogenation of carbonyl compounds (*e.g.*, ketones, aldehydes, esters and CO_2; Scheme 1-9), dehydrogenation of formic acid, and alkyne semihydrogenation.[29]
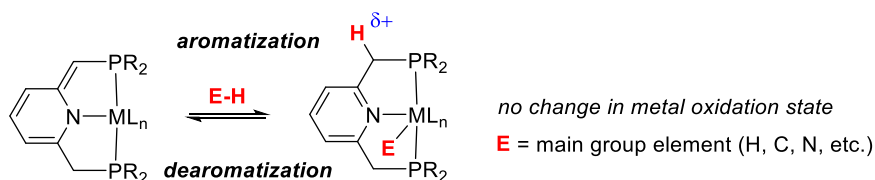
Figure 1-3. Bond activation by metal-ligand cooperativity involving pyridine aromatization/dearomatization.
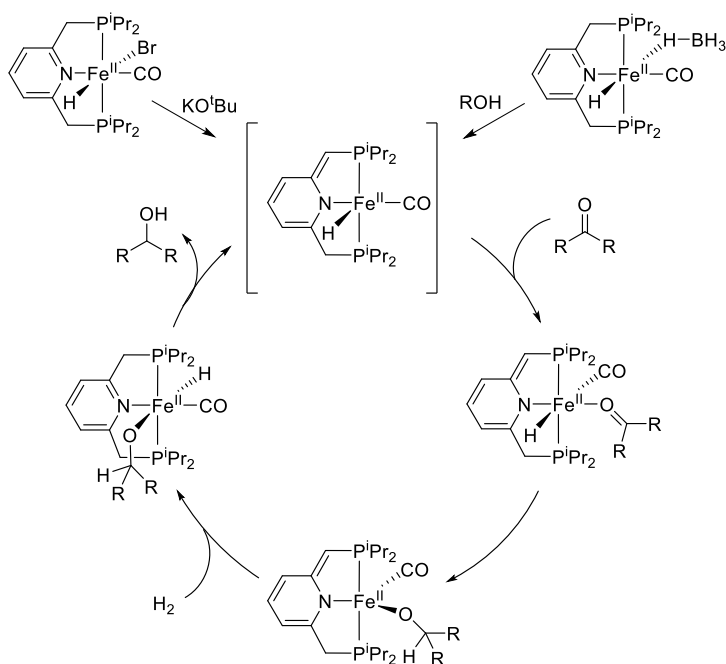
Scheme 1-9. Both (^{i}Pr-PNP)Fe(H)(Br)(CO) and (^{i}Pr-PNP)Fe(H)(CO)(HBH$_3$) are precatalysts for the hydrogenation of ketones to alcohols *via* metal-ligand cooperativity involving pyridine aromatization/dearomatization.

While cooperativity involving the transfer of a proton from the metal center to an electronegative donor has been utilized extensively, an alternative strategy where a hydride is transferred from the metal to an electropositive donor has not been rigorously investigated. Peters and coworkers[30] have investigated the synthesis and reactivity of first row metal complexes supported by PBP ligation (Figure 1-1, **J**), and have shown that Co and Ni PBP species undergo reversible H$_2$ addition across the M-B bond (Scheme 1-10a).[30] The utility of such PBP species in olefin hydrogenation was demonstrated,[30b] and the complex (^{t}Bu-PBP)NiH showed enhanced catalytic activity when compared with analogues where the boryl unit was substituted by a phenyl or amine donor, which is consistent with M-B cooperativity. Given the electropositive nature of Si, one can envision that such reversible hydride transfer involving M-Si species may also play a role in hydrofunctionalization catalysis (Scheme 1-10b). In this regard, Chapters 4 and 5 will

discuss the synthesis of PSiP iron pincer complexes, and their utility in hydrogenation catalysis.
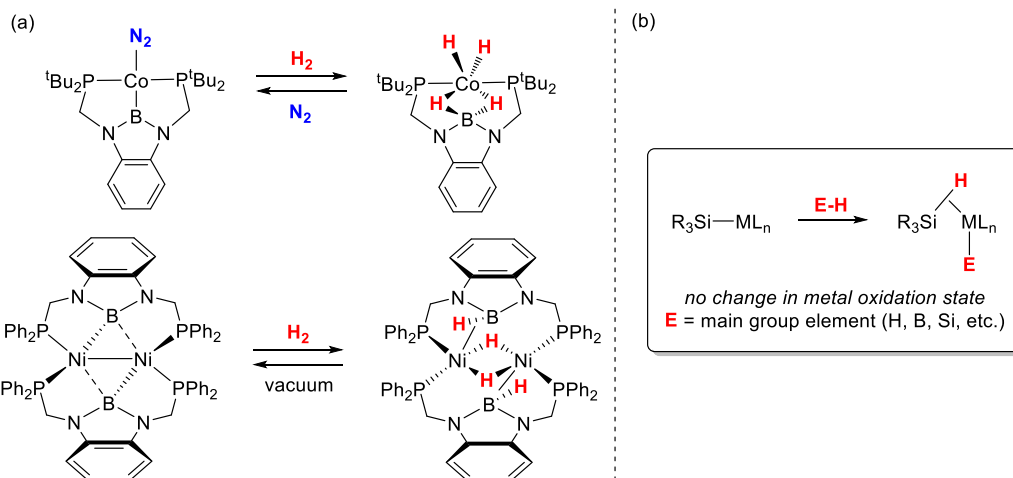
Scheme 1-10. (a) Both Co and Ni PBP species undergo reversible H_2 addition across the M-B bond; (b) potential reversible hydride transfer involving M-Si species.

1.3 Advancements in Bis(phosphino)silyl Pincer Metal Chemistry

In an effort to access new and highly reactive classes of pincer complexes, research in the Turculet group has focused on developing the chemistry of bis(phosphino)silyl "PSiP" pincer species (Figure 1-1, **K** and **L**).[31] In comparison with the closely related PCP derivatives, the increased electron-donating character of Si relative to C is anticipated to lead to a more electron-rich metal center in the case of PSiP ligation. In addition, the stronger *trans*-labilizing ability of Si can better promote the generation of coordinatively unsaturated complexes, allowing for more reactive species to be accessible. Such features have been demonstrated to lead to significant structural and reactivity differences between PCP- and PSiP-supported metal complexes. Indeed, PSiP ligation has been utilized to prepare unprecedented four-coordinate, trigonal pyramidal Ru^{II} complexes, and computational studies have confirmed the key role of the strongly σ-donating silyl group in enforcing the unusual coordination geometry.[32] The first part of the thesis will focus on

13

the synthesis of Rh and Ir complexes supported by a new class of bis(phosphino)silyl pincer-type ancillary ligands that feature an indolyl backbone (^{i}Pr-PSiP^{Ind}, Figure 1-1, **L**). Previous work in the Turculet group has shown that Ir complexes supported by related PSiP ligation (Figure 1-1, **K**) with a phenylene-derived ligand backbone are able to undergo challenging E-H (E = C, N) bond activation reactions (Scheme 1-11).[31, 33] More specifically, coordinatively unsaturated (Cy-PSiP)Ir^I when generated in benzene solution readily undergoes reversible C-H oxidative addition of benzene to form (Cy-PSiP)IrH(Ph) at room temperature (Scheme 1-11).[33a] Furthermore, when generated in cyclohexane solution (Cy-PSiP)Ir^I undergoes N-H oxidative addition of various amines including ammonia, *tert*-butylamine and aniline to form amido hydride complexes of the type (Cy-PSiP)Ir(H)(NHR) (R = H, alkyl, aryl) that are resistant to N-H reductive elimination (Scheme 1-11).[33b] The analogous (Cy-PSiP)Rh^I complex proved unreactive toward such oxidative addition chemistry. Subsequent studies on the insertion of unsaturated substrates into the Ir-amido linkages to develop new hydroamination protocols proved challenging, with insertion only observed with xylyl isocyanide.[33c] The work detailed herein aims to build on these results, with the investigation of ^{i}Pr-PSiP^{Ind}-supported Rh and Ir complexes in N-H bond activation, as well as the insertion of unsaturated substrates into metal-amido linkages for catalytic applications.
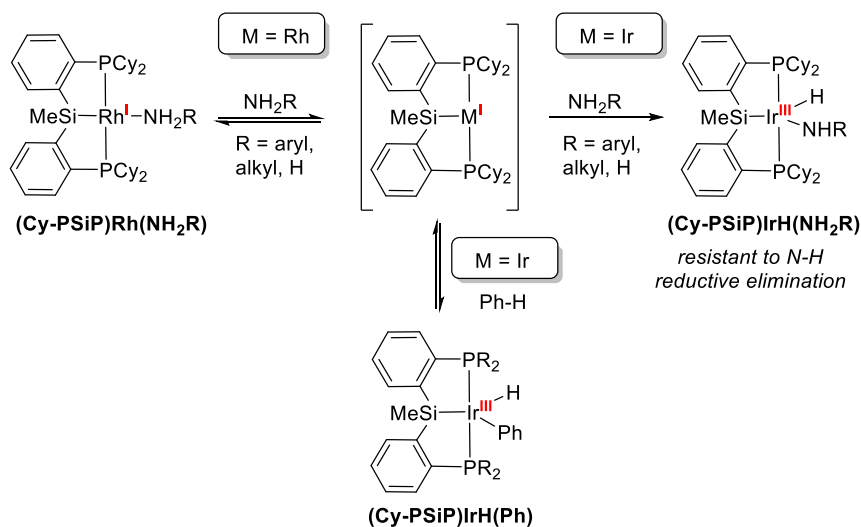
Scheme 1-11. C-H and N-H oxidative addition by (Cy-PSiP)Ir^I.

Bis(phosphino)silyl PSiP ligation has shown to not only be applicable to 4d- and 5d-metals, but also to 3d-metals. Silicon can behave in a cooperative manner by participating in hydride transfer processes (M to Si) to form η^2-(Si-H) complexes. Such hydride transfer can be integral to catalytic reactivity, as 3d-metals typically favor lower oxidation states and may not undergo conventional two-electron pathways, such as oxidative addition and reductive elimination. In this regard, metal-to-Si hydride transfer and the formation of η^2-(Si-H)-bound species involving both Cy-PSiP and ^{i}Pr-PSiP^{Ind} ligation have been previously reported. Iwasawa and co-workers[34] have investigated Ph-PSiP (PSiP = κ^3-(2-Ph$_2$PC$_6$H$_4$)$_2$SiMe) Group 10 metal hydride complexes formed upon treatment of M(PPh$_3$)$_4$ (M = Ni, Pd, Pt) with (Ph-PSiP)H. While the corresponding Pt^{II} complex (Ph-PSiP)PtH(PPH$_3$) features a terminal hydride ligand coordinated *trans*-to Si, the Pd and Ni derivatives were identified as η^2-(Si-H) M^0 complexes (Figure 1-3a).[34] Related reactivity involving interconversion of a terminal (Cy-PSiP)Ni^{II} hydride complex with the corresponding η^2-(Si-H) Ni^0 species was reported by Hazari and co-workers (Figure 1-3b).[35]

15
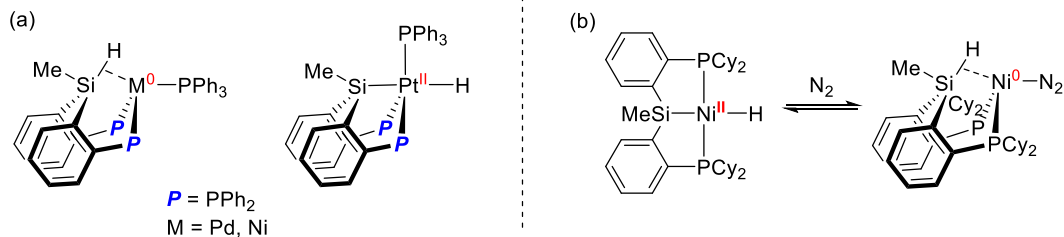
(a) (Ph-PSiP)M (M = Pd, Ni) complexes exhibit η^2-(Si-H) interactions while the Pt analogue does not; (b) reversible Si-H bond formation facilitated by N_2 cordination to (Cy-PSiP)Ni.

In a more recent report, Turculet and co-workers[36] reported on (^{i}Pr-PSiP^{Ind})MH (M = Ni, Pd, Pt) species and showed that while the Pd and Pt derivatives feature terminal hydride ligands, (^{i}Pr-PSiP^{Ind})NiH undergoes interconversion with the corresponding η^2-(Si-H) Ni^0 species in a dynamic process that is temperature and solvent dependent, as well as dependent on the nature of other coordinating species (*i.e.* N_2, PMe$_3$, DMAP; Scheme 1-12). The Ni hydride species was found to be catalytically active in the hydroboration of CO_2 to the formaldehyde level to provide the bis(boryl) acetal PinBOCH$_2$OBPin with high yield and selectivity.[36]
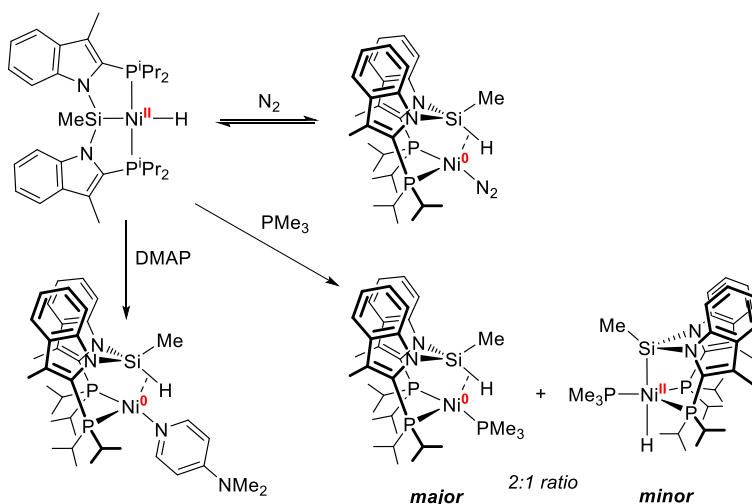
Scheme 1-12. (^{i}Pr-PSiP^{Ind})NiH undergoes Si-H reductive elimination in the presence of an L donor (*i.e.*, N_2, PMe$_3$, DMAP) to form an η^2-(Si-H) complex.

Given the apparent inclination of 3*d*-metal PSiP complexes to form η^2-(Si-H)

species, the utility of such complexes in hydrofunctionalization catalysis (i.e., hydrogenation, hydroboration, hydrosilylation) is an ongoing interest in the Turculet group, as the potential for metal-Si cooperativity may lead to useful reactivity. The combination of Earth-abundant $3d$-metal catalysts, and atom-economical hydrofunctionalization reactions is particularly appealing from the standpoint of developing sustainable synthetic methods. In this regard, the second part of the thesis will focus on the synthesis of Fe complexes supported by both Cy-PSiP and ^{i}Pr-PSiP^{Ind} ligation (Figure 1-1, **K** and **L**), with applications in alkyne hydrogenation catalysis.

Initial work on the synthesis and reactivity of (Cy-PSiP)Fe complexes reported by the Turculet group demonstrated that (Cy-PSiP)FeH(N$_2$)$_2$ (Figure 1-5) is an active olefin-hydrogenation catalyst, and that such reactions may procced *via* the formation of polyhydride species that feature η^2-(Si-H) coordination.[37] Treatment of (Cy-PSiP)Fe(PMe$_3$)(H) with H$_2$ led to the formation of an Fe^{II} dihydride complex (Cy-PSi(μ-H)P^{Me})FeH$_2$(PMe$_3$) containing an η^2-(Si-H) fragment (Figure 1-5). Variable temperature NMR spectroscopy revealed that all three hydride positions exchange on the NMR timescale. In an effort to further explore the applications of such reactivity in catalysis, the utility of (Cy-PSiP)FeH(N$_2$)$_2$ and related species in alkyne hydrogenation was evaluated and is detailed in this thesis. Unusual selectivity was observed such that alkynes are preferentially hydrogenated in the presence of an Fe-bromide precatalyst, while alkenes do not react. Preliminary computational studies of this reactivity in collaboration with Dr. Erin Johnson (Dalhousie) support an unusual Fe-carbene mediated mechanism, in which hydride transfer involving the silicon moiety in the Cy-PSiP ligand plays an integral role. The synthesis and catalytic applications of Fe complexes bearing ^{i}Pr-PSiP^{Ind} ligation was also explored in an effort to study ligand effects on reactivity.

17
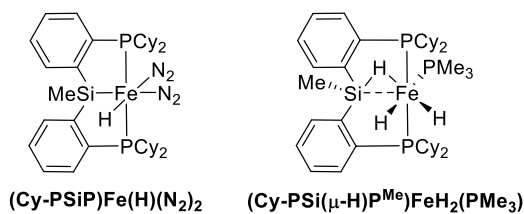
Figure 1-5. Cy-PSiP Fe complexes with applications in olefin-hydrogenation and formation of η^2-(Si-H) interactions.

The studies of bis(phosphino)silyl pincer coordination chemistry and catalysis presented in this thesis address reactivity challenges associated with the development of increasingly sustainable methodologies for chemical synthesis. The discovery of effective $3d$-metal catalysts is a highly sought-after goal in the quest to achieve increased sustainability in synthesis. The development of ligand design strategies that can enable breakthroughs in this regard is of fundamental importance. As such, this thesis aims to further the applicability of PSiP ligation for atom-economical Fe catalysis, wherein silyl-metal cooperativity may play a role in achieving unique reactivity. While Earth-abundant $3d$-metal catalysts are highly desirable, the utility of precious metal complexes for targeted, challenging reactivity applications cannot yet be discounted. In this context, the continued investigation of N-H bond oxidative addition involving Rh and Ir bis(phosphino)silyl pincer complexes presented herein targets the development of new, atom-efficient amination startegies that would be of tremendous utility for the sustainable synthesis of nitrogen-containing pharmaceuticals, fine chemicals, and materials.

Chapter 2: Synthesis of Rhodium and Iridium Complexes Supported by Bis(indolylphosphino)silyl Pincer Ligation: Competitive N-H and C-H Bond Activation by an Ir(I) Species

This chapter contains information from the following publication: Hollenhorst, H.; McDonald, R.; Ferguson, M.; Turculet, L., Synthesis of Rhodium and Iridium Complexes Supported by Bis(indolylphosphino)silyl Pincer Ligation: Competitive N–H and C–H Bond Activation by an Ir(I) Species. *Organometallics* **2021**, *40* (16), 2768-2784. All synthetic work was conducted by Helia Hollenhorst. X-Ray crystallographic data was obtained and refined by Dr. Robert McDonald and Dr. Michael Ferguson of the University of Alberta X-ray Crystallography Laboratory, Edmonton, AB. All elemental analysis was obtained by Galbraith Laboratories.

2.1 Introduction

2.1.1 N-H Bond Activation by Late 4*d*- and 5*d*-Transition Metals

Reactivity involving the metal-mediated cleavage of N-H bonds *via* oxidative addition has been pursued extensively,[10a, 10c, 38] as such a process may have utility in the development of new transition metal catalyzed amination reactions. The prevalence of amino functional groups in many pharmaceuticals, fine chemicals and other such high-profile synthetic targets has driven the pursuit of catalytic amination reactions that are increasingly efficient and selective. While reactions such as C-N cross coupling and alkene hydroamination have largely dominated this field, such reactions do not typically involve direct, metal-mediated N-H bond cleavage steps. Indeed, well-documented examples of N-H bond oxidative addition of amines are exceedingly rare,[20, 28b, 39] largely due to the ability of amines to form stable Werner-type coordination complexes. The development of metal complexes that undergo facile N-H oxidative addition involving simple amine substrates may thus lead to new reactions for the synthesis of amine derivatives that are

19

complementary to existing methodologies.

While some progress has been made toward the development of synthetic protocols that utilize N-H oxidative addition as an elementary step, this effort is limited due to the scarcity of metal complexes that can mediate this challenging bond activation. Since the early 2000s, Ir pincer complexes have been investigated in this regard, and have demonstrated a relative aptitude for N-H bond oxidative addition.[18a, 20, 39-40] Hartwig and co-workers demonstrated that the *in situ* generated pincer species (^{t}Bu-PCP)Ir^I (**2-1**) reacts with aniline to afford an Ir^{III} anilido complex resulting from N-H bond oxidative addition (**2-2**, Scheme 2-1, **A**).[18a] The analogous parent amido complex resulting from N-H bond cleavage in ammonia proved to be thermodynamically less stable than the reductive elimination product, (^{t}Bu-PCP)Ir(NH$_3$) (**2-3**). In addition, exposure of **2-2** to benzene resulted in the formation of an equilibrium mixture containing the anilido complex and the phenyl hydride species **2-4** resulting from reductive elimination of aniline and oxidative addition of a benzene C-H bond. These results indicate that although N-H bond oxidative addition occurs in this system, the reaction is readily reversible, which complicates the development of subsequent reactivity involving the Ir-NHR fragment.

Due to the instability of the amido hydride complexes formed, Goldman and Hartwig developed a related Ir^I complex featuring an aliphatic pincer ligand backbone, [(^{t}Bu$_2$P(CH$_2$)$_2$)$_2$CH]Ir^I which was proposed to increase the electron density on the metal center, in hopes of stabilizing the Ir^{III} oxidation state.[18b] Treatment of the propene complex [(^{t}Bu$_2$P(CH$_2$)$_2$)$_2$CH]Ir(CH$_2$=CHMe) (**2-5a**) with excess ammonia at room temperature led to the generation of the desired Ir^{III} parent amido complex **2-6** with evolution of propene (Scheme 2-1, **B**).[18b] Complex **2-6** is a rare example of an isolable, monomeric amido hydride complex resulting from N-H bond oxidative addition of ammonia. Unfortunately,

facile N-H reductive elimination was also observed in this system upon exposure of the amido hydride complex to 1-pentene (Scheme 2-1, **2-5b**), which also renders challenging the development of further functionalization chemistry, such as insertion of an alkene or alkyne into the Ir-*N* bond.
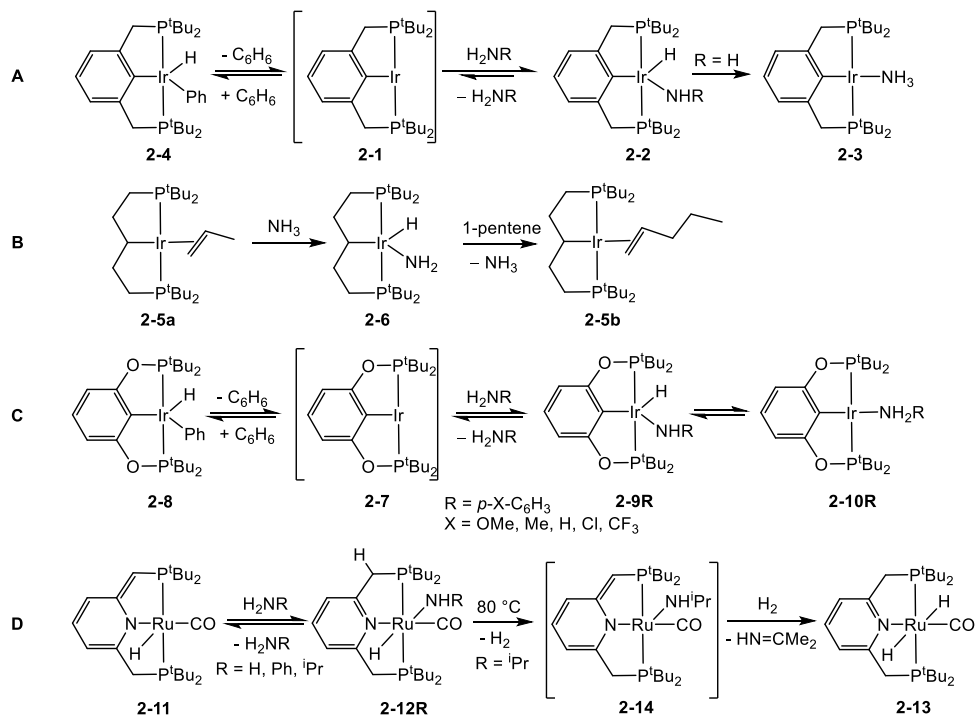
Scheme 2-1. N-H oxidative addition, and competitive reductive elimination, with (PCP)-, (POCOP)- and (PNP)M (M = Ir, Ru) complexes.

Hartwig and co-workers[40] have also investigated the N-H oxidative addition of hydrazines and have reported on the synthesis of hydrazido hydride Ir pincer complexes supported by PCP ligation. Initial studies showed that treatment of either **2-4** or **2-5a** with benzophenone hydrazone led to the formation of the stable N-H oxidative addition products of the form (PCP)Ir(H)(NHN=CPh$_2$) within minutes at room temperature. The hydrazido hydride complexes were not susceptible to reductive elimination, even in the presence of excess benzene or 1-pentene. N-H bond oxidative addition of 1-aminopiperidine was also

mediated by such (PCP)Ir species, however, upon mild heating, a second N-H bond activation was observed, forming an Ir aminonitrene complex of the type (PCP)Ir(N=NC$_5$H$_{10}$) and H$_2$.

Brookhart and co-workers[19] investigated the reactivity of (^{t}Bu-POCOP)Ir^I (**2-7**) in the oxidative addition of N-H bonds. They demonstrated that treatment of *in situ* generated **2-7** (Scheme 2-1, **C**) with a variety of anilines in benzene solution produced three products in equilibrium – (^{t}Bu-POCOP)Ir(H)(Ph) (**2-8**), (^{t}Bu-POCOP)Ir(H)(NHR) (**2-9R**) and the Lewis base adduct (^{t}Bu-POCOP)Ir(NH$_2$R) (**2-10R**, R = *p*-X-C$_6$H$_3$; X = OMe, Me, H, Cl, or CF$_3$). Equilibrium constants were found to be dependent on the *para*-substituent of the aniline. Electron donating groups in the *para* position increased the basicity of the aniline, resulting in a product distribution that favors the Ir^I adduct **2-10R**. Electron withdrawing groups in the *para* position decreased the basicity of the aniline, thereby rendering the N-H activation product **2-9R** as the favored species. The observed product mixtures indicate that once again this system appears to also be plagued by facile N-H reductive elimination. Related N-H bond activation studies with benzamides yielded products of the type (^{t}Bu-POCOP)Ir(H)(NHC(O)Ar).[19] X-Ray crystallographic data indicated significant interaction between the carbonyl group and the Ir center, thereby stabilizing the complex, and minimizing the occurrence of N-H reductive elimination.

An alternative mechanistic pathway involving metal-ligand cooperativity for the Ru-mediated N-H activation of amines and ammonia has been reported by Milstein and co-workers (Scheme 2-1, **D**).[28b] This reactivity utilizes a strategy of reversible aromatization/dearomatization of a pyridine based PNP ligand that the Milstein group has used extensively for E-H activation applications.[26a, 28, 41] The reactions take place *via* E-H oxidative addition with hydrogen transfer to the unsaturated ligand arm as determined with

mechanistic as well as computational investigations.[28b, 42] Treatment of (^{t}Bu-PNP)Ru(H)(CO) (**2-11**) with aniline led to proton transfer to the unsaturated ligand arm and aromatization of the pyridine unit to afford [(^{t}Bu-PNP)H]Ru(H)(NHPh)(CO) (**2-12Ph**). The related reaction of **2-11** with NH$_3$ (1 atm) led to coordination of NH$_3$, followed by the transfer of one H$^+$ from NH$_3$ to the ligand backbone, resulting in formation of a metal amido within 5 minutes to afford [(^{t}Bu-PNP)H]Ru(H)(NH$_2$)(CO) (**2-12H**). When ND$_3$ (1 atm) was used in place of NH$_3$, ^{2}H incorporation was observed into the ligand backbone and Ir-ND$_2$ positions. After 16 h at room temperature, complete ^{2}H incorporation was observed in the methylene positions on the ligand arms (adjacent to P), with 70% of the complex converted to Ru-*D* over Ru-*H*. Similar conditions executed with isopropylamine led to formation of the corresponding N-H activation product **2-12^{i}Pr**. When this complex was heated for 1 week at 80 °C, the formation of [(^{t}Bu-PNP)H]Ru(H)$_2$(CO) (**2-13**) was observed. This reactivity was proposed to involve H$_2$ elimination from **2-12^{i}Pr** to form the unsaturated dearomatized intermediate (^{t}Bu-PNP)Ru(NH^{i}Pr)(CO) (**2-14**), which was postulated on the basis of DFT studies.[43] Subsequent β-hydride elimination in **2-14** involving the N-^{i}*Pr* group generates isopropylimine and (^{t}Bu-PNP)Ru(H)(CO), which can then react with H$_2$ to form **2-13**.

While pincer ligation to late metal centers has been shown to aid N-H oxidative addition processes, the synthesis of stable amido hydride complexes for further amine functionalization remains a challenge. In this regard, studying the effects of ligand design on metal reactivity may aid in better understanding the elementary reaction steps involved in alternative hydroamination methodologies involving N-H activation.

2.1.2 N-H Bond Activation by Bis(phosphino)silyl Rh and Ir Complexes

Research in the Turculet group targets the synthesis of transition metal complexes

supported by silyl based PSiP pincer ligation (Figure 1-1, **K** & **L**). The decreased electronegativity of Si by comparison to C is predicted to render PSiP complexes more electron rich relative to PCP analogues. In the context of late transition metal chemistry, such electron rich metal centers may undergo oxidative addition processes more readily.[18c] The strongly σ-donating silyl group also exerts a significant *trans*-influence, more pronounced than Me or H,[44] that can support coordinative unsaturation at the metal center. The Turculet group introduced tridentate bis(phosphino)silyl ligands featuring an *ortho*-phenylene backbone (R-PSiP = $(2-R_2PC_6H_4)_2SiMe$, R= alkyl or aryl; Figure1-1, **K**) and demonstrated that such ligands are readily metalated *via* Si-H bond activation to afford a variety of reactive pincer complexes.[31-33, 36, 39, 45]

In the context of Group 9 metal chemistry, five-coordinate Rh and Ir complexes of the type (Cy-PSiP)MH(Cl) (**2-15a**, M = Rh; **2-15b**, M = Ir) proved readily accessible and were dehydrohalogenated *in situ* to provide access to reactive (Cy-PSiP)M^I (**2-16a**, M = Rh; **2-16b**, M = Ir) species that could be trapped as isolable 16-electron complexes of the type (Cy-PSiP)ML (**2-17a**, M = Rh, L = PMe$_3$; **2-17b**, M = Ir, L = C_2H_4; Scheme 2-2).[33a] The proposed 14-electron species **2-16a**, **b** are not isolable, and as such their formulation is tentative. In the case of **2-16b**, when generated in cyclohexane-d_{12} solution, evidence for a possible Ir-*H* was observed by ^{1}H NMR spectroscopy, suggesting that reversible metalation of the Cy-PSiP ligand (**2-18**) may play a role in the reactivity. While *in-situ* generated **2-16a** is relatively inert, **2-16b** is able to undergo room temperature C-H bond activation of benzene to afford (Cy-PSiP)IrH(Ph) (**2-19Cy**), which also undergoes arene exchange.[39] While sp^2-CH oxidative addition proved facile, no observation of sp^3-CH activation was observed, such that the reaction of *in situ* generated **2-16b** with toluene generated only products resulting from C-H activation in the *meta* and *para*-positions of

the arene.
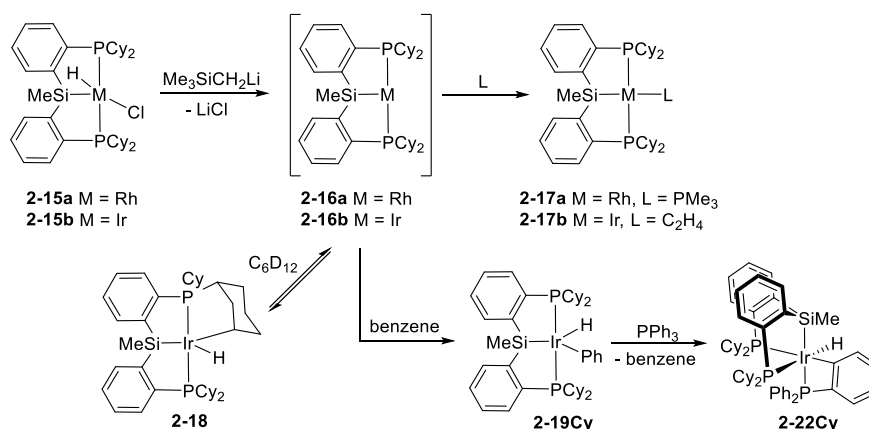
Scheme 2-2. Generation of (Cy-PSiP)M^I (M = Rh, Ir) and reactivity with CH bonds.

Following the report by the Turculet group on arene C-H oxidative addition by (Cy-PSiP)Ir, Shimada and co-workers[46] demonstrated that in the presence of a hydrogen acceptor, such as TBE, complexes of the type (R-PSiP)Ir(H)$_4$ (**2-20R**, R = Cy, ^{i}Pr, ^{t}Bu) also undergo C-H bond activation of benzene to afford (R-PSiP)IrH(Ph). Treatment of **2-20Cy** with excess norbornene resulted in the formation of (Cy-PSiP)Ir(η^2-norbornene) (**2-21**), which is consistent with the dehydrogenation of such tetrahydride precursors in the presence of alkenes to generate Ir^I species. Furthermore, treatment of **2-19R** with 1 equiv. of PPh$_3$ resulted in reductive elimination of benzene and coordination and metalation of PPh$_3$, to afford six coordinate species of the type (R-PSiP)IrH[κ^2-C$_6$H$_4$(PPh$_2$)] (**2-22R**, Scheme 2-2).

The Turculet group extended the reactivity of (Cy-PSiP)M (M = Rh, Ir) species to the oxidative addition of N-H bonds (Scheme 2-3).[33b] *In situ* generated **2-16b** was found to undergo N-H bond oxidative addition of anilines and ammonia under mild conditions, resulting in the formation of mononuclear Ir^{III} amido hydride complexes of the type (Cy-PSiP)Ir(H)(NHR') (**2-23R'**, R' = aryl, H), which could be readily isolated. Reactivity

studies revealed that, in comparison to previously reported (PCP)Ir and (POCOP)Ir systems (*vide supra*), **2-23R'** proved to be significantly more resistant to N-H bond reductive elimination, even in the presence of alkene and arene substrates. This is an important feature, as the insertion of alkenes or alkynes into either the M-*H* or Ir-*N* bonds of **2-23R'** represents a step toward possible catalytic amination chemistry. Subsequent work[33c] further revealed that (R-PSiP)Ir (R = Cy, ^{i}Pr) also mediated the oxidative addition of N-H bonds in primary alkyl amines that lack β-H's (R' = ^{t}Bu, Ad), hydrazine derivatives H_2N-NR"$_2$ (**2-24R"**, R"$_2$ = C_5H_{10}, $(CH_2CH_2)_2NMe$), and benzamides $H_2N(C=O)R'''$ (**2-25R'''**, R''' = Ph, C_6F_5). However, the Rh^I analogue **2-16a** was generally unable to undergo N-H bond oxidative addition under similar conditions, instead forming the corresponding adducts (Cy-PSiP)Rh(NH$_2$R') (**2-26R'**, R' = aryl, alkyl, H).[33b]
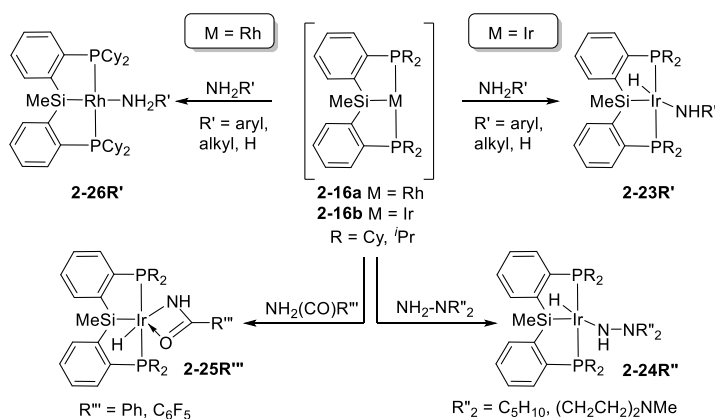
Scheme 2-3. N-H oxidative addition *via* (R-PSiP)M (R = Cy, ^{i}Pr; M = Rh, Ir).

While coordinatively unsaturated (Cy-PSiP)Ir species generated *in situ* were demonstrated to mediate N-H oxidative addition of various amines,[33b] subsequent studies for the insertion of alkenes and alkynes into the metal-amido linkages to develop catalytic chemistry were largely unsuccessful.[33c] As ligand design has proven to be an effective route for tuning reactivity at a metal center, it is possible that modifications to PSiP ligand design

may facilitate both N-H bond oxidative addition and subsequent insertion chemistry in the resulting complexes. Toward this end, this chapter details efforts to access new (PSiP)M (M = Rh, Ir) species featuring a 3-methylindole derived silyl pincer ligand, ^{i}Pr-PSiP^{Ind} (Scheme 2-4), with the goal of studying ligand effects on N-H bond activation reactivity. The strategy employed in this regard (Scheme 2-4) was to: (i) determine whether complexes of the type (^{i}Pr-PSiP^{Ind})MH(NHR) (R = H, alkyl, aryl) are synthetically feasible by exploring salt metathesis routes utilizing LiNHR reagents; (ii) investigate whether coordinatively and electronically unsaturated (^{i}Pr-PSiP^{Ind})M^I intermediates can be accessed from (^{i}Pr-PSiP^{Ind})MH(Cl); and (iii) study the reactivity of (^{i}Pr-PSiP^{Ind})M^I substrates with a variety of amines to see whether N-H oxidative addition occurs.
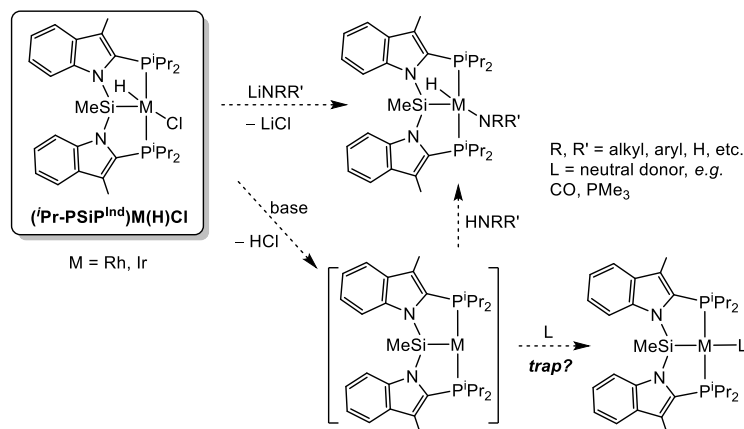
Scheme 2-4. Strategy for N-H bond activation studies using ^{i}Pr-PSiP^{Ind} pincer ligation.

2.2 Results and Discussion

2.2.1 Synthesis of (^{i}Pr-PSiP^{Ind})MH(Cl) (M = Rh, Ir) Precursor Complexes

The tertiary silane ligand precursor (^{i}Pr-PSiP^{Ind})H (**2-27**) was readily synthesized from commercially available 3-methylindole in 53% overall yield (Scheme 2-5; Table 2-1).[36, 47] The solid state structure of **2-27** was obtained by use of X-ray crystallographic techniques (Figure 2-1; Table 2-2) and confirmed the proposed connectivity. Treatment of

2-27 with 0.5 equiv. of [(COD)MCl]$_2$ (COD = 1,5-cyclooctadiene; M = Rh, Ir) afforded the corresponding (^{i}Pr-PSiP^{Ind})MH(Cl) (**2-28**, M = Rh; **2-29**, M = Ir; Scheme 2-2; Table 2-1) complexes in 95 and 70% yield, respectively, following heating in benzene solution for several days. NMR spectroscopic characterization of **2-28** and **2-29** (Table 2-1) was consistent with metalation of **2-27**, as indicated by the observation of a downfield-shifted M-*H* resonance in the corresponding ^{1}H NMR spectra of the isolated complexes, as well as the significant change in the ^{31}P and ^{29}Si NMR chemical shift for **2-27** *vs*. **2-28** and **2-29**. The observation of ^{31}P-^{103}Rh coupling in the ^{31}P{^{1}H} NMR spectrum of **2-28** ($^1J_{PRh}$ = 114 Hz) is further evidence of complexation. As well, the single ^{31}P{^{1}H} NMR resonance observed for each of **2-28** and **2-29** is indicative of chemically equivalent ^{31}P environments in each complex in solution.
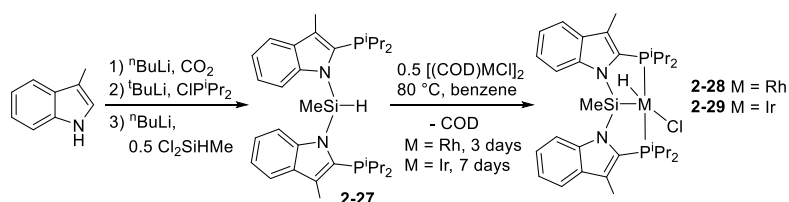
Scheme 2-5. Synthesis of the tertiary silane **2-27** and hydrido chloride complexes **2-28** and **2-29**.

28

Table 2-1. NMR spectroscopic data (ppm) for compounds **2-28** - **2-46** (benzene-d_6).

Compound		^{29}Si NMR	^{31}P{^{1}H} NMR	^{1}H NMR (hydride)	^{1}H NMR (N*H*)
(^{i}Pr-PSiP^{Ind})IrH(Cl)	**2-29**	-0.5	46.6	-22.44 (t)	n/a
(^{i}Pr-PSiP^{Ind})IrH(NHPh)	**2-31a**	8.9	41.5	-20.30 (t)	7.21
(^{i}Pr-PSiP^{Ind})IrH[NH(2,6-Me$_2$C$_6$H$_3$)]	**2-31b**	9.3	39.1	-20.02 (t)	6.32
(^{i}Pr-PSiP^{Ind})IrH[NH(2,6-^{i}Pr$_2$C$_6$H$_3$)]	**2-31c**	9.6	39.2	-19.78 (t)	7.03
(^{i}Pr-PSiP^{Ind})IrH[NH(p-FC$_6$H$_4$)]	**2-31d**	9.5	41.2	-20.42 (t)	7.12
(^{i}Pr-PSiP^{Ind})IrH[NH(p-OMeC$_6$H$_4$)]	**2-31e**	10.7	41.3	-20.20 (t)	7.52
(^{i}Pr-PSiP^{Ind})IrH[NH(p-MeC$_6$H$_4$)]	**2-31f**	9.98	41.3	-20.40 (t)	7.46
(^{i}Pr-PSiP^{Ind})IrH(NPh$_2$)	**2-32b**	0.9	40.9	-21.46 (t)	n/a
(^{i}Pr-PSiP^{Ind})IrH(NH^{t}Bu)	**2-33a**	11.8	40.8	-19.18 (t)	7.28
(^{i}Pr-PSiP^{Ind})IrH(NHAd)	**2-33b**	12.0	40.9	-19.07 (t)	7.18
(^{i}Pr-PSiP^{Ind})IrH(NH$_2$)	**2-34**	14.9	40.6	-19.17 (t)	5.42
(^{i}Pr-PSiP^{Ind})IrH[NH-N(CH$_2$CH$_2$)$_2$NMe]	**2-35a**	14.5	42.2 (AB q)	-19.08 (dd)	6.89 (d)
(^{i}Pr-PSiP^{Ind})IrH[NH-N(C$_5$H$_{10}$)]	**2-35b**	-	42.1 (AB q)	-19.03 (dd)	6.96 (d)
(^{i}Pr-PSiP^{Ind})IrH[NH(CO)Ph]	**2-37a**	8.3	35.5	-19.83 (br s)	5.90
(^{i}Pr-PSiP^{Ind})IrH[NH(CO)Me]	**2-37b**	8.1	35.2	-20.11 (br s)	4.65
[(^{i}Pr-PSiP^{Ind})Ir][a]	**2-40**	40.4	49.2	n/a	n/a
(^{i}Pr-PSiP^{Ind})Ir(C$_2$H$_4$)[a]	**2-41a**	-	44.7	n/a	n/a
(^{i}Pr-PSiP^{Ind})Ir(CO)$_2$	**2-41b**	35.2	32.0	n/a	n/a
(^{i}Pr-PSiP^{Ind})Ir(CO)	**2-41c**	75.3	55.6	n/a	n/a
(^{i}Pr-PSiP^{Ind})IrH(Cl)(CO)	**2-42**	38.4	29.6	n/a	n/a
(^{i}Pr-PSiP^{Ind})IrH(Ph)	**2-44**	-8.7	43.0	-10.60 (t)[a]	n/a
(^{i}Pr-PSiP^{Ind})IrH(Ph)(CO)	**2-45**	31.3	21.8	n/a	n/a
(^{i}Pr-PSiP^{Ind})IrH(2-FC$_6$H$_4$)	**2-46a**	-	45.3	-9.27 (app. q)	n/a
(^{i}Pr-PSiP^{Ind})IrH(2,5-F$_2$C$_6$H$_3$)	**2-46b**	-	45.1	-9.50 (dd)	n/a
(fac-κ^3-^{i}Pr-PSiP^{Ind})Ir(H)$_2$(NH=C$_6$H$_{10}$)[b]	**2-33c'**	21.4	23.1 (br)[c] 22.3 (br)[c]	-9.95 (m)	9.81
(fac-κ^3-^{i}Pr-PSiP^{Ind})IrH(κ^2-P,C-o-C$_6$H$_4$PPh$_2$)	**2-43**	25.0	28.8 (app. t) 7.2 (dd) -86.9 (dd)	-9.15 (app. dt)	n/a
(fac-κ^3-^{i}Pr-PSiP^{Ind})IrH(κ^2-N,C-o-C$_6$H$_4$NH$_2$)[a]	**2-31a'**	9.19	25.8 (d) 12.9 (d)	-6.64 (dd)	-
(fac-κ^3-^{i}Pr-PSiP^{Ind})IrH[κ^2-N,C-o-(p-FC$_6$H$_3$NH$_2$)]	**2-31d'**	9.05	23.8	-6.68 (app. q)	2.62
(fac-κ^3-^{i}Pr-PSiP^{Ind})IrH[κ^2-N,C-o-(p-OMeC$_6$H$_3$NH$_2$)]	**2-31e'**	-	25.5 (d) 13.3 (d)	-	-
(fac-κ^3-^{i}Pr-PSiP^{Ind})IrH[κ^2-N,C-o-(p-MeC$_6$H$_3$NH$_2$)]	**2-31f'**	-	24.5 (d) 13.3 (d)	-	-
(^{i}Pr-PSiP^{Ind})RhH(Cl)	**2-28**	38.9	44.2 (d)	-17.09 (dt)	n/a
(^{i}Pr-PSiP^{Ind})RhH(NHPh)	**2-30a**	39.8	46.6 (d)	-14.99 (app. q)	3.87
(^{i}Pr-PSiP^{Ind})RhH[NH(2,6-Me$_2$C$_6$H$_3$)]	**2-30b**	39.4	44.2 (d)	-15.12 (app. q)	2.85
(^{i}Pr-PSiP^{Ind})RhH[NH(2,6-^{i}Pr$_2$C$_6$H$_3$)]	**2-30c**	40.4	44.7 (d)	-15.83 (app. q)	5.25
(^{i}Pr-PSiP^{Ind})RhH(NPh$_2$)	**2-32a**	36.5	44.9 (d)	-17.04 (dt)	n/a
(^{i}Pr-PSiP^{Ind})RhH[NH(CO)Ph]	**2-36a**	48.2	48.8 (d)	-16.67 (m)	5.89
(^{i}Pr-PSiP^{Ind})RhH[NH(CO)Me]	**2-36b**	48.5	48.8 (d)	-16.90 (m)	4.67
[(^{i}Pr-PSiP^{Ind})Rh]$_2$(μ-N$_2$)	**2-38**	58.3	49.0 (d)	n/a	n/a
(^{i}Pr-PSiP^{Ind})Rh(PMe$_3$)	**2-39a**	63.4	57.3 (dd) 32.8 (dt)	n/a	n/a
(^{i}Pr-PSiP^{Ind})Rh(DMAP)	**2-39b**	60.8	40.9 (d)	n/a	n/a
(^{i}Pr-PSiP^{Ind})Rh(NH$_2$Ph)	**2-39c**	-	41.0 (d)	n/a	n/a

[a]Data acquired in cyclohexane-d_{12} solution. [b]Data acquired in THF-d_8 solution. [c] ^{31}P NMR data (^{1}H coupled).

X-Ray crystallographic characterization of **2-28** and **2-29** showed comparable coordination geometries and metrical parameters to those of the related (Cy-PSiP)MH(Cl) (M = Rh, Ir) complexes (Figure 2-1; Table 2-2).[33b, c] In the case of both **2-28** and **2-29**, a distorted five-coordinate structure is observed in the solid state (τ_5 = 0.27 for **2-28**, and 0.11 for **2-29**), with *trans*-disposed phosphino donors. For both structures, the hydrido ligand was located in the difference map and refined, and as previously noted for related five-coordinate Cy-PSiP hydrido complexes,[33a] a close Si···H contact (for **2-28**, Si···H = 2.15(4) Å; for **2-29**, Si···H = 2.187 Å; *cf.*, sum of van der Waals radii for Si and H[48] is 3.4 Å and the average Si-H bond in hydrosilanes[49] is typically set at 1.5 Å) was observed in each case, with the hydride ligand positioned *anti* relative to the Si-*Me*. Given the lack of accuracy in determining hydride positions in the vicinity of heavy elements with X-ray crystallographic techniques, this observation alone is not sufficient evidence to invoke a significant Si-H interaction. However, the consistency of this structural feature for five-coordinate hydride complexes with PSiP ligation is a notable trend. While no appreciable Si-H coupling was measured in solution for **2-29**, an Si-H coupling constant of 26 Hz was measured for the Rh analogue **2-28** (benzene-d_6). Computational studies[50] involving five-coordinate d^6 metal complexes have invoked M-L π-donor interactions as playing a key role in geometric distortions involving such complexes, and such interactions may indeed also contribute to the observed geometries in PSiP complexes that feature ligands capable of functioning as π-donors (*e.g.* chloro, amido).
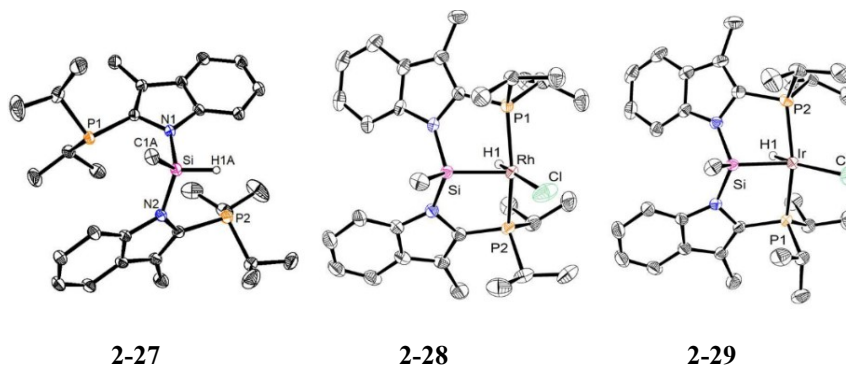
2-27   **2-28**   **2-29**

Figure 2-1. The crystallographically determined structures of **2-27**, **2-28**, and **2-29**, shown with 50% displacement ellipsoids. Most hydrogen atoms have been omitted for clarity.

Table 2-2. Selected bond distances (Å) and angles (deg.) for **2-27** - **2-29**.

2-27	2-28	2-29
Si-C(1A) 1.828(2)	Rh-P(1) 2.2858(11)	Ir-P(1) 2.2954(5)
Si-N(1) 1.7575(14)	Rh-P(2) 2.2965(10)	Ir-P(2) 2.3061(5)
Si-N(2) 1.7588(14)	Rh-H 1.27(4)	Ir-H 1.42(3)
Si-H(1A) 1.33(2)	Rh-Cl 2.4056(13)	Ir-Cl 2.3801(6)
C(1A)-Si-H(1A) 109.1(10)	Cl-Rh-H(1) 173.7(19)	Cl-Ir-H(1) 154.8(11)
N(1)-Si-N(2) 112.45(7)	Cl-Rh-Si 114.39(5)	Cl-Ir-Si 135.80(2)
	Si-Rh-H(1) 70.1(19)	Si-Ir-H(1) 69.1(11)
	P(1)-Rh-P(2) 157.59(4)	P(1)-Ir-P(2) 161.692(19)

2.2.2 Synthesis of (^{i}Pr-PSiP^{Ind})MH(NHR) Complexes (M = Rh, Ir)

The synthesis of Rh and Ir aryl- and alkylamido hydride complexes *via* a salt metathesis route was targeted initially, with the goal of determining the synthetic feasibility of such complexes. The anilido hydride complexes (^{i}Pr-PSiP^{Ind})MH(NRR') (Figure 2-2; M = Rh, R' = H: **2-30a** , R = Ph; **2-30b**, R = 2,6-Me$_2$C$_6$H$_3$; **2-30c**, R = 2,6-^{i}Pr$_2$C$_6$H$_3$; M = Ir, R' = H: **2-31a**, R = Ph; **2-31b**, R = 2,6-Me$_2$C$_6$H$_3$; **2-31c**, R = 2,6-^{i}Pr$_2$C$_6$H$_3$; **2-31d**, R = *p*-FC$_6$H$_4$; **2-31e**, R = *p*-OMeC$_6$H$_4$, **2-31f**, R = *p*-MeC$_6$H$_4$; M = Rh, R' = R = Ph, **2-32a**; M = Ir, R' = R = Ph, **2-32b**) were readily prepared by the reaction of either **2-28** or **2-29**, respectively, with 1 equiv. of the corresponding lithium anilide reagent Li(NRR'). These reactions occurred readily at room temperature within 15 – 60 minutes of mixing in benzene solution, with quantitative conversion observed by ^{31}P{^{1}H} NMR spectroscopy. While the

Ir complexes proved readily isolable in yields ranging from 76 - 97%, substantially lower isolated yields were often obtained for the Rh analogues, where N-H reductive elimination appears to play a more significant role (*vide infra*). NMR spectroscopic characterization (Table 2-1) of complexes **2-30** – **2-32** is consistent with the formation of C_s-symmetric anilido hydride complexes. No appreciable Si-H coupling constant (>10 Hz) was measured in solution for either **2-30a** or **2-31a**. Single crystal X-ray crystallographic data for **2-31a** - **c** (Figure 2-3, Table 2-3) support their formulation. In each case, the solid state structure indicates a five-coordinate metal center with coordination geometry similar to that of **2-28** and **2-29** (τ_5 = 0.088 for **2-31a**, 0.28 for **2-31b**, and 0.081 for **2-31c**), as well as related Cy-PSiP anilido hydride pincer complexes previously reported.[33] Acute Si-Ir-H1 angles are observed for all three structures, resulting in Si···H1 contacts ranging from 2.16–2.31 Å. A similarly acute H-Ir-C angle of 74.3° was observed for the related PCP pincer complex (ᵗBu-PCP)IrH(NHPh).[18a] The Ir-$N_{anilido}$ distances in **2-31a−c** are slightly shorter than those previously observed for (Cy-PSiP)IrH(NHPh) (2.056(2) Å), (Cy-PSiP)IrH(NH-2,6-Me$_2$C$_6$H$_3$) (2.077(3) Å),[33b] and (ᵗBu-PCP)IrH(NHPh) (2.082(2) Å).[18a] For each of **2-31a−c** the geometry at the anilido nitrogen is planar.
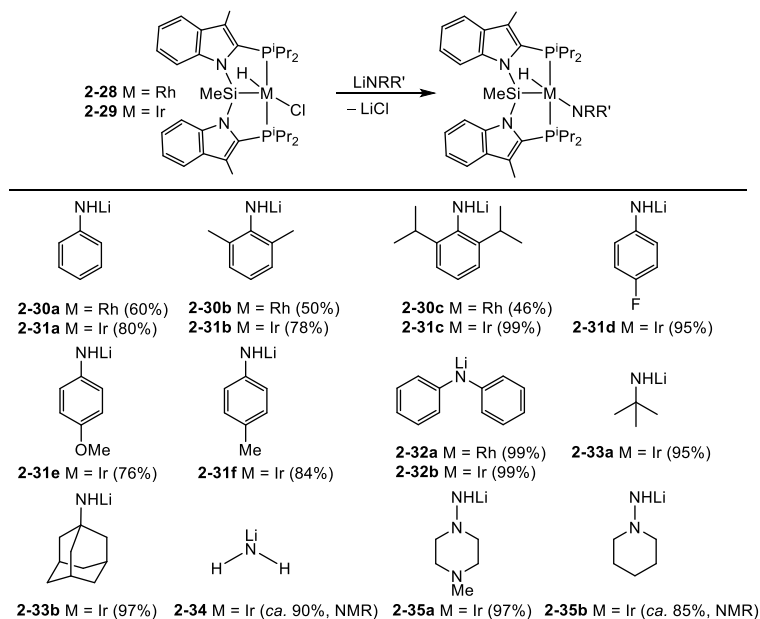
Figure 2-2. Synthesis of anilido, alkylamido, and hydrazido hydride complexes of Rh and Ir.

Interestingly, a minute amount of X-ray quality crystals obtained from a sample of crude **2-30a** revealed an alternative structure (**2-30a'**, Figure 2-3, Table 2-3) that features the NHPh group bound to Si, cleavage of a Si-N-indolyl bond, and transfer of the indolyl nitrogen donor to Rh to form a 4-membered Rh-N-C-P metallacycle (Figure 2-4). Complex **2-30a'** is not consistent with the solution spectroscopic data obtained for **2-30a**, as **2-30a'** features inequivalent phosphorus environments. As such, it appears that **2-30a'** does not represent the bulk compound and is likely a minor impurity. The formation of **2-30a'** is reminiscent of a related rearrangement previously observed for square planar (Cy-PSiP)MR (M = Ni, Pd; R = alkyl) complexes,[51] and serves to illustrate a possible decomposition pathway for such ^{i}Pr-PSiP^{Ind} complexes.

33

2-31a   2-31b   2-31c
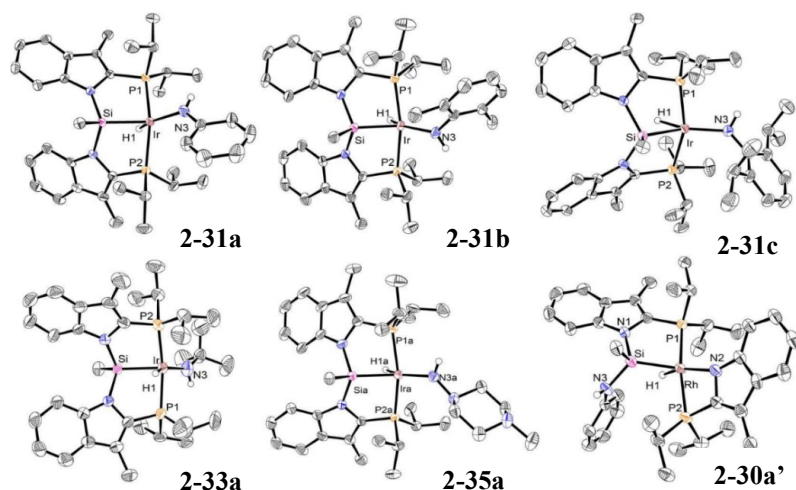
2-33a   2-35a   2-30a'

Figure 2-3. The crystallographically determined structures of **2-31a-c**, **2-33a**, **2-35a**, and **2-30a'** shown with 50% displacement ellipsoids. Most hydrogen atoms have been omitted for clarity.

Table 2-3. Selected bond distances (Å) and angles (deg.) for **2-31a-c**, **2-33a**, **2-35a**, and **2-30a'**.

2-31a	**2-31b**	**2-31c**
Ir-P(1) 2.2872(5)	Ir-P(1) 2.3040(11)	Ir-P(1) 2.2988(4)
Ir-P(2) 2.3056(5)	Ir-P(2) 2.3046(11)	Ir-P(2) 2.3108(4)
Ir-Si 2.2619(5)	Ir-Si 2.2571(11)	Ir-Si 2.2603(4)
Ir-N(3) 2.0336(19)	Ir-N(3) 2.019(4)	Ir-N(3) 2.0315(15)
Ir-H(1) 1.48(3)	Ir-H(1) 1.492(10)[b]	Ir-H(1) 1.56(2)
Si···H1 2.20	Si···H(1) 2.31	Si···H(1) 2.16
P(1)-Ir-P(2) 155.88(2)	P(1)-Ir-P(2) 162.67(4)	P(1)-Ir-P(2) 157.28(2)
Si-Ir-H(1) 71.5(10)	Si-Ir-H(1) 73(2)	Si-Ir-H(1) 67.5(9)
Si-Ir-N(3) 137.52(6)	Si-Ir-N(3) 141.09(12)	Si-Ir-N(3) 139.95(5)
N(3)-Ir-H(1) 150.6(10)	N(3)-Ir-H(1) 146(3)	N(3)-Ir-H(1) 152.4(9)
$\Sigma_{\angle s(N3)}$ = 359.8	$\Sigma_{\angle s(N3)}$ = 357.5[c]	$\Sigma_{\angle s(N3)}$ = 359.9

2-33a	**2-35a**[a]	**2-30a'**
Ir-P(1) 2.2956(13)	Ir-P(1) 2.2880(7)	Rh-P(1) 2.2876(11)
Ir-P(2) 2.2921(14)	Ir-P(2) 2.2815(7)	Rh-P(2) 2.3214(11)
Ir-Si 2.2579(12)	Ir-Si 2.2761(7)	Rh-Si 2.2431(12)
Ir-N(3) 1.997(5)	Ir-N(3) 1.982(2)	Rh-N(2) 2.130(4)
Ir-H(1) 1.36(5)	Ir-H(1) 1.50(3)	Rh-H(1) 1.42(5)
Si···H(1) 2.26	Si···H(1) 2.21	Si···H(1) 1.96(5)
P(1)-Ir-P(2) 152.50(5)	P(1)-Ir-P(2) 163.87(3)	P(1)-Rh-P(2) 169.75(4)
Si-Ir-H(1) 73(2)	Si-Ir-H(1) 68.1(13)	Si-Rh-H(1) 60(2)
Si-Ir-N(3) 131.66(16)	Si-Ir-N(3) 145.05(8)	Si-Rh-N(2) 132.6(1)
N(3)-Ir-H(1) 152(2)	N(3)-Ir-H(1) 146.6(13)	N(2)-Rh-H(1) 163(2)
$\Sigma_{\angle s(N3)}$ = 359.8[d]	$\Sigma_{\angle s(N3)}$ = 359.9	

[a]One of two crystallographically independent molecules. [b]Distance constrained during refinement: d(Ir–H1) = 1.50(1) Å. [c]Angles include distances constrained during refinement: d(Ir–H1) = 1.50(1) Å; d(N3–H3N) = 0.88(1) Å. [d]Average, taking into consideration positional disorder involving C2.

34
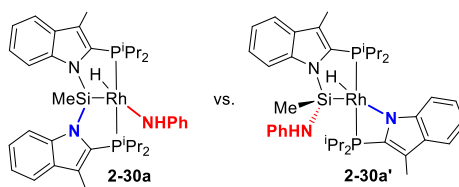
Figure 2-4. Isomers of (iPr-PSiPInd)RhH(NHPh), **2-30a** and **2-30a'**.

In an effort to extend the synthesis of Group 9 amido hydride complexes to alkyl and parent amido derivatives, complexes **2-28** and **2-29** were also treated with the corresonding LiNHR (R = tBu, 1-Ad, H) reagent (Figure 2-2). While reactions of this type involving **2-28** typically led to the formation of multiple unidentified products (by ^{1}H and ^{31}P NMR), analogous reactivity involving **2-29** led to the formation of amido complexes of the type (iPr-PSiPInd)IrH(NHR) (**2-33a**, R = tBu; **2-33b**, R = 1-Ad; **2-34**, R = H),which proved isolable in the case of **2-33a** and **2-33b** (Table 2-1). In the case of the parent amido derivative **2-34**, while the *in situ* formation of the targeted complex can be observed spectroscopically, attempts to isolate pure **2-34** resulted in the gradual decomposition of this complex to a mixture of unidentified species. As such, complex **2-34** could not be isolated in pure form. This observation stands in contrast to the relative stability of the analogous (Cy-PSiP)IrH(NH2) complex.[33b] As in the case of the related anilido derivatives, NMR spectroscopic characterization of **2-33a–b** and **2-34** (Table 2-1) is consistent with the formation of C_s-symmetric amido hydride species, as indicated by the observation of a downfield-shifted Ir-*H* resonance in the corresponding ^{1}H NMR spectra of these complexes, as well as a single ^{31}P{^{1}H} NMR resonance in each case. Once again, no appreciable Si-H coupling constant (>10 Hz) was measured in solution for **2-33a**. The solid-state structure of **2-33a** (Figure 2-3; Table 2-3) was determined by use of X-ray crystallographic techniques and is comparable to the related anilido hydride complexes **2-**

31a – c. (τ_5 = 0.0083). The Ir-N3 distance of 1.997(5) Å is in the range of those observed for the anilido derivatives and the geometry at the amido nitrogen is once again planar. Such examples of coordinatively unsaturated late metal alkylamido hydride complexes are exceedingly rare.[28b, 52]

The reactivity of alkylamido reagents containing β-hydrogens, such as Me$_2$NLi, ^{i}Pr$_2$NLi and (PhCH$_2$)HNLi, with **2-28** and **2-29** was also investigated, however such reactions led to the formation of multiple unidentified products (by ^{1}H and ^{31}P NMR) from which no pure material could be isolated. Interestingly, the reaction of **2-29** with 1 equiv. of LiNHCy in benzene solution led to the initial formation of an intermediate dihydride species **2-33c** (^{31}P{^{1}H} NMR: 44.8 ppm; ^{1}H NMR: Ir-H at -8.52 (dt, $^2J_{PH}$ = 16 Hz, $^2J_{HH}$ = 4 Hz) and -21.80 (dt, $^2J_{PH}$ = 19 Hz, $^2J_{HH}$ = 4 Hz) ppm), which appears to undergo a subsequent transformation to form a new dihydride product **2-33c'** that precipitates from solution over the course of the reaction. Complexes **2-33c** and **2-33c'** are tentatively assigned on the basis of NMR spectroscopic data as isomers of an Ir dihydride complex that features a cyclohexanimine ligand[18c] resulting from β-hydride elimination in a proposed cyclohexylamido hydride Ir intermediate (Scheme 2-6). While the NMR features of **2-33c** are consistent with a *cis*-dihydride Ir complex featuring *mer*-κ^3-^{i}Pr-PSiP^{Ind} coordination, the spectroscopic features of **2-33c'** suggest a *cis*-dihydride *fac*-κ^3-^{i}Pr-PSiP^{Ind} formulation leading to magnetically non-equivalent hydride and phosphino ligand environments. The ^{1}H NMR spectrum of **2-33c'** (THF-d_8) features a hydride resonance centered at -9.93 ppm (2 H) that exhibits second order effects, and a downfield-shifted N-H resonance at 9.84 ppm (1 H) that is assigned to the coordinated cyclohexanimine moiety. The ^{1}H{^{31}P} NMR spectrum of **2-33c'** features a singlet resonance at -9.93 ppm

36

corresponding to the magnetically equivalent hydride ligands in the absence of ^{31}P-coupling (Figure 2-5). In keeping with this scenario, while the ^{31}P{^{1}H} NMR spectrum of **2-33c'** features a single resonance at 22.5 ppm, the ^{31}P NMR spectrum features two resonances at 23.1 and 22.3 ppm, respectively (Figure 2-5). Collectively, these data are consistent with the proposed structure of **2-33c'**. Due to the poor solubility of **2-33c'**, it could not be effectively separated from the LiCl generated in the initial salt metathesis reaction.
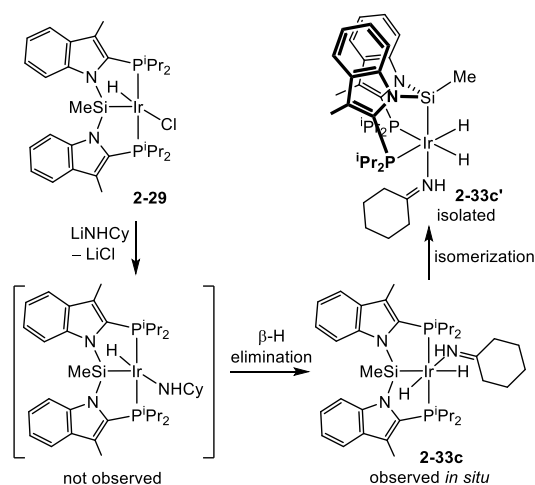
Scheme 2-6. β-Hydride elimination from an Ir cyclohexylamido intermediate.
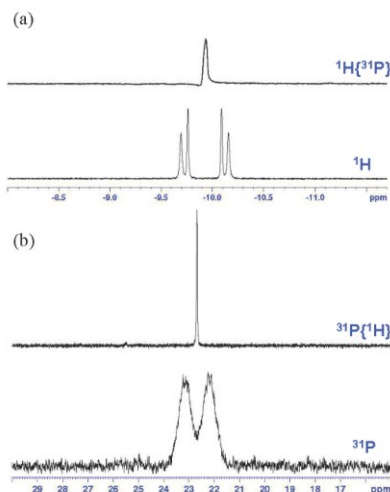
Figure 2-5. (a) ^{1}H and (b) ^{31}P NMR data for **2-33c'** (THF-d_8) highlighting magnetically non-equivalent hydride and phosphino ligand environments.

37

Having noted that alkylamido and anilido complexes supported by ^{i}Pr-PSiP^{Ind} ligation are accessible, further investigations targeted the synthesis of related hydrazido (Figure 2-2) and amidate complexes (Figure 2-6). In the case of Ir, the hydrazido complex (^{i}Pr-PSiP^{Ind})IrH(NH-NR$_2$) (**2-35a**, R$_2$ = (CH$_2$CH$_2$)$_2$NMe) was readily accessible by treatment of **2-29** with the corresponding LiNH-NR(CH$_2$CH$_2$)$_2$NMe. Related Ir hydrazido complexes supported by PCP[40] and PSiP[33c] ligation have been reported, and a comparison of NMR spectroscopic features for **2-35a** (Table 2-1) with these previous examples is consistent with the formulation of this complex as a hydrazido hydride species. A unique feature for such hydrazido pincer complexes is the observation of inequivalent phosphorus environments, as evidenced by the appearance of an AB quartet in the ^{31}P{^{1}H} NMR spectrum of **2-35a** (42.6 ppm, Δv_{AB} = 661 HZ, J_{AB} = 299 Hz). This phenomenon is likely a result of hindered rotation involving the hydrazido ligand, possibly due to increased N to Ir π-donation relative to related anilido and amido derivatives. X-Ray crystallographic data obtained for **2-35a** (Figure 2-3; Table 2-3) further confirms the formulation of this complex and reveals a solid-state structure (τ_5 = 0.29) that is analogous to the related anilido and alkylamido Ir species **2-31a** - **c** and **2-33a**. The Ir-N3 distance of 1.982(2) Å is somewhat shorter than that observed for the anilido derivatives (Ir-N3 = 2.0336(19) Å for **2-31a**, 2.019(4) for **2-31b**, and 2.0315(15) Å for **2-31c**), which may reflect the proposed increase in Ir-N π-bonding. The PCP pincer derivative [κ^3-(^{t}Bu$_2$P(CH$_2$)$_2$)$_2$CH]IrH(NH-NC$_5$H$_{10}$) features a comparably short Ir-N distance of 1.9875(18) Å.[40]

Treatment of **2-29** with LiNH-N(CH$_2$CH$_2$)$_2$CH$_2$ resulted in *ca.* 85% conversion (by ^{31}P NMR) to a product tentatively assigned as (^{i}Pr-PSiP^{Ind})IrH(NH-N(CH$_2$CH$_2$)$_2$CH$_2$ (**2-35b**; Figure 2-2; Table 2-1). The mixture also contained *ca.* 15% (by ^{31}P NMR) of an

additional (^{i}Pr-PSiP^{Ind})Ir product (^{31}P{^{1}H} NMR: 44.4 ppm (br s), ^{1}H NMR: Ir-H at -22.27

ppm) that could not be effectively separated from **2-35b**. Heating of the reaction mixture

up to 60 °C in THF did not result in the complete conversion to **2-35b**. Related reactions

involving **2-28** formed complex mixtures containing multiple unidentified products (by ^{1}H

and ^{31}P NMR) from which no pure material could be isolated.

The amidate derivatives (^{i}Pr-PSiP^{Ind})MH(NH(CO)R) (M = Rh: **2-36a**, R = Ph; **2-

36b**, R = Me; M = Ir: **2-37a**, R = Ph; **2-37b**, R = Me) were prepared by a protonolysis route

involving treatment of either **2-30a** or **2-31a**, respectively, with 1 equiv. of either

benzamide or acetamide (Figure 2-6; Table 2-1). These complexes were found to be readily

isolable with yields varying from 75–95 %. Related POCOP[19] and PSiP[33c]-supported Ir

benzamidate complexes have been previously reported, and these exhibited bidentate

coordination of the amidate ligand in the solid state. While X-ray crystallographic

characterization of **2-36a,b** and **2-37a,b** has thus far proven elusive, these complexes are

tentatively assigned as six-coordinate species featuring bidentate amidate ligands, by

analogy with the previously reported analogues.
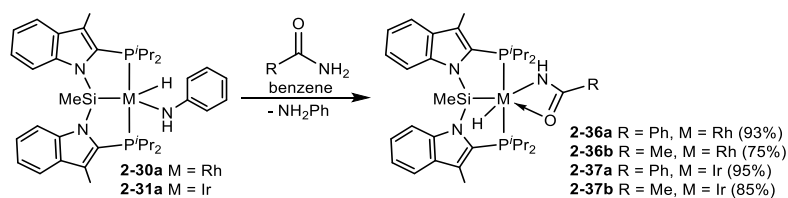
Figure 2-6. Synthesis of amidate hydride complexes.

Having found that a variety of Rh and Ir anilido, amido, hydrazido, and amidate

hydride complexes supported by the new indolylphosphino ^{i}Pr-PSiP^{Ind} ligation are

synthetically feasible and readily isolable, the relative thermal stability of these complexes

was evaluated. In previously reported examples of related PCP[18a] and POCOP-supported[19]

Ir amido and anilido hydride complexes, N-H reductive elimination was typically observed, such that the Ir^{III} amido hydride species were found to be in equilibrium with both Ir^I products of N-H reductive elimination as well as Ir^{III} phenyl hydride complexes resulting from subsequent C-H oxidative addition of benzene solvent (Scheme 2-1). By comparison, (Cy-PSiP)IrH(NHR) (R = aryl, alkyl, H) complexes were found to be resistant to such N-H reductive elimination processes, including in benzene solvent, in most cases even upon heating at temperatures up to 80 °C.[33b, c, 39] In the case of the ^{i}Pr-PSiP^{Ind} supported complexes described herein, the Rh and Ir complexes **2-30a – 2-37b** were found to be stable in the solid state at room temperature under an N_2 atmosphere for several weeks, as indicated by ^{1}H and ^{31}P NMR spectroscopy. Heating to 80 °C in either toluene-d_8 or benzene-d_6 solution led to N-H reductive elimination in **2-30a – 2-30c** within 6 h, to quantitatively form a new Rh-containing species (**2-38**, Scheme 2-7) that was subsequently identified as an N_2 adduct of (^{i}Pr-PSiP^{Ind})Rh involving coordination of N_2 from the reaction atmosphere (*vide infra*). No evidence of benzene activation was noted in these studies. By comparison, (^{i}Pr-PSiP^{Ind})Ir anilido and alkylamido hydride complexes **2-31a – 2-31c**, **2-33a**, **2-33b** and **2-34** proved much more robust when heated to 80 °C, and were resistant to N-H reductive elimination for up to one week of heating.

2.2.3 Synthesis of (^{i}Pr-PSiP^{Ind})M^I and (^{i}Pr-PSiP^{Ind})M(L) Species

Having shown that various Rh^{III} and Ir^{III} anilido, alkylamido, hydrazido, and amidate hydride complexes supported by ^{i}Pr-PSiP^{Ind} ligation are isolable, subsequent investigations targeted the synthesis of such complexes by N-H oxidative addition. Toward this end, the generation and characterization of coordinatively unsaturated (^{i}Pr-PSiP^{Ind})M^I (M = Rh, Ir) precursors was targeted. Treatment of **2-28** with 1 equiv. of Me$_3$SiCH$_2$Li at room temperature in benzene solution led to the rapid (upon mixing) and quantitative (by

^{1}H and ^{31}P NMR) formation of Me$_4$Si and a new (^{i}Pr-PSiP^{Ind})Rh species (**2-38**) that has been identified as an N$_2$ adduct of (^{i}Pr-PSiP^{Ind})Rh involving coordination of N$_2$ from the reaction atmosphere (Scheme 2-7; Table 2-1). Complex **2-38** also forms upon N-H reductive elimination in the Rh anilido species **2-30a−c** (*vide supra*, Scheme 2-7). The Raman spectrum of **2-38** features a relatively intense band at 2,073 cm^{-1}, which is consistent with an M-*N$_2$* stretching vibration (*cf.* ν_{NN} of 2,331 cm^{-1} for free N$_2$). While complex **2-38** is isolable it appears to decompose over the course of several days in the solid state at room temperature or upon extended exposure to vacuum. By comparison, the product resulting from analogous dehydrohalogenation of (Cy-PSiP)RhH(Cl) could not be isolated, though it served as a source of (Cy-PSiP)Rh^I and could be trapped by the addition of donors such as PMe$_3$.[33b] The solid state structure of **2-38** was determined by use of X-ray crystallographic techniques and reveals a dinuclear complex with an equivalent of N$_2$ bridging two (^{i}Pr-PSiP^{Ind})Rh moieties in an end-on fashion (Figure 2-7; Table 2-4).
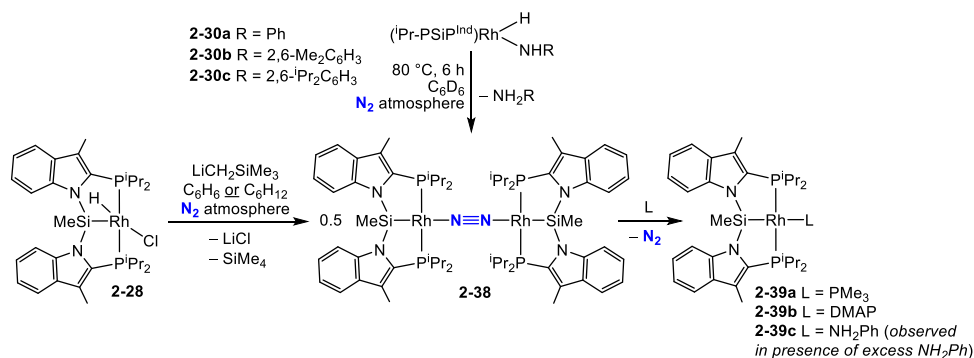
Scheme 2-7. Generation and trapping of (^{i}Pr-PSiP^{Ind})Rh^I species.

Dehydrohalogenation of **2-28** by treatment with Me$_3$SiCH$_2$Li in the presence of alternative L-donors resulted in the quantitative (by ^{31}P NMR) formation of isolable adducts formulated as (^{i}Pr-PSiP^{Ind})RhL (**2-39a**, L = PMe$_3$; **2-39b**, L = DMAP; Scheme 2-7; Table 2-1). Complex **2-39b** was crystallographically characterized (Figure 2-7; Table 2-

4), confirming the assignment of this complex as a four-coordinate species featuring distorted square planar coordination geometry at the Rh center ($\tau_4 = 0.33$, $\tau'_4 = 0.29$).

2-38   **2-39b**   **2-43**
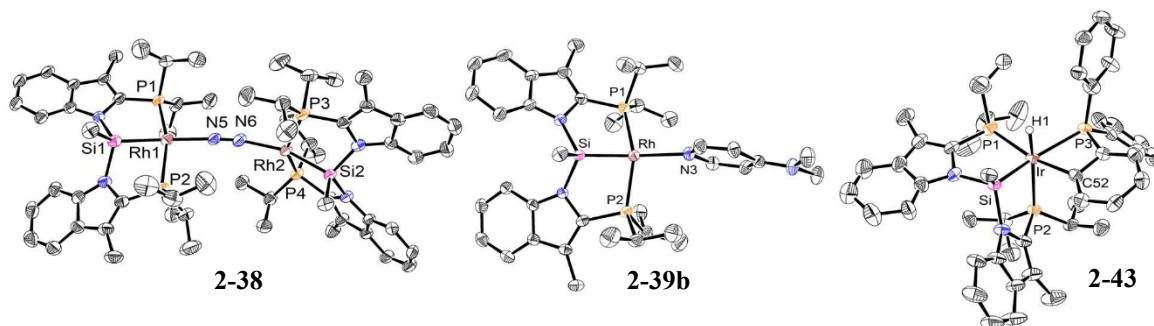
Figure 2-7. The crystallographically determined structures of **2-38**, **2-39b**, and **2-43** shown with 50% displacement ellipsoids. Most hydrogen atoms have been omitted for clarity.

Table 2-4. Selected bond distances (Å) and angles (deg.) for **2-38**, **2-39b**, and **2-43**.

2-38	2-39b	2-43
Rh(1)-P(1) 2.2707(11)	Rh-P(1) 2.2609(7)	Ir-P(1) 2.2878(19)
Rh(1)-P(2) 2.2819(12)	Rh-P(2) 2.2746(7)	Ir-P(2) 2.3977(16)
Rh(1)-Si(1) 2.2796(14)	Rh-Si 2.2282(8)	Ir-P(3) 2.490(2)
Rh(1)-N(5) 2.055(4)	Rh-N(3) 2.230(2)	Ir-Si 2.2620(17)
Rh(2)-P(3) 2.2968(11)	P(1)-Rh-P(2) 150.66(3)	Ir-C(52) 2.164(7)
Rh(2)-P(4) 2.2873(11)	P(1)-Rh-Si 83.67(3)	Ir-H(1) 1.497(10)[a]
Rh(2)-Si(2) 2.2513(12)	P(1)-Rh-N(3) 102.05(7)	P(1)-Ir-P(2) 108.43(8)
Rh(2)-N(6) 2.077(4)	Si-Rh-N(3) 162.89(7)	Si-Ir-H(1) 83(3)
N(5)-N(6) 1.094(6)		P(2)-Ir-H(1) 164(3)
P(1)-Rh(1)-P(2) 157.78(5)		Si-Ir-P(3) 154.27(6)
Si(1)-Rh(1)-N(5) 176.86(12)		P(1)-Ir-C(52) 163.91(19)
Si(2)-Rh(2)-N(6) 159.31(13)		
P(3)-Rh(2)-P(4) 146.14(5)		
Rh(1)-N(5)-N(6) 176.3(4)		
Rh(2)-N(6)-N(5) 168.1(4)		

[a]Distance constrained to 1.50(1) Å during refinement.

By comparison, treatment of **2-29** with 1 equiv. of Me$_3$SiCH$_2$Li at room temperature in cyclohexane-d_{12} solution led to the rapid (upon mixing) and quantitative (by ^{1}H and ^{31}P NMR) formation of Me$_4$Si and a new (^{i}Pr-PSiP^{Ind})Ir species (**2-40**; Scheme 2-8; Table 2-1). Attempts to isolate this complex resulted in decomposition such that no clean material

could be isolated. *In-situ*-generated **2-40** was also observed to decompose over the course of an hour at room temperature in cyclohexane solution. The $^{31}P\{^1H\}$ NMR spectrum of **2-40** features a characteristic resonance at 49.2 ppm, and the ^1H NMR spectrum (cyclohexane-d_{12}) contains no evidence for an Ir-H. While the NMR features observed for **2-40** support the formulation of this complex as a C_s-symmetric Ir^I species, this complex is likely stabilized by additional coordination, as three-coordinate, 14-electron (^iPr-PSiP^{Ind})Ir is anticipated to be highly reactive. Previous studies into the dehydrohalogenation of (Cy-PSiP)IrH(Cl) revealed that a similarly reactive species was generated.[33b, c] However, a broad Ir-H ^1H NMR resonance was observed suggesting that ligand metalation processes might be implicated in the stabilization of (Cy-PSiP)Ir. As no such evidence was noted for **2-40**, other possible stabilizing features include potential agostic interactions involving P^iPr groups, although no NMR or IR evidence for such interactions was observed. Alternatively, given the observation that N$_2$ coordinates to (^iPr-PSiP^{Ind})Rh, it is possible that **2-40** also exists as an N$_2$ adduct. However, we were unable to observe an N$_2$ stretch for **2-40** by use of solution IR techniques. Morales-Morales, Jensen and co-workers[53] have reported the related N$_2$-bridged dinuclear complex [(^tBu-PCP)Ir]$_2(\mu$-N$_2)$ (ν_{NN} = 2078 cm^{-1}).
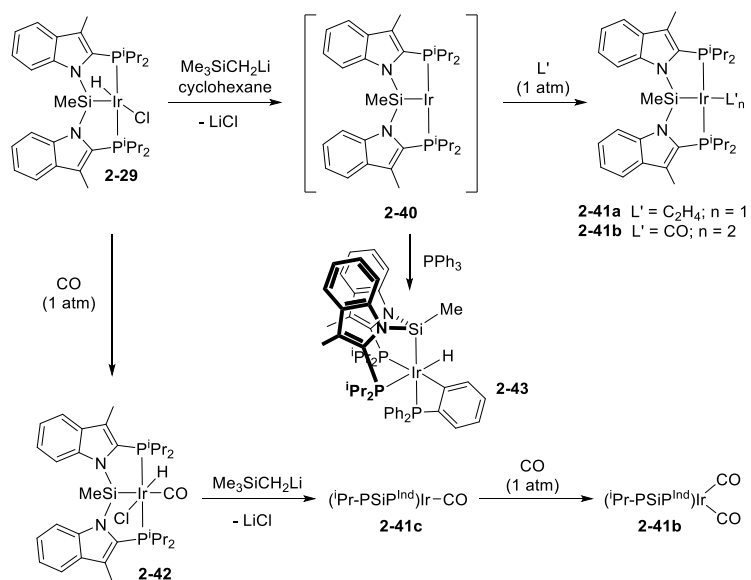
Scheme 2-8. Generation and trapping of (^{i}Pr-PSiP^{Ind})Ir^I species.

As the highly reactive nature of **2-40** precludes the isolation of this compound, efforts to trap this postulated Ir^I species by treatment of *in situ* generated **2-40** (cyclohexane-d_{12}) with two electron donors were attempted (Scheme 2-8). While such reactivity proceeded smoothly for **2-38**, treatment of **2-40** with DMAP or PMe$_3$ led to the formation of multiple products from which no pure material could be isolated. The reaction of **2-40** with ethylene (1 atm) led to the formation of a single new product (**2-41a**) whose NMR features are consistent with the formulation (^{i}Pr-PSiP^{Ind})Ir(C$_2$H$_4$) (Scheme 2-8). The latter complex, generated *in situ*, gives rise to a ^{31}P{^{1}H) NMR resonance at 44.7 ppm as well as a singlet ^{1}H NMR resonance at 2.02 ppm (4 H) that is consistent with 1 equiv. of bound ethylene. Attempts to isolate this species were unsuccessful, likely due to the highly reactive nature of this complex. Attempts to access such an ethylene adduct by treatment of **2-29** with ethylene and subsequent dehydrohalogenation with Me$_3$SiCH$_2$Li also proved unsuccessful. The observed formation of **2-41a** from *in situ* generated **2-40** does, however, suggest that **2-40** is a viable source of (^{i}Pr-PSiP^{Ind})Ir^I. This Ir^I species was also successfully

trapped with CO (1 atm) to form isolable (^{i}Pr-PSiP^{Ind})Ir(CO)$_2$ (**2-41b**; Scheme 2-8, Table 2-1). The monocarbonyl complex (^{i}Pr-PSiP^{Ind})Ir(CO) (**2-41c**) could also be synthesized by initial treatment of **2-29** with CO (1 atm) to form (^{i}Pr-PSiP^{Ind})Ir(H)(Cl)(CO) (**2-42**), and subsequent dehydrohalogenation with Me$_3$SiCH$_2$Li. Storage of **2-41c** under an N$_2$ atompshere at -35 °C for more than 1 week resulted in the gradual formation of **2-41b**. Furthermore, treatment of **2-41c** with CO immediately led to the quantitative formation of **2-41b** (Scheme 2-8).

Treatment of *in situ* generated **2-40** (cyclohexane-d_{12}) with 1 equiv. of PPh$_3$ led to the formation of a Ir^{III} cyclometallated PPh$_3$ complex (**2-43**; Scheme 2-8, Table 2-1), likely *via* coordination of PPh$_3$ to Ir, followed by C-H oxidative addition of a phenyl substituent. The solid-state structure of **2-43** confirmed the formulation of this complex (Figure 2-7, Table 2-4). Interestingly, the ^{i}Pr-PSiP^{Ind} ligand in **2-43** is coordinated in a facial manner, featuring *cis*-disposed phosphino donors. This binding mode is confirmed by ^{31}P{^{1}H} NMR analysis of **2-43**, as inequivalent ^{31}P resonances are observed (28.8 ppm (apparent t), 7.16 ppm (dd), -86.9 ppm (dd)), with small $^2J_{PPcis}$ of 16 and 32 Hz (Table 2-1). Similar reactivity involving metalation of PPh$_3$ by (R-PSiP)Ir (R = Cy, ^{i}Pr, ^{t}Bu) was previously reported by Shimada and co-workers.[46]

2.2.4 C-H Bond Oxidative Addition Reactions Involving (^{i}Pr-PSiP^{Ind})Ir^I

Generation of **2-40** by treatment of **2-29** with Me$_3$SiCH$_2$Li in benzene solution led to the rapid formation of a new (^{i}Pr-PSiP^{Ind})Ir complex **2-44** that features a ^{31}P{^{1}H} NMR resonance at 43.0 ppm (Table 2-1). Given that the analogous reaction with (Cy-PSiP)IrH(Cl) results in formation of the phenyl hydride complex (Cy-PSiP)IrH(Ph) due to C-H bond activation of the benzene solvent by (Cy-PSiP)Ir,[33a] the direct synthesis of (^{i}Pr-PSiP^{Ind})IrH(Ph) was pursued in order to determine if a similar C-H bond cleavage process

can be invoked. Treatment of **2-29** with 1 equiv. of PhLi in benzene-d_6 solution indeed generated **2-44** (by ^{31}P NMR), which is thus formulated as (^{i}Pr-PSiP^{Ind})IrH(Ph) (Scheme 2-9). The ^{1}H NMR spectrum of freshly generated **2-44** (benzene-d_6) features an Ir-*H* resonance at -10.45 ppm. Over the course of 30 min. in benzene-d_6 solution at room temperature, deuterium incorporation into the Ir-*H* and Ir-*Ph* positions was observed due to exchange with the deuterated solvent involving reversible C-H reductive elimination/benzene-d_6 oxidative addition in **2-44** (Scheme 2-9). While complex **2-44** remained stable in benzene solution for the purposes of NMR characterization, attempts to isolate this complex led to decomposition to form multiple unidentified products. Upon exposure of **2-44** to CO (1 atm) the 18-electron complex (^{i}Pr-PSiP^{Ind})IrH(Ph)(CO) (**2-45**) formed quantitatively (^{31}P NMR). Unlike **2-44**, complex **2-45** was readily isolated in 93% yield, and no deuterium incorporation into the Ir-*H* and Ir-*Ph* positions was observed in benzene-d_6 solution.

By comparison, the analogous reaction involving dehydrohalogenation of **2-28** in benzene solution does not lead to C-H bond activation of the benzene solvent (*vide supra*), even upon heating at 60 °C for several days, resulting instead in the formation of the N$_2$ adduct **2-38** (Scheme 2-7). It is possible that N$_2$ coordination to Rh may hinder subsequent oxidative addition chemistry. This observation is consistent with the reactivity of the related (Cy-PSiP)Rh, which is similarly inert to arene C-H bond oxidative addition.[33c] However, generation of **2-38** in benzene, followed by three freeze-pump-thaw cycles resulted in the formation of multiple unidentified products at room temperature, as observed by ^{31}P NMR spectroscopy.
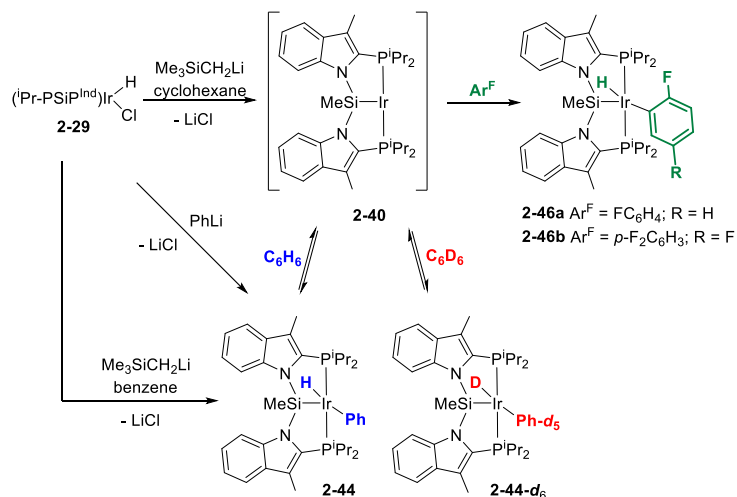
Scheme 2-9. Arene sp^2-C-H bond activation *via* **2-40**.

In an effort to further probe the propensity of (^{i}Pr-PSiP^{Ind})Ir^I to undergo sp^2-CH bond oxidative addition of arenes, the reactivity of *in situ* generated **2-40** with fluorobenzene and *p*-difluorobenzene, respectively, was explored (Scheme 2-9). Fluorinated arenes feature an increase in C-H bond strength relative to the parent arenes, and as a result CH-bond oxidative addition can be more challenging.[54] Treatment of **2-40** with excess fluorobenzene or *p*-difluorobenzene in cyclohexane solution initially led to the formation of multiple products (by ^{31}P NMR), likely due to arene C-H activation in either the *ortho*, *meta*, and/or *para* positions in the case of fluorobenzene. Heating the reaction mixture for 1 day at 75 °C resulted in conversion to a single major product (**2-46a**, FC$_6$H$_5$ activation; **2-46b**, *p*-F$_2$C$_6$H$_4$ activation; Scheme 2-9; Table 2-1). Both **2-46a** and **2-46b** were isolable upon scale-up of the reaction. The isolated complexes each feature chemically equivalent phosphino donors, as indicated by the presence of a single ^{31}P{^{1}H} NMR resonance for each (at 45.3 ppm for **2-46a** and 45.1 ppm for **2-46b**), consistent with *mer*-PSiP coordination in solution. The ^{1}H NMR spectra (benzene-d_6) of **2-46a** and **b** each feature a hydride resonance (apparent quartet) integrating to 1 H at - 9.27 and - 9.50 ppm,

respectively. Furthermore, the ^{1}H$\{^{31}$P$\}$ NMR spectrum in each case features a doublet in the hydride region, which is assigned to hydride-fluorine coupling (J_{HF} = 17 Hz for **2-46a**). Such H-F coupling suggests that metalation in **2-46a** has occurred *ortho* to a fluorine substituent, such that an H-F interaction may occur *via* either a close intramolecular H···F contact involving the Ir hydride, coordination of the *ortho*-F to Ir, or possibly even a long-range through-bond coupling. The selective activation of sp^2-CH bonds *ortho* to fluorine substituents has been described previously, and a significant thermodynamic driving force for this selectivity has been invoked. The ^{19}F$\{^1$H$\}$ NMR spectra of **2-20a** and **b** are consistent with metalation of the corresponding fluoroarene, most notably in the case of **2-20b**, for which inequivalent ^{19}F NMR resonances are observed at -102.2 and -122.7 ppm (two d, J_{FF} = 21 Hz).[55]

Interestingly, addition of a Lewis base such as NEt$_3$ or THF (both in excess) to *in situ* generated **2-40** (cyclohexane-d_{12}), followed by the addition of excess fluorobenzene or *p*-difluorobenzene appears to facilitate the *ortho*-metalation of these arenes, resulting in quantitative conversion to **2-46a** and **b**, respectively, within 1 h at 75 °C. It is possible that the added Lewis base coordinates weakly to the highly reactive Ir^I intermediate in the oxidative addition process, and thereby facilitates such reactivity. While there are previous reports of C-H activation of fluoroarenes by (POCOP)Ir[56] and (PCP)Ir systems,[55] multiple days of heating up to 120 °C or UV irradiation are typically required to facilitate this reactivity and to obtain a single isomer.[57] These results exemplify the propensity of *in situ* generated **2-40** to undergo sp^2-C-H oxidative addition reactions.

2.2.5 Investigation of N-H Bond Oxidative Addition by (^{i}Pr-PSiP^{Ind})M^I (M = Rh, Ir)

To investigate the ability of Rh^I and Ir^I species to mediate N-H bond oxidative addition of amines, complexes **2-38** or **2-40** were first generated *in situ* (in benzene or

cyclohexane solution, respectively) and their formation was confirmed by ^{31}P{^{1}H} NMR spectroscopy. The reaction mixtures were then treated with an amine substrate and the reaction progress was monitored by ^{31}P{^{1}H} and ^{1}H NMR spectroscopy (Scheme 2-10).

Treatment of **2-38** with 20 equiv. of H$_2$NPh led to the quantitative (by ^{31}P NMR) generation of a new species assigned as the σ-aniline adduct (^{i}Pr-PSiP^{Ind})Rh(NH$_2$Ph) (**2-39c**; Scheme 2-7, Table 2-1). The ^{1}H NMR spectrum of **2-39c** lacks the characteristic Rh*H* resonance associated with the anilido hydride derivative **2-30a**, indicating that N-H oxidative addition has not occurred. The ^{31}P{^{1}H} NMR resonance associated with **2-39c** is also shifted in comparison with the resonance associated with the N$_2$ adduct **2-38** (41.0 ppm for **2-39c**, *cf*. 49.0 ppm for **2-38**). While complex **2-39c** was observed spectroscopically in the presence of excess aniline (*ca*. 20 equiv.), this compound did not survive isolation attempts, as **2-38** was obtained after excess aniline was removed under vacuum. No evidence for N-H oxidative addition to afford **2-30a** was apparent after heating a sample of **2-39c** in the presence of *ca*. 20 equiv. of aniline at 70 °C for several days. This observation is in agreement with the reactivity previously observed for (Cy-PSiP)Rh, which was similarly unreactive towards N-H oxidative addition despite the apparent stability of Rh^{III} complexes of the type (Cy-PSiP)RhH(NHR).[33b, c]
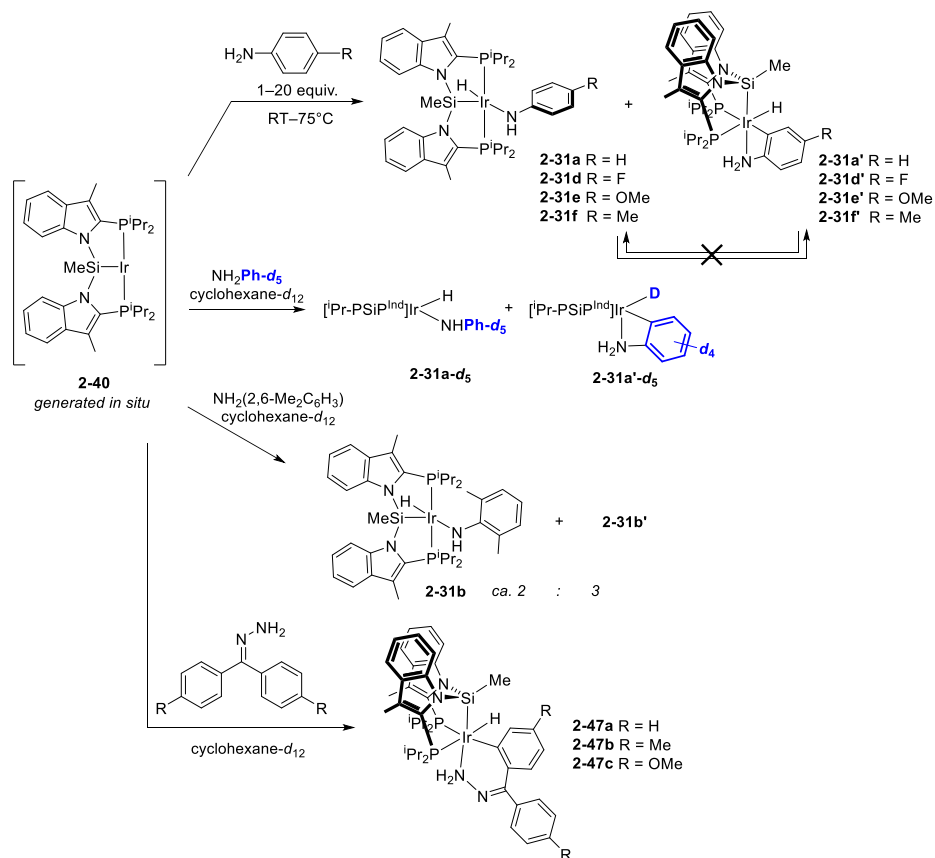
Scheme 2-10. Competitive N-H and C-H bond oxidative addition *via* (^{i}Pr-PSiP^{Ind})Ir^I.

By comparison, the Ir^I species **2-40** was found to be much more reactive than the Rh analogue. Treatment of *in situ* generated **2-40** with 1 equiv. of H$_2$NPh at room temperature in cyclohexane solution led to the formation of a mixture containing the desired N-H activation product (^{i}Pr-PSiP^{Ind})Ir(H)(NHPh) **2-31a**, as well as an additional species (**2-31a'**) that is assigned as the product of *ortho*-metallation of the aniline substrate (*ca.* 1:3 ratio of **2-31a**:**2-31a'** on the basis of ^{31}P NMR; Scheme 2-10). The ratio of **2-31a**:**2-31a'** was found to vary slightly in the presence of excess aniline, such that a 1:2 ratio was obtained when 20 equiv. H$_2$NPh were employed. Upon standing at room temperature, small amounts of precipitate were observed in such reactions. Attempts to heat reaction mixtures containing **2-31a** and **2-31a'** in an effort to drive the reaction in the direction of either of these products resulted in the apparent decomposition of **2-31a'** to multiple unidentified

products while **2-31a** appeared to remain intact. Variation of the reaction solvent to either benzene, THF or Et$_2$O did not favor the formation of **2-31a**. In the case where the phenyl hydride complex **2-44-d$_6$** was generated *in situ* (by treatment of **2-29** with 1 equiv. of LiCH$_2$SiMe$_3$ in benzene-d$_6$ solution) and treated with 20 equiv. of aniline, an 8:1 ratio of **2-31a'**: **2-44-d$_6$** was observed within 40 minutes of mixing, with no evidence for the formation of **2-31a**. Interestingly, while previous studies involving the reactivity of pincer Ir^I species with aniline derivatives in benzene solution have shown that equilibria involving reversible N-H oxidative addition and C-H oxidative addition of the benzene solvent are established (Scheme 2-1), C-H bond activation of the aniline substrate, as observed herein, does not appear to generally play a significant role in the reactivity of such species.

Attempts to isolate **2-31a'** from reaction mixtures that also contained **2-31a** or **2-44** have thus far been unsuccessful, and as such this species has been characterized *in situ*. Complex **2-31a'** features inequivalent phosphorus environments, as indicated by the observation of two ^{31}P{^{1}H} NMR resonances at 25.8 and 12.9 ppm (d, $^2J_{PP}$ = 12 Hz), respectively (Table 2-1). The ^{1}H NMR spectrum of **2-31a'** (cyclohexane-d$_{12}$) features a hydride resonance at -6.64 ppm (dd, 1 H, $^2J_{HP}$ = 22, 130 Hz). On the basis of these data, it appears that **2-31a'** likely adopts a structure featuring *fac*-PSiP coordination in solution, likely enforced by coordination of the aniline -NH$_2$ group to Ir to afford an 18-electron complex (Scheme 2-10). Such a structure is analogous to that observed for the related complex **2-43** (Scheme 2-8), which exhibited similar NMR features (Table 2-1). The reactivity of **2-40** with aniline was further probed by using the isotopically labeled aniline substrate H$_2$NPh-d$_5$. Treatment of **2-40** with H$_2$NPh-d$_5$ led to deuterium incorporation exclusively in the hydride position associated with **2-31a'**, and not in that associated with **2-31a** (Figure 2-8). This experiment supports the proposal of competitive arene C-H/C-D

and aniline N-H activation pathways in the reaction of **2-40** with aniline. Interestingly, no evidence for the formation of arene C-H activation products was observed in similar reactions involving (Cy-PSiP)Ir, which formed exclusively the anilido hydride product associated with N-H oxidative addition. As the Ir anilido complexes **2-31a–f** are readily isolated and appear to be quite stable, the proposed C-H activation pathway appears to be independent of a pathway involving N-H oxidative addition of the aniline, though it is likely that these reactions share a common intermediate, such as an Ir^I σ-aniline adduct.
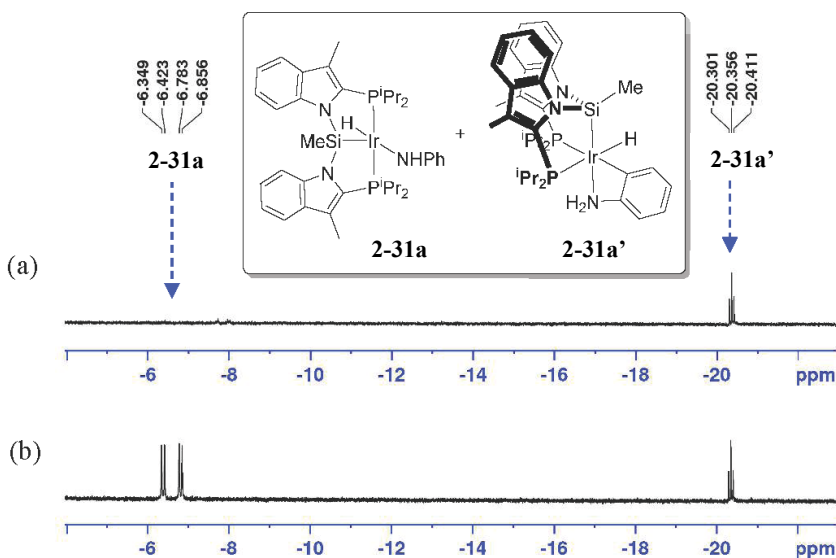
Figure 2-8. ^{1}H NMR spectra (cyclohexane-d_{12}) in the hydride region for product mixtures generated upon treatment of **2-40** with (a) H$_2$NPh-d_5 and (b) H$_2$NPh, consistent with ^{2}H incorporation exclusively into the Ir-H of **2-31a'**.

In an effort to further understand this reactivity and potentially inhibit *ortho*-metalation of the aniline substrate, studies involving a variety of substituted anilines were conducted (Scheme 2-10). Treatment of **2-40** with 1 equiv. of H$_2$N(C$_6$F$_5$) in cyclohexane led to the formation of multiple unidentified products (by ^{31}P NMR) from which no pure material could be isolated. A comparable reaction with 1 equiv. of H$_2$N(2,6-Me$_2$C$_6$H$_3$) led to formation of **2-31b** as a minor product (*ca.* 40% by ^{31}P NMR; Table 2-1). The major

product of this reaction (**2-31b'**, *ca*. 60%) features inequivalent phosphine environments, as indicated by the observation of two ^{31}P{^{1}H} NMR resonances at 27.1 and 4.24 ppm (d, $^2J_{PP}$ = 10 Hz), as well as an Ir-*H* ^{1}H NMR resonance at –9.50 ppm (dd, $^2J_{HP}$ = 20, 142 Hz). These spectroscopic features are similar to those observed for **2-31a'**. As such, it may be that **2-31b'** is a structurally related analogue of **2-31a'** involving metalation of an *ortho*-methyl substituent on the aniline substrate. However, complex **2-31b'** has eluded isolation attempts thus far.

Having noted the effects of *ortho*-substitution on the reactivity of aniline derivatives with **2-40**, *para*-substituted aniline substrates were also investigated to study possible electronic effects on this reactivity (Scheme 2-10). Treatment of *in situ* generated **2-40** with 1 - 20 equiv. of H$_2$N(*p*-FC$_6$H$_4$) at room temperature in cyclohexane solution resulted in the formation of a substantial amount of beige precipitate within 40 minutes of addition. NMR analysis of this reaction mixture indicated a sole species present in the supernatant solution, which is tentatively assigned as (^{i}Pr-PSiP^{Ind})IrH[HN(*p*-FC$_6$H$_4$)] (**2-31d**), the anilido hydride complex resulting from NH-bond oxidative addition. Complex **2-31d** gives rise to a ^{31}P{^{1}H} NMR resonance at 39.1 ppm, as well as a ^{1}H NMR resonance at –20.2 ppm ($^2J_{HP}$ = 16 Hz) that corresponds to the Ir-*H* (Table 2-1). The precipitate was isolated and redissolved in benzene-d_6. NMR spectroscopic analysis of this material is consistent with its formulation as the product of *ortho*-metalation (relative to NH$_2$) of the aniline substrate (**2-31d'**; Table 2-1). The ^{31}P{^{1}H} NMR spectrum of **2-31d'** features two doublet resonances at 23.8 and 13.5 ppm ($^2J_{PP}$ = 10 Hz), respectively. As previously observed for related complexes, the ^{1}H NMR spectrum (benzene-d_6) of **2-31d'** features a characteristic Ir-*H* resonance at -6.68 ppm (dd, 1 H, $^2J_{HP}$ = 22 and 127 Hz), as well as a resonance at 2.62 ppm (br s, 2 H) that corresponds to the N*H$_2$* group. Unlike **2-31a'** and **2-31b'**, complex **2-**

31d' is isolable, and was obtained in 93% yield in a preparative-scale experiment that utilized 1 equiv. of the aniline substrate, which indicates that while traces of **2-31d** are observed in solution, the major product of the reaction of **2-40** with $H_2N(4\text{-}FC_6H_4)$ is **2-31d'**.

The reactivity of **2-40** with $H_2N(p\text{-}OMeC_6H_4)$ and $H_2N(p\text{-}MeC_6H_4)$ was also probed to investigate the effect of electron donating substituents on NH- *vs*. CH-bond activation of anilines (Scheme 2-10). As was observed in the case of $H_2N(p\text{-}FC_6H_4)$, the formation of a precipitate was noted in both reactions upon addition of the aniline to *in situ* generated **2-40** in cyclohexane solution. Treatment of **2-40** in cyclohexane with 1 equiv. $H_2N(p\text{-}OMeC_6H_3)$ resulted in the rapid (within 30 min. of addition) formation of a single product by ^{31}P NMR of a complex (**2-31e'**) that features inequivalent phosphine environments (observed as doublets at 25.5 and 13.3 ppm, $^2J_{PP}$ = 12 Hz), as well as an Ir-H ^1H NMR resonance at –6.74 ppm (dd, $^2J_{HP}$ = 22 and 127 Hz). Given that the spectroscopic features observed for **2-31e'** are similar to those observed in reactivity involving both the parent aniline and $H_2N(p\text{-}FC_6H_4)$, it is plausible that this complex also resulted from preferrential sp^2-CH activation of the aniline substrate, and as such **2-31e'** is tentatively formulated as a six coordinate complex featuring *ortho*-metallation (relative to NH_2) of the arene and amine coordination. While no formation of **2-31e** resulting from N-H oxidative addition was initially observed in the reaction mixture, gradual formation of **2-31e** (30% by ^{31}P NMR) was noted after 1 h at room temperature. Longer reaction times (up to 2 days at room temperature) did not result in significant conversion to **2-31e**. Rather, the formation of a new unidentified product that gives rise to a $^{31}P\{^1H\}$ NMR resonance at 30.3 ppm (s) and does not contain an associated Ir-H ^1H NMR resonance was observed. Unlike in the case of **2-31d'**, attempts to isolate **2-31e'** were not successful. Similarly, treatment of **2-40** with

$H_2N(4\text{-}MeC_6H_3)$ resulted in the rapid (within 30 min. of addition) formation of the N-H oxidative addition product **2-31f** (*ca*. 44% by ^{31}P NMR), as well as a complex (**2-31f'**) that features inequivalent phosphine environments (observed as doublets at 24.5 and 13.3 ppm, $^2J_{PP}$ = 12 Hz), as well as an Ir-*H* ^{1}H NMR resonance –20.4 ppm ($^2J_{HP}$ = 17 Hz). Complex **2-31f'** is tentatively assigned as a six coordinate product of arene CH-bond activation, analogous to **2-31a'**, **d'**, and **e'** on the basis of the similar NMR features observed for these complexes. As in the case of **2-31a'** and **2-31e'**, **2-31'** could not be successfully isolated.

Further repeated attempts to observe (^{i}Pr-PSiP^{Ind})Ir mediated NH-bond activation involving alkylamines, such as H_2N^tBu and $H_2N(1\text{-}Ad)$, or NH_3 under various reaction conditions were generally unsuccessful, leading to the formation of complex mixtures containing multiple products (by ^{31}P NMR) from which pure material could not be isolated. For example, treatment of *in situ* generated **2-40** with H_2N^tBu in cyclohexane solution led to the formation of a mixture of unidentified products, in which the major species present (**2-33a'**; *ca*. 59%) features inequivalent phosphorus environments giving rise to ^{31}P{^{1}H} NMR resonances at 15.3 and 13.6 ppm (d, $^2J_{PP}$ = 11 Hz), as well as an Ir-*H* ^{1}H NMR resonance at –6.97 ppm (dd, $^2J_{HP}$ = 22 and 135 Hz). No evidence was obtained for the formation of the N-H oxidative addition product **2-33a**, and attempts to isolate **2-33a'** proved unsuccessful. In the case of ammonia, treatment of *in situ* generated **2-40** with ammonia gas (*ca*. 1 atm) in cyclohexane solution led to the formation of a precipitate. The *in situ* ^{31}P{^{1}H} NMR spectrum of the reaction mixture indicated the presence of multiple unidentified products in the supernatant solution. ^{1}H and ^{31}P NMR analysis of the precipitated material (redissolved in benzene-d_6) also revealed the presence of multiple unknown species. No evidence for the formation of the N-H oxidative addition product **2-34** was observed (by ^{31}P NMR). While changing the reaction solvent to Et_2O resulted in a

55

homogenous reaction mixture, ^{31}P NMR analysis once again revealed an intractable mixture of products with no evidence for the formation of **2-34**. It should be noted that when complex **2-34** (synthesized from **2-29** and LiNH$_2$, *vide supra*) was treated with an excess of NH$_3$ (1 atm) in benzene solution, a complex mixture of unidentified products was also observed by ^{31}P NMR analysis, suggesting that complex **2-34** is reactive in the presence of excess NH$_3$. In an effort to add a stoichiometric equivalent of NH$_3$ to (^{i}Pr-PSiP^{Ind})Ir, *in situ* generated **2-40** was treated with 1 equiv. of a 0.5 M NH$_3$ solution in dioxane. However, a complex mixture of products resulted once again, with no evidence for the formation of **2-34**. The reactivity of **2-40** with alkylamines and ammonia stands in contrast to that of (Cy-PSiP)Ir, which undergoes facile NH-oxidative addition with such substrates.[33b, c]

Having noted that hydrazido and amidate hydride complexes such as **2-35a,b**, **2-36a,b**, and **2-37a,b** are accessible and thermally stable (*vide supra*), the reactivity of **2-38** and **2-40** with amide and hydrazine-derived substrates was probed. In this regard, treatment of *in situ* generated **2-38** and **2-40** with benzamide and acetamide was found to produce complex mixtures comprised of multiple unidentified products (by ^{31}P NMR), with no evidence of N-H oxidative addition. Treatment of **2-40** with either 1-amino-4-methylpiperazine or the structurally similar substrate N-aminopiperidine in cyclohexane-d_{12} resulted in the formation of multiple unidentified products, with no evidence for the formation of **2-35a** or **2-35b**, respectively. Furthermore, treatment of **2-40** with 1 equiv. of benzophenone hydrazone in cyclohexane solution appears to result in preferential CH-bond activation of the hydrazone substrate, giving rise to an isolable Ir hydride species (**2-47a**; Scheme 2-10) that features inequivalent phosphorus environments giving rise to ^{31}P{^{1}H} NMR resonances at 20.4 and 11.1 ppm (d, $^2J_{PP}$ = 15 Hz), as well as an Ir-*H* ^{1}H NMR

56

resonance at -9.66 ppm (dd, $^2J_{HP}$ = 24 and 116 Hz). The ^{1}H NMR spectrum of **2-47a** also contains a resonance at 5.32 ppm that corresponds to the intact N-N*H$_2$* protons of the substrate, consistent with a lack of N-H oxidative addition. The *para*-methyl and -methoxy substituted benzophenone hydrazone substrates reacted in a similar manner with **2-40** to afford isolable complexes (*p*-Me, **2-47b**; *p*-OMe, **2-47c**) that exhibit NMR features comparable to those observed for **2-47a** (Table 2-1).

2.3 Conclusion

The synthetic viability of Group 9 amido, anilido, hydrazido, and amidate hydride complexes supported by ^{i}Pr-PSiP^{Ind} ligation has been established and the resultant complexes are typically sufficiently stable to be isolated and characterized. While the synthesis of five-coordinate anilido hydride complexes of both Rh and Ir proved to be facile, the preparation of analogous alkylamido complexes was more challenging, and evidence for β-hydride elimination processes was obtained (for M = Ir). However, Ir amido hydride complexes lacking β-hydrogen substituents were found to be viable synthetic targets, including *tert*-butylamido, adamantylamido, and the parent amido complexes. The propensity of such anilido and amido hydride complexes to undergo N-H bond reductive elimination was evaluated, and it was observed that the Ir complexes are thermally robust while the Rh analogues undergo relatively facile reductive elimination. The stability of such coordinatively unsaturated pincer anilido and alkylamido Ir complexes stands in contrast to previously reported PCP and POCOP analogues, which undergo N-H reductive elimination much more readily.[18-19]

Dehydrohalogenation of (^{i}Pr-PSiP^{Ind})MH(Cl) (M = Rh, Ir) provides access to 14-electron intermediates of the type (^{i}Pr-PSiP^{Ind})M^I, which in the case of M = Rh were

successfully trapped by simple donor ligands (*e.g.* N$_2$, PMe$_3$, DMAP) to afford isolable 16-electron adducts. Such Rh^I species proved unreactive towards both arene CH-bonds and N-H oxidative addition of aniline. The Ir^I species generated upon dehydrohalogenation of (^{i}Pr-PSiP^{Ind})IrH(Cl) proved significantly more reactive and more challenging to observe and characterize. Attempts to trap this species with an added donor ligand, as in the case of the Rh analogue, were generally not successful, although carbonyl adducts and a metalated PPh$_3$ complex were isolated. In benzene solution, dehydrohalogenation of (^{i}Pr-PSiP^{Ind})IrH(Cl) resulted in C-H bond activation of the solvent to afford (^{i}Pr-PSiP^{Ind})IrH(Ph), which undergoes facile arene exchange with benzene-d_6. Activation of fluorobenzene and *para*-difluorobenzene was also observed to form products derived from sp^2-CH-bond oxidative addition, with selectivity for *ortho*-metalation of fluoroarenes. When generated in cyclohexane solution, (^{i}Pr-PSiP^{Ind})Ir reacts with aniline to afford a mixture of N-H and C-H bond oxidative addition products. Although the observation of arene exchange involving (^{i}Pr-PSiP^{Ind})IrH(Ph) suggests that sp^2-C-H bond oxidative addition is reversible, attempts to drive similar reactivity with aniline in the direction of N-H bond oxidative addition by applying heat, changing solvents, and altering the substitution of the aniline aromatic ring were generally unsuccessful. Other substrates containing an N-H functionality, such as alkylamines, ammonia, and benzamide proved similarly resistant to N-H oxidative addition and typically produced complicated reaction mixtures from which no pure material could be isolated.

The reactivity of Group 9 metal complexes supported by ^{i}Pr-PSiP^{Ind} differs from that of related Rh and Ir complexes supported by Cy-PSiP ligation.[33b, c] Most notably, although both PSiP ligands provide access to thermally stable five-coordinate anilido, alkylamido, and hydrazido hydride complexes, (Cy-PSiP)Ir undergoes facile and selective

N-H oxidative addition of anilines, alkylamines, ammonia, and hydrazine derivatives to high conversion, while in the case of (^{i}Pr-PSiP^{Ind})Ir, N-H oxidative addition typically accounts for only the minor portion of the products formed, with competitive C-H bond activation of the amine substrate often comprising the major product. In the case of aniline derivatives, attempts to block the readily metalated *ortho*-position with Me substituents resulted in the apparent activation of an *ortho*-Me group. Thus, a pathway involving CH-bond oxidative addition by (^{i}Pr-PSiP^{Ind})Ir^I appears to be more favourable than in the case of (Cy-PSiP)Ir^I. Notably, it appears that for (^{i}Pr-PSiP^{Ind})Ir, products resulting from NH- and CH-oxidative addition of aniline substrates do not interconvert, despite the likely scenario that they share a 16-electron aniline adduct as a common intermediate. Collectively, these results establish that even subtle modification to the PSiP ligand backbone can influence the preferred course of reactivity (*i.e.*, C-H vs. N-H activation) in derived Ir complexes, and provide further insights into the reaction pathways that are implicated in N-H oxidative addition chemistry.

2.4 Experimental Section

2.4.1 General Considerations

All experiments were conducted under nitrogen in a glovebox or using standard Schlenk techniques. Dry, oxygen-free solvents were used unless otherwise indicated. All non-deuterated solvents were deoxygenated by sparging with nitrogen. Benzene, toluene and pentane were subsequently passed through a double column purification system (one activated alumina column and one column packed with activated Q-5). Tetrahydrofuran and diethyl ether were purified by distillation from Na/benzophenone. All purified solvents were stored over 4 Å molecular sieves. Benzene-d_6 and cyclohexane-d_{12} were degassed via three freeze-pump-thaw cycles and stored over 4 Å molecular sieves. All other reagents

were purchased from commercial suppliers and used as received. Unless otherwise stated, ^{1}H, ^{13}C, ^{31}P, ^{15}N, and ^{29}Si NMR characterization data were collected at 300K with chemical shifts reported in parts per million downfield of SiMe$_4$ (for ^{1}H, ^{13}C, and ^{29}Si), or 85% H$_3$PO$_4$ in D$_2$O (for ^{31}P). Chemical shift ranges are cited to indicate overlapping resonances. ^{1}H and ^{13}C NMR chemical shift assignments are based on data obtained from ^{13}C-DEPTQ, ^{1}H-^{1}H COSY, ^{1}H-^{13}C HSQC, and ^{1}H-^{13}C HMBC NMR experiments. ^{29}Si NMR assignments are based on ^{1}H-^{29}Si HMQC and ^{1}H-^{29}Si HMBC experiments (including for J_{SiH} determination). In some cases, fewer than expected unique ^{13}C NMR reso-nances were observed, despite prolonged acquisition times. The following abbreviations were utilized to assign NMR data: s = singlet; d = doublet; t = triplet; q = quartet; dvt = doublet of virtual triplets; m = multiplet; br = broad. Please note that a ^{13}C NMR shift at ca. 110 ppm is due to an instrument artefact. Infrared spectra were recorded for thin films or Nujol mulls using NaCl plates at a resolution of 4 cm^{-1}. Raman spectra were recorded using a Thermo Nicolet NXR 9650 spectrometer at 2 cm^{-1} resolution.

2.4.2 Synthetic Details and Characterization Data

(^{i}Pr-PSiP^{Ind})H (2-27). The compound 2-(dipropan-2-ylphosphanyl)-3-methyl-1H-indole (4.00 g, 16.7 mmol) was dissolved in ca. 100 ml THF and cooled to -78 ^{o}C. To this solution, ^{n}BuLi (10.1 ml, 16.7 mmol) was added dropwise and the resulting reaction mixture was stirred for 20 min. at -78 °C. The reaction mixture was then allowed to warm to room temperature over the course of an hour. The solution was again cooled to -78 °C, and Cl$_2$SiHMe (0.84 ml, 8.09 mmol) was added at once by syringe. The mixture was allowed to reach room temperature over the course of 18 h, during which a white precipitate was formed. The volatile components were then removed *in vacuo* and benzene (ca. 60 mL) was added to the residue. The resulting slurry was then filtered through Celite. The

filtrate solution was collected and the volatile components were removed *in vacuo*. The remaining residue was triturated with pentane (4 × 3 mL) and subsequently washed with pentane (3 × 4 mL) to afford **2-27** (3.21 g, 74% yield) as an off-white solid. ^{1}H NMR (500 MHz, benzene-d_6): δ 7.56 (apparent d, 4 H, J = 8 Hz, H_{arom}), 7.20 (overlapping resonances, 1 H, Si*H*), 7.18–7.09 (overlapping resonances, 4 H, H_{arom}), 2.27 (s, 6 H, Indole-*Me*), 2.24–2.18 (m, 4 H, PC*H*Me$_2$), 1.18 (s, 3 H, Si*Me*), 1.05–0.95 (overlapping resonances, 12 H, PCH*Me$_2$*), 0.78–0.74 (overlapping resonances, 6 H, PCH*Me$_2$*), 0.68–0.64 (overlapping resonances, 6 H, PCH*Me$_2$*). ^{13}C{^{1}H} NMR (126 MHz, benzene-d_6): δ 143.3 (C_{arom}), 136.1 (C_{arom}), 133.4 (C_{arom}), 123.2 (CH_{arom}), 120.5 (CH_{arom}), 118.9 (CH_{arom}), 115.5 (CH_{arom}), 25.9 (apparent d, J_{CP} = 9 Hz, P*C*HMe$_2$), 25.2 (apparent d, J_{CP} = 9 Hz, P*C*HMe$_2$), 22.1 (m, PCH*Me$_2$*), 21.4 (m, PCH*Me$_2$*), 11.1 (Indole-*Me*), 4.5 (Si*Me*). ^{31}P{^{1}H} NMR (202 MHz, benzene-d_6): δ -8.5. ^{29}Si NMR (100 MHz, benzene-d_6): δ -27.3 ($^1J_{SiH}$ = 271 Hz). Anal. Calcd for C$_{31}$H$_{46}$N$_2$P$_2$Si: C, 69.37; H, 8.64; N, 5.22. Found: C, 69.47; H, 8.89; N, 5.25.

(^{i}Pr-PSiP^{Ind})RhH(Cl) (2-28). A solution of **2-27** (0.40 g, 0.75 mmol) in ca. 25 mL of benzene was added to solid [Rh(COD)Cl]$_2$ (0.18 g, 0.37 mmol). The reaction mixture was placed in a thick walled Schlenk vessel sealed with a Teflon stopcock and was heated at 80 °C for 3 days with magnetic stirring. The volatile components of the reaction mixture were subsequently removed in vacuo and the remaining residue was triturated with pentane (5 × 4 mL) and then washed with pentane (3 × 3 mL) and dried in vacuo to afford **2-28** (0.51 g, 95% yield) as a yellow solid. Single crystals of **2-28** suitable for X-ray diffraction analysis were obtained from a con-centrated benzene solution at room temperature. ^{1}H NMR (300 MHz, benzene-d_6): δ 7.90 (m, 2 H, H_{arom}), 7.55 (m, 2 H, H_{arom}), 7.18–7.14 (4 H, H_{arom}), 2.95 (m, 2 H, PCHMe$_2$), 2.39 (m, 2 H, PCHMe$_2$), 2.19 (s, 6 H, indole-*Me*), 1.48–1.31 (12 H, PCHMe$_2$), 1.13 (dvt, 6 H, J_{HH} = J_{HP} = 8 Hz, PCHMe$_2$), 0.95 (s, 3 H, Si*Me*),

0.91 (dvt, 6 H, J_{HH} = 7 Hz, J_{HP} = 9 Hz, PCHMe₂), -17.09 (dt, 1 H, $^1J_{RhH}$ = 26 Hz, $^2J_{HP}$ = 14 Hz, RhH). ^{13}C{^{1}H} NMR (75.5 MHz, benzene-d_6): δ 141.0 (C$_{arom}$), 135.5 (C$_{arom}$), 134.2 (C$_{arom}$), 123.1 (CH$_{arom}$), 121.8 (C$_{arom}$), 120.6 (CH$_{arom}$), 119.5 (CH$_{arom}$), 116.1 (CH$_{arom}$), 28.2 (apparent t, J_{CP} = 13 Hz, PCHMe₂), 26.2 (apparent t, J_{CP} = 13 Hz, PCHMe₂), 20.7 (PCHMe₂), 20.4 (PCHMe₂), 19.3 (PCHMe₂), 19.0 (PCHMe₂), 11.0 (indole-*Me*), 7.8 (Si*Me*). ^{31}P{^{1}H} NMR (121.5 MHz, benzene-d_6): δ 44.2 (d, $^1J_{PRh}$ = 109 Hz). ^{29}Si NMR (99.4 MHz, benzene-d_6): δ 38.9 ($^2J_{SiH}$ = 26 Hz). Anal. Calcd for C₃₁H₄₆ClN₂P₂RhSi·(C₆H₆)₀.₅: C, 57.18; H, 6.92; N, 3.92. Found: C, 57.15; H, 6.94; N, 3.88.

(ᶦPr-PSiP^{Ind})IrH(Cl) (2-29). A solution of **2-27** (0.40 g, 0.75 mmol) in ca. 20 mL of benzene was added to solid [Ir(COD)Cl]₂ (0.25 g, 0.37 mmol). The reaction mixture was placed in a thick walled Schlenk vessel sealed with a Teflon stopcock and heated at 80 °C for 7 days with magnetic stirring. The volatile components of the reaction mixture were then removed in vacuo and the residue was triturated with pentane (6 × 3 mL) and subsequently washed with pentane (3 × 3 mL) and dried in vacuo to afford **2-29** (0.40 g, 70% yield) as a yellow solid. Single crystals of **2-29** suitable for X-ray diffraction analysis were obtained from a concentrated Et₂O solution at -35 °C. ^{1}H NMR (300 MHz, benzene-d_6): δ 7.95 (m, 2 H, H$_{arom}$), 7.53 (m, 2 H, H$_{arom}$), 7.20–7.11 (4 H, H$_{arom}$), 3.18 (m, 2 H, PC*H*Me₂), 2.69 (m, 2 H, PC*H*Me₂), 2.18 (s, 6 H, indole-*Me*), 1.36 (dvt, 6 H, J_{HH} = 7 Hz, J_{HP} = 10 Hz, PCH*Me₂*), 1.25 (dvt, 6 H, J_{HH} = 7 Hz, J_{HP} = 11 Hz, PCH*Me₂*), 1.08 (dvt, 6 H, J_{HH} = 7 Hz, J_{HP} = 8 Hz, PCH*Me₂*), 0.93–0.81 (9 H, PCH*Me₂* + Si*Me*; the Si*Me* resonance was identified at 0.87 ppm in a ^{1}H-^{13}C HSQC experiment), -22.44 (t, 1 H, $^2J_{HP}$ = 14 Hz, Ir*H*). ^{13}C{^{1}H} NMR (75.5 MHz, benzene-d_6): δ 140.6 (C$_{arom}$), 135.9 (C$_{arom}$), 135.5 (C$_{arom}$), 123.3 (*C*H$_{arom}$), 121.0 (C$_{arom}$), 120.7 (*C*H$_{arom}$), 119.9 (*C*H$_{arom}$), 116.4 (*C*H$_{arom}$), 28.9 (apparent t, J_{CP} = 15 Hz, PCHMe2), 26.5 (apparent t, J_{CP} = 16 Hz, PCHMe2), 20.5

(PCH*Me2*), 20.4 (PCH*Me2*), 19.4 (PCH*Me2*), 19.3 (PCH*Me2*), 11.2 (indole-*Me*), 5.0 (Si*Me*). ^{31}P{^{1}H} NMR (121.5 MHz, benzene-d_6): δ 46.6 (s). ^{29}Si NMR (99.4 MHz, benzene-d_6): δ -0.5 ($^2J_{SiH}$ = 3 Hz). Anal. Calcd for $C_{31}H_{46}ClIrN_2P_2Si$: C, 48.71; H, 6.07; N, 3.66. Found: C, 48.64; H, 5.80; N, 3.40.

General procedure for the synthesis of LiNHR and LiNRR' salts. The amine (for H$_2$NPh, 147 μL, 1.61 mmol) was dissolved in ca. 7 mL of pentane and the solution was cooled to -35 °C. To this pre-cooled solution, one equiv. of ^{n}BuLi (2.5 M in hexanes, 644 μL, 1.61 mmol) was added dropwise by microsyringe. The formation of a white precipitate was observed. The volatile components of the reaction mixture were subsequently removed under vacuum and the remaining solid residue was washed (3 × 2 ml) with pentane and dried in vacuo to afford LiNRR' as a white solid in near-quantitative yield.

PhLi. Iodobenzene (82 μL, 0.74 mmol) was dissolved in ca. 6 mL of pentane and cooled to –35 ºC. The solution was treated with 2.5 M ^{n}BuLi (324 μL, 0.81 mmol) added dropwise by microsyringe. A white precipitate formed immediately upon addition. The supernatant solution was removed by pipette and the remaining solid was washed with pentane (3 × 2 mL) and evaporated to dryness, to afford PhLi in quantitative yield.

(^{i}Pr-PSiP^{Ind})RhH(NHPh) (2-30a). A solution of **2-28** (0.058 g, 0.086 mmol) in ca. 6 mL of benzene was treated with LiNHPh (0.090 g, 0.086 mmol). An immediate color change from yellow to dark red was observed. The reaction mixture was magnetically stirred for 15 minutes at room temperature and was subsequently filtered through Celite. The filtrate solution was collected, and the volatile components were removed in vacuo. The remaining residue was triturated with pentane (3 × 2 mL) and subsequently washed with pentane (3 × 3 mL) and dried in vacuo to afford **2-30a** (0.040 g, 63%) as a purple solid. A minute quantity of single crystals of **2-30a'**, a decomposition product of **2-30a**,

suitable for X-ray diffraction analysis was obtained from a concentrated pentane solution of **2-30a** at room temperature over the course of severeal days. ^{1}H NMR (300 MHz, benzene-d_6): δ 7.92 (m, 2 H, H$_{arom}$), 7.56 (m, 2 H, H$_{arom}$), 7.25–7.16 (6 H, H$_{arom}$), 6.66 (t, 1 H, $^3J_{HH}$ = 7 Hz, H$_{arom}$), 6.56 (d, 2 H, $^3J_{HH}$ = 7 Hz, H$_{arom}$), 3.87 (br s, 1 H, N*H*), 2.52 (m, 2 H, PC*H*Me$_2$), 2.40 (m, 2 H, PC*H*Me$_2$), 2.22 (s, 6 H, indole-*Me*), 1.28 (dvt, 6 H, J_{HH} = 7 Hz, J_{HP} = 9 Hz PCH*Me$_2$*), 1.11–0.94 (21 H, PCH*Me$_2$* + Si*Me*; the Si*Me* resonance was identified at 1.00 ppm in a ^{1}H-^{13}C HSQC experiment), -14.99 (apparent q, 1 H, *J* = 17 Hz, Rh*H*). ^{13}C{^{1}H} NMR (75.5 MHz, benzene-d_6): δ 163.9 (C$_{arom}$), 140.9 (C$_{arom}$), 135.4 (C$_{arom}$), 134.8 (C$_{arom}$), 129.2 (*C*H$_{arom}$), 123.1 (*C*H$_{arom}$), 120.7 (*C*H$_{arom}$), 120.3 (C$_{arom}$), 119.7 (*C*H$_{arom}$), 117.2 (*C*H$_{arom}$), 116.4 (*C*H$_{arom}$), 112.5 (*C*H$_{arom}$), 28.9 (apparent t, J_{CP} = 12 Hz, P*C*HMe$_2$), 26.9 (apparent t, J_{CP} = 14 Hz, P*C*HMe$_2$), 21.1 (PCH*Me$_2$*), 20.4 (PCH*Me$_2$*), 19.2 (PCH*Me$_2$*), 19.1 (PCH*Me$_2$*), 11.3 (indole-*Me*), 8.1 (Si*Me*). ^{31}P{^{1}H} NMR (121.5 MHz, benzene-d_6): δ 46.6 (d, $^1J_{PRh}$ = 113 Hz). ^{29}Si NMR (99.4 MHz, benzene-d_6): δ 39.8 ($^2J_{SiH}$ = 3 Hz). Anal. Calcd for C$_{37}$H$_{52}$N$_3$P$_2$RhSi: C, 60.73; H, 7.16; N, 5.74. Found: C, 60.45; H, 7.02; N, 5.48.

(ᶦPr-PSiP^{Ind})RhH[NH(2,6-Me$_2$C$_6$H$_3$)] (2-30b). A solution of **2-28** (0.074 g, 0.15 mmol) in ca. 6 mL of benzene was treated with LiNH(2,6-Me$_2$C$_6$H$_3$) (0.014 g, 0.15 mmol). An immediate color change from yellow to dark red was observed. The reaction mixture was magnetically stirred for 40 minutes at room temperature and was subsequently filtered through Celite. The filtrate solution was collected, and the volatile components were removed in vacuo. The remaining residue was triturated with pentane (4 × 2 mL) and subsequently washed with pentane (5 × 3 ml) and dried in vacuo to afford **2-30b** (0.056 g, 50 %) as a purple solid. ^{1}H NMR (300 MHz, benzene-d_6): δ 7.82 (m, 2 H, H$_{arom}$), 7.56 (m, 2 H, H$_{arom}$), 7.20–7.13 (6 H, H$_{arom}$), 6.58 (t, 1 H, $^3J_{HH}$ = 7 Hz, H$_{arom}$), 2.85 (br s, 1 H, N*H*), 2.51–2.33 (10 H, PC*H*Me2 + 2,6-*Me$_2$*C$_6$H$_3$; the 2,6-*Me$_2$*C$_6$H$_3$ resonance was identified at

64

2.37 ppm in a ^{1}H-^{13}C HSQC experiment), 2.22 (s, 6 H, indole-Me), 1.19 (dvt, 6 H, J_{HH} = 7

Hz, J_{HP} = 11 Hz, PCHMe_2), 1.09–0.97 (15 H, PCHMe_2 + SiMe; the SiMe resonance was

identified at 0.99 ppm in a ^{1}H-^{13}C HSQC experiment), 0.91 (dvt, 6 H, J_{HH} = 7 Hz, J_{HP} = 8

Hz, PCHMe_2), -15.12 (apparent q, 1 H, J = 17 Hz, RhH). ^{13}C{^{1}H} NMR (75.5 MHz,

benzene-d_6): δ 162.4 (C_{arom}), 140.8 (C_{arom}), 135.6 (C_{arom}), 134.8 (C_{arom}), 128.6 (CH_{arom}),

124.9 (C_{arom}), 121.3 (C_{arom}), 120.5 (C_{arom}), 123.0 (CH_{arom}), 120.8 (CH_{arom}), 119.4 (CH_{arom}),

116.7 (CH_{arom}), 111.6 (CH_{arom}), 29.1 (apparent t, J_{CP} = 11 Hz, P$CH$$Me_2$), 27.7 (apparent t,

J_{CP} = 14 Hz, P$CH$$Me_2$), 20.7 (PCH$Me_2$), 20.4 (PCH$Me_2$), 20.3 (PCH$Me_2$), 19.3 (2,6-

Me_2C$_6$H$_3$), 19.1 (PCHMe_2), 11.3 (indole-Me), 7.0 (SiMe). ^{31}P{^{1}H} NMR (121.5 MHz,

benzene-d_6): δ 44.2 (d, $^1J_{PRh}$ = 112 Hz). ^{29}Si{^{1}H} NMR (99.4 MHz, benzene-d_6): δ 39.4.

Anal. Calcd for C$_{39}$H$_{56}$N$_3$P$_2$RhSi: C, 61.65; H, 7.43; N, 5.53. Found: C, 61.32; H, 7.39; N,

5.68.

(^{i}Pr-PSiP^{Ind})RhH[NH(2,6-^{i}Pr$_2$C$_6$H$_3$)] (2-30c). A solution of 2-28 (0.076 g, 0.11

mmol) in ca. 4 mL of benzene was added to a slurry of LiNH(2,6-^{i}Pr$_2$C$_6$H$_3$) (0.021 g, 0.11

mmol) in ca. 4 mL benzene at room temperature. An immediate color change from yellow

to dark red was observed within 15 min of addition. After 35 minutes of stirring at room

temperature the reaction mixture was filtered through Celite. The filtrate solution was

collected, and the volatile components were removed in vacuo. The remaining residue was

triturated with pentane (3 × 2 mL) and dried in vacuo to afford crude 2-30c as a dark red

solid (0.042 g, 46 % crude yield). It should be noted that crude 2-30c contains variable

amounts of 2-38 as well as H$_2$N(2,6-^{i}Pr$_2$C$_6$H$_3$) contaminants due to facile N-H reductive

elimination in 2-30c. The amount of these contaminants was found to increase with longer

reaction times as well as prolonged exposure to vacuum during workup/isolation. ^{1}H NMR

(300 MHz, benzene-d_6): δ 8.02 (d, 2 H, J_{HH} = 8 Hz, H$_{arom}$), 7.54 (d, 2 H, J_{HH} = 9 Hz, H$_{arom}$),

7.26–7.16 (6 H, H_{arom}), 7.04 (t, 1 H, $^3J_{HH}$ = 8 Hz, H_{arom}), 5.25 (br s, 1 H, NH), 4.11 (sept, 1 H, $^3J_{HH}$ = 4 Hz, 2,6-$^iPr_2C_6H_3$), 4.00 (sept, 1 H, $^3J_{HH}$ = 4 Hz, 2,6-$^iPr_2C_6H_3$), 2.51–2.31 (4 H, PCHMe$_2$), 2.23 (s, 6 H, indole-Me), 1.38 (d, 6 H, $^3J_{HH}$ = 4 Hz, 2,6-$^iPr_2C_6H_3$) 1.33–1.28 (12 H, PCHMe_2 + 2,6-$^iPr_2C_6H_3$), 1.22 (s, 3 H, SiMe), 1.01–0.86 (18 H, PCHMe_2), -15.83 (apparent q, 1 H, J = 17 Hz, RhH). ^{13}C{^{1}H} NMR (75.5 MHz, benzene-d_6): δ 159.2 (C_{arom}), 141.3 (C_{arom}), 140.9 (C_{arom}), 140.6 (C_{arom}), 135.9 (C_{arom}), 135.6 (C_{arom}), 123.0 (CH_{arom}), 121.9 (CH_{arom}), 121.8 (CH_{arom}), 120.6 (CH_{arom}), 120.1 (C_{arom}), 119.6 (CH_{arom}), 119.5 (CH_{arom}), 116.3 (CH_{arom}), 28.5 (2,6-$^iPr_2C_6H_3$), 28.0 (2,6-$^iPr_2C_6H_3$), 27.5 (apparent t, J_{CP} = 14 Hz, PCHMe$_2$), 26.5 (apparent t, J_{CP} = 14 Hz, PCHMe$_2$), 23.7 (2,6-$^iPr_2C_6H_3$), 23.6 (2,6-$^iPr_2C_6H_3$), 20.5 (PCHMe_2), 20.3 (PCHMe_2), 19.5 (PCHMe_2), 18.9 (PCHMe_2), 11.5 (indole-Me), 8.3 (SiMe). ^{31}P{^{1}H} NMR (121.5 MHz, benzene-d_6): δ 44.7 (d, $^1J_{PRh}$ = 117 Hz). ^{29}Si{^{1}H} NMR (99.4 MHz, benzene-d_6): δ 40.4. Satisfactory elemental analysis data could not be obtained for **2-30c** due to N-H reductive elimination leading to the formation of variable amounts of **2-38** and H_2N(2,6-$^iPr_2C_6H_3$) contaminants during workup/isolation.

(^{i}Pr-PSiP^{Ind})IrH(NHPh) (2-31a). A solution of **2-29** (0.21 g, 0.31 mmol) dissolved in ca. 16 mL of benzene was treated with LiNHPh (0.029 g, 0.31 mmol). The reaction mixture was magnetically stirred at room temperature and an immediate color change from yellow to orange was observed. After stirring for 40 minutes, the mixture was filtered through Celite. The filtrate solution was collected, and the volatile components were removed in vacuo. The remaining residue was washed with pentane (4 × 2 mL) and dried under vacuum to afford **2-31a** (0.21 g, 80%) as an orange solid. Single crystals of **2-31a** suitable for X-ray diffraction analysis were obtained from a concentrated pentane solution at -35 °C. ^{1}H NMR (500 MHz, benzene-d_6): δ 8.18 (d, 2 H, J_{HH} = 8 Hz, H_{arom}), 7.56 (d, 2 H, J_{HH} = 8 Hz, H_{arom}), 7.26–7.16 (7 H, H_{arom} + NH; the NH resonance was identified at 7.21

ppm in a ^{1}H-^{15}N HMQC experiment), 7.05 (d, 2 H, J_{HH} = 8 Hz, H$_{arom}$), 6.88 (t, 1 H, J_{HH} = 7 Hz, H$_{arom}$), 2.72 (m, 2 H, PCHMe$_2$), 2.45 (m, 2 H, PCHMe$_2$), 2.26 (s, 6 H, indole-Me), 1.26 (s, 3 H, SiMe), 1.12 (dvt, 6 H, J_{HH} = 7 Hz, J_{HP} = 9 Hz, PCHMe_2), 1.02–0.94 (18 H, PCHMe_2), -20.30 (t, 1 H, $^2J_{HP}$ = 17 Hz, IrH). ^{13}C{^{1}H} NMR (125.8 MHz, benzene-d_6): δ 164.0 (C$_{arom}$), 140.8 (C$_{arom}$), 136.4 (C$_{arom}$), 135.9 (C$_{arom}$), 128.4 (CH$_{arom}$), 122.9 (CH$_{arom}$), 122.3 (CH$_{arom}$), 120.3 (CH$_{arom}$), 119.8 (CH$_{arom}$), 119.6 (C$_{arom}$), 118.8 (CH$_{arom}$), 116.1 (CH$_{arom}$), 28.5 (apparent t, J_{CP} = 12 Hz, PCHMe$_2$), 25.4 (apparent t, J_{CP} = 17 Hz, PCHMe$_2$), 20.4 (PCHMe_2), 20.0 (PCHMe_2), 19.7 (PCHMe_2), 18.6 (PCHMe_2), 11.7 (indole-Me), 6.47 (SiMe). ^{31}P{^{1}H} NMR (121.5 MHz, benzene-d_6): δ 41.5. ^{29}Si{^{1}H} NMR (99.4 MHz, benzene-d_6): δ 8.9. Anal. Calcd for C$_{37}$H$_{52}$IrN$_3$P$_2$Si: C, 54.12; H, 6.38; N, 5.12. Found: C, 53.96; H, 6.29; N, 5.30.

(^{i}Pr-PSiP^{Ind})IrH[NH(2,6-Me$_2$C$_6$H$_3$)] (2-31b). A solution of **2-29** (0.099 g, 0.13 mmol) in ca. 10 mL of benzene was treated with LiNH(2,6-Me$_2$C$_6$H$_3$) (0.017 g, 0.13 mmol). An immediate color change from yellow to orange was observed. The reaction mixture was allowed to stir at room temperature for 40 minutes, and was subsequently filtered through Celite. The filtrate solution was collected, and the volatile components were removed in vacuo. The remaining residue was triturated with pentane (3 × 2 mL) and subsequently washed with pentane (3 × 2 mL) and dried in vacuo to afford **2-31b** (0.085 g, 78% yield) as an orange solid. Single crystals of **2-31b** suitable for X-ray diffraction analysis were obtained from a concentrated pentane solution at -35 °C. ^{1}H NMR (300 MHz, benzene-d_6): δ 8.15 (d, J_{HH} = 8 Hz, 2 H, H$_{arom}$), 7.57 (d, 2 H, J_{HH} = 8 Hz, H$_{arom}$), 7.23–7.13 (6 H, H$_{arom}$), 6.89 (t, 1 H, J_{HH} = 7 Hz, H$_{arom}$), 6.32 (br s, 1 H, NH), 2.69–2.56 (5 H, PCHMe$_2$ + 2,6-Me_2C$_6$H$_3$), 2.49 (s, 3 H, 2,6-Me_2C$_6$H$_3$), 2.28 – 2.18 (s, 8 H, indole-Me + PCHMe$_2$), 1.21 (s, 3 H, SiMe), 1.13 (dvt, 6 H, J_{HH} = 7 Hz, J_{HP} = 11 Hz, PCHMe_2), 0.98–0.81 (18 H, PCHMe_2),

-20.02 (t, 1 H, $^2J_{HP}$ = 17 Hz, IrH). ^{13}C{^{1}H} NMR (75.5 MHz, benzene-d_6): δ 162.0 (C$_{arom}$), 140.7 (C$_{arom}$), 136.9 (C$_{arom}$), 136.0 (C$_{arom}$), 132.8 (C$_{arom}$), 130.9 (C$_{arom}$), 127.9 (CH$_{arom}$), 127.6 (CH$_{arom}$), 122.8 (CH$_{arom}$), 121.0 (CH$_{arom}$), 120.3 (CH$_{arom}$), 119.8 (CH$_{arom}$), 119.1 (C$_{arom}$), 116.3 (CH$_{arom}$), 27.4 (apparent t, J_{CP} = 13 Hz, PCHMe$_2$), 25.8 (apparent t, J_{CP} = 17 Hz, PCHMe$_2$), 21.3 (2,6-Me_2C$_6$H$_3$), 20.3 (2,6-Me_2C$_6$H$_3$), 20.2 (PCHMe$_2$), 19.8 (PCHMe$_2$), 19.3 (PCHMe$_2$), 18.8 (PCHMe$_2$), 11.6 (indole-Me), 5.42 (SiMe). ^{31}P{^{1}H} NMR (121.5 MHz, benzene-d_6): δ 39.1. ^{29}Si{^{1}H} NMR (99.4 MHz, benzene-d_6): δ 9.3. Anal. Calcd for C$_{39}$H$_{56}$IrN$_3$P$_2$Si: C, 55.16; H, 6.65; N, 4.95. Found: C, 55.68; H, 6.68; N, 4.85. Although these results in %C are outside the range viewed as establishing analytical purity, they illustrate the best values obtained to date for this complex.

(^{i}Pr-PSiP^{Ind})IrH[NH(2,6-^{i}Pr$_2$C$_6$H$_3$)] (2-31c). A solution of 2-29 (0.074 g, 0.097 mmol) in ca. 7 mL of benzene was treated with LiNH(2,6-^{i}Pr$_2$C$_6$H$_3$) (0.018 g, 0.097 mmol). An immediate color change from yellow to orange was observed. The reaction mixture was stirred for 1 h at room temperature and was subsequently filtered through Celite. The filtrate solution was collected, and the volatile components were removed in vacuo. The remaining residue was triturated with pentane (3 × 2 mL) and washed with pentane (3 × 4 mL) and dried in vacuo to afford 2-31c (0.090 g, 99 % yield) as an orange-red solid. Single crystals of 2-31c suitable for X-ray diffraction analysis were obtained from a concentrated pentane solution at -35 °C. ^{1}H NMR (500 MHz, benzene-d_6): δ 8.15 (d, 2 H, J_{HH} = 8 Hz, H$_{arom}$), 7.57 (d, 2 H, J_{HH} = 8 Hz, H$_{arom}$), 7.26–7.14 (6 H, H$_{arom}$), 7.07 (t, 1 H, J_{HH} = 8 Hz, H$_{arom}$), 7.03 (br s, 1 H, NH), 4.33 (sept, 1 H, $^3J_{HH}$ = 7 Hz, 2,6-^{i}Pr$_2$C$_6$H$_3$), 4.13 (sept, 1 H, $^3J_{HH}$ = 7 Hz, 2,6-^{i}Pr$_2$C$_6$H$_3$), 2.66 (m, 2 H, PCHMe$_2$), 2.37 (sept, 2 H, $^3J_{HH}$ = 7 Hz, PCHMe$_2$), 2.28 (s, 6 H, indole-Me), 1.30 (d, 6 H, $^3J_{HH}$ = 7 Hz, 2,6-^{i}Pr$_2$C$_6$H$_3$), 1.26 (d, 6 H, $^3J_{HH}$ = 7 Hz, 2,6-^{i}Pr$_2$C$_6$H$_3$) 1.25–1.17 (9 H, PCHMe$_2$ + SiMe; the SiMe resonance was identified at 1.22

68

ppm in a ^{1}H-^{13}C HSQC experiment), 0.96 (m, 12 H, PCHMe_2), 0.87 (dvt, 6 H, $J_{HH} = J_{HP} =$ 8 Hz, PCHMe_2), -19.78 (t, 1 H, $^2J_{HP} = 17$ Hz, IrH). ^{13}C{^{1}H} NMR (125.8 MHz, benzene-d_6): δ 159.3 (C$_{arom}$), 144.0 (C$_{arom}$), 142.9 (C$_{arom}$), 141.0 (C$_{arom}$), 137.7 (C$_{arom}$), 136.3 (C$_{arom}$), 123.3 (CH_{arom}), 123.0 (CH_{arom}), 122.1 (CH_{arom}), 122.0 (CH_{arom}), 120.6 (CH_{arom}), 120.1 (CH_{arom}), 119.2 (C$_{arom}$), 116.6 (CH_{arom}), 28.7 (2,6-$^iPr_2$C$_6$H$_3$), 28.3 (2,6-$^iPr_2$C$_6$H$_3$), 28.2 (apparent t, $J_{CP} = 12$ Hz, PCHMe_2), 26.6 (apparent t, $J_{CP} = 17$ Hz, PCHMe$_2$), 24.0 (2,6-$^iPr_2$C$_6$H$_3$), 23.9 (2,6-$^iPr_2$C$_6$H$_3$), 20.6 (PCHMe_2), 20.5 (PCHMe_2), 19.8 (PCHMe_2), 19.3 (PCHMe_2), 11.5 (indole-Me), 5.6 (SiMe). ^{31}P{^{1}H} NMR (202.5 MHz, benzene-d_6): δ 39.2. ^{29}Si{^{1}H} NMR (99.4 MHz, benzene-d_6): δ 9.6. Anal. Calcd for C$_{43}$H$_{64}$IrN$_3$P$_2$Si: C, 57.05; H, 7.13; N, 4.64. Found: C, 56.63; H, 7.02; N, 4.55. Although these results in %C are outside the range viewed as establishing analytical purity, they illustrate the best values obtained to date for this complex.

(^{i}Pr-PSiP^{Ind})IrH[NH(4-FC$_6$H$_4$)] (2-31d). A solution of 2-29 (0.10 g, 0.14 mmol) in ca. 8 mL benzene and the mixture was treated with LiNH(4-FC$_6$H$_4$) (0.016 g, 0.14 mmol). An instant color change from yellow to orange was observed. The mixture was allowed to stir for 2 h at room temperature and was then filtered through Celite. The filtrate solution was evaporated to dryness and the residue was triturated with pentane (3 × 2 mL). The remaining material was washed with pentane (3 × 2 mL) and dried in vacuo to afford 2-31d (0.11 g, 95 % yield) as a yellow-orange powder. ^{1}H NMR (300 MHz, benzene-d_6): δ 8.18 (apparent d, $J = 8$ Hz, 2 H, H$_{arom}$), 7.55 (apparent d, $J = 8$ Hz, 2 H, H$_{arom}$), 7.27–7.17 (overlapping resonances, 4 H, H$_{arom}$), 7.12 (s, NH), 6.87 (s, 2 H, H$_{arom}$), 6.84 (s, 2 H, H$_{arom}$), 2.72–2.62 (overlapping resonances, 2 H, PCHMe$_2$), 2.30–2.20 (overlapping resonances, 2 H, PCHMe$_2$), 2.24 (s, 6H, Indole-Me), 1.25 (s, 3 H, SiMe), 1.09 – 0.84 (overlapping resonances, 24 H, PCHMe_2), -20.42 (t, 1 H, $^2J_{HP} = 16$ Hz, IrH). ^{13}C{^{1}H} NMR (125.8 MHz,

benzene-d_6): δ 160.3 (C_{arom}), 159.4 (C_{arom}), 140.9 (C_{arom}), 136.7 (C_{arom}), 136.3 (C_{arom}), 135.8 (C_{arom}), 123.7 (CH_{arom}, $J_{\text{CF}} = 8$ Hz), 122.9 (CH_{arom}), 120.4 (CH_{arom}), 119.8 (CH_{arom}), 116.1 (CH_{arom}), 114.5 (CH_{arom}, $J_{\text{CF}} = 22$ Hz), 28.2 (apparent t, $^1J_{\text{CP}} = 13$ Hz, PCHMe$_2$), 25.1 (apparent t, $^1J_{\text{CP}} = 17$ Hz, PCHMe$_2$), 20.3 (CHMe_2), 20.0 (CHMe_2), 19.6 (CHMe_2), 18.5 (CHMe_2), 11.8 (Indole-Me), 6.58 (SiMe). ^{31}P{^{1}H} NMR (121.5 MHz, benzene-d_6): δ 41.2. ^{29}Si NMR (99.4 MHz, benzene-d_6): δ 9.5. ^{19}F{^{1}H} NMR (282.3 MHz, benzene-d_6): δ -126.1.

(^{i}Pr-PSiP$^{\text{Ind}}$)IrH[NH(4-OMeC$_6$H$_4$)] (2-31e). A solution of **2-29** (0.086 g, 0.11 mmol) in ca. 8 mL benzene was treated with LiNH(4-OMeC$_6$H$_4$) (0.015 g, 0.11 mmol). An immediate color change from yellow to dark orange was observed. The reaction mixture was allowed to stir at room temperature for 1.5 h and was subsequently filtered through Celite. The filtrate solution was evaporated to dryness and the residue was triturated with pentane (3 × 2 mL) and washed with pentane (3 × 3 mL). The remaining material was dried under vacuum to afford **2-31e** (0.071 g, 76 % yield) as a yellow-orange solid. ^{1}H NMR (300 MHz, benzene-d_6): δ 8.24 (apparent d, $J = 8$ Hz, 2 H, H$_{\text{arom}}$), 7.57 (apparent d, $J = 8$ Hz, 2 H, H$_{\text{arom}}$), 7.52 (apparent t, $J = 6$ Hz, NHAr), 7.29–7.17 (overlapping resonances, 4 H, H$_{\text{arom}}$), 7.08 (apparent d, $J = 9$ Hz, 2 H, H$_{\text{arom}}$), 6.86 (apparent d, $J = 9$ Hz, 2 H, H$_{\text{arom}}$), 3.44 (s, 3H, OMe), 2.78–2.64 (overlapping resonances, 2 H, PCHMe$_2$), 2.35–2.22 (overlapping resonances, 2 H, PCHMe$_2$), 2.28 (s, 6H, Indole-Me), 1.33 (s, 3 H, SiMe), 1.18–1.10 (overlapping resonances, 6 H, PCHMe_2), 1.04–0.95 (overlapping resonances, 6 H, PCHMe_2), - 20.2 (t, 1 H, $^2J_{\text{HP}} = 17$ Hz, IrH). ^{13}C{^{1}H} NMR (125.8 MHz, benzene-d_6): δ 157.8 (C_{arom}), 154.6 (C_{arom}), 140.9 (C_{arom}), 136.7 (C_{arom}), 136.0 (C_{arom}), 124.6 (CH_{arom}), 122.9 (CH_{arom}), 120.2 (CH_{arom}), 119.8 (CH_{arom}), 119.5 (C_{arom}), 116.2 (CH_{arom}), 113.6 (CH_{arom}), 27.9 (apparent t, $^1J_{\text{CP}} = 13$ Hz, PCHMe$_2$), 24.9 (apparent t, $^1J_{\text{CP}} = 17$ Hz,

PC*H*Me$_2$), 20.4 (CH*Me$_2$*), 20.2 (CH*Me$_2$*), 19.6 (CH*Me$_2$*), 18.5 (CH*Me$_2$*), 11.8 (Indole-*Me*), 6.8 (Si*Me*). ^{31}P{^{1}H} NMR (121.5 MHz, benzene-d_6): δ 41.3. ^{29}Si NMR (99.4 MHz, benzene-d_6): δ 10.7.

(^{i}Pr-PSiP^{Ind})IrH[NH(4-MeC$_6$H$_4$)] (2-31f). A solution of **2-29** (0.099 g, 0.13 mmol) in ca. 12 mL benzene was treated with LiNH(4-MeC$_6$H$_4$) (0.015 g, 0.13 mmol). An immediate color change from yellow to dark orange was observed. The reaction mixture was allowed to stir at room temperature for 1.5 h and was subsequently filtered through Celite. The filtrate solution was evaporated to dryness and the residue was triturated with pentane (3 × 2 mL) pentane and washed with pentane (2 × 3 mL). The remaining material was dried under vacuum to afford **2-31f** (0.091 g, 84 % yield) as an orange solid. ^{1}H NMR (300 MHz, benzene-d_6): δ 8.22 (apparent d, J = 8 Hz, 2 H, H$_{arom}$), 7.56 (apparent d, J = 8 Hz, 2 H, H$_{arom}$), 7.46 (apparent t, J = 5 Hz, N*H*Ar), 7.28–7.17 (overlapping resonances, 4 H, H$_{arom}$), 7.04 (s, 4 H, H$_{arom}$), 2.76–2.64 (overlapping resonances, 2 H, PC*H*Me$_2$), 2.47–2.35 (overlapping resonances, 2 H, PC*H*Me$_2$), 2.26 (s, 6H, Indole-*Me*), 1.31 (s, 3 H, Si*Me*), 1.16–0.92 (overlapping resonances, 24 H, PCH*Me$_2$*), -20.4 (t, 1 H, $^2J_{HP}$ = 17 Hz, Ir*H*). ^{13}C{^{1}H} NMR (125.8 MHz, benzene-d_6): δ 161.7 (*C*$_{arom}$), 140.9 (*C*$_{arom}$), 137.1 (*C*$_{arom}$), 136.6 (*C*$_{arom}$), 135.9 (*C*$_{arom}$), 128.9 (*C*H$_{arom}$), 122.9 (*C*H$_{arom}$), 122.8 (*C*H$_{arom}$), 120.2 (*C*H$_{arom}$), 119.7 (*C*H$_{arom}$), 119.5 (*C*$_{arom}$), 116.1 (*C*H$_{arom}$), 28.3 (apparent t, $^1J_{CP}$ = 13 Hz, PC*H*Me$_2$), 25.1 (apparent t, $^1J_{CP}$ = 17 Hz, PC*H*Me$_2$), 20.4 (CH*Me$_2$*), 20.2 (CH*Me$_2$*), 19.6 (CH*Me$_2$*), 18.6 (CH*Me$_2$*), 11.8 (Indole-*Me*), 6.6 (Si*Me*). ^{31}P{^{1}H} NMR (121.5 MHz, benzene-d_6): δ 41.3. ^{29}Si NMR (99.4 MHz, benzene-d_6): δ 9.98.

(^{i}Pr-PSiP^{Ind})RhH(NPh$_2$) (2-32a). A solution of **2-28** (0.083 g, 0.12 mmol) in ca. 8 mL of benzene was treated with LiNPh$_2$ (0.021 g, 0.12 mmol). An immediate color change

from yellow to orange to dark purple was observed. The reaction mixture was magnetically stirred for 1.5 h at room temperature and was subsequently filtered through Celite. The filtrate solution was collected, and the volatile components were removed in vacuo. The remaining residue was triturated with pentane (3 × 2 mL) and subsequently washed with pentane (2 × 3 mL) and dried in vacuo to afford **2-32a** (0.10 g, 99 % yield) as a purple solid. ^{1}H NMR (300 MHz, benzene-d_6): δ 7.74 (m, 2 H, H$_{arom}$), 7.57 (m, 2 H, H$_{arom}$), 7.21–7.12 (12 H, H$_{arom}$), 6.73 (m, 2 H, H$_{arom}$), 2.57 (m, 2 H, PCHMe$_2$), 2.41 (m, 2 H, PCHMe$_2$), 2.22 (s, 6 H, indole-Me), 1.17 (dvt, 6 H, J_{HH} = 7 Hz, J_{HP} = 10 Hz, PCHMe_2), 1.03 (dvt, 6 H, J_{HH} = 7 Hz, J_{HP} = 8 Hz, PCHMe_2), 0.95 (s, 3 H, SiMe), 0.93–0.80 (12 H, PCHMe_2), -17.04 (dt, 1 H, $^1J_{HRh}$ = 19 Hz, $^2J_{HP}$ = 16 Hz, RhH). ^{13}C{^{1}H} NMR (75.5 MHz, benzene-d_6): δ 157.4 (C$_{arom}$), 141.2 (C$_{arom}$), 136.4 (C$_{arom}$), 133.3 (C$_{arom}$), 129.4 (CH$_{arom}$), 128.6 (CH$_{arom}$), 123.2 (CH$_{arom}$), 121.5 (C$_{arom}$), 121.1 (CH$_{arom}$), 119.6 (CH$_{arom}$), 117.4 (CH$_{arom}$), 116.5 (CH$_{arom}$), 29.7 (apparent t, J_{CP} = 13 Hz, PCHMe$_2$), 27.1 (apparent t, J_{CP} = 12 Hz, PCHMe$_2$), 21.2 (PCHMe_2), 20.3 (PCHMe_2), 19.0 (PCHMe_2), 18.0 (PCHMe_2), 11.6 (indole-Me), 8.95 (SiMe). ^{31}P{^{1}H} NMR (121.5 MHz, benzene-d_6): δ 44.9 (d, $^1J_{RhP}$ = 58 Hz). ^{29}Si{^{1}H} NMR (99.4 MHz, benzene-d_6): δ 36.5. Anal. Calcd for C$_{43}$H$_{56}$N$_3$P$_2$RhSi: C, 63.93; H, 6.99; N, 5.20. Found: C, 63.55; H, 7.23; N, 5.17.

(^{i}Pr-PSiP^{Ind})IrH(NPh$_2$) (2-32b). A solution of **2-29** (0.070 g, 0.092 mmol) in ca. 7 mL of benzene was treated with LiNPh2 (0.016 g, 0.092 mmol). An immediate color change from yellow to red to dark purple was observed. The reaction mixture was stirred for 1 h at room temperature and was subsequently filtered through Celite. The filtrate solution was collected, and the volatile components were removed in vacuo. The remaining residue was triturated with pentane (6 × 3 mL) and washed with pentane (2 × 3 mL) and dried in vacuo to afford **2-32b** (0.082 g, 99 % yield) as a purple solid. ^{1}H NMR (300 MHz,

benzene-d_6): δ 7.81 (m, 2 H, H_{arom}), 7.56 (m, 2 H, H_{arom}), 7.21–7.12 (8 H, H_{arom}), 6.99 (d, 4 H, J_{HH} = 7 Hz, H_{arom}), 6.75 (t, 2 H, J_{HH} = 7 Hz, H_{arom}), 2.68 (m, 2 H, PCHMe$_2$), 2.55 (m, 2 H, PCHMe$_2$), 2.22 (s, 6 H, indole-Me), 1.13 (dvt, 6 H, J_{HH} = 9 Hz, J_{HP} = 7 Hz, PCHMe_2), 0.98 (dvt, 6 H, J_{HH} = 9 Hz, J_{HP} = 7 Hz, PCHMe_2), 0.95–0.83 (9 H, PCHMe_2 + SiMe; the SiMe resonance was identified at 0.92 ppm in a ^{1}H-^{13}C HSQC experiment), 0.78 (dvt, 6 H, J_{HH} = 9 Hz, J_{HP} = 7 Hz, PCHMe_2), -21.46 (t, 1 H, $^2J_{HP}$ = 16 Hz, IrH). ^{13}C{^{1}H} NMR (75.5 MHz, benzene-d_6): δ 157.8 (C_{arom}), 140.8 (C_{arom}), 136.4 (C_{arom}), 134.5 (C_{arom}), 129.5 (CH_{arom}), 123.1 (CH_{arom}), 120.9 (CH_{arom}), 120.3 (C_{arom}), 119.8 (CH_{arom}), 119.0 (CH_{arom}), 117.4 (CH_{arom}), 117.2 (CH_{arom}), 30.0 (apparent t, J_{CP} = 17 Hz, PCHMe$_2$), 28.4 (apparent t, J_{CP} = 14 Hz, PCHMe$_2$), 20.4 (PCHMe_2), 20.3 (PCHMe_2), 19.0 (PCHMe_2), 18.0 (PCHMe_2), 11.6 (indole-Me), 6.60 (SiMe). ^{31}P{^{1}H} NMR (121.5 MHz, benzene-d_6): δ 40.9. ^{29}Si{^{1}H} NMR (99.4 MHz, benzene-d_6): δ 0.9. Anal. Calcd for $C_{43}H_{56}IrN_3P_2Si$: C, 57.57; H, 6.29; N, 4.68. Found: C, 57.25; H, 6.42; N, 4.77.

(^{i}Pr-PSiP^{Ind})IrH(NH^{t}Bu) (2-33a). A solution of 2-29 (0.060g, 0.079 mmol) in ca. 6 mL of benzene was treated with LiNH^{t}Bu (0.0062 g, 0.079 mmol). An instant color change from yellow to orange was observed. The reaction mixture was stirred for 1 h at room temperature and was subsequently filtered through Celite. The filtrate solution was collected, and the volatile components were removed in vacuo. The remaining residue was triturated with pentane (2 × 3 mL) and washed with pentane (3 × 2 mL) and dried in vacuo to afford 2-33a (0.060 g, 95 % yield) as an orange solid. Single crystals of 2-33a suitable for X-ray diffraction analysis were obtained from a concentrated pentane solution at -35 °C. ^{1}H NMR (300 MHz, benzene-d_6): δ 8.24 (d, 2 H, J_{HH} = 8 Hz, H_{arom}), 7.53 (d, 2 H, J_{HH} = 7 Hz, H_{arom}), 7.30–7.13 (5 H, H_{arom} + NH; the NH resonance was identified at 7.28 ppm in a ^{1}H-^{15}N HMQC experiment), 2.84–2.57 (4 H, PCHMe$_2$), 2.29 (s, 6 H, indole-Me), 1.43

(s, 9 H, NH^tBu), 1.38 (s, 3 H, SiMe), 1.18 (m, 6 H, PCHMe_2), 1.07–0.96 (18 H, PCHMe_2), -19.18 (t, 1 H, $^2J_{HP}$ = 19 Hz, IrH). ^{13}C{^{1}H} NMR (75.5 MHz, benzene-d_6): δ 140.7 (C$_{arom}$), 136.1 (C$_{arom}$), 122.6 (CH_{arom}), 120.0 (CH_{arom}), 119.5 (CH_{arom}), 118.6 (C$_{arom}$), 116.0 (CH_{arom}), 58.6 (NHCMe$_3$), 35.7 (NHCMe_3), 24.2 (apparent t, J_{CP} = 20 Hz, PCHMe$_2$), 20.6 (PCHMe_2), 20.4 (PCHMe_2), 18.3 (PCHMe_2), 11.9 (indole-Me), 7.32 (SiMe). ^{31}P{^{1}H} NMR (121.5 MHz, benzene-d_6): δ 40.8. ^{29}Si{^{1}H} NMR (59.6 MHz, benzene-d_6): δ 11.8 ($^2J_{SiH}$ = 6 Hz). Anal. Calcd for C$_{35}$H$_{56}$IrN$_3$P$_2$Si: C, 52.48; H, 7.05; N, 5.25. Found: C, 52.16; H, 6.88; N, 5.03.

(^{i}Pr-PSiP^{Ind})IrH(NHAd) (2-33b). A solution of **2-29** (0.061 g, 0.080 mmol) in ca. 6 mL of benzene was treated with LiNHAd (0.0013 g, 0.080 mmol). An immediate color change from yellow to orange was observed. The reaction mixture was stirred for 1 h at room temperature and was subsequently filtered through Celite. The filtrate solution was collected, and the volatile components were removed in vacuo. The remaining residue was triturated with pentane (3 × 2 mL) and washed with pentane (2 × 3 mL) and dried in vacuo to afford **2-33b** (0.072 g, 97 %) as an orange solid. ^{1}H NMR (300 MHz, benzene-d_6): δ 8.25 (d, 2 H, J_{HH}= 8 Hz, H$_{arom}$), 7.55 (d, 2 H, J_{HH} = 8 Hz, H$_{arom}$), 7.25–7.14 (5 H, H$_{arom}$ + NH; the NH resonance was identified at 7.18 ppm in a ^{1}H-^{15}N HMQC experiment), 2.86–2.64 (4 H, PCHMe$_2$), 2.31 (s, 6 H, indole-Me), 2.15 (m, 3 H, NHAd), 1.84 (m, 6 H, NHAd), 1.68 (m, 6 H, NHAd), 1.39 (s, 3 H, SiMe), 1.22 (dvt, 6 H, J_{HH} = 7 Hz, J_{HP} = 9 Hz, PCHMe_2), 1.11–0.99 (18 H, PCHMe_2), -19.07 (t, 1 H, $^2J_{HP}$ = 19 Hz, IrH). ^{13}C{^{1}H} NMR (75.5 MHz, benzene-d_6): δ 140.7 (C$_{arom}$), 136.1 (C$_{arom}$), 122.6 (CH_{arom}), 120.1 (CH_{arom}), 119.6 (CH_{arom}), 118.7 (C$_{arom}$), 116.1 (CH_{arom}), 58.0 (NHAd), 49.6 (NHAd), 37.2 (NHAd), 31.3 (NHAd), 24.3 (apparent t, J_{CP} = 17 Hz, PCHMe$_2$), 20.7 (PCHMe_2), 20.5 (PCHMe_2), 18.3 (PCHMe_2), 12.0 (indole-Me), 7.5 (SiMe). ^{31}P{^{1}H} NMR (121.5 MHz, benzene-d_6): δ 40.9. ^{29}Si NMR (99.4

MHz, benzene-d_6): δ 12.0. Anal. Calcd for C$_{41}$H$_{62}$IrN$_3$P$_2$Si: C, 56.01; H, 7.11; N, 4.78. Found: C, 55.69; H, 6.86; N, 4.84.

(^{i}Pr-PSiP^{Ind})IrH(NH$_2$) (2-34). A solution of **2-29** (0.072 g, 0.094 mmol) in ca. 7 mL of THF was treated with LiNH2 (0.013 g, 0.56 mmol). The resulting yellow solution was stirred for 1 h at room temperature. The reaction mixture was then filtered through Celite. The filtrate solution was collected, and the volatile components were removed in vacuo. The remaining residue was triturated with pentane (2 × 3 mL) and subsequently washed with pentane (3 × 3 mL) and dried in vacuo to afford **2-34** (0.065 g, 94% crude yield) as a yellow solid. Attempts to further purify **2-34** resulted in the gradual decomposition of this complex to a mixture of unidentified species. ^{1}H NMR (300 MHz, benzene-d_6): δ 8.18 (d, J_{HH} = 8 Hz, 2 H, H$_{arom}$), 7.61 (m, 2 H, H$_{arom}$), 7.28–7.18 (4 H, H$_{arom}$), 5.42 (br s, 2 H, N*H$_2$*), 2.64–2.47 (4 H, PC*H*Me$_2$), 2.32 (s, 6 H, indole-*Me*), 1.28–0.92 (27 H, PCH*Me$_2$* + Si*Me*; the Si*Me* resonance was identified at 1.10 ppm in a ^{1}H-^{13}C HSQC experiment), -19.17 (t, $^2J_{HP}$ = 15 Hz, Ir*H*). ^{13}C{^{1}H} NMR (75.5 MHz, benzene-d_6): δ 140.8 (C$_{arom}$), 136.7 (C$_{arom}$), 122.8 (*C*H$_{arom}$), 120.1 (*C*H$_{arom}$), 119.8 (*C*H$_{arom}$), 118.9 (C$_{arom}$), 116.4 (*C*H$_{arom}$), 28.6 (apparent t, J_{CP} = 13 Hz, PC HMe$_2$), 25.6 (apparent t, J_{CP} = 17 Hz, PCHMe$_2$), 20.6–20.3 (PCH*Me$_2$*), 19.6 (PCH*Me$_2$*), 11.4 (indole-*Me*), 6.9 (Si*Me*). ^{31}P{^{1}H} NMR (121.5 MHz, benzene-d_6): δ 40.6 (s). ^{29}Si{^{1}H} NMR (99.4 MHz, benzene-d_6): δ 14.9.

Generation of (*fac*-κ^3-^{i}Pr-PSiP^{Ind})Ir(H)$_2$(NH=C$_6$H$_{10}$) (2-33c'). A solution of **2-29** (0.048 g, 0.062 mmol) in ca. 5 mL of benzene was treated with LiNHCy (0.0065 g, 0.062 mmol). A color change from yellow to red was observed over the course of 30 minutes at room temperature. The reaction mixture was stirred at room temperature for 2 days over the course of which the formation of an off-white precipitate was noted. The volatile components of the reaction mixture were removed in vacuo. The remaining residue

was triturated with pentane (3 × 2 mL) and washed with pentane (3 × 2 mL) to afford a beige solid (0.050 g) composed of **2-33c'** and residual LiCl. Due to the insolubility of **2-33c'** in most solvents, LiCl could not be separated efficiently from this material. ^{1}H NMR (300 MHz, THF-d_8): δ 9.81 (br s, 1 H, N*H*), 7.81 (d, 2 H, J_{HH} = 8 Hz, H$_{arom}$), 7.42 (d, 2 H, J_{HH} = 8 Hz, H$_{arom}$), 7.04 (t, 2 H, J_{HH} = 7 Hz, H$_{arom}$), 6.95 (t, 2 H, J_{HH} = 7 Hz, H$_{arom}$), 2.97 (m, 2 H, PC*H*Me$_2$), 2.81 (t, 2 H, J_{HH} = 6 Hz, NH=C$_6$H$_{10}$), 2.73 (m, 2 H, PC*H*Me$_2$), 2.46 (s, 6 H, indole-*Me*), 2.42 (t, 2 H, J_{HH} = 6 Hz, NH=C$_6$H$_{10}$), 1.75–1.56 (overlapping resonances, 6 H, NH=C$_6$H$_{10}$), 1.22 (dd, 6 H, $^3J_{HH}$ = 7 Hz, $^3J_{PH}$ = 12 Hz, PCH*Me$_2$*), 1.08 (dd, 6 H, $^3J_{HH}$ = 7 Hz, $^3J_{PH}$ = 16 Hz, PCH*Me$_2$*), 0.98 – 0.85 (overlapping resonances, 15 H, PCH*Me$_2$* + Si*Me*; the Si*Me* resonance was identified at 0.92 ppm in a ^{1}H-^{13}C HSQC experiment), -9.93 (second order m, 2 H, Ir*H$_2$*). ^{13}C{^{1}H} NMR (75.5 MHz, THF-d_8): δ 188.4 (NH=*C*), 141.2 (C$_{arom}$), 140.6 (C$_{arom}$), 136.9 (C$_{arom}$), 122.4 (*C*H$_{arom}$), 119.8 (*C*H$_{arom}$), 119.4 (*C*H$_{arom}$), 116.0 (C$_{arom}$), 115.4 (*C*H$_{arom}$), 42.5 (NH=*C$_6$*H$_{10}$), 38.9 (NH=*C$_6$*H$_{10}$), 33.5 (m, P*C*HMe$_2$), 30.3 (m, P*C*HMe$_2$), 28.4 (NH=*C$_6$*H$_{10}$), 26.9 (NH=*C$_6$*H$_{10}$), 26.4 (NH=*C$_6$*H$_{10}$), 21.8 (m, PCH*Me$_2$*), 21.0 (PCH*Me$_2$*), 20.7 (m, PCH*Me$_2$*), 19.6 (PCH*Me$_2$*), 11.6 (indole-*Me*), 8.6 (Si*Me*). ^{31}P{^{1}H} NMR (122 MHz, THF-d_8): δ 22.5 (s). ^{31}P NMR (122 MHz, THF-d_8): 23.1 (br, 1 P), 22.3 (br, 1 P). ^{29}Si{^{1}H} NMR (100 MHz, THF-d_8): δ 21.4.

([i]Pr-PSiP[Ind])IrH[NH-N(CH$_2$CH$_2$)$_2$NMe] (2-35a). A solution of **2-29** (0.094 g, 0.12 mmol) in ca. 10 mL of benzene and was treated with Li[NH-N(CH$_2$CH$_2$)$_2$NMe] (0.011 g, 0.12 mmol) in ca. 5 mL benzene. A gradual color change from yellow to orange was observed over the course of 1 h at room temperature. The reaction mixture was then filtered through Celite. The filtrate solution was collected, and the volatile components were removed in vacuo. The remaining residue was triturated with pentane (2 × 3 mL) and subsequently washed with pentane (3 × 3 mL) and dried in vacuo to afford **2-35a** (0.099 g,

96%) as an orange solid. ^{1}H NMR (300 MHz, benzene-d_6): δ 8.25 (d, 1 H, J_{HH} = 8 Hz, H$_{arom}$), 8.23 (d, 1 H, J_{HH} = 8 Hz, H$_{arom}$), 7.65–7.55 (2 H, H$_{arom}$), 7.34–7.17 (4 H, H$_{arom}$), 6.89 (apparent d, J = 8 Hz, 1 H, NH), 3.56 (m, 1 H, PCHMe$_2$), 3.40–1.95 (overlapping resonances, 20 H, PCHMe$_2$ + indole-Me + N(CH_2CH_2)$_2$NMe + NMe; PCHMe$_2$resonances were identified at 2.83, 2.56, and 2.42 ppm in a ^{1}H-^{13}C HSQC experiment; indole-Me resonances were identified at 2.41 and 2.31 ppm in a ^{1}H-^{13}C HSQC experiment; the NMe resonance was identified at 2.16 ppm in a ^{1}H-^{13}C HSQC experiment; broad N(CH_2CH_2)$_2$NMe resonances were identified at 3.14 and 2.41 ppm in a ^{1}H-^{13}C HSQC experiment), 1.35 – 0.87 (overlapping resonances, 27 H, PCHMe_2 + SiMe; the SiMe resonance was identified at 1.21 ppm in a ^{1}H-^{13}C HSQC experiment), -19.08 (dd, $^2J_{PH}$ = 15, 17 Hz, 1 H, IrH). ^{13}C{^{1}H} NMR (75.5 MHz, benzene-d_6): δ 141.3 (C$_{arom}$), 141.1 (C$_{arom}$) 138.7–136.0 (overlapping resonances, C$_{arom}$), 123.2 (CH_{arom}), 122.9 (CH_{arom}), 120.4 CH_{arom}), 120.3 (CH_{arom}), 120.1 (CH_{arom}), 120.0 (CH_{arom}), 119.4–119.3 (C$_{arom}$), 116.6 (CH_{arom}), 116.5 (CH_{arom}), 62.3 (m, N(CH_2CH_2)$_2$NMe), 56.0 (N(CH$_2$CH$_2$)$_2$NMe), 46.3 (NMe), 28.2–27.3 (overlapping resonances, PCHMe$_2$; two resonances centered at 27.9 and 27.6 ppm were identified in a ^{1}H-^{13}C HSQC experiment), 25.3–23.8 (overlapping resonances, PCHMe$_2$; two resonances centered at 25.1 and 23.9 ppm were identified in a ^{1}H-^{13}C HSQC experiment), 21.0–20.4 (overlapping resonances, PCHMe_2), 19.6–19.3 (overlapping resonances, PCHMe_2), 18.5–18.4 (overlapping resonances, PCHMe_2), 12.3 (indole-Me), 11.9 (indole-Me), 7.5 (SiMe). ^{31}P{^{1}H} NMR (121.5 MHz, benzene-d_6): δ 42.2 (AB q, v_A = 45.0 ppm, v_B = 39.4 ppm, $^2J_{AB}$ = 297 Hz). ^{29}Si{^{1}H} NMR (99.4 MHz, benzene-d_6): δ 14.5. Anal. Calcd for $C_{36}H_{58}IrN_5P_2Si$: C, 51.28; H, 6.93; N, 8.31. Found: C, 51.03; H, 6.78; N, 8.05.

(^{i}Pr-PSiP^{Ind})IrH(NH-N(CH$_2$CH$_2$)$_2$CH$_2$) (2-35b). Complex **2-29** (0.067 g, 0.089 mmol) was dissolved in ca. 10 mL THF and was added to Li(NH(N(CH$_2$CH$_2$)$_2$CH$_2$) (0.009 g, 0.089 mmol) in ca. 5 mL THF. A gradual color change from yellow to orange was observed within 1 h of stirring. ^{31}P{^{1}H} NMR spectroscopy revealed the presence of *ca.* 85% (by ^{31}P NMR) of the desired product **2-35b** with the presence of a minor product (*ca.* 15 % by ^{31}P NMR). Purification efforts including washing and crystallizations with various solvents were unsuccessful. The *in situ* data for the major product obtained are as follows: ^{1}H NMR (300 MHz, benzene-d_6): δ 8.24 (apparent d, J = 8 Hz, 2 H, H$_{arom}$), 7.96 (m, 1 H, H$_{arom}$), 7.63 – 7.55 (overlapping resonances, 2 H), 7.31 – 7.14 (overlapping resonances, 2H, H$_{arom}$), 6.96 (apparent d, J = 7 Hz), 3.53 (m, 1 H, PC*H*Me$_2$), 3.22 (m, 1 H, PC*H*Me$_2$), 2.76 (m, 1 H, PC*H*Me$_2$), 2.53 (m, 1 H, PC*H*Me$_2$), 2.41 (s, 3H, Indole-*Me*), 2.31 (s, 3 H, Indole-*Me*), 1.85 – 0.86 (overlapping resonances, 34 H, PCH*Me$_2$*NH(N(C$_2$*H$_4$*)$_2$CH$_2$, NH(N(C$_2$*H$_4$*)$_2$NCH$_3$), 1.21 (s, 3 H, Si*Me*), -19.03 (apparent dd, J_{HP} = 17, 15 Hz, 1 H, Ir*H*). ^{31}P{^{1}H} NMR (122 MHz, benzene-d_6): δ 42.07 (ABq) Δv_{AB} = 666 Hz, J_{AB} = 297 Hz.

(^{i}Pr-PSiP^{Ind})RhH(NH(CO)Ph) (2-36a). A room temperature solution of **2-30a** (0.070 g, 0.096 mmol) in ca. 6 mL of benzene was transferred to a vial containing benzamide (0.012 g, 0.096 mmol). A color change from dark red to yellow was observed. The resulting solution was allowed to stand at room temperature for 1 h. The volatile components of the reaction mixture were then removed in vacuo. The remaining residue was triturated with pentane (3 × 2 mL) and subsequently washed with pentane (3 × 3 mL) and dried in vacuo to afford **2-30a** (0.055 g, 75%) as a yellow solid. ^{1}H NMR (300 MHz, benzene-d_6): δ 7.96 (m, 2 H, H$_{arom}$), 7.82 (m, 2 H, H$_{arom}$), 7.62 (m, 2 H, H$_{arom}$), 7.30–7.08 (overlapping resonances, 7 H, H$_{arom}$), 5.89 (br s, 1 H, N*H*), 2.63–2.43 (overlapping resonances, 4 H, PC*H*Me$_2$), 2.29 (s, 6 H, indole-*Me*), 1.54 (dvt, 6 H, J_{HH} = J_{HP} = 7 Hz,

PCH*Me₂*), 1.17–0.91 (overlapping resonances, 18 H, PCH*Me₂*), 0.85 (s, 3 H, Si*Me*), -16.67 (m, 1 H, Rh*H*). $^{13}C\{^1H\}$ NMR (75.5 MHz, benzene-d_6): δ 175.7 (*C*=O), 141.3 (C$_{arom}$), 138.3 (C$_{arom}$), 136.4 (C$_{arom}$), 130.0 (*CH*$_{arom}$), 127.0 (*CH*$_{arom}$), 123.1 (*CH*$_{arom}$), 120.9 (*CH*$_{arom}$), 119.8 (*CH*$_{arom}$), 119.7 (C$_{arom}$), 117.2 (*CH*$_{arom}$), 30.0 (apparent t, J_{CP} = 12 Hz, P*C*HMe₂), 28.8 (apparent t, J_{CP} = 15 Hz, P*C*HMe₂), 21.3 (PCH*Me₂*), 20.8 (PCH*Me₂*), 20.1 (PCH*Me₂*), 19.1 (PCH*Me₂*), 11.4 (indole-*Me*), 6.4 (Si*Me*). $^{31}P\{^1H\}$ NMR (121.5 MHz, benzene-d_6): δ 48.8 (d, $^1J_{RhP}$ = 109 Hz). $^{29}Si\{^1H\}$ NMR (99.4 MHz, benzene-d_6): δ 48.2. Anal. Calcd for C$_{38}$H$_{52}$N$_3$OP$_2$RhSi: C, 60.07; H, 6.90; N, 5.53. Found: C, 60.02; H, 6.94; N, 5.35.

(^{i}Pr-PSiP^{Ind})RhH(NH(CO)CH₃) (2-36b). A room temperature solution of **2-30a** (0.014 g, 0.019 mmol) in ca. 0.75 mL of benzene-d_6 was transferred to a vial containing acetamide (0.001 g, 0.019 mmol). A color change from black-red to yellow was observed within 1 h of mixing. Quantitative conversion to **2-36b** was determined by use of $^{31}P\{^1H\}$ NMR spectroscopy. The product was characterized *in situ* as exposure to vacuum led to decomposition, preventing the isolation of **2-36b**. ^{1}H NMR (300 MHz, benzene-d_6): δ 7.91–7.87 (overlapping resonances, 2 H, H$_{arom}$), 7.58–7.54 (overlapping resonances, 2 H, H$_{arom}$), 7.16–7.10 (overlapping resonances, 4 H, H$_{arom}$), 4.67 (br s, 1 H, N*H*), 2.63–2.43 (overlapping resonances, 4 H, PC*H*Me₂), 2.26 (s, 6 H, Indole-*Me*), 1.68 (s, OC*Me*), 1.48–0.93 (overlapping resonances, 24 H, PCH*Me₂*), 0.69 (s, 3 H, Si*Me*), -16.9 (m, 1 H, Rh*H*). $^{13}C\{^1H\}$ NMR (75.5 MHz, benzene-d_6): δ 178.2 (*C*O$_{amide}$), 147.4 (C$_{arom}$), 140.6 (C$_{arom}$), 138.8 (C$_{arom}$), 136.2 (C$_{arom}$), 122.4 (*CH*$_{arom}$), 120.1 (*CH*$_{arom}$), 119.3 (*CH*$_{arom}$), 116.5 (*CH*$_{arom}$), 29.8 (apparent t, J_{CP} = 11 Hz, P*C*HMe₂), 28.6 (apparent t, J_{CP} = 15 Hz, P*C*HMe₂), 25.7 (OC*Me*), 21.0 (CH*Me₂*), 18.4 (CH*Me₂*), 19.8 (CH*Me₂*), 19.0 (CH*Me₂*), 10.7 (Indole-*Me*), 5.7 (Si*Me*). $^{31}P\{^1H\}$ NMR (121.5 MHz, benzene-d_6): δ 48.8 (d, $^2J_{PP}$ = 110). ^{29}Si NMR (99.4 MHz, benzene-d_6): δ 48.5.

(ⁱPr-PSiP^{Ind})IrH(NH(CO)Ph) (2-37a). A room temperature solution of **2-31a** (0.054 g, 0.066 mmol) in ca. 6 mL of benzene was transferred to a vial containing benzamide (0.008 g, 0.066 mmol). A color change from red-orange to yellow was observed. The resulting solution was allowed to stand at room temperature for 1 h. The volatile components of the reaction mixture were then removed in vacuo. The remaining residue was triturated with pentane (3 × 2 mL) and subsequently washed with pentane (3 × 3 mL) and dried in vacuo to afford **2-37a** (0.053 g, 95% yield) as a yellow-orange solid. ^{1}H NMR (300 MHz, benzene-d_6): δ 8.10 (d, J_{HH} = 8 Hz, 2 H, H$_{arom}$), 7.77 – 7.62 (overlapping resonances, 4 H, H$_{arom}$), 7.34–7.13 (overlapping resonances, 7 H, H$_{arom}$), 5.90 (br s, 1 H, N*H*), 2.93–2.63 (overlapping resonances, 4 H, PC*H*Me$_2$), 2.31 (s, 6 H, indole-*Me*), 1.53 (dvt, 6 H, J_{HH} = J_{HP} = 8 Hz, PCH*Me$_2$*), 1.19–0.95 (overlapping resonances, 18 H, PCH*Me$_2$*), 0.88 (s, 3 H, Si*Me*), -19.83 (br s, 1 H, Ir*H*). ^{13}C{^{1}H} NMR (75.5 MHz, benzene-d_6): δ 77.1 (C=O), 140.9 (C$_{arom}$), 139.0 (C$_{arom}$), 137.9 (C$_{arom}$), 136.6 (C$_{arom}$), 130.5 (*C*H$_{arom}$), 126.5 (*C*H$_{arom}$) 123.0 (*C*H$_{arom}$), 120.6 (*C*H$_{arom}$), 120.0 (*C*H$_{arom}$), 118.9 (C$_{arom}$), 117.2 (*C*H$_{arom}$), 30.3 (apparent t, J_{CP} = 14 Hz, P*C*HMe$_2$), 29.0 (apparent t, J_{CP} = 17 Hz, P*C*HMe2), 21.2 (CH*Me$_2$*), 20.4 (CH*Me$_2$*), 20.0 (CH*Me$_2$*), 19.0 (CH*Me$_2$*), 11.4 (indole-*Me*), 4.5 (Si*Me*). ^{31}P{^{1}H} NMR (121.5 MHz, benzene-d_6): δ 35.5. ^{29}Si{^{1}H} NMR (99.4 MHz, benzene-d_6): δ 8.3. Anal. Calcd for C$_{38}$H$_{52}$IrN$_3$OP$_2$Si: C, 53.75; H, 6.17; N, 4.95. Found: C, 54.30; H, 6.28; N, 4.97. Although these results in %C are outside the range viewed as establishing analytical purity, they illustrate the best values obtained to date for this complex.

(ⁱPr-PSiP^{Ind})IrH(NH(CO)CH$_3$) (2-37b). A room temperature solution of **2-31a** (0.054 g, 0.066 mmol) in ca. 6 mL of benzene was transferred to a vial containing acetamide (0.004 g, 0.066 mmol). A color change from red-orange to yellow was observed. The

resulting solution was allowed to stand at room temperature for 1 h. The volatile components of the reaction mixture were then removed in vacuo. The remaining residue was triturated with pentane (3 × 2 mL) and subsequently washed with pentane (3 × 3 mL) and dried in vacuo to afford **2-37b** (0.044 g, 85% yield). ^{1}H NMR (300 MHz, benzene-d_6): δ 8.04 (d, 2 H, J_{HH} = 8 Hz, H$_{arom}$), 7.63 (m, 2 H, H$_{arom}$), 7.29–7.17 (overlapping resonances, 4 H, H$_{arom}$), 4.65 (br s, 1 H, N*H*), 2.83 (m, 2 H, PC*H*Me$_2$), 2.67 (m, 2 H, PC*H*Me$_2$) 2.32 (s, 6 H, indole-*Me*), 1.54 (s, 3 H, O=C*Me*), 1.44 (dvt, 6 H, J_{HH} = J_{HP} = 8 Hz, PCH*Me$_2$*), 1.16 (dvt, 6 H, J_{HH} = J_{HP} = 8 Hz, PCH*Me$_2$*), 1.05-0.91 (overlapping resonances, 12 H, PCH*Me$_2$*), 0.73 (s, 3 H, Si*Me*), -20.11 (br s, 1 H, Ir*H*). ^{13}C{^{1}H} NMR (75.5 MHz, benzene-d_6): δ 179.4 (C=O), 140.8 (C$_{arom}$), 138.1 (C$_{arom}$), 136.6 (C$_{arom}$), 122.9 (*C*H$_{arom}$), 120.6 (*C*H$_{arom}$), 119.9 (*C*H$_{arom}$), 118.9 (C$_{arom}$), 117.2 (*C*H$_{arom}$), 30.4 (apparent t, J_{CP} = 14 Hz, P*C*HMe$_2$), 29.0 (apparent t, J_{CP} = 18 Hz, P*C*HMe$_2$), 27.4 (O=C*Me*), 21.1 (CH*Me$_2$*), 20.4 (CH*Me$_2$*), 20.1 (CH*Me$_2$*), 18.8 (CH*Me$_2$*), 11.4 (indole-*Me*), 4.3 (Si*Me*). ^{31}P{^{1}H} NMR (121.5 MHz, benzene-d_6): δ 35.2. ^{29}Si{^{1}H} NMR (99.4 MHz, benzene-d_6): δ 8.1. Anal. Calcd for C$_{33}$H$_{50}$IrN$_3$OP$_2$Si: C, 50.36; H, 6.40; N, 5.34. Found: C, 50.42; H, 6.45; N, 5.47.

[(^{i}Pr-PSiP^{Ind})Rh]$_2$(μ-N$_2$) (2-38). A solution of **2-28** (0.035 g, 0.052 mmol) in ca. 0.75 mL of benzene-d_6 was treated with Me$_3$SiCH$_2$Li (0.005 g, 0.052 mmol). An immediate color change from yellow to orange was observed; the resulting solution was allowed to stand at room temperature for 20 minutes. The solution was subsequently filtered through Celite and evaporated to dryness. The remaining residue was triturated with pentane (3 × 2 mL), and the orange residue was dried under vacuum to afford **2-38** (0.032 g, 95%) as an orange solid. While **2-38** was found to be isolable, decomposition of this material was observed in the solid state over the course of several days, as well as upon prolonged exposure to vacuum. X-Ray quality crystals of **2-38** were obtained from a concentrated

pentane solution at -35 °C. ^{1}H NMR (300 MHz, benzene-d_6): δ 7.91 (m, 2 H, H$_{arom}$), 7.68 (m, 2 H, H$_{arom}$), 7.26–7.20 (overlapping resonances, 4 H, H$_{arom}$), 2.68–2.46 (overlapping resonances, 4 H, PCHMe$_2$), 2.40 (s, 6 H, indole-Me), 1.32 (m, 12 H, PCHMe_2), 1.06 (m, 12 H, PCHMe_2), 0.86 (s, 3 H, SiMe). ^{13}C{^{1}H} NMR (75.5 MHz, benzene-d6): δ 140.9 (C$_{arom}$), 137.2 (C$_{arom}$), 122.4 (CH$_{arom}$), 120.3 (CH$_{arom}$), 119.4 (CH$_{arom}$), 117.8 (C$_{arom}$), 117.5 (CH$_{arom}$), 30.7 (apparent t, J_{CP} = 13 Hz, PCHMe$_2$), 29.9 (apparent t, J_{CP} = 11 Hz, PCHMe2), 22.0 (m, PCHMe_2), 21.7-21.4 (overlapping resonances, PCHMe_2), 11.3 (indole-Me), 8.3 (SiMe). ^{31}P{^{1}H} NMR (121.5 MHz, benzene-d_6): δ 49.0 (d, $^1J_{PRh}$ = 159 Hz). ^{29}Si{^{1}H} NMR (99.4 MHz, benzene-d_6): δ 58.3. Raman (solid state, cm^{-1}): 2073 (μ-N$_2$, s). The gradual decomposition of this material in the solid state precluded the acquisition of CHN elemental analysis data.

(^{i}Pr-PSiP^{Ind})Rh(PMe$_3$) (2-39a). A solution of **2-28** (0.057 g, 0.084 mmol) in ca. 5 mL of benzene was treated with Me$_3$SiCH$_2$Li (0.008 g, 0.084 mmol). An immediate color change from yellow to red was observed. The reaction mixture was subsequently treated with PMe$_3$ (8.6 μL, 0.084 mmol). After standing for 15 minutes at room temperature, the solution was filtered through Celite. The filtrate solution was collected and evaporated to dryness. The remaining residue was triturated with pentane (3 × 2 mL) and washed with pentane (3 × 2 mL), then dried under vacuum to afford **2-39a** (0.024 g, 40% yield) as a red-orange solid. ^{1}H NMR (300 MHz, benzene-d_6): δ 8.04 (m, 2 H, H$_{arom}$), 7.65 (m, 2 H, H$_{arom}$), 7.26–7.18 (overlapping resonances, 4 H, H$_{arom}$), 2.64 (m, 2 H, PCHMe$_2$), 2.44 (s, 6 H, indole-Me), 2.33 (apparent sept, $^3J_{HH}$ = 7 Hz, 2 H, PCHMe$_2$), 1.22 (dd, $^2J_{HP}$ = 5 Hz, $^3J_{HRh}$ = 1 Hz, 9 H, PMe_3), 1.13 (s, 3 H, SiMe), 1.11–0.96 (overlapping resonances, 24 H, PCHMe_2). ^{13}C{^{1}H} NMR (75.5 MHz, benzene-d_6): δ 141.0 (C$_{arom}$), 140.3 (C$_{arom}$), 138.2 (C$_{arom}$), 122.3 (CH$_{arom}$), 120.2 (CH$_{arom}$), 119.4 (CH$_{arom}$), 117.2 (CH$_{arom}$), 116.6 (C$_{arom}$), 32.2

(apparent t, J_{CP} = 10 Hz, PCHMe$_2$), 27.9 (apparent t, J_{CP} = 13 Hz, PCHMe$_2$), 22.7 (d, $^2J_{CP}$ = 14 Hz, PMe_3), 21.9-21.1 (overlapping resonances, PCHMe_2), 20.0 (PCHMe_2), 12.6 (indole-Me), 9.3 (SiMe). ^{31}P{^{1}H} NMR (121.5 MHz, benzene-d_6): δ 57.3 (dd, 2 P, $^1J_{PRh}$ = 128 Hz, $^2J_{PP}$ = 27 Hz, PSiP), 32.8 (dt, 1 P, $^1J_{PRh}$ = 125 Hz, $^2J_{PP}$ = 27 Hz, PMe$_3$). ^{29}Si{^{1}H} NMR (99.4 MHz, benzene-d_6): δ 63.4. Anal. Calcd for C$_{34}$H$_{54}$N$_2$P$_3$RhSi: C, 57.14; H, 7.62; N, 3.92. Found: C, 57.26; H, 7.35; N, 3.70.

(^{i}Pr-PSiP^{Ind})Rh(DMAP) (2-39b). A solution of **2-28** (0.059 g, 0.088 mmol) in ca. 5 mL of benzene was treated with Me$_3$SiCH$_2$Li (0.008 g, 0.088 mmol). An immediate color change from yellow to red was observed. The reaction mixture was treated with 4-dimethylaminopyridine (0.011 g, 0.088 mmol). A color change from dark red to orange-yellow was observed, and the resulting solution was allowed to stand at room temperature for 20 minutes. The reaction mixture was then filtered through Celite, and the filtrate solution was collected. The solvent was removed in vacuo, and the remaining residue was subsequently triturated with pentane (3 × 2 mL) and washed with pentane(3 × 3 mL). The residue was dried under vacuum to afford **2-39b** (0.058 g, 87% yield) as a yellow-orange solid. X-Ray quality crystals of **2-39b** were obtained from a concentrated pentane solution at -35 °C. ^{1}H NMR (500 MHz, benzene-d_6): δ 8.53 (d, 2 H, J_{HH} = 6 Hz, H$_{arom}$), 8.11 (m, 2 H, H$_{arom}$), 7.75 (m, 2 H, H$_{arom}$), 7.29–7.23 (overlapping resonances, 4 H, H$_{arom}$), 5.92 (d, 2 H, J_{HH} = 6 Hz, H$_{arom}$), 2.70 (m, 2 H, PCHMe$_2$), 2.63 (m, 2 H, PCHMe$_2$), 2.53 (s, 6 H, indole-Me), 2.08 (s, 6 H, NMe_2), 1.28 (m, 12 H, PCHMe_2), 1.21 (apparent q, J = 7 Hz, 6 H, PCHMe_2), 0.97 (s, 3 H, SiMe), 0.91 (apparent q, J = 7 Hz, 6 H, PCHMe_2). ^{13}C{^{1}H} NMR (125.8 MHz, benzene-d_6): δ 153.4 (C$_{arom}$), 152.5 (CH$_{arom}$), 141.2 (C$_{arom}$), 139.9 (m, C$_{arom}$), 137.4 (C$_{arom}$), 121.9 (CH$_{arom}$), 119.5 (CH$_{arom}$), 119.1 (CH$_{arom}$), 117.7 (CH$_{arom}$), 115.6 (C$_{arom}$), 106.9 (CH$_{arom}$), 38.9 (NMe_2), 29.7 (apparent t, J_{CP} = 10 Hz, PCHMe$_2$), 28.6

(apparent t, J_{CP} = 10 Hz, PCHMe₂), 21.8 (PCH*Me₂*), 21.5 (PCH*Me₂*), 21.1 (PCH*Me₂*), 20.2 (apparent t, J_{CP} = 5 Hz, PCH*Me₂*), 12.2 (indole-*Me*), 9.5 (Si*Me*). ³¹P{¹H} NMR (202.5 MHz, benzene-d_6): δ 40.9 (d, ¹J_{PRh} = 165 Hz). ²⁹Si{¹H} NMR (99.4 MHz, benzene-d_6): δ 60.8. Anal. Calcd for C₃₈H₅₅N₄P₂RhSi: C, 59.99; H, 7.29; N, 7.36. Found: C, 59.75; H, 7.23; N, 7.05.

(ⁱPr-PSiPᴵⁿᵈ)Rh(NH₂Ph) (2-39c). A solution of **2-28** (0.010 g, 0.015 mmol) in ca. 0.75 mL of cyclohexane-d_{12} was treated with Me₃SiCH₂Li (0.0014 g, 0.015 mmol). An immediate color change from yellow to orange-red was observed. The complete conversion of **2-28** to **2-38** was confirmed by ³¹P{¹H} NMR spectroscopy and aniline (27 μL, 0.30 mmol) was then added dropwise by micro-syringe. A color change from orange to yellow was observed within 10 minutes of addition. Quantitative conversion to **2-39c** was confirmed by in situ ³¹P{¹H} NMR spectroscopy. Attempts to isolate **2-39c** resulted in the quantitative conversion of this complex to the N₂ adduct **2-38**. ¹H NMR (500 MHz, cyclohexane-d_{12}): δ 7.51 (m, 2 H, H$_{arom}$), 7.41 (m, 2 H, H$_{arom}$), 6.93 (overlapping with NH₂Ph resonances, 4 H, H$_{arom}$), 2.60 (br m, 2 H, PC*H*Me₂), 2.39 (s, 6 H, Indole-*Me*), 1.27 (m, 6 H, PCH*Me₂*), 1.11 (apparent q, J = 7 Hz, 6 H, PCH*Me₂*), 0.95-0.84 (overlapping resonances, 12 H, PCH*Me₂*), 0.68 (s, 3 H, Si*Me*). ³¹P{¹H} NMR (121.5 MHz, cyclohexane-d_{12}): δ 41.0 (d, ¹J_{PRh} = 169 Hz).

Generation of [(ⁱPr-PSiPᴵⁿᵈ)Ir] (2-40). A solution of **2-29** (0.010 g, 0.013 mmol) in ca. 0.75 mL cyclohexane-d_{12} was treated with Me₃SiCH₂Li (0.001 g, 0.013 mmol). An immediate color change from yellow to red was observed. ¹H and ³¹P{¹H} NMR analysis of the reaction mixture within 5 minutes of addition indicated the complete consumption of **2-29** with concomitant formation of SiMe₄ and a new (ⁱPr-PSiPᴵⁿᵈ)Ir species assigned as **2-40**. Gradual decomposition of **2-40** in cyclohexane was observed within 1 h of mixing.

The highly reactive nature of **2-40** precluded its isolation, and as a result NMR data for this compound was obtained in situ. ^{1}H NMR (300 MHz, cyclohexane-d_{12}): δ 7.59–7.42 (overlapping resonances, 4 H, H$_{arom}$), 6.99 (m, 4 H, H$_{arom}$), 3.38 (br m, 1 H, PCHMe$_2$), 2.95 (br overlapping resonances, 3 H, PCHMe$_2$), 2.50 (s, 6 H, indole-Me), 1.30–1.07 (br overlapping resonances, 24 H, PCHMe_2), 0.66 (s, 3 H, SiMe). ^{31}P{^{1}H} NMR (121.5 MHz, cyclohexane-d_{12}): δ 49.2. ^{29}Si{^{1}H} NMR (99.4 MHz, cyclohexane-d_{12}): δ 40.4.

Generation of ([i]Pr-PSiP[Ind])Ir(C$_2$H$_4$) (2-41a). A solution of **2-29** (0.011 g, 0.014 mmol) in ca. 0.75 mL of cyclohexane-d_{12} was treated with Me$_3$SiCH$_2$Li (0.001 g, 0.014 mmol). An instant color change from yellow to orange to red was observed, and the contents were transferred to a J-Young NMR tube. ^{1}H and ^{31}P{^{1}H} NMR analysis of the reaction mixture within 5 minutes of addition indicated the complete consumption of **2-29** with concomitant formation of SiMe$_4$. The reaction mixture was subsequently degassed via three freeze-pump-thaw cycles, and ethylene (1 atm) was introduced. An instant color change from dark orange to yellow was observed. ^{31}P{^{1}H} NMR analysis of the reaction mixture indicated quantitative formation of **2-41a**. Due to the highly reactive nature of **2-41a** attempts to scale up and isolate this compound were not successful, and as such it was characterized *in situ*. ^{1}H NMR (300 MHz, cyclohexane-d_{12}): δ 7.59–7.56 (overlapping resonances, 2 H, H$_{arom}$), 7.45–7.42 (overlapping resonances, 2 H, H$_{arom}$), 7.04–6.99 (overlapping resonances, 4 H, H$_{arom}$), 3.59–3.44 (overlapping resonance, 2 H, PCHMe$_2$), 2.93–2.79 (overlapping resonance, 2 H, PCHMe$_2$), 2.52 (s, 6 H, Indole-Me), 2.05 (s, 4 H, IrC$_2$$H_2$), 1.41–0.91 (overlapping resonances, 24 H, PCHMe_2). ^{31}P{^{1}H} NMR (121.5 MHz, cyclohexane-d_{12}): δ 46.0.

(**^{i}Pr-PSiP^{Ind})Ir(CO)$_2$ (2-41b).** A solution of **2-29** (0.11 g, 0.14 mmol) in ca. 10 mL of cyclohexane and treated with Me$_3$SiCH$_2$Li (0.014g, 0.14 mmol). An instant color change from yellow to orange-red was observed. Complete consumption of **2-29** and formation of **2-40** was confirmed by ^{31}P{^{1}H} NMR spectroscopy. The reaction mixture was then transferred to a thick-walled glass vessel with a Teflon stopcock and was degassed via three freeze-pump-thaw cycles. CO (1 atm) was then introduced to the flask and an immediate color change from red to yellow was observed. The reaction mixture was evaporated under reduced pressure and the remaining residue was washed with pentane and (3 × 2 mL). The remaining material was dried under vacuum to afford **2-41b** (0.054g, 48% yield) as a yellow solid. ^{1}H NMR (500 MHz, benzene-d_6): δ 7.94 (apparent d, 2 H, J_{HH} = 7 Hz, H$_{arom}$), 7.54 (apparent d, 2 H, J_{HH} = 7 Hz, H$_{arom}$), 7.21–7.14 (overlapping resonances, 4 H, H$_{arom}$), 2.44–2.35 (overlapping resonances, 2 H, PC*H*Me$_2$), 2.30–2.25 (overlapping resonances, 2 H, PC*H*Me$_2$), 2.24 (s, 6 H, Indole-*Me*), 1.21 (s, 3 H, Si*Me*), 1.11–0.99 (overlapping resonances, 12 H, PCH*Me$_2$*), 0.73–0.67 (overlapping resonances, 12 H, PCH*Me$_2$*). ^{13}C{^{1}H} NMR (125.8 MHz, benzene-d_6): δ 185.1 (apparent t, J_{CP} = 10 Hz, *C*O), 182.2 (apparent t, J_{CP} = 30 Hz, *C*O), 148.1 (*C*$_{arom}$), 140.9 (*C*$_{arom}$), 137.6 (*C*$_{arom}$), 123.3 (*CH*$_{arom}$), 120.5 (*C*$_{arom}$), 119.9 (*CH*$_{arom}$), 117.2 (*CH*$_{arom}$), 115.7 (*CH*$_{arom}$), 32.1 (apparent t, J_{CP} = 19 Hz, P*C*HMe$_2$), 31.9 (apparent t, J_{CP} = 13 Hz, P*C*HMe$_2$), 21.5 (CH*Me$_2$*), 20.6 (CH*Me$_2$*), 19.8 (CH*Me$_2$*), 19.4 (CH*Me$_2$*), 10.9 (Indole-*Me*), 7.48 (Si*Me*). ^{31}P{^{1}H} NMR (121.5 MHz, benzene-d_6): δ 32.0. ^{29}Si NMR (99.4 MHz, benzene-d_6): δ 35.2.

(**^{i}Pr-PSiP^{Ind})Ir(H)(Cl)(CO) (2-42).** A solution of **2-29** (0.098g, 0.13 mmol) in ca. 20 mL THF was transferred to a thick-walled glass vessel with a Teflon stopcock and was degassed via three freeze-pump-thaw cycles. CO (1 atm) was then introduced to the flask and a color change from yellow to pale yellow was observed within 30 min of addition.

The reaction mixture was evaporated to dryness and the remaining solid was washed with pentane (4 × 2 mL). The remaining material was dried under vaccum to afford **2-42** (0.10 g, 98% yield) as a tan solid. ^{1}H NMR (300 MHz, benzene-d_6): δ 7.86 – 7.83 (overlapping resonances, 2 H, H_{arom}), 7.58–7.56 (overlapping resonances, 2 H, H_{arom}), 7.18–7.12 (overlapping resonances, 4 H, H_{arom}), 2.86 (m, 2 H, PC*H*Me$_2$), 2.38 (m, 2 H, PC*H*Me$_2$), 2.21 (s, 6 H, Indole-*Me*), 1.58–1.50 (overlapping resonances, 6 H, PCH*Me$_2$*), 1.24–1.17 (overlapping resonances, 6 H, PCH*Me$_2$*), 1.06–0.98 (overlapping resonances, 6 H, PCH*Me$_2$*), 0.88 (s, 3 H, Si*Me*), 0.62–0.54 (overlapping resonances, 6 H, PCH*Me$_2$*), -18.9 (t, 1 H, $^2J_{HP}$ = 15 Hz, Ir*H*). ^{13}C{^{1}H} NMR (125.8 MHz, benzene-d_6): δ 139.2 (*C*O), 135.5 (*C*$_{arom}$), 133.9 (*C*$_{arom}$), 133.4 (*C*$_{arom}$), 121.3 (*C*H$_{arom}$), 119.0 (*C*H$_{arom}$), 118.0 (*C*H$_{arom}$), 117.6 (*C*$_{arom}$), 115.4 (*C*H$_{arom}$), 29.8 (apparent t, $^2J_{CP}$ = 16 Hz, P*C*HMe$_2$), 28.6 (apparent t, $^2J_{CP}$ = 19 Hz, P*C*HMe$_2$), 18.7 (CH*Me$_2$*), 18.2 (CH*Me$_2$*), 17.8 (CH*Me$_2$*), 17.6 (CH*Me$_2$*), 9.02 (Indole-*Me*), 0.49 (Si*Me*). ^{31}P{^{1}H} NMR (121.5 MHz, benzene-d_6): δ 29.6. ^{29}Si NMR (99.4 MHz, benzene-d_6): δ 38.4.

(^{i}**Pr-PSiP^{Ind})Ir(CO) (2-41c).** Complex **2-42** (0.098g, 0.12 mmol) was placed under vacuum overnight to ensure removal of any excess CO and was subsequently dissolved in ca. 15 mL benzene. The solution was treated with Me$_3$SiCH$_2$Li (0.012g, 0.12 mmol). A color change from yellow to orange to red was observed within five minutes of addition. The resulting reaction mixture was allowed to stir at room temperature for 2 h. The solution was then filtered through Celite and evaporated to dryness. The remaining solid was washed with pentane (3 × 2 mL) and dried under vaccum to afford to obtain **2-41c** (0.050g, 55% yield) as a red solid. Storage of **2-41c** under an N$_2$ atompshere leads to the gradual formation of **2-41b**. ^{1}H NMR (500 MHz, benzene-d_6): δ 7.92–7.90 (overlapping resonances, 2 H, H_{arom}), 7.57–7.55 (overlapping resonances, 2 H, H_{arom}), 7.18–7.13

(overlapping resonances, 2 H, H_{arom}), 7.09–7.08 (overlapping resonances, 2 H, H_{arom}), 2.68–2.61 (overlapping resonances, 2 H, PC*H*Me$_2$), 2.58–2.53 (overlapping resonances, 2 H, PC*H*Me$_2$), 2.26 (s, 6 H, Indole-*Me*), 1.19–1.13 (overlapping resonances, 12 H, PCH*Me$_2$*), 0.86–0.79 (overlapping resonances, 12 H, PCH*Me$_2$*), 0.70 (s, 3 H, Si*Me*). ^{13}C{^{1}H} NMR (125.8 MHz, benzene-d_6): δ 205.4 (*CO*), 140.9 (C_{arom}), 138.1 (C_{arom}), 137.9 (C_{arom}), 122.9 (*CH*$_{arom}$), 120.5 (*CH*$_{arom}$), 120.0 (*CH*$_{arom}$), 118.1 (C_{arom}), 117.0 (*CH*$_{arom}$), 31.7 (apparent t, J_{CP} = 15 Hz, P*C*HMe$_2$), 30.4 (apparent t, J_{CP} = 18 Hz, P*C*HMe$_2$), 21.6 (CH*Me$_2$*), 21.0 (CH*Me$_2$*), 20.9 (CH*Me$_2$*), 20.3 (CH*Me$_2$*), 11.2 (Indole-*Me*), 6.72 (Si*Me*). ^{31}P{^{1}H} NMR (121.5 MHz, benzene-d_6): δ 55.6. ^{29}Si NMR (99.4 MHz, benzene-d_6): δ 75.3.

(*fac*-κ^3-^{i}Pr-PSiP^{Ind})IrH(κ^2-*P,C-o*-C$_6$H$_4$PPh$_2$) (2-43). A solution of **2-29** (0.083 g, 0.11 mmol) in ca. 5 mL of benzene was treated with Me$_3$SiCH$_2$Li (0.010 g, 0.11 mmol) dissolved in ca. 4 mL of benzene. An immediate color change from yellow to dark orange was observed. An aliquot of the reaction mixture was analyzed by use of ^{31}P{^{1}H} NMR spectroscopy to confirm the complete consumption of **2-29**. The reaction mixture was subsequently treated with PPh$_3$ (0.028 g, 0.11 mmol) resulting in a color change to dark red. After standing at room temperature for 40 minutes, the reaction mixture was filtered through Celite. The filtrate solution was collected and evaporated to dryness. The remaining residue was triturated with pentane (3 × 3 mL) and washed with pentane (2 × 2 mL) to obtain **2-43** (0.10 g, 95% yield) as an off-white solid. X-Ray quality crystals of **2-43** (featuring a pentane solvate) were obtained from a concentrated pentane solution at -35 °C. ^{1}H NMR (300 MHz, benzene-d_6): δ 8.49 (d, 1 H, J_{HH} = 8 Hz, H_{arom}), 8.31 (d, 1 H, J_{HH} = 8 Hz, H_{arom}), 8.07 (t, 2 H, J_{HH} = 8 Hz, H_{arom}), 7.69 (d, 1 H, J_{HH} = 8 Hz, H_{arom}), 7.60–6.84 (overlapping resonances, 13 H, H_{arom}), 6.74–6.45 (overlapping resonances, 4 H, H_{arom}), 3.11 (sept, 1 H, PC*H*Me$_2$), 2.37 (apparent d, $^4J_{HP}$ = 1 Hz, 3 H, indole-*Me*), 2.35-2.04

(overlapping resonances, 6 H, PC*H*Me$_2$ + indole-*Me*; three PC*H*Me$_2$ resonances were identified at 2.30, 2.27, and 2.12 ppm, and the indole-*Me* resonance was identified at 2.27 ppm in a ^{1}H-^{13}C HSQC experiment), 1.63 (apparent d, 3 H, $^4J_{HP}$ = 2 Hz, Si*Me*), 1.47–1.27 (overlapping resonances, 9 H, PCH*Me*$_2$), 0.82–0.33 (overlapping resonances, 12 H, PCH*Me*$_2$), 0.16 (dd, $^3J_{HH}$ = 7 Hz, $^3J_{HP}$ = 15 Hz, 3 H, PCH*Me*$_2$), -9.15 (apparent dt, 1 H, $^2J_{HP}$ = 115, 22 Hz, Ir*H*). ^{13}C{^{1}H} NMR (75.5 MHz, benzene-d_6): δ 156.8 (apparent d, $^2J_{CP}$ = 54 Hz, C$_{arom}$), 142.6-135.8 (overlapping resonances, C$_{arom}$), 134.8 (*CH*$_{arom}$), 134.7 (*CH*$_{arom}$), 133.0 (C$_{arom}$), 132.0 (apparent d, J_{CP} = 10 Hz, *CH*$_{arom}$), 131.5 (*CH*$_{arom}$) 130.5 (*CH*$_{arom}$), 130.1-127.6 (overlapping resonances, *CH*$_{arom}$), 123.7 (apparent d, J_{CP} = 8 Hz, *CH*$_{arom}$), 122.7 (apparent d, J_{CP} = 7 Hz, *CH*$_{arom}$), 120.5 (*CH*$_{arom}$), 120.3 (*CH*$_{arom}$), 119.7 (C$_{arom}$), 116.8 (C$_{arom}$), 115.6 (*CH*$_{arom}$), 115.2 (*CH*$_{arom}$), 32.3 (d, $^1J_{CP}$ = 19 Hz, P*C*HMe$_2$), 31.1 (d, $^1J_{CP}$ = 36 Hz, P*C*HMe$_2$), 27.3 (d, $^1J_{CP}$ = 17 Hz, P*C*HMe$_2$), 26.8 (d, $^1J_{CP}$ = 20 Hz, P*C*HMe$_2$), 23.5-22.6 (overlapping resonances, PCH*Me*$_2$), 20.4-19.4 (overlapping resonances, PCH*Me*$_2$), 18.7 (PCH*Me*$_2$), 18.1 (PCH*Me*$_2$), 12.4 (indole-*Me*), 11.8 (indole-*Me*), 7.2 (Si*Me*). ^{31}P{^{1}H} NMR (121.5 MHz, benzene-d_6): δ 28.8 (apparent t, $^2J_{PP}$ = 16 Hz, *P*SiP), 7.2 (dd, $^2J_{PP}$ = 16, 32 Hz, *P*SiP), -86.9 (dd, $^2J_{PP}$ = 16, 32 Hz, κ^2-*P*,*C*-*o*-C$_6$H$_4$*P*Ph$_2$). ^{29}Si{^{1}H} NMR (99.4 MHz, benzene-d_6): δ 25.0. Anal. Calcd for C$_{54}$H$_{72}$IrN$_2$P$_3$Si·(C$_5$H$_{12}$): C, 61.05; H, 6.83; N, 2.64. Found: C, 59.80; H, 6.79; N, 2.79.

(**^{i}Pr-PSiP^{Ind}**)**IrH(Ph) (2-44).** *Method 1*: A solution of **2-29** (0.023 g, 0.030 mmol) in ca. 0.75 ml of benzene-d_6 was treated with PhLi (0.003 g, 0.030 mmol). An immediate color change from yellow to orange was observed. Complete consumption of **2-29** and formation of **2-44** was confirmed by use of ^{1}H and ^{31}P{^{1}H} NMR spectroscopy within 10 minutes of mixing. Deuterium incorporation into the Ir*H* and Ir*Ph* positions due to exchange with the benzene-d_6 solvent was observed by ^{1}H NMR spectroscopy within 30

min of addition of PhLi at room temperature. *Method 2*: A solution of **2-29** (0.010 g, 0.013 mmol) in ca. 0.75 mL of benzene-d_6 was treated with Me$_3$SiCH$_2$Li (0.001 g, 0.013 mmol). An immediate color change from yellow to dark red was observed. Complete consumption of **2-29** and formation of **2-44** was confirmed by use of ^{1}H and ^{31}P{^{1}H} NMR spectroscopy within 10 minutes of addition. The highly reactive nature of **2-44** precluded its isolation, and as a result NMR data for this compound was obtained *in situ*. ^{1}H NMR (300 MHz, cyclohexane-d_{12}): δ 7.82 (d, J_{HH} = 7 Hz, 2 H, H$_{arom}$), 7.48 (m, 2 H, H$_{arom}$), 7.17–7.06 (overlapping resonances, 6 H, H$_{arom}$), 6.97 (m, 2 H, H$_{arom}$), 6.67 (t, J_{HH} = 7 Hz, H$_{arom}$), 3.04-2.85 (overlapping resonances, 4 H, PC*H*Me$_2$), 2.44 (s, 6 H, indole-*Me*), 1.43 (m, 6 H, PCH*Me$_2$*), 1.25 (dvt, 6 H, J_{HH} = 8 Hz, J_{HP} = 7 Hz, PCH*Me$_2$*), 0.96 (dvt, 6 H, J_{HH} = 9 Hz, J_{HP} = 7 Hz, PCH*Me$_2$*), 0.88 (s, 3 H, Si*Me*), 0.81 dvt, 6 H, J_{HH} = 9 Hz, J_{HP} = 7 Hz, PCH*Me$_2$*) -10.60 (t, 1 H, $^2J_{HP}$ = 17 Hz, Ir*H*). ^{31}P{^{1}H} NMR (121.5 MHz, cyclohexane-d_{12}): δ 43.0. ^{1}H NMR (300 MHz, benzene-d_6): δ 8.05 (d, J_{HH} = 8 Hz, 2 H, H$_{arom}$), 7.58 (m, 2 H, H$_{arom}$), 7.25-7.18 (overlapping resonances, 4 H, H$_{arom}$), 2.78–2.53 (overlapping resonances, 4 H, PC*H*Me$_2$), 2.23 (s, 6 H, indole-*Me*), 1.25 (m, 6 H, PCH*Me$_2$*), 1.08 (dvt, 6 H, J_{HH} = 8 Hz, J_{HP} = 7 Hz, PCH*Me$_2$*), 0.99 (s, 3 H, Si*Me*), 0.87 (m, 6 H, PCH*Me$_2$*), 0.76 (m, 6 H, PCH*Me$_2$*), -10.46 (t, $^2J_{HP}$ = 17 Hz, Ir*H*). ^{13}C{^{1}H} NMR (75.5 MHz, benzene-d_6): δ 140.5 (C$_{arom}$), 136.6 (C$_{arom}$), 135.6 (C$_{arom}$), 123.3 (*C*H$_{arom}$), 120.8 (*C*H$_{arom}$), 120.1 (*C*H$_{arom}$), 116.7 (*C*H$_{arom}$), 31.6 (m, P*C*HMe$_2$), 29.1 (m, P*C*HMe$_2$), 21.8-18.8 (overlapping resonances, PCH*Me$_2$*), 18.3 (PCH*Me$_2$*), 11.4 (indole-*Me*), 5.3 (Si*Me*). ^{29}Si{^{1}H} NMR (99.4 MHz, benzene-d_6): δ -8.7.

(ᶦPr-PSiP^{Ind})Ir(H)(Ph)(CO) (2-45). A solution of **2-29** (0.095 g, 0.12 mmol) in ca. 15 mL benzene was treated Me$_3$SiCH$_2$Li (0.012 g, 0.12 mmol). An instant color change from yellow to orange was observed. Complete consumption of **2-29** and formation of **2-**

44 was observed by $^{31}P\{^{1}H\}$ NMR spectroscopy. The reaction mixture was then transferred to a thick-walled glass vessel with a Teflon stopcock and was degassed via three freeze-pump-thaw cycles. CO (1 atm) was then introduced and a color change from orange to yellow was observed. The reaction mixture was then filtered through Celite and evaporated to dryness. The remaining material was then triturated with pentane (2 × 2 mL) and the residue was dried under vacuum to aford **2-45** (0.093 g, 93 % yield) as a beige powder. ^{1}H NMR (300 MHz, benzene-d_6): δ 7.98–7.95 (overlapping resonances, 2 H, H$_{arom}$), 7.64–7.61 (overlapping resonances, 2 H, H$_{arom}$), 7.25–7.13 (overlapping resonances, 9 H, H$_{arom}$), 2.93 (m, 2 H, PC*H*Me$_2$), 2.66 (m, 2 H, PC*H*Me$_2$), 2.29 (s, 6 H, Indole-*Me*), 1.04–0.94 (overlapping resonances, 6 H, PCH*Me$_2$*), 0.90–0.82 (overlapping resonances, 6 H, PCH*Me$_2$*), 0.69 (s, 3 H, Si*Me*), -9.66 (t, 1 H, $^{2}J_{HP}$ = 19 Hz, Ir*H*). $^{13}C\{^{1}H\}$ NMR (125.8 MHz, benzene-d_6): δ 148.0 (*CO*), 141.8 (*C*$_{arom}$), 136.8 (*C*$_{arom}$), 137.7 (*C*$_{arom}$), 123.0 (*CH*$_{arom}$), 122.4 (*CH*$_{arom}$), 120.8 (*CH$_{arom}$*), 120.0 (*CH$_{arom}$*), 119.1 (*C*$_{arom}$), 117.7 (*CH$_{arom}$*), 26.0 (apparent t, $^{2}J_{CP}$ = 16 Hz, P*C*HMe$_2$), 27.1 (apparent t, $^{2}J_{CP}$ = 19 Hz, P*C*HMe$_2$), 19.2 (CH*Me$_2$*), 18.6 (CH*Me$_2$*), 18.0 (CH*Me$_2$*), 17.5 (CH*Me$_2$*), 11.8 (Indole-*Me*), 6.2 (Si*Me*). $^{31}P\{^{1}H\}$ NMR (121.5 MHz, benzene-d_6): δ 21.8. ^{29}Si NMR (99.4 MHz, benzene-d_6): δ 31.3.

(^{i}Pr-PSiP^{Ind})IrH(2-FC$_6$H$_4$) (2-46a). A solution of **2-29** (0.11 g, 0.14 mmol) in ca. 15 mL of cyclohexane was treated with Me$_3$SiCH$_2$Li (0.014 g, 0.14 mmol). An instant color change from yellow to orange to red was observed. $^{31}P\{^{1}H\}$ NMR analysis of the reaction mixture confirmed complete consumption of **2-29** and formation of **2-40**. Triethylamine (1 drop) was then added to the mixture, which was allowed to stir at room temperature for 30 minutes. An excess of fluorobenzene (0.15 mL, 1.5 mmol) was then added to the dark red solution. The reaction mixture was then heated at 75 °C for 1 h, resulting in a color change to yellow-orange. The mixture was then filtered through Celite and evaporated to dryness.

91

The remaining material was triturated with pentane (3 × 2 mL) and washed with pentane (2 × 3 mL). The residue was dried under vacuum to afford **2-46a** (0.098 g, 85 %) as a yellow-orange powder. ^{1}H NMR (300 MHz, benzene-d_6): δ 8.01–8.00 (overlapping resonances, 2 H, H_{arom}), 7.92 (m, 1 H, H_{arom}), 7.61–7.57 (overlapping resonances, 2 H, H_{arom}), 7.24–7.13 (overlapping resonances, 5 H, H_{arom}), 7.02–6.97 (overlapping resonances, 2 H, H_{arom}), 2.75 (m, 2 H, PC*H*Me$_2$), 2.56 (m, 2 H, PC*H*Me$_2$), 2.23 (s, 6 H, Indole-*Me*), 1.40–1.27 (overlapping resonances, 6 H, PCH*Me$_2$*), 1.12–1.05 (overlapping resonances, 6 H, PCH*Me$_2$*), 0.95 (s, 3 H, Si*Me*), 0.89–0.78 (overlapping resonances, 12 H, PCH*Me$_2$*), -9.27 (apparent q, J = 17 Hz, 1 H, Ir*H*). ^{13}C{^{1}H} NMR (75.5 MHz, benzene-d_6): δ 168.3 (C_{arom}), 165.4 (C_{arom}), 140.0 (C_{arom}), 142.2 (apparent d, J_{CF} = 26 Hz, CH_{arom}), 135.7 (C_{arom}), 124.6 (CH_{arom}), 123.8 (C_{arom}), 123.0 (CH_{arom}), 122.9 (CH_{arom}), 120.5 (CH_{arom}), 119.7 (CH_{arom}), 119.4 (C_{arom}), 116.4 (CH_{arom}), 113.2 (apparent d, J_{CF} = 26 Hz, CH_{arom}), 31.6 (apparent t, J_{CP} = 16 Hz, PC*H*Me$_2$), 29.3 (apparent t, J_{CP} = 16 Hz, PC*H*Me$_2$), 20.6 (PCH*Me$_2$*), 20.4 (PCH*Me$_2$*), 19.2 (PCH*Me$_2$*), 17.8 (PCH*Me$_2$*), 10.9 (Indole-*Me*), 4.6 (Si*Me*). ^{31}P{^{1}H} NMR (121.5 MHz, benzene-d_6): δ 45.3. ^{19}F{^{1}H} NMR (282.3 MHz, benzene-d_6): δ -94.7.

(^{i}Pr-PSiP^{Ind})IrH(2,5-F$_2$C$_6$H$_3$) (2-46b). A solution of **2-29** (0.055 g, 0.07 mmol) in ca. 15 mL of cyclohexane was treated with Me$_3$SiCH$_2$Li (0.007 g, 0.07 mmol). An instant color change from yellow to orange to red was observed. ^{31}P{^{1}H} NMR analysis of the reaction mixture confirmed complete consumption of **2-29** and formation of **2-40**. Triethylamine (2 drops) was then added to the mixture, which was allowed to stir at room temperature for 30 minutes. An excess of *p*-difluorobenzene (0.15 mL, 1.18 mmol) was then added to the dark red solution. The reaction mixture was then heated at 75 °C for 1 h, resulting in a color change to yellow-orange. The mixture was then filtered through Celite

and evaporated to dryness. The remaining material was triturated with pentane (3 × 2 mL) pentane and washed with pentane (3 × 3 mL). The residue was dried under vacuum to afford **2-47b** (0.047 g, 80 %) as a yellow-orange powder. ^{1}H NMR (300 MHz, benzene-d_6): δ 7.94–7.90 (overlapping resonances, 2 H, H$_{arom}$), 7.73 (m, 1 H, H$_{arom}$), 7.58–7.54 (overlapping resonances, 2 H, H$_{arom}$), 7.19–7.14 (overlapping resonances, 4 H, H$_{arom}$), 6.71 (m, 1 H, H$_{arom}$), 6.62 (m, 1 H, H$_{arom}$), 2.70 (m, 2 H, HPC*H*Me$_2$), 2.57 (m, 2 H, PC*H*Me$_2$), 2.20 (s, 6 H, Indole-*Me*), 1.33–0.74 (overlapping resonances, 24 H, PCH*Me$_2$*), 0.88 (s, 3 H, Si*Me*), -9.50 (apparent q, $J = 17$ Hz, 1 H, Ir*H*). ^{13}C{^{1}H} NMR (75.5 MHz, benzene-d_6): δ 142.2 (apparent d, $J_{CF} = 26$ Hz, *CH*$_{arom}$), 140.1 (*C*$_{arom}$), 139.7 (*C*$_{arom}$), 135.7 (*C*$_{arom}$), 135.5 (*C*$_{arom}$), 135.1 (*C*$_{arom}$), 127.2 (*C*$_{arom}$), 127.0 (*C*$_{arom}$), 123.3 (*C*$_{arom}$), 123.2 (CH$_{arom}$), 120.6 (CH$_{arom}$), 120.0 (*C*$_{arom}$), 119.7 (CH$_{arom}$), 116.5 (CH$_{arom}$), 112.8 (*CH*$_{arom}$), 109.3 (*CH*$_{arom}$), 31.6 (apparent t, $J_{CP} = 15$ Hz, PCHMe$_2$), 29.4 (apparent t, $J_{CP} = 17$ Hz, PCHMe$_2$), 20.6 (PCH*Me$_2$*), 20.3 (PCH*Me$_2$*), 19.3 (PCH*Me$_2$*), 17.9 (PCH*Me$_2$*), 11.0 (Indole-*Me*), 4.43 (Si*Me*). ^{31}P{^{1}H} NMR (122 MHz, benzene-d_6): δ 45.1. ^{19}F{^{1}H} NMR (282.3 MHz, benzene-d_6): δ –102.2 (d, $J_{FF} = 21$ Hz), -122.7 (d, $J_{FF} = 21$ Hz).

Generation of (*fac*-κ^3-^{i}Pr-PSiP^{Ind})IrH(κ^2-*N,C-o*-C$_6$H$_4$NH$_2$) (2-31a'). A solution of **2-3** (0.060 g, 0.079 mmol) in ca. 0.75 mL cyclohexane-d_{12} was treated with Me$_3$SiCH$_2$Li (0.0074 g, 0.079 mmol). An immediate color change from yellow to red was observed. The reaction mixture was analyzed by use of ^{1}H and ^{31}P{^{1}H} NMR spectroscopy to confirm the complete consumption of **2-29**. Aniline (7.2 μL, 0.079 mmol) was then added to the reaction mixture at room temperature. ^{1}H and ^{31}P{^{1}H} NMR analysis of the resulting reaction mixture within 20 minutes of aniline addition indicated the formation of **2-31a'** as the major product and **2-31a** as the minor product (*ca*. 3:1 ratio, on the basis of ^{31}P NMR). Attempts to isolate **2-31a'** from this mixture resulted in its decomposition to form multiple

unidentified products. Characteristic *in situ* NMR data is provided for **2-31a'**. ^{1}H NMR (300 MHz, cyclohexane-d_{12}): δ -6.64 (dd, 1 H, $^2J_{HP}$ = 22, 130 Hz, Ir*H*). ^{1}H NMR (300 MHz, benzene-d_6): δ -6.57 (dd, 1 H, $^2J_{HP}$ = 21, 128 Hz, Ir*H*). ^{31}P{^{1}H} NMR (122 MHz, cyclohexane-d_{12}): δ 25.8 (d, $^2J_{PP}$ = 12 Hz, 1 P), 12.9 (d, $^2J_{PP}$ = 12 Hz, 1 P). ^{29}Si NMR (99.4 MHz, benzene-d_6): δ 9.19.

(*fac*-κ^3-^{i}Pr-PSiP^{Ind})IrH[κ^2-*N,C-o*-(*p*-FC$_6$H$_3$NH$_2$)] (2-31d'). A solution of **2-29** (0.072 g, 0.09 mmol) in ca. 8 mL of cyclohexane was treated with Me$_3$SiCH$_2$Li (0.009 g, 0.09 mmol). An instant color change from yellow to orange to red was observed. Consumption of **2-29** and formation of **2-40** was observed by ^{31}P{^{1}H} NMR spectroscopy. *Para*-fluoroaniline (0.009 mL, 0.09 mmol) was then added to the mixture by microsyringe. Within a few minutes, formation of an orange-brown solution containing a significant amount of beige precipitate was noted. ^{31}P{^{1}H} NMR analysis of the reaction mixture indicated complete consumption of **2-40** within 30 minutes of aniline addition. The reaction mixture was evaporated to dryness. The remaining solid was dissolved in ca. 5 mL of benzene and filtered through Celite. The filtrate solution was evaporated to dryness and the residue was triturated with pentane (2 × 3 mL) and washed with pentane (3 × 3 mL). The remaining material was dried under vacuum to afford **2-31d'** (0.070 g, 93 %) as a beige solid. ^{1}H NMR (300 MHz, benzene-d_6): δ 8.18–8.11 (overlapping resonance, 2 H, H$_{arom}$), 7.62–7.54 (overlapping resonances, 2 H, H$_{arom}$), 7.39 (m, 1 H, H$_{arom}$), 7.31–7.12 (overlapping resonances, 5 H, H$_{arom}$), 6.55 (m, 1 H, H$_{arom}$), 5.87 (m, 1 H, H$_{arom}$), 2.96–2.71 (overlapping resonances, 2 H, PC*H*Me$_2$), 2.62 (s, 2 H, *H*$_2$NAr), 2.39 (m, 1 H, PC*H*Me$_2$), 2.33 (s, 3H, Indole-*Me*), 2.29 (s, 3H, Indole-*Me*), 2.14 (m, 1 H, PC*H*Me$_2$), 1.33 (s, 3 H, Si*Me*), 1.06–0.37 (overlapping resonances, 24 H, PCH*Me$_2$*), -6.68 (dd, 1 H, $^2J_{HP}$ = 22 and 127 Hz, Ir*H*). ^{13}C{^{1}H} NMR (125.8 MHz, benzene-d_6): δ 135.9 (*C*H$_{arom}$), 125.6 (*C*H$_{arom}$),

124.5 (CH_{arom}), 124.6 (C_{arom}), 123.9 (C_{arom}), 123.1 (CH_{arom}), 122.7 (C_{arom}), 120.5 (CH_{arom}), 119.9 (C_{arom}), 119.6 (C_{arom}), 117.7 (CH_{arom}), 116.7 (CH_{arom}), 114.6 (C_{arom}), 107.3 (C_{arom}), 30.2 (PCHMe$_2$), 29.7 (PCHMe$_2$), 28.7 (PCHMe$_2$), 26.2 (PCHMe$_2$), 21.5 (CHMe_2), 21.0 (CHMe_2), 20.8 (CHMe_2), 20.5 (CHMe_2), 19.4 (CHMe_2), 19.0 (CHMe_2), 18.5 (CHMe_2), 18.3 (CHMe_2), 11.7 (Indole-Me), 11.9 (Indole-Me), 4.4 (SiMe). ^{31}P{^{1}H} NMR (121.5 MHz, benzene-d_6): δ 23.8 (d, $^2J_{PP}$ = 8 Hz, 1 P), 13.5 (d, $^2J_{PP}$ = 12 Hz, 1 P). ^{29}Si NMR (99.4 MHz, benzene-d_6): δ 9.05. ^{19}F{^{1}H} NMR (282.3 MHz, benzene-d_6): δ -115.4.

Generation of (*fac*-κ³-^{i}Pr-PSiP^{Ind})IrH[κ²-*N*,*C*-*o*-(*p*-OMeC$_6$H$_3$NH$_2$)] (2-31e'). A solution of **2-3** (0.014 g, 0.02 mmol) in ca. 0.75 mL of cyclohexane-d_{12} was treated with Me$_3$SiCH$_2$Li (0.0017 g, 0.02 mmol). An instant color change from yellow to orange to red was observed. The complete consumption of **2-29** and formation of **2-40** was confirmed by ^{31}P{^{1}H} NMR spectroscopy. The reaction mixture was then treated with *para*-anisidine (0.002 g, 0.02 mmol) resulting in an instant color change from red to cloudy yellow. Spectroscopic data for **2-31e'** was obtained *in situ*, as attempts to isolate this compound resulted in the formation of multiple unidentified products. ^{31}P{^{1}H} NMR (121.5 MHz, benzene-d_6): δ 25.5 (d, $^2J_{PP}$ = 12 Hz, 1 P), 13.3 (d, $^2J_{PP}$ = 12 Hz, 1 P).

Generation of (*fac*-κ³-^{i}Pr-PSiP^{Ind})IrH[κ²-*N*,*C*-*o*-(*p*-MeC$_6$H$_3$NH$_2$)] (2-31f'). A solution of **2-29** (0.011 g, 0.01 mmol) in ca. 0.75 mL of cyclohexane-d_{12} was treated with Me$_3$SiCH$_2$Li (0.001 g, 0.01 mmol). An instant color change from yellow to orange to red was observed. The complete consumption of **2-29** and formation of **2-40** was confirmed by ^{31}P{^{1}H} NMR spectroscopy. The reaction mixture was then treated with *para*-toluidine (0.0015 g, 0.02 mmol) resulting in an instant color change from red to cloudy yellow. Spectroscopic data for **2-31f'** was obtained *in situ*, as attempts to isolate this compound

resulted in the formation of multiple unidentified products. $^{31}P\{^1H\}$ NMR (121.5 MHz, benzene-d_6): δ 24.5 (d, $^2J_{PP}$ = 17 Hz, 1 P), 13.3 (d, $^2J_{PP}$ = 17 Hz, 1 P).

(*fac*-κ³-^{i}Pr-PSiP^{Ind})IrH[κ²-*N,C-o*-(C_6H_4(CPh=N-*N*H₂))] (2-47a). A solution of **2-29** (0.086 g, 0.11 mmol) in ca. 5 mL of cyclohexane was treated with Me₃SiCH₂Li (0.011 g, 0.11 mmol). An instant color change from yellow to dark red was observed. The complete consumption of **2-29** and formation of **2-40** was confirmed by $^{31}P\{^1H\}$ NMR spectroscopy. The reaction mixture was then treated with benzophenone hydrazone (0.022 g, 0.11 mmol), and a color change from red to orange was observed. $^{31}P\{^1H\}$ NMR analysis of the reaction mixture 1 h post addition showed complete consumption of **2-40** and quantitative formation of **2-37a**. The reaction mixture was filtered through Celite and evaporated to dryness. The remaining residue was washed with pentane (3 × 3 mL), and the solid material obtained was dried under vacuum to afford **2-37a** (0.052 g, 50% yield) as a yellow solid. ^1H NMR (500 MHz, benzene-d_6): δ 8.49 (apparent d, J = 8 Hz, 1 H, H_{arom}), 8.28 (apparent d, J = 9 Hz, 1 H, H_{arom}), 7.71 (apparent d, J = 8 Hz, 1 H, H_{arom}), 7.61 (apparent d, J = 8 Hz, 1 H, H_{arom}), 7.51 (apparent t, J = 8 Hz, 1 H, H_{arom}), 7.35 (apparent t, J = 8 Hz, 1 H, H_{arom}), 7.24–7.13 (overlapping resonances, 10 H, H_{arom}), 6.76 (apparent d, J = 8 Hz, 1 H, H_{arom}), 6.64 (apparent t, J = 8 Hz, 1 H, H_{arom}), 6.44 (apparent t, J = 8 Hz, 1 H, H_{arom}), 5.32 (s, 2 H, H_2N-N=CPh), 3.16 (m, 1 H, PCHMe₂), 2.71 (m, 1 H, PCHMe₂), 2.63 (m, 1 H, PCHMe₂), 2.43 (s, 3 H, Indole-*Me*), 2.31 (s, 3 H, Indole-*Me*), 2.24 (m, 1 H, PCHMe₂), 1.39 (s, 3H, Si*Me*), 1.38–0.31 (overlapping resonances, 24 H, PCH*Me₂*), -9.66 (dd, $^2J_{HP}$ = 24 Hz, 116 Hz, 1 H, IrH). $^{13}C\{^1H\}$ NMR (125.8 MHz, toluene-d_8): δ 165.8 (C_{arom}), 148.8 (C_{arom}), 142.2 (C_{arom}), 140.4 (C_{arom}), 139.2 (CH_{arom}), 136.9 (C_{arom}), 133.8 (C_{arom}), 129.8 (CH_{arom}), 129.5 (CH_{rom}), 129.4 (CH_{arom}), 129.3 (CH_{arom}), 128.7 (CH_{arom}), 123.3 (CH_{arom}), 123.2 (CH_{arom}), 121.0 (CH_{arom}), 120.2 (CH_{arom}), 120.0 (CH_{arom}), 119.8

(CH_{arom}), 119.1 (C_{arom}), 116.2 (C_{arom}), 115.5 (CH_{arom}), 30.6 (PCHMe₂), 30.4 (PCHMe₂),

26.2 (PCHMe₂), 11.6 (PCHMe₂), 22.6 (CHMe_2), 21.6 (CHMe_2), 20.0 (CHMe_2), 19.9

(CHMe_2), 19.3 (CHMe_2), 19.0 (CHMe_2), 18.8 (CHMe_2), 18.5 (CHMe_2), 12.1 (Indole-Me),

11.6 (Indole-Me), 4.9 (SiMe). ^{31}P{^{1}H} NMR (202.5 MHz, benzene-d_6): δ 20.4 (d, $^2J_{PP}$ = 15

Hz, 1 P), 11.1 (d, $^2J_{PP}$ = 15 Hz, 1 P). ^{29}Si NMR (99.4 MHz, benzene-d_6): δ 20.4. Anal. Calcd

for $C_{44}H_{57}IrN_4P_2Si$: C, 57.18; H, 6.22; N, 6.06. Found: C, 56.77; H, 6.38; N, 5.88.

(fac-κ³-^{i}Pr-PSiP^{Ind})IrH[κ²-N,C-o-(3-MeC_6H_3(C(p-tolyl)N=NH₂))] **(2-47b).** A

solution of **2-3** (0.11 g, 0.14 mmol) in ca. 15 mL of cyclohexane was treated with

Me₃SiCH₂Li (0.014 g, 0.14 mmol). An instant color change from yellow to dark red was

observed. Analysis of the reaction mixture by ^{31}P{^{1}H} NMR spectroscopy confirmed the

complete consumption of **2-29** and formation of **2-40**. The reaction mixture was then

treated with 4,4'-dimethylbenzophenone hydrazone (0.033 g, 0.14 mmol), resulting in a

color change from red to orange. ^{31}P{^{1}H} NMR analysis of the reaction mixture 1 h post

addition showed complete consumption of **2-40** and quantitative formation of **2-47b**. The

reaction mixture was filtered through Celite and evaporated to dryness. The remaining

residue was triturated with pentane (3 × 2 mL) washed with pentane (3 × 3 mL), and the

solid material obtained was dried under vacuum to afford **2-47b** (0.13 g, 95% yield) as a

yellow-orange powder. ^{1}H NMR (300 MHz, benzene-d_6): δ 8.45 (apparent d, J = 8 Hz, 1

H, H_{arom}), 8.23 (apparent d, J = 8 Hz, 1 H, H_{arom}), 7.78 (apparent d, J = 8 Hz, 1 H, H_{arom}),

7.70–7.65 (overlapping resonances, 3 H, H_{arom}), 7.59–7.50 (overlapping resonances, 2 H,

H_{arom}), 7.34 (m, 1 H, H_{arom}), 7.24–7.19 (overlapping resonances, 3 H, H_{arom}), 6.94 (apparent

d, J = 8 Hz, 1 H, H_{arom}), 6.56 (apparent d, J = 8 Hz, 1 H, H_{arom}), 4.60 (br s, 2 H, H_2N-

N=CAr), 3.11 (m, 2 H, PCHMe₂), 2.61 (m, 1 H, PCHMe₂), 2.63 (m, 1 H, PCHMe₂), 2.41

(s, 3 H, Indole-Me), 2.25 (s, 3 H, Indole-Me), 2.01 (s, 3 H, Me-C_{arom}), 1.73 (s, 1 H, Me-

C$_{arom}$), 1.68–1.59 (overlapping resonances, 6 H, PC*H*Me$_2$), 1.42 (s, 3 H, Si*Me*), 1.26–0.17 (overlapping resonances, 18 H, PCHM*e$_2$*), -8.11 (dd, $^2J_{HP}$ = 23 Hz, 115 Hz, 1 H, Ir*H*). ^{31}P{^{1}H} NMR (122.5 MHz, benzene-*d$_6$*): δ 29.3 (d, $^2J_{PP}$ = 15 Hz, 1 P), 13.9 (d, $^2J_{PP}$ = 15 Hz, 1 P). ^{29}Si NMR (99.4 MHz, benzene-*d$_6$*): δ 1.42.

(*fac*-κ^3-^{i}Pr-PSiP^{Ind})IrH[κ^2-*N,C-o*-(3-OMe*C*$_6$H$_3$(C(*p*-OMeC$_6$H$_4$)N=*N*H$_2$))]   (2-47c). A solution of **2-3** (0.095 g, 0.12 mmol) in ca. 12 mL of cyclohexane was treated with Me$_3$SiCH$_2$Li (0.012 g, 0.12 mmol). An instant color change from yellow to dark red was observed. Analysis of the reaction mixture by ^{31}P{^{1}H} NMR spectroscopy confirmed the complete consumption of **2-29** and formation of **2-40**. The reaction mixture was then treated with 4,4'-dimethoxybenzophenone hydrazone (0.032 g, 0.12 mmol), resulting in a color change from red to orange. ^{31}P{^{1}H} NMR analysis of the reaction mixture 1 h post addition showed complete consumption of **2-40** and quantitative formation of **2-47c**. The reaction mixture was filtered through Celite and evaporated to dryness. The remaining residue was triturated with pentane (3 × 2 mL) and washed with pentane (3 × 3 mL), and the solid material obtained was dried under vacuum to afford **2-47c** (0.11 g, 94% yield) as an orange solid. ^{1}H NMR (300 MHz, benzene-*d$_6$*): δ 8.35 (apparent d, *J* = 8 Hz, 1 H, H$_{arom}$), 8.18 (apparent d, *J* = 8 Hz, 1 H, H$_{arom}$), 7.86 (apparent d, *J* = 9 Hz, 3 H, H$_{arom}$), 7.79 (apparent d, 1 H, H$_{arom}$), 7.71 (apparent d , *J* = 8 Hz, 1 H, H$_{arom}$), 7.60 (apparent t, *J* = 9 Hz, 2 H, H$_{arom}$), 7.39 (apparent d, *J* = 8 Hz, 1 H, H$_{arom}$), 7.29–6.57 (overlapping resonances, 5 H, H$_{arom}$), 3.22 (s, 3 H, OC*H$_3$*), 3.14 (m, 1 H, PC*H*Me$_2$), 2.83 (s, 3 H, Indole-*Me*), 2.63 (m, 1 H, PC*H*Me$_2$), 2.44 (s, 3 H, OC*H$_3$*), 2.38 (m, 1 H, PC*H*Me$_2$), 2.22 (s, 3 H, Indole-*Me*), 1.75–1.62 (overlapping resonances, 6 H, PC*H*Me$_2$), 1.37 (s, 3H, Si*Me*), 1.30–0.79 (overlapping resonances, 12 H, PC*H*Me$_2$), 0.37–0.15 (overlapping resonances, 6 H, PCHM*e$_2$*), -8.13 (dd, $^2J_{HP}$ = 22 Hz, 115 Hz, 1 H, Ir*H*). ^{31}P{^{1}H} NMR (121.5 MHz, benzene-

d_6): δ 29.8 (d, $^2J_{PP}$ = 15 Hz, 1 P), 14.2 (d, $^2J_{PP}$ = 15 Hz, 1 P). ^{29}Si NMR (99.4 MHz, benzene-d_6): δ 12.4.

Crystallographic Solution and Refinement Details. Crystallographic data were obtained between 173(2) and 193(2) K on either a Bruker D8/APEX II CCD or a Bruker PLATFORM/APEX II CCD diffractometer using either CuKα (λ = 1.54178 Å, microfocus source) or graphite monochromated MoKα (λ = 0.71073 Å; for **2-29**, **2-35a**, and **2-43**) radiation employing samples that were mounted in inert oil and transferred to a cold gas stream on the diffractometer. Programs for diffractometer operation, data collection, and data reduction (including SAINT) were supplied by Bruker. Data reduction, correction for Lorentz−polarization, and absorption correction were each performed. Structure solution was achieved by either intrinsic phasing methods or Patterson search/structure expansion. All structures were refined by use of full-matrix least-squares procedures (on F^2) with R_1 based on $F_o^2 \geq 2\sigma(F_o^2)$ and wR_2 based on $F_o^2 \geq -3\sigma(F_o^2)$.

Unless otherwise indicated, all nonhydrogen atoms were refined with anisotropic displacement parameters. One equiv. of C_6H_6 was located in the asymmetric unit for **2-31a**, and was refined anisotropically. Half an equiv. of Et_2O was located in the asymmetric unit for **2-31b**, and was refined anisotropically with an occupancy factor of 0.5 for O1S and C1S-C4S. In the case of **2-33a**, disorder involving the N-^{t}Bu group and a P-^{i}Pr substituent was identified. The disordered N-^{t}Bu group was modeled over two positions, such that C2A-C5a were refined with an occupancy factor of 0.64 and C2B-C5B were refined with an occupancy factor of 0.36. The disordered P-^{i}Pr substituent was modeled over two positions, such that C41A-C43A were refined with an occupancy factor of 0.60 and C41B-C43B were refined with an occupancy factor of 0.40. In both cases pairs of atoms were refined with an equivalent anisotropic displacement parameter. The disordered N-^{t}Bu group

was restrained to have approximately the same geometry by use of the *SHELXL* SAME instruction. Additionally, an anti-bumping restraint was applied to the H3N···H41B (of the minor orientation of the disordered isopropyl group) distance. In the case of **2-35a**, two cystallographically-independent molecules (A and B) were located in the asymmetric unit; for convenience, only molecule A is discussed in the text. Half an equiv. of *n*-pentane was located in the asymmetric unit for **2-38**. Atoms of the inversion-disordered solvent *n*-pentane molecule (C1S–C5S) were refined with an occupancy factor of 0.5 and a common isotropic displacement parameter. Distances within the *n*-pentane molecule were constrained during refinement: d(C1S–C2S) = d(C2S–C3S) = d(C3S–C4S) = d(C4S–C5S) = 1.52(1) Å; d(C1S···C3S) = d(C2S···C4S) = d(C3S···C5S) = 2.43(1) Å. In the case of **2-39b**, the crystal used for data collection was found to display non-merohedral twinning. Both components of the twin were indexed with the program *CELL_NOW* (Bruker AXS Inc., Madison, WI, 2004). The second twin component can be related to the first component by 180° rotation about the [0 1 0] axis in both real and reciprocal space. Integrated intensities for the reflections from the two components were written into a *SHELXL-2014* HKLF 5 reflection file with the data integration program *SAINT* (version 8.34A), using all reflection data (exactly overlapped, partially overlapped and non-overlapped). The refined value of the twin fraction (*SHELXL-2014* BASF parameter) was 0.4574 (12). In addition, half an equiv. of C_6H_6 was located in the asymmetric unit for **2-39b**, and was refined anisotropically (C1S-C3S). Lastly, for **2-43** attempts to refine peaks of residual electron density as disordered or partial-occupancy solvent *n*-pentane carbon atoms were unsuccessful. The data were corrected for disordered electron density through use of the SQUEEZE procedure as implemented in *PLATON* (Spek, A. L. *Acta Crystallogr.* **2015**, *C71*, 9–18. *PLATON* - a multipurpose crystallographic tool. Utrecht University, Utrecht,

The Netherlands). A total solvent-accessible void volume of 731 $Å^3$ with a total electron count of 141 (consistent with 4 molecules of solvent *n*-pentane, or one molecule per formula unit of the Ir complex) was found in the unit cell. Further, the Ir complex for **10** is disordered across two different mirror planes, located at (x, 0, z) (upon which the Ir atom is located) and (x, 0.5, z) (upon which the atom C17 is located). Details of this can be found in the deposited CIF. The following distances were constrained during refinement of **2-43**: (a) d(C41–C42) = d(C41–C43) = d(C44–C45) = d(C44–C46) = 1.52(1) Å; (b) d(C42…C43) = d(C45…C46) = 2.52(1) Å.

The M-*H* (H1; M = Rh or Ir) in each of **2-28**, **2-29**, **2-30a'**, **2-31a-c**, **2-33a**, **2-35a**, and **2-43** and the N-*H* (H3N) in each of **2-30a'**, **2-31a-c**, **2-33a**, and **2-35a** were located in the difference map and refined isotropically. For **2-31b**, the Ir–H1 (1.50(1) Å) and N3–H3N (0.88(1) Å) distances were constrained during refinement. The Ir-H1 distance in **10** (1.50(1) Å) was also constrained during refinement. Otherwise, all hydrogen atoms were added at calculated positions and refined by use of a riding model employing isotropic displacement parameters based on the isotropic displacement parameter of the attached atom.

Chapter 3: Reactivity of (ⁱPr-PSiP^Ind)M (M = Rh, Ir) Amido Hydride Complexes with Unsaturated Substrates: Progress Toward Insertion Reactions

In this chapter, all synthetic work was conducted by Helia Hollenhorst. X-Ray crystallographic data and refinement was conducted by Dr. Michael Ferguson and Dr. Yuqiao Zhou of the University of Alberta X-ray Crystallography Laboratory, Edmonton, AB.

3.1 Introduction

3.1.1 Insertion Chemistry of Unsaturated Substrates into Late Metal-Amido Bonds

The functionalization of simple amines by use of selective and efficient catalytic processes is an area of ongoing research interest, given the prevalence of amines in fine chemicals and pharmaceuticals. Catalytic hydroamination involving olefin activation (Figure 3-1, **A**) is well-precedented, while examples of related reactivity involving N-H oxidative addition to a metal center are rare (Figure 3-1, **B**),[10a, 10c, 38a, b, 58] yet such methodology may provide unique reactivity and/or selectivity advantages over traditional hydroamination catalysis. Major obstacles in developing such chemistry include the challenge posed by N-H oxidative addition of amines to a metal center, as well as the insertion of unsaturated substrates into the M-N bond and subsequent C-H reductive elimination to obtain the functionalized amine (Figure 3-1, **B**). While olefin insertion into a M-*N* bond is believed to be more favourable than insertion into the M-H bond,[59] examples of migratory insertion involving a late metal amido linkage are rare.[10a] β-Hydride elimination subsequent to olefin insertion may result in either olefin isomerization (for M-H insertion) or oxidative amination and enamine formation (for M-N insertion).[10a]
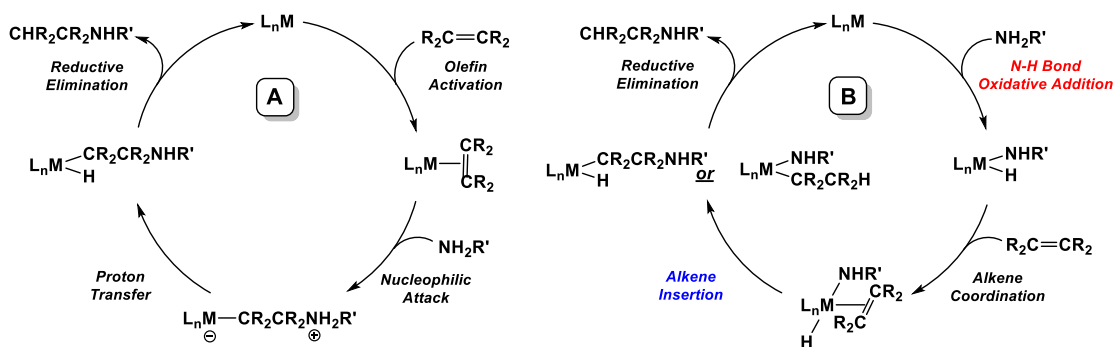
Figure 3-1. Catalytic cycles of hydroamination *via* olefin activation (**A**), or alternatively, *via* N-H oxidative addition and olefin insertion (**B**).

The insertion of acrylonitrile into the Pt-*N* linkage of *trans*-PtH(NHPh)(PEt$_3$)$_2$ and subsequent C-H reductive elimination to form 3-anilinopropionitrile as the hydroamination product has been observed stoichiometrically, requiring prolonged reaction times and elevated temperatures.[60] However, the development of this reaction into a catalytic process was hindered by the inaptitude for N-H oxidative addition. Both intra- and intermolecular insertion of alkenes into Pd-N bonds has been reported.[61] Remarkably, in the case of the latter process, Hartwig and co-workers have reported the insertion of ethylene into the Pd-*N* bond of isolated Pd amido complexes, with evidence for an intermediate that features ethylene coordinated to the Pd center (Scheme 3-1).[61d, e]
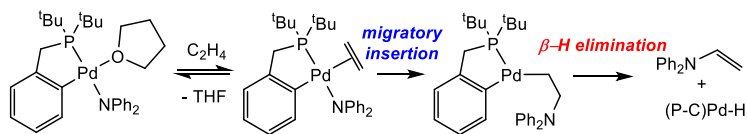
Scheme 3-1. Stoichiometric insertion of ethylene into a Pd-amido bond *via* a Pd^{II} amido alkene intermediate.

Beller and co-workers[62] reported on the oxidative amination/hydroamination of aromatic olefins with morpholine and *N*-arylpiperazines mediated by cationic [Rh(cod)$_2$]BF$_4$ / 2 PPh$_3$, and noted that the insertion of the olefin into the Rh-*N* bond resulting from amine activation is likely to be the rate-determining step. Subsequently,

Hartwig and co-workers[63] demonstrated that the anilido complex (PEt₃)₃Rh(NHAr) reacts with excess (15-30 equiv.) styrene, 1-hexene, or 1-propene to generate products containing new C-N bonds, resulting from insertion of the olefin into the Rh-anilido bond.

Iridium has featured prominently in studies of reactivity involving the insertion of unsaturated substrates into M-amido linkages with applications in catalytic hydroamination. Milstein was the first to report on the catalytic hydroamination of norbornene *via* a route involving N-H oxidative addition of aniline to an Ir^I center, however, catalytic performance was relatively poor (TON of only 2 to 6 after 48 h in refluxing THF).[20] More recently, improved reactivity involving the Ir-catalyzed enantioselective hydroamination of norbornene derivatives *via* an N-H activation pathway has been developed by Hartwig and co-workers (Scheme 3-2a).[64] The active catalyst in this system is proposed to be a monomeric, neutral Ir anilido complex, with the unusual feature that the anilido ligand functions as both an ancillary and reactive ligand. In a subsequent report involving a related Ir catalyst that undergoes α-olefin insertion into an Ir-benzamide bond, competitive C-H reductive elimination to form the *N*-alkylamide and β-hydride elimination to form the enamide were reported (Scheme 3-2b).[65] Such competitive pathways illustrate potential complications that may arise during such amination reactivity.
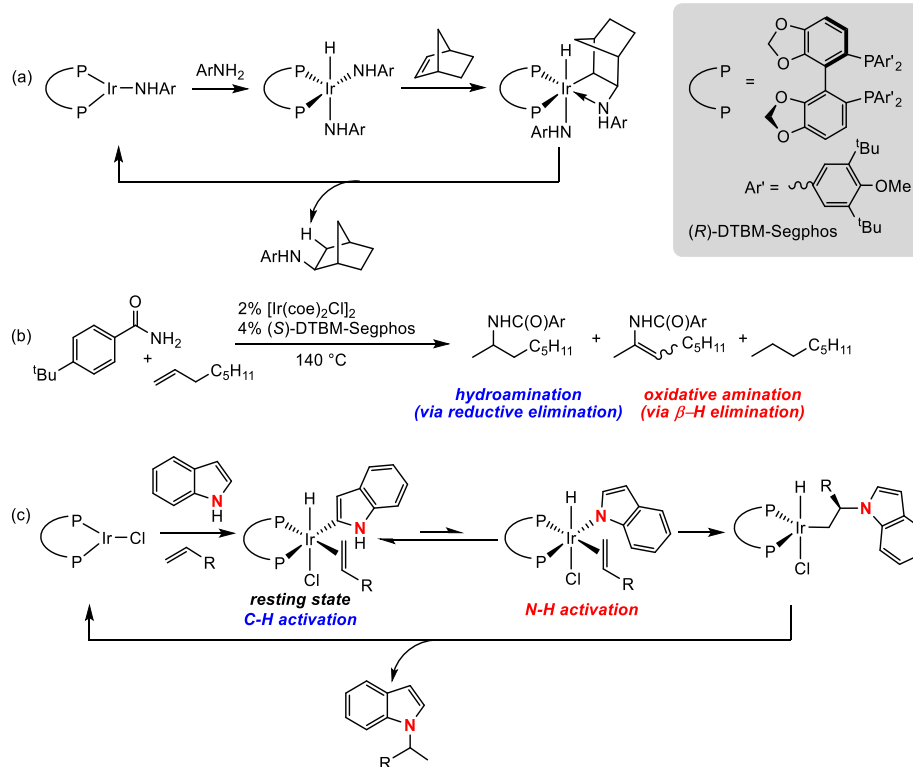
Scheme 3-2. Recent examples of Ir-catalyzed hydroamination catalysis where olefin insertion into an Ir-amido linkage has been invoked.

Hartwig and coworkers have also reported on the Ir-catalyzed hydroamination of olefins with indoles (Scheme 3-2c).[66] Mechanistic studies support a pathway involving migratory insertion into the Ir-*N* bond of an *N*-indolyl complex resulting from N-H activation of indole. However, the catalyst resting state was determined to result from α-C-H activation of the indole. Computational and experimental studies confirmed that olefin insertion into the Ir-*N* bond is faster than the insertion into the Ir-*C* bond, leading to the observed hydroamination products. More recently, Hartwig and co-workers[67] have extended their Ir hydroamination catalysis to asymmetric addition of an amine across internal alkenes to afford chiral amines with high enantioselectivity.

The insertion of unsaturated substrates into metal-amido linkages is not limited to alkenes and alkynes but can also involve other substrates such as CO_2 for the formation of

carbamates, which have potential application in the synthesis of pharmaceuticals, agrochemicals, insecticides, and polymers such as polyurethanes (Figure 3-2).[68] The formation of the $N–CO_2$ bond would facilitate the synthesis of carbamic acid derivatives without the use of phosgene, which is currently employed for this purpose. This reactivity also has potential application in the development of CO_2 capture technology. The mechanism for such CO_2 insertion is postulated to feature nucleophilic attack of the amido nitrogen on the carbon atom of the CO_2 molecule.[69] The stoichiometric insertion of CO_2 into M-*N* linkages of transition metal complexes, including Ir examples, has been reported, but remains relatively rare for platinum group metal amido species.[59c, 70] An early example involving Ru^{II} was reported by Hartwig, Bergman, and Andersen (Scheme 3-3a).[70a] Low temperature NMR data supports a mechanism where attack of CO_2 by the Ru-amido initially forms an N-bound carbamato species, which subsequently rearranges to form the O-bound product. A related Pt^{II} example in which an N-bound carbamato complex rearranges to the O-bound isomer was reported by Roundhill and co-workers (Scheme 3-3b).[71] More recently, Hazari and co-workers[72] reported a (PCP)Ni^{II} pincer example of CO_2 insertion into a Ni-amido bond, and also postulated a rearrangement of the initially formed N-bound carbamato ligand to the O-bound isomer (Scheme 3-3c). Related Ni pincer examples featuring POCOP- and PSiP-supported anilido complexes were subsequently reported.[73]
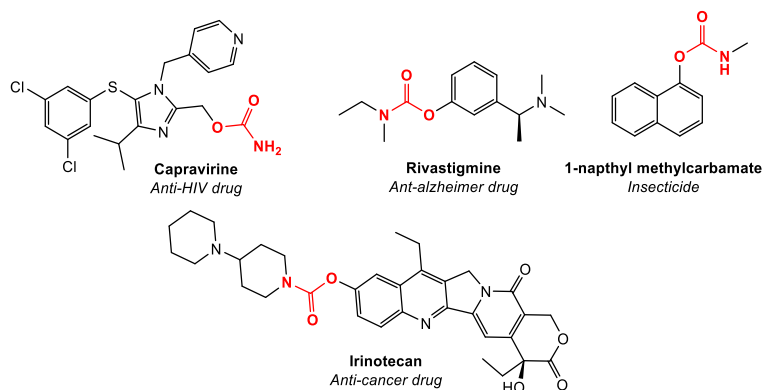
Figure 3-2. Examples of carbamates in active pharmaceuticals and insecticides.
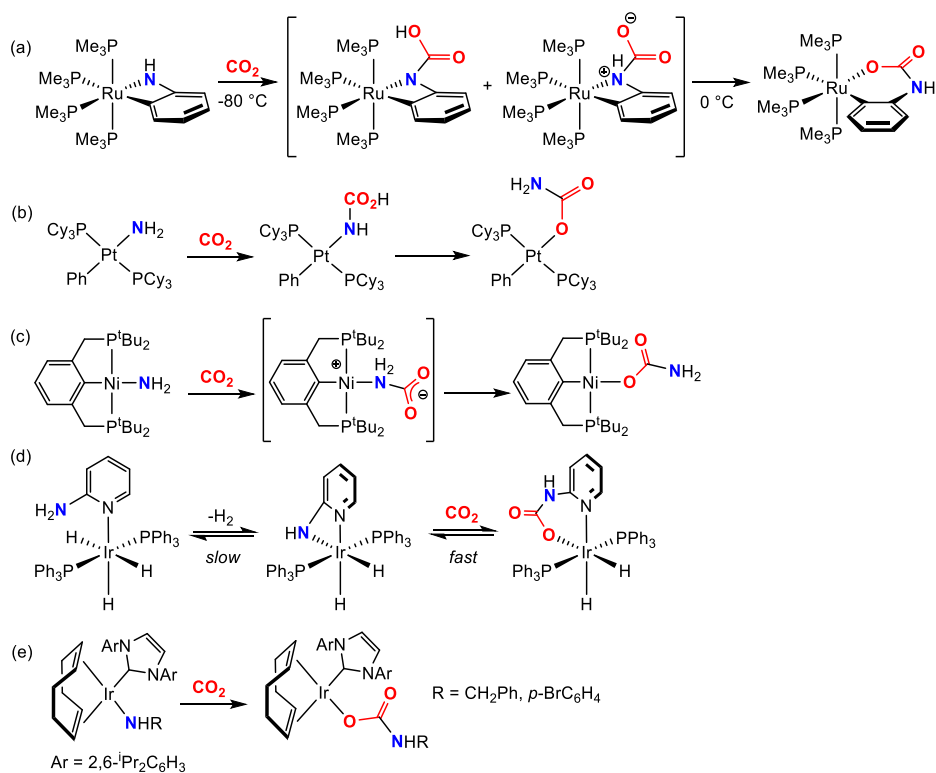
Scheme 3-3. Examples of CO_2 insertion into a late transition metal amido linkage.

A handful of examples involving the reaction of Ir-amido species with CO_2 have been reported. Treatment of an Ir^{III} trihydride complex containing a 2-aminopyridine ligand with CO_2 resulted in the formation of a carbamato complex with the concomitant evolution of H_2 (Scheme 3-3d).[70d] The insertion process is reversible in the presence of H_2. Computational studies support a step-wise mechanism for CO_2 insertion that, as in

previously reported examples,[69] proceeds *via* initial nucleophilic attack of the Ir-anilido on CO_2 to form an N-bound carbamato species that subsequently rearranges to the O-bound carbamato complex. In accordance, the rate of reaction was found to be dependent on the nucleophilicity of the amide, with more nucleophilic amides leading to faster rates. Surprisingly, CO_2 insertion into the Ir-H bond to afford a formate complex was not observed,[70d] even though a related $(PNP)Ir(H)_3$ complex lacking a pendant NH_2 group has been shown to produce a formate complex upon treatment with CO_2.[74] Nolan and co-workers[70f] have also reported an example of an Ir^I-NHC amido complex that undergoes facile CO_2 insertion into the Ir-N bond to afford carbamato species.

3.1.2 Reactivity of Bis(phosphino)silyl Rh and Ir Complexes with Unsaturated Substrates

While some progress has been made toward the development of synthetic protocols that utilize N-H oxidative addition and insertion reactions as elementary steps, this effort is limited due to the scarcity of metal complexes that can mediate these challenging reactions. As discussed in Chapter 2, Ir^I pincer complexes have demonstrated a relative aptitude for N-H bond oxidative addition.[18a, b, 19, 33b, 40] In particular, the Turculet group has demonstrated that Ir^I bis(phosphino)silyl pincer complexes can readily undergoes N-H oxidative addition of ammonia, as well as alkyl and aryl amines.[33b] Reactivity studies revealed that, in comparison to previously reported $(PCP)Ir$[18a, 40] and $(POCOP)Ir$[19] systems, (Cy-PSiP)IrH(NHR) (R = H, alkyl, aryl) proved to be significantly more resistant to N-H bond reductive elimination under thermal conditions.[33b, c]

Computational studies by Leitner and co-workers[75] on the feasibility of catalytic hydroamination of ethylene with ammonia mediated by either (Cy-PSiP)Ir or (^{t}Bu-PCP)Ir highlighted the key role of ligand design in this chemistry. The authors calculated several

mechanistic possibilities by which the hydroamination of ammonia may occur. Once ethylene has inserted into the Ir-amido bond, a σ-bond metathesis step may occur, whereby one proton of a newly coordinated ammonia molecule is transferred to the metal bonded carbon atom, generating a new amido ligand and releasing the product (Scheme 3-4, **A**). Alternatively, C-H reductive elimination of the insertion product followed by coordination and oxidative addition of an incoming ammonia molecule can result in reformation of the amido hydride complex (Scheme 3-4, **B**). Their investigation concluded that the energy barriers for this reaction are generally too high to be feasible with either (Cy-PSiP)Ir or (ᵗBu-PCP)Ir catalysts. However, the energetic spans for cycles starting with (ᵗBu-PCP)IrH(NH$_2$) are close to or higher than 40 kcal mol^{-1}, while the barriers for cycles with (Cy-PSiP)IrH(NH$_2$) are significantly lower in some cases, with the lowest energy span being 33.4 kcal mol^{-1}. (Ph-PSiP)Ir was found to be the most likely to mediate this process catalytically with an energy span of 27.1 kcal mol^{-1} for cycle **B**, as shown in Scheme 3-4.[75] Unfortunately, coordinatively unsaturated (Ph-PSiP)Ir complexes of the type that may engage in N-H activation processes have thus far not been accessible experimentally. While such Ph-PSiP derivatives are not currently available, it is possible that more straightforward modification of the (PSiP)Ir design could skew the barriers for such reactivity sufficiently to favor catalytic turnover.
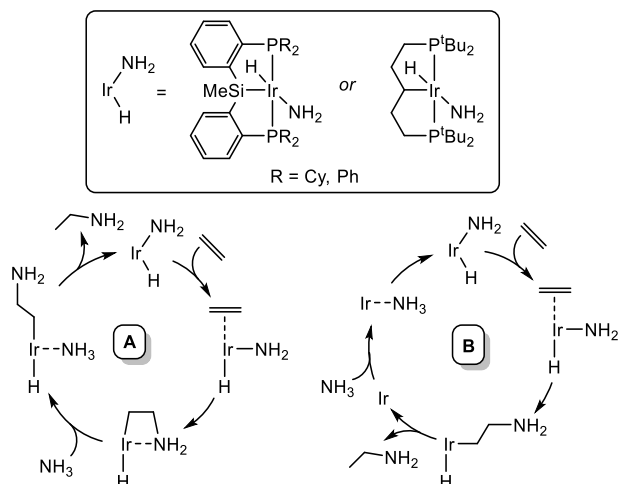
Scheme 3-4. Potentially operative catalytic cycles for Ir-mediated hydroamination of ethylene with ammonia.

Unfortunately, the direct insertion of simple alkenes and alkynes into the Ir-NHR bond of (Cy-PSiP)IrH(NHR) (R = H, alkyl, aryl) complexes proved elusive (Scheme 3-5).[33c] A variety of substrates were studied in this regard, including norbornene, ethylene, and 1-hexene. While no reaction was observed with ethylene, in the case of 1-hexene, isomerization to internal hexenes was observed, consistent with insertion of the alkene into the Ir-*H* rather than the Ir-*N* linkage. The parent amido complex (Cy-PSiP)IrH(NH$_2$) reacted with an excess of norbornene upon heating (2 d, 70 °C) to eliminate ammonia and afford the corresponding norbornene adduct as a mixture of isomers. Similar reactivity was observed with alkynes such as 1-hexyne, which generally formed Ir^I alkyne adducts with reductive elimination of ammonia. Insertion into the Ir-*N* linkage was observed exclusively in the case of xylyl isocyanide, a polar and highly reactive substrate (Scheme 3-5).[33c]
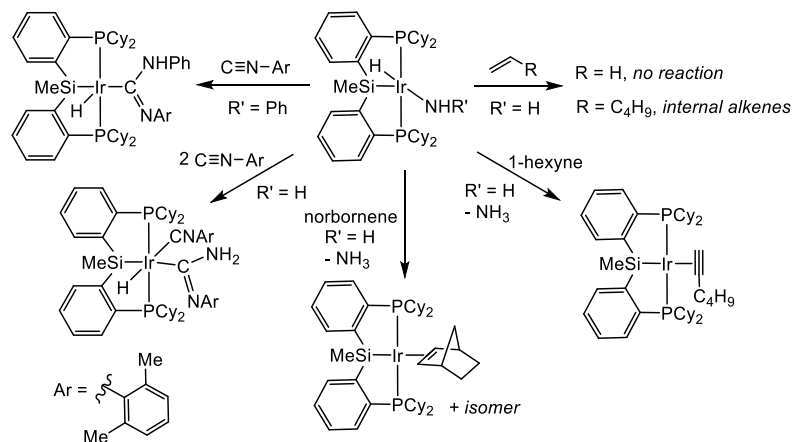
Scheme 3-5. Attempted insertion reactions with (Cy-PSiP)Ir(H)(NHR').

In an effort to access Ir silyl pincer species that might show improved reactivity in this regard, the synthesis of Ir complexes supported by the new 3-methyl indole derived silyl pincer ligand [i]Pr-PSiP[Ind] (Figure 1-1, **L**) has been pursued (*vide infra*). The results presented in Chapter 2 of this document show that complexes of the type ([i]Pr-PSiP[Ind])M(H)(NHR) (M = Rh, Ir; R = alkyl, aryl, H) are indeed accessible, and in the case of Ir are resistant to N-H reductive elimination.[76] Attempts to access such complexes *via* N-H bond oxidative addition resulted in mixtures of products resulting from both N-H and intramolecular C-H activation of the amine substrate. Nonetheless, the ability of such amido complexes to undergo insertion reactions was probed extensively, in an effort to determine whether [i]Pr-PSiP[Ind] ligation is better able to facilitate insertion processes involving pre-formed Rh and Ir amido species.

3.2 Results and Discussion

3.2.1 Reactivity of ([i]Pr-PSiP)MH(NHR) (M = Rh, Ir; R = aryl, alkyl, H) with Unsaturated Substrates

In the course of these studies, the complexes **2-30a**, **2-31a**, **2-33a**, **2-33b** and **2-34** were treated with 1 – 20 equiv. of various unsaturated substrates (Table 3-1) in benzene solution at room temperature, and the reactions were monitored by ^{31}P and ^{1}H NMR

spectroscopy. Reactions treated with a gaseous substrate (*i.e.* CO, CO_2, C_2H_4) involved the addition of *ca.* 1 atm of the gas to a previously degassed solution of the metal complex.

In the case of **2-30a**, treatment with either xylyl isocyanide, norbornene, 1,5-COD, α-methylstyrene, acetophenone, CO, ethylene, or 1-phenyl-1-propyne resulted in reductive elimination of aniline and quantitative conversion (by ^{1}H and ^{31}P NMR) over the course of several minutes to Rh^I adducts of the type (^{i}Pr-PSiP^{Ind})RhL (L = unsaturated substrate; Scheme 3-6).

Table 3-1. Unsaturated substrates tested for insertion reactivity.

Alkenes	Alkynes	Other
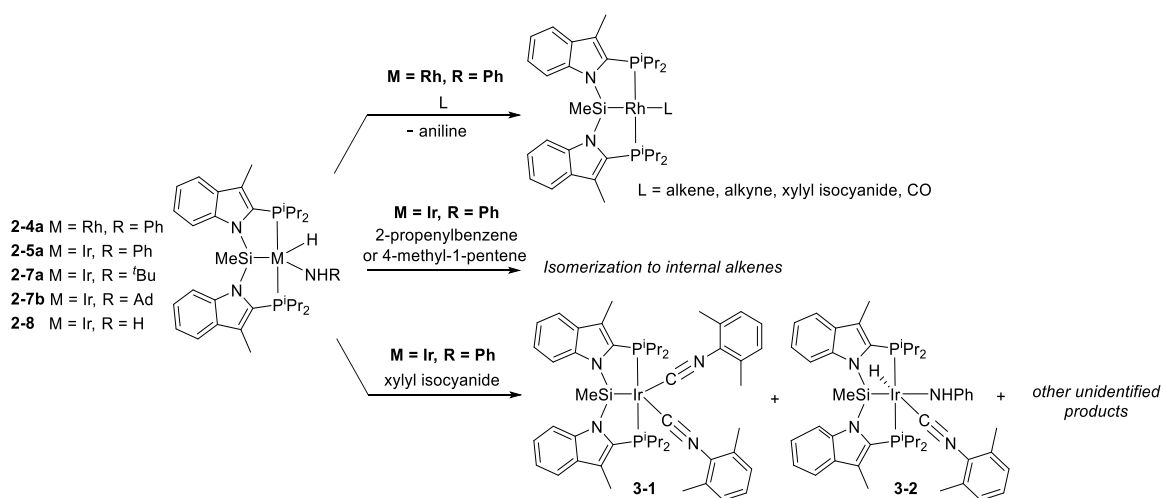
Scheme 3-6. Summary of insertion reactions with (^{i}Pr-PSiP^{Ind})M (M = Rh, Ir) amido complexes.

112

With rare exception, similar treatment of the Ir amido species **2-31a**, **2-33a**, **2-33b** and **2-34** with various unsaturated substrates (Table 3-1) typically resulted in the formation of complex mixtures containing multiple unidentified products (by ^{31}P NMR). Given the propensity of the (^{i}Pr-PSiP^{Ind})Ir system to undergo C-H oxidative addition (as described in Chapter 2 of this document), possible complications may arise due to N-H reductive elimination followed by C-H activation of the substrate, which may then lead to further reactivity. For example, while previously reported[33c] (Cy-PSiP)IrH(NH$_2$) reacted with 20 equiv. of norbornene (nbn) to afford reductive elimination of ammonia and the formation of (Cy-PSiP)Ir(nbn), treatment of **2-34** with either 1 or 20 equiv. of norbornene led to the formation of multiple unidentifiable products. Comparatively, no reaction was observed upon treatment of **2-31a** and **2-33a** with either 1 or 20 equiv. of norbornene, including after heating for 3 days at 65 °C in benzene-d_6.

While heating of (Cy-PSiP)IrH(NHR) (R = H, alkyl, aryl) with diphenylacetylene (1 or 10 equiv.) resulted in partial formation of the Ir^I-alkyne adduct (Cy-PSiP)Ir(DPA) (DPA = diphenylacetylene) resulting from N-H reductive elimination and coordination of the alkyne to Ir,[33c] no reactivity was observed upon treatment of **2-31a**, **2-33a** or **2-34** with DPA (1 or 10 equiv.) after heating for 2 days at 65 °C. Complexes **2-31a** and **2-33a** were similarly unreactive toward 1-phenyl-1-propyne upon heating at 70 °C for 2 days.

As in the case of related (Cy-PSiP)Ir species[33c], treatment of **2-31a** with 2-propenylbenzene and 4-methyl-1-pentene resulted in isomerization to internal alkenes within minutes at room temperature (Scheme 3-6), presumably *via* alkene insertion into the Ir-*H* followed by β-hydride elimination. While insertion of xylyl isocyanide into the Ir-*N* bond of (Cy-PSiP)Ir(H)(NHR) (R = H, Ph) was successful, treatment of **2-31a** with 1 equiv. of xylyl isocyanide resulted in a mixture of products, one of which was identified as (^{i}Pr-

PSiP^{Ind})Ir(C≡NAr)$_2$ (**3-1**, Ar = 2,6-Me$_2$C$_6$H$_3$, Scheme 3-6; < 50 % yield by ^{31}P NMR), the product resulting from reductive elimination of aniline and coordination of 2 equiv. of xylyl isocyanide to the Ir center. Complex **3-1** could also be synthesized by treatment of *in situ* generated (^{i}Pr-PSiP^{Ind})Ir (**2-40**) with 2 equiv. of xylyl isocyanide in cyclohexane solution. The solid-state structure of **3-1** was determined by use of X-ray crystallographic techniques (Figure 3-3, Table 3-2), confirming the formulation of this complex as a five-coordinate adduct of xylyl isocyanide. Furthermore, a minute amount of crystalline material was obtained from a reaction mixture containing **2-31a** and xylyl isocyanide, and X-ray crystallographic analysis of this material revealed a six-coordinate complex formulated as (^{i}Pr-PSiP^{Ind})Ir(H)(NHPh)(CNAr) (**3-2**, Ar = 2,6-Me$_2$C$_6$H$_3$, Figure 3-3; Table 3-2), the xylyl isocyanide adduct of the anilido hydride complex **2-31a**. Complex **3-2** may be an intermediate in the formation of **3-1**. Unfortunately, **3-2** could not be independently synthesized, only as a side product from a mixture also containing **3-1**. Bergman and co-workers[77] have reported on the insertion of isocyanates and carbodiimides into the N-H bond of the Ir-amido ligand in [Ir(Cp*)(PMe$_3$)(Ph)(NH$_2$)]; aryl isocyanides resulted in the reductive elimination of the amine. The insertion of nitriles, carbodiimides, isocyanates, and benzaldehyde into the Ru-*N* bond of (PCP)Ru(CO)(PMe$_3$)(NHPh) to form κ^2-N,N or κ^2-N-O ligands was also previously reported.[78]
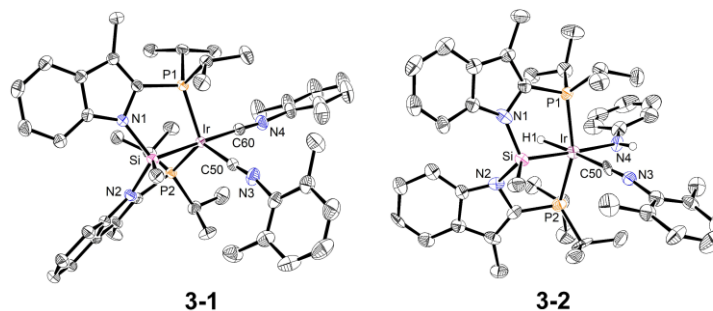
3-1   **3-2**

Figure 3-3. The crystallographically determined structures of **3-1** and **3-2** shown with 50% displacement ellipsoids. Most hydrogen atoms have been omitted for clarity.

Table 3-2. Selected bond distances (Å) and angles (deg.) for **3-1** and **3-2**.

3-1		3-2	
Ir-P(1) 2.3114(4)	P(1)-Ir-P(2) 120.232(15)	Ir-P(1) 2.315(3)	P(1)-Ir-P(2) 157.24(10)
Ir-P(2) 2.3204(4)	P(1)-Ir-C(50) 114.54(6)	Ir-P(2) 2.332(3)	Si-Ir-N(4) 174.4(2)
Ir-Si 2.3546(5)	P(2)-Ir-C(50) 122.30(5)	Ir-Si 2.293(3)	C(50)-Ir-H(1) 163(5)
Ir-C(50) 1.9307(18)	Si-Ir-C(60) 178.83(5)	Ir-N(4) 2.222(9)	Si-Ir-C(50) 99.1(3)
Ir-C(60) 1.972(2)	C(50)-Ir-C(60) 92.40(8)	Ir-C(50) 1.992(11)	Si-Ir-H(1) 65(5)
		Ir-H(1) 1.551(10)	

In an attempt to promote the insertion of unsaturated species into Ir-amido linkages, **2-30a** and **2-31a** were treated with the Lewis acid $B(C_6F_5)_3$. It was anticipated that the Lewis acid may coordinate to the amido N, and that the resulting adduct may undergo insertion reactions more readily. This proposal was inspired by early studies of N-H oxidative addition by Milstein and co-workers,[20] who reported that the Ir-catalyzed hydroamination of norbornene with aniline required the stoichiometric addition of the Lewis acid $ZnCl_2$ to achieve catalytic turnover. Addition of 1 equiv. of $B(C_6F_5)_3$ to either **2-30a** or **2-31a** resulted in the quantitative formation of a new ^iPr-PSiP^{Ind} Ir complex in each case, as indicated by ^{31}P NMR analysis of the reaction mixtures. However, treatment of the *in situ* generated $B(C_6F_5)_3$ adducts with various substrates listed in Table 3-1 did not lead to promising results.

3.2.2 Insertion of CO_2 into Ir-Amido Linkages of (^{i}Pr-PSiP)IrH(NHR) (R = alkyl, aryl) and (Cy-PSiP)IrH(NHR) (R = H, alkyl, aryl)

While insertion reactions involving simple alkene and alkyne substrates proved to be generally challenging, complexes **2-30a**, **2-31a**, **2-33a**, and **2-33b** reacted cleanly with CO_2 (1 atm) in either benzene or THF to afford quantitative conversion to the respective carbamato hydride species (**3-3**, **3-4a**–**c**, Scheme 3-7), respectively. The ^{1}H NMR spectra of **3-3** and **3-4a**–**c** feature M-H resonances, indicating that CO_2 did not insert into the M-H bond. Interestingly, treatment of **2-34** with CO_2 (1 atm) resulted in the formation of multiple unidentified products (by ^{31}P NMR). Furthermore, the parent (Cy-PSiP)IrH(NHR) (R = H, ^{t}Bu, Ph) complexes likewise reacted cleanly with CO_2 (1 atm) in either benzene or THF to afford complexes of the type (Cy-PSiP)IrH[O(CO)NHR] (R = Ph; **3-5a**, R = ^{t}Bu, **3-5b**, R = H, **3-5c**; Scheme 3-7). The solid state structures of **3-5a** and **3-5b** were obtained by use of X-ray crystallographic techniques and confirm their formulation as six-coordinate carbamato hydride specie featuring a κ^2 interaction between the carbonyl and the Ir center (Figure 3-4, Table 3-3).
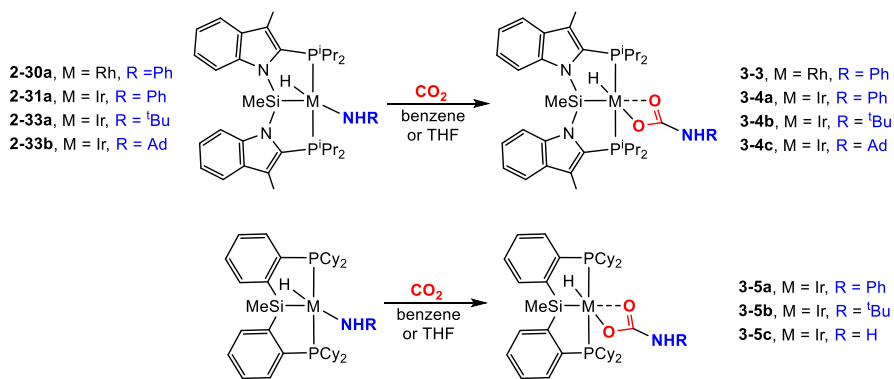
Scheme 3-7. Successful insertion of CO_2 into the Ir-amido linkages with both the (Cy-PSiP)- and (^{i}Pr-PSiP) Ir amido hydride complexes.

3-5a   **3-5b**
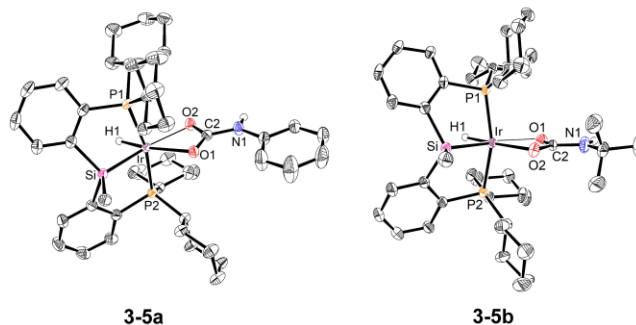
Figure 3-4. Crystallographically determined structures of **3-5a** and **3-5b** thermal ellipsoids shown at the 50% probability level. Most hydrogen atoms have been omitted for clarity.

Table 3-3. Selected bond distances (Å) and angles (deg.) for **3-5a** and **3-5b**.

3-5a		3-5b	
Ir-H 1.53(2)	P(1)-Ir-P(2) 167.483(14)	Ir-H 1.59(4)	P(1)-Ir-P(2) 160.95(3)
Ir-P(1) 2.3053(4)	Si-Ir-H 76.3(8)	Ir-P(1) 2.2879(7)	Si-Ir-H 75.2(15)
Ir-P(2) 2.3055(4)	O(1)-Ir-O(2) 57.92(4)	Ir-P(2) 2.2810(7)	O(1)-Ir-O(2) 58.12(8)
Ir-Si 2.2793(5)	Si-Ir-O(1) 116.75(3)	Ir-Si 2.2692(8)	Si-Ir-O(1) 167.70(6)
Ir-O(1) 2.2599(11)	Si-Ir-O(2) 174.63(3)	Ir-O(1) 2.319(2)	Si-Ir-O(2) 109.60(6)
Ir-O(2) 2.2953(12)	P(1)-Ir-O(1) 94.93(3)	Ir-O(2) 2.229(2)	P(1)-Ir-O(1) 98.65(6)
	P(2)-Ir-O(1) 95.10(3)		P(2)-Ir-O(1) 96.44(6)
	P(1)-Ir-O(2) 96.53(3)		P(1)-Ir-O(2) 95.31(6)
	P(2)-Ir-O(2) 95.13(3)		P(2)-Ir-O(2) 100.67(6)
	P(1)-Ir-H 86.8(8)		P(1)-Ir-H 80.5(15)
	P(2)-Ir-H 85.2(8)		P(2)-Ir-H 80.4(15)

3.2.3 Reactivity of (PSiP)Ir Carbamato Hydride Complexes

While several examples of pincer Ir amido complexes reacting with CO_2 exist, further reactivity beyond this point is limited. As such, the reactivity of (Cy-PSiP)- and (iPr-PSiP[Ind])-ligated Ir carbamate complexes (**3-4a–c** and **3-5a-c**) with various boranes and silanes was investigated. In this regard, **3-4a** and **3-5a** were individually treated with a variety of different boranes (HBPin, PhB(OH)$_2$, PhBPin, 9-BBN, HBCat; 1 and 20 equiv, benzene) and silanes (Ph$_3$SiH, Ph$_2$SiH$_2$, tBuMe$_2$SiH, Me$_2$PhSiH; 1 and 20 equiv, benzene) While PhBPin and PhB(OH)$_2$) were largely unreactive, even upon heating at 100 °C in toluene, complex **3-4a** reacted with 1 equiv. of HBPin at room temperature to afford a

complex mixture of products from which no pure material could be isolated. While **3-4a** was largely unreactive toward silanes, treatment of **3-5a** with silanes typically resulted in the formation of multiple unidentified products. Attempts to use a Lewis acid (*i.e.*, $B(C_6F_5)_3$) to promote reactivity of the carbamato species with boranes and silanes did not lead to improved reactivity.

No reaction was observed upon treatement of either **3-4a** or **3-5a** with Mg^0 or Zn^0, including at elevated temperatures (65 °C, benzene) or in THF for multiple days. Treatment of **3-5a** with either Me_2Zn or MeOTf resulted in a complex mixture of products from which no pure material could be isolated. However, the Rh carbamato complex **3-3** reacted cleanly with MeOTf to afford (^{i}Pr-PSiP^{Ind})Rh(H)(OTf) (**3-6**) quantitatively (by ^{31}P NMR). The organic product could not be identified at this time. This same complex can also be obtained by treatment of **2-28** with AgOTf in benzene solution. Treatment of **3-4a** and **3-5a** with PhMgBr in benzene-d_6 led to quantitative conversion to (Cy-PSiP)IrH(Ph)[33a] and (^{i}Pr-PSiP^{Ind})IrH(Ph) (**2-44**) (by ^{31}P NMR), respectively. The formation of MgO(CO)NHPh in these reactions could not be confirmed.

3.3 Conclusion

In summary, it appears that Ir^{III} amido hydride complexes supported by Cy-PSiP- or ^{i}Pr-PSiP^{Ind}-ligation do not readily undergo Ir-*N* insertion processes with unsaturated substrates such as alkenes and alkynes. In some cases, desired insertion reactivity is hampered by amine N-H reductive elimination and either coordination of the substrate to the Ir^I center or potential C-H activation of such substrates by (^{i}Pr-PSiP^{Ind})Ir^I to form complex mixtures of products. Evidence for the insertion of terminal alkenes into the Ir-*H* bond has been observed for both ligand systems, with subsequent alkene isomerization *via* facile β-hydride elimination rather than C-N bond reductive elimination. More activated

substrates that feature polar C=X bonds, such as xylyl isocyanide and CO_2, have shown some promising reactivity regarding Ir-N insertion. While xylyl isocyanide is able to insert into the Ir-amido linkage in (Cy-PSiP)IrH(NHR) (R = H, Ph), the analogous reaction of **2-31a** with xylyl isocyanide resulted in a mixture of products including an Ir[I] xylylisocyande adduct resulting from N-H reductive elimination and an Ir[III] adduct in which the isocyanide simply coordinates to the metal center without undergoing insertion. Several Cy-PSiP- and [i]Pr-PSiP[Ind]-supported carbamato hydride complexes were readily synthesized by insertion of CO_2 into the M-amido linkage. However, attempts for further functionalization of such complexes have been unsuccessful thus far. Computational studies by Leitner and-coworkers[75] suggest that PSiP-ligand design can play a key role in the development of Ir pincer complexes that can undergo both N-H oxidative addition and subsequent insertion into the Ir-N bond. While such complexes have proven out of reach experimentally thus far, the study of PSiP derivatives with alternative substitution at the phosphino donors may provide access to complexes that can mediate such reactivity more readily.

3.4 Experimental Section

3.4.1 General Considerations

All experiments were conducted under nitrogen in a glovebox or using standard Schlenk techniques. Dry, oxygen-free solvents were used unless otherwise indicated. All non-deuterated solvents were deoxygenated by sparging with nitrogen. Benzene, toluene and pentane were subsequently passed through a double column purification system (one activated alumina column and one column packed with activated Q-5). Tetrahydrofuran and diethyl ether were purified by distillation from Na/benzophenone. All purified solvents were stored over 4 Å molecular sieves. Benzene-d_6 and cyclohexane-d_{12} were degassed via three freeze-pump-thaw cycles and stored over 4 Å molecular sieves. All other reagents

were purchased from commercial suppliers and used as received. The tertiary silane (^{i}Pr-PSiP^{Ind})H was prepared according to a previously published procedure.[36] Unless otherwise stated, ^{1}H, ^{13}C, ^{31}P, and ^{29}Si NMR characterization data were collected at 300K with chemical shifts reported in parts per million downfield of SiMe$_4$ (for ^{1}H, ^{13}C, and ^{29}Si), or 85% H$_3$PO$_4$ in D$_2$O (for ^{31}P). Chemical shift ranges are cited to indicate overlapping resonances. ^{1}H and ^{13}C NMR chemical shift assignments are based on data obtained from ^{13}C-DEPTQ, ^{1}H-^{1}H COSY, ^{1}H-^{13}C HSQC, and ^{1}H-^{13}C HMBC NMR experiments. ^{29}Si NMR assignments are based on ^{1}H-^{29}Si HMQC and ^{1}H-^{29}Si HMBC experiments (including for J_{SiH} determination). In some cases, fewer than expected unique ^{13}C NMR resonances were observed, despite prolonged acquisition times. The following abbreviations were utilized to assign NMR data: s = singlet; d = doublet; t = triplet; q = quartet; m = multiplet; br = broad. Please note that a ^{13}C NMR shift at ca. 110 ppm is due to an instrument artefact. X-Ray crystallographic data was collected and refined on a fee-for-service basis by Drs. Michael J. Ferguson and Yuqiao Zhou of the University of Alberta X-ray Crystallography Laboratory, Edmonton, AB.

3.4.2 Synthetic Details and Characterization Data

(^{i}Pr-PSiP^{Ind})Ir[CN(2,6-Me$_2$C$_6$H$_3$)]$_2$ (3-1). A solution of 2-29 (0.015 g, 0.02 mmol) in *ca.* 0.5 mL cyclohexane-d_{12} was treated with Me$_3$SiCH$_2$Li (0.019 g, 0.02 mmol). An immediate color change from yellow to orange to red was observed and ^{31}P{^{1}H} NMR spectroscopy indicated the complete consumption of 2-29 and formation of 2-40. A solution of 2,6-xylyl isocyanide (0.005 g, 0.04 mmol) in *ca.* 0.5 mL of cyclohexane-d_{12} was then added dropwise to the reaction mixture. Within 30 min of addition, ^{31}P{^{1}H} NMR spectroscopy indicated the complete consumption of 2-40 and formation of 3-1, which was characterized *in situ*. ^{1}H NMR (300 MHz, benzene-d_6): δ 7.66–7.93 (overlapping

resonances, 2 H, H$_{arom}$), 7.39–7.36 (overlapping resonances, 2 H, H$_{arom}$), 6.99–6.92 (overlapping resonances, 4 H, H$_{arom}$), 6.92–6.80 (overlapping resonances, 6 H, H$_{arom}$), 2.77–2.67 (overlapping resonances, 4 H, PC*H*Me$_2$), 2.46 (s, 6 H, Indole-*Me*), 2.40 (s, 6 H, 2,6-*Me$_2$*C$_6$H$_3$), 2.20 (s, 6 H, 2,6-*Me$_2$*C$_6$H$_3$), 1.33–0.85 (overlapping resonances, 24 H, PCH*Me$_2$*), 1.43 (s, 3 H, Si*Me*). ^{31}P{^{1}H} NMR (121.5 MHz, benzene-*d$_6$*): δ 30.0. ^{29}Si NMR (99.4 MHz, benzene-*d$_6$*): δ 38.2.

(**^{i}Pr-PSiP^{Ind})Ir(H)(NHPh)[CN(2,6-Me$_2$C$_6$H$_3$)] (3-2).** A solution of 2,6-xylyl isocyanide (0.007 g, 0.052 mmol) in ca. 3.5 mL of benzene was added dropwise to a solution of **2-31a** (0.043 g, 0.052 mmol) in ca. 3.5 mL of benzene at room temperature. An instant color change from dark orange to yellow-orange was observed. Analysis by ^{1}H and ^{31}P{^{1}H} NMR spectroscopy suggest formation of **3-2**. ^{1}H NMR (300 MHz, benzene-*d$_6$*): δ 7.99–7.96 (overlapping resonances, 2 H, H$_{arom}$), 7.64–7.61 (overlapping resonances, 2 H, H$_{arom}$), 7.29–7.21 (overlapping resonances, 6 H, H$_{arom}$), 6.77–6.66 (overlapping resonances, 5 H, H$_{arom}$), 6.48 (apparent t, 1 H, *J* = 7 Hz, H$_{arom}$), 3.17–3.08 (overlapping resonances, 2 H, PC*H*Me$_2$), 2.77–2.67 (overlapping resonances, 2 H, PC*H*Me$_2$), 2.31 (s, 12 H, Indole-*Me*, 2,6-*Me$_2$*C$_6$H$_3$), 1.32–0.81 (overlapping resonances, 24 H, PCH*Me$_2$*), 0.71 (s, 3 H, Si*Me*), -9.62 (t, 1 H, ^{2}*J$_{HP}$* = 19 Hz, Ir*H*). ^{31}P{^{1}H} NMR (121.5 MHz, benzene-*d$_6$*): δ 23.8. ^{29}Si NMR (99.4 MHz, benzene-*d$_6$*): δ 22.9.

(**^{i}Pr-PSiP^{Ind})RhH[O(CO)NHPh] (3-3).** A solution of **2-30a** (0.072 g, 0.098 mmol) in ca. 10 mL benzene was transferred to a 100 mL thick-walled flask adapted with a Teflon stopcock. The solution was degassed *via* three freeze-pump-thaw cycles. CO$_2$ (1 atm) was then introduced and an instant color change from dark orange to light yellow was observed. Quantitative conversion to **3-3** was observed by ^{31}P{^{1}H} NMR spectroscopy. The reaction mixture was then evaporated to dryness and the remaining material was triturated with

121

pentane (3 × 2 mL). The remiaing solid was dried under vacuum to afford **3-3** (0.074 g, 97 % yield) as a beige powder. ^{1}H NMR (300 MHz, benzene-d_6): δ 7.92–7.89 (overlapping resonances, 2 H, H_{arom}), 7.62–7.59 (overlapping resonances, 2 H, H_{arom}), 7.53 (apparent d, 2 H, J = 8 Hz, H_{arom}), 7.21–7.11 (overlapping resonances, 6 H, H_{arom}), 6.80 (apparent t, 1 H, J = 7 Hz, H_{arom}), 6.57 (br s, 1 H, N*H*), 2.65–2.45 (overlapping resonances, 4 H, PC*H*Me$_2$), 2.26 (s, 6 H, Indole-*Me*), 1.56–1.48 (overlapping resonances, 6 H, PCH*Me$_2$*), 1.33–1.26 (overlapping resonances, 6 H, PCH*Me$_2$*), 1.15–1.07 (overlapping resonances, 6 H, PCH*Me$_2$*), 1.04–0.96 (overlapping resonances, 6 H, PCH*Me$_2$*), 0.95 (s, 3 H, Si*Me*), -19.7 (dt, 1 H, $^1J_{RhH}$ = 24 Hz, $^2J_{HP}$ = 16 Hz, Rh*H*). ^{13}C{^{1}H} NMR (75.5 MHz, benzene-d_6): δ 159.7 (*C*O), 139.4 (C_{arom}), 139.1 (C_{arom}), 134.0 (C_{arom}), 133.6 (C_{arom}), 133.2 (C_{arom}), 127.2 (*C*H$_{arom}$), 121.0 (*C*H$_{arom}$), 119.4 (*C*H$_{arom}$), 118.8 (*C*H$_{arom}$), 118.3 (C_{arom}), 117.6 (*C*H$_{arom}$), 115.2 (*C*H$_{arom}$), 114.9 (*C*H$_{arom}$), 27.5 (apparent t, $^2J_{CP}$ = 12 Hz, P*C*HMe$_2$), 26.2 (apparent t, $^2J_{CP}$ = 15 Hz, P*C*HMe$_2$), 18.7 (PCH*Me$_2$*), 18.5 (PCH*Me$_2$*), 17.7 (PCH*Me$_2$*), 16.9 (PCH*Me$_2$*), 9.1 (Indole-*Me*), 3.56 (Si*Me*). ^{31}P{^{1}H} NMR (121.5 MHz, benzene-d_6): δ 46.3 (d, $^1J_{RhP}$ = 110 Hz). ^{29}Si NMR (100 MHz, benzene-d_6): δ 47.9.

(^{i}Pr-PSiP^{Ind})IrH[O(CO)NHPh] (3-4a). A solution of **2-31a** (0.056 g, 0.068 mmol) in ca. 10 mL of benzene was transferred to a 100 mL thick-walled flask adapted with a Teflon stopcock. The solution was degassed *via* three freeze-pump-thaw cycles. CO_2 (1 atm) was then introduced into the reaction flask and an instant color change from dark orange to light yellow was observed. Quantitative conversion to **3-4a** was observed by ^{31}P{^{1}H} NMR spectroscopy. The reaction mixture was then evaporated to dryness and the remaining material was triturated with pentane (3 × 2 mL). The remaining solid was dried under vacuum to afford **3-4a** (0.057 g, 97 % yield) as a beige powder. ^{1}H NMR (300 MHz, benzene-d_6): δ 8.03–7.99 (overlapping resonances, 2 H, H_{arom}), 7.64–7.61 (overlapping

resonances, 2 H, H$_{arom}$), 7.46 (apparent d, 2 H, J = 8 Hz, H$_{arom}$), 7.24–7.2 (overlapping

resonances, 4 H, H$_{arom}$), 7.10 (apparent t, 2 H, J = 8 Hz, H$_{arom}$), 6.79 (apparent t, 1 H, J = 8

Hz, H$_{arom}$), 6.40 (br s, 1 H, NH), 2.92–2.63 (overlapping resonances, 4 H, PCHMe$_2$), 2.29

(s, 6 H, Indole-Me), 1.52–1.43 (overlapping resonances, 6 H, PCHMe_2), 1.31–1.23

(overlapping resonances, 6 H, PCHMe_2), 1.15–1.07 (overlapping resonances, 6 H,

PCHMe_2), 1.02–0.95 (overlapping resonances, 6 H, PCHMe_2), 0.90 (s, 3 H, SiMe), - 25.6

(br t, 1 H, $^2J_{HP}$ = 16 Hz, IrH). ^{13}C{^{1}H} NMR (125.8 MHz, benzene-d_6): δ 163.3 (CO), 140.6

(C_{arom}), 140.0 (C_{arom}), 136.4 (C_{arom}), 136.1 (C_{arom}), 129.2 (CH_{arom}), 122.8 (CH_{arom}), 121.9

(CH_{arom}), 120.5 (CH_{arom}), 119.7 (CH_{arom}), 119.4 (C_{arom}), 117.4 (CH_{arom}), 116.9 (CH_{arom}),

30.1 (PCHMe$_2$), 28.3 (PCHMe$_2$), 20.4 (PCHMe_2), 20.2 (PCHMe_2), 19.6 (PCHMe_2), 18.7

(PCHMe_2), 11.1 (Indole-Me), 3.30 (SiMe). ^{31}P{^{1}H} NMR (121.5 MHz, benzene-d_6): δ 38.2.

^{29}Si NMR (100 MHz, benzene-d_6): δ 7.59.

(^{i}Pr-PSiP^{Ind})IrH[O(CO)NH^{t}Bu] (3-4b). A solution of **2-33a** (0.056 g, 0.07 mmol)

in ca. 15 mL benzene was transferred to a thick-walled flask adapted with a Telfon

stopcock. The solution was degassed *via* three freeze-pump-thaw cycles. CO$_2$ (1 atm) was

then introduced to the flask. Quantitative conversion to **3-4b** was observed by ^{31}P{^{1}H}

NMR spectroscopy within 30 min of CO$_2$ addition. The reaction mixture was evaporated

to dryness to afford **3-4b** (0.056 g, 95% yield) as an orange powder. ^{1}H NMR (300 MHz,

benzene-d_6): δ 8.06–8.03 (overlapping resonances, 2 H, H$_{arom}$), 7.66–7.62 (overlapping

resonances, 2 H, H$_{arom}$), 7.24–7.21 (overlapping resonances, 4 H, H$_{arom}$), 4.15 (s, 1 H, NH),

2.91 (m 2 H, PCHMe$_2$), 2.72 (m 2 H, PCHMe$_2$), 2.34 (s, 6 H, Indole-Me), 1.55–1.34

(overlapping resonances, 8 H, PCHMe_2), 1.24 (s, 9 H, NHCMe_3), 1.22–1.14 (overlapping

resonances, 8 H, PCHMe_2), 1.03–0.95 (overlapping resonances, 8 H, PCHMe_2), 0.89 (s, 3

H, SiMe), -25.2 (br s, 1 H, IrH). ^{13}C{^{1}H} NMR (125.8 MHz, benzene-d_6): δ 166.4 (CO$_2$),

140.6 (C_{arom}), 137.1 (C_{arom}), 136.2 (C_{arom}), 122.7 (CH_{arom}), 120.3 (CH_{arom}), 119.7 (CH_{arom}), 118.9 (C_{arom}), 116.9 (CH_{arom}), 49.03 (NHCMe_3), 34.4 (PCHMe$_2$), 29.9 (PCHMe$_2$), 22.7 (PCHMe$_2$), 20.5 (PCHMe$_2$), 19.7 (PCHMe$_2$), 19.1 (PCHMe$_2$), 14.26 (NHCMe_3), 11.13 (Indole-Me), 3.28 (SiMe). ^{31}P{^{1}H} NMR (121.5 MHz, benzene-d_6): δ 37.6. ^{29}Si NMR (99.4 MHz, benzene-d_6): δ 9.30.

(^{i}Pr-PSiP^{Ind})IrH[O(CO)NHAd] (3-4c). A solution of 2-33b (0.055 g, 0.06 mmol) in ca. 10 mL benzene was transferred to a thick-walled flask adapted with a Teflon stopcock. The solution was degassed *via* three freeze-pump-thaw cycles and CO_2 (1 atm) was introduced to the flask. An immediate color change from orange to light-pink-orange was observed. Quantitative conversion to 3-4c was observed by ^{31}P{^{1}H} NMR spectroscopy within 30 min of CO_2 addition. The reaction mixture was evaporated to dryness and the remaining material was triturated with pentane (2 × 3 mL). The remaining solid was dried under vacuum to afford 3-4c (0.053 g, 96 % yield) as a pink-orange solid. ^{1}H NMR (300 MHz, benzene-d_6): δ 8.05–8.01 (overlapping resonances, 2 H, H$_{arom}$), 7.65–7.61 (overlapping resonances, 2 H, H$_{arom}$), 7.23–7.19 (overlapping resonances, 4 H, H$_{arom}$), 4.12 (s, 1 H, NH), 2.94 (m 2 H, PCHMe$_2$), 2.74 (m 2 H, PCHMe$_2$), 2.34 (s, 6 H, Indole-Me), 1.95 (s, 10 H, NHC$_{10}H_{15}$), 1.54–0.95 (overlapping resonances, 24 H, PCHMe_2), 1.54–0.95 (overlapping resonances, 5 H, NHC$_{10}H_{15}$), 0.89 (s, 3 H, SiMe), -25.3 (br t, 1 H, IrH). ^{13}C{^{1}H} NMR (125.8 MHz, benzene-d_6): δ 166.1 (CO_2), 140.6 (C_{arom}), 137.0 (C_{arom}), 136.2 (C_{arom}), 122.7 (CH_{arom}), 120.3 (CH_{arom}), 119.6 (CH_{arom}), 118.9 (C_{arom}), 116.9 (CH_{arom}), 43.0 (NHC$_{10}H_{15}$), 30.1 (PCHMe$_2$), 28.3 (PCHMe$_2$), 20.4 (CH$_{alkyl}$), 20.1 (CH$_{alkyl}$), 19.7 (CH$_{alkyl}$), 19.2 (CH$_{alkyl}$), 11.1 (Indole-Me), 3.31 (SiMe). ^{31}P{^{1}H} NMR (121.5 MHz, benzene-d_6): δ 37.7. ^{29}Si NMR (99.4 MHz, benzene-d_6): δ 9.32.

(Cy-PSiP)IrH[O(CO)NHPh] (3-5a). A solution of (Cy-PSiP)IrH(NHPh) (0.053 g, 0.06 mmol) in benzene-d_6 was transferred to a 100 mL thick-walled flask adapted with a Teflon stopcock. The solution was degassed *via* three freeze-pump-thaw cycles and CO_2 (1 atm) was introduced to the flask. An immediate color change from orange to yellow was observed, and the reaction was allowed to proceed for another hour. The reaction mixture was evaporated to dryness and the remaining material was triturated with pentane (2 × 3 mL) and then washed with pentane (4 × 3 mL). The remaining solid was dried under vacuum to afford **3-5a** as a beige solid (0.045 g, 82 % yield). $^{31}P\{^1H\}$ NMR (121.5 MHz, benzene-d_6): δ 52.7.

Crystallographic Solution and Refinement Details. Crystallographic data were obtained at 173(2) K on a Bruker D8/APEX II CCD diffractometer using CuKα (λ = 1.54178 Å, microfocus source) radiation employing samples that were mounted in inert oil and transferred to a cold gas stream on the diffractometer. Programs for diffractometer operation, data collection, and data reduction (including SAINT) were supplied by Bruker. Data reduction, correction for Lorentz−polarization, and absorption correction were each performed. Structure solution was achieved by either intrinsic phasing methods or Patterson search/structure expansion. All structures were refined by use of full-matrix least-squares procedures (on F^2) with R_1 based on $F_o^2 \geq 2\sigma(F_o^2)$ and wR_2 based on $F_o^2 \geq -3\sigma(F_o^2)$.

Unless otherwise indicated, all nonhydrogen atoms were refined with anisotropic displacement parameters. For **3-1**, 2.5 equiv. of cyclohexane solvent were located in the asymmetric until and were refined in a satisfactory manner with anisotropic displacement parameters. For **3-2**, an equiv. of disordered benzene solvent was located in the asymmetric unit. The carbon atoms of the disordered benzene molecule were split into two sets of six atoms, with occupancy factors of 60% (C1SA-C6SA) and 40% (C1SB-C6SB), and were

125

refined isotropically as idealized hexagons with C–C bond lengths of 1.390 Å and C–C–C bond angles of 120.0º. In the case of **3-5a**, two equiv. of benzene solvent were found in the asymmetric unit and were refined in a satisfactory manner with anisotropic displacement parameters. The Ir-*H* (H1) and N-*H* (H4N for **3-2,** H1N for **3-5a** and **3-5b**) atoms were located in the difference map and refined isotropically in each case. For **3-2**, the Ir–H1 (1.55(1) Å) and N4–H4N (0.88(1) Å) distances were constrained during refinement. Otherwise, all hydrogen atoms were added at calculated positions and refined by use of a riding model employing isotropic displacement parameters based on the isotropic displacement parameter of the attached atom.

Chapter 4: Unusual Selectivity in Alkyne Hydrogenation Catalyzed by Bis(Phosphino)silyl Iron Species

In this chapter, all synthetic work was conducted by Helia Hollenhorst. DFT calculations were conducted by Dr. Erin Johnson at Dalhousie University with collaboration. X-Ray crystallographic data was collected and refined by Dr. Michael J. Ferguson of the University of Alberta X-ray Crystallography Laboratory, Edmonton, AB. Elemental Analysis was conducted by Galbraith Laboratories, Inc. and ANALEST at the University of Toronto.

4.1 Introduction

4.1.1 Iron Pincer Complexes in the Hydrogenation of Alkynes

Catalytic hydrogenation is a fundamental reaction with applications in the synthesis of fine chemicals and pharmaceuticals.[79] Hydrogenation protocols involving the use of platinum group metal catalysts have been pursued extensively, due in part to the highly active and selective nature of such catalysts.[9] However, the low abundance, high cost,[4-5] and environmental impact associated with the extraction of platinum group metals has driven recent interest toward the development of alternative, base metal catalysts.[80] Although interest abounds, examples of homogenous, selective hydrogenation catalysts that feature abundant base metals such as iron are scarce.[81] In many ways iron is an ideal candidate for the development of new, sustainable catalysts, as it is readily accessed due to its high abundance in the Earth's crust.[7] Yet numerous challenges are associated with the synthesis of well-defined iron pre-catalysts for synthetic applications, in large part due to the prevalence of often unpredictable one electron chemistry.[6, 8]

In the context of alkene hydrogenation, Fe pincer complexes have emerged as leading candidates for catalyst development. Particularly noteworthy are

127

bis(imino)pyridine (PDI) Fe pincer complexes (Figure 1-1, **H**)[21d, 23] and related CNC *N*-heterocyclic carbene derivatives (Figure 1-1, **I**)[24-25, 82] that Chirik and co-workers have utilized to develop highly active alkene hydrogenation catalysts. The redox-active nature of PDI ligands, which can accept up to three electrons in the π-system according to DFT calculations, plays an integral role in the observed reactivity, whereby iron is able to mediate reactions without the need for higher oxidation states.[21c, 23g] Such ligands have been touted as enabling noble-metal-like reactivity in base metals such as iron, which highlights the importance of ligand design in effective Fe catalysis.[83]

The development of homogeneous iron catalysts for the reduction of alkynes is particularly challenging, due to issues of chemo- and stereo-selectivity. Possible outcomes include semihydrogenation to afford either *E*- or *Z*-alkenes, as well as complete reduction to the corresponding alkane (Scheme 4-1). As such alkyne hydrogenation often results in mixtures of products.
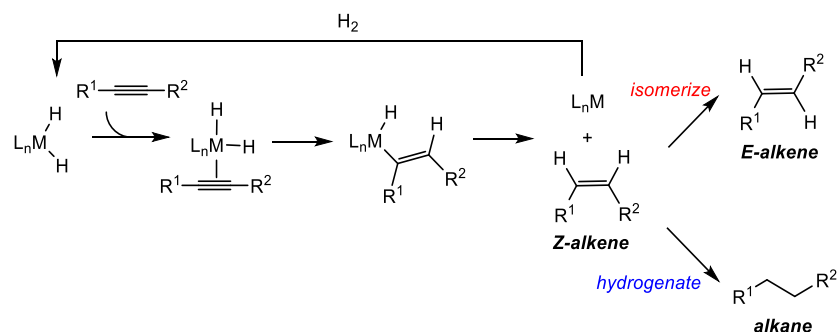
Figure 4-1. Possible pathways in alkyne hydrogenation chemistry.

In the context of Fe-catalysis, in 2004 Chirik and co-workers[23a] reported that (^{iPr}PDI)Fe(N$_2$)$_2$ (Figure 4-2), which is active in alkene-hydrogenation, can also fully hydrogenate diphenylacetylene and 2-butyne to bibenzyl and butane, respectively. ^{1}H NMR data of the reaction *in situ* revealed initial formation of the *Z*-alkene, which is subsequently hydrogenated to the alkane product. Terminal alkynes such as trimethylsilylacetylene could

not be hydrogenated, resulting in a mixture of products. Concurrently in 2004, Peters and co-workers[84] reported on tris(phosphino)borate-supported iron alkyl pre-catalysts ($^{Ph}BP^{iPr3}$)FeR (R = Me, Bn; Figure 4-2) in the hydrogenation of alkenes. 2-Pentyne was also fully hydrogenated to pentane, whereby monitoring of the reaction *in situ* by ^{1}H NMR spectroscopy indicated formation of *cis*-2-pentene as an intermediate. However, in the case of phenylacetylene only small amounts of styrene and ethylbenzene were observed. Complications arising from reductive dimerization, trimerization, cyclotrimerization, and polymerization were evident for both phenylacetylene and acetylene,[84] indicating some possible competing reactions in this type of chemistry.

Ar = 2,6-^{i}Pr$_2$C$_6$H$_3$

Chirik, 2004
2 examples

Peters, 2004
1 example

R = Me, Bn
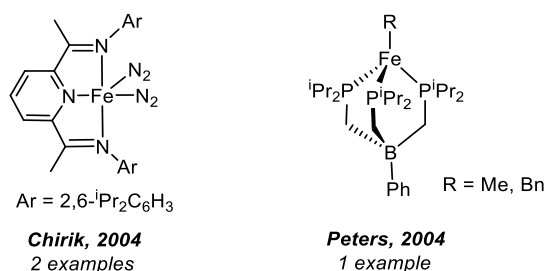
Figure 4-2. Homogenous iron complexes applied in the complete hydrogenation of alkynes to afford alkanes.

In 2013, Milstein and co-workers[85] reported on the semi-hydrogenation of internal alkynes to *E*-alkenes using an acridine-based (PNP)Fe^{II} imino borohydride pincer pre-catalyst (Figure 4-3). Alkynes featuring bulky or electron withdrawing substituents displayed decreased reactivity as a result of weaker coordination of the alkyne to the Fe center. Reactivity with *Z*-stilbene indicated isomerization to the *E*-stilbene isomer, which suggests that the diphenylacetylene derivatives are initially hydrogenated to *Z*-alkenes and then isomerized to the *E*-alkene product.[85] The reactivity observed is likely facilitated by metal-ligand cooperativity, involving dearomatization/aromatization of the central ring in the acridine ligand.[29f]

Milstein, 2013   **Kirchner, 2019**
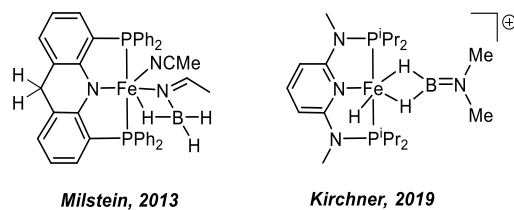
Figure 4-3. Homogenous iron complexes active in the semi-hydrogenation of alkynes.

More recently, Kirchner and co-workers[86] reported on the semi-hydrogenation of internal alkynes and complete hydrogenation of terminal alkynes involving a cationic Fe^{II} bis(σ-B-H) amino borane complex (Figure 4-3). Diphenyl and dialkyl alkynes were selectively semihydrogenated to afford the corresponding *Z*-alkenes. Further hydrogenation to the respective alkanes was not observed in any cases despite increased catalyst loading or higher pressures. However, terminal alkynes could be fully hydrogenated to the corresponding alkane. The selectivity observed was investigated mechanistically for 1-phenylpropyne and phenylacetylene. While the mechanistic steps were the same for the reduction of both 1-phenylpropyne and phenylacetylene, an important difference between the two pathways is the relative value of the highest barrier of H_2 addition. While the highest barrier for 1-phenylpropyne was the second addition of H_2 to hydrogenate the alkene to the alkane, the opposite was observed with phenylacetylene where the first barrier for hydrogenation of the alkyne was higher (15 kcal mol^{-1}) than the second hydrogenation of the alkene (12 kcal mol^{-1}). The selectivity was attributed to the stability of the η^2-alkene complexes formed prior to the second addition of H_2. Calculations indicate that the η^2-alkene complex of the terminal alkene (styrene) is more stable than for the internal alkene (1-phenylpropene). Therefore, the second hydrogenation step for the formation of the alkane is more favourable with the terminal alkene, rather than dissociation as in the case of the internal alkene.[86]

4.1.2 Development of Bis(phosphino)silyl Iron Pincer Complexes

The Turculet group is interested in studying the effects of ligand design on metal reactivity, particularly with bis(phosphino)silyl (PSiP) pincer ligation, which have been applied to Group 8, 9 and 10 transition metals.[31-33, 34-36, 46, 73b, 87] In the context of $3d$-metals such as iron, a key feature of the PSiP ligand design is the ability of silicon to participate in reactivity *via* the formation of η^2-(Si-H) complexes, which may lead to enhanced reactivity.[36, 87b, c, 87e] The formation of such silane complexes is particularly favorable for first row $3d$-metals, whose contracted d-orbitals do not effectively engage in backdonation with the Si-H bond, leading to the stabilization of η^2-(Si-H) species.[88] Multiple examples of η^2-Si-H coordination involving PSiP ligation have been reported with group 10 metals.[34-36, 87c] Iwasawa and co-workers[34] reported on η^2-(Si-H) interactions involving Ph-PSiP ligated Pd and Ni species (Figure 4-4); the analogous Pt complex is a terminal hydride. Similar structures involving η^2-(Si-H) interactions with Ni have also been observed by Hazari and coworkers,[35, 87c] and Turculet and co-workers (Figure 4-4).[36]

2011 Iwasawa (R = Ph)
2014 Hazari (R = Ph, Me)

2016 Hazari (L = N₂, CO)

2017 Turculet
(L = N₂, DMAP, PMe₃)
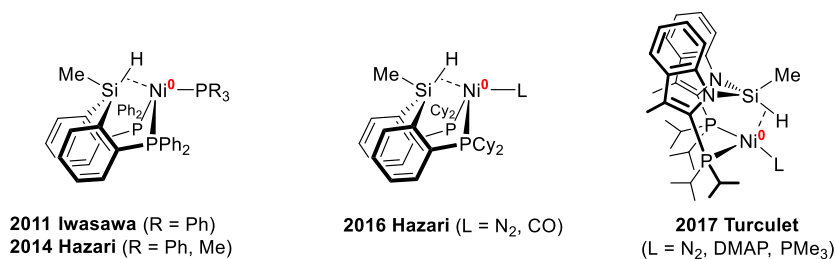
Figure 4-4. Examples of η^2-(Si-H) coordination involving PSiP-ligated Ni species.

The formation of η^2-(Si-H) complexes with PSiP-ligated base metals has also been observed with iron. In 2018, Turculet and co-workers[37] reported that treatment of (Cy-PSiP)FeCl(PMe₃) (**4-1·PMe₃**) with NaEt₃BH under an N₂ atmosphere resulted in the initial formation of diamagnetic (Cy-PSiP)FeH(PMe₃) (**4-2**) and gradual formation of (Cy-PSiP)FeH(PMe₃)(N₂) (**4-3**, Scheme 4-1). Complex **4-2** features an acute Si-Fe-H angle of

75(2)° in the solid state, and an Si···H distance of 2.48 Å, which is less than the sum of the van der Waals radii for these atoms (3.4 Å). However, the J_{SiH} value of 19 Hz obtained for **4-2** falls within a range where it is not possible to make a definitive assignment of η^2-(Si–H) coordination (while accepted values of J_{SiH} for η^2-silane complexes range from ca. 40–70 Hz, lower values are possible in some circumstances).[48, 89] When the mixture of **4-2** and **4-3** was either left in benzene solution (over several days) or exposed to H_2 (1 atm, 18 h, 65 °C), a diamagnetic η^2-(Si-H) complex of an Fe^{II} dihydride complex was obtained (**4-4**, Scheme 4-1). Complex **4-3** features an acute Si–Fe–H^1 angle of 50.7(14)° involving the η^2-(Si-H) moiety, and the Si···H^1 distance of ca. 1.73 Å is much less than the sum of the van der Waals radii of the two atoms, strongly supporting an Si–H interaction in the solid state. The short Si···H^2 distance of 2.34 Å may be indicative of a potential secondary Si···H interaction.[48] The measure J_{SiH} value of 65 Hz (for H^1) is consistent with an η^2-(Si-H) interaction that persists in solution.
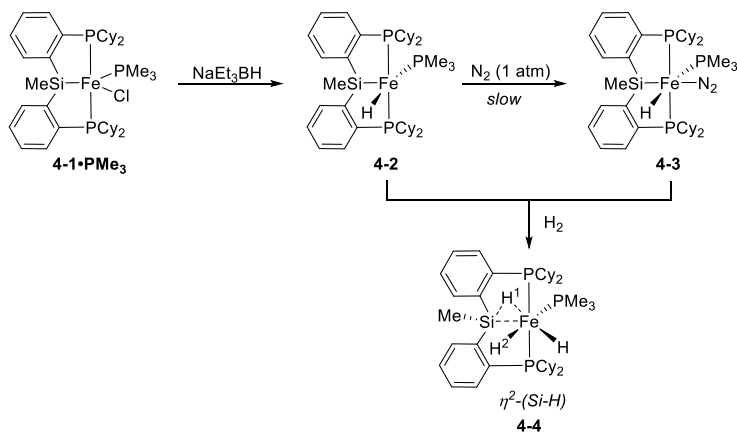
Scheme 4-1. Synthesis of (Cy-PSiP)Fe hydride complexes that feature nonclassical η^2-(Si-H) interactions.

A related iron-hydride bis(dinitrogen) complex (Cy-PSiP)Fe(H)(N2)2 (**4-5**, Figure 4-5) was found to be catalytically active in alkene hydrogenation catalysis under relatively

mild conditions (5 mol % Fe, 10 atm H_2, 65 °C, 4 h).[37] A variety of terminal and multiply substituted alkenes were readily reduced, including challenging *tri*substituted alkene substrates, and functional groups such as esters and ethers were well-tolerated by the catalyst. Complex **4-5** features an Si···H distances of 2.44 Å in the solid state and a J_{SiH} value of 70 Hz was measured in solution, suggesting the possibility of a nonclassical Si···H interaction in this complex. The reactivity of **4-5** toward the hydrogenation of diphenylacetylene was also investigated. In this regard, under the standard catalytic conditions employed (5 mol% Fe, 10 atm H_2, 65 °C, 4 h), a mixture of 42% *trans*-stilbene and 36% bibenzyl was obtained with no formation of the *cis*-stilbene isomer.[37] An increase in reaction temperature to 90 °C (toluene solution, 6 h) resulted in 92% conversion to the fully reduced bibenzyl.
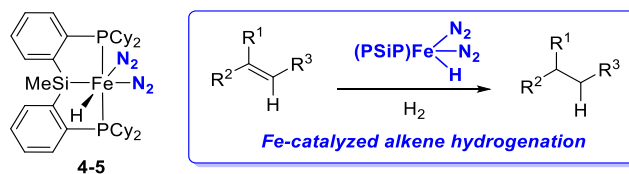
Figure 4-5. Alkene-hydrogenation catalyst (Cy-PSiP)FeH(N_2)$_2$ (**4-5**).

The observation of *E*-selectivity in the (Cy-PSiP)Fe-mediated hydrogenation of diphenylacetylene prompted further investigations of alkyne hydrogenation in this system. In this regard, this chapter will discuss the synthesis of Cy-PSiP ligated iron complexes and their utility as pre-catalysts for alkyne hydrogenation. Dr. Erin Johnson (Dalhousie) collaborated on this project, providing computational insight into the mechanism of (PSiP)Fe-catalyzed alkyne hydrogenation.

4.2 Results and Discussion

4.2.1 PSiP Iron Coordination Chemistry: Synthesis of [(Cy-PSiP)FeBr]$_2$(MgBr$_2$)

With the goal of further exploring the reactivity of **4-5**, a more streamlined synthesis of this complex was initially targeted. While the reported synthesis of this complex, involving treatment of (Cy-PSiP)FeCl(py) (**4-1·py**) with NaEt$_3$BH (Scheme 4-6),[37] is reproducible, the lability of the pyridine ligand in **4-1·py** at times complicated the ability to isolate pure **4-5** in high yield. In a previous study,[37] the Turculet group has shown that the synthesis of four-coordinate Fe^{II} complexes of the type (Cy-PSiP)FeX (X = Cl, Br) is challenging. These complexes were initially targeted by treatment of the tertiary silane (Cy-PSiP)H with various FeX$_2$ sources and bases to induce metalation (Scheme 4-6). A broad range of bases were studied in this regard, including amines. However, these attempts were largely unsuccessful as the resulting paramagnetic products proved difficult to isolate in pure form. In one case, a minute amount of X-ray quality crystals of monomeric (Cy-PSiP)FeBr (**4-6Br**) were obtained from treatment of (Cy-PSiP)H with FeBr$_2$ and 1 equiv. of MeMgBr at low temperature, supporting the feasibility of complexes with this formulation (Scheme 4-2). Related attempts to generate (Cy-PSiP)FeCl (**4-6Cl**) by treatment of (Cy-PSiP)H with FeCl$_2$(THF)$_{1.5}$ and 1 equiv. of BnMgCl led to isolation of a small amount of the Fe^{III} complex (Cy-PSiP)FeCl$_2$ (**4-7**, Scheme 4-2). The isolation of an Fe^{III} complex from this reaction implicates undesired one-electron processes. In a similar vein, the reaction of (Cy-PSiP)H with FeBr$_2$ and 2 equiv. of MeMgBr led instead to isolation of an (η^6-arene)Fe(I)-methyl complex, (**4-8**, Scheme 4-2), a result of a one-electron reduction process.
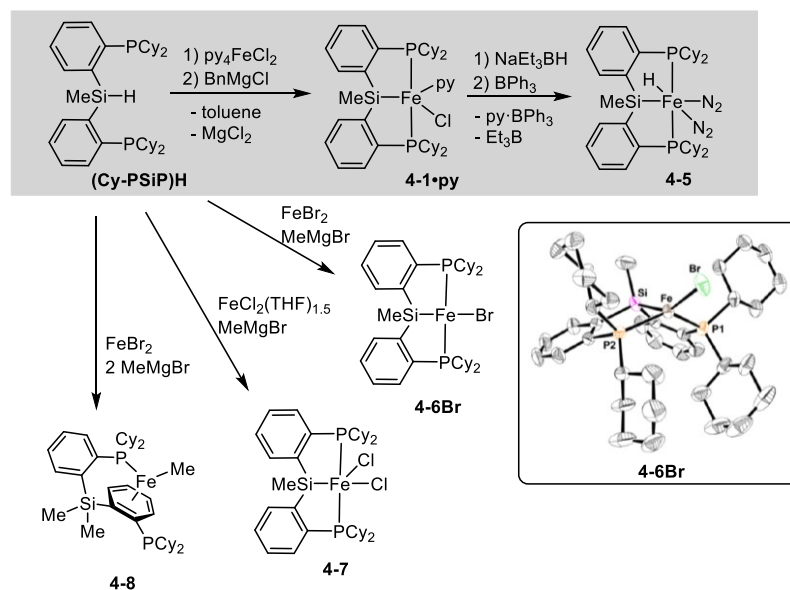
Scheme 4-2. Previously reported synthesis of (Cy-PSiP)Fe species.

Given the observed reactivity, it seemed evident that an additional L donor (L = neutral 2 electron donor) is required to stabilize complexes of the type (Cy-PSiP)FeX. In this context, the synthesis of 16 electron Fe^{II} complexes of the type (Cy-PSiP)FeX(L) was investigated by exploring various combinations of L donors (*i.e.*, PPh_3, PCy_3, DMAP, MeCN), X groups (*i.e.,* Cl, Br, Me, Ph, CH_2TMS, CH_2Ph), and bases (*i.e.* NEt_3, Cs_2CO_3, ^nBuLi, BnMgCl, BnMgBr, MeMgBr, MeLi, PhLi, $LiCH_2SiMe_3$, $LiCH_2Ph$, $NaEt_3BH$). Strong two electron donors such as PMe_3 and CO were strategically avoided as they may eventually hinder catalytic performance. Most attempts to generate (Cy-PSiP)FeX(L) by such routes resulted in the formation of multiple paramagnetic products from which no clean material could be isolated. Promising reactivity was observed when $FeCl_2$ was treated with 1 equiv. of either PCy_3 or DMAP, followed by the addition of 1 equiv. of each (Cy-PSiP)H and BnMgCl in THF (Scheme 4-3). ^{31}P and ^1H NMR spectroscopy of the reaction mixture indicated complete consumption of (Cy-PSiP)H and the formation of a paramagnetic product. While this complex could be successfully isolated, its partial

135

solubility in pentane was not ideal for the purpose of purification. Use of FeBr$_2$ in this reaction afforded comparably clean reactivity and a pentane-insoluble paramagnetic product (**4-9**) whose ^{1}H NMR spectrum was very similar to that of the FeCl$_2$-derived complex.
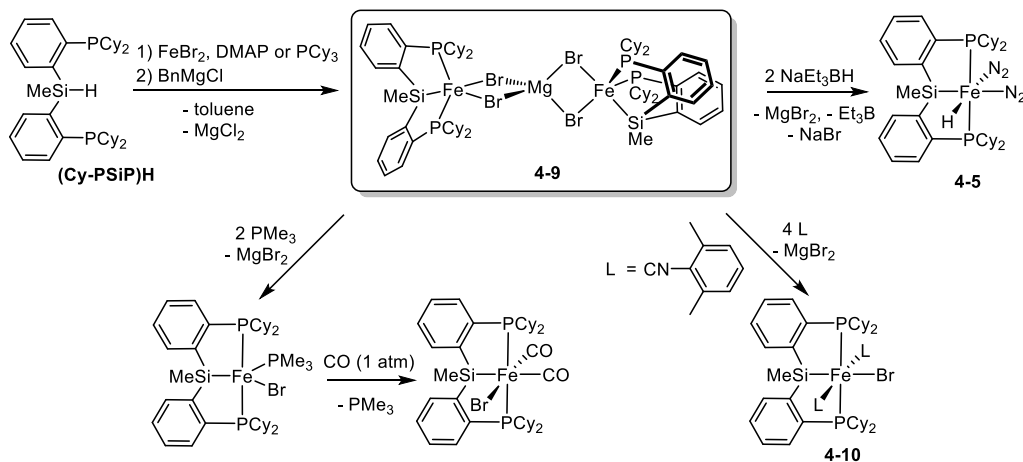
Scheme 4-3. Synthesis and derivatization of [(Cy-PSiP)FeBr]$_2$(MgBr$_2$) (**4-9**).

The solid state structure of **4-9** obtained by use of single crystal X-ray diffraction techniques reveals a trinuclear complex comprised of two (Cy-PSiP)FeBr moieties coordinated to a MgBr$_2$ fragment (Figure 4-6, Table 4-1). Each Fe center features approximate trigonal bipyramidal coordination geometry (τ_5 = 0.70 and 0.74 for Fe1 and Fe2, respectively), with Si and Br in the apical positions. The central Mg exhibits approximate tetrahedral coordination geometry. Multiple elemental analyses (C, H, N) all confirmed the formulation of the bulk material, while chloride analysis indicated the absence of chloride in the sample, consistent with loss of 1 equiv. MgCl$_2$ (chlorides from BnMgCl) per complex formed. Evans method in benzene solution indicated an effective magnetic moment of 4.71 μ_B, consistent with a total of four unpaired electrons, two per Fe center (S = 1 ground state for each Fe center; *cf.* μ_{eff} of 2.93 μ_B for **4-1·py**).

4-9   **4-10**
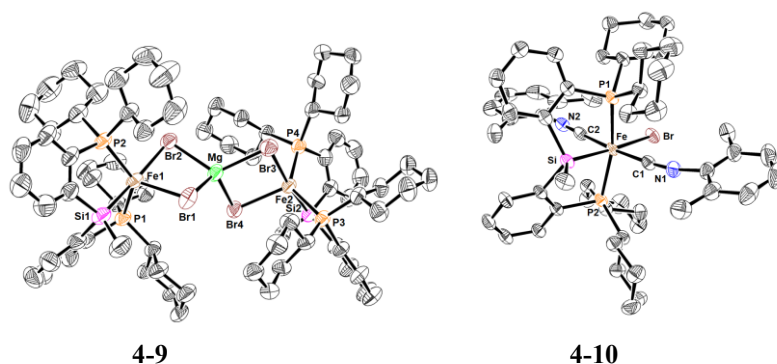
Figure 4-6. Crystallographically determined structures of **4-9** and **4-10** with thermal ellipsoids shown at the 50% probability level. Hydrogen atoms have been omitted for clarity.

Table 4-1. Selected bond distances (Å) and angles (deg.) for **4-9** and **4-10**.

4-9	**4-10**
P(1)-Fe(1) 2.317(2)	P(1)-Fe 2.2778(7)
P(2)-Fe(1) 2.319(2)	P(2)-Fe 2.2767(7)
Si(1)-Fe(1) 2.314(2)	Si-Fe 2.2891(7)
Br(1)-Fe(1) 2.5669(13)	Fe-C(1) 1.834(3)
Br(2)-Fe(1) 2.5770(13)	Fe-C(2) 1.849(2)
	Fe-Br 2.5337(4)
P(1)-Fe(1)-P(2) 132.05(8)	P(1)-Fe-Br 98.38(2)
P(1)-Fe(1)-Si(1) 81.27(7)	P(2)-Fe-Br 93.70(2)
P(2)-Fe(1)-Si(1) 81.41(8)	Si-Fe-Br 171.43(2)
Si(1)-Fe(1)-Br(1) 93.19(6)	Si-Fe-C(1) 100.08(8)
Si(1)-Fe(1)-Br(2) 174.27(8)	Si-Fe-C(2) 85.49(7)

The synthesis of **4-9** is reproducible, and high yielding (84% isolated yield). In the absence of added DMAP or PCy$_3$, the material obtained has similar ^{1}H NMR features to those of **4-9**, but also contains additional impurities that were not easily separated from the crude mixture. As such, while the role of added DMAP or PCy$_3$ is not immediately clear given that these species do not feature in the final product of the reaction, we speculate that the added Lewis base can potentially stabilize an intermediate in the formation of **4-9**. Operationally, the use of DMAP is preferred in the synthesis of **4-9**, as free DMAP proved easier to remove by pentane washing of the crude product. As well, BnMgCl was determined to be a more effective base than BnMgBr in this synthesis, affording higher

137

yields of pure **4-9** with no issues of halide scrambling as determined by elemental analysis of the isolated product. Complex **4-9** was found to be stable in the solid state for more than 6 months at room temperature and no decomposition was observed by ^{31}P or ^{1}H NMR spectroscopy when the sample was heated at 65 °C for 4 h in benzene-d_6.

The diiron complex **4-9** functions as a convenient source of (Cy-PSiP)FeBr (**4-6Br**) upon loss of MgBr$_2$. While **4-9** does not react directly with CO, treatment with 2 equiv. of PMe$_3$ led to the formation of the paramagnetic complex (Cy-PSiP)FeBr(PMe$_3$), the chloride analogue of which has been previously reported by the Turculet group (Scheme 4-3).[37] Subsequent treatment of (Cy-PSiP)FeBr(PMe$_3$) with CO (1 atm) led to the loss of PMe$_3$ and formation of diamagnetic (Cy-PSiP)FeBr(CO)$_2$, the chloride analogue of which has previously reported (Scheme 4-4). Treatment of **4-9** with 4 equiv. of xylyl isocyanide (CNAr) led to the formation of (Cy-PSiP)FeBr(CNAr)$_2$ (**4-10**) (Scheme 4-3), which is also diamagnetic and was successfully characterized by NMR spectroscopy and X-ray crystallography (Figure 4-6, Table 4-1). While the previously reported synthesis of the alkene hydrogenation pre-catalyst **4-5** proved challenging,[37] treatment of **4-9** with 2 equiv. NaEt$_3$BH led to the reproducible synthesis of **4-5** with a significantly improved yield of 89% (Scheme 4-3).

4.2.2 Alkyne Hydrogenation Catalysis

Having developed an improved method for the synthesis of **4-5** (Scheme 4-3), its performance in alkyne semi-hydrogenation was initially investigated. However, despite many efforts to optimize the conversion of diphenylacetylene to *trans*-stilbene, **4-5** gave inconsistent results in this type of reactivity. Remarkably, when **4-9** was used as the pre-catalyst (5 mol% Fe, 1 atm H$_2$, 30 °C, 4 h) nearly quantitative reduction of diphenylacetylene to bibenzyl was obtained in benzene-d_6 solution (93% conversion by ^{1}H

NMR with ferrocene internal standard; 5% *cis*-stilbene was also generated) was obtained (Scheme 4-4). Thus, it appears that the diiron complex is much more reactive for the complete hydrogenation of diphenylacetylene to bibenzyl than the hydride pre-catalyst **4-5**, which required 10 atm H_2 with heating at 90 °C for 6 h to afford 92% conversion to bibenzyl at an equal Fe loading. Control reactions were conducted for the hydrogenation of diphenylacetylene involving all possible combinations of $FeBr_2$, $FeCl_2$, DMAP, $MgCl_2$, $MgBr_2$ and (Cy-PSiP)H in both benzene-d_6 and THF solution (5 mol% Fe, 1 atm H_2, 30 °C, 4 h). In all cases, no reaction of the diphenylacetylene was observed by ^{1}H NMR spectroscopy. Multiple catalytic trials at varying conditions using different batches of the pre-catalyst **4-9** consistently indicated that **4-9** hydrogenates diphenylacetylene to bibenzyl with no significant formation of *cis*- or *trans*-stilbene.
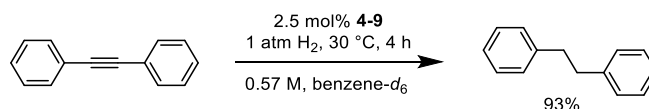
Scheme 4-4. Complete hydrogenation of diphenylacetylene to bibenzyl catalyzed by **4-9** under mild conditions. ^{1}H NMR yield obtained using ferrocene as an internal standard (an average of multiple runs).

Interestingly, a stoichiometric reaction of **4-9** with H_2 (1 atm) resulted in no significant change (by ^{1}H and ^{31}P NMR). Furthermore, the reaction of **4-9** and 2 equiv. of diphenylacetylene resulted in no major change (by ^{31}P and ^{1}H NMR) either. However, treatment of **4-9** with a large excess of diphenylacetylene, as per catalytic conditions, led to a rapid color change from dark-purple to red, likely due to the dissociation of $MgBr_2$ and coordination of diphenylacetylene to the iron center.

The reactivity observed in the hydrogenation of diphenylacetylene to bibenzyl under mild conditions, led to the investigation of other alkynes with various forms of substitution (Scheme 4-5). All catalytic reactions were run as duplicates (or triplicates in

some cases), and the conversion to product was measured by ^{1}H NMR integration vs.

ferrocene as an internal standard with an NMR relaxation delay of 60 seconds.
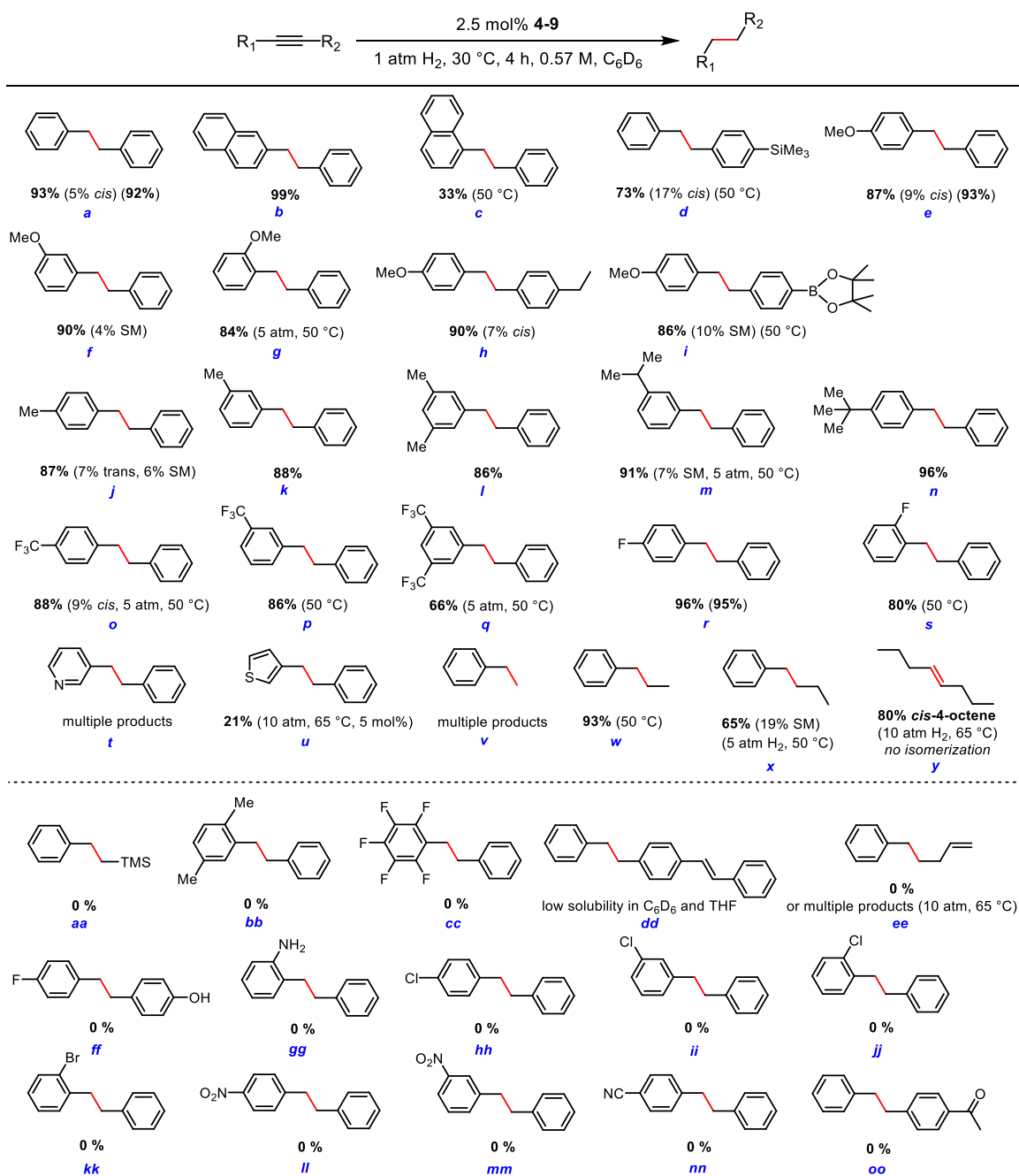
Scheme 4-5. Substrate scope for hydrogenation catalysis by **4-9**. Conversion to product determined on the basis of ^{1}H NMR integration vs. ferrocene as an internal standard (average of two runs). Isolated yields in parantheses; these were obtained with 2.5 mol% **4-9**, 5 atm 30 °C, 4 h.

Of the substrates that afforded high conversion (>80%) to the corresponding alkane, general trends that were observed include selectivity for diaryl alkynes with relatively electron-donating substituents and no steric hindrance. In accordance with this trend, diaryl alkynes that feature substituents in the *ortho*-position were generally less reactive, such that in the case of OMe substitution of one aryl ring, the *para*- and *meta*-isomers (substrates *e* and *f*, respectively; Scheme 4-5) displayed near quantitative conversion to the corresponding alkane under the standard conditions (5 mol% Fe, 1 atm H_2, 30 °C, 4 h), while the *ortho*-isomer (substrate *g*) required harsher conditions (5 atm H_2, 50 °C, 4 h) to achieve comparable conversion. Similarly, in the case of dimethyl substitution of one aryl ring (substrates *f* and *bb*), the 3,5-Me_2 isomer achieved 86% conversion under standard conditions, while the 2,5-Me_2 isomer was unreactive.

The effects of electron-donating and electron-withdrawing substituents on the diaryl alkyne substrates are well-illustrated by substrates that contain a single substituent in the *para*-position of one aryl ring. Thus, the *para*-OMe and -Me derivatives (**e** and **f**, Scheme 4-5) that feature donating substituents achieve 87% and 90% conversion, respectively under standard conditions, while the *para*-CF_3 derivative (**o**) requires 5 atm H_2 and heating to 50 °C for 4 h to achieve comparable reactivity. The *para*-NO_2 and -CN derivatives (**ll** and **nn**) are completely unreactive. Also, in accordance with this trend, the *meta*-CF_3 substituted derivative (**p**) is slightly more reactive than the *para*-isomer (**o**), achieving 86% conversion with only heating to 50 °C for 4 h and no pressure increase. Entry **q**, which features 3,5-$(CF_3)_2$ substitution is slightly more deactivated, requiring 5 atm H_2 and heating at 50 °C for 4 h to reach 66% conversion to the corresponding alkane. Surprisingly, the *para*-F derivative (**r**) achieves 96% conversion under standard conditions and the *ortho*-F isomer (**s**) reaches 80% conversion with only heating to 50 °C for 4 h and no pressure

increase. By comparison, Cl and Br substitution in one aryl ring (substrates **hh**–**kk**) is not well tolerated, achieveing no conversion to product.

To further probe the scope of **4-9**-mediated alkyne hydrogenation, alkynes that do not feature diaryl substitution were evaluated. Phenylacetylene (substrate **v**, Scheme 4-5) afforded multiple products under the standard hydrogenation conditions, suggesting that terminal alkynes are not well-tolerated. By comparison 1-phenyl-1-propyne (**w**) and 1-phenyl-1-butyne (**x**) afforded 93% (50 °C) and 65% (5 atm H_2, 50 °C) conversion, respectively, which suggests that alkyl substitution in the alkyne substrate hinders reactivity relative to diaryl derivatives. In accordance with this trend, the reactivity of 4-octyne (**y**) was diminshed significantly, with little reaction observed under standard conditions. Interestingly, at higher pressure and temperature (10 atm H_2, 65 °C, 4h), 80% conversion of 4-octyne to *cis*-4-octene was obtained, with no evidence for subsequent isomerization.

Substrates that were not well-tolerated in this reactivity include alkynes featuring heteroaromatic substituents such as pyridine and thiophene derivatives (substrates **t** and **u**, Scheme 4-5). As well, subtrates containing OH, NH_2, and acetyl functionalities proved unreactive (**ff**, **gg**, and **oo**), as did a C_6F_5-substituted aryl alkyne (**cc**).

Lastly, isolated yields were obtained for substrates **a**, **e**, and **r** (Scheme 4-5). For preparative-scale reactions, an increase in H_2 pressure to 5 atm was necessary to obtain yields comparable to the yields determined on the basis of ^{1}H NMR integration, likely due to issues of scale and efficiency of H_2 transfer into solution.

4.2.3 Reactivity of [(Cy-PSiP)FeBr]$_2$(MgBr$_2$) with Alkenes

To further investigate the reactivity of **4-9** in hydrogenation reactions, the reactivity toward alkene hydrogenation was probed. Surprisingly, no conversion of alkenes to alkanes was observed with either 1-octene, *cis*-4-octene, *trans*-4-octene, styrene, or *cis*-stilbene (5

mol% Fe, 1 atm H_2, 30 °C , 4 h), including under the somewhat more forcing conditions originally reported for **4-5**-mediated alkene hydrogenation (2.5 mol % **4-9**, 10 atm H_2, 65 °C , 4 h),[37] with the exception of *cis*-stilbene, for which 20% conversion to bibenzyl was obtained under the latter conditions (Scheme 4-6). The observed reactivity was particularly intriguing given that *cis*-stilbene would be considered a likely intermediate in the complete hydrogenation of diphenylacetylene to bibenzyl.
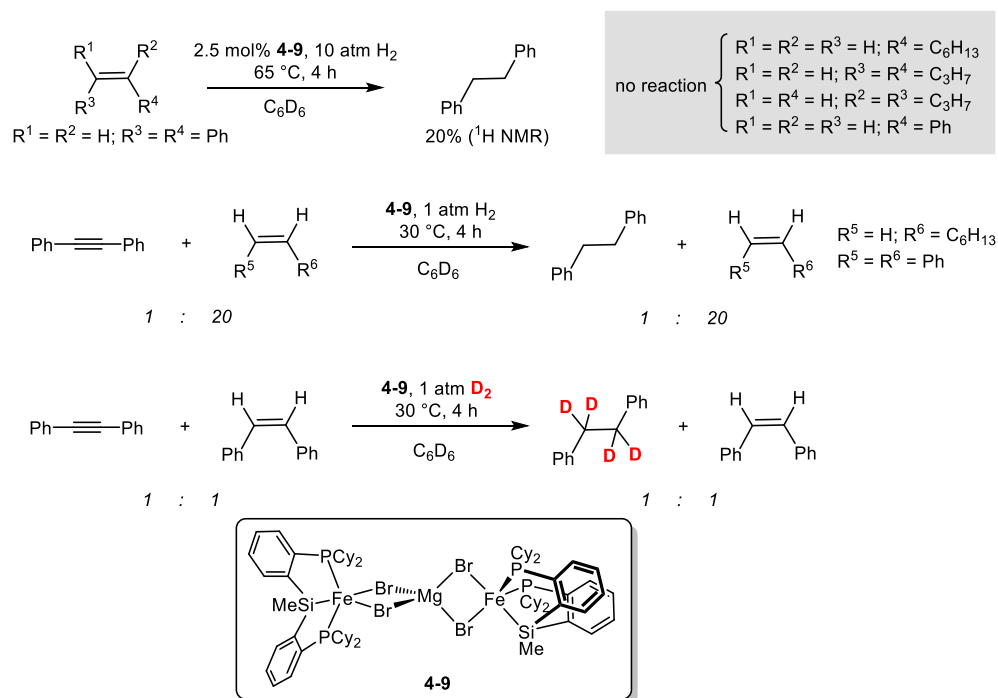
Scheme 4-6. Reactivity of [(Cy-PSiP)FeBr$_2$(MgBr$_2$)] (**4-9**) with respect to alkene hydrogenation.

It was speculated that a more strongly donating alkyne substrate may be necessary to coordinate to the Fe center in **4-9** and promote its dissociation into (Cy-PSiP)FeBr (**4-6Br**) and MgBr$_2$. In an effort to probe this possibility, **4-9** was treated with 1 equiv. of diphenylacetylene and 20 equiv. of either 1-octene or *cis*-stilbene in benzene-d_6, and the reaction mixtures were exposed to 1 atm H_2 and heated at 30 °C for 4 hours (Scheme 4-6). This led to quantitative conversion of diphenylacetylene to bibenzyl (by ^{1}H NMR), with no

conversion of either 1-octene or *cis*-stilbene to their respective alkanes. In a related experiment, treatment of **4-9** with a 1:1 mixture of diphenylacetylene and *cis*-stilbene and exposure to 1 atm of D_2 afforded exclusively Ph-CD_2-CD_2-Ph, with no evidence for the formation of Ph-CHD-CHD-Ph (by ^{1}H and ^{13}C NMR) after 4 h at 30 °C (Scheme 4-6). This result lends further support to the hypothesis that *(Cy-PSiP)FeBr exhibits exclusive selectivity for alkyne reduction, with no ability to reduce the intermediate alkenes associated with a typical metal-mediated hydrogenation cycle.*

This remarkable selectivity of alkyne over alkene hydrogenation using a homogenous iron catalyst is unprecedented. In order to better understand this unusual selectivity, DFT computational studies were conducted in collaboration with Dr. Erin Johnson (Dalhousie).

4.2.4 Computational Studies on the Mechanism of Alkyne Hydrogenation

Catalytic hydrogenation mechanisms involving platinum group metals have been widely explored, and the elementary steps typically involved in such reactivity are well defined. A classic hydrogenation mechanism in this context typically involves H_2 oxidative addition, coordination of the substrate, migratory insertion of the substrate into a M-H bond, and subsequent reductive elimination of the product. In the case of alkyne hydrogenation, this leads to the formation of the *Z*-alkene product, which can undergo metal-mediated isomerization to the *E*-isomer in some cases. Full reduction of the alkyne is achieved by subsequent hydrogenation of the alkene intermediate. However, hydrogenation mechanisms for first-row transition metals such as iron are relatively underexplored and may exhibit different elementary steps in comparison to platinum group metals. Unlike the case of 4*d*- and 5*d*-metals, depending on ligand field considerations, the metal can adopt different spin states leading to different reactivity manifolds. One-electron

chemistry that is often characteristic of 3*d*-metals can be much more challenging to predict than well-established two-electron processes, such as oxidative addition and reductive elimination associated with platinum group metal reactivity. In addition, 3*d*-metals tend to favor lower oxidation states, and as such may preferrentially undergo σ-bond metathesis reactions over traditional oxidative addition.

As demonstrated experimentally, complex **4-9** functions as a source of (Cy-PSiP)FeBr (**4-6Br**), which forms *via* dissociation of $MgBr_2$. Given the large molecular weight of the diiron complex, the dissociation energy of the analogous dimethylphosphino complex [(Me-PSiP)FeBr]$_2$(MgBr$_2$) (**4-9^{Me}**) to 2 equiv. of (Me-PSiP)FeBr was evaluated using DFT methods. The diiron complex **4-9^{Me}** was determined to have a dissociation enthalpy of 58.6 kcal mol^{-1} (Scheme 4-7). The dissociation enthalpy of **4-9** is anticipated to be comparable, although perhaps slightly higher due to greater dispersion stabilization of the dimer imparted by the dicyclohexylphosphino groups. The driving force for this dissociation may be a result of net loss of solid $MgBr_2$, which due to its lattice energy, is irreversible.
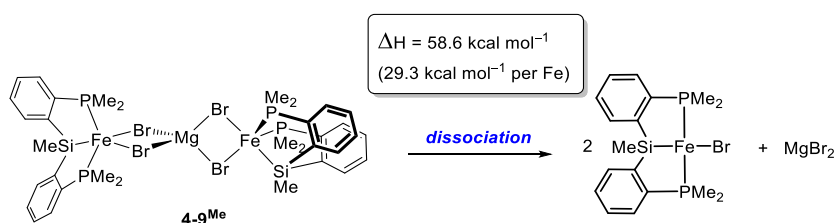
Scheme 4-7. Dissociation enthalpy calculated for [(Me-PSiP)FeBr$_2$](MgBr$_2$) (**4-9^{Me}**).

The DFT optimized structure of **4-6Br** was in good agreement with previously obtained X-ray diffraction data for this complex.[37] The triplet spin state was determined to be the ground state for **4-6Br**, and subsequent calculations were conducted with the iron

complexes in the triplet state. We also hypothesized that the bromine moiety remains coordinated to the iron center throughout the hydrogenation cycle.

Given the experimental results obtained for the synthesis of **4-10** by addition of 4 equiv. of xylyl isocyanide to **4-9**, the enthalpy associated with the coordination of 2 equiv. of xylyl isocyanide to **4-6Br** was evaluated using DFT methods. This process was determined to have an exothermic enthalpy of -59.9 kcal mol^{-1} (Scheme 4-8), consistent with a highly favorable interaction.
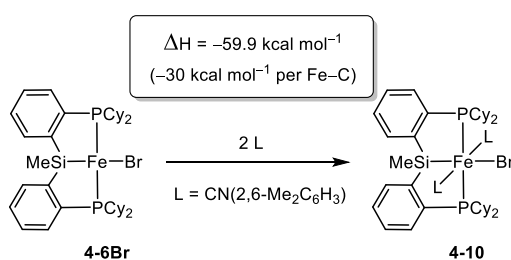
Scheme 4-8. Determination of enthalpy associated with the coordination of 2 equiv. of xylyl isocyanide to **4-6Br**.

Subsequent calculations targeted the binding enthalpy of diphenylacetylene to **4-6Br** in comparison to 1-octene and *cis*-stilbene, given that catalytic hydrogenation was only observed for diphenylacetylene. In this regard, the binding enthalpy of diphenylacetylene to **4-6Br** is -16.3 kcal mol^{-1}, which is indicative of a fairly strong coordination. Comparatively, the binding enthalpy of 1-octene to **4-6Br** is only -5.1 kcal/mol. Hence, 1-octene does not bind strongly enough to the iron center for subsequent reactivity to occur. The binding enthalpy of *cis*-stilbene to **4-6Br** is also indicative of weak coordination, resulting in the formation of a van der Waals complex.

Having determined experimentally that **4-9** does not readily react with H$_2$ (1 atm in benzene-d_6 at room temperature), the enthalpy associated with the coordination of H$_2$ to **4-6Br** to form the corresponding σ-complex was evaluated. A high endothermic enthalpy of

13.8 kcal mol^{-1} was calculated for this process, which precludes H_2 coordination and subsequent oxidative addition by **4-6Br**. Rather, the favorable coordination of diphenylacetylene is more likely to occur prior to an H_2 activation step. Sterically unencumbered alkynes featuring electron-donating groups are reduced more readily than bulky, electron-poor alkynes which support the idea that alkyne coordination to the Fe centre plays an important role in catalysis. With this in mind, DFT methods were applied to determine the energies associated with potential catalytic intermediates for diphenylacetylene hydrogenation mediated by **4-6Br**.

Considering experimental observations that show exclusive selectivity for alkyne hydrogenation over alkene hydrogenation, as well as the computationally determined weak binding of *cis*-stilbene to **4-6Br**, we postulated that unlike a typical alkyne hydrogenation cycle, the hydrogenation of diphenylacetylene by **4-6Br** may likely proceed without the intermediate formation of *cis*-stilbene. Although little precedent for such a mechanism is known, a relevant example involving Ru-mediated alkyne hydrogenation was recently reported by Fürstner and co-workers.[90] While investigating the mechanism of *trans*-selective alkyne semi-hydrogenation mediated by Cp*RuCl(COD) (Cp* = C_5Me_5), Fürstner and co-workers discovered an unusual mechanistic manifold involving geminal H_2 transfer to a single C atom of the alkyne substrate, while the second C atom is converted to a Ru-carbene. The Ru carbene intermediate is capable of a second H_2 activation step, which results in the formation of a Ru alkyl hydride species that can undergo subsequent reductive elimination to afford the fully reduced alkane product. This represents a unique example of an alkyne hydrogenation mechanism that does not require the formation of a semi-hydrogenated alkene intermediate. On the basis of this example, we postulated a related mechanism for the hydrogenation of diphenylacetylene by **4-6Br** (Scheme 4-9).

Initial coordination of the alkyne to **4-6Br** leads to intermediate **I** with the PSiP ligand facially disposed, which undergoes a conformational change, favouring a meridional geometry in **II**. Subsequent H_2 activation, potentially assisted by Si, leads to the formation of an Fe(II)-metallacyclopropene intermediate (**III**, Scheme 4-9). Transfer of the hydride to the sp^2-C of the metallacyclopropene (C_α) would lead to formation of the stilbene adduct **IV**. However, the geometry of the metallacyclopropene hinders hydride transfer to C_α, which would require a rotation about the Fe-(sp^2-C) bond (Figure 4-7). Instead, hydride transfer to C_β leads to the formation of an Fe(II) carbene species **V**. A conformational change in **V** leads to a facial geometry, thereby generating intermediate **VI** which is able to undergo a second H_2 activation step to afford the Fe alkyl complex **VII**. C-H reductive elimination in **VII** provides the reduced bibenzyl product, thereby regenerating **4-6Br**. In this proposed mechanism, the reactivity of the metallacyclopropene species **III** determines the selectivity of the hydrogenation reaction. The involvement of an Fe(II) carbene intermediate, though unusual, is not unprecedented. Isolable iron carbene complexes have been reported previously, most commonly supported by *N*-heterocyclic carbene-based ligands.[91] Other examples of iron carbene complexes featuring cyclopentadienyl-, tetrapyrrolic-, and PDI-based ancillary ligands have also been reported, and have found application in carbene transfer reactions and cyclopropanation.[23m, 91-92] Related cyclopentadienyl ruthenium carbene complexes have also been reported and are implicated in the *trans*-selective hydroboration, hydrogermylation, hydrostannation, and hydrogenation reactions of alkynes.[90]
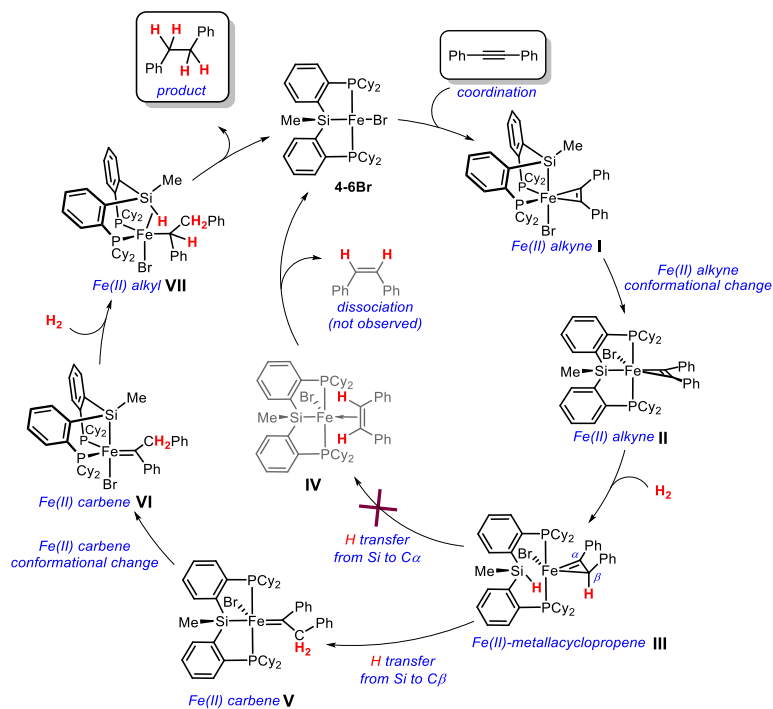
Scheme 4-9. Proposed cycle for the hydrogenation of diphenylacetylene by **4-6Br**.

The enthalpies associated with the intermediates depicted in Scheme 4-9 are shown in Figure 4-8. Although this computational study remains in-progress, the enthalpy values obtained thus far are consistent with a favorable, energetically downhill process. On-going DFT calculations by Dr. Erin Johnson suggest that H_2 addition to (Cy-PSiP)FeBr(DPA) (**II**, DPA = diphenylacetylene) occurs *via* a concerted transition state in which Si, Fe, and the alkyne carbon each participate in H_2 activation to directly form the Fe(II) metallacyclopropene species **III** (**TS1**, Figure 4-8). The concerted formation of the metallacyclopropene intermediate from **II** was determined to be more energetically feasible than a step-wise process involving the formation of an Fe hydride intermediate. The transition state for the formation of the iron carbene intermediate **V** from **III** is also concerted (**TS2**, Figure 4-8). The Si-H in **III** is transferred directly to Fe, which mediates hydride migration to C_β to complete the geminal addition of the first H_2 equivalent to diphenylacetylene. While both transition state calculations are energetically feasible and

149

result in intermediates that are thermodynamically downhill, the addition of H_2 is the limiting step ($\Delta H^{\ddagger} = 21.4$ kcal mol^{-1}), which is consistent with experimental observations that a large headspace of H_2 is required for the catalysis to reach completion. Furthermore, the transition states calculated thus far highlight the key role of Si in H_2 activation and hydride transfer to the substrate, lending support to the notion that metal-silyl cooperativity can enable unique reactivity in $3d$-metal catalysis.
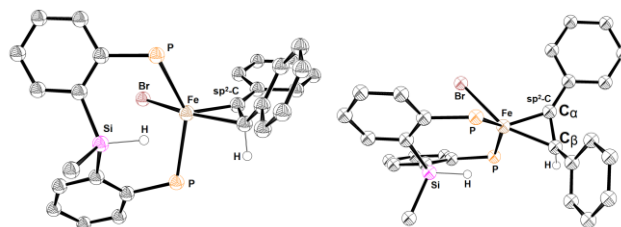
Figure 4-7. DFT calculated *cif* structures for intermediate **II** from two different viewpoints. Most hydrogen atoms and the cyclohexyl groups have been removed for clarity.
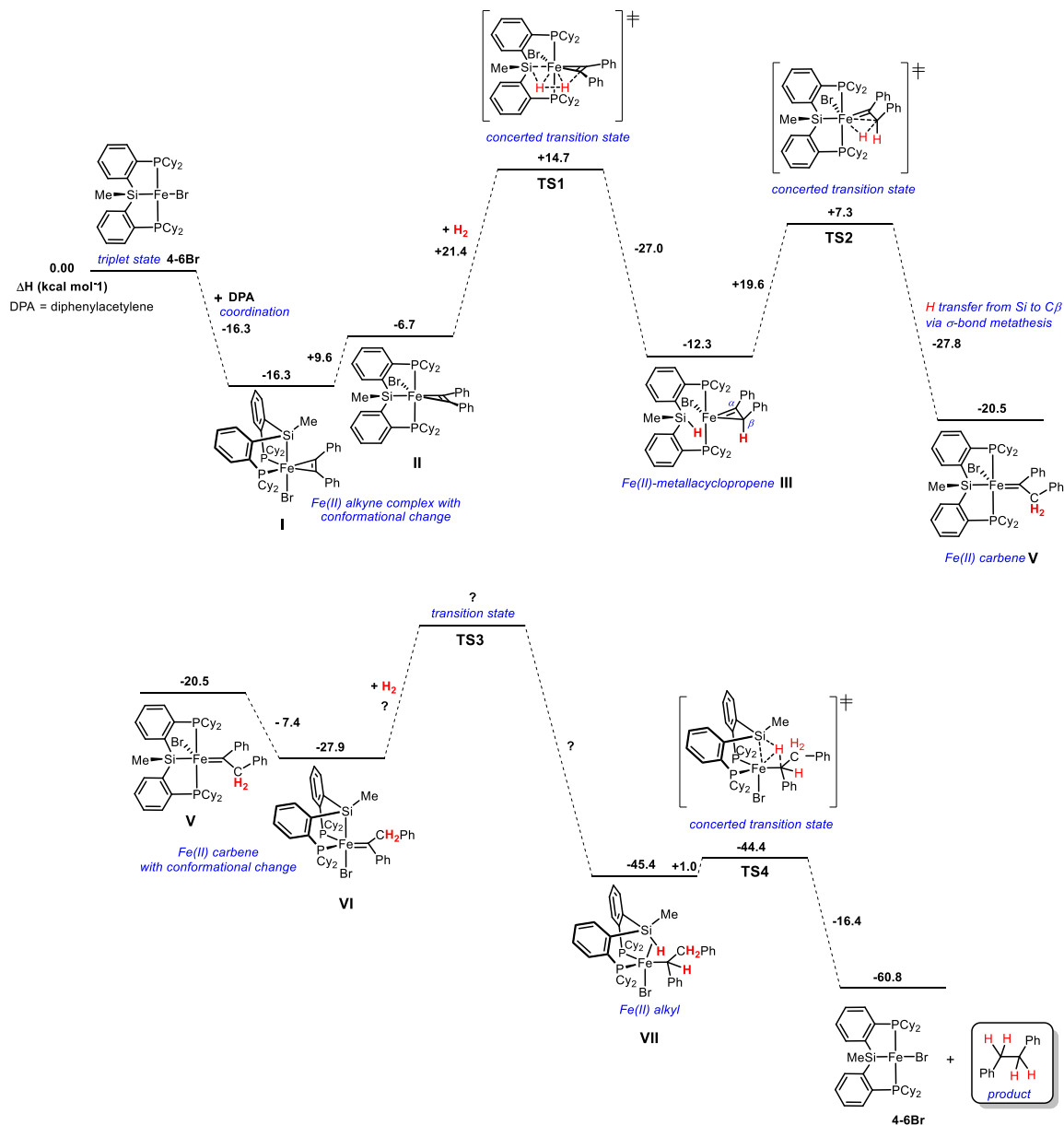
Figure 4-8. Enthalpies (ΔH, kJ/mol) of intermediates and transition states in the hydrogenation of diphenylacetylene to bibenzyl by **4-6Br**.

4.3 Conclusion

A direct, one pot synthesis of the MgBr$_2$-bridged diiron complex [(Cy-PSiP)FeBr](MgBr$_2$) (**4-9**) was developed. Complex **4-9** can dissociate MgBr$_2$ to function as an effective source of (Cy-PSiP)FeBr (**4-6Br**), and is a readily accessed precursor for the synthesis of (Cy-PSiP)Fe^{II} derivatives, such as (Cy-PSiP)FeH(N$_2$)$_2$. Furthermore, **4-9** was found to be a highly effective pre-catalyst for the complete hydrogenation of

151

diarylalkynes to the corresponding alkanes under mild conditions. Although **4-9** was active in the hydrogenation of alkynes, alkenes were found to be largely unreactive. This unusual selectivity led us to investigate the mechanism of this reaction using DFT methods in collaboration with Dr. Erin Johnson (Dalhousie). Although these studies are on-going, results obtained thus far implicate metal-silyl cooperativity as playing a key role in H_2 activation, and in the transfer of hydride equivalents to the coordinated alkyne fragment. Furthermore, an unususal mechanism involving geminal transfer of H_2 to a single alkyne carbon *via* Fe(II) metallacyclopropene and Fe(II) carbene intermediates has been determined to be thermodynamically downhill and is thus far in agreement with experimental observations. This mechanism has little precedent in organometallic reactivity, with only a Ru example having been reported previously. Mechanistic insight gained from these studies will guide the development of further novel reactivity facilitated by PSiP-ligated 3d-metal species.

4.4 Experimental

4.4.1 General Considerations: Synthesis

All experiments were conducted under nitrogen in a glovebox or Parr Bomb apparatus using standard Schlenk techniques. Dry, oxygen-free solvents were used unless otherwise indicated. All non-deuterated solvents were deoxygenated by sparging with nitrogen. Benzene was subsequently passed through a double column purification system (one activated alumina column and one column packed with activated Q-5). Tetrahydrofuran was purified by distillation from Na/benzophenone. All purified solvents were stored over 4 Å molecular sieves. Benzene-d_6 was degassed *via* sparging for 30 minutes and stored over 4 Å molecular sieves. All other reagents were purchased from commercial suppliers and used as received. The tertiary silane (Cy-PSiP)H was prepared

according to a previously published procedure.[33a] [1]H, ^{13}C, ^{31}P, and ^{29}Si NMR characterization data were collected at 300K with chemical shifts reported in parts per million downfield of $SiMe_4$ (for ^{1}H, ^{13}C, and [29]Si), or 85% H_3PO_4 in D_2O (for ^{31}P). Chemical shift ranges are cited to indicate overlapping resonances. The following abbreviations were utilized to assign NMR data: s = singlet; d = doublet; t = triplet; q = quartet; m = multiplet; br = broad; dm = doublet of multiplets; apt = apparent. Solution magnetic moment measurements were determined by use of the Evans method.[93] Please note that a ^{13}C NMR shift at ca. 110 ppm is due to an instrument artifact. X-Ray crystallographic data was collected and refined on a fee-for-service basis by Dr. Michael J. Ferguson of the University of Alberta X-ray Crystallography Laboratory, Edmonton, AB.

4.4.2 General Considerations: Computational Studies

All calculations were performed with the B3LYP density functional[1,2] and the XDM dispersion correction[3,4] using the Gaussian 09 program,[5] interfaced with postG.[6] All Fe-containing species were modeled as triplet states. Geometry optimizations and frequency calculations used a mixed basis set, with 6-31G* assigned to C and H atoms, and 6-31+G* assigned to all other elements. Evaluations of the thermal enthalpy corrections assumed an ideal gas at 298.15 K with a molar volume of 1 L. Single-point energy calculations were performed using the 6-311+G(2d,2p) basis set. The XDM damping parameters were set to $a_1 = 0$, $a_2 = 3.7737$ Å for the optimizations and $a_1 = 0.4376$, $a_2 = 2.1607$ Å for the single-point energies.

References for DFT calculations:

1. Becke, A. D. Density-functional thermochemistry. III. The role of exact exchange, *J. Chem. Phys.* **1993**. 98, 5648-5652.

2. Lee, C., Yang, W., Parr, R. G. Development of the Colle-Salvetti correlation-energy formula into a functional of the electron density. *Phys. Rev.* **1988**. B 37, 785-789.

3. Otero de la Roza, A., Johnson, E. R. Non-Covalent Interactions and Thermochemistry using XDM-Corrected Hybrid and Range-Separated Hybrid Density Functionals, *J. Chem. Phys.* **2013**. 138, 204109-1 – 204109-13.

4. Johnson, E. R. The Exchange-Hole Dipole Moment Dispersion Model, in Non-Covalent Interactions in Quantum Chemistry and Physics. **2017**. Ch. 5, 169-194.

5. M. J. Frisch et al. Gaussian 09 Revision B.01 Gaussian Inc. Wallingford CT **2009**.

6. The postG code is available from http://schooner.chem.dal.ca

4.4.3 Synthetic Details and Characterization Data

4.4.3.1 Synthesis of Iron Complexes

(Cy-PSiP)FeH(N$_2$)$_2$ (4-5). A solution of **4-9** (0.080 g, 0.05 mmol) in ca. 4 mL of benzene was treated with two equiv. NaEt$_3$BH (1 M in toluene; 0.10 mL, 0.10 mmol) added dropwise at room temperature. An immediate color change from purple-black to yellow was observed. The reaction mixture was filtered through Celite, and the volatile component of the reaction mixture were removed under vacuum. with benzene and evaporated to dryness to afford **4-5** (0.089 mml, 89% yield) as a beige powder.

[(Cy-PSiP)FeBr](MgBr$_2$) (4-9). FeBr$_2$ (0.12 g, 0.57 mmol) was treated with a solution of DMAP (0.070 g, 0.57 mmol) in ca. 5 mL of THF. The reaction mixture was allowed to stir for 20 minutes at room temperature. A solution of (Cy-PSiP)H (0.34 g, 0.57 mmol) ca. 10 mL of THF was added to the magentically stirred reaction mixture, and the resulting solution was allowed to react at room temperature for 20 minutes. BnMgCl (1.4 M in toluene; 0.41 mL, 0.57 mmol) was diluted with ca. 2 mL of THF and was subsequently added dropwise to the magentically stirred reaction mixture. An immediate color change

from beige to dark grey to black-red was observed. The mixture was stirred for 18 h at room temperature. Subsequently, the volatile components of the reaction mixture were removed under vacuum and the remaining residue was triturated with pentane (4 × 3 mL). The remaining material was dissolved in a 2:1 mixture of benzene:pentane and filtered through Celite. The filtrate solution was evaporated to dryness. The remaining residue was washed with pentane (3 × 3 mL) and dried under vacuum to afford **4-9** (0.48 mmol, 84% yield) as a grey-blue paramagnetic solid. μ_{eff} (benzene-d_6): 4.71 μ_B (S = 1 ground state for each Fe center). ^{1}H NMR (300 MHz, benzene-d_6): δ 32.4, 20.2, 15.6, 14.5, 13.0, 8.42, 7.50, 7.22, 5.54, 4.25, 3.87, 3.46, 2.30, 1.37, 1.28, 1.26, 1.23, 0.42, 0.01, -0.68, -1.47, -1.76, -4.84, -10.1, -14.3, -32.2, -54.6, -77.6. Anal. Calcd for $C_{73}H_{107}Br_4Fe_2MgP_4Si_2$: C, 54.11; H, 6.66. Found: C, 54.18; H, 6.48; N, < 0.5; Cl, < 0.5.

(Cy-PSiP)FeBr[CN(2,6-Me₂C₆H₃)]₂ (4-10). A solution of xylyl isocyanide (0.020 g, 0.15 mmol) in ca. 2 mL of benzene was added to a a solution of **4-9** (0.12 g, 0.075 mmol) in ca. 3 mL of benzene. An immediate color change from purple-black to yellow-orange was observed. The reaction mixture was allowed to react for 2 h at room temperature and was subsequently evaporated to dryness. The remaining residue was washed with pentane (3 × 3 mL) and dried under vacuum to afford **4-10** (0.15 mmol, 93% yield) as a yellow-orange powder. ^{1}H NMR (300 MHz, benzene-d_6) δ 8.36 (apt d., J_{HH} = 7 Hz, 2 H, H$_{arom}$), 7.57 (m, 3 H, H$_{arom}$), 7.33 (m, 2 H, H$_{arom}$), 7.24 (m, 2 H, H$_{arom}$), 6.86–6.78 (4 H, H$_{arom}$), 6.67 (m, 1 H, H$_{arom}$), 3.02 (br s., 2 H, P*Cy₂*), 2.75 (s, 6 H, CN(*Me₂*C₆H₃)), 2.57 (s, 6 H, CN(*Me₂*C₆H₃)), 2.37 – 1.18 (22 H, P*Cy₂*). ^{31}P {^{1}H} NMR (121.5 MHz, benzene-d_6): δ 78.7. Anal. Calcd for $C_{55}H_{73}BrFeN_2P_2Si$: C, 66.86; H, 7.45; N, 2.84. Found: C, 66.71; H, 7.40; N, 2.78.

Crystallographic Solution and Refinement Details. Crystallographic data were obtained at 193(2)K (for **4-9**) and 173(2) K (for **4-10**) on a Bruker D8/APEX II CCD diffractometer using CuKα (λ = 1.54178 Å, microfocus source) radiation employing samples that were mounted in inert oil and transferred to a cold gas stream on the diffractometer. In the case of **4-9**, data were collected with the detector set at three different positions. Low-angle (detector 2θ = −33°) data frames were collected using a scan time of 5 seconds, medium-angle (detector 2θ = 75°) frames using a scan time of 30 seconds, and high-angle (detector 2θ = 117°) frames using a scan time of 45 seconds. Programs for diffractometer operation, data collection, and data reduction (including SAINT) were supplied by Bruker. Data reduction, correction for Lorentz−polarization, and absorption correction were each performed. Structure solution was achieved by intrinsic phasing methods. All structures were refined by use of full-matrix least-squares procedures (on F^2) with R_1 based on $F_o^2 \geq 2\sigma(F_o^2)$ and wR_2 based on $F_o^2 \geq -3\sigma(F_o^2)$.

Unless otherwise indicated, all nonhydrogen atoms were refined with anisotropic displacement parameters. For **4-9**, the C–C distances within cyclohexyl group (C111 to C116) were restrained to be approximately the same by use of the *SHELXL* **SADI** instruction. Furthermore, 1.25 equiv. of pentane solvate were located in the asymmetric unit for **4-9**. The solvent pentane molecules were restrained to have the same refined C–C and C$\cdots$C distances by use of the **DFIX** instruction; further, the ADPs of the pentane molecules were restrained by the rigid bond restraint **RIGU**. Finally, atoms C6S to C10S were constrained to have equivalent ADPs. The pentane atoms were refined with partial occupancies as follows: C1S-C5S were refined anisotropically with occupancy of 0.75; C6S-C10S were refined with occupancy of 0.50 and equivalent anisotropic displacement

parameters. For **4-10**, one equiv. of pentane solvent was located in the asymmetric unit. The pentane solvate was modeled over two positions with refined occupancies of 0.667(8) (C1S-C5S) and 0.333(8) (C1SB-C5SB). The C–C distance within the disordered solvent pentane molecules were restrained to be approximately the same by the *SHELXL* **SADI** instruction. All hydrogen atoms were added at calculated positions and refined by use of a riding model employing isotropic displacement parameters based on the isotropic displacement parameter of the attached atom.

4.4.3.2 General Procedure for Alkyne Hydrogenation Catalysis

In a glovebox, the alkyne (0.11 mmol) was weighed into a 1 dram vial, to which 0.10 mL of benzene-d_6 was added. A catalyst stock solution of **4-9** (28.5 M) was prepared and 2.5 mol% of [(Cy-PSiP)FeBr]$_2$(MgBr$_2$) (0.10 mL) was added to the vial followed by a stir bar. The vial was sealed with a septa cap and punctured with one 18 gauge needle. The vial was then placed inside a 400 mL-sized Parr bomb and sealed. The Parr bomb was purged with hydrogen, then pressurized with hydrogen (1 atm, unless otherwise stated), and was subsequently placed in an oil bath to heat at 30 °C (unless otherwise stated; internal temperature was monitored *via* a thermocouple) for 4 h. The reaction was then exposed to air, and ferrocene was added as an internal standard (stock solution in benzene-d_6, 0.095 M unless otherwise stated, 300 μL). The reaction mixture was then filtered through a silica plug which was subsequently washed with 1 mL of benzene-d_6. ^{1}H NMR spectra containing the internal standard were obtained at a (16 scans, 60 second delay).

Scale-ups: In a glovebox, the alkyne (0.57 mmol) was weighed into a 1 dram vial, to which 0.50 mL of benzene-d_6 was added. A catalyst stock solution of **4-9** (28.5 M) was prepared and 2.5 mol% of [(Cy-PSiP)FeBr](MgBr$_2$) (0.50 mL) was added to the vial

followed by a stir bar. The vial was sealed with a septa cap and punctured with three 18 gauge needles. The vial was then placed inside a 400 mL-sized Parr bomb and sealed. The Parr bomb was purged with hydrogen, then pressurized with hydrogen (5 atm), and was subsequently placed in an oil bath to heat at 30 °C (internal temperature was monitored via a thermocouple) for 4 h. The reaction was then exposed to air and the contents were filtered through a silica plug which was subsequently washed with 2 mL of benzene. The collected benzene solutions were combined and evaporated to dryness. and the remaining residue was weighed to determine isolated yield. No further purification was necessary due to quantitative product formation.

4.4.3.3 General Synthesis of Alkynes: Sonogashira Cross-Coupling Reactions

In a glovebox, the aryl iodide (17 mmol) was weighed into a 4 dram vial, to which $PdCl_2$ (2 mol%, 0.34 mmol, 0.061 g) and PPh_3 (6 mol%, 1.02 mmol, 0.27 g) were added, followed by CuI (2 mol%, 0.34 mmol, 0.065 g) and phenylacetylene (17 mmol). Triethylamine (3 mL) was then added, followed by THF (ca. 20 mL total). The reaction mixture was transferred to a thick walled glass vessel sealed with a Teflon stopcock and was heated at 80 °C for 18 h. Water (ca. 40 mL) was then added to the glass vessel, and the contents were transferred to a separatory funnel and extracted with ethyl acetate (3 × 15 mL). The organic extracts were collected, combined, and evaporated to dryness. The crude materiall was purified by column chromatography with ethyl acetate/hexanes. Optimization of the reactions was not pursued.

4.4.3.4 Characterization Data of Alkyne Starting Materials

Diphenylacetylene
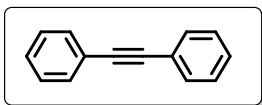
^{1}H NMR (300 MHz, benzene-d_6) δ 7.53 – 7.49 (4 H, H$_{arom}$), 7.04 – 6.97 (6 H, H$_{arom}$). ^{13}C{^{1}H} (75.5 MHz, benzene-d_6) δ 132.0 (C$_{arom}$), 128.7 (C$_{arom}$), 128.5 (C$_{arom}$), 123.9 (C$_{arom}$), 90.2 (C$_{alkyne}$).

2-(2-phenylethynyl)naphthalene
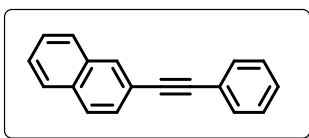
^{1}H NMR (500 MHz, benzene-d_6) δ 7.99 (apt. s, 1H, H$_{arom}$), 7.60 – 7.56 (3 H, H$_{arom}$), 7.51 – 7.45 (3 H, H$_{arom}$), 7.19 – 7.17 (2 H, H$_{arom}$), 7.06 – 7.01 (3 H, H$_{arom}$). ^{13}C{^{1}H} (125.7 MHz, benzene-d_6) δ 133.6 (C$_{arom}$), 133.3 (C$_{arom}$), 132.0 (CH$_{arom}$), 128.8 (CH$_{arom}$), 128.7 (CH$_{arom}$), 128.5 (CH$_{arom}$), 128.4 (CH$_{arom}$), 128.2 (CH$_{arom}$), 126.9 (CH$_{arom}$), 126.8 (CH$_{arom}$), 124.1 (C$_{arom}$), 121.1 (C$_{arom}$), 90.7 (C$_{alkyne}$), 90.5 (C$_{alkyne}$). Two overlapping peaks with benzene-d_6.

1-(2-phenylethynyl)naphthalene
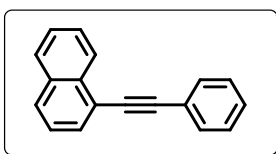
^{1}H NMR (500 MHz, benzene-d_6) δ 8.69 (apt. d, J_{HH} = 8 Hz, 1 H, H$_{arom}$), 7.71 (apt. dd, J_{HH} = 7 Hz, 1 Hz, 1 H, H$_{arom}$), 7.58 – 7.55 (3 H, H$_{arom}$), 7.51 (J_{HH} = 8 Hz, 1 H, H$_{arom}$), 7.39 (m, 1 H), 7.26 (m, 1 H), 7.10 (apt. t, J_{HH} = 8 Hz, 1 H), 7.05 – 7.01 (3 H, H$_{arom}$). ^{13}C{^{1}H} (125.7 MHz, benzene-d_6) δ 133.9 (C$_{arom}$), 133.8 (C$_{arom}$), 132.0 (CH$_{arom}$), 130.8 (CH$_{arom}$), 129.1 (CH$_{arom}$), 128.7 (CH$_{arom}$), 128.6 (CH$_{arom}$), 127.1 (CH$_{arom}$), 126.7 (CH$_{arom}$), 126.6 (CH$_{arom}$), 125.6 (CH$_{arom}$), 124.0 (C$_{arom}$), 121.5 (C$_{arom}$), 95.1 (C$_{alkyne}$), 88.4 (C$_{alkyne}$).

(4-trimethylsilylphenyl)phenylacetylene
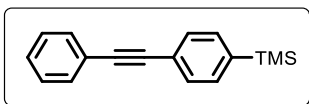
^{1}H NMR (500 MHz, benzene-d_6) δ 7.61 (apt. d, J_{HH} = 8 Hz, 2 H, H$_{arom}$), 7.54 (m, 2 H, H$_{arom}$), 7.34 (apt. d, J_{HH} = 8 Hz, 2 H, H$_{arom}$), 7.02 – 6.98 (3 H, H$_{arom}$), 0.15 (s, 9 H, Si*Me₃*). ^{13}C{^{1}H} (125.7 MHz, benzene-d_6) δ 141.1 (C$_{arom}$), 133.7 (CH$_{arom}$), 132.0 (CH$_{arom}$), 131.2 (CH$_{arom}$), 128.7 (CH$_{arom}$), 128.5 (CH$_{arom}$), 124.3 (C$_{arom}$), 124.0 (C$_{arom}$), 90.7 (C$_{alkyne}$), 90.4 (C$_{alkyne}$), -1.25 (Si*Me₃*).

Phenylacetylene
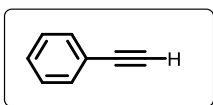
^{1}H NMR (500 MHz, benzene-d_6) δ 7.40 (m, 2 H, H$_{arom}$), 6.95 – 6.89 (3 H, H$_{arom}$), 2.73 (s, 1 H, C$_{alkyne}$*H*). ^{13}C{^{1}H} (125.7 MHz, benzene-d_6) δ 132.4 (CH$_{arom}$), 128.8 (CH$_{arom}$), 128.5 (CH$_{arom}$), 122.8 (C$_{arom}$), 83.9 (C$_{alkyne}$), 77.8 (*C*$_{alkyne}$H).

1-phenyl-1-propyne
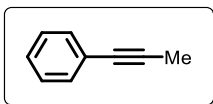
^{1}H NMR (500 MHz, benzene-d_6) δ 7.46 (m, 2 H, H$_{arom}$), 7.02 – 6.95 (3 H, H$_{arom}$), 1.66 (s, 3 H, C$_{alkyne}$*Me*). ^{13}C{^{1}H} (125.7 MHz, benzene-d_6) δ 131.9 (CH$_{arom}$), 128.5 (CH$_{arom}$), 127.7 (CH$_{arom}$), 124.9 (C$_{arom}$), 86.1 (C$_{alkyne}$), 60.5 (C$_{alkyne}$), 4.0 (C$_{alkyne}$*Me*).

1-phenyl-1-butyne
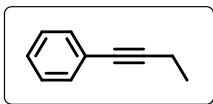
^{1}H NMR (500 MHz, benzene-d_6) δ 7.47 (m, 2 H, H$_{arom}$), 7.02 – 6.95 (3 H, H$_{arom}$), 2.15 (q, 2 H, $^3J_{HH}$ = 7 Hz, C*H₂*), 1.00 (t, 3 H, $^3J_{HH}$ = 7 Hz, C*H₃*). ^{13}C{^{1}H} (125.7 MHz, benzene-d_6) δ 131.9 (CH$_{arom}$), 128.5 (CH$_{arom}$), 127.7 (CH$_{arom}$), 124.9 (C$_{arom}$), 91.9 (C$_{alkyne}$), 80.8 (C$_{alkyne}$), 14.0 (C*H₂*), 13.3 (C*H₃*).

## 1-methoxy-4-(2-phenylethynyl)-benzene
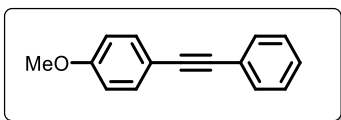
^{1}H NMR (500 MHz, benzene-d_6) δ 7.56 (m, 2 H, H$_{arom}$), 7.47 (m, 2 H, H$_{arom}$), 7.04 – 6.96 (3 H, H$_{arom}$), 6.61 (m, 2 H, H$_{arom}$), 3.18 (s, 3 H, OMe). ^{13}C{^{1}H} (125.7 MHz, benzene-d_6) δ 160.2 (C$_{arom}$), 133.5 (CH$_{arom}$), 131.9 (CH$_{arom}$), 128.7 (CH$_{arom}$), 124.4 (C$_{arom}$), 116.0 (C$_{arom}$), 114.5 (CH$_{arom}$), 90.4 (C$_{alkyne}$), 88.9 (C$_{alkyne}$), 54.8 (OMe).

1-methoxy-3-(2-phenylethynyl)-benzene
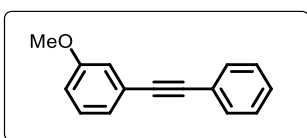
^{1}H NMR (500 MHz, benzene-d_6) δ 7.53 (m, 2 H, H$_{arom}$), 7.23 – 7.17 (2 H, H$_{arom}$), 7.03 – 6.95 (4 H, H$_{arom}$), 6.72 (1 H, H$_{arom}$), 3.21 (s, 3 H, OMe). ^{13}C{^{1}H} (125.7 MHz, benzene-d_6) δ 160.1 (C$_{arom}$), 132.0 (CH$_{arom}$), 129.8 (CH$_{arom}$), 128.7 (CH$_{arom}$), 128.5 (CH$_{arom}$), 125.0 (CH$_{arom}$), 124.5 (C$_{arom}$), 123.9 (C$_{arom}$), 116.8 (CH$_{arom}$), 115.5 (CH$_{arom}$), 90.3 (C$_{alkyne}$), 89.9 (C$_{alkyne}$), 54.7 (OMe).

1-methoxy-2-(2-phenylethynyl)-benzene
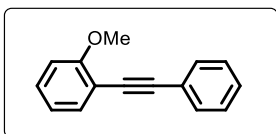
^{1}H NMR (500 MHz, benzene-d_6) δ 7.58 – 7.54 (3 H, H$_{arom}$), 7.01 – 6.93 (3 H, H$_{arom}$), 6.71 (m, 1 H, $^3J_{HH}$ = 8 Hz, H$_{arom}$), 6.45 (apt. d, 1 H, $^3J_{HH}$ = 8 Hz, H$_{arom}$), 3.32 (s, 3 H, OMe). ^{13}C{^{1}H} (125.7 MHz, benzene-d_6) δ 160.7 (C$_{arom}$), 133.9 (CH$_{arom}$), 132.0 (CH$_{arom}$), 129.8 (CH$_{arom}$), 128.6 (CH$_{arom}$), 128.2 (CH$_{arom}$), 124.5 (C$_{arom}$), 120.7 (CH$_{arom}$), 113.5 (C$_{arom}$), 111.1 (CH$_{arom}$), 94.1 (C$_{alkyne}$), 87.0 (C$_{alkyne}$), 55.3 (OMe).

1-ethyl-4-[2-(4-methoxyohenyl)ethynyl]-benzene
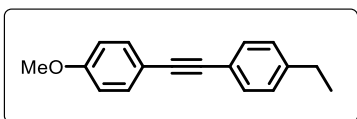
^{1}H NMR (500 MHz, benzene-d_6) δ 7.55 (apt. d, 2 H, $^3J_{HH}$ = 8 Hz, H$_{arom}$), 7.50 (apt. d, 2 H, $^3J_{HH}$ = 8 Hz, H$_{arom}$), 6.91 (apt. d, 2 H, $^3J_{HH}$ = 8 Hz, H$_{arom}$), 6.61 (m, 2 H, H$_{arom}$), 3.19 (s, 3 H, OMe), 2.35 (q, 2 H, $^3J_{HH}$ = 8 Hz, CH_2), 1.00 (t, 3 H, $^3J_{HH}$ = 8 Hz, CH_3). ^{13}C{^{1}H} (125.7

MHz, benzene-d_6) δ 160.1 (C$_{arom}$), 144.4 (C$_{arom}$), 133.4 (CH$_{arom}$), 131.9 (CH$_{arom}$), 128.3 (CH$_{arom}$), 121.7 (C$_{arom}$), 116.3 (C$_{arom}$), 114.4 (CH$_{arom}$), 89.7 (C$_{alkyne}$), 89.1 (C$_{alkyne}$), 54.8 (OMe), 29.0 (CH_2), 15.4 (CH_3).

2-[4-[2-(4-methoxyphenyl)ethynyl]phenyl]-4,4,5,5-tetramethyl-1,3,2-dioxaborolane
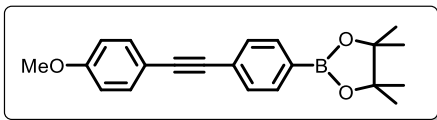
^{1}H NMR (500 MHz, benzene-d_6) δ 8.06 (apt. d, 2 H, $^3J_{HH}$ = 8 Hz, H$_{arom}$), 7.59 (apt. d, 2 H, $^3J_{HH}$ = 8 Hz, H$_{arom}$), 7.45 (apt. d, 2 H, $^3J_{HH}$ = 9 Hz, H$_{arom}$), 6.60 (apt. d, 2 H, H$_{arom}$), 3.18 (s, 3 H, OMe), 1.10 (s, 12 H, BPin). ^{13}C{^{1}H} (125.7 MHz, benzene-d_6) δ 160.3 (C$_{arom}$), 135.4 (CH$_{arom}$), 133.5 (CH$_{arom}$), 131.2 (CH$_{arom}$), 127.2 (C$_{arom}$), 116.0 (C$_{arom}$), 114.4 (CH$_{arom}$), 91.8 (C$_{alkyne}$), 89.2 (C$_{alkyne}$), 83.9 (BPin), 54.8 (OMe), 25.0 (BPin).

1-methyl-4-(2-phenylethynyl)-benzene
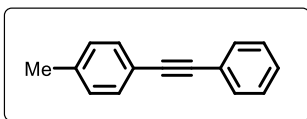
^{1}H NMR (500 MHz, benzene-d_6) δ 7.54 (m, 2 H, H$_{arom}$), 7.47 (m, 2 H, H$_{arom}$), 7.03 – 6.96 (m, 2 H, H$_{arom}$), 6.83 (apt. d, 2 H, $^3J_{HH}$ = 8 Hz, H$_{arom}$), 1.99 (s, 3 H, Me). ^{13}C{^{1}H} (125.7 MHz, benzene-d_6) δ 138.5 (C$_{arom}$), 131.9 (CH$_{arom}$), 129.5 (CH$_{arom}$), 128.6 (CH$_{arom}$), 124.2 (C$_{arom}$), 121.0 (C$_{arom}$), 90.4 (C$_{alkyne}$), 89.6 (C$_{alkyne}$), 21.3 (Me).

1-methyl-3-(2-phenylethynyl)-benzene
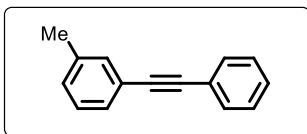
^{1}H NMR (300 MHz, benzene-d_6) δ 7.54 (m, 2 H, H$_{arom}$), 7.41 – 7.34 (m, 2 H, H$_{arom}$), 7.04 – 6.95 (m, 4 H, H$_{arom}$), 6.84 (m, 1 H, H$_{arom}$), 1.99 (s, 3 H, Me). ^{13}C{^{1}H} (75.5 MHz, benzene-d_6) δ 138.2 (C$_{arom}$), 132.7 (CH$_{arom}$), 131.9 (CH$_{arom}$), 129.4 (CH$_{arom}$), 129.1 (CH$_{arom}$), 128.7 (CH$_{arom}$), 128.4 (CH$_{arom}$), 124.1 (C$_{arom}$), 123.8 (C$_{arom}$), 90.5 (C$_{alkyne}$), 89.8 (C$_{alkyne}$), 21.1 (Me).

1,3-dimethyl-5-(2-phenylethynyl)-benzene
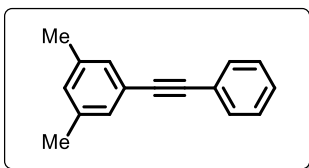
^{1}H NMR (500 MHz, benzene-d_6) δ 7.56 (m, 2 H, H$_{arom}$), 7.22 (s, 2 H, H$_{arom}$), 7.05 – 6.97 (3 H, H$_{arom}$), 6.69 (s, 1 H, H$_{arom}$), 2.02 (s, 6 H, *Me*). ^{13}C{^{1}H} (125.7 MHz, benzene-d_6) δ 138.0 (CH$_{arom}$), 132.0 (CH$_{arom}$), 130.5 (C$_{arom}$), 129.9 (CH$_{arom}$), 128.7 (CH$_{arom}$), 124.3 (C$_{arom}$), 123.7 (C$_{arom}$), 90.8 (C$_{alkyne}$), 89.5 (C$_{alkyne}$), 21.0 (*Me*).

1-(1-methylethyl)-3-(2-phenylethynyl)-benzene
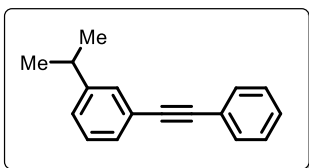
^{1}H NMR (500 MHz, benzene-d_6) δ 7.56 – 7.53 (3 H, H$_{arom}$), 7.44 (m, 1 H, H$_{arom}$), 7.05 – 6.95 (5 H, H$_{arom}$), 2.62 (m, 1 H, C*H*Me$_2$), 1.06 (s, 3 H, *Me*), 1.05 (s, 3 H, *Me*). ^{13}C{^{1}H} (125.7 MHz, benzene-d_6) δ 149.2 (C$_{arom}$), 132.0 (CH$_{arom}$), 130.2 (CH$_{arom}$), 129.6 (CH$_{arom}$), 128.8 (CH$_{arom}$), 128.7 (CH$_{arom}$), 128.4 (CH$_{arom}$), 127.0 (C$_{arom}$), 124.1 (C$_{arom}$), 123.9 (C$_{arom}$), 90.7 (C$_{alkyne}$), 89.8 (C$_{alkyne}$), 34.3 (*C*HMe$_2$), 23.9 (CH*Me$_2$*).

1-(1,1-dimethylethyl)-4-(2-phenylethynyl)-benzene
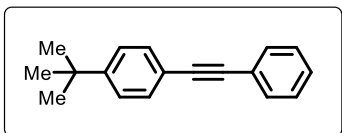
^{1}H NMR (300 MHz, benzene-d_6) δ 7.59 – 7.54 (4 H, H$_{arom}$), 7.16 – 7.13 (2 H, H$_{arom}$), 7.01 – 6.99 (3 H, H$_{arom}$), 1.13 (s, 9 H, C*Me$_3$*). ^{13}C{^{1}H} (75.5 MHz, benzene-d_6) δ 151.6 (C$_{arom}$), 132.0 (CH$_{arom}$), 131.9 (CH$_{arom}$), 128.6 (CH$_{arom}$), 128.3 (CH$_{arom}$), 125.8 (CH$_{arom}$), 124.2 (C$_{arom}$), 121.1 (C$_{arom}$), 90.4 (C$_{alkyne}$), 89.6 (C$_{alkyne}$), 34.7 (*C*Me$_3$), 23.9 (C*Me$_3$*).

1,4-dimethyl-2-(2-phenylethynyl)-benzene
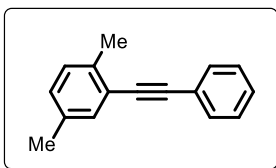
^{1}H NMR (500 MHz, benzene-d_6) δ 7.56 (m, 2 H, H$_{arom}$), 7.22 (s, 2 H, H$_{arom}$), 7.04 – 6.99 (3 H, H$_{arom}$), 2.02 (s, 6 H, 2Me). ^{13}C{^{1}H} (125.7 MHz, benzene-d_6) δ 138.0 (CH$_{arom}$), 131.9 (CH$_{arom}$), 130.5 (C$_{arom}$), 129.9 (CH$_{arom}$), 128.7 (CH$_{arom}$), 128.3 (C$_{arom}$), 124.3 (C$_{arom}$), 123.7 (C$_{arom}$), 90.8 (C$_{alkyne}$), 89.5 (C$_{alkyne}$), 21.0 (2Me).

1-(2-phenylethynyl)-4-(trifluoromethyl)-benzene
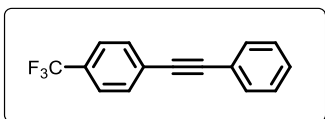
^{1}H NMR (500 MHz, benzene-d_6) δ 7.49 – 7.47 (2 H, H$_{arom}$), 7.25 (m, 2 H, H$_{arom}$), 7.15 (m, 2 H, H$_{arom}$), 7.01 – 6.99 (3 H, H$_{arom}$). ^{19}F{^{1}H} (470.6 MHz, benzene-d_6) δ -62.6. ^{13}C{^{1}H} (125.7 MHz, benzene-d_6) δ 132.1 (CH$_{arom}$), 132.0 (CH$_{arom}$), 130.0 (q, $^2J_{CF}$ = 32 Hz, CCF$_3$), 129.0 (CH$_{arom}$), 128.8 (CH$_{arom}$), 127.4 (C$_{arom}$), 125.5 (m, CH$_{arom}$), 124.7 (q, $^1J_{CF}$ = 272 Hz, CF$_3$), 123.1 (C$_{arom}$), 92.4 (C$_{alkyne}$), 88.6 (C$_{alkyne}$).

1-(2-phenylethynyl)-3-(trifluoromethyl)-benzene
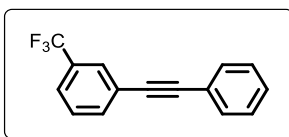
^{1}H NMR (300 MHz, benzene-d_6) δ 7.72 (s, 1 H, H$_{arom}$), 7.48 – 7.45 (2 H, H$_{arom}$), 7.31 (apt. d, 1 H, $^3J_{HH}$ = 8 Hz, H$_{arom}$), 7.13 (apt. d, 3 H, $^3J_{HH}$ = 8 Hz, H$_{arom}$), 7.03 – 6.99 (3 H, H$_{arom}$), 6.74 (apt. t, 1 H, $^3J_{HH}$ = 8 Hz, H$_{arom}$). ^{19}F{^{1}H} (282.4 MHz, benzene-d_6) δ -62.7. ^{13}C{^{1}H} (75.5 MHz, benzene-d_6) δ 134.8 (CH$_{arom}$), 132.0 (CH$_{arom}$), 131.1 (q, $^2J_{CF}$ = 33 Hz, CCF$_3$), 129.1 (CH$_{arom}$), 128.9 (CH$_{arom}$), 128.7 (CH$_{arom}$), 128.6 (m, C$_{arom}$), 124.8 (C$_{arom}$), 124.7 (C$_{arom}$), 124.4 (q, $^1J_{CF}$ = 272 Hz, CF$_3$), 123.2 (C$_{arom}$), 91.6 (C$_{alkyne}$), 88.4 (C$_{alkyne}$).

1-(2-phenylethynyl)-3,5-bis(trifluoromethyl)-benzene
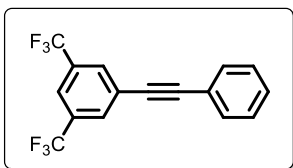
^{1}H NMR (500 MHz, benzene-d_6) δ 7.59 (s, 2 H, H$_{arom}$), 7.54 (s, 1 H, H$_{arom}$), 7.48 – 7.46 (2 H, H$_{arom}$), 7.05 – 7.03 (3 H, H$_{arom}$). ^{19}F{^{1}H} (470.6 MHz, benzene-d_6) δ -63.0. ^{13}C{^{1}H} (125.7 MHz, benzene-d_6) δ 132.1 (CH$_{arom}$), 132.0 (q, $^2J_{CF}$ = 33 Hz, CCF$_3$), 131.6 (br, CH$_{arom}$), 129.5 (CH$_{arom}$), 128.9 (CH$_{arom}$), 126.0 (C$_{arom}$), 123.4 (q, $^1J_{CF}$ = 272 Hz, CF$_3$), 122.5 (C$_{arom}$), 121.5 (CH$_{arom}$), 93.3 (C$_{alkyne}$), 86.9 (C$_{alkyne}$).

1,2,3,4,5-pentafluoro-6-(2-phenylethynyl)-benzene
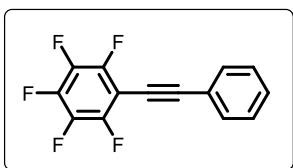
^{1}H NMR (500 MHz, benzene-d_6) δ 7.41 – 7.39 (2 H, H$_{arom}$), 6.96 – 6.90 (3 H, H$_{arom}$). ^{19}F{^{1}H} (470.6 MHz, benzene-d_6) δ -137.2 (m, 2 H), -153.5 (apt. t, $^3J_{FF}$ = 21 Hz, 1 H), -162.4 (m, 2 H). ^{13}C{^{1}H} (125.7 MHz, benzene-d_6) δ 147.4 (dm, $^1J_{CF}$ = 252 Hz, CF), 141.5 (dm, $^1J_{CF}$ = 256 Hz, CF), 137.8 (dm, $^1J_{CF}$ = 245 Hz, CF), 132.1 (CH$_{arom}$), 129.8 (CH$_{arom}$), 128.8 (CH$_{arom}$), 121.9 (C$_{arom}$), 100.5 (C$_{arom}$), 102.1 (C$_{alkyne}$), 73.6 (C$_{alkyne}$).

1-fluoro-4-(2-phenylethynyl)-benzene
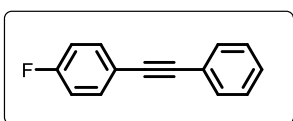
^{1}H NMR (500 MHz, benzene-d_6) δ 7.51 – 7.49 (2 H, H$_{arom}$), 7.25 – 7.22 (3 H, H$_{arom}$), 7.03 – 6.98 (3 H, H$_{arom}$), 6.61 (apt t, J = 9 Hz, 2 H, H$_{arom}$). ^{19}F{^{1}H} (470.6 MHz, benzene-d_6) δ -137.2 (m, 2 H), -153.5 (apt. t, $^3J_{FF}$ = 21 Hz, 1 H), -162.4 (m, 2 H). ^{13}C{^{1}H} (125.7 MHz, benzene-d_6) δ 162.9 (d, $^1J_{CF}$ = 249 Hz, CF), 133.8 (apt. d, J_{CF} = 9 Hz, CH$_{arom}$), 131.9 (CH$_{arom}$), 128.7 (CH$_{arom}$), 128.6 (CH$_{arom}$), 123.8 (C$_{arom}$), 119.9 (apt. d, $^4J_{CF}$ = 4 Hz, C$_{arom}$), 115.9 (apt. d, J_{CF} = 22 Hz, CH$_{arom}$), 89.8 (C$_{alkyne}$), 89.0 (C$_{alkyne}$).

1-fluoro-2-(2-phenylethynyl)-benzene
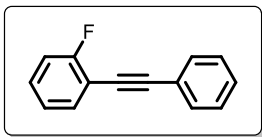
^{1}H NMR (500 MHz, benzene-d_6) δ 7.50 – 7.48 (2 H, H$_{arom}$), 7.33 (m, 1 H, H$_{arom}$), 6.97 – 6.96 (3 H, H$_{arom}$), 6.76 – 6.72 (2 H, H$_{arom}$), 6.64 (m, 1 H, H$_{arom}$). ^{19}F{^{1}H} (470.6 MHz, benzene-d_6) δ -109.6. ^{13}C{^{1}H} (125.7 MHz, benzene-d_6) δ 163.2 (d, $^1J_{CF}$ = 252 Hz, CF), 133.7 (CH$_{arom}$), 132.0 (CH$_{arom}$), 130.1 (apt. d, J_{CF} = 8 Hz, CH$_{arom}$), 128.8 (CH$_{arom}$), 128.6 (CH$_{arom}$), 124.1 (apt. d, J_{CF} = 4 Hz, CH$_{arom}$), 123.5 (C$_{arom}$), 115.7 (apt. d, J_{CF} = 21 Hz, CH$_{arom}$), 112.5 (apt. d, J_{CF} = 17 Hz, C$_{arom}$), 95.3 (C$_{alkyne}$), 83.4 (C$_{alkyne}$).

1-chloro-4-(2-phenylethynyl)-benzene
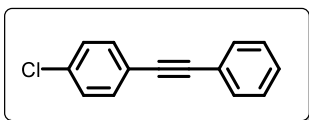
^{1}H NMR (500 MHz, benzene-d_6) δ 7.49 0 7.47 (2 H, H$_{arom}$), 7.16 – 7.15 (2 H, H$_{arom}$), 7.02 – 6.98 (3 H, H$_{arom}$), 6.93 – 6.91 (2 H, H$_{arom}$). ^{13}C{^{1}H} (125.7 MHz, benzene-d_6) δ 134.6 (CCl), 133.1 (CH$_{arom}$), 131.9 (CH$_{arom}$), 129.0 (CH$_{arom}$), 128.7 (CH$_{arom}$), 123.6 (C$_{arom}$), 122.2 (C$_{arom}$), 91.0 (C$_{alkyne}$), 89.0 (C$_{alkyne}$).

1-chloro-3-(2-phenylethynyl)-benzene
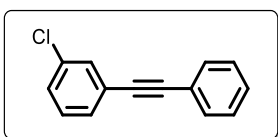
^{1}H NMR (500 MHz, benzene-d_6) δ 7.47 – 7.45 (3 H, H$_{arom}$), 7.17 (m, 1 H, H$_{arom}$), 7.02 – 6.98 (3 H, H$_{arom}$), 6.94 (m, 1 H, H$_{arom}$), 6.66 (apt. t, J_{HH} = 8 Hz, 1 H, H$_{arom}$). ^{13}C{^{1}H} (125.7 MHz, benzene-d_6) δ 134.6 (CCl), 132.0 (CH$_{arom}$), 131.9 (CH$_{arom}$), 129.9 (CH$_{arom}$), 129.8 (CH$_{arom}$), 128.8 (CH$_{arom}$), 128.7 (CH$_{arom}$), 125.6 (C$_{arom}$), 123.4 (C$_{arom}$), 91.3 (C$_{alkyne}$), 88.6 (C$_{alkyne}$).

1-chloro-2-(2-phenylethynyl)-benzene
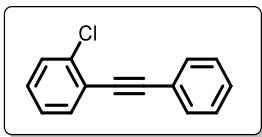
^{1}H NMR (300 MHz, benzene-d_6) δ 7.54 (m, 2 H, H$_\text{arom}$), 7.35 (m, 1 H, H$_\text{arom}$), 7.11 (m, 1 H, H$_\text{arom}$), 6.98 (m, 3 H, H$_\text{arom}$), 6.68 (m, 2 H, H$_\text{arom}$). ^{13}C{^{1}H} (75.5 MHz, benzene-d_6) δ 136.4 (CCl), 133.5 (CH$_\text{arom}$), 132.1 (CH$_\text{arom}$), 129.6 (CH$_\text{arom}$), 129.4 (CH$_\text{arom}$), 128.8 (CH$_\text{arom}$), 128.7 (CH$_\text{arom}$), 126.6 (CH$_\text{arom}$), 123.8 (C$_\text{arom}$), 123.5 (C$_\text{arom}$), 95.4 (C$_\text{alkyne}$), 86.9 (C$_\text{alkyne}$).

1-bromo-2-(2-phenylethynyl)-benzene
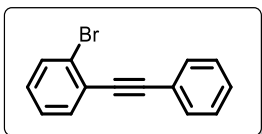
^{1}H NMR (500 MHz, benzene-d_6) δ 7.56 – 7.54 (2 H, H$_\text{arom}$), 7.32 (m, 2 H, H$_\text{arom}$), 7.00 – 6.99 (3 H, H$_\text{arom}$), 6.74 (m, 1 H, H$_\text{arom}$), 6.59 (m, 1 H, H$_\text{arom}$). ^{13}C{^{1}H} (125.7 MHz, benzene-d_6) δ 140.5 (CBr), 133.5 (CH$_\text{arom}$), 132.8 (CH$_\text{arom}$), 132.1 (CH$_\text{arom}$), 129.5 (CH$_\text{arom}$), 128.8 (CH$_\text{arom}$), 128.7 (CH$_\text{arom}$), 128.6 (CH$_\text{arom}$), 127.1 (CH$_\text{arom}$), 126.2 (CH$_\text{arom}$), 126.0 (C$_\text{arom}$), 123.5 (C$_\text{arom}$), 94.7 (C$_\text{alkyne}$), 88.8 (C$_\text{alkyne}$).

1-nitro-4-(2-phenylethynyl)-benzene
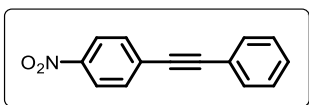
^{1}H NMR (500 MHz, benzene-d_6) δ 7.66 (apt. d, J_HH = 8 Hz, 2 H, H$_\text{arom}$), 7.46 – 7.45 (m, 2 H, H$_\text{arom}$), 7.05 – 6.99 (5 H, H$_\text{arom}$). ^{13}C{^{1}H} (125.7 MHz, benzene-d_6) δ 147.4 (CNO$_2$), 132.2 (CH$_\text{arom}$), 132.0 (CH$_\text{arom}$), 129.7 (C$_\text{arom}$), 129.4 (CH$_\text{arom}$), 128.8 (CH$_\text{arom}$), 123.7 (CH$_\text{arom}$), 122.8 (C$_\text{arom}$), 94.6 (C$_\text{alkyne}$), 88.3 (C$_\text{alkyne}$).

1-nitro-3-(2-phenylethynyl)-benzene
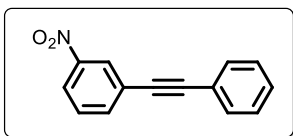
^{1}H NMR (500 MHz, benzene-d_6) δ 8.16 (m, 1 H, H$_\text{arom}$), 7.61 (m, 1 H, H$_\text{arom}$), 7.47 – 7.46 (3 H, H$_\text{arom}$), 7.22 (m, 2 H, H$_\text{arom}$), 7.03 – 7.01 (5 H, H$_\text{arom}$), 6.56 (apt. t, J_HH = 8 Hz, 2 H, H$_\text{arom}$). ^{13}C{^{1}H} (125.7 MHz, benzene-d_6) δ 148.1 (CNO$_2$), 136.2 (CH$_\text{arom}$), 131.6 (CH$_\text{arom}$),

167

128.8 (CH$_{arom}$), 128.7 (CH$_{arom}$), 128.4 (CH$_{arom}$), 127.9 (C$_{arom}$), 126.1 (CH$_{arom}$), 124.6 (C$_{arom}$), 122.4 (CH$_{arom}$), 91.8 (C$_{alkyne}$), 87.2 (C$_{alkyne}$).

4-(2-phenylethynyl)-benzonitrile
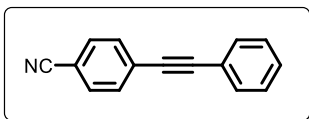
^{1}H NMR (500 MHz, benzene-d_6) δ 7.46 – 7.44 (2 H, H$_{arom}$), 7.02 – 6.99 (5 H, H$_{arom}$), 6.80 (m, 2 H, H$_{arom}$). ^{13}C{^{1}H} (125.7 MHz, benzene-d_6) δ 132.0 (CH$_{arom}$), 131.9 (CH$_{arom}$), 129.2 (CH$_{arom}$), 128.8 (CH$_{arom}$), 127.7 (C$_{arom}$), 122.9 (C$_{arom}$), 118.4 (*C*N), 112.2 (*C*CN), 93.8 (CH$_{alkyne}$), 88.5 (CH$_{alkyne}$).

3-(2-phenylethynyl)-pyridine
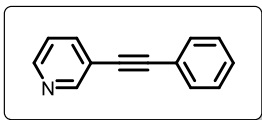
^{1}H NMR (500 MHz, benzene-d_6) δ 8.92 (apt. s, 1 H, H$_{arom}$), 8.35 (m, 1 H, H$_{arom}$), 7.46 – 7.43 (2 H, H$_{arom}$), 7.36 (m, 1 H, H$_{arom}$), 7.01 – 6.99 (3 H, H$_{arom}$), 6.56 (m, 1 H, H$_{arom}$). ^{13}C{^{1}H} (125.7 MHz, benzene-d_6) δ 152.8 (CH$_{arom}$), 149.1 (CH$_{arom}$), 138.0 (CH$_{arom}$), 132.0 (CH$_{arom}$), 128.9 (CH$_{arom}$), 128.8 (CH$_{arom}$), 123.2 (C$_{arom}$), 122.9 (CH$_{arom}$), 120.6 (C$_{arom}$), 93.0 (C$_{alkyne}$), 86.9 (C$_{alkyne}$).

3-(2-phenylethynyl)-thiophene
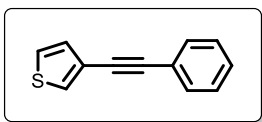
^{1}H NMR (500 MHz, benzene-d_6) δ 7.51 – 7.49 (2 H, H$_{arom}$), 7.19 (m, 1 H, H$_{arom}$), 7.04 (m, 1 H, H$_{arom}$), 7.01 – 6.97 (3 H, H$_{arom}$), 6.69 (m, 1 H, H$_{arom}$). ^{13}C{^{1}H} (125.7 MHz, benzene-d_6) δ 131.9 (CH$_{arom}$), 130.1 (CH$_{arom}$), 128.9 (CH$_{arom}$), 128.7 (CH$_{arom}$), 128.4 (CH$_{arom}$), 125.6 (CH$_{arom}$), 123.9 (C$_{arom}$), 122.9 (C$_{arom}$), 89.6 (C$_{alkyne}$), 85.4 (C$_{alkyne}$).

4.4.3.5 Characterization Data of Alkane Products

1,1'-(1,2-ethanediyl)bis-benzene
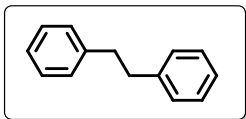
Yield: **93 %**; Isolated Yield: **92 %**

^{1}H NMR (500 MHz, benzene-d_6) δ 7.15 – 7.12 (4 H, H$_{arom}$), 7.08 – 7.05 (2 H, H$_{arom}$), 7.01 – 6.99 (4 H, H$_{arom}$), 2.74 (s, 4 H, H$_{alkane}$). ^{13}C{^{1}H} (125.7 MHz, benzene-d_6) δ 142.0 (C$_{arom}$), 128.8 (CH$_{arom}$), 128.6 (CH$_{arom}$), 126.2 (CH$_{arom}$), 38.2 (CH$_{alkane}$).

2-(2-phenylethyl)-naphthalene
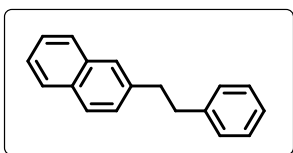
Yield: **99%**

^{1}H NMR (500 MHz, benzene-d_6) δ 7.66 – 7.59 (3 H, H$_{arom}$), 7.42 (s, 1 H, H$_{arom}$), 7.29 – 7.25 (2 H, H$_{arom}$), 7.15 – 7.03 (6 H, H$_{arom}$), 2.91 – 2.80 (4 H, H$_{alkane}$). ^{13}C{^{1}H} (125.7 MHz, benzene-d_6) δ 142.0 (C$_{arom}$), 139.5 (C$_{arom}$), 134.3 (C$_{arom}$), 132.7 (C$_{arom}$), 128.8 (CH$_{arom}$), 128.7 (CH$_{arom}$), 127.7 (CH$_{arom}$), 127.0 (CH$_{arom}$), 126.3 (CH$_{arom}$), 126.2 (CH$_{arom}$), 125.5 (CH$_{arom}$), 38.3 (CH$_{alkane}$), 38.1 (CH$_{alkane}$).

1-(2-phenylethyl)-4-(trimethylsilyl)-benzene
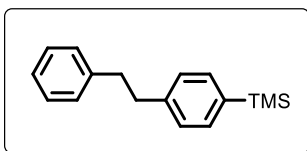
Yield: **73 %**

^{1}H NMR (500 MHz, benzene-d_6) δ 7.44 (apt. d, J_{HH} = 8 Hz, 2 H, H$_{arom}$), 7.31 (apt. s, 1 H, H$_{arom}$), 7.14 – 7.13 (2 H, H$_{arom}$), 7.09 – 7.08 (2H, H$_{arom}$), 7.04 – 7.02 (2 H, H$_{arom}$), 2.79 (s, 4 H, H$_{alkane}$), 0.23 (s, 9 H, Si*Me₃*). ^{13}C{^{1}H} (125.7 MHz, benzene-d_6) δ 142.8 (C$_{arom}$), 142.0 (C$_{arom}$), 137.5 (C$_{arom}$), 133.8 (CH$_{arom}$), 129.3 (CH$_{arom}$), 128.8 (CH$_{arom}$), 128.6 (CH$_{arom}$), 128.4 (CH$_{arom}$), 126.2 (CH$_{arom}$), 38.16 (CH$_{alkane}$), -0.96 (Si*Me₃*).

Propylbenzene
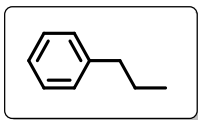
Yield: **93 %**

^{1}H NMR (300 MHz, benzene-d_6) δ 7.20 – 7.15 (2 H, H$_{arom}$), 7.10 – 7.04 (3 H, H$_{arom}$), 2.43 (apt. t, $^{3}J_{HH}$ = 8 Hz, H$_{alkane}$), 1.51 (m, 2 H, H$_{alkane}$), 0.82 (apt. t, $^{3}J_{HH}$ = 7 Hz, 3 H, H$_{alkane}$). ^{13}C{^{1}H} (125.7 MHz, benzene-d_6) δ 142.7 (C$_{arom}$), 128.8 (CH$_{arom}$), 128.6 (CH$_{arom}$), 126.0 (CH$_{arom}$), 38.3 (CH$_{alkane}$), 24.9 (CH$_{alkane}$), 13.9 (CH$_{alkane}$).

Butylbenzene
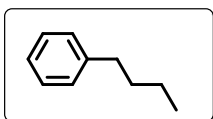
Yield: **65 %**

^{1}H NMR (500 MHz, benzene-d_6) δ 7.19 – 7.18 (2 H, H$_{arom}$), 7.09 – 7.06 (3 H, H$_{arom}$), 2.47 (t, 2 H, H$_{alkane}$), 1.48 (m, 2 H, H$_{alkane}$), 1.23 (m, 2 H, H$_{alkane}$), 0.84 (t, 3 H, H$_{alkane}$). ^{13}C{^{1}H} (125.7 MHz, benzene-d_6) δ 143.0 (C$_{arom}$), 128.8 (CH$_{arom}$), 128.6 (CH$_{arom}$), 126.0 (CH$_{arom}$), 36.0 (CH$_{alkane}$), 34.0 (CH$_{alkane}$), 22.6 (CH$_{alkane}$), 14.1 (CH$_{alkane}$).

1-methoxy-4-(2-phenylethyl)-benzene
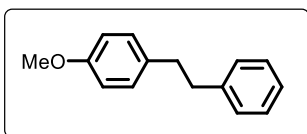
Yield: **87 %**

Isolated Yield: **93 %**

^{1}H NMR (500 MHz, benzene-d_6) δ 7.16 – 7.14 (2 H, H$_{arom}$), 7.08 (m, 1 H, H$_{arom}$), 7.03 (m, 2 H, H$_{arom}$), 6.93 – 6.92 (2 H, H$_{arom}$), 6.77 – 6.76 (2 H, H$_{arom}$), 3.33 (s, 3 H, O*Me*), 2.76 (m, 4 H, H$_{alkane}$). ^{13}C{^{1}H} (125.7 MHz, benzene-d_6) δ 158.6 (C$_{arom}$), 142.1 (C$_{arom}$), 133.9 (C$_{arom}$), 129.7 (CH$_{arom}$), 128.9 (CH$_{arom}$), 128.6 (CH$_{arom}$), 126.2 (CH$_{arom}$), 114.2 (CH$_{arom}$), 54.8 (O*Me*), 38.5 (CH$_{alkane}$), 37.3 (CH$_{alkane}$).

1-methoxy-3-(2-phenylethyl)-benzene
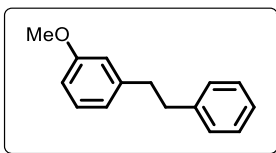
Yield: **90 %**

^{1}H NMR (500 MHz, benzene-d_6) δ 7.15 – 7.12 (2 H, H$_{arom}$), 7.09 – 7.06 (2 H, H$_{arom}$), 7.00 (m, 2 H, H$_{arom}$), 6.73 – 6.68 (3 H, H$_{arom}$), 3.34 (s, 3 H, O*Me*), 2.76 (apt. s, 4 H, H$_{alkane}$). ^{13}C{^{1}H} (125.7 MHz, benzene-d_6) δ 160.4 (*C*OMe), 143.6 (C$_{arom}$), 142.0 (C$_{arom}$), 129.6 (CH$_{arom}$), 128.8 (CH$_{arom}$), 128.6 (CH$_{arom}$), 126.2 (CH$_{arom}$), 121.2 (CH$_{arom}$), 114.8 (CH$_{arom}$), 111.7 (CH$_{arom}$), 54.7 (O*Me*), 38.2 (CH$_{alkane}$), 38.1 (CH$_{alkane}$).

1-methoxy-2-(2-phenylethyl)-benzene
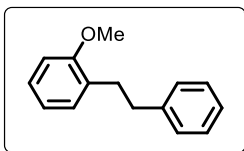
Yield: **84 %**

^{1}H NMR (300 MHz, benzene-d_6) δ 7.12 – 7.00 (7 H, H$_{arom}$), 6.82 (m, 1 H, H$_{arom}$), 6.55 (m, 1 H, H$_{arom}$), 3.31 (s, 3 H, O*Me*), 3.03 – 2.87 (4 H, H$_{alkane}$). ^{13}C{^{1}H} (75.5 MHz, benzene-d_6) δ 157.9 (*C*OMe), 124.7 (C$_{arom}$), 130.3 (CH$_{arom}$), 129.3 (C$_{arom}$), 128.9 (CH$_{arom}$), 128.6 (CH$_{arom}$), 127.5 (CH$_{arom}$), 126.1 (CH$_{arom}$), 120.8 (CH$_{arom}$), 110.5 (CH$_{arom}$), 54.8 (O*Me*), 36.7 (CH$_{alkane}$), 33.0 (CH$_{alkane}$).

1-ethyl-4-[2-(4-methoxyphenyl)ethyl]-benzene
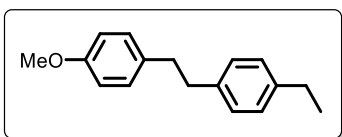
Yield: **90 %**

^{1}H NMR (300 MHz, benzene-d_6) δ 7.29 (apt. s, 3 H, H$_{arom}$), 7.16 (m, 1 H, H$_{arom}$), 7.09 (m, 2 H, H$_{arom}$), 6.90 (m, 2 H, H$_{arom}$), 3.45 (s, 3 H, O*Me*), 2.92 (apt. s, 4 H, H$_{alkane}$), 2.60 (q, $^3J_{HH}$ = 8 Hz, 2 H, C*H$_2$*Me), 1.24 (t, $^3J_{HH}$ = 8 Hz, 3 H, CH$_2$*Me*). ^{13}C{^{1}H} (125.7 MHz, benzene-d_6) δ 158.6 (*C*OMe), 141.8 (C$_{arom}$), 139.4 (C$_{arom}$), 134.1 (C$_{arom}$), 129.7 (CH$_{arom}$), 128.9 (CH$_{arom}$), 128.1 (CH$_{arom}$), 114.2 (CH$_{arom}$), 54.8 (O*Me*), 38.2 (CH$_{alkane}$), 37.5 (CH$_{alkane}$), 28.9 (*C*H$_2$CH$_3$), 15.9 (CH$_2$*C*H$_3$).

2-[4-[2-(4-methoxyphenyl)ethyl]phenyl]-4,4,5,5-tetramethyl-1,3,2-dioxaborolane
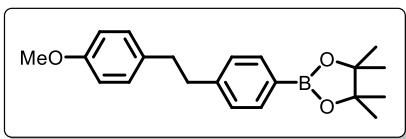
Yield: **86 %**

^{1}H NMR (300 MHz, benzene-d_6) δ 8.14 (apt. d, J_{HH} = 8 Hz, 2 H, H$_{arom}$), 7.08 (apt. d, J_{HH} = 8 Hz, 2 H, H$_{arom}$), 6.89 (m, 2 H, H$_{arom}$), 6.74 (m, 2 H, H$_{arom}$), 3.32 (s, 3 H, OMe), 2.72 (apt. s, 4 H, H$_{alkane}$), 1.13 (s, 12 H, BPin). ^{13}C{^{1}H} (125.7 MHz, benzene-d_6) δ 158.6 (C$_{arom}$), 145.6 (C$_{arom}$), 135.6 (CH$_{arom}$), 133.9 (C$_{arom}$), 130.7 (C$_{arom}$), 129.7 (CH$_{arom}$), 128.5 (CH$_{arom}$), 114.1 (CH$_{arom}$), 83.6 (BPin), 54.8 (OMe), 38.7 (CH$_{alkane}$), 37.1 (CH$_{alkane}$), 25.0 (BPin).

1-methyl-4-(2-phenylethyl)-benzene
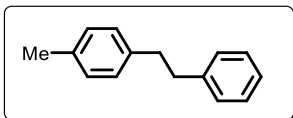
Yield: **87 %**

^{1}H NMR (500 MHz, benzene-d_6) δ 7.15 – 7.13 (2 H, H$_{arom}$), 7.07 (m, 1 H, H$_{arom}$), 7.03 – 7.01 (2 H, H$_{arom}$), 6.99 – 6.94 (4 H, H$_{arom}$), 2.77 (apt. s, 4 H, H$_{alkane}$), 2.14 (s, 3 H, Me). ^{13}C{^{1}H} (125.7 MHz, benzene-d_6) δ 142.1 (C$_{arom}$), 139.0 (C$_{arom}$), 135.4 (C$_{arom}$), 129.3 (CH$_{arom}$), 128.8 (CH$_{arom}$), 128.7 (CH$_{arom}$), 128.6 (CH$_{arom}$), 126.2 (CH$_{arom}$), 38.4 (CH$_{alkane}$), 37.8 (CH$_{alkane}$), 21.1 (Me).

1-methyl-3-(2-phenylethyl)-benzene
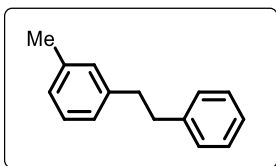
Yield: **88 %**

^{1}H NMR (500 MHz, benzene-d_6) δ 7.15 – 7.14 (2 H, H$_{arom}$), 7.12 – 7.07 (2 H, H$_{arom}$), 7.05 – 7.03 (2 H, H$_{arom}$), 6.92 – 6.86 (3 H, H$_{arom}$), 2.77 (apt. s, 4 H, H$_{alkane}$), 2.15 (s, 3 H, Me). ^{13}C{^{1}H} (125.7 MHz, benzene-d_6) δ 142.2 (C$_{arom}$), 142.0 (C$_{arom}$), 137.8 (C$_{arom}$), 129.6 (CH$_{arom}$), 128.8 (CH$_{arom}$), 128.6 (CH$_{arom}$), 128.5 (CH$_{arom}$), 127.0 (CH$_{arom}$), 126.2 (CH$_{arom}$), 125.9 (CH$_{arom}$), 38.3 (CH$_{alkane}$), 38.2 (CH$_{alkane}$), 21.4 (Me).

1,3-dimethyl-5-(2-phenylethyl)-benzene
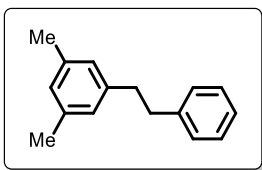
Yield: **86 %**

^{1}H NMR (500 MHz, benzene-d_6) δ 7.18 – 7.15 (2 H, H$_{arom}$), 7.09 – 7.06 (3 H, H$_{arom}$), 6.74 – 6.73 (3 H, H$_{arom}$), 2.84 – 2.76 (4 H, H$_{alkane}$), 2.17 (s, 6 H, 2*Me*). [13]C{[1]H} (125.7 MHz, benzene-d_6) δ 142.3 (*C*Me), 141.9 (C$_{arom}$), 137.7 (C$_{arom}$), 128.8 (CH$_{arom}$), 128.6 (CH$_{arom}$), 127.9 (CH$_{arom}$), 126.8 (CH$_{arom}$), 126.2 (CH$_{arom}$), 38.5 (CH$_{alkane}$), 38.3 (CH$_{alkane}$), 21.4 (*Me*).

1-(1-methylethyl)-3-(2-phenylethyl)-benzene
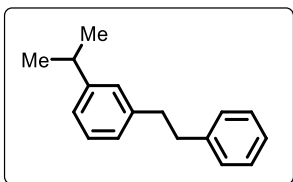
Yield: **91 %**

^{1}H NMR (500 MHz, benzene-d_6) δ 7.15 – 7.13 (3 H, H$_{arom}$), 7.07 (m, 1 H, H$_{arom}$), 7.03 – 6.99 (3 H, H$_{arom}$), 6.95 – 6.91 (2 H, H$_{arom}$), 2.79 (apt. s, 4 H, H$_{alkane}$), 2.73 (m, 1 H, C*H*Me$_2$), 1.17 (s, 3 H, CH*Me$_2$*), 1.16 (s, 3 H, CH*Me$_2$*). [13]C{[1]H} (125.7 MHz, benzene-d_6) δ 149.0 (C$_{arom}$), 142.1 (C$_{arom}$), 142.0 (C$_{arom}$), 128.9 (CH$_{arom}$), 128.7 (CH$_{arom}$), 128.6 (CH$_{arom}$), 127.1 (CH$_{arom}$), 126.3 (CH$_{arom}$), 126.2 (CH$_{arom}$), 124.3 (CH$_{arom}$), 38.4 (CH$_{alkane}$), 34.5 (*C*HMe$_2$), 24.1 (CH*Me$_2$*).

1-(1,1-dimethylethyl)-4-(2-phenylethyl)-benzene
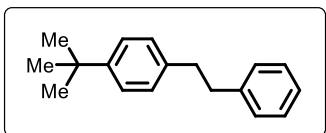
Yield: **96 %**

^{1}H NMR (300 MHz, benzene-d_6) δ 7.26 (m, 2 H, H$_{arom}$), 7.15 – 7.13 (2 H, H$_{arom}$), 7.09 – 7.03 (5 H, H$_{arom}$), 2.80 (apt. s, 4 H, H$_{alkane}$), 1.25 (s, 8 H, C*Me$_3$*). [13]C{[1]H} (75.5 MHz, benzene-d_6) δ 148.7 (C$_{arom}$), 142.2 (C$_{arom}$), 139.1 (C$_{arom}$), 128.8 (CH$_{arom}$), 128.6 (CH$_{arom}$), 128.5 (CH$_{arom}$), 126.2 (CH$_{arom}$), 125.5 (CH$_{arom}$), 38.3 (CH$_{alkane}$), 37.7 (CH$_{alkane}$), 34.4 (*C*Me$_3$), 31.6 (C*Me$_3$*).

1-(2-phenylethyl)-4-(trifluoromethyl)-benzene
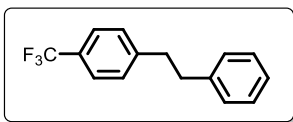
Yield: **88 %**

^{1}H NMR (500 MHz, benzene-d_6) δ 7.30 (apt. d, J_{HH} = 8 Hz, 2 H, H$_{arom}$), 7.15 – 7.12 (2 H, H$_{arom}$), 7.07 (m, 1 H, H$_{arom}$), 6.92 (apt. d, J_{HH} = 8 Hz, 2 H, H$_{arom}$), 6.73 (apt. d, J_{HH} = 8 Hz, 2 H), 2.57 (m, 4 H, H$_{alkane}$). ^{19}F {^{1}H} (282.4 MHz, benzene-d_6) δ -62.0. ^{13}C{^{1}H} (75.5 MHz, benzene-d_6) δ 145.9 (C$_{arom}$), 141.3 (C$_{arom}$), 129.1 (CH$_{arom}$), 128.7 (CH$_{arom}$), 128.0 (apt. q, $^1J_{CF}$ = 288.3 Hz, CF$_3$), 126.5 (CH$_{arom}$), 125.4 (m, CH$_{arom}$), 37.6 (CH$_{alkane}$), 37.5 (CH$_{alkane}$). CCF$_3$ signals hidden in baseline.

1-(2-phenylethyl)-3-(trifluoromethyl)-benzene
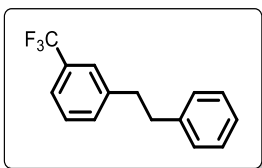
Yield: **86 %**

^{1}H NMR (300 MHz, benzene-d_6) δ 7.26 – 7.23 (2 H, H$_{arom}$), 7.13 – 7.06 (3 H, H$_{arom}$), 6.91 – 6.81 (4 H, H$_{arom}$), 2.54 (apt. s, 4 H, H$_{alkane}$). ^{19}F {^{1}H} (282.4 MHz, benzene-d_6) δ -62.2. ^{13}C{^{1}H} (75.5 MHz, benzene-d_6) δ 142.9 (C$_{arom}$), 141.2 (C$_{arom}$), 132.1 (CH$_{arom}$), 128.9 (CH$_{arom}$), 128.7 (CH$_{arom}$), 128.6 (CH$_{arom}$), 127.0 (apt. q, $^2J_{CF}$ = 15 Hz, CCF$_3$), 126.4 (CH$_{arom}$), 125.5 (m, CH$_{arom}$), 123.0 (m, CH$_{arom}$), 37.6 (CH$_{alkane}$), 37.5 (CH$_{alkane}$). CF$_3$ signals hidden in baseline.

1-(2-phenylethyl)-3,5-bis(trifluoromethyl)-benzene
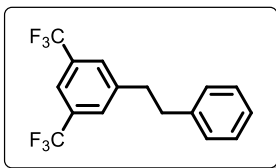
Yield: **66 %**

^{1}H NMR (500 MHz, benzene-d_6) δ 7.60 (apt. s, 1 H, H$_{arom}$), 7.16 – 1.15 (3 H, H$_{arom}$), 7.11 (m, 2 H, H$_{arom}$), 6.81 – 6.79 (2 H, H$_{arom}$), 2.36 (s, 4 H, H$_{alkane}$). ^{19}F{^{1}H} (470.6 MHz, benzene-d_6) δ -62.6. ^{13}C{^{1}H} (125.7 MHz, benzene-d_6) δ 144.4 (CH$_{arom}$), 140.4 (CH$_{arom}$), 131.6 (q, $^2J_{CF}$ = 33 Hz, CCF$_3$), 129.0 (br, CH$_{arom}$), 128.7 (CH$_{arom}$), 128.6 (CH$_{arom}$), 126.7 (C$_{arom}$), 124.0 (q, $^1J_{CF}$ = 274 Hz, CF$_3$), 120.0 (C$_{arom}$), 37.05 (CH$_{alkane}$).

1-fluoro-4-(2-phenylethyl)-benzene
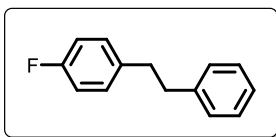
Yield: **96 %**; Isolated Yield: **95 %**

^{1}H NMR (500 MHz, benzene-d_6) δ 7.16 – 7.12 (2 H, H$_{arom}$), 7.07 (m, 1 H, H$_{arom}$), 6.96 (apt. d, J = 8 Hz, 2 H, H$_{arom}$), 6.79 – 6.75 (2 H, H$_{arom}$), 6.71 – 6.69 (2 H, H$_{arom}$), 2.64 – 2.58 (4 H, H$_{alkane}$). ^{19}F $\{^1$H$\}$ (470.6 MHz, benzene-d_6) δ -117.4. ^{13}C$\{^1$H$\}$ (75.5 MHz, benzene-d_6) δ 161.8 (d, $^1J_{CF}$ = 243 Hz, CF), 141.6 (C$_{arom}$), 137.5 (C$_{arom}$), 130.2 (d, J_{CF} = 8 Hz), 128.8 (CH$_{arom}$), 128.6 (CH$_{arom}$), 126.3 (CH$_{arom}$), 115.3 (apt. d, J_{CF} = 21 Hz), 38.1 (CH$_{alkane}$), 37.2 (CH$_{alkane}$).

1-fluoro-3-(2-phenylethyl)-benzene
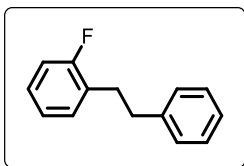
Yield: **80 %**

^{1}H NMR (300 MHz, benzene-d_6) δ 7.14 – 6.96 (5 H, H$_{arom}$), 6.86 – 6.75 (4 H, H$_{arom}$), 2.84 – 2.74 (4 H, H$_{alkane}$). ^{19}F $\{^1$H$\}$ (282.4 MHz, benzene-d_6) δ -118.9. ^{13}C$\{^1$H$\}$ (75.5 MHz, benzene-d_6) δ 161.7 (d, $^1J_{CF}$ = 244 Hz, CF), 141.7 (C$_{arom}$), 131.0 (d, $^2J_{CF}$ = 5 Hz, CH$_{arom}$), 129.0 (apt. d, $^2J_{CF}$ = 13 Hz, C$_{arom}$), 128.8 (CH$_{arom}$), 128.6 (CH$_{arom}$), 127.9 (CH$_{arom}$), 126.3 (CH$_{arom}$), 124.1 (d, J_{CF} = 4 Hz, CH$_{arom}$), 115.4 (d, $^2J_{CF}$ = 22 Hz, CH$_{arom}$), 36.7 (CH$_{alkane}$), 31.4 (CH$_{alkane}$).

Chapter 5: Synthesis and Reactivity of Indolyl(phosphino)silyl Iron Pincer Complexes

In this chapter, all synthetic work was conducted by Helia Hollenhorst. X-Ray crystallographic data was collected and refined by Dr. Michael J. Ferguson and Dr. Yuqiao Zhou of the University of Alberta X-ray Crystallography Laboratory, Edmonton, AB. Elemental analysis was obtained through Galbraith Laboratories, Inc. and ANALEST at the University of Toronto.

5.1 Introduction

In the interest of developing sustainable synthetic methods, homogenous, selective hydrogenation catalysts that feature Earth-abundant 3d-metals such as iron are highly sought-after.[5-8] As described in Chapter 4 of this document, Fe pincer complexes have emerged as leading candidates for catalyst development, and bis(phosphino)silyl iron pincer complexes supported by Cy-PSiP ligation have been shown to be effective pre-catalysts for alkene[37] and alkyne hydrogenation chemistry. Computational and experimental results detailed in Chapter 4 implicate silyl-metal cooperativity that can facilitate catalytic processes involving hydride transfer *via* the formation of η^2-(Si-H) species. This chapter details efforts to explore the coordination chemistry and reactivity of related (^{i}Pr-PSiP^{Ind})Fe complexes, with the goal of furthering the understanding of ligand effects on the chemistry exhibited by such PSiP-ligated iron complexes in order to better understand their utility in hydrofunctionalization catalysis.

5.2 Results and Discussion

5.2.1 Synthesis of Indolyl(phosphino)silyl Pincer Iron Complexes

The synthesis of ^{i}Pr-PSiP^{Ind} supported iron pincer complexes was initially attempted using the methodologies previously established for the synthesis of (Cy-PSiP)Fe species

(see Chapter 4).[37] Treatment of $(py)_4FeCl_2$ (py = pyridine) with the tertiary silane precursor

(^{i}Pr-PSiP^{Ind})H (2-27), followed by addition of 1 equiv. of BnMgCl in THF led to the

formation of paramagnetic (^{i}Pr-PSiP^{Ind})FeCl(py) (5-1, Scheme 5-1), which was

characterized by elemental analysis and X-ray crystallography (Figure 5-1, Table 5-1). An

alternative method involving the addition of 1 equiv. of pyridine to $FeCl_2$ in THF, followed

by the adition of 2-27 and BnMgCl also afforded 5-1, and proved to be operationally

simpler to carry out due to the absence of excess pyridine in the reaction mixture. While

the analogous complex (Cy-PSiP)FeCl(py) (4-1·py) has been previously reported,[37] the

lability of the py ligand in 4-1·py hindered the ability to isolate and fully characterize this

complex, as pyridine loss was observed upon exposure to vacuum. By comparison, 5-1

proved much more amenable to manipulation.
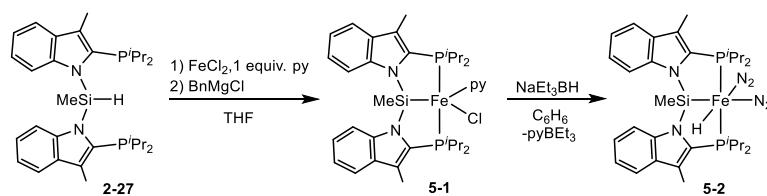
Scheme 5-1. Synthesis of paramagnetic 5-1 and diamagnetic 5-2.
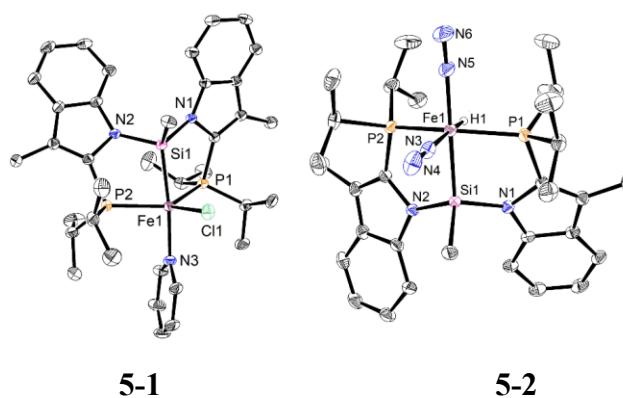
5-1   5-2

Figure 5-1. Crystallographically determined structures of 5-1 and 5-2 with thermal
ellipsoids shown at the 50% probability level. Most hydrogen atoms are omitted for
clarity.

Table 5-1. Selected bond distances (Å) and angles (deg.) for **5-1** and **5-2**.

5-1		5-2	
Fe-P(1) 2.3324(10)	P(1)-Fe-P(2) 135.95(4)	Fe-P(1) 2.2032(8)	P(1)-Fe-P(2) 148.94(3)
Fe-P(2) 2.3239(10)	P(1)-Fe-Si 81.04(4)	Fe-P(2) 2.2171(8)	P(1)-Fe-Si 84.04(3)
Fe-Si 2.2800(11)	P(2)-Fe-Si 80.18(4)	Fe-Si 2.2655(8)	P(2)-Fe-Si 85.66(3)
Fe-Cl 2.3104(10)	Si-Fe-Cl 90.34(4)	Fe-H 1.35(3)	Si-Fe-N(3) 89.57(9)
Fe-N(3) 2.073(3)	Si-Fe-N(3) 172.95(9)	Fe-N(3) 1.824(3)	Si-Fe-N(5) 178.25(10)
		Fe-N(5) 1.879(3)	Si···H 2.53

Treatment of **5-1** with 1 equiv. of NaEt$_3$BH in benzene solution led to the formation of the diamagnetic hydride complex (^{i}Pr-PSiP^{Ind})FeH(N$_2$)$_2$ (**5-2**, Scheme 5-1). Complex **5-2** is analogous to the previously reported (Cy-PSiP)FeH(N$_2$)$_2$ (**4-5**).[37] While the synthesis of **4-5** requires the addition of BPh$_3$ for the removal of pyridine, BEt$_3$ generated from NaEt$_3$BH was found to be a strong enough Lewis acid for the synthesis of **5-2** without the need for addition of BPh$_3$. The ^{1}H NMR spectrum of **5-2** (benzene-d_6) features a characteristic Fe-*H* resonance at -15.3 ppm (t, $^2J_{HP}$ = 62 Hz; *cf.* -16.3 ppm, $^2J_{PH}$ = 59 Hz for **4-5**). By use of IR spectroscopy, N-N stretching frequencies of 2144 cm^{-1} and 2085 cm^{-1} were measured for **5-2**. The solid state structure of **5-2** was determined by use of single crystal X-ray diffraction techniques and confirms the formulation of this complex as a bis(N$_2$) adduct of a (^{i}Pr-PSiP^{Ind})FeH (Figure 5-1, Table 5-1). While most metrical parameters determined for **5-2** are comparable to those observed for the analogous complex **4-5**, the Si···H distance of 2.53 Å in **5-2** is somewhat longer than the distance of 2.35 Å in **4-5** (Table 5-2). Exposure of **5-2** to vacuum results in the formation of multiple unidentified paramagnetic species, as indicated by broadening of the baseline in the ^{1}H NMR spectrum of **5-2**.

Table 5-2. Selected bond distances (Å) for **5-2** in comparison to **4-5**.

5-2	4-5
Fe-N(3) 1.824(3)	Fe-N(1) 1.8368(12)
Fe-N(5) 1.879(3)	Fe-N(3) 1.8654(12)
Fe-Si 2.2655(8)	Fe-Si 2.2844(4)
Fe-P(1) 2.2032(8)	Fe-P(1) 2.2268(3)
Fe-P(2) 2.2171(8)	Fe-P(2) 2.2147(3)
Fe-H(1) 1.35(3)	Fe-H(1) 1.418(19)
Si···H 2.53	Si···H 2.35

An attempt to synthesize an iron-benzyl complex by treatment of $FeCl_2$ with 1 equiv. of pyridine, followed by the addition of the silane **2-27** and 2 equiv. of BnMgCl in THF afforded a mixture of multiple unidentified products ($^{31}P\{^1H\}$ and ^1H NMR). A minute amount of crystalline material obtained from the crude product mixture was characterized by single X-ray diffraction techniques, revealing an unusual decomposition product **5-3** (Figure 5-2). Cleavage of the Si-N linkage in the ^iPr-PSiP^{Ind} ligand backbone has produced three phosphinoindolyl fragments that are coordinates in a κ^2-P,N manner to two Fe centers in a trigonal paddlewheel configuration. Fe1 features P,P,N-coordination, with two phosphino ligands and one coordinated indolyl ring, while Fe2 features P,N,N-coordination, with one phosphino ligand and two coordinated indolyl rings. The Fe1-Fe2 distance of 2.3056(6) Å is significantly less than the sum of covalent radii for two Fe centers (2.74 Å), consistent with the presence of an Fe-Fe bond. Related diiron complexes featuring trigonal paddlewheel configurations have been reported previously.[94] Although the mechanism associated with the formation of this complex is currently unknown, the structure of **5-3** gives insight into some of the reaction complications that may arise in the synthesis of iron complexes supported by ^iPr-PSiP^{Ind} ligation.

5-3
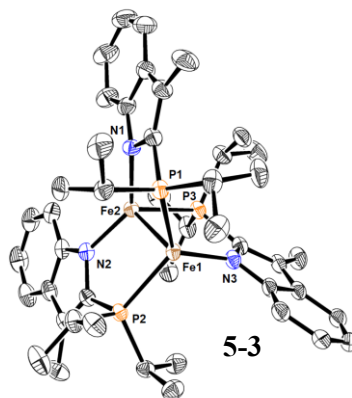
Figure 5-2. Crystallographically determined structures of **5-3** with thermal ellipsoids shown at the 50% probability level. Hydrogen atoms are omitted for clarity. Selected interatomic distances (Å) and angles (deg.) for **5-3** (one of two crystallographically independent molecules): Fe(1)-Fe(2) 2.3056(6), Fe(1)-P(1) 2.4217(8), Fe(1)-P(2) 2.3930(7), Fe(1)-N(3) 1.979(2), Fe(2)-P(3) 2.4497(7), Fe(2)-N(1) 1.972(2), Fe(2)-N(2) 1.996(2), P(1)-Fe(1)-P(2) 124.92(3), P(1)-Fe(1)-N(3) 118.65(6), P(2)-Fe(1)-N(3) 115.76(6), P(3)-Fe(2)-N(1) 106.98(6), P(3)-Fe(2)-N(2) 110.58(6), N(1)-Fe(2)-N(2) 135.24(9).

In an effort to prepare a diiron complex analogous to [(Cy-PSiP)FeBr]$_2$(MgBr$_2$) (**4-9**), the reaction of FeBr$_2$ with 1 equiv. of DMAP in THF solution, followed by the addition of the silane **2-27** and 1 equiv. of BnMgCl was carried out. The paramagnetic diiron complex [(^{i}Pr-PSiP^{Ind})FeBr]$_2$MgBr$_2$(THF) (**5-4**, Scheme 5-2) was obtained in 90% yield *via* this route, and was characterized by elemental analysis and X-ray crystallography (Figure 5-3, Table 5-3). As in the case of **4-9**, either PCy$_3$ or DMAP could be used in the synthesis of **5-4** with similar yields of product obtained in both cases. Heating **5-4** in benzene-d_6 solution at 65 °C for 4 h resulted in no change, as indicated by ^{1}H and ^{31}P{^{1}H} NMR analysis, indicative of the relative thermal stability of **5-4**. While **5-4** was found to exhibit similar coordination geometry to **4-9** in the solid state, a notable structural difference is the coordination of one molecule of THF to Mg in **5-4**. A comparison of the bond distances in **5-4** versus those in **4-9** (Table 5-3) indicates somewhat shorter Fe-Br distances in **5-4** which are accompanied by longer Mg-Br distances.
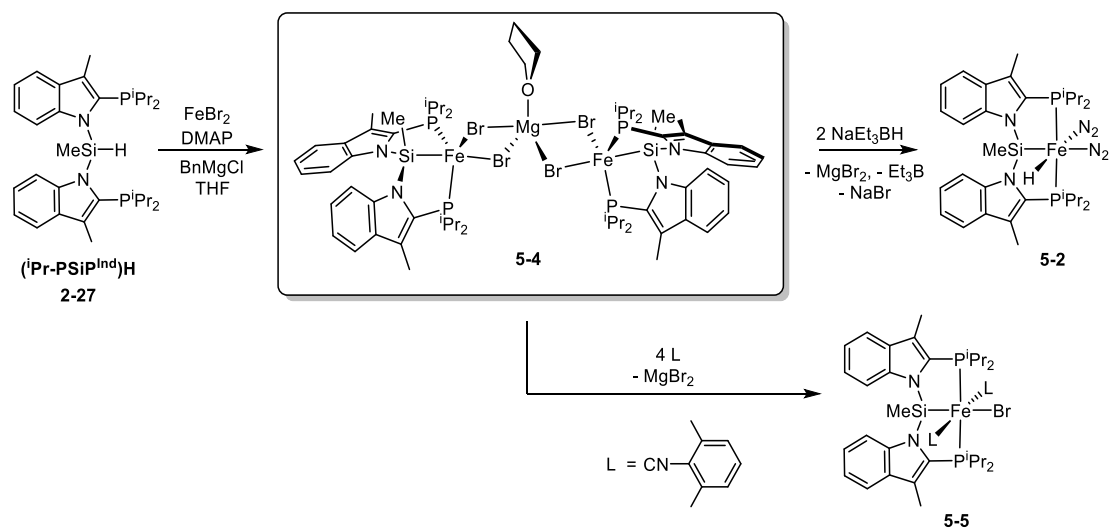
Scheme 5-2. Synthesis of dimeric Mg-bridged indolyl(phosphino)silyl iron complex **5-3**.
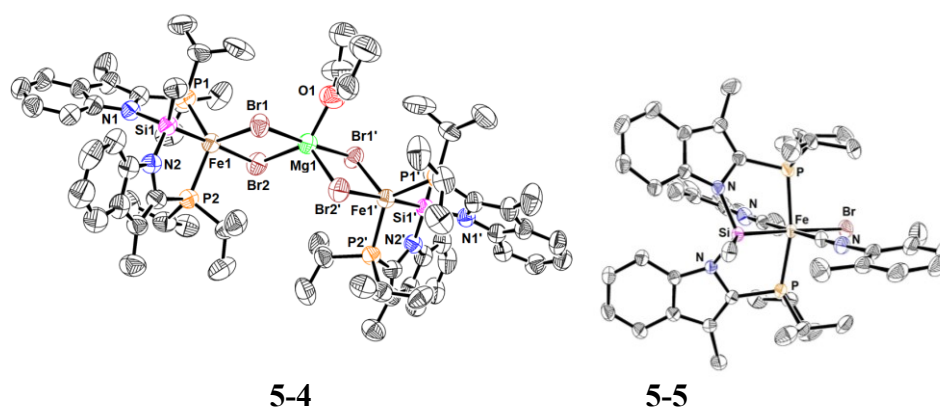
Figure 5-3. Crystallographically determined structures of **5-4** and **5-5** with thermal ellipsoids shown at the 50% probability level. Hydrogen atoms are omitted for clarity.

Table 5-3. Selected bond distances (Å) and angles (deg) for **5-4** in comparison to **4-4**, as well as for **5-5**.

5-4	4-4	5-5
Fe(1)-Si(1) 2.273(3)	Fe(1)-Si(1) 2.314(2)	Fe-Br 2.5422(3)
Fe(1)-Br(2) 2.5099(16)	Fe(1)-Br(2) 2.5770(13)	Fe-P(1) 2.2548(5)
Fe(1)-Br(1) 2.5262(16)	Fe(1)-Br(1) 2.5669(13)	Fe-P(2) 2.2576(6)
Fe(1)-P(1) 2.318(3)	Fe(1)-P(1) 2.317(2)	Fe-Si 2.2341(5)
Fe(1)-P(2) 2.312(3)	Fe(1)-P(2) 2.319(2)	Fe-C(3) 1.8400(19)
Mg(1)-Br(1) 2.6415(10)	Mg(1)-Br(1) 2.479(3)	Fe-C(4) 1.8221(19)
Mg(1)-Br(2) 2.529(3)	Mg(1)-Br(2) 2.487(3)	N(3)-C(3) 1.171(3)
Mg(1)-Br(1') 2.6415(10)	Mg(1)-Br(3) 2.484(3)	N(4)-C(4) 1.168(3)
Mg(1)-Br(2') 2.529(3)	Mg(1)-Br(4) 2.448(3)	Br-Fe-Si 176.021(18)
Mg(1)-O(1) 2.037(16)	P(1)-Fe(1)-P(2) 132.05(8)	P(1)-Fe-P(2) 166.95(2)
P(1)-Fe(1)-P(2) 128.81(11)		C(3)-Fe-C(4) 178.97(9)

Treatment of **5-4** with 4 equiv. of xylyl isocyanide led to the quantitative formation of the diamagnetic complex (^{i}Pr-PSiP^{Ind})FeBr(CNAr)$_2$ (**5-5**, Ar = 2,6-Me$_2$C$_6$H$_3$, Scheme 5-2) by dissociation of MgBr$_2$(THF), indicating that much like **4-9**, complex **5-4** can serve as a source of 2 equiv. of (^{i}Pr-PSiP^{Ind})FeBr. The solid state structure of complex **5-5** was determined by use of single crystal X-ray diffrection techniques, and is essentially isostructural with the Cy-PSiP analogue **4-10** (Figure 5-3, Table 5-3). Furthermore, when **5-4** was treated with 1 atm of CO in benzene-d_6 solution, analysis of the reaction mixture by ^{1}H NMR and ^{31}P{^{1}H} NMR spectroscopy indicated complete consumption of **5-4** and formation of a new paramagnetic Fe species. By comparison **4-9** was unreactive toward CO under similar conditions (see Chapter 4). Lastly, as in the case of the parent Cy-PSiP system, treatment of **5-4** with 2 equiv. of NaEt$_3$BH in benzene solution led to the formation of **5-2** (Scheme 5-2), which could be isolated in 25% *via* this route.

5.2.2 Investigation of Alkene and Alkyne Hydrogenation by (^{i}Pr-PSiP^{Ind}) Iron Complexes

The utility of the iron hydride complex **5-2** as a pre-catalyst in alkene hydrogenation was evaluated using the optimized reaction conditions developed for **4-5** (5 mol% Fe, 10

atm H$_2$, 65 °C, 4 h, benzene-d_6 solution).[37] The hydrogenation of *cis*-4-octene, ethylidenecyclohexane, ethyl butanoate, *cis*-stilbene, and diphenylacetylene was attempted (Scheme 5-3). Unfortunately, while these substrates were readily reduced when **4-5** was used as the source of Fe, the performance of **5-2** was inferior, affording low conversion of starting material in all cases.
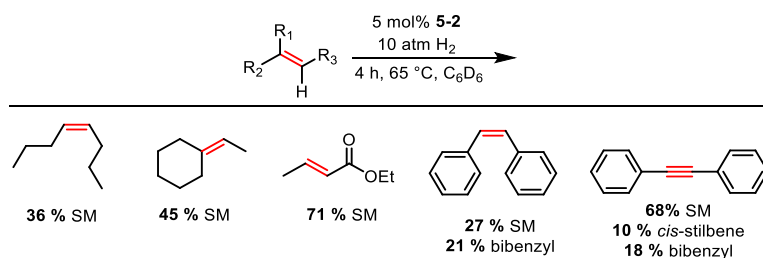
Scheme 5-3. Substrate scope probed for olefin-hydrogenation by **5-2**, indicating low conversions.

The reactivity of **5-4** was likewise probed in alkyne hydrogenation chemistry under the same optimized reaction conditions developed for **4-9** (5 mol % Fe, 1 atm H$_2$, 30 °C, 4 h, benzene-d_6 solution). The substrates tested included diphenylacetylene, 1-phenylpropyne, 4-octyne, and *cis*-stilbene (Scheme 5-4). Unfortunately, **5-4** was found to be unreactive in the hydrogenation of these substrates. Under more forcing reaction conditions of (5 mol % Fe, 10 atm H$_2$, 60 °C, 4 h, 0.228 M in benzene-d_6) diphenylacetylene was hydrogenated to afford ca. 91% bibenzyl and 9% *cis*-stilbene (by ^{1}H NMR integration relative to ferrocene as an internal standard). Under the same conditions ca. 37% conversion of 1-phenylpropyne to propyl benzene could be obtained, with the remainder being unreacted alkyne starting material.

183
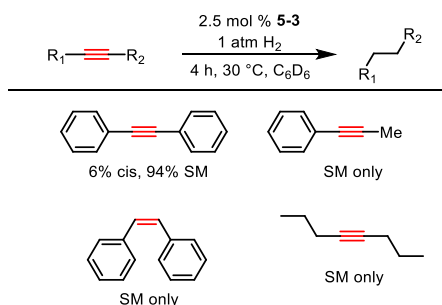
Scheme 5-4. Attempted alkyne hydrogenation reactions with **5-4** using optimized conditions for **4-4** indicate low conversion of starting material.

5.3 Conclusion

The coordination chemistry and reactivity of (^{i}Pr-PSiP^{Ind})Fe complexes was investigated in an effort to expand the library of PSiP-ligated Fe species for application in hydrofunctionalization catalysis. The synthetic strategies developed for the preparation of (Cy-PSiP)Fe complexes were found to be generally applicable to the synthesis of (^{i}Pr-PSiP^{Ind})Fe analogues. An N_2-stabilized iron hydride complex **5-2** analogous to (Cy-PSiP)FeH(N_2)$_2$ proved accessible, although **5-2** appeared to decompose upon exposure to vacuum. A diiron complex featuring two (^{i}Pr-PSiP^{Ind})FeBr moieties coordinated to one MgBr$_2$(THF) moiety (**5-4**) analogous to fragment **4-9** was also readily synthesized in high yield. While (Cy-PSiP)FeH(N_2)$_2$ and [(Cy-PSiP)FeBr]$_2$(MgBr$_2$) are effective catalysts for alkene and alkyne hydrogenation, respectively, their (^{i}Pr-PSiP^{Ind})Fe analogues were found to be significantly less active in such reactivity. Although the source of the discrepancy in catalytic activity between Cy-PSiP- and ^{i}Pr-PSiP^{Ind}-ligated complexes is not known, these observations highlight the profound impact of ligand design on metal reactivity.

5.4 Experimental Section

5.4.1 General Considerations

All experiments were conducted under nitrogen in a glovebox or Parr Bomb apparatus using standard Schlenk techniques. Dry, oxygen-free solvents were used unless otherwise indicated. All non-deuterated solvents were deoxygenated by sparging with nitrogen. Benzene was subsequently passed through a double column purification system (one activated alumina column and one column packed with activated Q-5). Tetrahydrofuran was purified by distillation from Na/benzophenone. All purified solvents were stored over 4 Å molecular sieves. Benzene-d_6 was degassed *via* sparging for 30 minutes and stored over 4 Å molecular sieves. All other reagents were purchased from commercial suppliers and used as received. The tertiary silane (Cy-PSiP)H was prepared according to a previously published procedure.[33a] ^{1}H, ^{13}C, ^{31}P, and ^{29}Si NMR characterization data were collected at 300K with chemical shifts reported in parts per million downfield of SiMe$_4$ (for ^{1}H, ^{13}C, and ^{29}Si), or 85% H$_3$PO$_4$ in D$_2$O (for ^{31}P). Chemical shift ranges are cited to indicate overlapping resonances. The following abbreviations were utilized to assign NMR data: s = singlet; d = doublet; t = triplet; q = quartet; m = multiplet; br = broad; dm = doublet of multiplets; apt = apparent. Please note that a ^{13}C NMR shift at ca. 110 ppm is due to an instrument artifact. X-Ray crystallographic data was collected and refined on a fee-for-service basis by Drs. Michael J. Ferguson and Yuqiao Zhou of the University of Alberta X-ray Crystallography Laboratory, Edmonton, AB.

5.4.2 Synthetic Details and Characterization Data

(^{i}Pr-PSiP^{Ind})FeCl(py) (5-1). A suspension of FeCl$_2$ (0.047 g, 0.37 mmol) in ca. 3 mL of THF was treated with pyridine (0.030 mL, 0.37 mmol), and the reaction mixture was allowed to stir magnetaically for 20 minutes at room temperature. A solution of (^{i}Pr-PSiP^{Ind})H (0.20 g, 0.37 mmol) in ca. 3 mL of THF was added to the reaction mixture, which was allowed to stir for another 20 minutes at room temperature. BnMgCl (1.4 M in THF, 0.27 mL, 0.37 mmol) was diluted with 2 mL of THF and added dropwise to the reaction mixture while stirring. A color change from yellow-beige to orange was observed. The reaction mixture was allowed to stir for an additional 18 h at room temperature. The mixture was subsequently evaporated to dryness and the remainingresidue was triturated with pentane (4 × 3 mL). The material obtained was dissolved in ca. 5 mL of 2:1 benzene:pentane and filtered through Celite. The volatile components of the filtrate solution were removed under vacuum and the remaining residue was triturated with pentane (4 × 3 mL) and washed with pentane (3 × 2 mL). The remaining solid was dried under vacuum to afford 5-1 (0.16 g, 62% yield) as an orange powder. ^{1}H NMR (300 MHz, benzene-d_6): δ 72.9, 65.6, 31.2, 15.1, 13.1, 9.55, 9.17, 8.24, 7.86, 7.40, 7.29, 6.89, 4.23, 3.59, 1.64, 1.29, 1.26, 1.24, -3.26, -6.23, -0.78, -28.4, -45.5, -61.6.

(^{i}Pr-PSiP^{Ind})FeH(N$_2$)$_2$ (5-2). *Method 1:* A room temperature solution of 5-1 (0.047 g, 0.07 mmol) in ca. 5 mL of benzene was treated with NaEt$_3$BH (1 M in toluene, 0.067 mL, 0.07 mmol) diluted with 2 mL benzene, which was added dropwise while stirring. A color change from orange to yellow was observed and the reaction mixture was allowed to stir magentically for an additional 18 h at room temperature. The mixture was then filtered through Celite and evaporated to dryness. The remaining residue was triturated with

pentane (3 × 2 mL) and washed with pentane (1 x 2 mL), and the material remaining was dried under vacuum to obtain crude **5-2** as a beige solid. Crystallization of this material from a concentrated ether solution at -35 °C afforded **5-2** as a beige crystalline solid in ca. 20 % yield. Subsequent exposure of this material to vacuum results in partial decomposition. *Method 2:* A solution of **5-4** (0.083 g, 0.12 mmol) in ca. 5 mL of benzene was treated with NaEt$_3$BH (1 M in toluene, 0.12 mL, 0.12 mmol), which was added dropwise while stirring. A color change from orange to yellow was observed and the reaction mixture was allowed to react for an additional 18 h at room temperature. The mixture was then filtered through Celite and evaporated to dryness. The remaining residue was triturated with pentane (3 × 2 mL) and washed with pentane (2 × 2 mL) to obtain crude **5-2** as a beige solid that was recrystallized from ether at -35 °C to afford **5-2** in ca. 25 % yield. Exposure fo this material to vacuum led to partial decomposition. ^{1}H NMR (300 MHz, benzene-d_6): δ 7.97 (m, 2 H, H$_{arom}$), 7.67 (m, 2 H, H$_{arom}$), 7.22 (m, 4 H, H$_{arom}$), 2.79–2.60 (4 H, CHMe$_2$), 2.34 (s, 6 H, Indole-Me), 1.44–0.93 (24 H, CHMe_2), 0.69 (SiMe), -15.3 (t, $^2J_{HP}$ = 62 Hz, 1 H, Fe-H). ^{13}C{^{1}H} NMR: (75.5 MHz, benzene-d_6): δ 141.4 (C$_{arom}$), 136.7 (C$_{arom}$), 122.6 (CH$_{arom}$), 120.5 (CH$_{arom}$), 119.7 (C$_{arom}$), 119.5 (CH$_{arom}$), 117.3 (C$_{arom}$), 117.1 (CH$_{arom}$), 32.1 (apt. m, CHMe$_2$), 31.6 (apt. m, CHMe$_2$), 22.7 (CHMe_2), 20.2 (CHMe$_2$), 19.7 (CHMe_2), 19.5 (CHMe$_2$), 14.3 (CHMe_2), 11.1 (CHMe_2), 10.0 (Indole-Me), 3.88 (SiMe). ^{31}P{^{1}H} (121.5 MHz, benzene-d_6): δ 72.2. ^{29}Si NMR (99.4 MHz, benzene-d_6): δ 75.8. IR (thin film, cm^{-1}): 2279 (FeH), 2144 (FeN_2), 2085 (FeN_2).

[(^{i}Pr-PSiP^{Ind})FeBr]$_2$MgBr$_2$(THF) (5-4). A suspension of FeBr$_2$ (0.11 g, 0.49 mmol) in ca. 3 mL of THF was treated with a solution of dimethylaminopyridine (0.060 g, 0.49 mmol) in ca, 2 mL of THF. The reaction mixture was allowed to stir at room

temperature for 20 minutes. A solution of (^{i}Pr-PSiP^{Ind})H (0.264 g, 0.49 mmol) in ca. 4 mL of THF was added to the reaction mixture, which was subsequently allowed to stir magentically for another 20 minutes at room temperature. BnMgCl (1.4 M in THF, 0.35 mL, 0.49 mmol) was diluted with 2 mL of THF and added dropwise to the reaction mixture. A color change from beige to red was observed. The reaction mixture was allowed to stir for an additional for 18 h at room temperature, at which point the volatile components were removed under vacuum. The remaining residue was triturated with pentane (4 × 3 mL) and the remaining material was dissolved in ca. 5 mL of 2:1 benzene:pentane and then filtered through Celite. The filtrate solution was solution was evaporated to dryness, and the remaining residue was triturated with pentane (3 × 3 mL) and washed with pentane (3 × 3 mL). The solid residue was dried under vacuum to afford **5-4** (0.36 g, 91% yield) as an orange powder. ^{1}H NMR: (300 MHz, benzene-d_6): δ 73.6, 16.7, 14.4, 10.2, 8.57, 7.91, 7.53, 6.07, 4.03, 3.66, 3.21, 2.87, 2.58, 2.28, 1.92, 1.52, 1.41, 1.22, 0.86, -3.28, -6.77, -48.2, -57.2. Anal. Calcd for $C_{66}H_{98}Br_4Fe_2MgN_4OP_4Si_2$: C, 49.57; H, 6.18; N, 3.50. Found: C, 50.80; H, 5.88; N, 3.97.

(^{i}Pr-PSiP^{Ind})FeBr[CN(2,6-Me$_2$C$_6$H$_3$)]$_2$ (5-5). A solution of **5-4** (0.081 g, 0.05 mmol) in ca. 5 mL of benzene was treated with a solution of xylyl isocyanide (0.026 g, 0.19 mmol) in ca. 2 mL of benzene. An instant color change from red to lighter orange was observed and the mixture was allowed to stir magentically at room temperature for 2 h. The reaction mixture was then filtered through Celite and evaporated to dryness. The residue was triturated with pentane (3 × 2 mL) and washed with pentane (3 × 3 mL). The remaining material was dried under vacuum to afford **5-5** (0.081 g, 87% yield) as an orange powder. ^{1}H NMR (300 MHz, benzene-d_6): δ 8.06 (d, J_{HH} = 8 Hz, 2 H, H$_{arom}$), 7.65 (d, J_{HH} = 8 Hz, 2

H, H$_{arom}$), 7.35 (t, J_{HH} = 8 Hz, 2 H, H$_{arom}$), 7.28 (t, J_{HH} = 8 Hz, 2 H, H$_{arom}$), 6.74 (s, 3 H,

H$_{arom}$), 6.61 (br. s, 1 H, H$_{arom}$), 6.61 (br. s, 1 H, H$_{arom}$), 6.48 (t, J_{HH} = 8 Hz, 1 H, H$_{arom}$), 6.19

(br. s, 1 H, H$_{arom}$), 3.88 (m, 2 H, C*H*Me$_2$), 2.79–2.60 (overlapping resonances, br, 10 H,

C*H*Me$_2$, 2,6-*Me*$_2$C$_6$H$_3$), 2.31 (s, 6 H, Indole-*Me*), 1.51 (m, 6 H, CH*Me*$_2$), 1.30 (m, 6 H,

CH*Me*$_2$), 1.20 (m, 6 H, CH*Me*$_2$), 1.07 (m, 6 H, CH*Me*$_2$), 0.77 (s, 3 H, Si*Me*). ^{13}C{^{1}H} NMR

(125.8 MHz, benzene-*d*$_6$): δ 187.0 (*C*NAr), 179.2 (*C*NAr), 141.6 (C$_{arom}$), 138.7 (C$_{arom}$),

136.7 (C$_{arom}$), 129.9 (C$_{arom}$), 128.7 (C$_{arom}$), 127.3 (CH$_{arom}$), 126.9 (CH$_{arom}$), 122.1 (CH$_{arom}$),

120.6 (CH$_{arom}$), 119.8 (CH$_{arom}$), 119.5 (CH$_{arom}$), 117.9 (CH$_{arom}$), 29.6 (t, $^2J_{CP}$ = 10 Hz,

*C*HMe$_2$), 29.1 (t, $^2J_{CP}$ = 10 Hz, *C*HMe$_2$), 20.9 (CH*Me*$_2$), 20.8 (CH*Me*$_2$), 20.5 (br, 2,6-

Me$_2$C$_6$H$_3$), 20.0 (*C*HMe$_2$), 19.8 (*C*HMe$_2$), 19.4 (br, 2,6-*Me*$_2$C$_6$H$_3$), 17.5 (br, 2,6-*Me*$_2$C$_6$H$_3$),

11.5 (Indole-*Me*), 7.34 (Si*Me*). ^{31}P{^{1}H} (202.5 MHz, benzene-*d*$_6$): δ 61.6. ^{29}Si NMR (300

MHz, benzene-*d*$_6$): δ 82.3. Anal. Calcd for C$_{49}$H$_{65}$BrFeN$_4$P$_2$Si: C, 63.02; H, 6.80; N, 6.00.

Found: C, 62.88; H, 6.74; N, 6.05.

Crystallographic solution and refinement details. Crystallographic data were

obtained between 173(2)-193(2)K on either a Bruker D8/APEX II CCD or a Bruker

PLATFORM/APEX II CCD diffractometer equipped with a CCD area detector using either

graphite-monochromated Mo Kα (λ = 0.71073 Å) radiation (for **5-1** and **5-2**) or Cu Kα (λ

= 1.54184 Å, microfocus source) radiation (for **5-3**, **5-4**, and **5-5**) employing samples that

were mounted in inert oil and transferred to a cold gas stream on the diffractometer. In the

case of **5-4**, data were collected with the detector set at three different positions. Low-angle

(detector 2θ = –33º) data frames were collected using a scan time of 5 seconds, medium-

angle (detector 2 θ = 75º) frames using a scan time of 15 seconds, and high-angle (detector

2 θ = 117º) frames using a scan time of 30 seconds. Programs for diffractometer operation,

data collection, and data reduction (including SAINT) were supplied by Bruker. Data reduction, correction for Lorentz polarization, and absorption correction were each performed. In all cases structure solution was achieved by use of intrinsic phasing methods. All structures were refined by use of full-matrix least-squares procedures (on F^2) with R_1 based on $F_o^2 \geq 2\sigma(F_o^2)$ and wR_2 based on $F_o^2 \geq -3\sigma(F_o^2)$.

Unless otherwise indicated, all non-hydrogen atoms were refined with anisotropic displacement parameters. In the case of **5-3**, two crystallographically independent diiron molecules (A and B) were found in the asymmetric unit; for convenience, only molecule A is discussed in the text. For **5-4**, primed atoms are related to unprimed ones by a 2-fold rotation axis at $1/2$, y, $1/4$. Disorder involving a P^iPr substituent was identified. The corrersponding carbon atoms were modeled over two positions (C31-C33, refined with an occupancy of 0.754(19) and C31A-C33A, refined with an occupancy 0.246(19)). Pairs of atoms (C31 and C31A, C32 and C32A, and C33 and C33A) were refined with common anisotropic displacement parameters. The corresponding P–C, C–C, P···C, and C···C distances within both components of the disordered isopropyl group were restrained to be approximately equal by use of the *SHELXL* **SADI** instruction. Additionally, the rigid-bond restraint (**RIGU**) was applied to improve the quality of the anisotropic displacement parameters of the carbon atoms of the disordered isopropyl group. Disorder was also identifed for the Mg-bound THF molecule, this was addressed by constraining occupancies of the atoms in question (O1, C51-C54) to be 0.5. The rigid-bond restraint was also applied to the carbon atom ADPs of the disordered tetrahydrofuran molecule. A disordered molecule of pentane solvent was also identified in the asymmetric unit, and the occupancies of the corresponding carbon atoms (C1S-C5S) were constrained to be 0.5. Finally, the

disordered pentane molecule was restrained by both **SADI** (C–C and C···C distances) and **RIGU**. In the case of **5-5**, all four P^{i}Pr groups were disordered and the following sets of bond length restraints (**SADI**, 182 restraints) were applied: all <u>P</u>–<u>C</u>H(Me2) distances were restrained to be approximately the same; all C–C distances within the isopropyl groups; all P···C$_{iPr}$ distances (i.e <u>P</u>–C–(<u>C</u>H$_3$)$_2$; and all C···C distances within the isopropyl groups. Additionally, the rigid bond restraint (**RIGU**, 132 restraints) was applied to improve the anisotropic displacement parameters of the carbon atoms of the isopropyl groups. The carbon atoms in question were refined anisotropically over two positions: C51-C56, refined with an occupancy of 0.603(5); C51A-C56A, refined with an occupancy 0.397(5); C61-C66, refined with an occupancy of 0.726(4); and C61A-C66A, refined with an occupancy of 0.274(4). The Fe-*H* in **5-2** was located in the difference map and refined isotropically. Otherwise, all hydrogen atoms were added at calculated positions and refined by use of a riding model employing isotropic displacement parameters based on the isotropic displacement parameter of the attached atom.

Chapter 6: Conclusions and Future Work

6.1 Overview

The development of efficient, selective homogenous catalysts for chemical synthesis is highly sought after. Precious metal (*i.e.*, Ru, Rh, Ir, Pd, Pt) catalysts have been widely studied in this regard.[9] Despite their efficacy, such catalysts are limited by the decreasing availability, and associated high cost, of the late $4d$- and $5d$-transition metals.[4-5] Mining and processing of ores containing such metals is also highly energy intensive, generating large quantities of CO_2 emissions. Faced with the pressing need to develop increasingly sustainable synthetic processes, two approaches emerge for catalyst development: (1) transition to the utilization of Earth-abundant $3d$-metals, such Mn, Fe, Co, and Ni; and (2) refine the efficacy of precious metal catalysts for targeted, challenging reactivity applications that remain beyond the reach of the $3d$-metals. Both approaches require innovation in ancillary ligand design in order to be successful.

Tridentate pincer ligation has emerged as a privileged class of highly tunable ancillary ligands that are compatible with late $3d$-, $4d$- and $5d$-metals and can support highly reactive complexes for applications in bond activation and catalysis. The research presented in this thesis has utilized bis(phosphino)silyl (PSiP) pincer ligand design to tackle reactivity issues involving both precious $4d$- and $5d$-metals (Rh and Ir) as well as $3d$-metal (Fe) catalysis. Chapters 2 and 3 focused on the synthesis and reactivity of electron-rich indolyl(phosphino)silyl (^{i}Pr-PSiP^{Ind}) Rh and Ir complexes for applications in N-H oxidative addition and insertion reactions for possible amine functionalization processes. Silyl pincer ligands have shown to be particularly effective in supporting platinum group metal complexes that can engage in the activation of strong bonds, in part due to the strongly σ-donating silyl fragment. Chapters 4 and 5 focused on the synthesis of (PSiP)Fe complexes

for application in hydrogenation catalysis. In the context of $3d$-metals such as iron, PSiP ligation can support reactivity by silyl-metal cooperativity, whereby Si can participate in hydride transfer reactions to form η^2-(Si-H) species. Such metal-silyl cooperativity may play a key role in hydrofunctionalization catalysis mediated by $3d$-metals by facilitating bond activation reactivity that does not require oxidative addition. Indeed, preliminary DFT calculations carried out in collaboration with Dr. Erin Johnson (Dalhousie) on the mechanism of (Cy-PSiP)Fe-catalyzed alkyne hydrogenation implicate metal-silyl cooperativity as playing a key role in H_2 activation and hydride transfer to the coordinated alkyne.

6.2 Summary and Future Work for Chapters 2 and 3

The synthesis of indolyl(phosphino)silyl (^{i}Pr-PSiP^{Ind}) Ir and Rh complexes was targeted for the development of N-H oxidative addition reactivity. Possible applications of such reactivity include the development of new hydroamination methodologies involving N-H oxidative addition, which may offer unique selectivity relative to existing amination catalysis. Several challenges are associated with this type of process, which is comprised of N-H oxidative addition, insertion of an alkene or alkyne into the M-N bond, and subsequent reductive elimination of the functionalized amine product. As a result, examples of hydroamination involving N-H oxidative addition to a late metal center are exceedingly rare. The Turculet group has previously shown that (Cy-PSiP)Ir^I is able to mediate facile N-H oxidative addition of ammonia, as well as alkyl- and arylamines to form Ir amido hydride complexes of the type (Cy-PSiP)IrH(NHR) (R = H, alkyl, aryl) that are resistant to reductive elimination.[33b] However, subsequent studies on the insertion of unsaturated substrates into the metal-amido linkages of (Cy-PSiP)IrH(NHR) were largely unsuccessful, with insertion into the Ir-amido linkage only observed with xylyl isocyanide.[33c] Chapters 2

and 3 of this thesis focused on developing the reactivity of ^{i}Pr-PSiP^{Ind}-ligated complexes in N-H oxidative addition and subsequent insertion reactions, in an effort to potentially identify more easily accessed pathways for possible amine functionalization. A library of (^{i}Pr-PSiP^{Ind})MH(NHR) (M = Rh, R = aryl; M = Ir, R = H, alkyl, aryl) complexes were synthesized *via* a salt metathesis route. This confirmed the synthetic feasibility of such complexes and provided some understanding of the relative stability of such coordinatively unsaturated complexes. It was found that (^{i}Pr-PSiP^{Ind})IrH(NHR) complexes are significantly more resistant to N-H reductive elimination than the Rh analogues, which is important for subsequent reactivity involving amine functionalization. The synthesis of such amido hydride complexes *via* N-H oxidative addition to coordinatively unsaturated (PSiP)M^I species was subsequently pursued.

While (Pr-PSiP^{Ind})Rh^I proved unreactive towards amine activation, treatment of (^{i}Pr-PSiP^{Ind})Ir^I with aniline resulted in competitive N-H and C-H bond oxidative addition, involving the formation of the amido hydride complex (^{i}Pr-PSiP^{Ind})IrH(NHPh) and the *ortho*-C-H activated aniline complex (*fac*-κ^3-^{i}Pr-PSiP^{Ind})IrH(κ^2-*N*,*C*-*o*-C$_6$H$_4$NH$_2$) (Scheme 6-1). Tuning of electronic factors by utilizing *para*-substitution in the aniline substrate (*p*-F, -OMe, and -Me) did not favor N-H oxidative addition. Similarly, the introduction of *ortho*-substituents on the aniline with the goal of blocking *ortho*-metalation did not promote N-H activation reactivity. Although C-H and N-H bond activation manifolds are likely linked by a common intermediate, such as an Ir^I-aniline adduct, and despite the facts that (^{i}Pr-PSiP^{Ind})IrH(Ph) undergoes facile arene exchange and (^{i}Pr-PSiP^{Ind})IrH(NHR) complexes are thermodynamically stable, it appears that for (^{i}Pr-PSiP^{Ind})Ir products resulting from NH- and CH-oxidative addition of aniline, substrates do not readily interconvert.

194
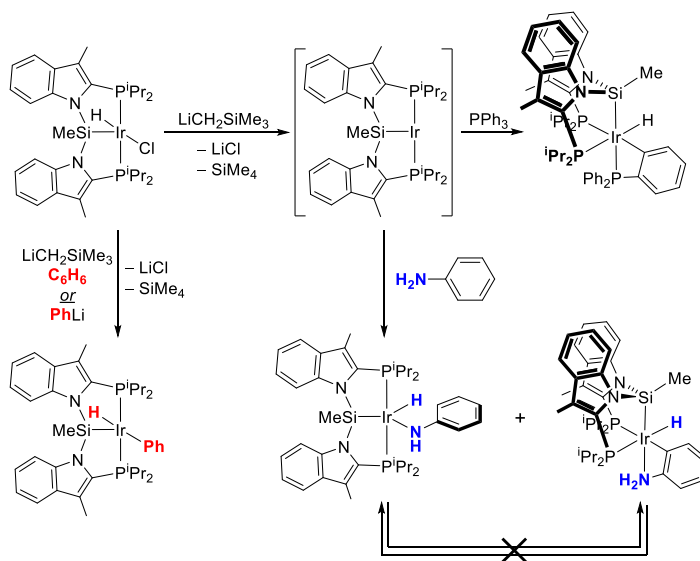
Scheme 6-1. N-H and C-H bond oxidative addition by (^{i}Pr-PSiP^{Ind})Ir^I.

Subsequent studies targeted the reactivity of (^{i}Pr-PSiP^{Ind})MH(NHR) (M = Rh, R =

aryl; M = Ir, R = H, alkyl, aryl) with unsaturated substrates, in an effort to identify insertion

into the M-amido linakge. This reactivity proved quite challenging. Examples of alkene

insertion into the Ir-H bond and subsequent β-hydride elimination to form isomerization

products were observed in some cases. However, CO_2 was found to successfully insert into

the Ir-*N* bond of both (^{i}Pr-PSiP^{Ind})- and (Cy-PSiP)-ligated amido hydride complexes to

form isolable carbamato hydride complexes (Scheme 6-2).
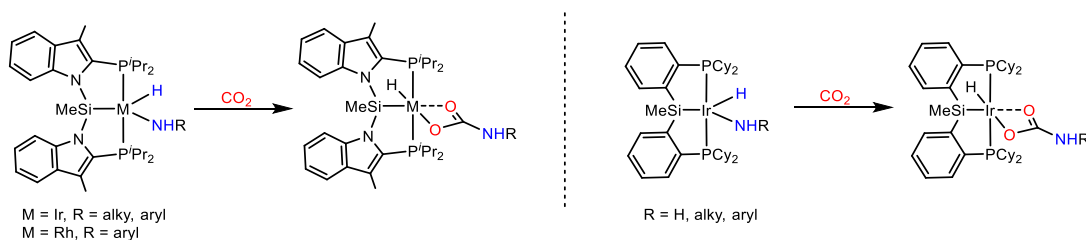
Scheme 6-2. Insertion of CO_2 into the Ir-*N* bond for ^{i}Pr-PSiP^{Ind} and Cy-PSiP-ligated
amido hydride complexes.

The effect of PSiP ligand design on the elementary reaction steps involving N-H

oxidative addition and the insertion of an unsaturated substrate into the M-amido bond of

195

Rh and Ir complexes has not been fully determined, and further investigation is necessary. The investigation of new silyl pincer motifs may lead to the discovery of catalytically viable reactivity. Leitner and co-workers[75] have reported extensive computational studies that suggest Ph-PSiP ligation may support Ir species that can undergo catalytic hydroamination of ethylene with ammonia *via* N-H oxidative addition. While the synthesis of (Ph-PSiP)Ir complexes proved experimentally challenging, indolyl-derived phenyl-phosphino silyl pincer ligation (Ph-PSiP[Ind], Figure 6-1) may prove more suitable in this regard. Further modification of the L donors in the LSiL framework can also be pursed experimentally, such as by the development of PSiN or PSiS ligation (Figure 6-1), which may better balance competing oxidative addition and reductive elimination processes.
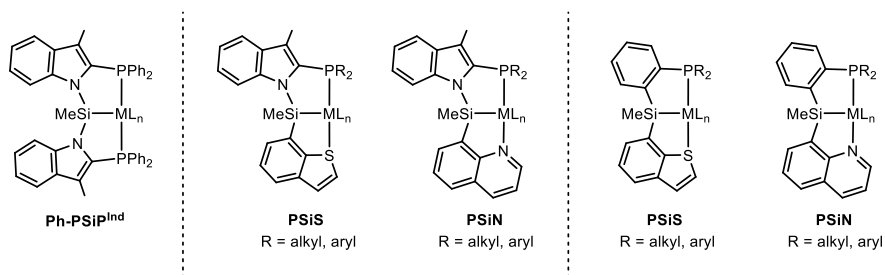
Figure 6-1. Alternative silyl pincer ligands to investigate in N-H oxidative addition and insertion reactions with M = Ir, Rh.

6.3 Summary and Future Work for Chapters 4 and 5

In the second half of this thesis, the synthesis of PSiP iron complexes supported by Cy-PSiP and [i]Pr-PSiP[Ind] ligation, respectively, was explored. The application of the ensuing complexes in hydrogenation catalysis was also investigated. The Turculet group had previously shown that (Cy-PSiP)FeH(N$_2$)$_2$ is an active pre-catalyst for alkene hydrogenation with good substrate tolerance.[37] In an effort to develop the reactivity of this pre-catalyst with alkyne substrates, an improved synthesis of (Cy-PSiP)FeH(N$_2$)$_2$ was developed. In the course of these investigations, a new diiron complex bridged by MgBr$_2$

was discovered. [(Cy-PSiP)FeBr]$_2$(MgBr$_2$) can be readily synthesized in one pot and can be stored indefinitely with no sign of decomposition. This diiron complex serves as a source of the elusive four-coordinate complex (Cy-PSiP)FeBr, which is generated upon dissociation of MgBr$_2$. The hydrido complex (Cy-PSiP)FeH(N$_2$)$_2$ can be readily obtained *via* [(Cy-PSiP)FeBr]$_2$(MgBr$_2$) with improved yield relative to the previously employed synthetic protocol.

The diiron complex [(Cy-PSiP)FeBr]$_2$(MgBr$_2$) itself was found to be highly active in the complete hydrogenation of diarylalkynes under especially mild conditions (5 mol% Fe, 1 atm H$_2$, 30 °C, 4 h) (Scheme 6-3). Surprisingly, [(Cy-PSiP)FeBr]$_2$MgBr$_2$ appears to be a more effective pre-catalyst for this reactivity than (Cy-PSiP)FeH(N$_2$)$_2$, even though the latter complex features an Fe-H and what are likely fairly labile N$_2$ ligands. Interestingly, the diiron complex was found to be unreactive towards the hydrogenation of alkenes, including 1-octene and *cis*-stilbene, even at elevated temperatures and pressures. Computational studies in collaboration with Dr. Erin Johnson (Dalhousie) aimed to elucidate the mechanism of the reaction in order to better understand the origin of the observed selectivity. The calculations indicate that the ability for a substrate to be hydrogenated is dependent on its ability to bind strongly enough to (Cy-PSiP)FeBr (generated upon dissociation of MgBr$_2$ from the diiron complex). Diphenylacetylene binds more strongly to the Fe centre in comparison to 1-octene, and *cis*-stilbene, and therefore gets preferentially hydrogenated. While several diphenylacetylene derivatives could be fully hydrogenated, substrates containing strongly electron withdrawing groups such as nitro groups could not be tolerated, likely due to the substrate not being able to bind strongly enough to the Fe centre. Similar reactivity findings were previously reported by Milstein and co-workers involving iron-catalyzed alkyne semi-hydrogenation.[85]
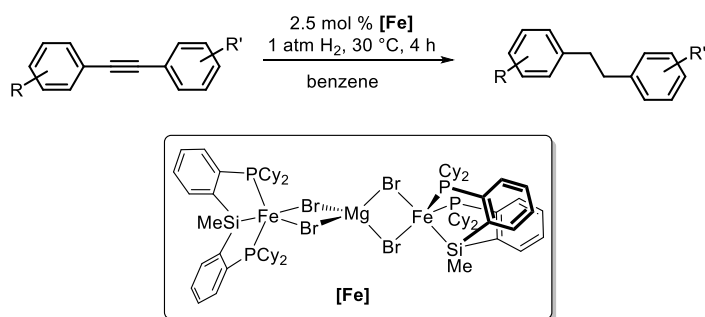
Scheme 6-3. Alkyne hydrogenation by [(Cy-PSiP)FeBr]$_2$(MgBr$_2$).

Furthermore, while diphenylacetylene derivatives involving steric hindrance in the *meta* and *para* position were well tolerated in the hydrogenation catalysis, *ortho*-methyl substitution hindered reactivity. Given the substantial steric bulk of the dicyclohexylphosphino donors in Cy-PSiP, decreasing the steric bulk in the ligand by using isopropylphosphino or ethylphosphino substitution may also allow for improved reactivity (Figure 6-2).
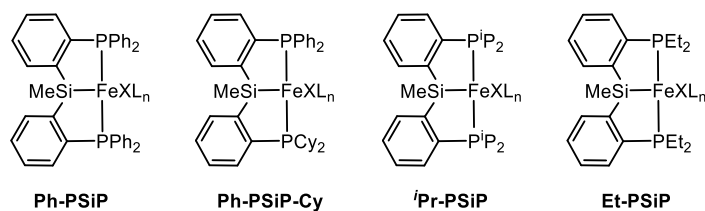
Figure 6-2. Alternative PSiP pincer ligands with iron for potential hydrogenation catalysis.

The selectivity observed for the hydrogenation of alkynes was further investigated by computational studies, which suggest that metal-silyl cooperativity involving the Cy-PSiP ligand plays an important role in the mechanism of hydrogenation. This involves hydride transfer to silicon and formation of η^2-(Si-H) species *via* Si-Fe bond cleavage. Silyl-mediated H-transfer is implicated in the formation of key intermediates along the reaction pathway, including an Fe[II]-metallacyclopropene species and an unusual Fe[II]-carbene resulting from the geminal addition of H$_2$ to the coordinated alkyne (Figure 6-3).

198

A subsequent H_2 activation step generates an Fe^{II}-alkyl complex that leads to the direct formation of bibenzyl. While a similar mechanism has been postulated for Cp*Ru-mediated (Cp* = C_5Me_5) alkyne hydrogenation,[90d] this remains a highly unusual hydrogenation mechanism that is entirley unprecedented for iron.

Fe(II)-metallacyclopropene **III**   *Fe(II) carbene* **IV**   *Fe(II) alkyl* **V**
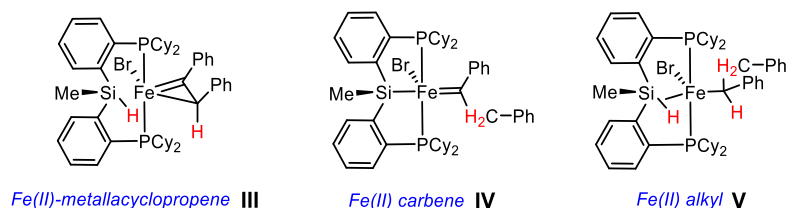
Figure 6-3. Examples of key interemediates calculated for alkyne hydrogenation by [(Cy-PSiP)FeBr]$_2$(MgBr$_2$) *via* (Cy-PSiP)FeBr.

Given the propensity of [(Cy-PSiP)FeBr]$_2$(MgBr$_2$) to mediate the hydrogenation of alkynes, the investigation of other types of synthetically useful alkyne hydrofunctionalization reactivity (*e.g.*, hydroboration, hydrosilylation, hydrostannation) is certainly worthwhile (Scheme 6-4). Preliminary studies with diphenylacetylene derivatives indicate that [(Cy-PSiP)FeBr]$_2$(MgBr$_2$) is indeed active in the hydroboration of alkynes. Due to the increased steric demand of hydrofunctionalization reagents relative to H_2, tuning of the ligand steric features (Figure 6-2) is likely to play an important role in achieving catalytic reactivity.
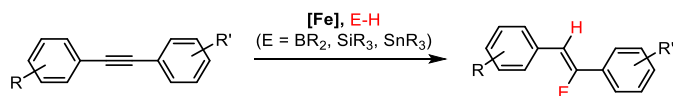
Scheme 6-4. Hydrofunctionalization of biaryl alkynes with [(Cy-PSiP)FeBr]$_2$(MgBr$_2$) as a possible path of investigation.

Chapter 5 focused on the synthesis of ^{i}Pr-PSiP^{Ind}-ligated iron complexes. While complexes such as (^{i}Pr-PSiP^{Ind})FeH(N$_2$)$_2$ and [(^{i}Pr-PSiP^{Ind})FeBr]$_2$MgBr$_2$(THF) proved synthetically accessible and exhibited similar structural features to the analogous (Cy-PSiP)Fe complexes, they proved do be significantly less reactive in alkene and alkyne

hydrogenation catalysis. Although this discrepancy was observed in the case of iron catalysis, the utility of this ligand platform for other types of base-metal-mediated reactivity remains to be studied. In this regard, the synthesis of Co and Mn derivatives may lead to the discovery of useful catalytic reactivity.

6.4 Conclusion

PSiP pincer ligation has proven suitable for the synthesis of late 3d-, 4d-, and 5d-metal complexes with applications in bond activation and catalysis (Figure 6-4). Silicon plays an important role in the reactivity of the ensuing (PSiP)M complexes. As a strong σ-donor towards metals such as Rh and Ir, silyl ligation promotes N-H and C-H oxidative addition by Ir[I] that can lead to coordinatively unsaturated amido hydride complexes that are resistant to reductive elimination. Furthermore, PSiP ligation can support base metal complexes that mediate E-H activation *via* metal-silyl cooperativity (Figure 6-4), which is a promising strategy for enabling base-metal catalyzed hydrofunctionalization reactivity. While the studies presented in this document support the feasibility of these ligand design concepts, the modular nature of the pincer ligand can be utilized in future studies to further tune reactivity at the metal center with the goal of accessing increasingly effective catalysts.
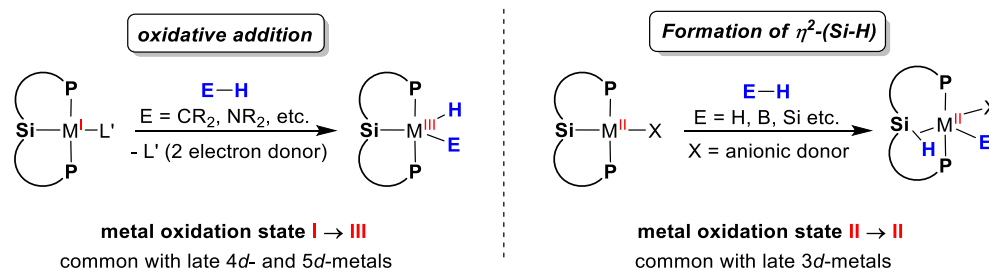
Figure 6-4. PSiP ligation with late 3d-, 4d- and 5d-metals.

References

1.   (a) B., S. K., Searching for New Reactivity (Nobel Lecture). *Angew. Chem., Int. Ed.* **2002,** *41*, 2024 - 2032; (b) Knowles, W. S., Asymmetric Hydrogenation (Nobel Lecture). *Angew. Chem., Int. Ed.* **2002,** *41*, 1998-2007; (c) Noyori, R., Asymmetric Catalysis: Science and Opportunities (Nobel Lecture). *Angew. Chem., Int. Ed.* **2002,** *41*, 2008 - 2022.

2.   (a) Chauvin, Y., Olefin Metathesis: The Early Days (Nobel Lecture). *Angew. Chem., Int. Ed.* **2006,** *45*, 3740-3765; (b) Grubbs, R. H., Olefin-Metathesis Catalysts for the Preparation of Molecules and Materials (Nobel Lecture). *Angew. Chem., Int. Ed.* **2006,** *45* (23), 3760-5; (c) Schrock, R. R., Multiple Metal-Carbon Bonds for Catalytic Metathesis Reactions (Nobel Lecture). *Angew. Chem., Int. Ed.* **2006,** *45* (23), 3748-3759.

3.   Wu, X. F.; Anbarasan, P.; Neumann, H.; Beller, M., From Noble Metal to Nobel Prize: Palladium-Catalyzed Coupling Reactions as Key Methods in Organic Synthesis. *Angew. Chem., Int. Ed.* **2010,** *49* (48), 9047-9050.

4.   Daily Metal Prices. https://www.dailymetalprice.com/.

5.   Price pressures on metals. *Nat. Catal.* **2019,** *2* (9), 735.

6.   Fürstner, A., Iron Catalysis in Organic Synthesis: A Critical Assessment of What It Takes To Make This Base Metal a Multitasking Champion. *ACS.* **2016,** *2* (11), 778-789.

7.   Frey, P. A.; Reed, G. H., The Ubiquity of Iron. *ACS Chem. Biol.* **2012,** *7* (9), 1477-1481.

8.   Ludwig, J. R.; Schindler, C. S., Catalyst: Sustainable Catalysis. *Chem* **2017,** *2* (3), 313-316.

9.   Hartley, F. R., Chemistry of the Platinum Group Metals: Recent Developments. *Elsevier.* **2013**.

10.   (a) Muller, T. E.; Beller, M., Metal-Initiated Amination of Alkenes and Alkynes. *Chem. Rev.* **1998,** *98*, 675-703; (b) Severin, R.; Doye, S., The catalytic hydroamination of alkynes. *Chem. Soc. Rev.* **2007,** *36* (9), 1407-1420; (c) Muller, T. E.; C., H. K.; Yus, M.; Foubelo, F.; Tada, M., Hydroamination: Direct Addition of Amines to Alkenes and Alkynes. *Chem. Rev.* **2008,** *108* (9), 3799 - 3892; (d) Huang, L.; Arndt, M.; Goossen, K.; Heydt, H.; Goossen, L. J., Late Transition Metal-Catalyzed Hydroamination and Hydroamidation. *Chem. Rev.* **2015,** *115* (7), 2596-2697.

11. Peris, E.; Crabtree, R. H., Key factors in pincer ligand design. *Chem. Soc. Rev.* **2018,** *47* (6), 1959-1968.

12. Moulton, C. J.; Shaw, B. L., Transition metal-carbon bonds. Part XLII. Complexes of nickel, palladium, platinum, rhodium and iridium with the tridentate ligand 2,6-bis[(di-t-butylphosphino)methyl]phenyl. *Dalton Trans.* **1976,** (11), 1020-1024.

13. (a) Gupta, M.; Hagen, C.; Kaska, W. C.; Cramer, R. E.; Jensen, C. M., Catalytic Dehydrogenation of Cycloalkanes to Arenes by a Dihydrido Iridium P-C-P Pincer Complex. *J. Am. Chem. Soc.* **1997,** *119* (4), 840 - 841; (b) Jensen, C. M., Iridium PCP pincer complexes: highly active and robust catalysts for novel homogeneous aliphatic dehydrogenations. *Chem. Commun.* **1999,** *24*, 2443-2449; (c) Liu, F.; Park, E. B.; Singh, B.; Jensen, C. M.; Goldman, A. S., Dehydrogenation of n-Alkanes Catalyzed by Iridium "Pincer" Complexes: Regioselective Formation of α-Olefins. *J. Am. Chem. Soc.* **1999,** *121*, 4086-4087.

14. (a) Choi, J.; MacArthur, A. H.; Brookhart, M.; Goldman, A. S., Dehydrogenation and related reactions catalyzed by iridium pincer complexes. *Chem. Rev.* **2011,** *111* (3), 1761-1779; (b) Findlater, M.; Choi, J.; Goldman, A. S.; Brookhart, M., Alkane Dehydrogenation. In Alkane C-H Activation by Single-Site Metal Catalysis, Pérez, P. J., Ed. Springer Netherlands: Dordrecht, **2012**, 113-141; (c) Gottker-Schnetmann, I.; White, P.; Brookhart, M., Iridium Bis(phosphinite) *p*-XPCP Pincer Complexes: Highly Active Catalyst for the Transfer Dehydrogenation of Alkanes. *J. Am. Chem. Soc.* **2004,** *126*, 1804 - 1811.

15. Burford, R. J.; Yeo, A.; Fryzuk, M. D., Dinitrogen activation by group 4 and group 5 metal complexes supported by phosphine-amido containing ligand manifolds. *Coord. Chem. Rev.* **2017,** *334*, 84-99.

16. Morales-Morales, D.; Jensen, C. M., The Chemistry of Pincer Compounds. Elsevier: 2007.

17. Liang, L., Metal complexes of chelating diarylamido phosphine ligands. *Coord. Chem. Rev.* **2006,** *250* (9-10), 1152-1177.

18.   (a) Kanzelberger, M.; Zhang, X.; Emge, T. J.; Goldman, A. S.; Zhao, J.; Incarvito, C.; Hartwig, J. F., Distinct Thermodynamics for the Formation and Cleavage of N−H Bonds in Aniline and Ammonia. Directly-Observed Reductive Elimination of Ammonia from an Isolated Amido Hydride Complex. *J. Am. Chem. Soc.* **2003,** *125* (45), 13644-13645; (b) Zhao, J.; Goldman, A. S.; Hartwig, J. F., Oxidative Addition of Ammonia to Form a Stable Monomeric Amido Hydride Complex. *Science.* **2005,** *307*, 1080 - 1083; (c) Wang, D. Y.; Choliy, Y.; Haibach, M. C.; Hartwig, J. F.; Krogh-Jespersen, K.; Goldman, A. S., Assessment of the Electronic Factors Determining the Thermodynamics of "Oxidative Addition" of C-H and N-H Bonds to Ir(I) Complexes. *J. Am. Chem. Soc.* **2016,** *138* (1), 149-163.

19.   Skyes, A. C.; White, P.; Brookhart, M., Reactions of Anilines and Benzamides with a 14-Electron Iridium(I) Bis(phosphinite) Complex: N-H Oxidative Addition versus Lewis Base Coordination. *Organometallics* **2006,** *25* (7), 1664-1675.

20.   Casalnuovo, A. L.; Calabrese, J. C.; D., M., Rational Design in Homogeneous Catalysis. Ir(I)-Catalyzed Addition of Aniline to Norbornylene via N-H Activation. *Inorg. Chem.* **1988,** *110* (20), 6744-6748.

21.   (a) de Bruin, B.; Bill, E.; Bothe, E.; Weyhermuller, T.; Wieghardt, K., Molecular and Electronic Structures of Bis(pyridine-2,6-diimine)metal Complexes [ML$_2$](PF$_6$)n (n = 0, 1, 2, 3; M = Mn, Fe, Co, Ni, Cu, Zn). *Inorg. Chem. Front.* **2000,** *39*, 2936-2947; (b) Bart, S. C.; Chlopek, K.; Bill, E.; Bouwkamp, M. W.; Lobkovsky, E.; Neese, F.; Wieghardt, K.; Chirik, P. J., Electronic Structure of Bis(imino)pyridine Iron Dichloride, Monochloride, and Neutral Ligand Complexes: A Combined Structural, Spectroscopic, and Computational Study. *J. Am. Chem. Soc.* **2006,** *128*, 13901-13912; (c) Chirik, P. J.; Wieghardt, K., Radical Ligands Confer Nobility on Base-Metal Catalysts. *Science.* **2010,** *327*, 794-795; (d) Stieber, S. C.; Milsmann, C.; Hoyt, J. M.; Turner, Z. R.; Finkelstein, K. D.; Wieghardt, K.; DeBeer, S.; Chirik, P. J., Bis(imino)pyridine Iron Dinitrogen Compounds Revisited: Differences in Electronic Structure Between Four- and Five-Coordinate Derivatives. *Inorg. Chem. Front.* **2012,** *51* (6), 3770-3785.

22.   Knijnenburg, Q.; Gambarotta, S.; Budzelaar, P. H., Ligand-centred reactivity in diiminepyridine complexes. *Dalton Trans.* **2006,** (46), 5442-8.

23.   (a) Bart, S. C.; Lobkovsky, M.; Chirik, P. J., Preparation and Molecular and Electronic Structures of Iron(0) Dinitrogen and Silane Complexes and Their Application to Catalytic Hydrogenation and Hydrosilation. *J. Am. Chem. Soc.* **2004,** *126*, 13794-13807; (b) Archer, A. M.; Bouwkamp, M. W.; Cortez, M.; Lobkovsky, E.; Chirik, P. J., Arene Coordination in Bis(imino)pyridine Iron Complexes: Identification of Catalyst Deactivation Pathways in Iron-Catalyzed Hydrogenation and Hydrosilation. *Organometallics* **2006,** *25* (18), 4270-4278; (c) Trovitch, R. J.; Lobkovsky, E.; Bill, E.; Chirik, P. J., Functional Group Tolerance and Substrate Scope in Bis(imino)pyridine Iron Catalyzed Alkene Hydrogenation. *Organometallics* **2008,** *27*, 1470-1478; (d) Trovitch, R. J.; Lobkovsky, E.; Bouwkamp, M. W.; Chirik, P. J., Carbon-Oxygen Bond Cleavage by Bis(imino)pyridine Iron Compounds: Catalyst Deactivation Pathways and Observation of Acyl C-O Bond Cleavage in Esters. *Organometallics* **2008,** *27* (23), 6264-6278; (e) Russell, S. K.; Lobkovsky, E.; Chirik, P. J., N-N Bond Cleavage in Diazoalkanes by a Bis(imino)pyridine Iron Complex. *J. Am. Chem. Soc.* **2009,** *131*, 36-37; (f) Russell, S. K.; Darmon, J. M.; Lobkovsky, E.; Chirik, P. J., Synthesis of Aryl-Substituted Bis(imino)pyridine Iron Dinitrogen Complexes. *Inorg. Chem. Front.* **2010,** *49* (6), 2782-2792; (g) Chirik, P. J., Preface: Forum on Redox-Active Ligands. *Inorg. Chem. Front.* **2011,** *50* (20), 9737-9740; (h) Russell, S. K.; Milsmann, C.; Lobkovsky, E.; Weyhermuller, T.; Chirik, P. J., Synthesis, Electronic Structure, and Catalytic Activity of Reduced Bis(aldimino)pyridine Iron Compounds: Experimental Evidence for Ligand Participation. *Inorg. Chem. Front.* **2011,** *50* (7), 3159-3169; (i) Darmon, J. M.; Turner, Z. R.; Lobkovsky, E.; Chirik, P. J., Electronic Effects in 4-Substituted Bis(imino)pyridines and the Corresponding Reduced Iron Compounds. *Organometallics* **2012,** *31* (6), 2275-2285; (j) Hojilla Atienza, C. C.; Tondreau, A. M.; Weller, K. J.; Lewis, K. M.; Cruse, R. W.; Nye, S. A.; Boyer, J. L.; Delis, J. G. P.; Chirik, P. J., High-Selectivity Bis(imino)pyridine Iron Catalysts for the Hydrosilylation of 1,2,4-Trivinylcyclohexane. *ACS Catal.* **2012,** *2* (10), 2169-2172; (k) Tondreau, A. M.; Hojilla Atienza, C. C.; Weller, K. J.; Nye, S. A.; Lewis, K. M.; Delis, J. G.; Chirik, P. J., Iron Catalysts for Selective Anti-Markovnikov Alkene Hydrosilylation Using Tertiary Silanes. *Science.* **2012,** *335*, 567 - 570; (l) Atienza, C. C.; Diao, T.; Weller, K. J.; Nye, S. A.; Lewis, K. M.; Delis, J. G.; Boyer, J. L.; Roy, A. K.; Chirik, P. J., Bis(imino)pyridine cobalt-catalyzed dehydrogenative silylation of alkenes: scope, mechanism, and origins of selective allylsilane formation. *J. Am. Chem. Soc.* **2014,** *136* (34), 12108-12118; (m) Russell, S. K.; Hoyt, J. M.; Bart, S. C.; Milsmann, C.; Stieber, S. C. E.; Semproni, S. P.; DeBeer, S.; Chirik, P. J., Synthesis, electronic structure and reactivity of bis(imino)pyridine iron carbene complexes: evidence for a carbene radical. *Chem.* **2014,** *5* (3), 1168-1174; (n) Joannou, M. V.; Hoyt, J. M.; Chirik, P. J., Investigations into the Mechanism of Inter- and Intramolecular Iron-Catalyzed [2+2] Cycloaddition of Alkenes. *J. Am. Chem. Soc.* **2020,** *142* (11), 5314-5330; (o) Kennedy, C. R.; Zhong, H.; Joannou, M. V.; Chirik, P. J., Pyridine(diimine) Iron Diene Complexes Relevant to Catalytic [2+2]-Cycloaddition Reactions. *ASC.* **2020,** *362* (2), 404-416; (p) Peterson, P. O.; Rummelt, S. M.; Wile, B. M.; Stieber, S. C. E.; Zhong, H.; Chirik, P. J., Direct Observation of Transmetalation from a Neutral Boronate Ester to a Pyridine(diimine) Iron Alkoxide. *Organometallics* **2020,** *39* (1), 201-205.

24. Monfette, S.; Turner, Z. R.; Semproni, S. P.; Chirik, P. J., Enantiopure C_1-Symmetric Bis(imino)pyridine Cobalt Complexes for Asymmetric Alkene Hydrogenation. *J. Am. Chem. Soc.* **2012,** *134* (10), 4561-4564.

25. Yu, R. P.; Darmon, J. M.; Hoyt, J. M.; Margulieux, G. W.; Turner, Z. R.; Chirik, P. J., High-Activity Iron Catalysts for the Hydrogenation of Hindered, Unfunctionalized Alkenes. *ACS Catal.* **2012,** *2* (8), 1760-1764.

26. (a) Schneider, S.; Meiners, J.; Askevold, B., Cooperative Aliphatic PNP Amido Pincer Ligands - Versatile Building Blocks for Coordination Chemistry and Catalysis. *Eur. J. Inorg. Chem.* **2012,** *2012* (3), 412-429; (b) Wei, Z.; Jiao, H., Bifunctional aliphatic PNP pincer catalysts for hydrogenation: mechanisms and scope. *Adv. Inorg.* **2019**, *73*, 323-384.

27. (a) Bornschein, C.; Werkmeister, S.; Wendt, B.; Jiao, H.; Alberico, E.; Baumann, W.; Junge, H.; Junge, K.; Beller, M., Mild and selective hydrogenation of aromatic and aliphatic (di)nitriles with a well-defined iron pincer complex. *Nat. Commun.* **2014,** *5*, 4111; (b) Lange, S.; Elangovan, S.; Cordes, C.; Spannenberg, A.; Jiao, H.; Junge, H.; Bachmann, S.; Scalone, M.; Topf, C.; Jungea, K.; Beller, M., Selective catalytic hydrogenation of nitriles to primary amines using iron pincer complexes. *Catal. Sci. Technol.* **2016,** *6*, 4768-4772.

28. (a) Schwartsburd, L.; Iron, M. A.; Konstantinovski, L.; Ben-Ari, E.; Milstein, D., A Dearomatized Anionic PNP Pincer Rhodium Complex: C–H and H–H Bond Activation by Metal–Ligand Cooperation and Inhibition by Dinitrogen. *Organometallics* **2011,** *30* (10), 2721-2729; (b) Khaskin, E.; Iron, M. A.; Shimon, L. J. W.; Zhang, J.; Milstein, D., N-H Activation of Amines and Ammonia by Ru via Metal-Ligand Cooperation. *J. Am. Chem. Soc.* **2010,** *132*, 8542-8543; (c) Ben-Ari, E.; Leitus, G.; Shimon, L. J. W.; Milstein, D., Metal-Ligand Cooperation in C-H and H_2 Activation by an Electron-Rich PNP Ir(I) System: Facile Ligand Dearomatization-Aromatization as Key Steps. *J. Am. Chem. Soc.* **2006,** *128*, 15390-15391.

29.   (a) Langer, R.; Diskin-Posner, Y.; Leitus, G.; Shimon, L. J.; Ben-David, Y.; Milstein, D., Low-Pressure Hydrogenation of Carbon Dioxide Catalyzed by an Iron Pincer Complex Exhibiting Noble Metal Activity. *Angew. Chem., Int. Ed.* **2011,** *50* (42), 9948-52; (b) Langer, R.; Leitus, G.; Ben-David, Y.; Milstein, D., Efficient Hydrogenation of Ketones Catalyzed by an Iron Pincer Complex. *Angew. Chem., Int. Ed.* **2011,** *50* (9), 2120-2124; (c) Langer, R.; Iron, M. A.; Konstantinovski, L.; Diskin-Posner, Y.; Leitus, G.; Ben-David, Y.; Milstein, D., Iron Borohydride Pincer Complexes for the Efficient Hydrogenation of Ketones under Mild, Base-Free Conditions: Synthesis and Mechanistic Insight. *Chem. Eur. J.* **2012,** *18* (23), 7196-209; (d) Zell, T.; Ben-David, Y.; Milstein, D., Unprecedented Iron-Catalyzed Ester Hydrogenation. Mild, Selective, and Efficient Hydrogenation of Trifluoroacetic Esters to Alcohols Catalyzed by an Iron Pincer Complex. *Angew. Chem., Int. Ed.* **2014,** *53* (18), 4685-9; (e) Zell, T.; Ben-David, Y.; Milstein, D., Highly efficient, general hydrogenation of aldehydes catalyzed by PNP iron pincer complexes. *Catal. Sci. Technol.* **2015,** *5*, 822-826; (f) Zell, T.; Milstein, D., Hydrogenation and dehydrogenation iron pincer catalysts capable of metal-ligand cooperation by aromatization/dearomatization. *Acc. Chem. Res* **2015,** *48* (7), 1979-1994.

30.   (a) Lin, T.; Peters, J. C., Boryl-Mediated Reversible H_2 Activation at Cobalt: Catalytic Hydrogenation, Dehydrogenation, and Transfer Hydrogenation. *J. Am. Chem. Soc.* **2013,** *135* (41), 15310-15313; (b) Lin, T.; Peters, J. C., Boryl–Metal Bonds Facilitate Cobalt/Nickel-Catalyzed Olefin Hydrogenation. *J. Am. Chem. Soc.* **2014,** *136* (39), 13672-13683.

31.   Turculet, L., PSiP Transition-Metal Pincer Complexes: Synthesis, Bond Activation, and Catalysis. In *Pincer and Pincer-Type Complexes*, Wiley-VCH Verlag GmbH & Co. KGaA: 2014; pp 149-188.

32.   MacInnis, M. C.; McDonald, R.; Ferguson, M. J.; Tobisch, S.; Turculet, L., Four-Coordinate, 14-Electron Ru(II) Complexes: Unusual Trigonal Pyramidal Geometry Enforced by Bis(phosphino)silyl Ligation. *J. Am. Chem. Soc.* **2011,** *133* (34), 13622-13633.

33.   (a) MacLean, D. F.; McDonald, R.; Ferguson, M. J.; Caddell, A. J.; Turculet, L., Room temperature benzene C-H activation by a new [PSiP]Ir pincer complex. *Chem. Commun.* **2008,** (41), 5146-5148; (b) Morgan, E.; MacLean, D. F.; McDonald, R.; Turculet, L., Rhodium and Iridium Amido Complexes Supported by Silyl Pincer Ligation: Ammonia N-H Bond Activation by a [PSiP]Ir Complex. *J. Am. Chem. Soc.* **2009,** *131*, 14234–14236; (c) Morgan, E. Rhodium and Iridium Pincer Complexes Supported by Bis(phosphino silyl Ligation: Applications in Bond Cleavage Chemistry. Dalhousie University, Halifax, Canada, 2013.

34. Takaya, J.; Iwasawa, N., Reaction of Bis(o-phosphinophenyl)silane with M(PPh$_3$)$_4$ (M = Ni, Pd, Pt): Synthesis and Structural Analysis of η^2-(Si–H) Metal(0) and Pentacoordinate Silyl Metal(II) Hydride Complexes of the Ni Triad Bearing a PSiP-Pincer Ligand. *Dalton Trans.* **2011,** *40*, 8814-8821.

35. Charboneau, D. J.; Balcells, D.; Hazari, N.; Lant, H. M. C.; Mayer, J. M.; Melvin, P. R.; Mercado, B. Q.; Morris, W. D.; Repisky, M.; Suh, H., Dinitrogen-Facilitated Reversible Formation of a Si–H Bond in a Pincer-Supported Ni Complex. *Organometallics* **2016,** *35* (18), 3154-3162.

36. Murphy, L. J.; Hollenhorst, H.; McDonald, R.; Ferguson, M.; Lumsden, M. D.; Turculet, L., Selective Ni-Catalyzed Hydroboration of CO$_2$ to the Formaldehyde Level Enabled by New PSiP Ligation. *Organometallics* **2017,** *36* (19), 3709-3720.

37. Murphy, L. J.; Ferguson, M. J.; McDonald, R.; Lumsden, M. D.; Turculet, L., Synthesis of Bis(phosphino)silyl Pincer-Supported Iron Hydrides for the Catalytic Hydrogenation of Alkenes. *Organometallics* **2018,** *37* (24), 4814-4826.

38. (a) Hartwig, J. F., Development of catalysts for the hydroamination of olefins. *Pure Appl. Chem.* **2004,** *76* (3), 507 - 516; (b) Hartwig, J. F., Carbon-heteroatom bond formation catalysed by organometallic complexes. *Nature.* **2008,** *455* (7211), 314-22; (c) Surry, D. S.; Buchwald, S. L., Biaryl phosphane ligands in palladium-catalyzed amination. *Angew. Chem., Int. Ed.* **2008,** *47* (34), 6338-6361; (d) Aubin, Y.; Fischmeister, C.; Thomas, C. M.; Renaud, J. L., Direct amination of aryl halides with ammonia. *Chem. Soc. Rev.* **2010,** *39* (11), 4130-45.

39. Morgan, E.; MacLean, D. F.; McDonald, R.; Turculet, L., Rhodium and Iridium Amido Complexes Supported by Silyl Pincer Ligation: Ammonia N-H Bond Activation by a [PSiP]Ir Complex. *J. Am. Chem. Soc.* **2009,** *131*, 14234-14236.

40. Huang, Z.; Zhou, J. S.; Hartwig, J. F., N-H Activation of Hydrazines by Iridium(I). Double N-H Activation to form Iridium Aminonitrene Complexes. *J. Am. Chem. Soc.* **2010,** *132* (33), 11458-11460.

41. Friedrich, A.; Drees, M.; Kass, M.; Herdtweck, E.; Schneider, S., Ruthenium Complexes with Cooperative PNP-Pincer Amine, Amido, Imine, and Enamido Ligands: Facile Ligand Backbone Functionalization Processes. *Inorg. Chem. Front.* **2010,** *49* (12), 5482-5494.

42. Gunanathan, C.; Milstein, D., Metal-Ligand Cooperation by Aromatization-Dearomatization: A New Paradigm in Bond Activation and "Green" Catalysis. *Acc. Chem. Res.* **2011,** *44* (8), 588-602.

43. Li, H.; Hall, M. B., Mechanism of the Formation of Carboxylate from Alcohols and Water Catalyzed by a Bipyridine-Based Ruthenium Complex: A Computational Study. *J. Am. Chem. Soc.* **2014,** *136* (1), 383-95.

44. Aizenberg, M.; Milstein, D., Facial (Methyl)(hydrido)(silyl) Complexes of Iridium: Synthesis, X-ray Structures, and Reductive Elimination Reactions. Facile Formation of Silametallacycles by Metalation of Silyl Ligands. *J. Am. Chem. Soc.* **1995,** *117*, 6456-6464.

45. (a) Mitton, S. J.; McDonald, R.; Turculet, L., Nickel and palladium silyl pincer complexes: unusual structural rearrangements that involve reversible Si-C(sp^3) and Si-C(sp^2) bond activation. *Angew. Chem., Int. Ed. Engl.* **2009,** *48* (45), 8568-71; (b) Mitton, S. J.; Turculet, L., Mild Reduction of Carbon Dioxide to Methane with Tertiary Silanes Catalyzed by Platinum and Palladium Silyl Pincer Complexes. *Chem. Eur. J.* **2012,** *18* (48), 15258-62; (c) Mitton, S. J.; McDonald, R.; Turculet, L., Facile intramolecular silicon–carbon bond activation at Pt^0 and Pt^{II} centers. *Polyhedron* **2013,** *52*, 750-754.

46. Fang, H.; Choe, Y. K.; Li, Y.; Shimada, S., Synthesis, Structure, and Reactivity of Hydridoiridium Complexes Bearing a Pincer-Type PSiP Ligand. *Chem. Asian J.* **2011,** *6* (9), 2512-2521.

47. Wassenaar, J.; Reek, J. N., INDOLPhos: novel hybrid phosphine-phosphoramidite ligands for asymmetric hydrogenation and hydroformylation. *Dalton Trans.* **2007,** (34), 3750-3.

48. Lachaize, S.; Sabo-Etienne, S., σ-Silane Ruthenium Complexes: The Crucial Role of Secondary Interactions. *Eur. J. Inorg. Chem.* **2006,** *2006* (11), 2115-2127.

49. Corey, J. Y., Reactions of Hydrosilanes with Transition Metal Complexes and Characterization of the Products. *Chem. Rev.* **2011,** *111* (863-1071).

50. Riehl, J.; Jean, Y.; Eisenstein, O.; Pelissier, M., Theoretical Study of the Structures of Electron-Deficient d^6 ML$_5$, Complexes. Importance of a π-Donating Ligand. *Organometallics* **1992,** *11*, 729-737.

51. Mitton, S. J.; McDonald, R.; Turculet, L., Nickel and Palladium Silyl Pincer Complexes: Unusual Structural Rearrangements that Involve Reversible Si-C(sp^3) and Si-C(sp^2) Bond Activation. *Angew. Chem., Int. Ed.* **2009,** *48* (45), 8568-8571.

52. Driver, M. S.; Hartwig, J. F., General N-H Activation of Primary Alkylamines by a Late Transition-Metal Complex. *J. Am. Chem. Soc.* **1996,** *118* (17), 4206-4207.

53. (a) Lee, D. W.; Kaska, W. C.; Jensen, C. M., Mechanistic Features of Iridium Pincer Complex Catalyzed Hydrocarbon Dehydrogenation Reactions: Inhibition upon Formation of a μ-Dinitrogen Complex. *Organometallics* **1998,** *17* (1), 1-3; (b) Lee, D. W.; Jensen, C. M.; Morales-Morales, D., Reactivity of Iridium PCP Pincer Complexes toward CO and CO_2. Crystal Structures of $IrH(k^2-O_2COH)\{C_6H_3-2,6-(CH_2PBu^{t2})_2\}$ and $IrH(C(O)OH)\{C_6H_3-2,6-(CH_2PBu^{t2})_2\}$,$H_2O$. *Organometallics* **2003,** *22* (23), 4744-4749.

54. (a) Clot, E.; Besora, M.; Maseras, F.; Mégret, C.; Eisenstein, O.; Oelckers, B.; Perutz, R. N., Bond energy M–C/H–C correlations. *Chem. Commun.* **2003,** (4), 490-491; (b) Clot, E.; Megret, C.; Eisenstein, O.; Perutz, R. N., Exceptional Sensitivity of Metal-Aryl Bond Energies to *ortho*-Fluorine Substituents: Influence of the Metal, the Coordination Sphere, and the Spectator Ligands on M-C/H-C Bond Energy Correlations. *J. Am. Chem. Soc.* **2009,** *131*, 7817-7827.

55. (a) Renkema, K. B.; Bosque, R.; Streib, W. E.; Maseras, F.; Eisenstein, O.; Caulton, K. G., Phosphine Dissociation Mediates C-H Cleavage of Fluoroarenes by $OsH(C_6H_5)(CO)(P^tBu_2Me)_2$. *J. Am. Chem. Soc.* **1999,** *121*, 10895-10907; (b) Ben-Ari, E.; Gandelman, M.; Rozenberg, H.; Shimon, L. J.; Milstein, D., Selective Ortho C-H Activation of Haloarenes by an Ir(I) System. *J. Am. Chem. Soc.* **2003,** *125*, 4714-4715; (c) Evans, M. E.; Burke, C. L.; Yaibuathes, S.; Clot, E.; Eisentein, O.; Jones, W. D., Energetics of C-H Bond Activation of Fluorinated Aromatic Hydrocarbons Using a [Tp′Rh(CNneopentyl)] Complex. *J. Am. Chem. Soc.* **2009,** *131*, 12464-13473; (d) Hauser, S. A.; Emerson-King, J.; Habershon, S.; Chaplin, A. B., UV-light promoted C–H bond activation of benzene and fluorobenzenes by an iridium(I) pincer complex. *Chem. Commun.* **2017,** *53*, 3634-3636.

56. Press, L. P.; Kosanovich, A. J.; McCulloch, B. J.; Ozerov, O. V., High-Turnover Aromatic C-H Borylation Catalyzed by POCOP-Type Pincer Complexes of Iridium. *J. Am. Chem. Soc.* **2016,** *138* (30), 9487-9497.

57. Fan, L.; Parkin, S.; Ozerov, O. V., Halobenzenes and Ir(I): Kinetic C-H Oxidative Addition and Thermodynamic C-Hal Oxidative Addition. *J. Am. Chem. Soc.* **2005,** *127* (48), 16772 - 16773

58. Van der Vlugt, J. I., Advances in selective activation and application of ammonia in homogeneous catalysis. *Chem. Soc. Rev.* **2010,** *39* (6), 2302-2322.

59. (a) Glueck, D. S.; Winslow, L. J. N.; Bergman, R. G., Iridium alkoxide and amide hydride complexes. Synthesis, reactivity, and the mechanism of oxygen-hydrogen and nitrogen-hydrogen reductive elimination. *Organometallics* **1991,** *10* (5), 1462-1479; (b) Schmeier, T. J.; Dobereiner, G. E.; Crabtree, R. H.; Hazari, N., Secondary Coordination Sphere Interactions Facilitate the Insertion Step in an Iridium(III) CO_2 Reduction Catalyst. *J. Am. Chem. Soc.* **2011,** *133* (24), 9274-9277; (c) Fernández-Alvarez, F. J.; Iglesias, M.; Oro, L. A.; Polo, V., CO_2 Activation and Catalysis Driven by Iridium Complexes. *ChemCatChem.* **2013,** *5* (12), 3481-3494.

60. Cowan, R. L.; Trogler, W. C., Regioselective Insertion of Acrylonitrile Into the Pt-N Bond of Hydrido(phenylamido)bis(triethylphosphine)-platinum(II). A Model Step for Olefin Amination. *Organometallics* **1987,** *6* (11), 2451-2453.

61. (a) Ney, J. E.; Wolfe, J. P., Palladium-catalyzed synthesis of N-aryl pyrrolidines from γ-(N-Arylamino) alkenes: evidence for chemoselective alkene insertion into Pd--N bonds. *Angew. Chem., Int. Ed.* **2004,** *43* (27), 3605-8; (b) Neukom, J. D.; Perch, N. S.; Wolfe, J. P., Intramolecular Alkene Aminopalladation Reactions of (dppf)Pd(Ar)[N(Ar¹)(CH₂)₃CH=CH₂] Complexes. Insertion of Unactivated Alkenes into Pd-N Bonds. *J. Am. Chem. Soc.* **2010,** *132*, 6276-6277; (c) Neukom, J. D.; Perch, N. S.; Wolfe, J. P., Intramolecular Insertion of Alkenes into Pd−N Bonds. Effects of Substrate and Ligand Structure on the Reactivity of (P−P)Pd(Ar)[N(Ar¹)(CH₂)₃CR=CHR′] Complexes. *Organometallics* **2011,** *30* (5), 1269-1277; (d) Hanley, P. S.; Markovic, D.; Hartwig, J. F., Intermolecular Insertion of Ethylene and Octene into a Palladium-Amide Bond. Spectroscopic Evidence for an Ethylene Amido Intermediate. *J. Am. Chem. Soc.* **2010,** *132* (6302-6303); (e) Hanley, P. S.; Hartwig, J. F., Intermolecular Migratory Insertion of Unactivated Olefins into Palladium-Nitrogen Bonds. Steric and Electronic Effects on the Rate of Migratory Insertion. *J. Am. Chem. Soc.* **2011,** *133* (39), 15661-73.

62. Beller, M.; Trauthwein, H.; Eichberger, M.; Breindl, C.; Herwig, J.; Muller, T. E.; Thiel, O. R., The First Rhodium-Catalyzed Anti-Markovnikov Hydroamination: Studies on Hydroamination and Oxidative Amination of Aromatic Olefins. *Chem. Eur. J.* **1999,** *5* (4), 1306-1319.

63. Zhao, P.; Krug, C.; Hartwig, J. F., Transfer of Amido Groups from Isolated Rhodium(I) Amides to Alkenes and Vinylarenes. *J. Am. Chem. Soc.* **2005,** *127*, 12066-12073.

64. Zhou, J.; Hartwig, J. F., Intermolecular, Catalytic Asymmetric Hydroamination of Bicyclic Alkenes and Dienes in High Yield and Enantioselectivity. *J. Am. Chem. Soc.* **2008,** *130*, 12220-12221.

65. Sevov, C. S.; Zhou, J.; Hartwig, J. F., Iridium-Catalyzed Intermolecular Hydroamination of Unactivated Aliphatic Alkenes with Amides and Sulfonamides. *J. Am. Chem. Soc.* **2012,** *134* (29), 11960-11963.

66. Sevov, C. S.; Zhou, J. S.; Hartwig, J. F., Iridium-Catalyzed, Intermolecular Hydroamination of Unactivated Alkenes with Indoles. *J. Am. Chem. Soc.* **2014,** *136* (8), 3200-3207.

67. Xi, Y.; Ma, S.; Hartwig, J. F., Catalytic asymmetric addition of an amine N-H bond across internal alkenes. *Nature.* **2020,** *588* (7837), 254-260.

68. Schilling, W.; Das, S., Transition Metal-Free Synthesis of Carbamates Using CO_2 as the Carbon Source. *ChemSusChem* **2020,** *13* (23), 6246-6258.

69. Leitner, W., The coordination chemistry of carbon dioxide and its relevance for catalysis: a critical survey. *Coord. Chem. Rev.* **1996,** *153*, 257-284.

70. (a) Hartwig, J. F.; Bergman, R. G.; Andersen, R. A., Insertion Reactions of Carbon Monoxide and Carbon Dioxide with Ruthenium Benzyl, Arylamido, and Aryloxide Complexes: A Comparison of the Reactivity of Ruthenium-Carbon, Ruthenium-Nitrogen, and Ruthenium-Oxygen Bonds. *J. Am. Chem. Soc.* **1991,** *113* (17), 6499-6508; (b) Yin, X.; Moss, J. R., Recent developments in the activation of carbon dioxide by metal complexes. *Coord. Chem. Rev.* **1998,** *181*, 27-59; (c) Ananikov, V. P.; Beletskaya, I. P., Alkyne and Alkene Insertion into Metal–Heteroatom and Metal–Hydrogen Bonds: The Key Stages of Hydrofunctionalization Process. *Top Organomet Chem.* **2012,** *43*, 1-19; (d) Dobereiner, G. E.; Wu, J.; Manas, M. G.; Schley, N. D.; Takase, M. K.; Crabtree, R. H.; Hazari, N.; Maseras, F.; Nova, A., Mild, Reversible Reaction of Iridium(III) Amido Complexes with Carbon Dioxide. *Inorg. Chem.* **2012,** *51* (18), 9683-93; (e) Truscott, B. J.; Nelson, D. J.; Slawin, A. M.; Nolan, S. P., CO_2 fixation employing an iridium(I)-hydroxide complex. *Chem. Commun.* **2014,** *50* (3), 286-8; (f) Vummaleti, S. V. C.; Talarico, G.; Nolan, S. P.; Cavallo, L.; Poater, A., Mechanism of CO_2 Fixation by Ir^I-X Bonds (X = OH, OR, N, C). *Eur. J. Inorg. Chem.* **2015,** *2015* (28), 4653-4657; (g) Hazari, N.; Heimann, J. E., Carbon Dioxide Insertion into Group 9 and 10 Metal-Element σ Bonds. *Inorg. Chem. Front.* **2017,** *56* (22), 13655-13678.

71. Park, S.; Rheingold, A. L.; Roundhill, D. M., Synthesis and Reaction Chemistry of Monomeric and Dimeric Amide Complexes of Platinum(II). *Organometallics* **1991,** *10* (3), 615-623.

72. Schmeier, T. J.; Nova, A.; Hazari, N.; Maseras, F., Synthesis of PCP-Supported Nickel Complexes and their Reactivity with Carbon Dioxide. *Chem. Eur. J.* **2012,** *18* (22), 6915-6927.

73.   (a) Hao, J.; Vabre, B.; Mougang-Soume, B.; Zargarian, D., Small Molecule Activation by POC(sp^3)OP-Nickel Complexes. *Chem. Eur. J.* **2014,** *20* (39), 12544-52; (b) Kim, J.; Park, K.; Lee, Y., Synthesis and characterization of a four-coordinate nickel carbamato species (MeSiP^{iPr2})Ni(OC(O)NHMes) generated from the reaction of (MeSiP^{iPr2})Ni(NHMes) with CO_2. *Inorganica Chim. Acta.* **2017,** *460*, 55-62.

74.   Tanaka, M.; Yamashita, M.; Nozaki, K., Catalytic Hydrogenation of Carbon Dioxide Using Ir(III)-Pincer Complexes. *J. Am. Chem. Soc.* **2009,** *131*, 12168-14169.

75.   Uhe, A.; Holscher, M.; Leitner, W., Analysis of Potential Molecular Catalysts for the Hydroamination of Ethylene with Ammonia: a DFT Study with [Ir(PCP)] and [Ir(PSiP)] Complexes. *Chem. Eur. J.* **2013,** *19* (3), 1020-1027.

76.   Hollenhorst, H.; McDonald, R.; Ferguson, M.; Turculet, L., Synthesis of Rhodium and Iridium Complexes Supported by Bis(indolylphosphino)silyl Pincer Ligation: Competitive N–H and C–H Bond Activation by an Ir(I) Species. *Organometallics* **2021**, *40* (16), 2768-2784.

77.   Rais, D.; Bergman, R. G., Synthesis and Reactivity of the Monomeric Late-Transition-Metal Parent Amido Complex [Ir(Cp*)(PMe$_3$)(Ph)(NH$_2$)]. *Chem. Eur. J* **2004,** *10* (16), 3970-3978.

78.   Gunnoe, T. B., Reactivity of Ruthenium(II) and Copper(I) Complexes that Possess Anionic Heteroatomic Ligands: Synthetic Exploitation of Nucleophilicity and Basicity of Amido, Hydroxo, Alkoxo, and Aryloxo Ligands for the Activation of Substrates that Possess Polar Bonds as well as Nonpolar C–H and H–H Bonds. *Eur. J. Inorg. Chem.* **2007,** *2007* (9), 1185-1203.

79.   Chaloner, P. A.; Esteruelas, M. A.; Joó, F.; Oro, L. A., *Homogeneous Hydrogenation*, Catalysis by Metal Complexes; Springer, **1994**. 10.1007/978-94-017-1791-5.

80.   Bullock, R. M., Catalysis without Precious Metals. *Wiley-WCH.* **2011**.

81.   Teichert, J. F., Homogenous Hydrogenation with Non-precious Catalysts. *Wiley-VCH.* **2010**.

82.   (a) Yu, R. P.; Darmon, J. M.; Milsmann, C.; Margulieux, G. W.; Stieber, S. C.; DeBeer, S.; Chirik, P. J., Catalytic Hydrogenation Activity and Electronic Structure Determination of Bis(arylimidazol-2-ylidene)pyridine Cobalt Alkyl and Hydride Complexes. *J. Am. Chem. Soc.* **2013,** *135* (35), 13168-84; (b) Darmon, J. M.; Yu, R. P.; Semproni, S. P.; Turner, Z. R.; Stieber, S. C.; DeBeer, S.; Chirik, P. J., Electronic Structure Determination of Pyridine N-Heterocyclic Carbene Iron Dinitrogen Complexes and Neutral Ligand Derivatives. *Organometallics* **2014,** *33* (19), 5423-5433.

83.   Alig, L.; Fritz, M.; Schneider, S., First-Row Transition Metal (De)Hydrogenation Catalysis Based On Functional Pincer Ligands. *Chem. Rev.* **2019,** *119* (4), 2681-2751.

84.   Daida, E. J.; Peters, J. C., Considering Fe$^{II/IV}$ Redox Processes as Mechanistically Relevant to the Catalytic Hydrogenation of Olefins by [PhBP^{iPr3}]Fe-H$_x$ Species. *Inorg. Chem. Front.* **2004,** *43*, 7474-7485.

85.   Srimani, D.; Diskin-Posner, Y.; Ben-David, Y.; Milstein, D., Iron Pincer Complex Catalyzed, Environmentally Benign, E-Selective Semi-Hydrogenation of Alkynes. *Angew. Chem., Int. Ed.* **2013,** *52* (52), 14131 –14134.

86.   Gorgas, N.; Brunig, J.; Stoger, B.; Vanicek, S.; Tilset, M.; Veiros, L. F.; Kirchner, K., Efficient Z-Selective Semihydrogenation of Internal Alkynes Catalyzed by Cationic Iron(II) Hydride Complexes. *J. Am. Chem. Soc.* **2019,** *141* (43), 17452-17458.

87.   (a) Takaya, J.; Kirai, N.; Iwasawa, N., Efficient Synthesis of Diborylalkenes from Alkenes and Diboron by a New PSiP-Pincer Palladium-Catalyzed Dehydrogenative Borylation. *J. Am. Chem. Soc.* **2011,** *133* (33), 12980-12983; (b) Wu, S.; Li, X.; Xiong, Z.; Xu, W.; Lu, Y.; Sun, H., Synthesis and Reactivity of Silyl Iron, Cobalt, and Nickel Complexes Bearing a [PSiP]-Pincer Ligand via Si–H Bond Activation. *Organometallics* **2013,** *32* (11), 3227-3237; (c) Suh, H.; Guard, L. M.; Hazari, N., Synthesis and reactivity of a masked PSiP pincer supported nickel hydride. *Polyhedron* **2014,** *84*, 37-43; (d) Imayoshi, R.; Nakajima, K.; Takaya, J.; Iwasawa, N.; Nishibayashi, Y., Synthesis and Reactivity of Iron- and Cobalt-Dinitrogen Complexes Bearing PSiP-Type Pincer Ligands toward Nitrogen Fixation. *Eur. J. Inorg. Chem.* **2017,** *2017* (32), 3769-3778; (e) Murphy, L. J.; Ruddy, A. J.; McDonald, R.; Ferguson, M. J.; Turculet, L., Activation of Molecular Hydrogen and Oxygen by PSiP Complexes of Cobalt. *Eur. J. Inorg. Chem.* **2018,** *2018* (40), 4481-4493.

88.   Nikonov, G. I., Recent Advances in Nonclassical Interligand Si---H Interactions. *Elsevier.* **2005,** *53*, 217.

89. Corey, J. Y., Reactions of Hydrosilanes with Transition Metal Complexes. *Chem. Rev.* **2016,** *116* (19), 11291-11435.

90. (a) Ding, S.; Song, L. J.; Chung, L. W.; Zhang, X.; Sun, J.; Wu, Y. D., Ligand-Controlled Remarkable Regio- and Stereodivergence in Intermolecular Hydrosilylation of Internal Alkynes: Experimental and Theoretical Studies. *J. Am. Chem. Soc.* **2013,** *135* (37), 13835-13842; (b) Sundararaju, B.; Fürstner, A., A *trans*-Selective Hydroboration of Internal Alkynes. *Angew. Chem., Int. Ed.* **2013,** *52* (52), 14050-14054; (c) Rummelt, S. M.; Fürstner, A., Ruthenium-catalyzed trans-selective hydrostannation of alkynes. *Angew. Chem., Int. Ed.* **2014,** *53* (14), 3626-3630; (d) Leutzsch, M.; Wolf, L. M.; Gupta, P.; Fuchs, M.; Thiel, W.; Fares, C.; Fürstner, A., Formation of Ruthenium Carbenes by Gem-Hydrogen Transfer to Internal Alkynes: Implications for Alkyne Trans-Hydrogenation. *Angew. Chem., Int. Ed.* **2015,** *54* (42), 12431-12436.

91. (a) Bézier, D.; Sortais, J.; Darcel, C., N-Heterocyclic Carbene Ligands and Iron: An Effective Association for Catalysis. *ASC.* **2013,** *355* (1), 19-33; (b) Riener, K.; Haslinger, S.; Raba, A.; Hogerl, M. P.; Cokoja, M.; Herrmann, W. A.; Kuhn, F. E., Chemistry of Iron N-Heterocyclic Carbene Complexes: Syntheses, Structures, Reactivities, and Catalytic Applications. *Chem. Rev.* **2014,** *114* (10), 5215-5272; (c) Johnson, C.; Albrecht, M., Piano-stool N-Heterocyclic Carbene Iron Complexes: Synthesis, Reactivity and Catalytic Applications. *Coord. Chem. Rev.* **2017,** *352*, 1-14.

92. (a) Fukumoto, K.; Sakai, A.; Oya, T.; Nakazawa, H., Desulfurization of N,N-dimethylthioformamide by hydrosilane with the help of an iron complex. Isolation and characterization of an iron-carbene complex as an intermediate of C=double bond cleavage. *Chem. Commun.* **2012,** *48* (32), 3809-11; (b) de Brito Sá, É.; Rodríguez-Santiago, L.; Sodupe, M.; Solans-Monfort, X., Toward Olefin Metathesis with Iron Carbene Complexes: Benefits of Tridentate σ-Donating Ligands. *Organometallics* **2016,** *35* (23), 3914-3923; (c) Batista, V. F.; Pinto, D. C. A.; Silva, A. M. S., Iron: A Worthy Contender in Metal Carbene Chemistry. *ACS Catal.* **2020,** *10* (17), 10096-10116.

93. (a) Evans, D. F., The Determination of the Paramagnetic Susceptibility of Substances in Solution by Nuclear Magnetic Resonance. *J. Am. Chem. Soc.* **1959**, 2003-2005; (b) Bain, G. A.; Berry, J. F., Diamagnetic Corrections and Pascal's Constants. *J. Chem. Educ.* **2008,** *85* (4), 532-536.

94. Hujon, F.; Lyngdoh, R. H. D.; King, R. B., Iron-Iron Bond Lengths and Bond Orders in Diiron Lantern-Type Complexes with High Spin Ground States. *Eur. J. Inorg. Chem.* **2021**, 848-860.

Appendix A: Chapter 2 Supporting Information

A-1: X-ray Crystallographic Information for Chapter 2

Table A1. Crystallographic Experimental Details for (^{i}Pr-PSiP^{Ind})H (**2-27**).

A. Crystal Data

formula	$C_{31}H_{46}N_2P_2Si$
formula weight	536.73
crystal dimensions (mm)	$0.34 \times 0.28 \times 0.18$
crystal system	orthorhombic
space group	*Pbca* (No. 61)
unit cell parameters^a	
a (Å)	15.566 (2)
b (Å)	15.398 (2)
c (Å)	25.945 (3)
V (Å^3)	6218.4 (14)
Z	8
ρ_{calcd} (g cm^{-3})	1.147
μ (mm^{-1})	0.200

B. Data Collection and Refinement Conditions

diffractometer	Bruker PLATFORM/APEX II CCD^b
radiation (λ [Å])	graphite-monochromated Mo Kα (0.71073)
temperature (°C)	–80
scan type	ω scans (0.3°) (20 s exposures)
data collection 2θ limit (deg)	55.10
total data collected	51277 ($-20 \le h \le 20$, $-19 \le k \le 20$, $-33 \le l \le 33$)
independent reflections	7167 ($R_{int} = 0.0481$)
number of observed reflections (*NO*)	5852 [$F_o^2 \ge 2\sigma(F_o^2)$]
structure solution method	intrinsic phasing (*SHELXT-2014^c*)
refinement method	full-matrix least-squares on F^2 (*SHELXL–2014^d*)
absorption correction method	Gaussian integration (face-indexed)
range of transmission factors	1.0000–0.9098
data/restraints/parameters	7167 / 1^e / 373
goodness-of-fit (S)^f [all data]	1.035
final *R* indices^g	
R_1 [$F_o^2 \ge 2\sigma(F_o^2)$]	0.0418
wR_2 [all data]	0.1182
largest difference peak and hole	0.588 and –0.500 e Å^{-3}

Table A1. Crystallographic Experimental Details for (^{i}Pr-PSiP^{Ind})H (**2-27**) (continued).

[a]Obtained from least-squares refinement of 7467 reflections with $4.86° < 2\theta < 41.24°$.

[b]Programs for diffractometer operation, data collection, data reduction and absorption correction were those supplied by Bruker.

[c]Sheldrick, G. M. *Acta Crystallogr.* **2015**, *A71*, 3–8.

[d]Sheldrick, G. M. *Acta Crystallogr.* **2015**, *C71*, 3–8.

[e]For the disordered Si–H hydrogen, the Si–H1A (75%) and Si–H1B (25%) distances were constrained to be equal (within 0.03 Å) during refinement.

[f]$S = [\Sigma w(F_o^2 - F_c^2)^2/(n - p)]^{1/2}$ (n = number of data; p = number of parameters varied; $w = [\sigma^2(F_o^2) + (0.0529P)^2 + 3.1865P]^{-1}$ where $P = [Max(F_o^2, 0) + 2F_c^2]/3$).

[g]$R_1 = \Sigma||F_o| - |F_c||/\Sigma|F_o|$; $wR_2 = [\Sigma w(F_o^2 - F_c^2)^2/\Sigma w(F_o^4)]^{1/2}$.
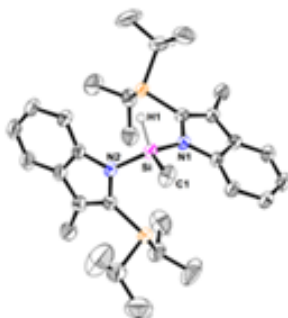
Figure A1. ORTEP diagram of (^{i}Pr-PSiP^{Ind})H (**2-27**).

Table A2. Crystallographic Experimental Details for (^{i}Pr-PSiP^{Ind})RhH(Cl) (**2-28**).

A. Crystal Data

formula	C$_{31}$H$_{46}$ClN$_2$P$_2$RhSi
formula weight	675.09
crystal dimensions (mm)	0.34 × 0.31 × 0.20
crystal system	orthorhombic
space group	$P2_12_12_1$ (No. 19)
unit cell parameters[a]	
a (Å)	10.6176 (5)
b (Å)	16.4722 (8)
c (Å)	18.6791 (8)

Table A2. Crystallographic Experimental Details for (^{i}Pr-PSiP$^{\text{Ind}}$)RhH(Cl) (**2-28**) (continued).

V (Å^3)	3266.9 (3)
Z	4
ρ_{calcd} (g cm^{-3})	1.373
μ (mm^{-1})	6.420

B. Data Collection and Refinement Conditions

diffractometer	Bruker D8/APEX II CCD[b]
radiation (λ [Å])	Cu Kα (1.54178) (microfocus source)
temperature (°C)	–100
scan type	ω and ϕ scans (1.0°) (5 s exposures)
data collection 2θ limit (deg)	148.28
total data collected	22615 ($-13 \leq h \leq 13$, $-19 \leq k \leq 20$, $-23 \leq l \leq 23$)
independent reflections	6580 ($R_{\text{int}} = 0.0303$)
number of observed reflections (*NO*)	6497 [$F_o^2 \geq 2\sigma(F_o^2)$]
structure solution method	Patterson/structure expansion (*DIRDIF–2008*[c])
refinement method	full-matrix least-squares on F^2 (*SHELXL–2014*[d])
absorption correction method	Gaussian integration (face-indexed)
range of transmission factors	0.4352–0.2175
data/restraints/parameters	6580 / 0 / 351
Flack absolute structure parameter[e]	0.055(9)
goodness-of-fit (*S*)[f] [all data]	1.024
final *R* indices[g]	
R_1 [$F_o^2 \geq 2\sigma(F_o^2)$]	0.0292
wR_2 [all data]	0.0723
largest difference peak and hole	2.136 and –0.883 e Å^{-3}

[a]Obtained from least-squares refinement of 9589 reflections with $7.16° < 2\theta < 147.64°$.

[b]Programs for diffractometer operation, data collection, data reduction and absorption correction were those supplied by Bruker.

[c]Beurskens, P. T.; Beurskens, G.; de Gelder, R.; Smits, J. M. M.; Garcia-Granda, S.; Gould, R. O. (2008). The *DIRDIF-2008* program system. Crystallography Laboratory, Radboud University Nijmegen, The Netherlands.

[d]Sheldrick, G. M. *Acta Crystallogr.* **2015**, *C71*, 3–8.

[e]Flack, H. D. *Acta Crystallogr.* **1983**, *A39*, 876–881; Flack, H. D.; Bernardinelli, G. *Acta Crystallogr.* **1999**, *A55*, 908–915; Flack, H. D.; Bernardinelli, G. *J. Appl. Cryst.* **2000**,

33, 1143–1148. The Flack parameter will refine to a value near zero if the structure is in the correct configuration and will refine to a value near one for the inverted configuration.

$^fS = [\Sigma w(F_o^2 - F_c^2)^2/(n - p)]^{1/2}$ (n = number of data; p = number of parameters varied; $w = [\sigma^2(F_o^2) + (0.0328P)^2 + 4.4282P]^{-1}$ where $P = [\text{Max}(F_o^2, 0) + 2F_c^2]/3$).

$^gR_1 = \Sigma||F_o| - |F_c||/\Sigma|F_o|$; $wR_2 = [\Sigma w(F_o^2 - F_c^2)^2/\Sigma w(F_o^4)]^{1/2}$.
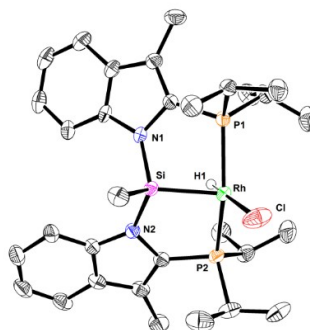
Figure A2. ORTEP diagram of (^{i}Pr-PSiP^{Ind})RhH(Cl) (**2-28**).

Table A3. Crystallographic Experimental Details for (^{i}Pr-PSiP^{Ind})IrH(Cl) (**2-29**).

A. Crystal Data

formula	C$_{31}$H$_{46}$ClIrN$_2$P$_2$Si
formula weight	764.38
crystal dimensions (mm)	0.42 × 0.22 × 0.19
crystal system	monoclinic
space group	$P2_1/n$ (an alternate setting of $P2_1/c$ [No. 14])
unit cell parameters^a	
$\quad a$ (Å)	17.9976 (10)
$\quad b$ (Å)	10.1313 (6)
$\quad c$ (Å)	18.1798 (10)
$\quad \beta$ (deg)	94.6154 (6)
$\quad V$ (Å^3)	3304.1 (3)
$\quad Z$	4
ρ_{calcd} (g cm^{-3})	1.537
μ (mm^{-1})	4.277

B. Data Collection and Refinement Conditions

Table A3. Crystallographic Experimental Details for (^{i}Pr-PSiP^{Ind})IrH(Cl) (**2-29**).

diffractometer	Bruker D8/APEX II CCD[b]
radiation (λ [Å])	graphite-monochromated Mo Kα (0.71073)
temperature (°C)	–100
scan type	ω scans (0.3°) (20 s exposures)
data collection 2θ limit (deg)	53.06
total data collected	26049 (-22 ≤ h ≤ 22, -12 ≤ k ≤ 12, -22 ≤ l ≤ 22)
independent reflections	6829 (R_{int} = 0.0143)
number of observed reflections (*NO*)	6397 [$F_o^2 \geq 2\sigma(F_o^2)$]
structure solution method	intrinsic phasing (*SHELXT-2014*[c])
refinement method	full-matrix least-squares on F^2 (*SHELXL–2014*[d])
absorption correction method	Gaussian integration (face-indexed)
range of transmission factors	0.5999–0.3378
data/restraints/parameters	6829 / 0 / 358
goodness-of-fit (*S*)[e] [all data]	1.042
final *R* indices[f]	
R_1 [$F_o^2 \geq 2\sigma(F_o^2)$]	0.0163
wR_2 [all data]	0.0406
largest difference peak and hole	0.946 and –0.400 e Å^{-3}

[a]Obtained from least-squares refinement of 9792 reflections with 4.62° < 2θ < 53.02°.

[b]Programs for diffractometer operation, data collection, data reduction and absorption correction were those supplied by Bruker.

[c]Sheldrick, G. M. *Acta Crystallogr.* **2015**, *A71*, 3–8. (*SHELXT-2014*)

[d]Sheldrick, G. M. *Acta Crystallogr.* **2015**, *C71*, 3–8. (*SHELXL-2014*)

[e]$S = [\Sigma w(F_o^2 - F_c^2)^2/(n - p)]^{1/2}$ (n = number of data; p = number of parameters varied; $w = [\sigma^2(F_o^2) + (0.0214P)^2 + 2.2886P]^{-1}$ where $P = [\text{Max}(F_o^2, 0) + 2F_c^2]/3$).

[f]$R_1 = \Sigma||F_o| - |F_c||/\Sigma|F_o|$; $wR_2 = [\Sigma w(F_o^2 - F_c^2)^2/\Sigma w(F_o^4)]^{1/2}$.
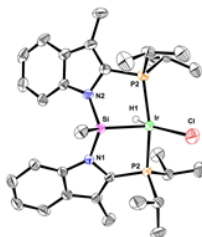
Figure A3. ORTEP diagram of (^{i}Pr-PSiP^{Ind})IrH(Cl) (**2-29**).

Table A4. Crystallographic Experimental Details for (^{i}Pr-PSiP^{Ind})IrH(NHPh) (**2-31a**).

A. Crystal Data

formula	$C_{43}H_{58}IrN_3P_2Si$
formula weight	899.15
crystal dimensions (mm)	$0.31 \times 0.23 \times 0.18$
crystal system	triclinic
space group	$P\bar{1}$ (No. 2)
unit cell parameters^a	
a (Å)	12.2127 (4)
b (Å)	12.5234 (4)
c (Å)	15.2342 (4)
α (deg)	103.9661 (6)
β (deg)	107.6365 (7)
γ (deg)	100.9991 (7)
V (Å^3)	2065.23 (11)
Z	2
ρ_{calcd} (g cm^{-3})	1.446
μ (mm^{-1})	7.510

B. Data Collection and Refinement Conditions

diffractometer	Bruker D8/APEX II CCD^b
radiation (λ [Å])	Cu Kα (1.54178) (microfocus source)
temperature (°C)	−100
scan type	ω and ϕ scans (1.0°) (5 s exposures)
data collection 2θ limit (deg)	148.14
total data collected	14776 ($-15 \leq h \leq 14$, $-15 \leq k \leq 15$, $-18 \leq l \leq 18$)
independent reflections	8006 ($R_{int} = 0.0147$)
number of observed reflections (*NO*)	7992 [$F_o^2 \geq 2\sigma(F_o^2)$]
structure solution method	Patterson/structure expansion (*DIRDIF–2008^c*)
refinement method	full-matrix least-squares on F^2 (*SHELXL–2014^d*)
absorption correction method	Gaussian integration (face-indexed)
range of transmission factors	0.5022–0.2374
data/restraints/parameters	8006 / 0 / 462
goodness-of-fit (*S*)^e [all data]	1.124
final *R* indices^f	

Table A4. Crystallographic Experimental Details for (*i*Pr-PSiP^Ind)IrH(NHPh) (**2-31a**) (continued).

$R_1 \ [F_o{}^2 \geq 2\sigma(F_o{}^2)]$	0.0192
wR_2 [all data]	0.0492
largest difference peak and hole	0.477 and -1.477 e Å^{-3}

[a]Obtained from least-squares refinement of 9770 reflections with $8.18° < 2\theta < 147.36°$.

[b]Programs for diffractometer operation, data collection, data reduction and absorption correction were those supplied by Bruker.

[c]Beurskens, P. T.; Beurskens, G.; de Gelder, R.; Smits, J. M. M.; Garcia-Granda, S.; Gould, R. O. (2008). The *DIRDIF-2008* program system. Crystallography Laboratory, Radboud University Nijmegen, The Netherlands.

[d]Sheldrick, G. M. *Acta Crystallogr.* **2015**, *C71*, 3–8.

[e]$S = [\Sigma w(F_o{}^2 - F_c{}^2)^2/(n - p)]^{1/2}$ (n = number of data; p = number of parameters varied; $w = [\sigma^2(F_o{}^2) + (0.0231P)^2 + 1.7493P]^{-1}$ where $P = [\text{Max}(F_o{}^2, 0) + 2F_c{}^2]/3$).

[f]$R_1 = \Sigma ||F_o| - |F_c||/\Sigma|F_o|$; $wR_2 = [\Sigma w(F_o{}^2 - F_c{}^2)^2/\Sigma w(F_o{}^4)]^{1/2}$.
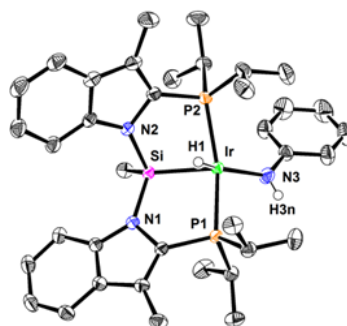
Figure A4. Crystallographic Experimental Details for (*i*Pr-PSiP^Ind)IrH(NHPh) (**2-31a**).

Table A5. Crystallographic Experimental Details for (*i*Pr-PSiP^Ind)Ir(H)[NH(2,6-*i*Pr$_2$C$_6$H$_3$)] (**2-31c**).

A. Crystal Data

formula	C$_{43}$H$_{64}$IrN$_3$P$_2$Si
formula weight	905.20
crystal dimensions (mm)	$0.25 \times 0.18 \times 0.13$
crystal system	monoclinic
space group	$P2_1/n$ (an alternate setting of $P2_1/c$ [No. 14])
unit cell parameters[a]	

Table A5. Crystallographic Experimental Details for (^{i}Pr-PSiP^{Ind})Ir(H)[NH(2,6-^{i}Pr$_2$C$_6$H$_3$)] (**2-31c**) (continued).

a (Å)	16.9980 (5)
b (Å)	13.4994 (4)
c (Å)	18.6961 (5)
β (deg)	100.3754 (9)
V (Å^3)	4219.9 (2)
Z	4
ρ_{calcd} (g cm^{-3})	1.425
μ (mm^{-1})	7.351

B. Data Collection and Refinement Conditions

diffractometer	Bruker D8/APEX II CCD[b]
radiation (λ [Å])	Cu Kα (1.54178) (microfocus source)
temperature (°C)	−100
scan type	ω and ϕ scans (1.0°) (5 s exposures)
data collection 2θ limit (deg)	147.90
total data collected	29209 (-21 ≤ h ≤ 21, -16 ≤ k ≤ 16, -23 ≤ l ≤ 23)
independent reflections	8542 (R_{int} = 0.0163)
number of observed reflections (*NO*)	8337 [$F_o^2 \geq 2\sigma(F_o^2)$]
structure solution method	Patterson/structure expansion (*DIRDIF–2008*[c])
refinement method	full-matrix least-squares on F^2 (*SHELXL–2014*[d])
absorption correction method	Gaussian integration (face-indexed)
range of transmission factors	0.5632–0.3370
data/restraints/parameters	8542 / 0 / 462
goodness-of-fit (*S*)[e] [all data]	1.048
final *R* indices[f]	
R_1 [$F_o^2 \geq 2\sigma(F_o^2)$]	0.0171
wR_2 [all data]	0.0437
largest difference peak and hole	0.347 and –0.756 e Å^{-3}

[a]Obtained from least-squares refinement of 9667 reflections with 10.16° < 2θ < 147.90°.

[b]Programs for diffractometer operation, data collection, data reduction and absorption correction were those supplied by Bruker.

[c]Beurskens, P. T.; Beurskens, G.; de Gelder, R.; Smits, J. M. M.; Garcia-Granda, S.; Gould, R. O. (2008). The *DIRDIF-2008* program system. Crystallography Laboratory, Radboud University Nijmegen, The Netherlands.

[d]Sheldrick, G. M. *Acta Crystallogr.* **2015**, *C71*, 3–8.

[e]$S = [\Sigma w(F_o^2 - F_c^2)^2/(n - p)]^{1/2}$ (n = number of data; p = number of parameters varied; w

Table A5. Crystallographic Experimental Details for (^{i}Pr-PSiP^{Ind})Ir(H)[NH(2,6-^{i}Pr$_2$C$_6$H$_3$)] (**2-31c**) (continued).

$= [\sigma^2(F_o^2) + (0.0210P)^2 + 3.0082P]^{-1}$ where $P = [\text{Max}(F_o^2, 0) + 2F_c^2]/3)$.

$^fR_1 = \Sigma||F_o| - |F_c||/\Sigma|F_o|$; $wR_2 = [\Sigma w(F_o^2 - F_c^2)^2/\Sigma w(F_o^4)]^{1/2}$.
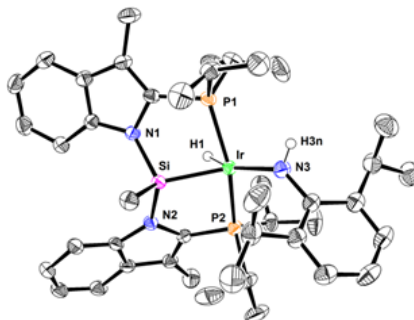
Figure A5. ORTEP diagram of (^{i}Pr-PSiP^{Ind})Ir(H)[NH(2,6-^{i}Pr$_2$C$_6$H$_3$)] (**2-31c**).

Table A6. Crystallographic Experimental Details for (^{i}Pr-PSiP^{Ind})IrH(NH^{t}Bu) (**2-33a**).

A. Crystal Data

formula	C$_{35}$H$_{56}$IrN$_3$P$_2$Si
formula weight	801.05
crystal dimensions (mm)	0.21 × 0.12 × 0.03
crystal system	monoclinic
space group	C2/c (No. 15)
unit cell parameters^a	
a (Å)	39.7688 (11)
b (Å)	13.4538 (4)
c (Å)	14.4543 (4)
β (deg)	104.5355 (15)
V (Å^3)	7486.1 (4)
Z	8
ρ_{calcd} (g cm^{-3})	1.421
μ (mm^{-1})	8.211

B. Data Collection and Refinement Conditions

diffractometer	Bruker D8/APEX II CCD^b
radiation (λ [Å])	Cu Kα (1.54178) (microfocus source)
temperature (°C)	–100
scan type	ω and ϕ scans (1.0°) (5 s exposures)
data collection 2θ limit (deg)	140.96
total data collected	124181 (-48 ≤ h ≤ 45,-16≤ k ≤ 16, -17≤l≤17)

Table A6. Crystallographic Experimental Details for (^{i}Pr-PSiP^{Ind})IrH(NH^{t}Bu) (**2-33a**) (continued).

independent reflections	6941 ($R_{int} = 0.0795$)
number of observed reflections (*NO*)	6380 [$F_o^2 \geq 2\sigma(F_o^2)$]
structure solution method	intrinsic phasing (*SHELXT-2014^c*)
refinement method	full-matrix least-squares on F^2 (*SHELXL–2014^d*)
absorption correction method	Gaussian integration (face-indexed)
range of transmission factors	0.8611–0.2820
data/restraints/parameters	6941 / 16^e / 443
goodness-of-fit (*S*)^e [all data]	1.170
final *R* indices^f	
R_1 [$F_o^2 \geq 2\sigma(F_o^2)$]	0.0361
wR_2 [all data]	0.0908
largest difference peak and hole	1.098 and –1.092 e Å^{-3}

^{a}Obtained from least-squares refinement of 9976 reflections with $6.96° < 2\theta < 140.22°$.

^{b}Programs for diffractometer operation, data collection, data reduction and absorption correction were those supplied by Bruker.

^{c}Sheldrick, G. M. *Acta Crystallogr.* **2015**, *A71*, 3–8. (*SHELXT-2014*)

^{d}Sheldrick, G. M. *Acta Crystallogr.* **2015**, *C71*, 3–8. (*SHELXL-2014*)

^{e}The disordered *tert*-butyl group was restrained to have approximately the same geometery by use of the *SHELXL* **SAME** instruction. Additionally, an anti-bumping restraint was applied to the H3N···H41B (of the minor orientation of the disordered isopropyl group) distance.

$^f S = [\Sigma w(F_o^2 - F_c^2)^2/(n - p)]^{1/2}$ (*n* = number of data; *p* = number of parameters varied; $w = [\sigma^2(F_o^2) + (0.0213P)^2 + 61.1963P]^{-1}$ where $P = [Max(F_o^2, 0) + 2F_c^2]/3$).

$^g R_1 = \Sigma||F_o| - |F_c||/\Sigma|F_o|$; $wR_2 = [\Sigma w(F_o^2 - F_c^2)^2/\Sigma w(F_o^4)]^{1/2}$.

Only the major orientations of the disordered *tert*-butyl and isopropyl groups are shown.
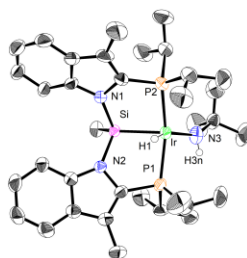
Figure A6. ORTEP diagram of (^{i}Pr-PSiP^{Ind})IrH(NH^{t}Bu) (**2-33a**).

Table A7. ORTEP diagram of (^{i}Pr-PSiP^{Ind})IrH(NH-N(CH$_2$CH$_2$)$_2$NMe) (**2-35a**).

A. Crystal Data

formula	C$_{36}$H$_{58}$IrN$_5$P$_2$Si
formula weight	843.10
crystal dimensions (mm)	$0.34 \times 0.21 \times 0.20$
crystal system	monoclinic
space group	$P2_1/c$ (No. 14)
unit cell parameters^a	
$\quad a$ (Å)	25.8898 (9)
$\quad b$ (Å)	12.5138 (5)
$\quad c$ (Å)	24.8225 (9)
$\quad \beta$ (deg)	108.4096 (5)
$\quad V$ (Å^3)	7630.4 (5)
$\quad Z$	8
ρ_{calcd} (g cm^{-3})	1.468
μ (mm^{-1})	3.646

B. Data Collection and Refinement Conditions

diffractometer	Bruker D8/APEX II CCD^b
radiation (λ [Å])	graphite-monochromated Mo Kα (0.71073)
temperature (°C)	-100
scan type	ω scans (0.3°) (15 s exposures)
data collection 2θ limit (deg)	56.61
total data collected	70164 ($-34 \le h \le 34$, $-16 \le k \le 16$, $-33 \le l \le 33$)
independent reflections	18766 (R_{int} = 0.0340)
number of observed reflections (*NO*)	15988 [$F_o^2 \ge 2\sigma(F_o^2)$]
structure solution method	Patterson/structure expansion (*DIRDIF–2008^c*)
refinement method	full-matrix least-squares on F^2 (*SHELXL–2014^d*)
absorption correction method	Gaussian integration (face-indexed)
range of transmission factors	0.6164–0.4196
data/restraints/parameters	18766 / 0 / 832
goodness-of-fit (*S*)^e [all data]	1.038
final *R* indices^f	
$\quad R_1$ [$F_o^2 \ge 2\sigma(F_o^2)$]	0.0269
$\quad wR_2$ [all data]	0.0667
largest difference peak and hole	3.159 and -0.806 e Å^{-3}

^{a}Obtained from least-squares refinement of 9918 reflections with $4.58° < 2\theta < 49.12°$.

Table A7. ORTEP diagram of (^{i}Pr-PSiP^{Ind})IrH(NH-N(CH$_2$CH$_2$)$_2$NMe) (**2-35a**) (continued).

[b]Programs for diffractometer operation, data collection, data reduction and absorption correction were those supplied by Bruker.

[c]Beurskens, P. T.; Beurskens, G.; de Gelder, R.; Smits, J. M. M.; Garcia-Granda, S.; Gould, R. O. (2008). The *DIRDIF-2008* program system. Crystallography Laboratory, Radboud University Nijmegen, The Netherlands.

[d]Sheldrick, G. M. *Acta Crystallogr.* **2015**, *C71*, 3–8.

[e]$S = [\Sigma w(F_o^2 - F_c^2)^2/(n - p)]^{1/2}$ (n = number of data; p = number of parameters varied; $w = [\sigma^2(F_o^2) + (0.0310P)^2 + 3.9900P]^{-1}$ where $P = [\text{Max}(F_o^2, 0) + 2F_c^2]/3$).

[f]$R_1 = \Sigma||F_o| - |F_c||/\Sigma|F_o|$; $wR_2 = [\Sigma w(F_o^2 - F_c^2)^2/\Sigma w(F_o^4)]^{1/2}$.

Perspective view of one of the two cystallographically-independent molecules of [{*k*3–MeSi(2-*i*Pr2P-3-Me-1*H*-indol-1-yl)2}IrH(4-methylpiperazin-1-amido)] shown.
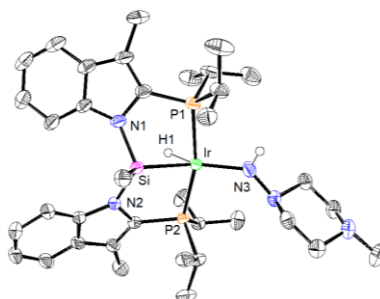
Figure A7. ORTEP diagram of (^{i}Pr-PSiP^{Ind})IrH(NH-N(CH$_2$CH$_2$)$_2$NMe) (**2-35a**).

Table A8. Crystallographic Experimental Details for (^{i}Pr-PSiP^{Ind})Rh(DMAP) (**2-39b**).

A. Crystal Data

formula	C$_{41}$H$_{58}$N$_4$P$_2$RhSi
formula weight	799.85
crystal dimensions (mm)	0.16 × 0.12 × 0.06
crystal system	monoclinic
space group	$P2_1/n$ (an alternate setting of $P2_1/c$ [No. 14])
unit cell parameters[a]	
a (Å)	9.64804 (13)
b (Å)	16.9264 (2)
c (Å)	25.0798 (3)
β (deg)	97.2958 (9)
V (Å^3)	4062.53 (9)
Z	4

Table A8. Crystallographic Experimental Details for (^{i}Pr-PSiP^{Ind})Rh(DMAP) (**2-39b**) (continued).

ρ_{calcd} (g cm^{-3})	1.308
μ (mm^{-1})	4.672

B. Data Collection and Refinement Conditions

diffractometer	Bruker D8/APEX II CCD^b
radiation (λ [Å])	Cu Kα (1.54178) (microfocus source)
temperature (°C)	–100
scan type	ω and ϕ scans (1.0°) (5 s exposures)
data collection 2θ limit (deg)	148.30
total data collected	262187 ($-12 \le h \le 12$, $-21 \le k \le 21$, $-31 \le l \le 31$)
independent reflections	8594 (R_{int} = 0.0985)
number of observed reflections (*NO*)	7651 [$F_o^2 \ge 2\sigma(F_o^2)$]
structure solution method	Patterson/structure expansion (*DIRDIF–2008^c*)
refinement method	full-matrix least-squares on F^2 (*SHELXL–2014^d*)
absorption correction method	multi-scan (*TWINABS*)
range of transmission factors	0.6626–0.4735
data/restraints/parameters	8594 / 0 / 448
goodness-of-fit (*S*)^e [all data]	1.052
final *R* indices^f	
R_1 [$F_o^2 \ge 2\sigma(F_o^2)$]	0.0366
wR_2 [all data]	0.0974
largest difference peak and hole	0.927 and –0.610 e Å^{-3}

^{a}Obtained from least-squares refinement of 9345 reflections with $6.32° < 2\theta < 147.02°$.

^{b}Programs for diffractometer operation, data collection, data reduction and absorption correction were those supplied by Bruker. The crystal used for data collection was found to display non-merohedral twinning. Both components of the twin were indexed with the program *CELL_NOW* (Bruker AXS Inc., Madison, WI, 2004). The second twin component can be related to the first component by 180º rotation about the [0 1 0] axis in both real and reciprocal space. Integrated intensities for the reflections from the two components were written into a *SHELXL-2014* HKLF 5 reflection file with the data integration program *SAINT* (version 8.34A), using all reflection data (exactly overlapped, partially overlapped and non-overlapped). The refined value of the twin fraction (*SHELXL-2014* BASF parameter) was 0.4574 (12).

^{c}Beurskens, P. T.; Beurskens, G.; de Gelder, R.; Smits, J. M. M.; Garcia-Granda, S.; Gould, R. O. (2008). The *DIRDIF-2008* program system. Crystallography Laboratory,

Table A8. Crystallographic Experimental Details for (^{i}Pr-PSiP^{Ind})Rh(DMAP) (**2-39b**) (continued).

Radboud University Nijmegen, The Netherlands.

[d]Sheldrick, G. M. *Acta Crystallogr.* **2015**, *C71*, 3–8.

[e]$S = [\Sigma w(F_o^2 - F_c^2)^2/(n - p)]^{1/2}$ (n = number of data; p = number of parameters varied; $w = [\sigma^2(F_o^2) + (0.0543P)^2 + 1.7650P]^{-1}$ where $P = [Max(F_o^2, 0) + 2F_c^2]/3$).

[f]$R_1 = \Sigma||F_o| - |F_c||/\Sigma|F_o|$; $wR_2 = [\Sigma w(F_o^2 - F_c^2)^2/\Sigma w(F_o^4)]^{1/2}$.
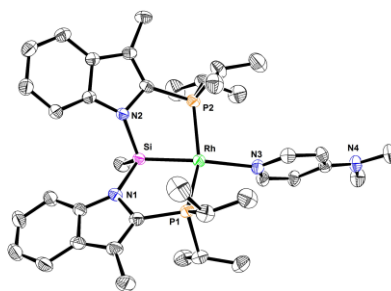
Figure A8. ORTEP diagram of (^{i}Pr-PSiP^{Ind})Rh(DMAP) (**2-39b**).

A-2: Selected NMR Data for Chapter 2

Figure A9. (a) $^{31}P\{^1H\}$, (b) ^1H, and (c) $^{13}C\{^1H\}$ NMR spectra (benzene-d_6) of (^{i}Pr-PSiP^{Ind})RhH(Cl) (**2-28**).
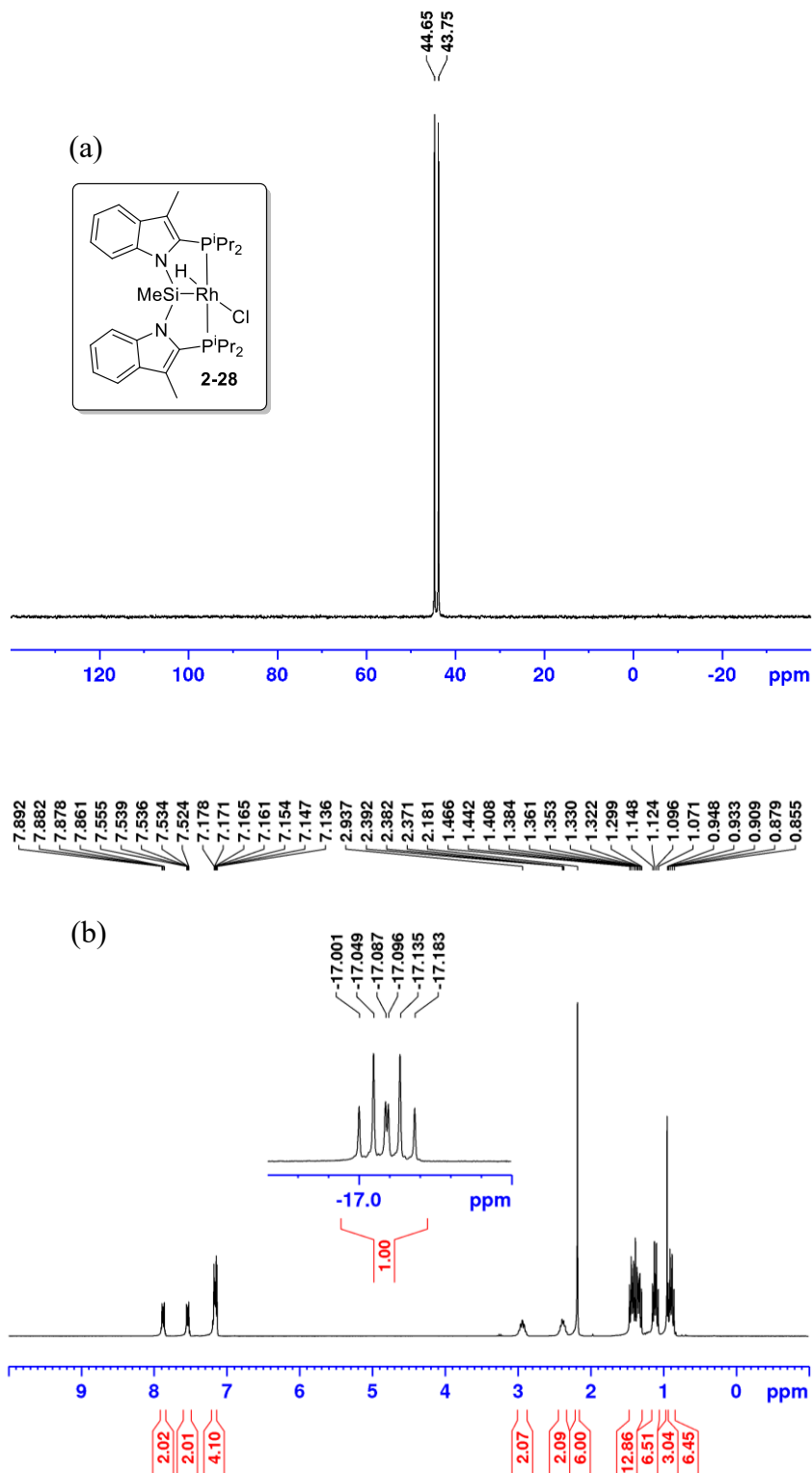
Figure A9. (continued) (a) $^{31}P\{^1H\}$, (b) ^1H, and (c) $^{13}C\{^1H\}$ NMR spectra (benzene-d$_6$) of (^iPr-PSiP^{Ind})RhH(Cl) (**2-28**).

(c)
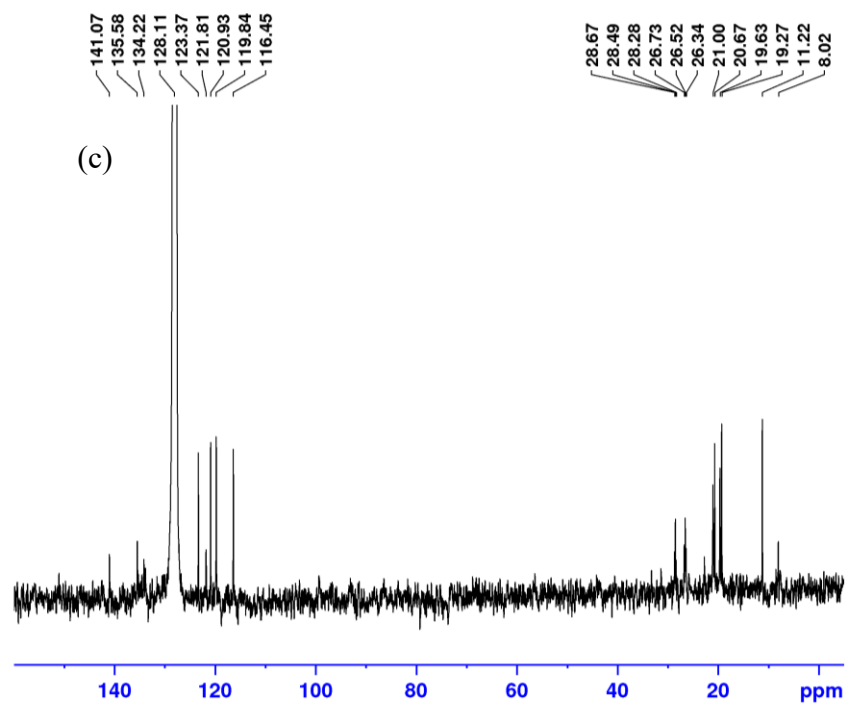
Figure A10. (a) $^{31}P\{^1H\}$, (b) ^1H, and (c) $^{13}C\{^1H\}$ NMR spectra (benzene-d_6) of (^{i}Pr-PSiP^{Ind})IrH(Cl) (**2-29**).
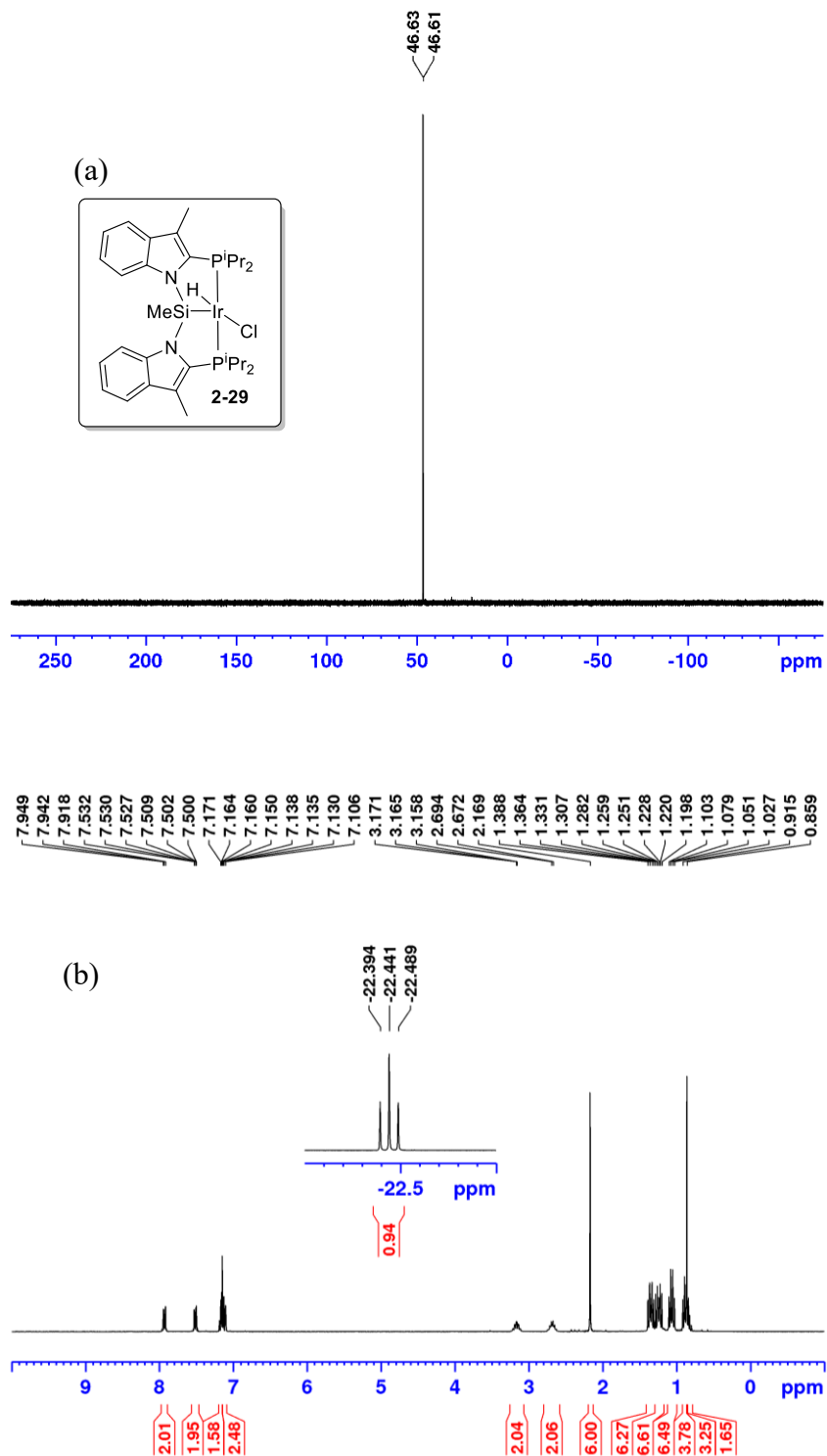
Figure A10. (continued) (a) $^{31}P\{^{1}H\}$, (b) ^{1}H, and (c) $^{13}C\{^{1}H\}$ NMR spectra (benzene-d_6) of (^{i}Pr-PSiP^{Ind})IrH(Cl) (**2-29**).
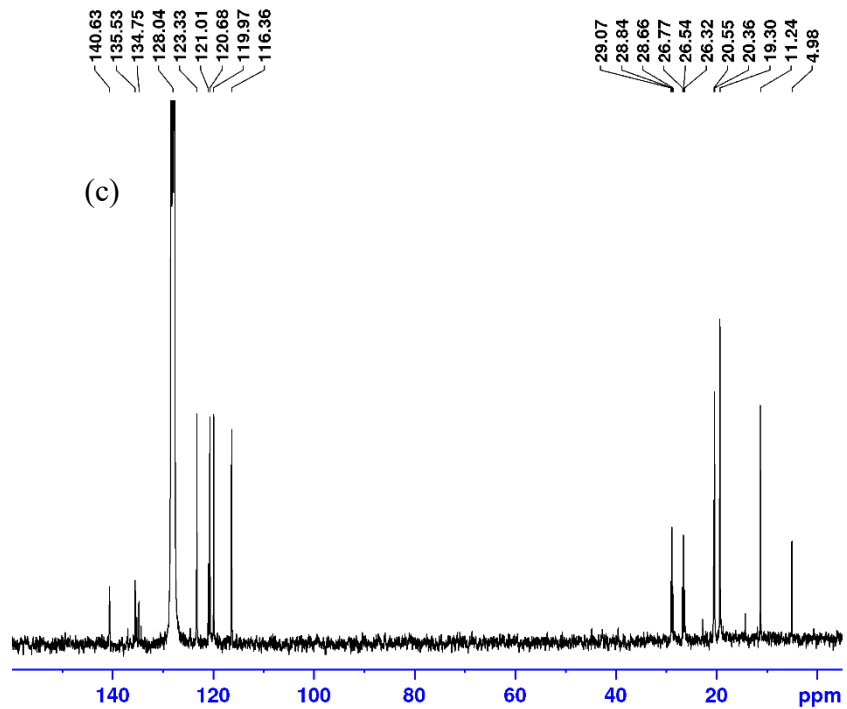
Figure A11. (a) $^{31}P\{^1H\}$, (b) ^1H, and (c) $^{13}C\{^1H\}$ NMR spectra (benzene-d_6) of (^{i}Pr-PSiP^{Ind})RhH(NHPh) (**2-30a**).
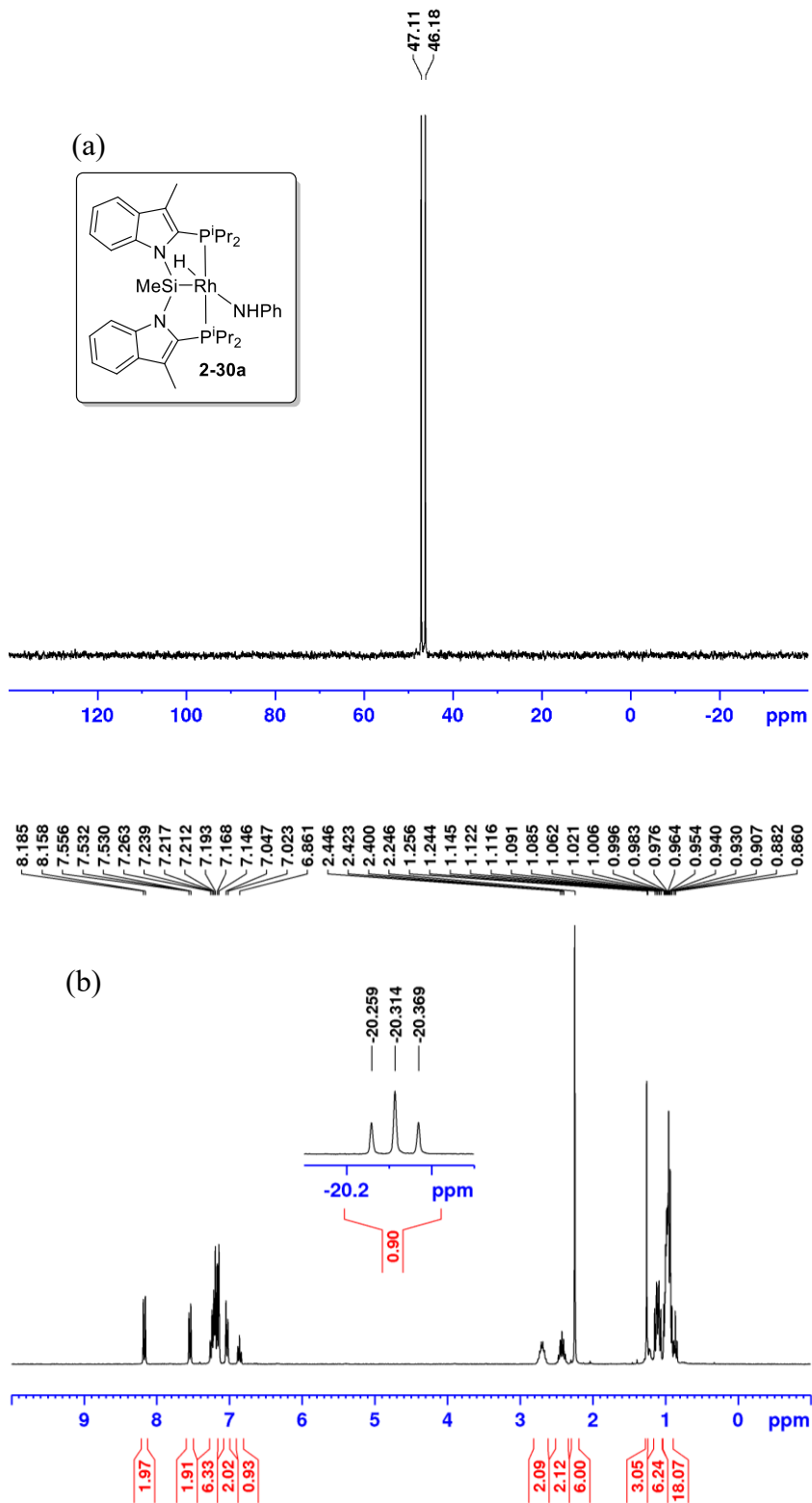
Figure A11. (continued) (a) $^{31}P\{^1H\}$, (b) ^1H, and (c) $^{13}C\{^1H\}$ NMR spectra (benzene-d_6) of (^{i}Pr-PSiP^{Ind})RhH(NHPh) (**2-30a**).
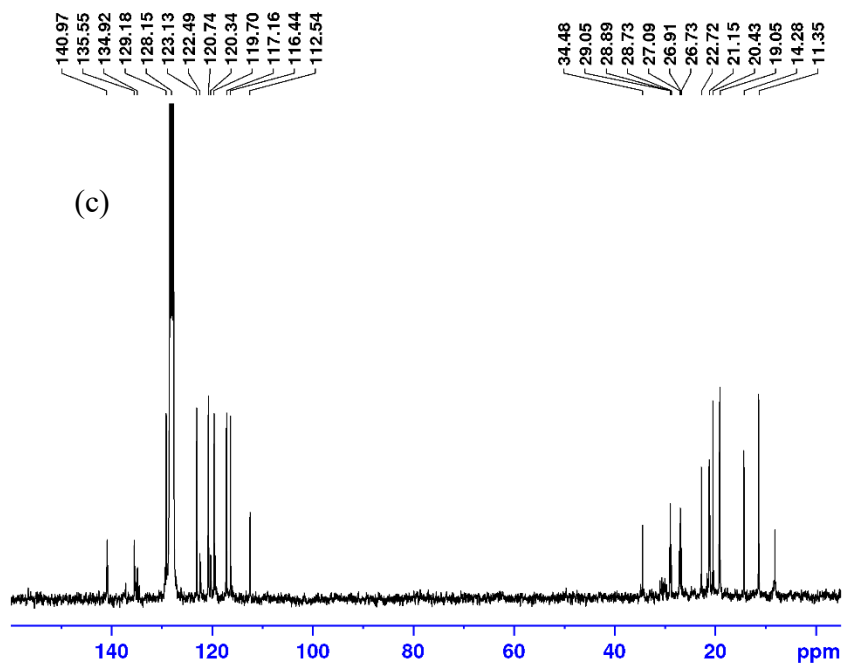
Figure A12. ^{1}H-^{29}Si HMBC NMR (500 × 99.4 MHz) spectrum of (^{i}Pr-PSiP^{Ind})RhH(NHPh) (**2-30a**; benzene-d_6); a scale factor of 7 was applied, such that $^2J_{SiH} = \Delta v/7$.
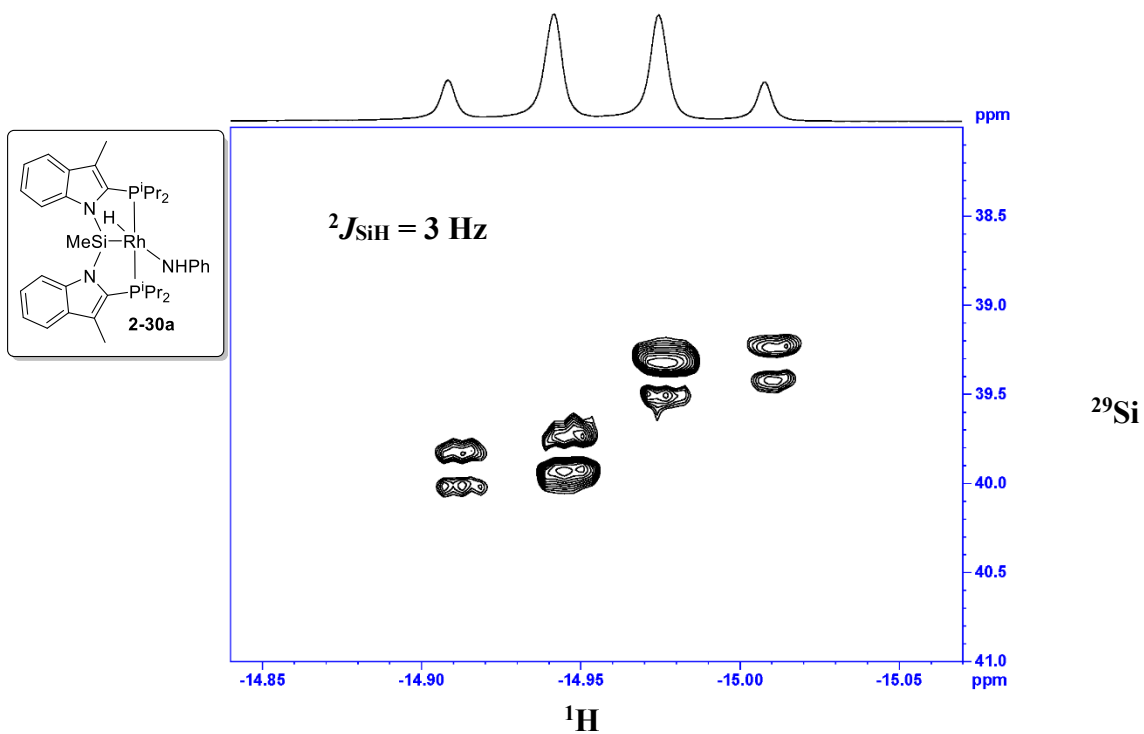
Figure A13. (a) $^{31}P\{^1H\}$, (b) ^1H, and (c) $^{13}C\{^1H\}$ NMR spectra (benzene-d_6) of (^iPr-PSiP^{Ind})RhH[NH(2,6-Me$_2$C$_6$H$_3$)] (**2-30b**).
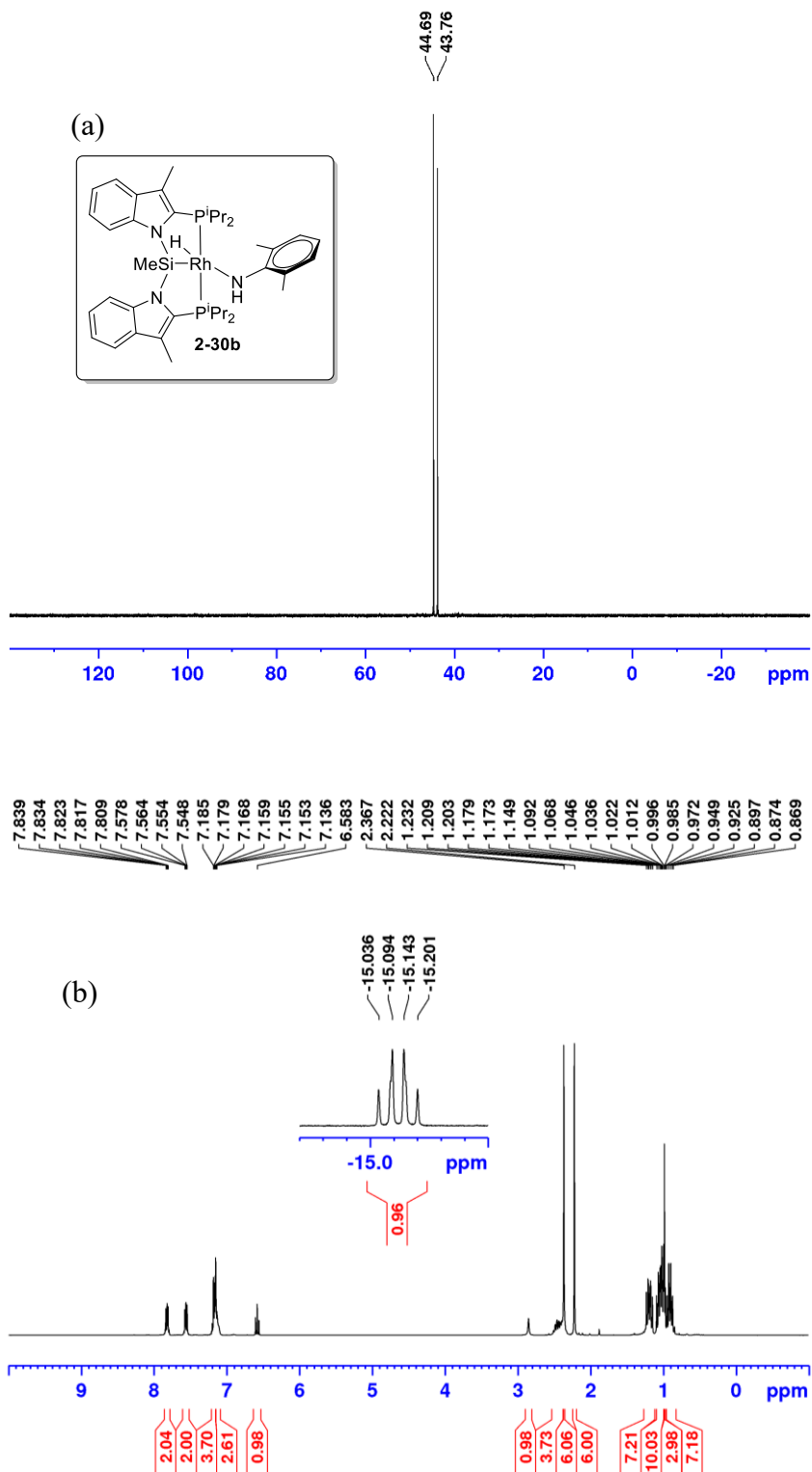
Figure A13. (continued) (a) $^{31}P\{^{1}H\}$, (b) ^{1}H, and (c) $^{13}C\{^{1}H\}$ NMR spectra (benzene-d_6) of (^{i}Pr-PSiP^{Ind})RhH[NH(2,6-Me$_2$C$_6$H$_3$)] (**2-30b**).
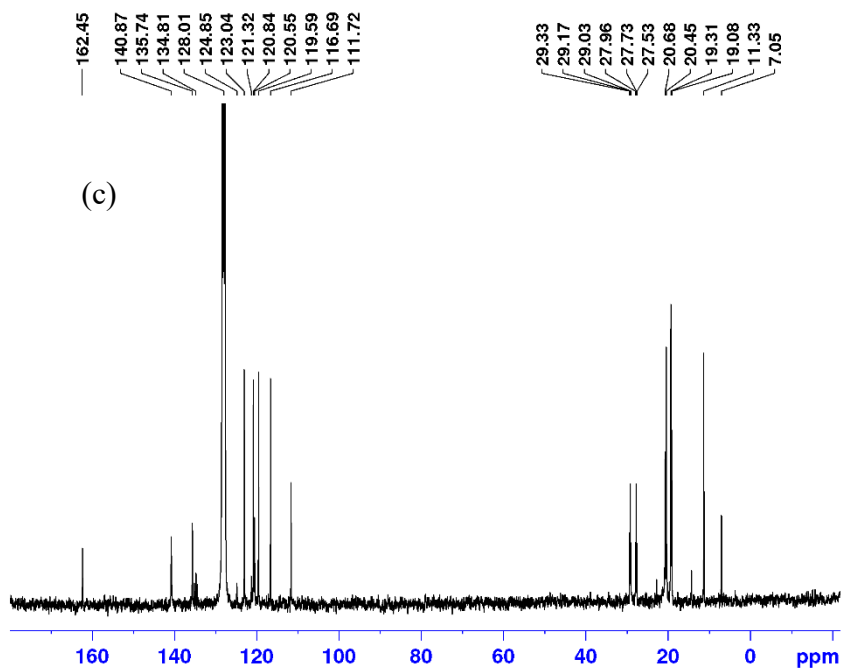
Figure A14. (a) $^{31}P\{^1H\}$, (b) ^1H, and (c) $^{13}C\{^1H\}$ NMR spectra (benzene-d_6) of (^{i}Pr-PSiP^{Ind})RhH[NH(2,6-^{i}Pr$_2$C$_6$H$_3$)] (**2-30c**).
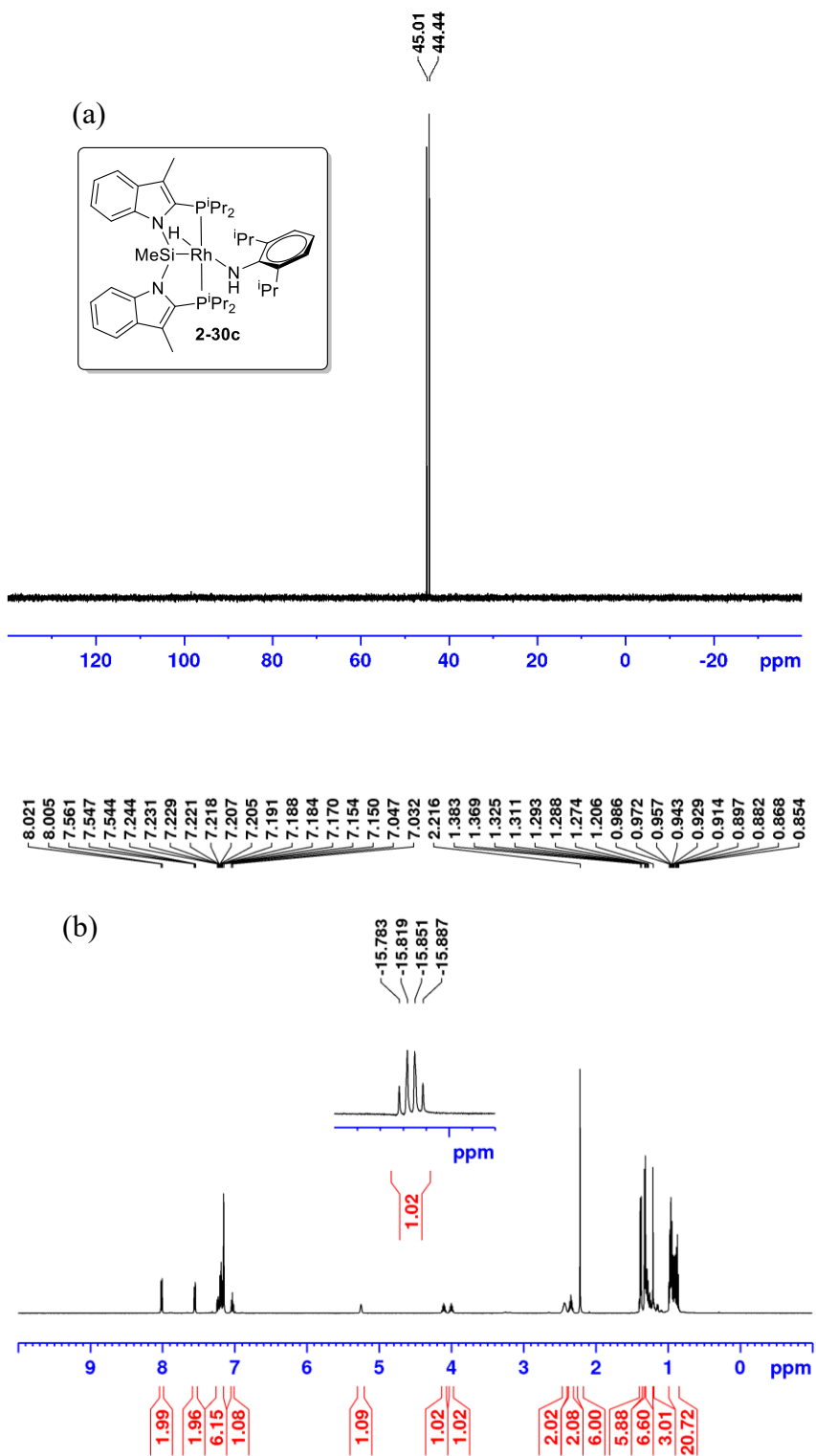
Figure A14. (continued) (a) $^{31}P\{^1H\}$, (b) ^1H, and (c) $^{13}C\{^1H\}$ NMR spectra (benzene-d_6) of (^iPr-PSiP^{Ind})RhH[NH(2,6-$^iPr_2C_6H_3$)] (**2-30c**).
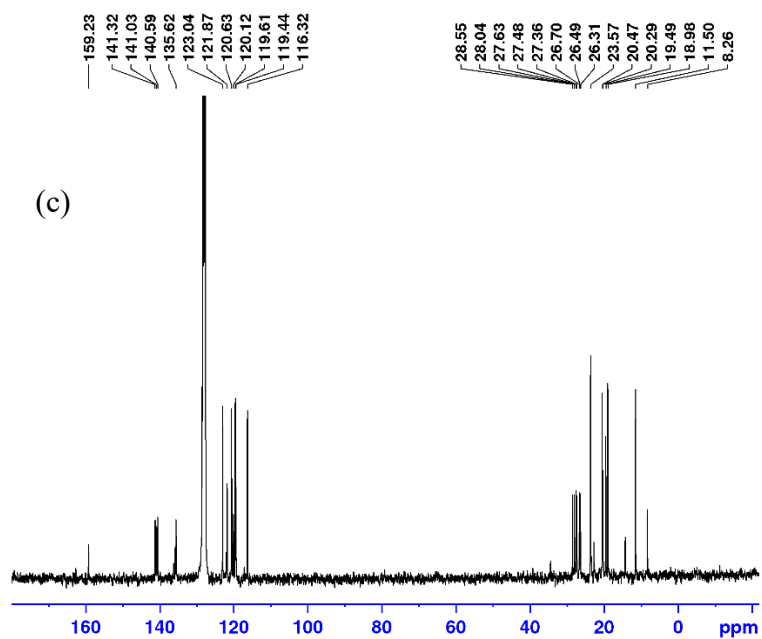
Figure A15. (a) $^{31}P\{^1H\}$, (b) ^1H, and (c) $^{13}C\{^1H\}$ NMR spectra (benzene-d_6) of (^{i}Pr-PSiP^{Ind})RhH(NPh$_2$) (**2-32a**).
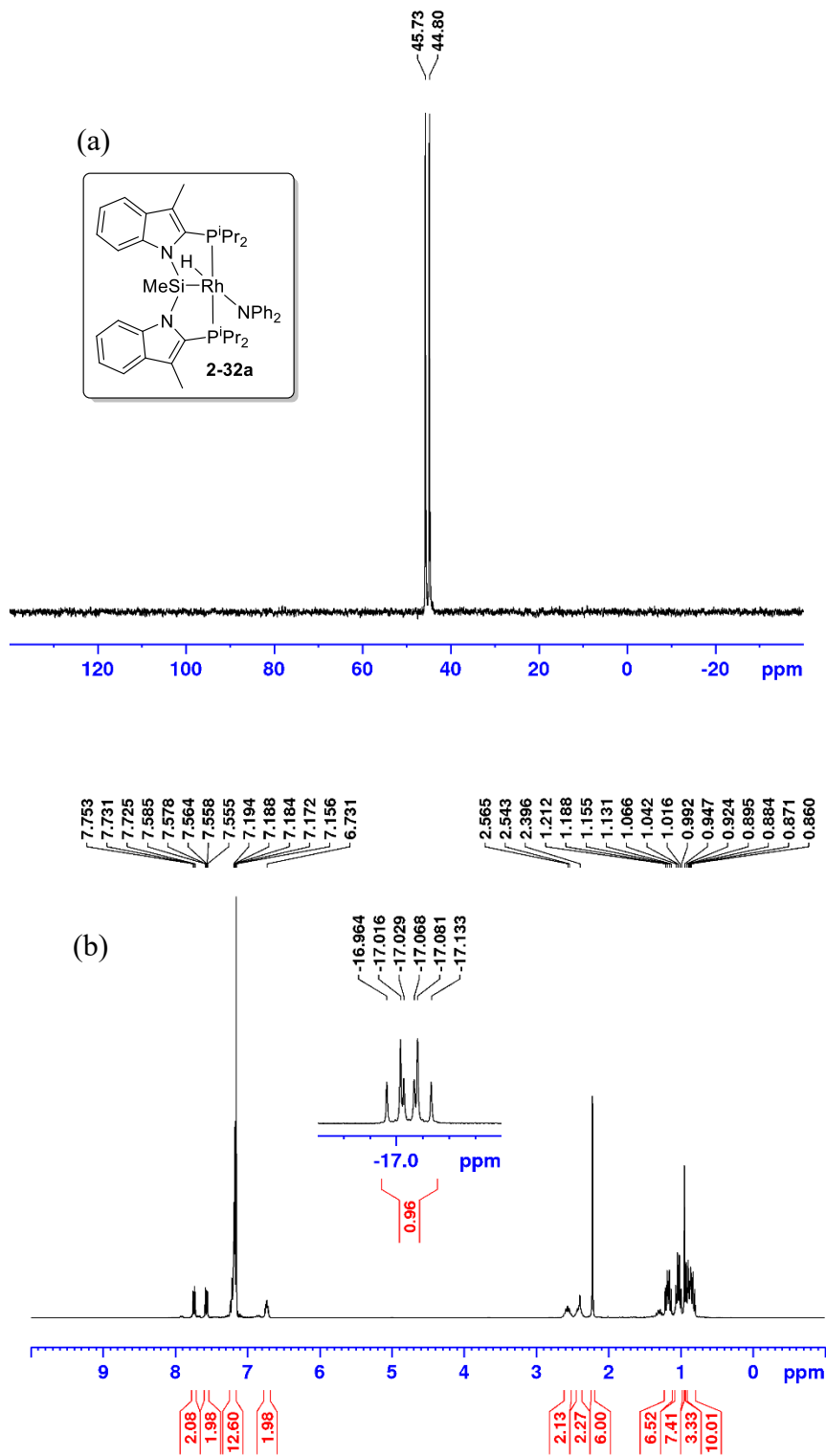
Figure A15. (continued) (a) $^{31}P\{^1H\}$, (b) ^1H, and (c) $^{13}C\{^1H\}$ NMR spectra (benzene-d_6) of (^iPr-PSiP^{Ind})RhH(NPh$_2$) (**2-32a**).
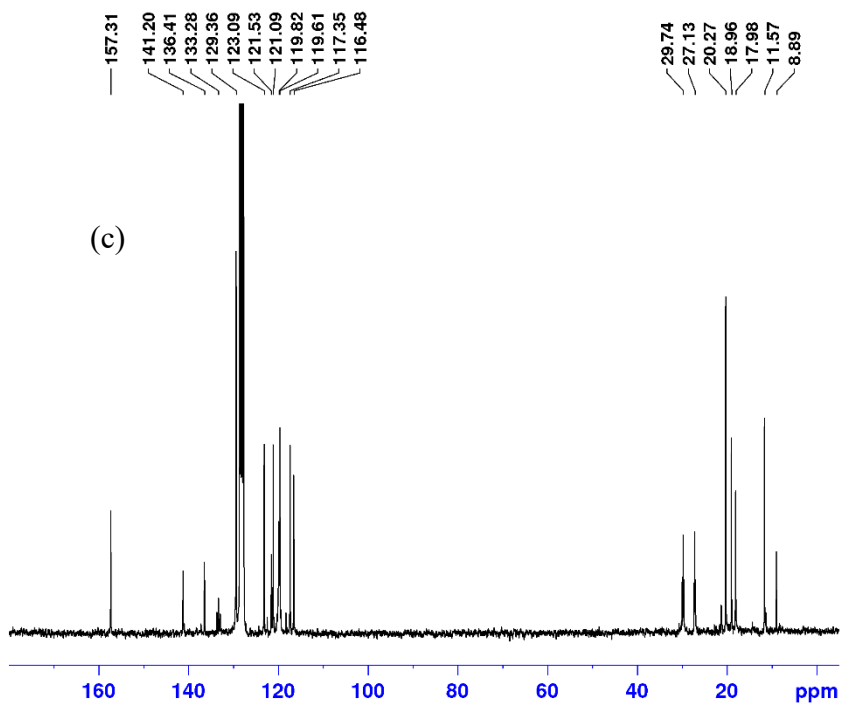
Figure A16. (a) $^{31}P\{^1H\}$, (b) ^1H, and (c) $^{13}C\{^1H\}$ NMR spectra (benzene-d_6) of (^{i}Pr-PSiP^{Ind})IrH(NHPh) (**2-31a**).
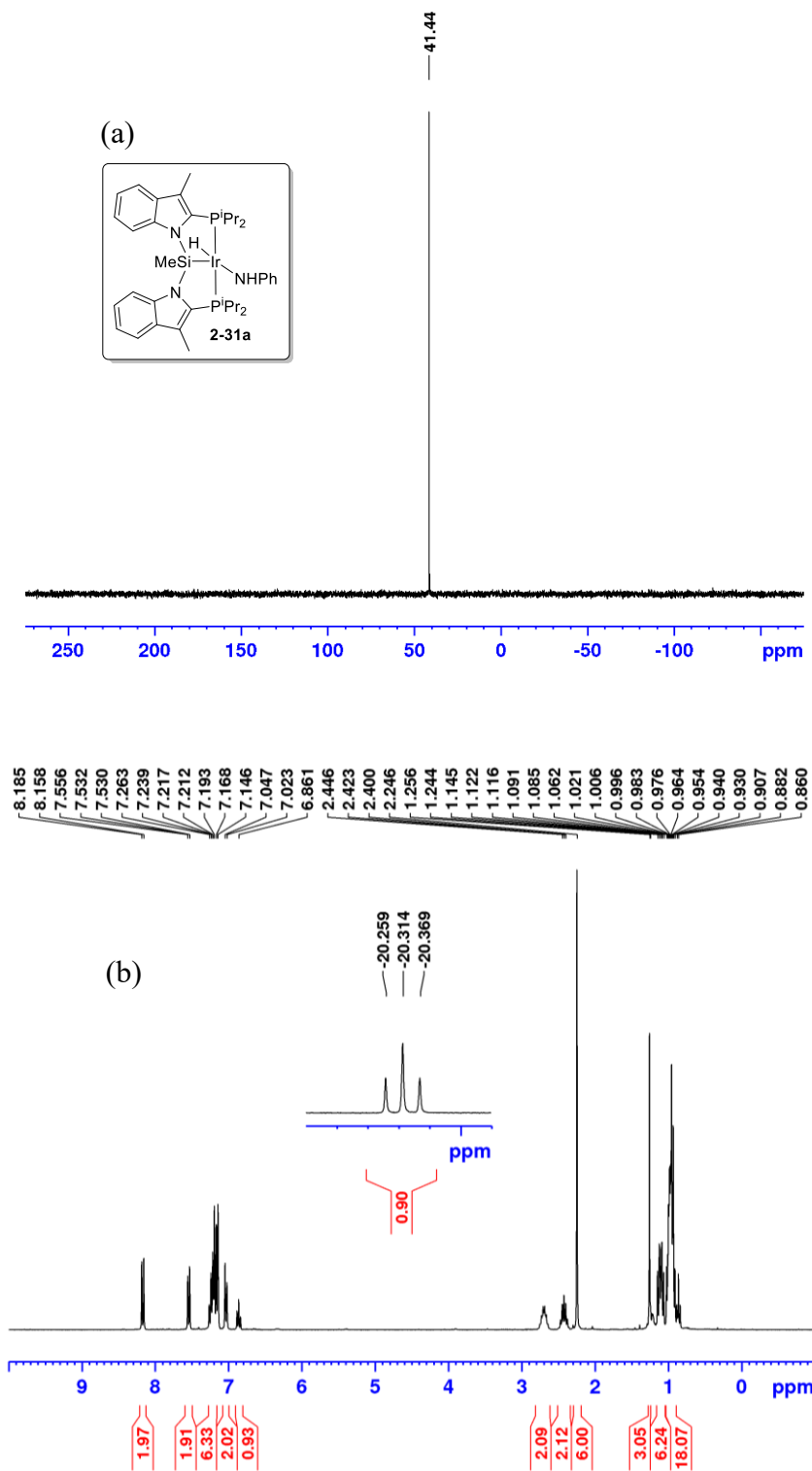
Figure A16. (continued) (a) $^{31}P\{^1H\}$, (b) ^1H, and (c) $^{13}C\{^1H\}$ NMR spectra (benzene-d_6) of (^{i}Pr-PSiP^{Ind})IrH(NHPh) (**2-31a**).
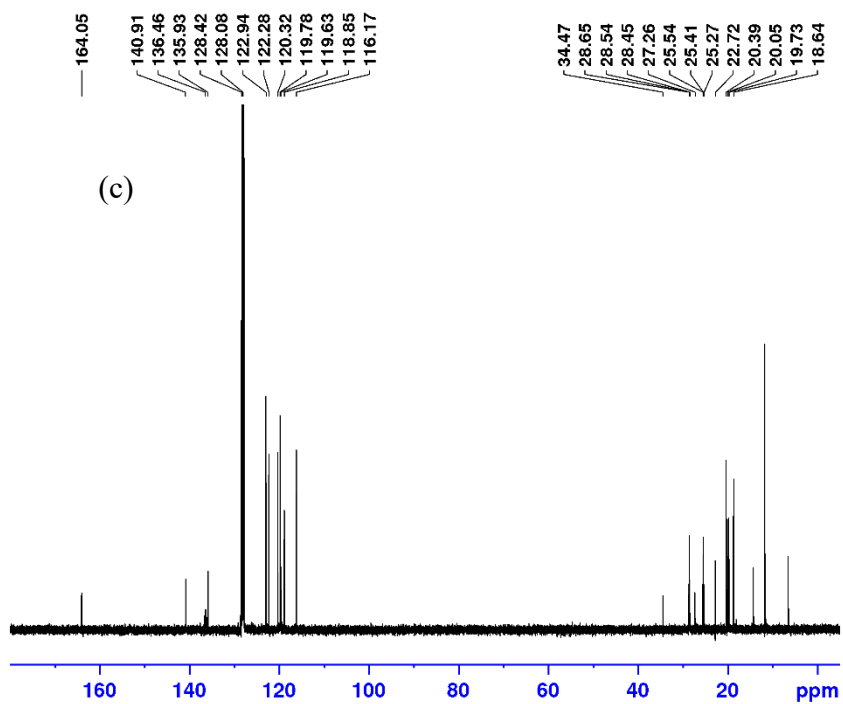
Figure A17. (a) $^{31}P\{^1H\}$, (b) ^1H, and (c) $^{13}C\{^1H\}$ NMR spectra (benzene-d_6) of (^{i}Pr-PSiP^{Ind})IrH[NH(2,6-Me$_2$C$_6$H$_3$)] (**2-31b**).
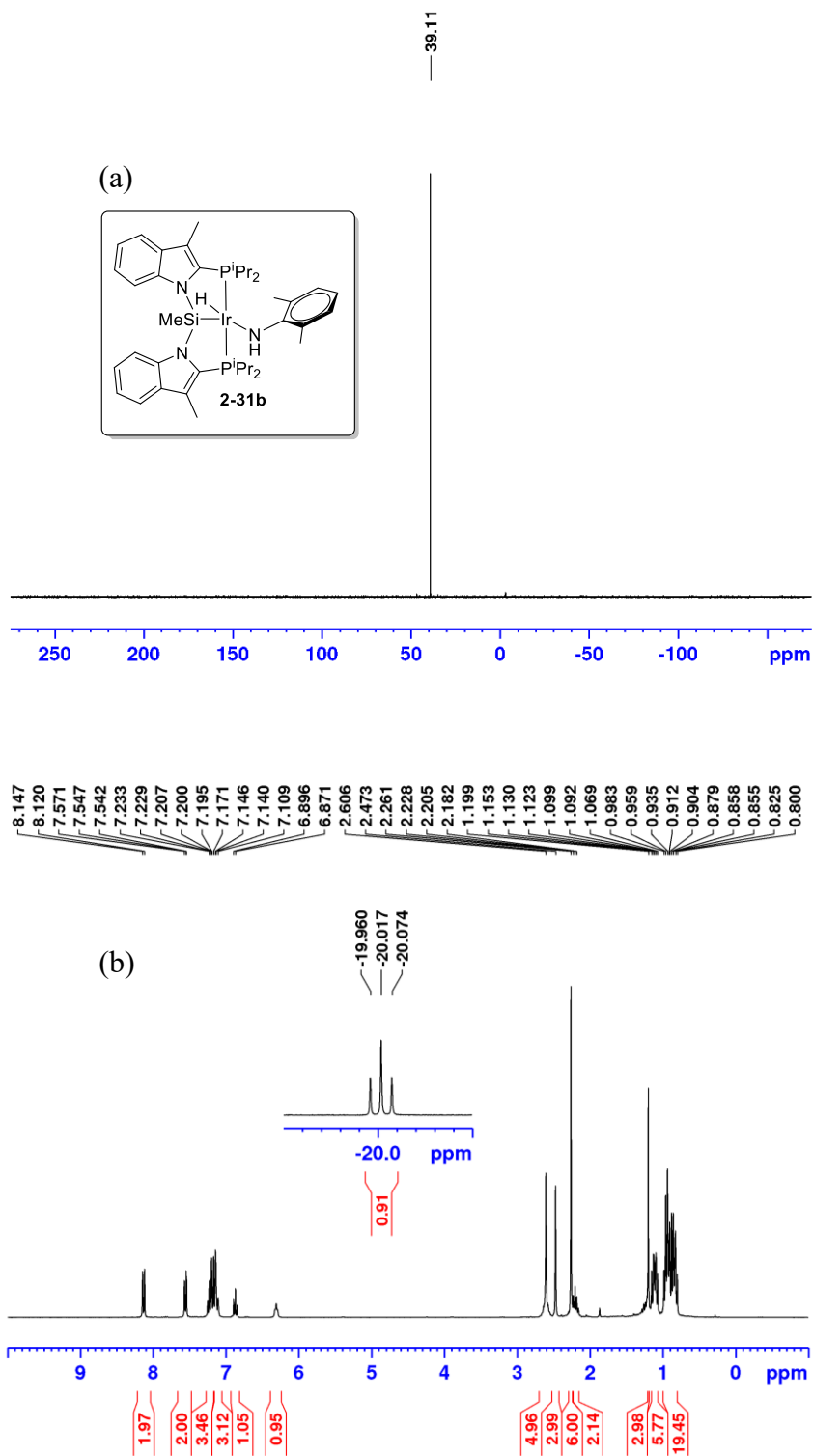
Figure A17. (continued) (a) $^{31}P\{^1H\}$, (b) ^1H, and (c) $^{13}C\{^1H\}$ NMR spectra (benzene-d_6) of (^{i}Pr-PSiP^{Ind})IrH[NH(2,6-Me$_2$C$_6$H$_3$)] (**2-31b**).
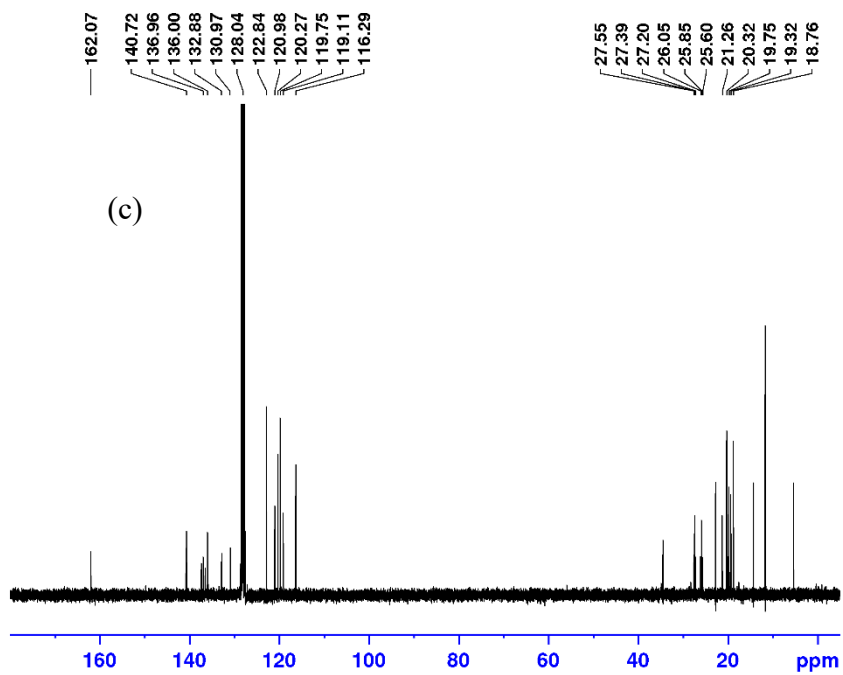
Figure A18. (a) $^{31}P\{^1H\}$, (b) ^1H, and (c) $^{13}C\{^1H\}$ NMR spectra (benzene-d_6) of (^{i}Pr-PSiP^{Ind})IrH[NH(2,6-^{i}Pr$_2$C$_6$H$_3$)] (**2-31c**).
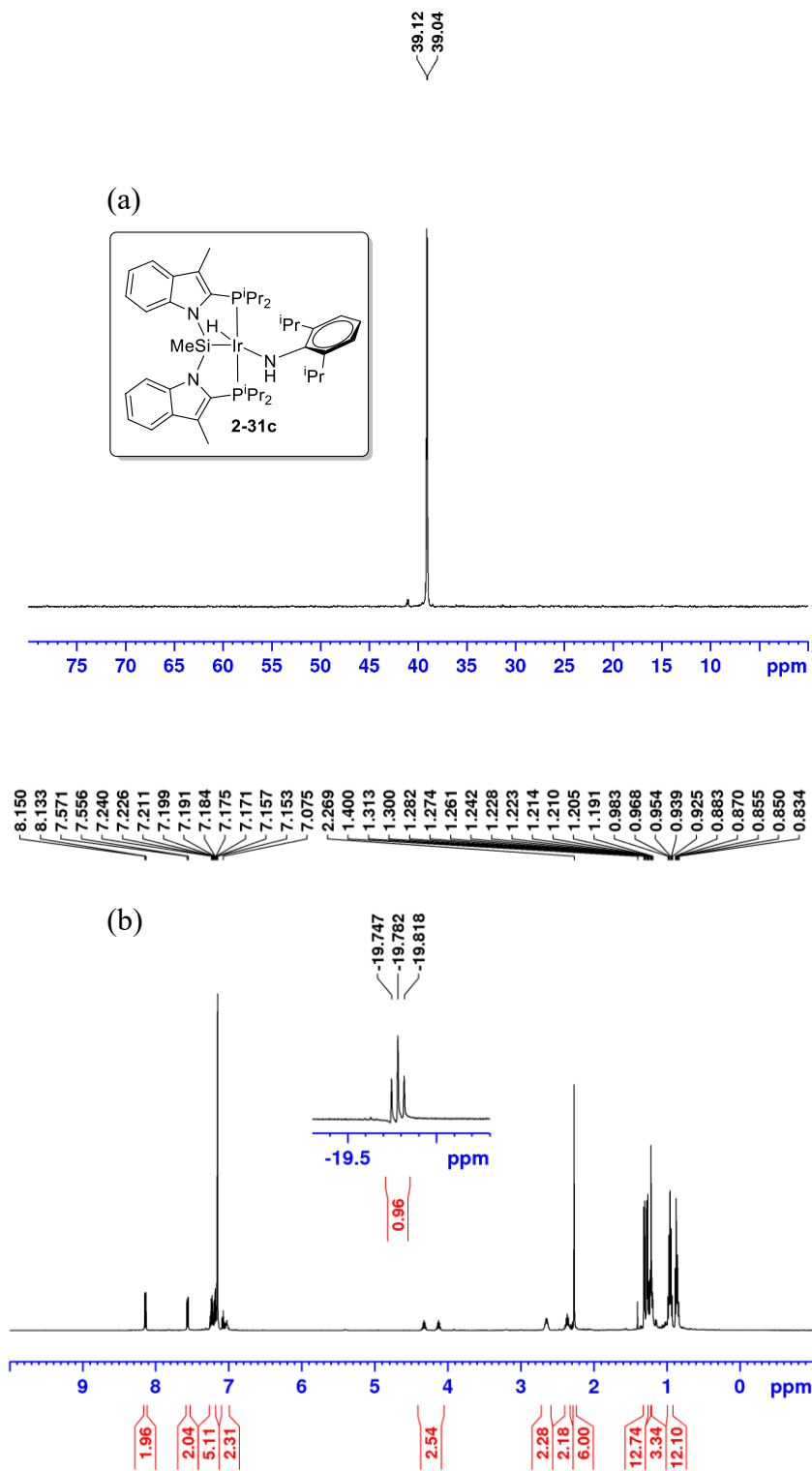
Figure A18. (continued) (a) $^{31}P\{^1H\}$, (b) ^1H, and (c) $^{13}C\{^1H\}$ NMR spectra (benzene-d_6) of (^iPr-PSiP^{Ind})IrH[NH(2,6-$^iPr_2C_6H_3$)] (**2-31c**).
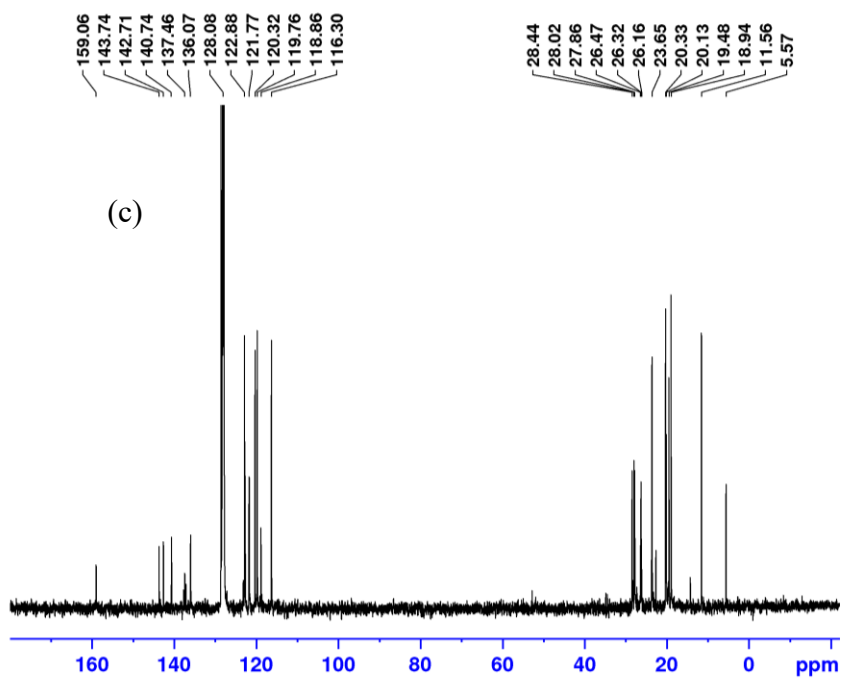
Figure A19. (a) $^{31}P\{^1H\}$, (b) ^1H, and (c) $^{13}C\{^1H\}$ NMR spectra (benzene-d_6) of (^{i}Pr-PSiP^{Ind})IrH(NPh$_2$) (**2-32b**).
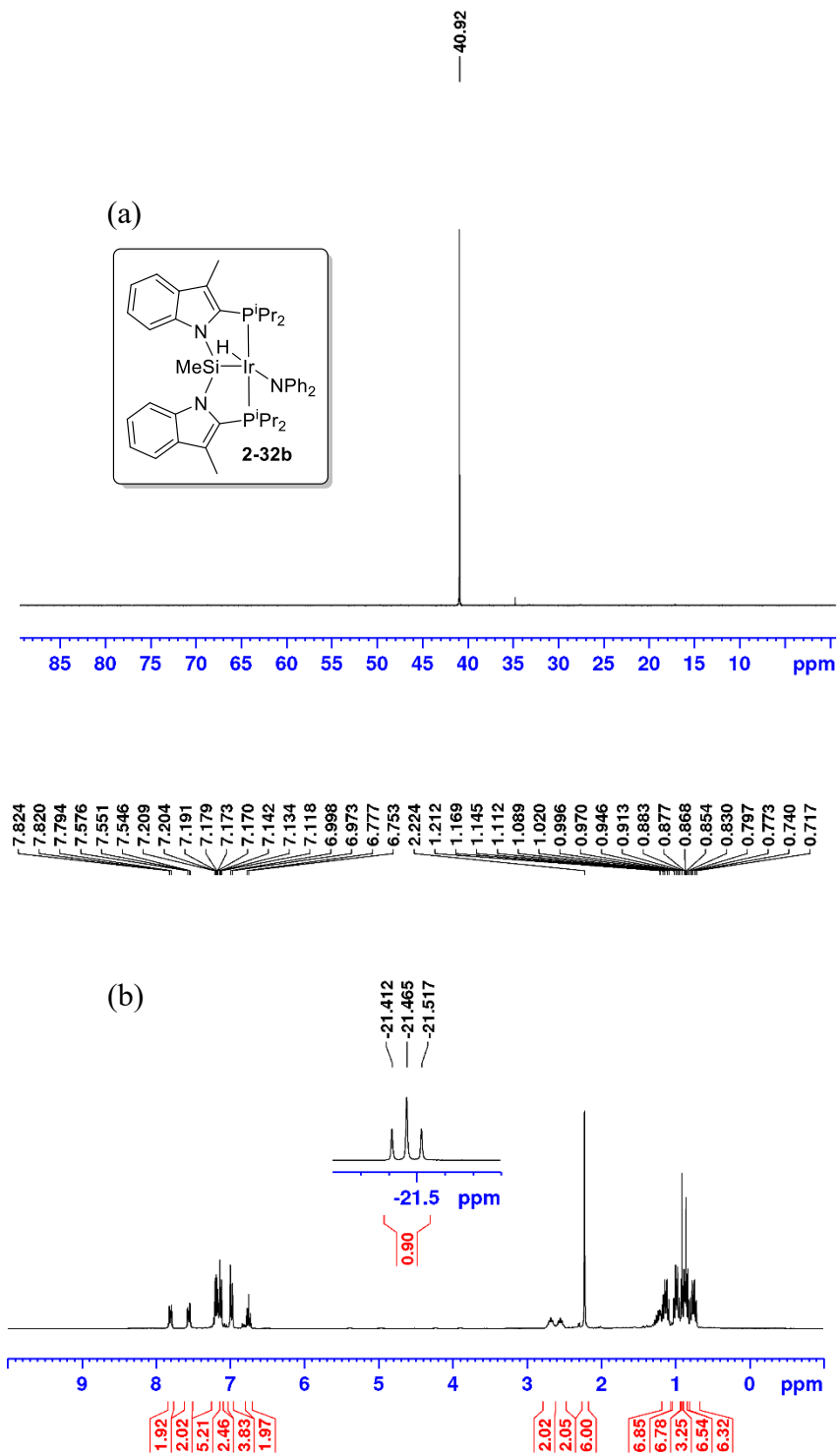
Figure A19. (continued) (a) $^{31}P\{^1H\}$, (b) ^1H, and (c) $^{13}C\{^1H\}$ NMR spectra (benzene-d_6) of (^{i}Pr-PSiP^{Ind})IrH(NPh$_2$) (**2-32b**).
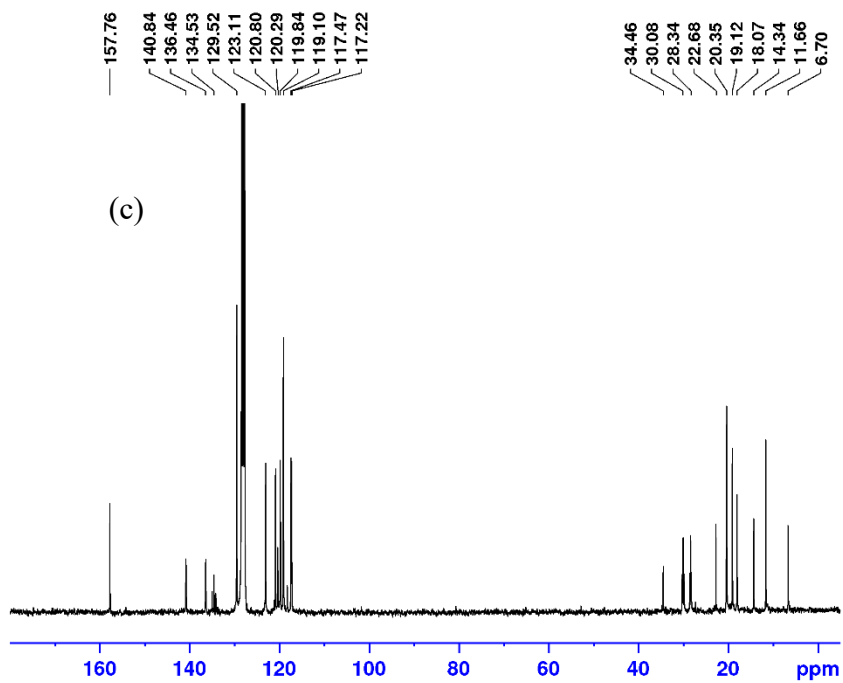
Figure A20. (a) $^{31}P\{^1H\}$, (b) ^1H, and (c) $^{13}C\{^1H\}$ NMR spectra (benzene-d$_6$) of (^{i}Pr-PSiP^{Ind})IrH(NH^{t}Bu) (**2-33a**).
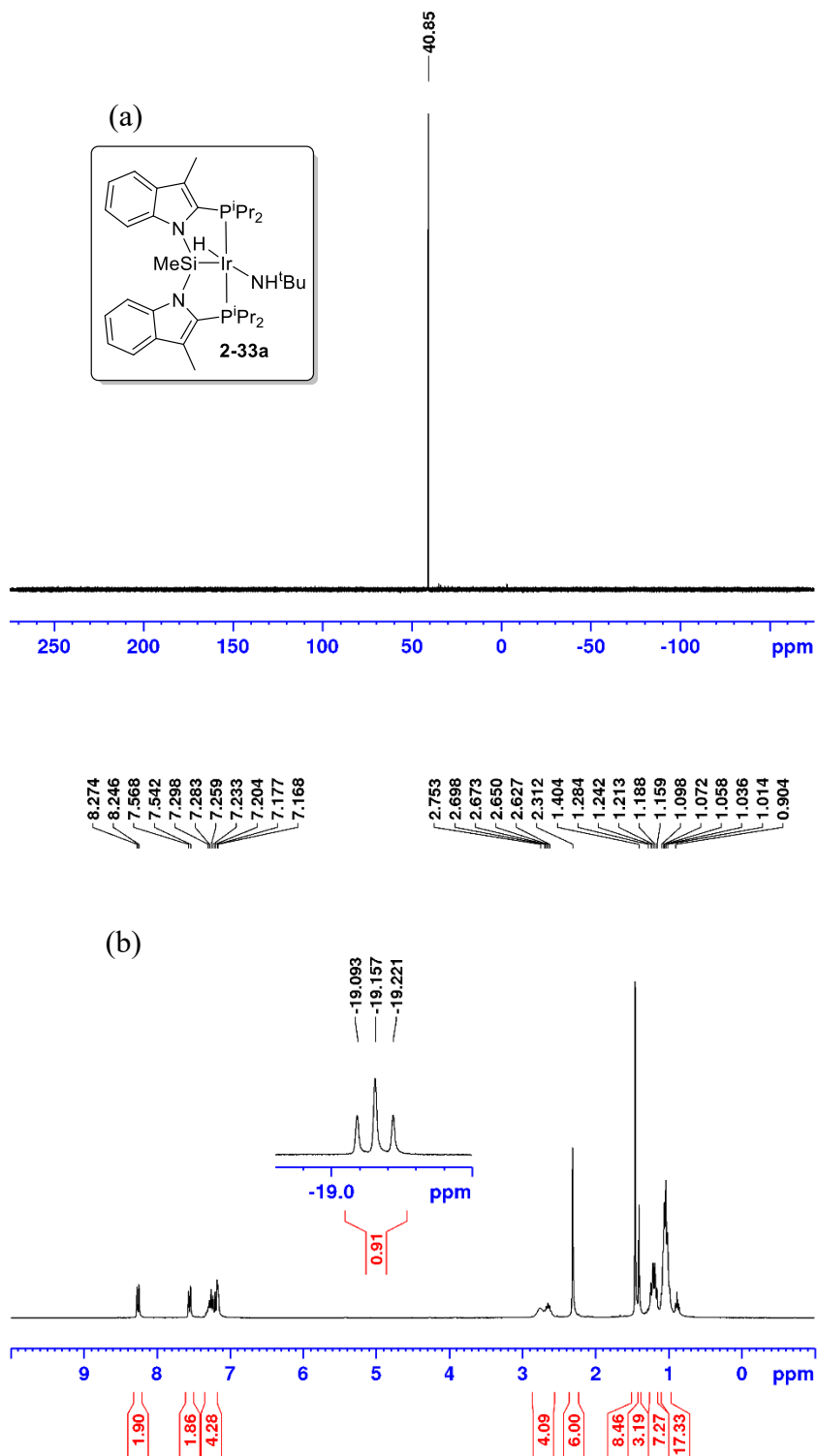
Figure A20. (continued) (a) $^{31}\text{P}\{^1\text{H}\}$, (b) ^1H, and (c) $^{13}\text{C}\{^1\text{H}\}$ NMR spectra (benzene-d_6) of (^{i}Pr-PSiP$^{\text{Ind}}$)IrH(NH^{t}Bu) (**2-33a**).
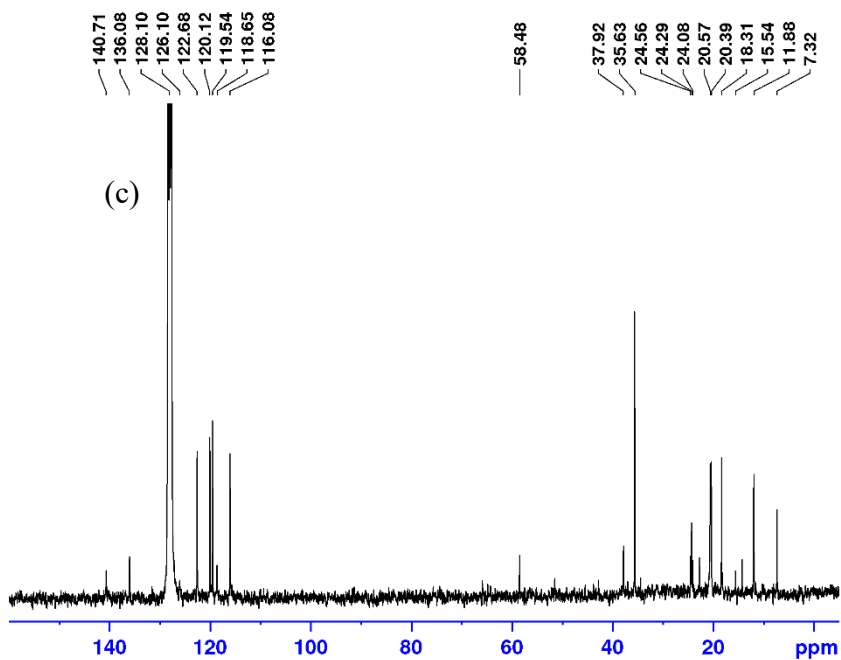
Figure A21. ^{1}H-^{29}Si HMBC NMR (300 × 59.6 MHz) spectrum of (^{i}Pr-PSiP$^{\text{Ind}}$)IrH(NH^{t}Bu) (**5a**; benzene-d_6); a scale factor of 4 was applied, such that $^2J_{\text{SiH}} = \Delta\nu/4$.
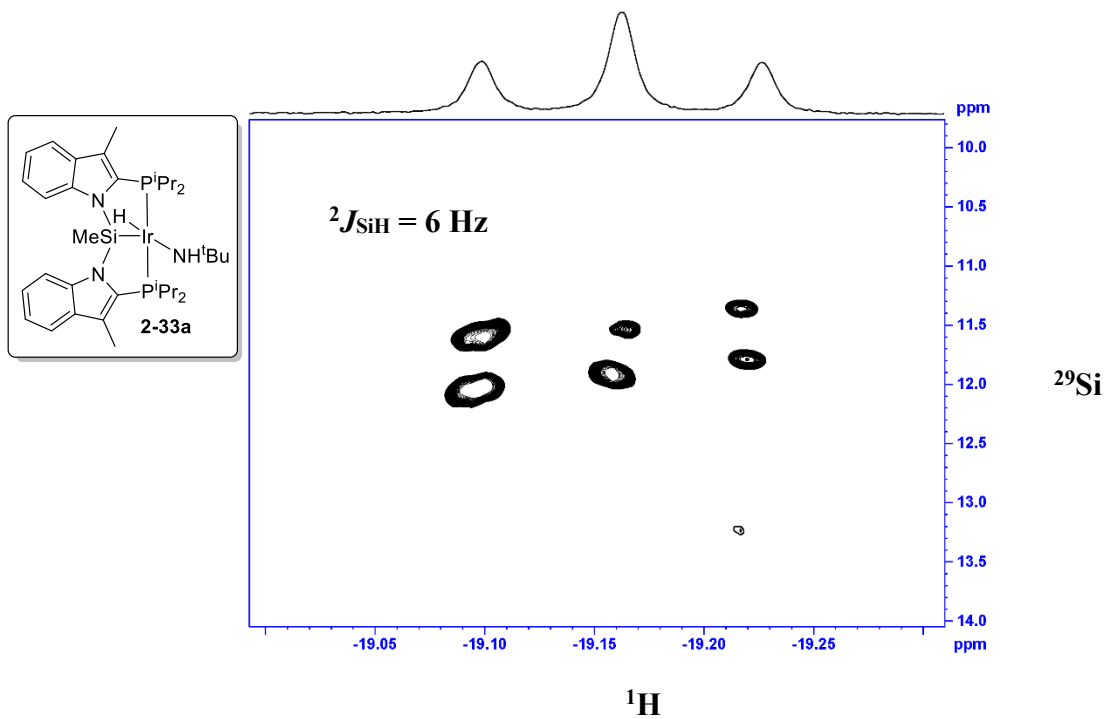
Figure A22. (a) $^{31}P\{^1H\}$, (b) ^1H, and (c) $^{13}C\{^1H\}$ NMR spectra (benzene-d_6) of (^{i}Pr-PSiP^{Ind})IrH(NHAd) (**2-33b**).

(a)

— 40.87

(b)
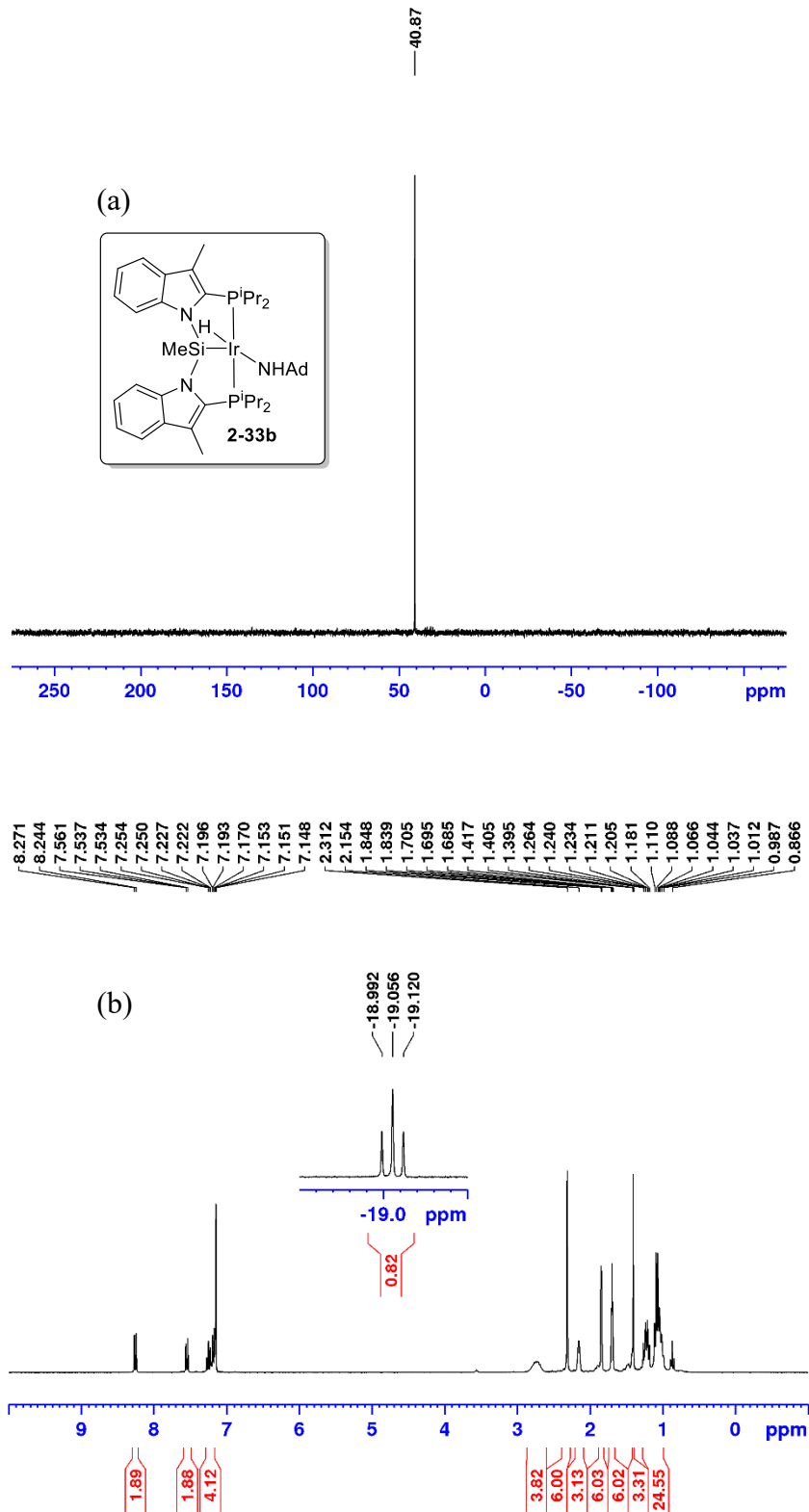
Figure A22. (continued) (a) $^{31}P\{^1H\}$, (b) ^1H, and (c) $^{13}C\{^1H\}$ NMR spectra (benzene-d_6) of (^{i}Pr-PSiP^{Ind})IrH(NHAd) (**2-33b**).
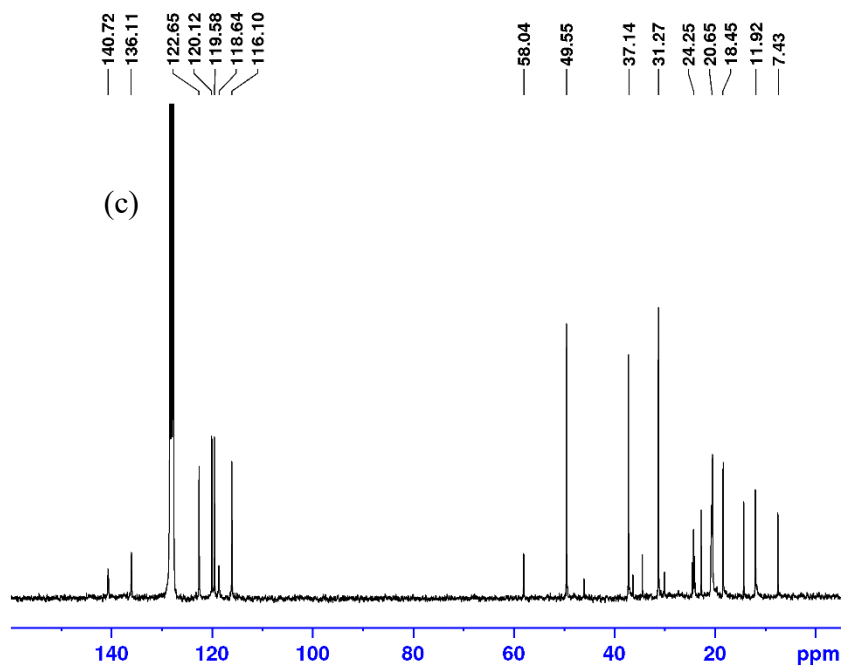
Figure A23. (a) $^{31}P\{^1H\}$, (b) ^1H, and (c) $^{13}C\{^1H\}$ NMR spectra (benzene-d_6) of crude (^{i}Pr-PSiP^{Ind})IrH(NH$_2$) (**2-34**).
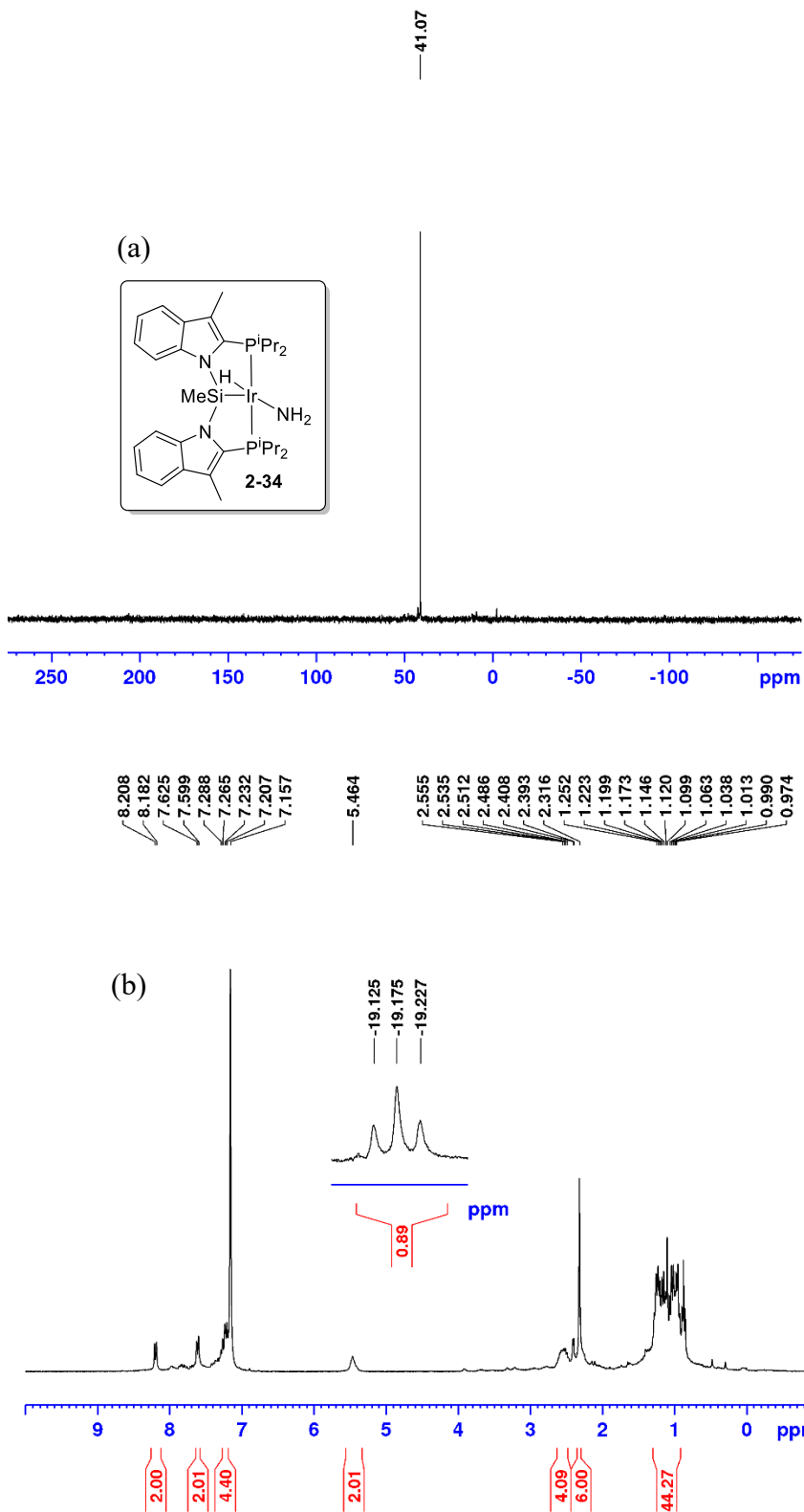
Figure A23. (continued) (a) $^{31}P\{^1H\}$, (b) ^1H, and (c) $^{13}C\{^1H\}$ NMR spectra (benzene-d_6) of crude (^{i}Pr-PSiP^{Ind})IrH(NH$_2$) (**2-34**).

(c)
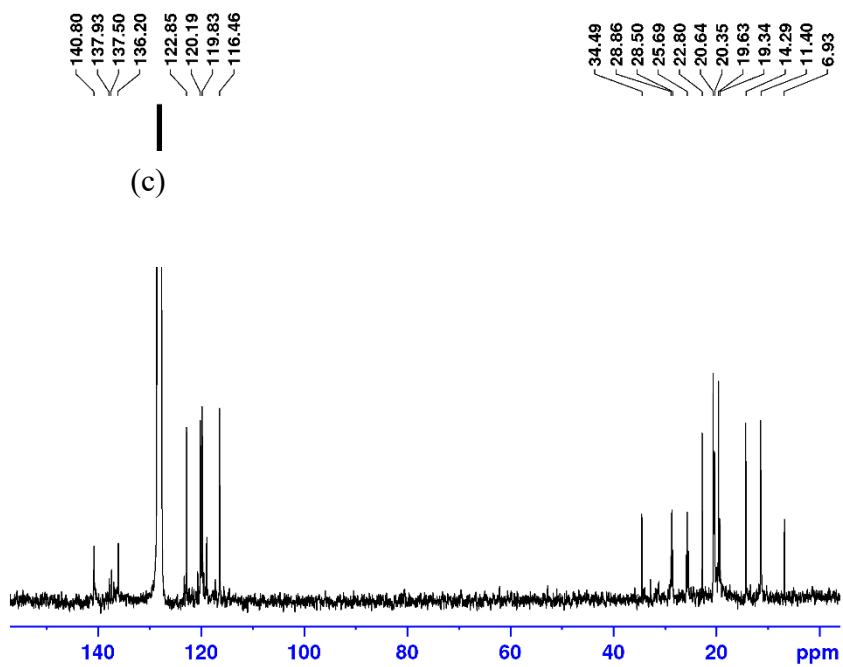
Figure A24. In situ (a) $^{31}P\{^1H\}$ and (b) ^1H NMR spectra (benzene-d$_6$) of the reaction mixture resulting from treatment of **2** with LiNHCy showing the formation of the proposed intermediate (mer-κ^3-^{i}Pr-PSiP^{Ind})Ir(H)$_2$(NH=C$_6$H$_{10}$) (**2-33c**).
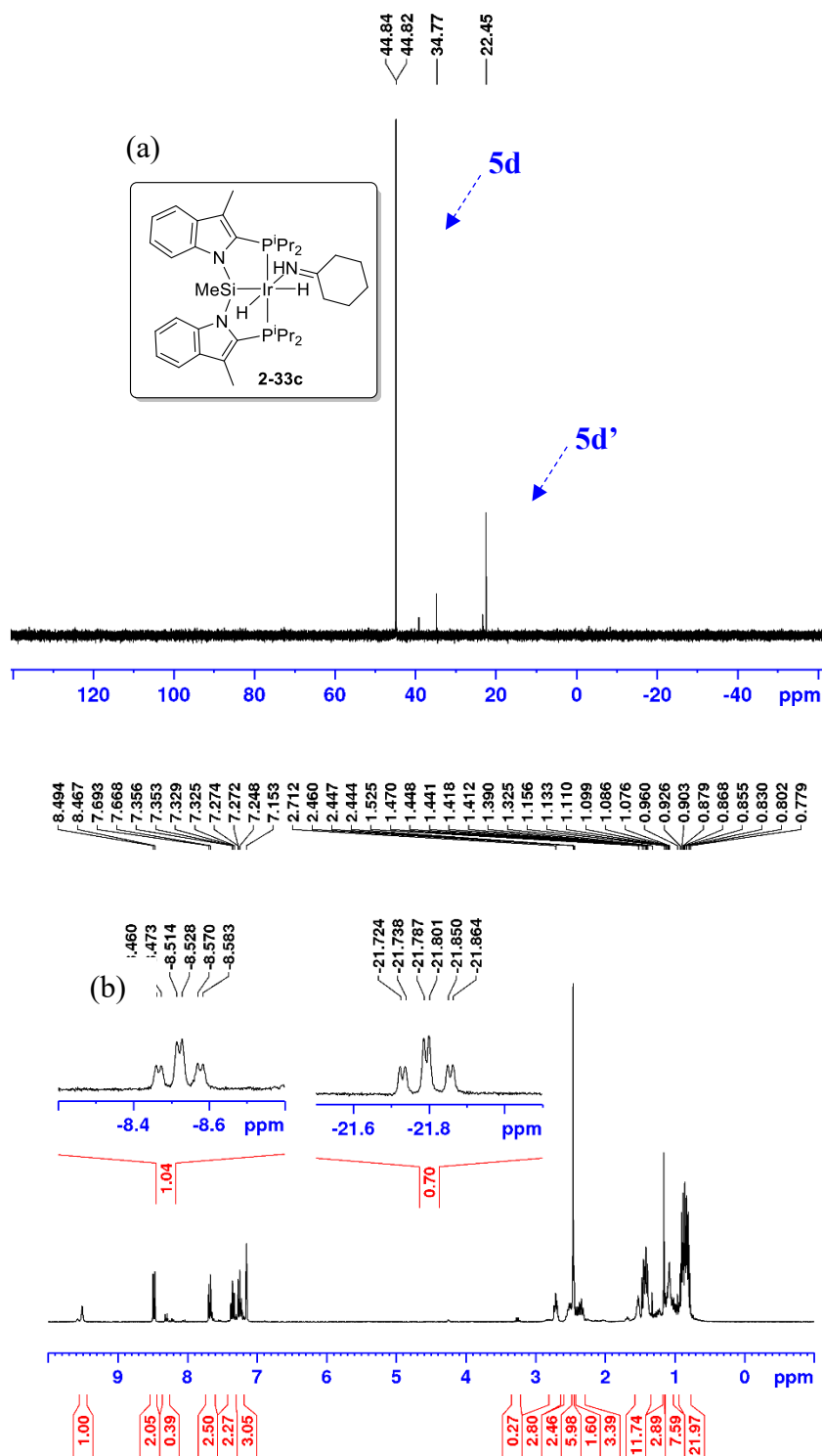
Figure A25. (a) $^{31}P\{^1H\}$, (b) ^1H, and (c) $^{13}C\{^1H\}$ NMR spectra (THF-d_8) of (fac-κ^3-^{i}Pr-PSiP^{Ind})Ir(H)$_2$(NH=C$_6$H$_{10}$) (**2-33c'**).
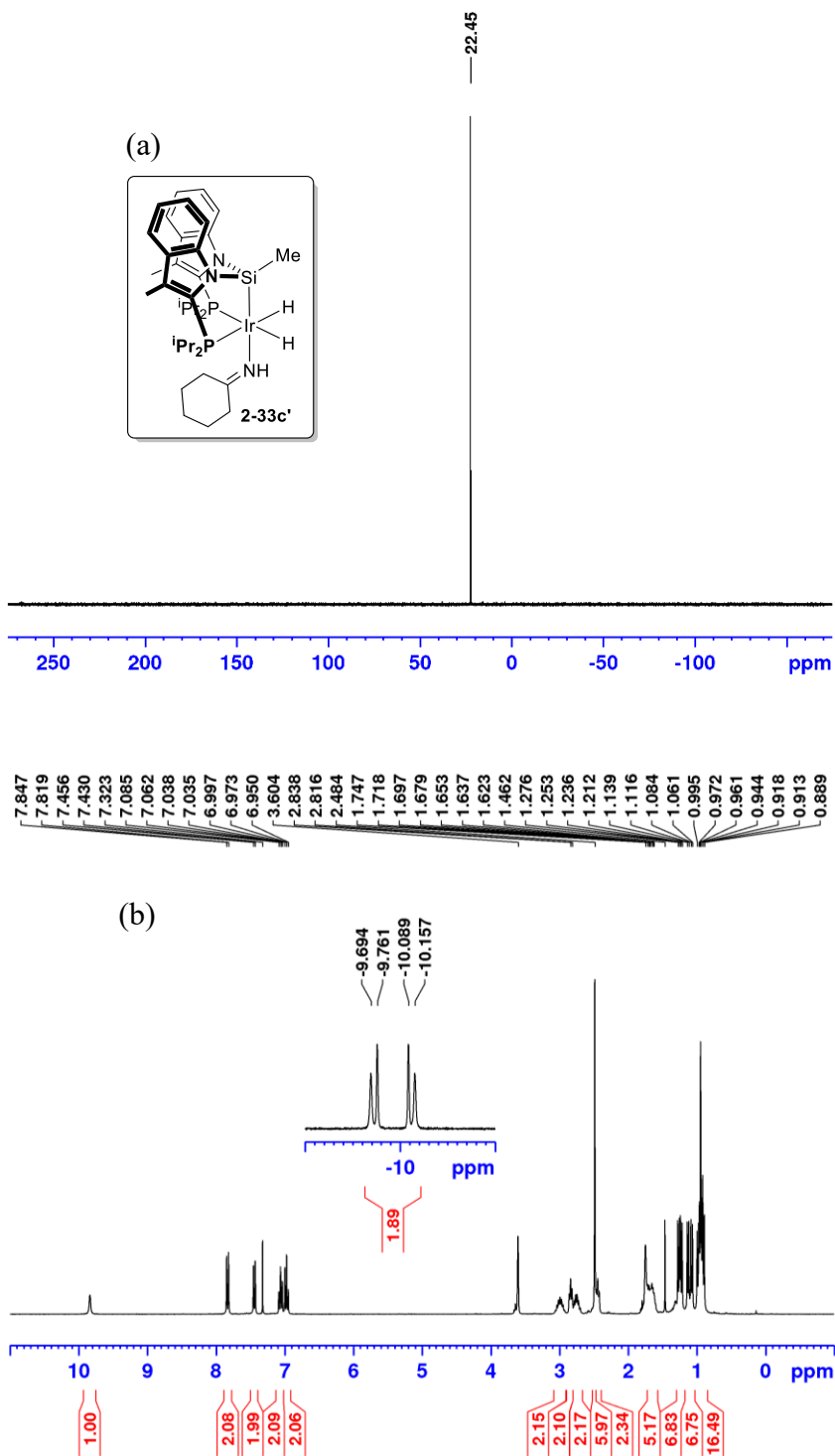
Figure A25. (continued) (a) $^{31}P\{^1H\}$, (b) ^1H, and (c) $^{13}C\{^1H\}$ NMR spectra (THF-d$_8$) of (fac-κ^3-^{i}Pr-PSiP^{Ind})Ir(H)$_2$(NH=C$_6$H$_{10}$) (**2-33c'**).
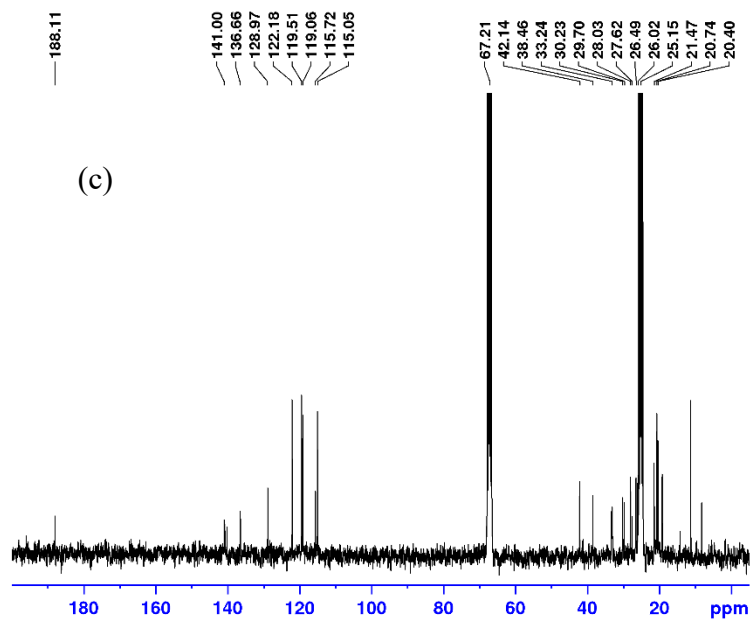
Figure A26. (a) ^1H and (b) ^{31}P NMR data for **2-33c'** (THF-d$_8$) highlighting magnetically non-equivalent hydride and phosphino ligand environments.

257
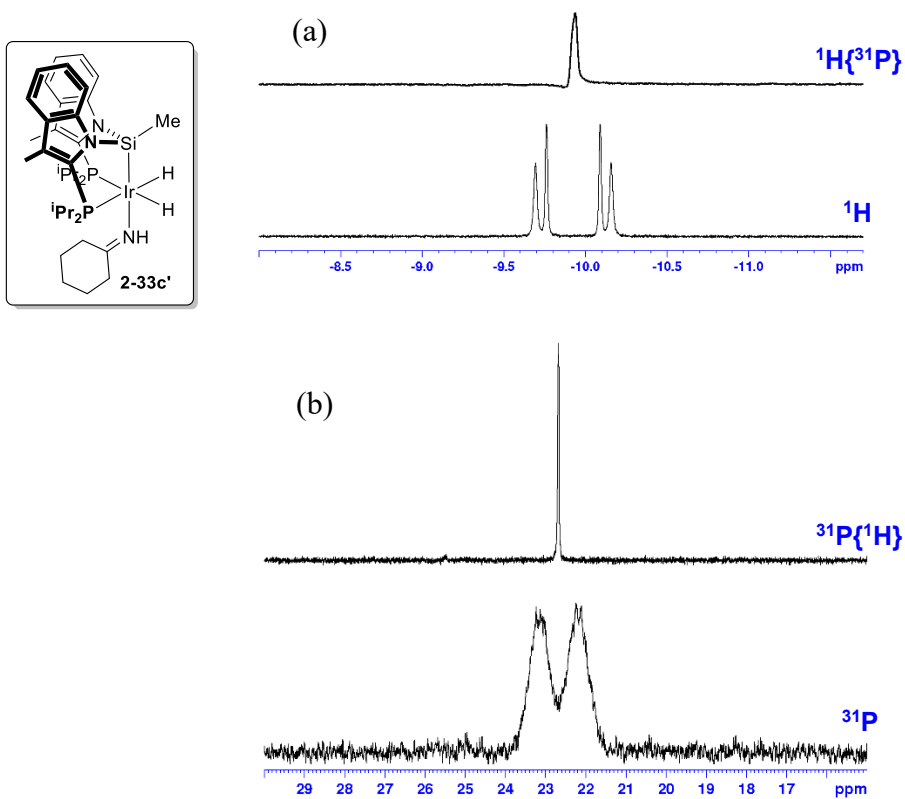
Figure A27. (a) $^{31}P\{^1H\}$, (b) ^1H, and (c) $^{13}C\{^1H\}$ NMR spectra (benzene-d_6) of (^{i}Pr-PSiP^{Ind})IrH[NH-N(CH$_2$CH$_2$)$_2$NMe] (**2-35a**).
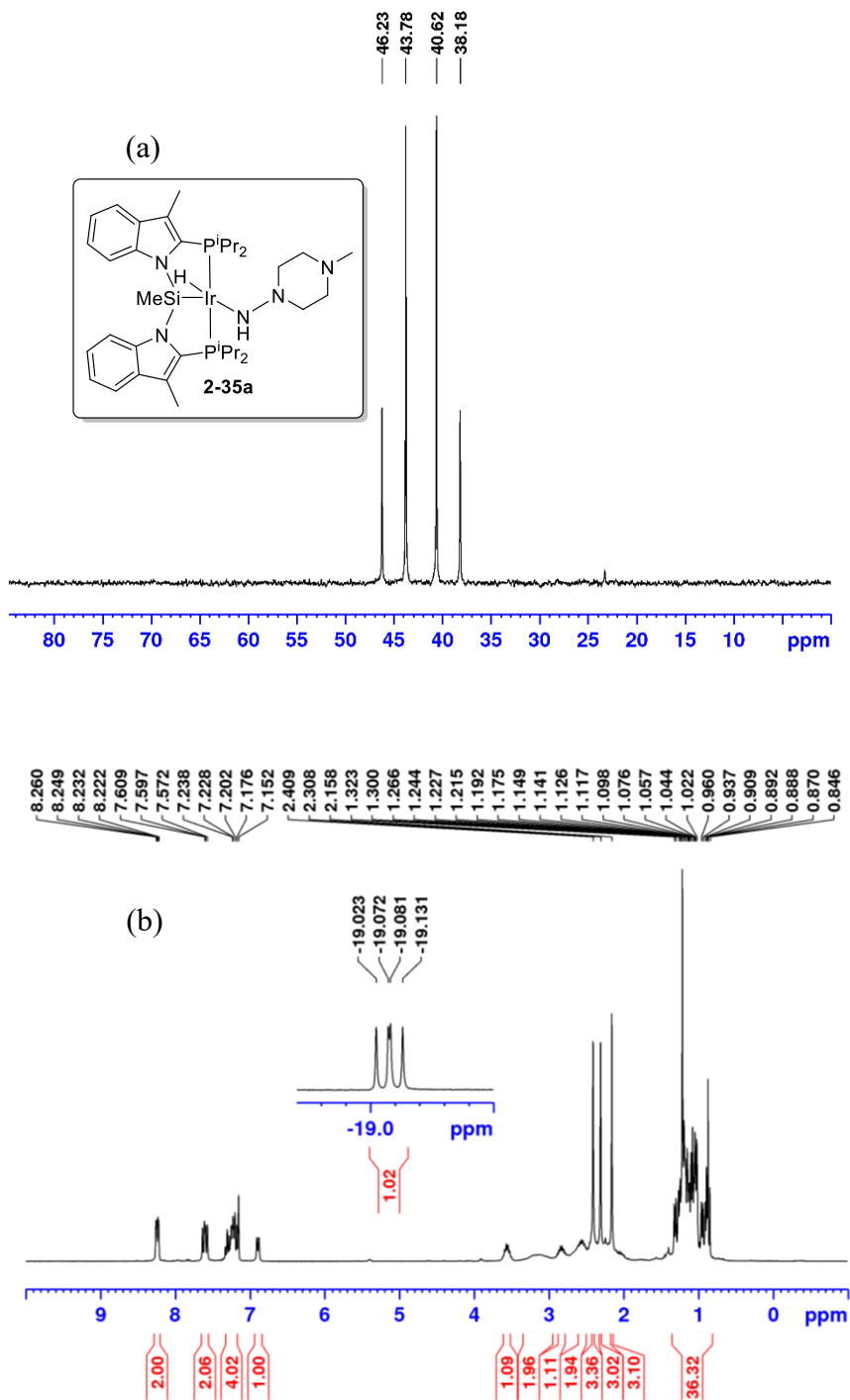
Figure A27. (continued) (a) $^{31}P\{^1H\}$, (b) ^1H, and (c) $^{13}C\{^1H\}$ NMR spectra (benzene-d_6) of (^iPr-PSiP^{Ind})IrH[NH-N(CH$_2$CH$_2$)$_2$NMe] (**2-35a**).
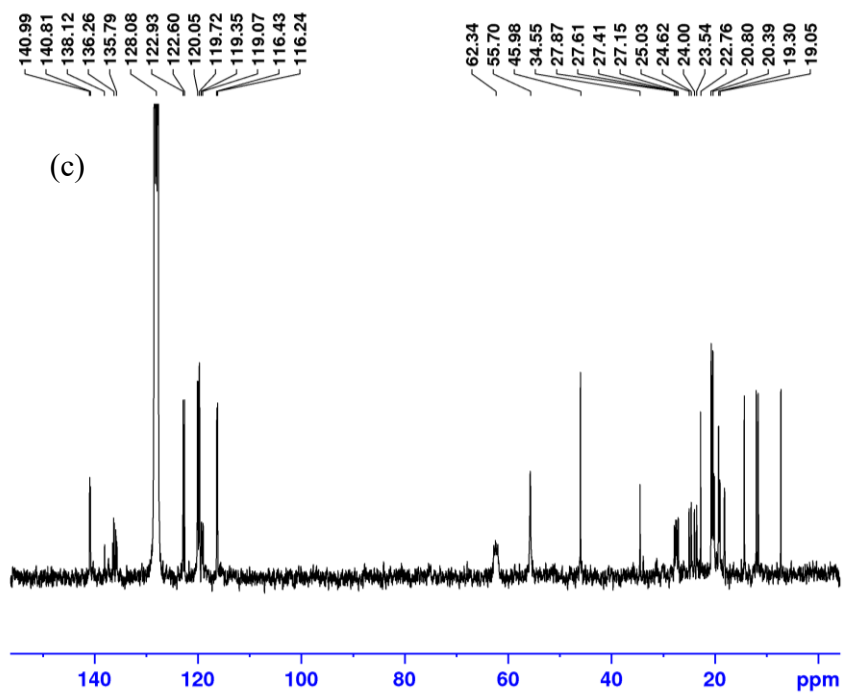
Figure A28. (a) $^{31}P\{^1H\}$, (b) ^1H, and (c) $^{13}C\{^1H\}$ NMR spectra (benzene-d_6) of (^{i}Pr-PSiP^{Ind})RhH(NH(CO)Ph) (**2-36a**).
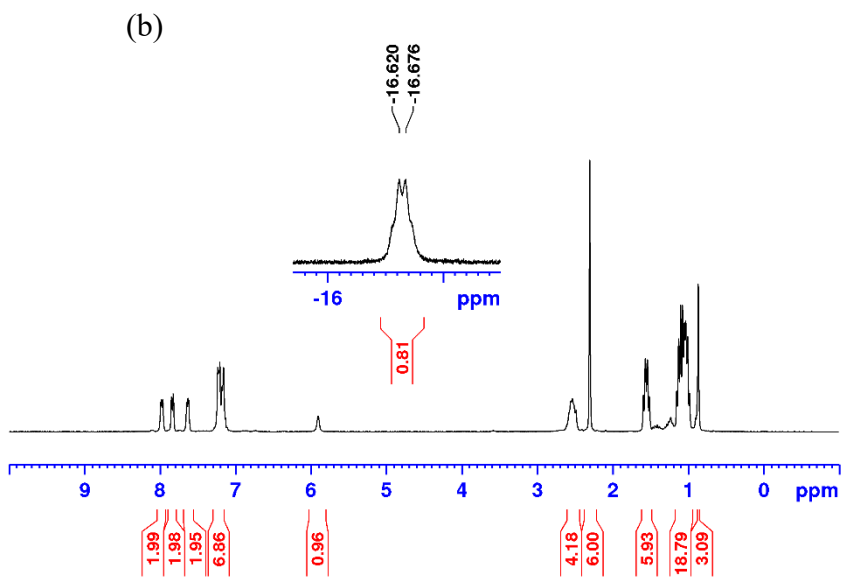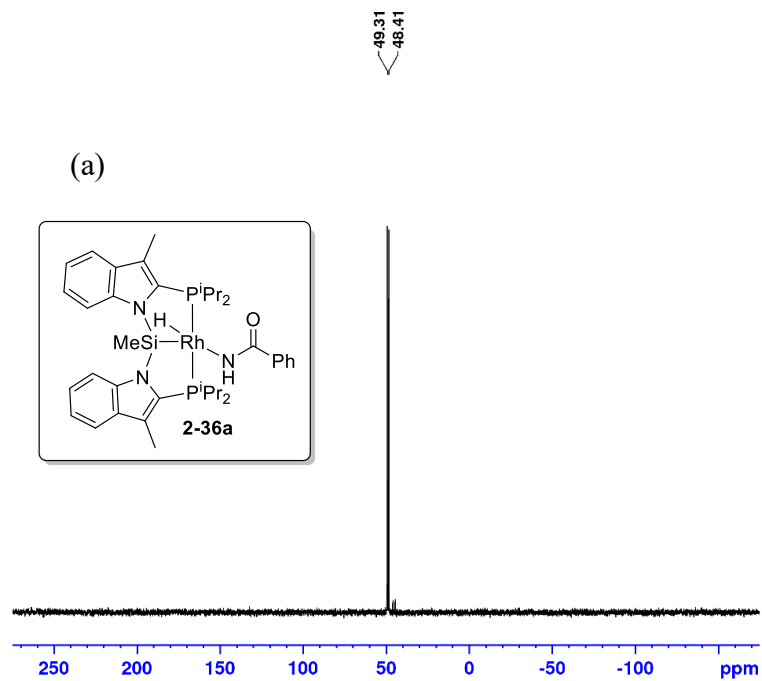
Figure A28. (continued) (a) $^{31}P\{^1H\}$, (b) ^1H, and (c) $^{13}C\{^1H\}$ NMR spectra (benzene-d_6) of (^{i}Pr-PSiP^{Ind})RhH(NH(CO)Ph) (**2-36a**).
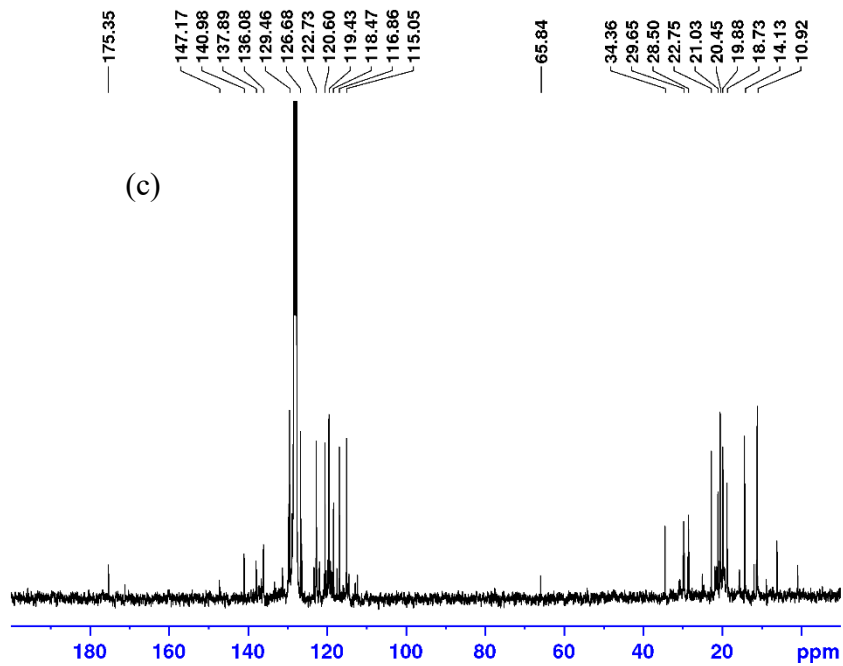
Figure A29. (a) $^{31}P\{^1H\}$, (b) ^1H, and (c) $^{13}C\{^1H\}$ NMR spectra (benzene-d_6) of (^{i}Pr-PSiP^{Ind})IrH(NH(CO)Ph) (**2-37a**).
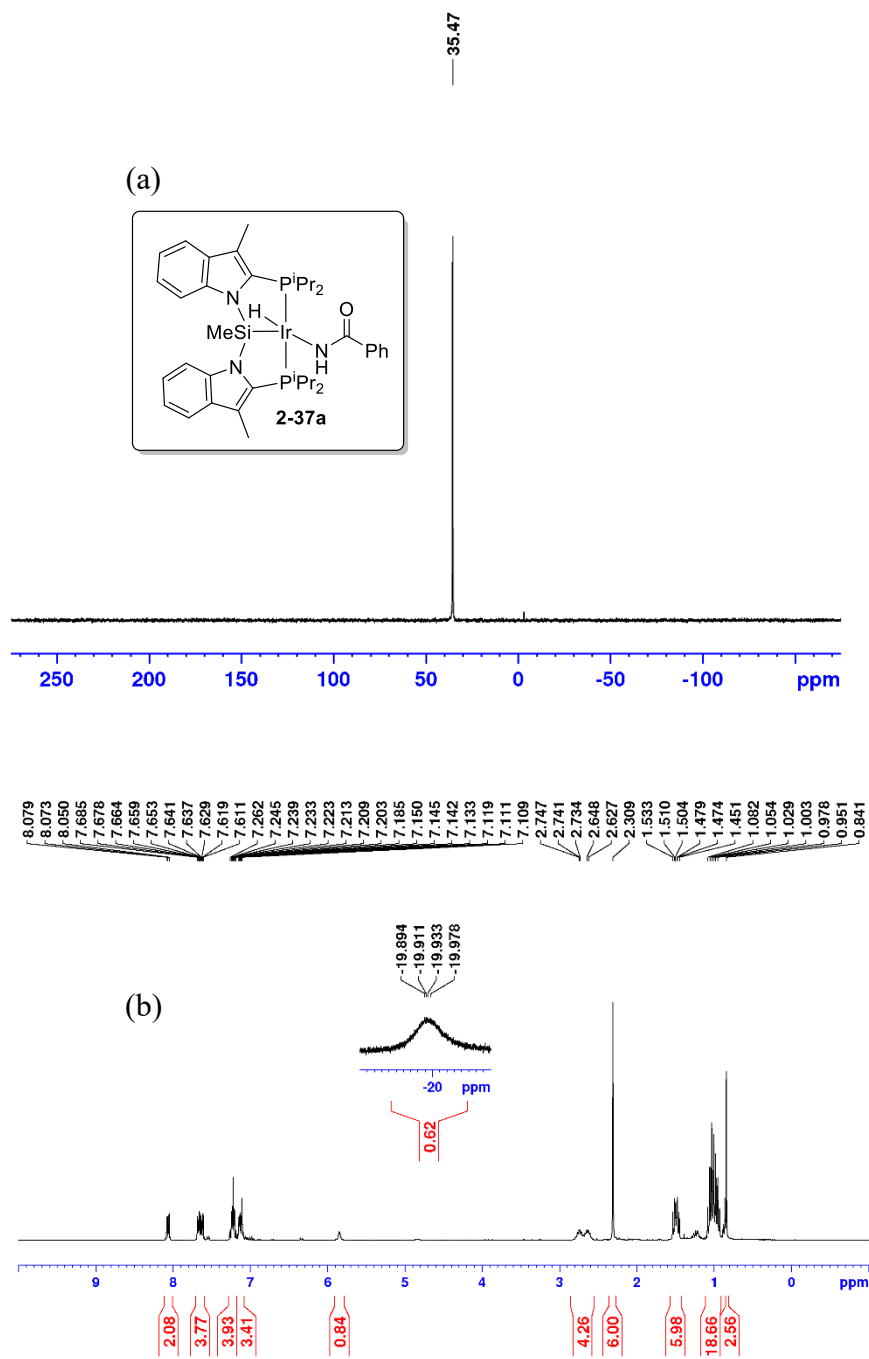
Figure A29. (continued) (a) $^{31}P\{^{1}H\}$, (b) ^{1}H, and (c) $^{13}C\{^{1}H\}$ NMR spectra (benzene-d_6) of (^{i}Pr-PSiP^{Ind})IrH(NH(CO)Ph) (**2-37a**).
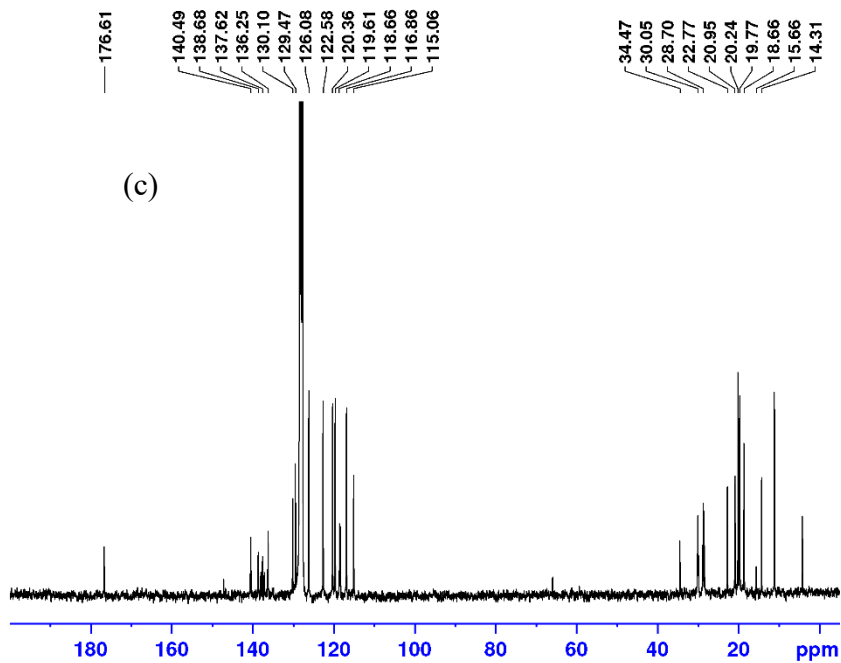
Figure A30. (a) $^{31}P\{^1H\}$, (b) ^1H, and (c) $^{13}C\{^1H\}$ NMR spectra (benzene-d_6) of (^{i}Pr-PSiP^{Ind})IrH(NH(CO)Me) (**2-37b**).
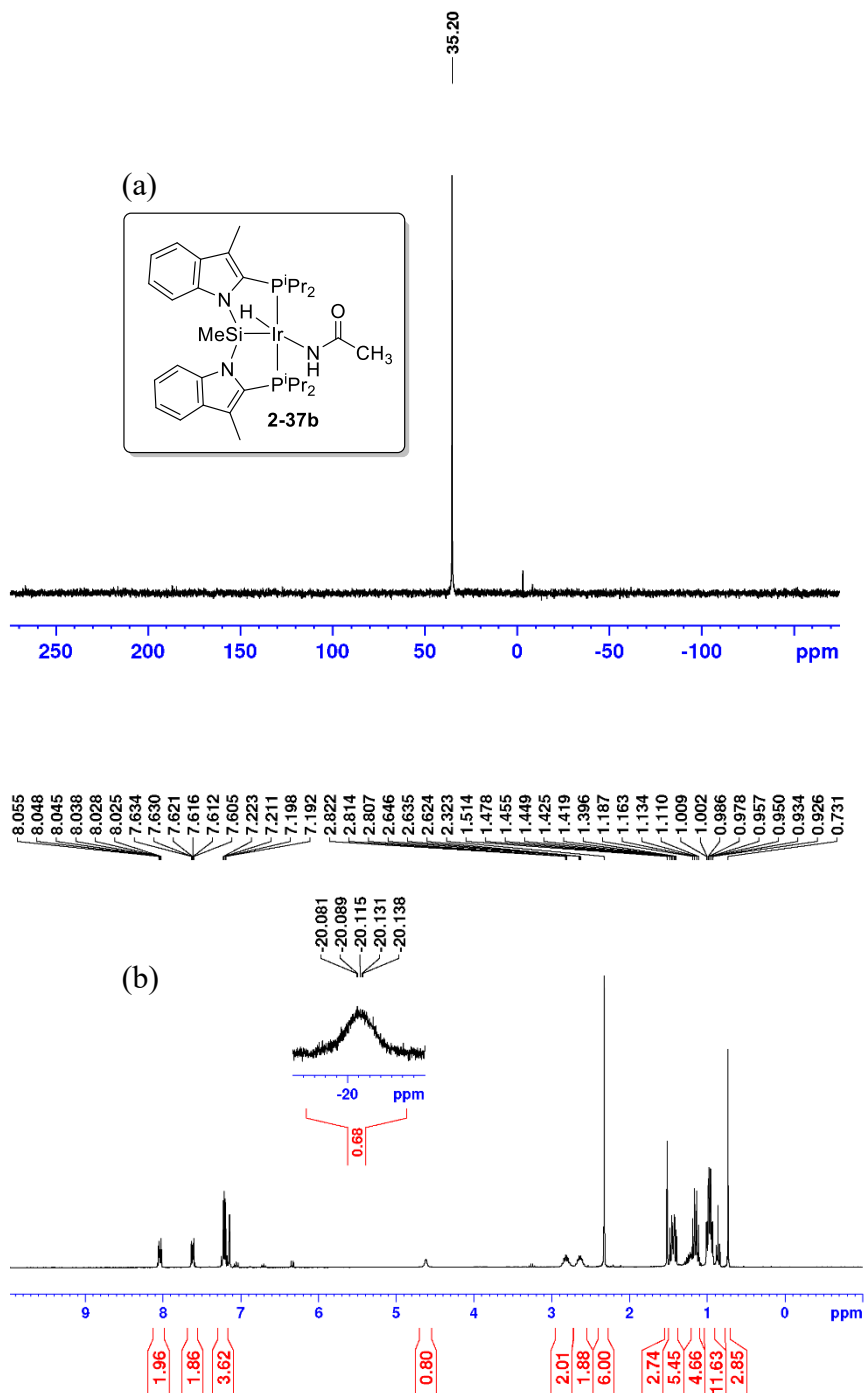
Figure A30. (continued) (a) $^{31}P\{^1H\}$, (b) ^1H, and (c) $^{13}C\{^1H\}$ NMR spectra (benzene-d_6) of (^iPr-PSiP^{Ind})IrH(NH(CO)Me) (**2-37b**).
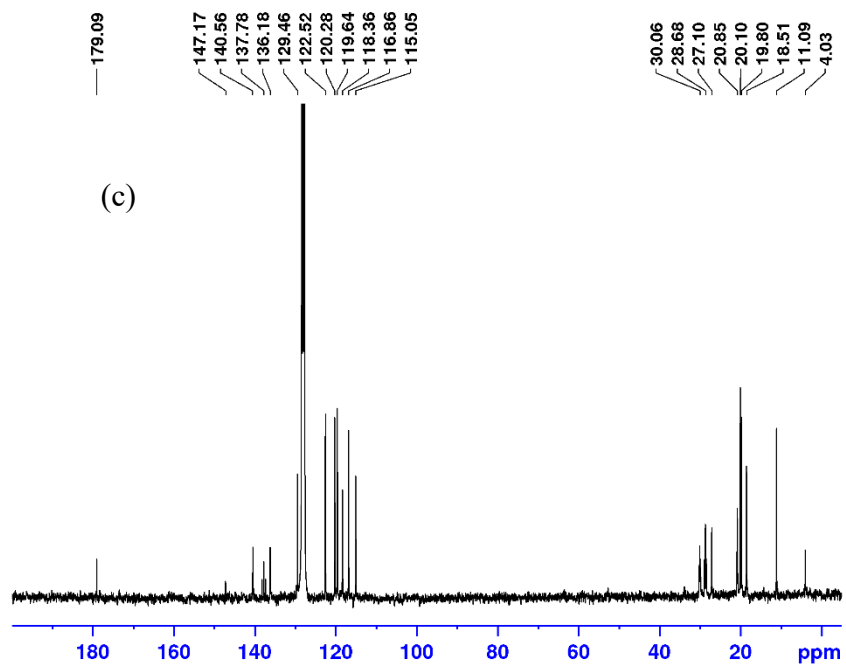
Figure A31. (a) $^{31}P\{^1H\}$, (b) ^1H, and (c) $^{13}C\{^1H\}$ NMR spectra (benzene-d_6), and (d) Raman (solid state, cm^{-1}) spectrum of [(^{i}Pr-PSiP^{Ind})Rh]$_2$(μ-N$_2$) (**2-38**).

(a)

2-38

(b)
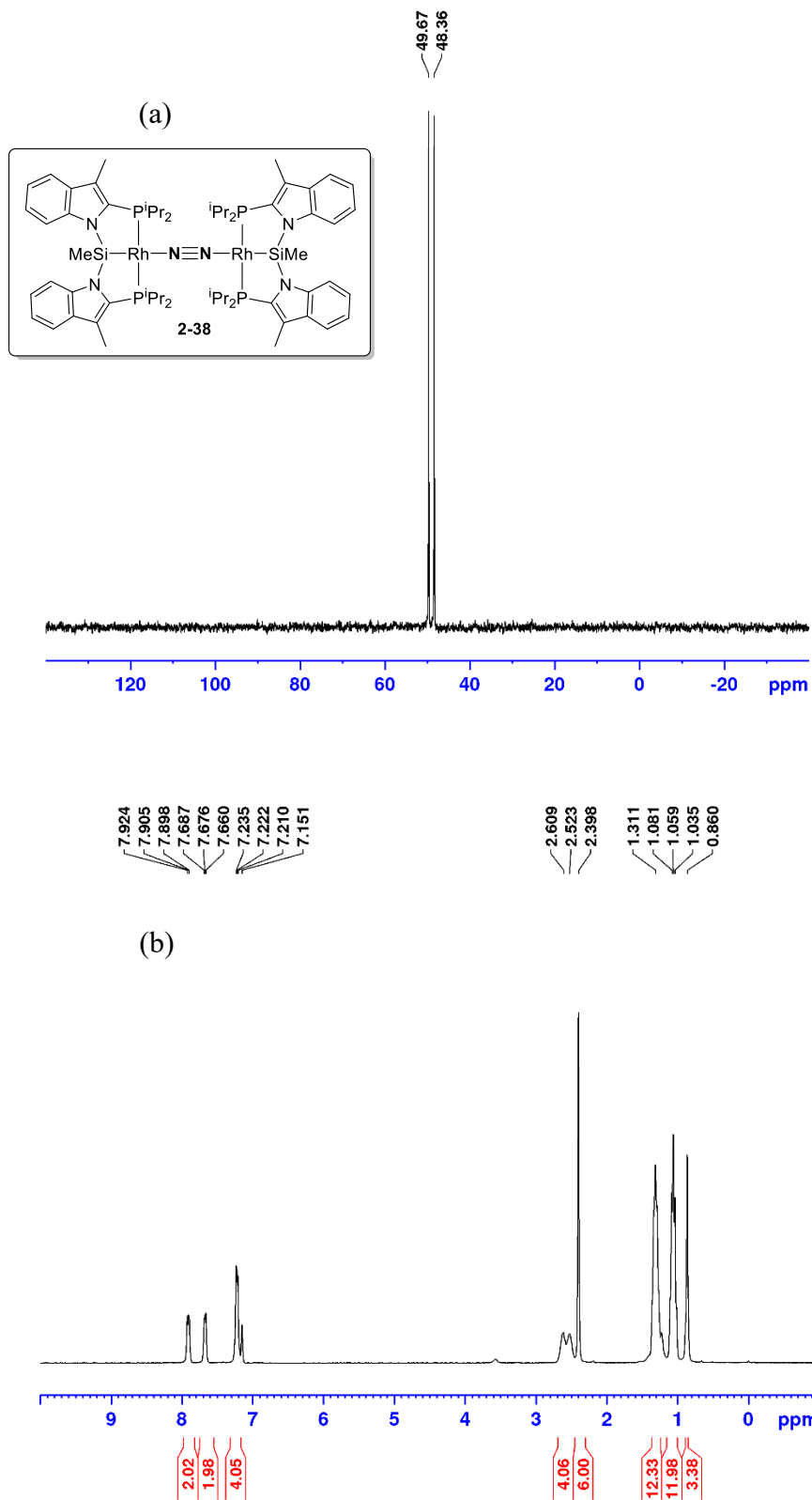
Figure A31. (continued) (a) $^{31}P\{^1H\}$, (b) ^1H, and (c) $^{13}C\{^1H\}$ NMR spectra (benzene-d_6), and (d) Raman (solid state, cm^{-1}) spectrum of [(^iPr-PSiP^{Ind})Rh]$_2$(μ-N$_2$) (**2-38**).
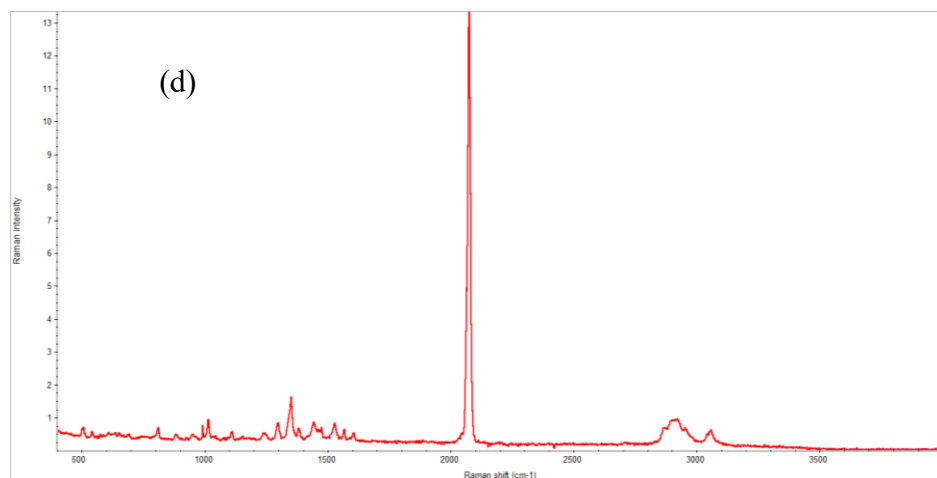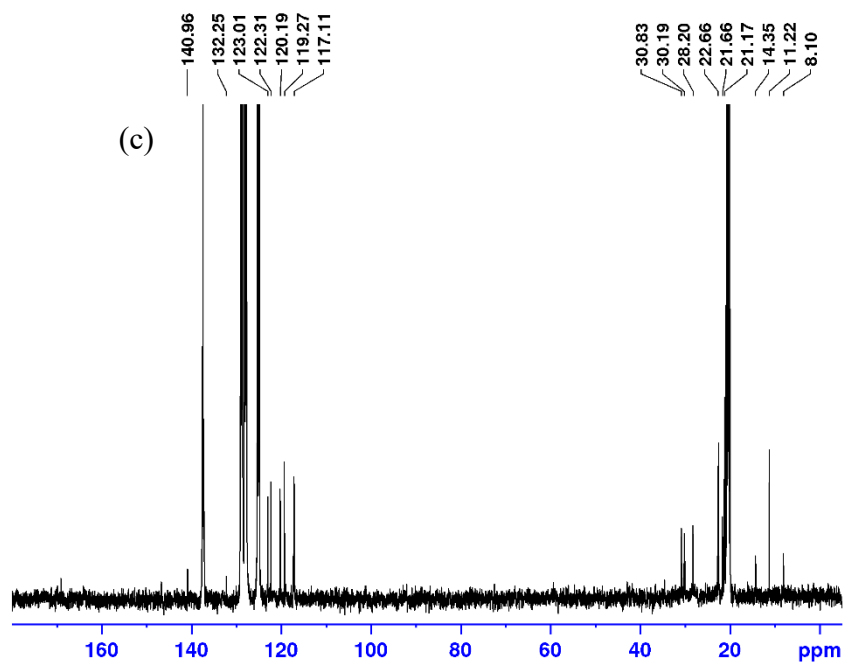
Figure A32. (a) $^{31}P\{^1H\}$, (b) ^1H, and (c) $^{13}C\{^1H\}$ NMR spectra (benzene-d_6) of (^{i}Pr-PSiP^{Ind})Rh(PMe$_3$) (**2-39a**).
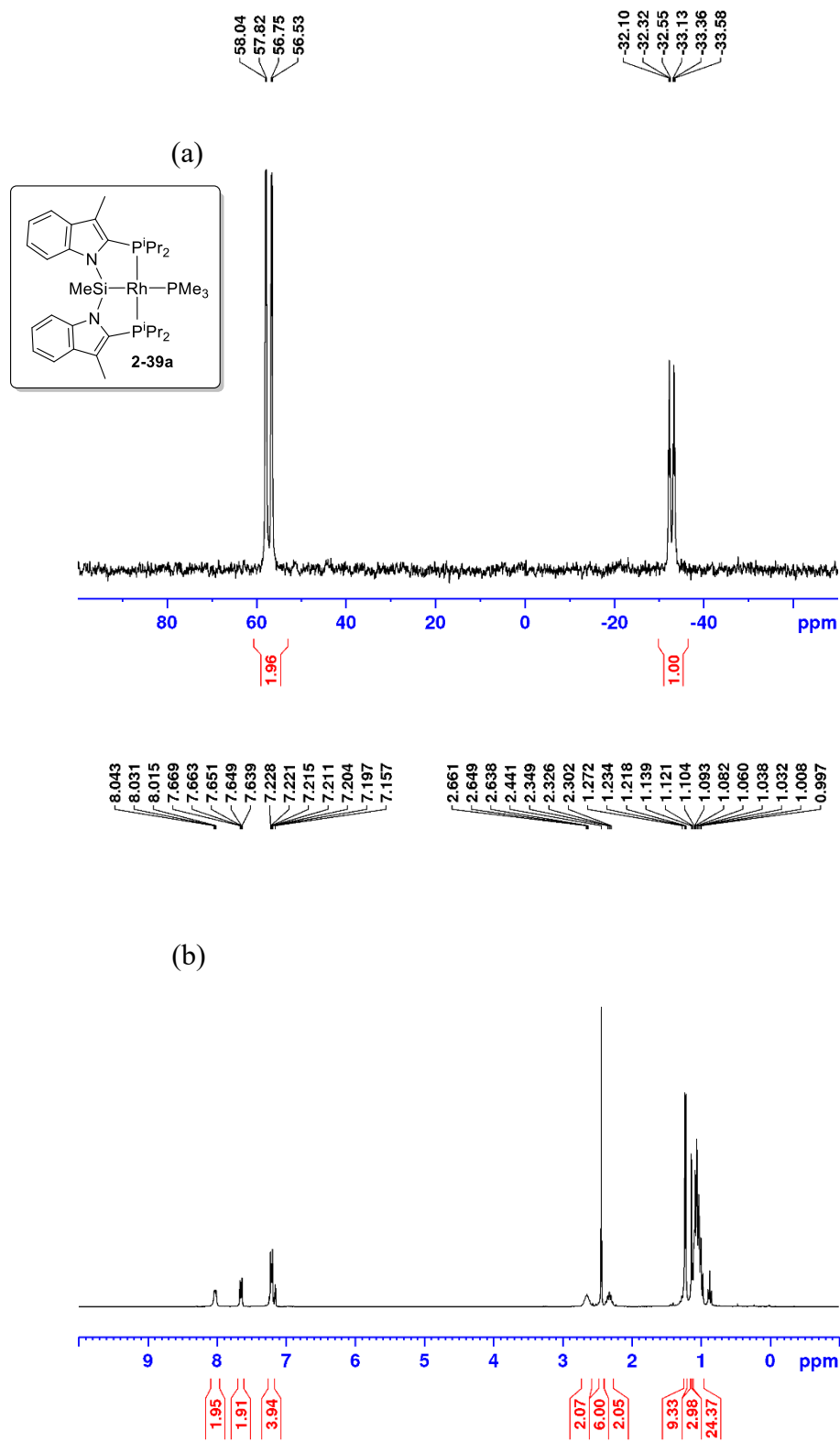
Figure A32. (continued) (a) $^{31}P\{^1H\}$, (b) ^1H, and (c) $^{13}C\{^1H\}$ NMR spectra (benzene-d_6) of (^iPr-PSiP^{Ind})Rh(PMe$_3$) (**2-39a**).
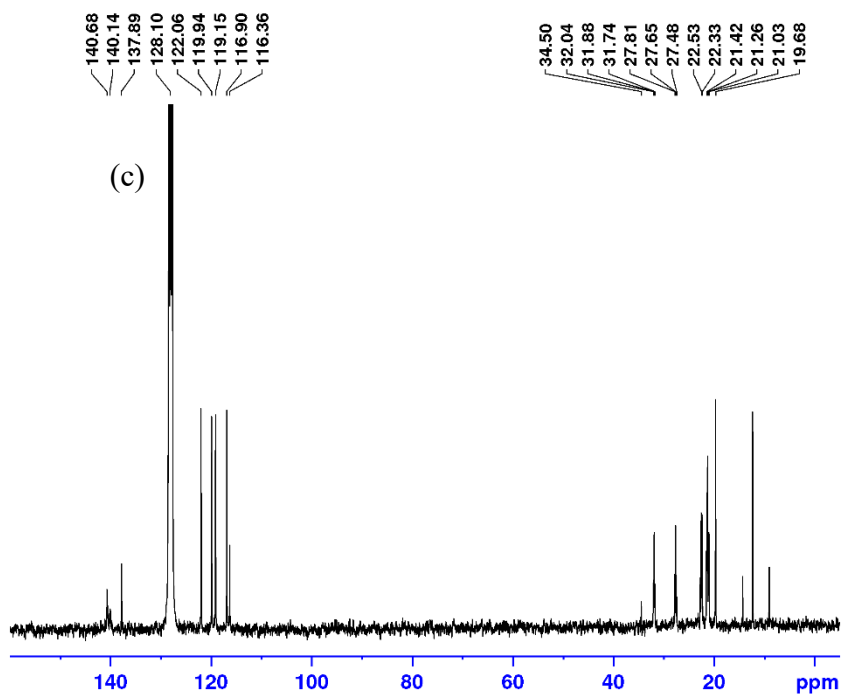
Figure A33. (a) $^{31}P\{^1H\}$, (b) ^1H, and (c) $^{13}C\{^1H\}$ NMR spectra (benzene-d_6) of (^{i}Pr-PSiP^{Ind})Rh(DMAP) (**2-39b**).
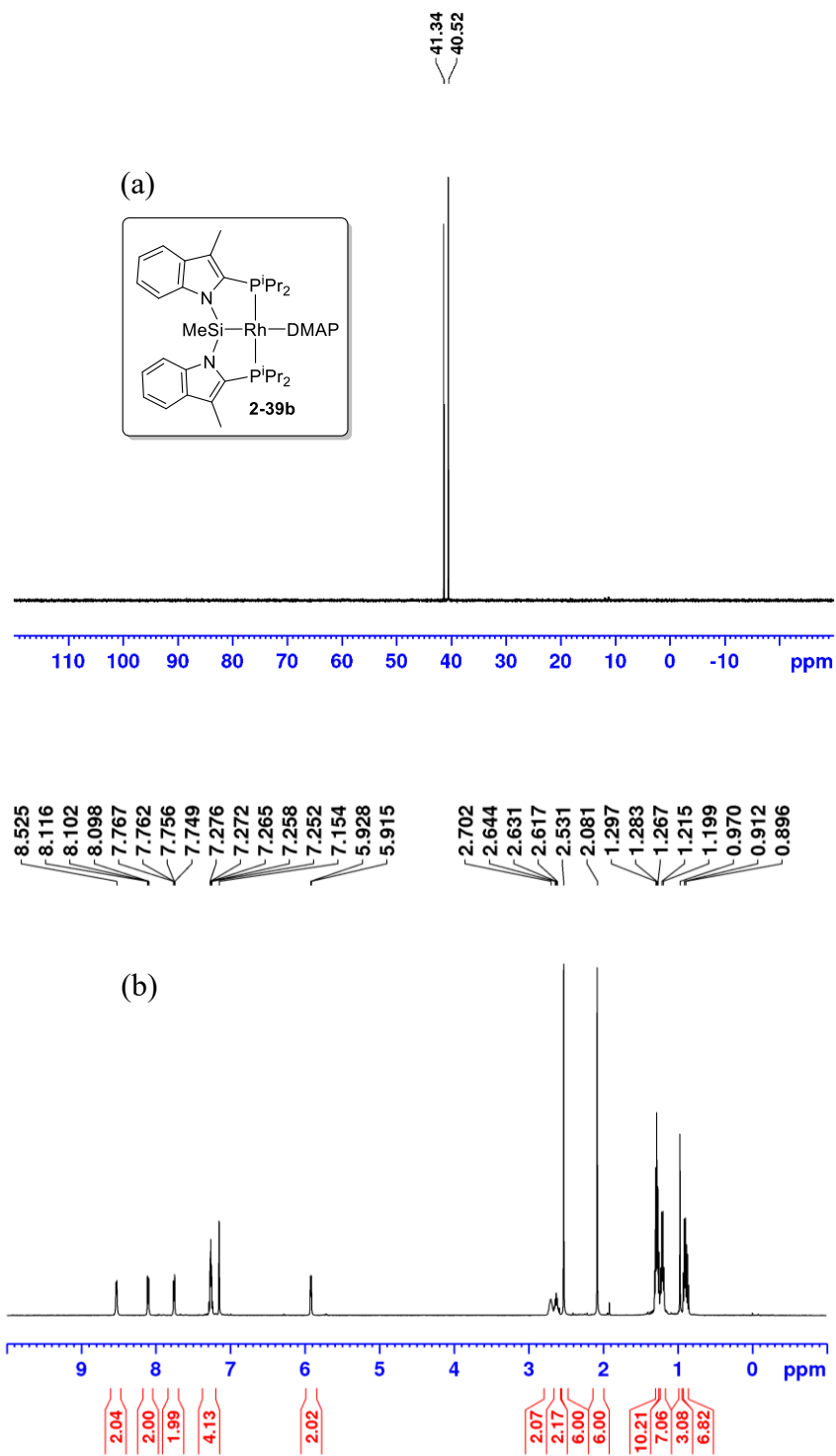
Figure A33. (continued) (a) $^{31}P\{^1H\}$, (b) ^1H, and (c) $^{13}C\{^1H\}$ NMR spectra (benzene-d_6) of (^{i}Pr-PSiP^{Ind})Rh(DMAP) (**2-39b**).
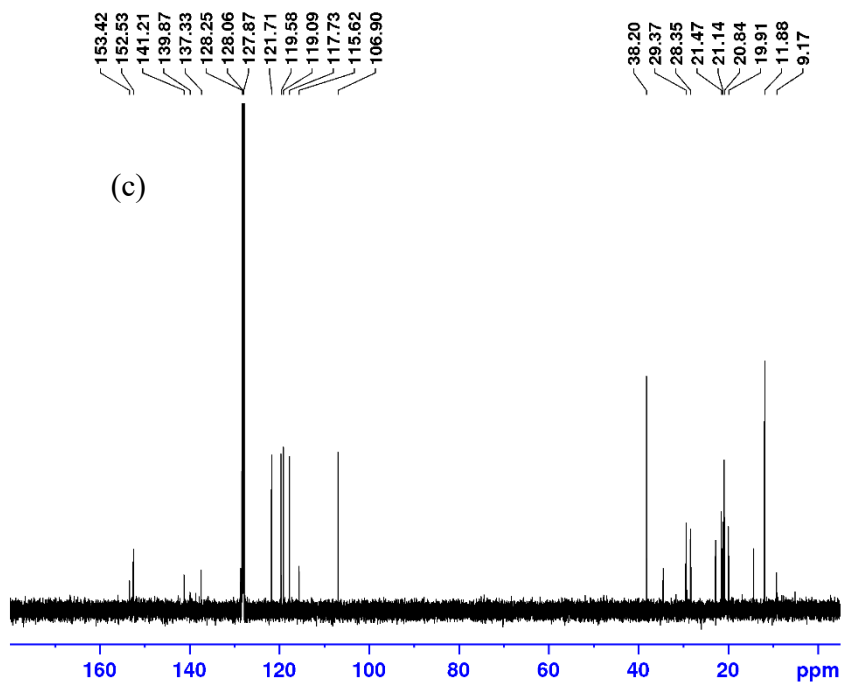
Figure A34. In situ (a) $^{31}P\{^1H\}$ and (b) ^1H NMR spectra (benzene-d_6) of (^iPr-PSiP^{Ind})Rh(NH$_2$Ph) (**2-39c**).
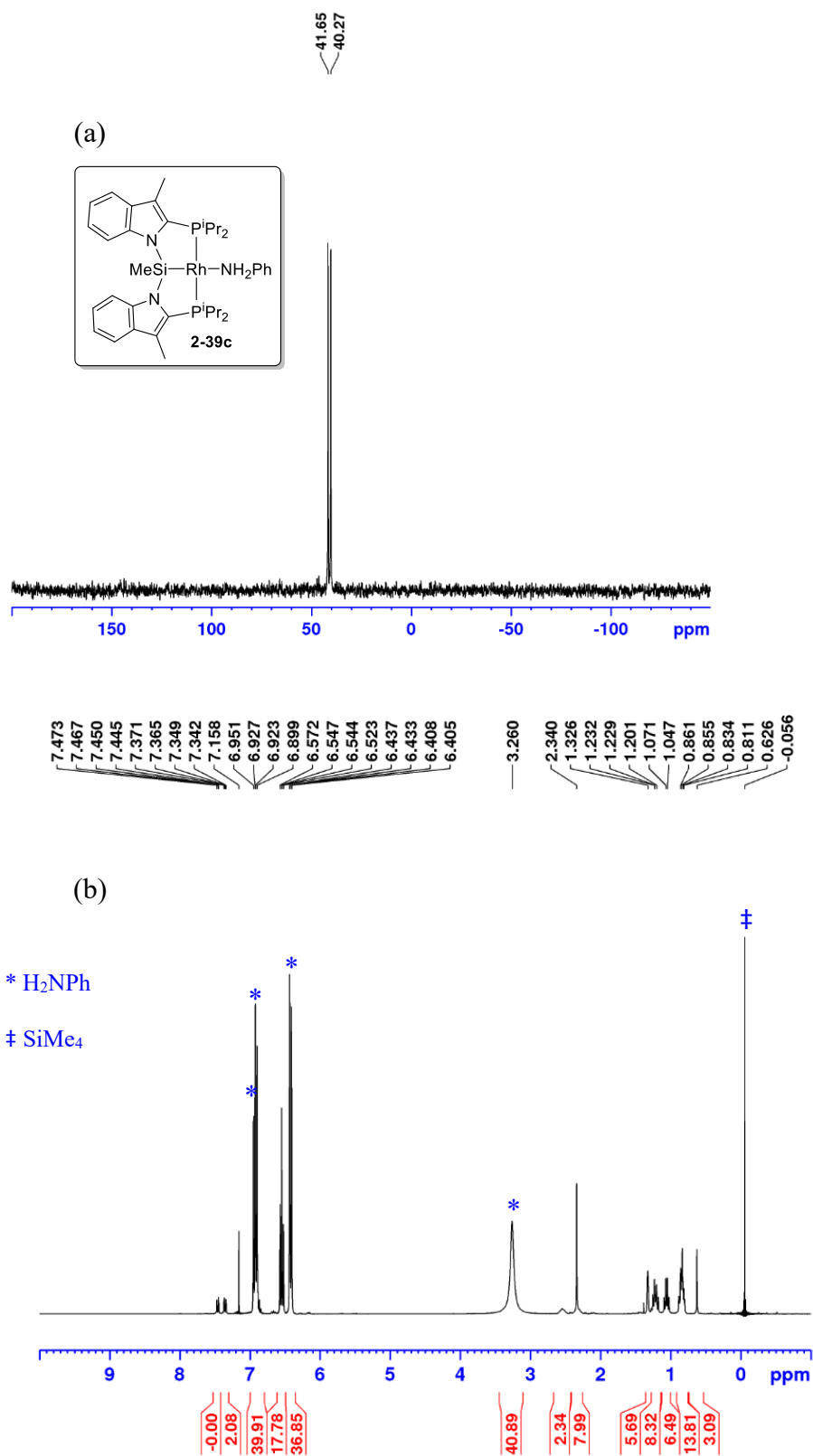
Figure A35. In situ (a) $^{31}P\{^1H\}$ and (b) ^1H NMR spectra (cyclohexane-d_{12}) of (^{i}Pr-PSiP^{Ind})Ir (**2-40**).
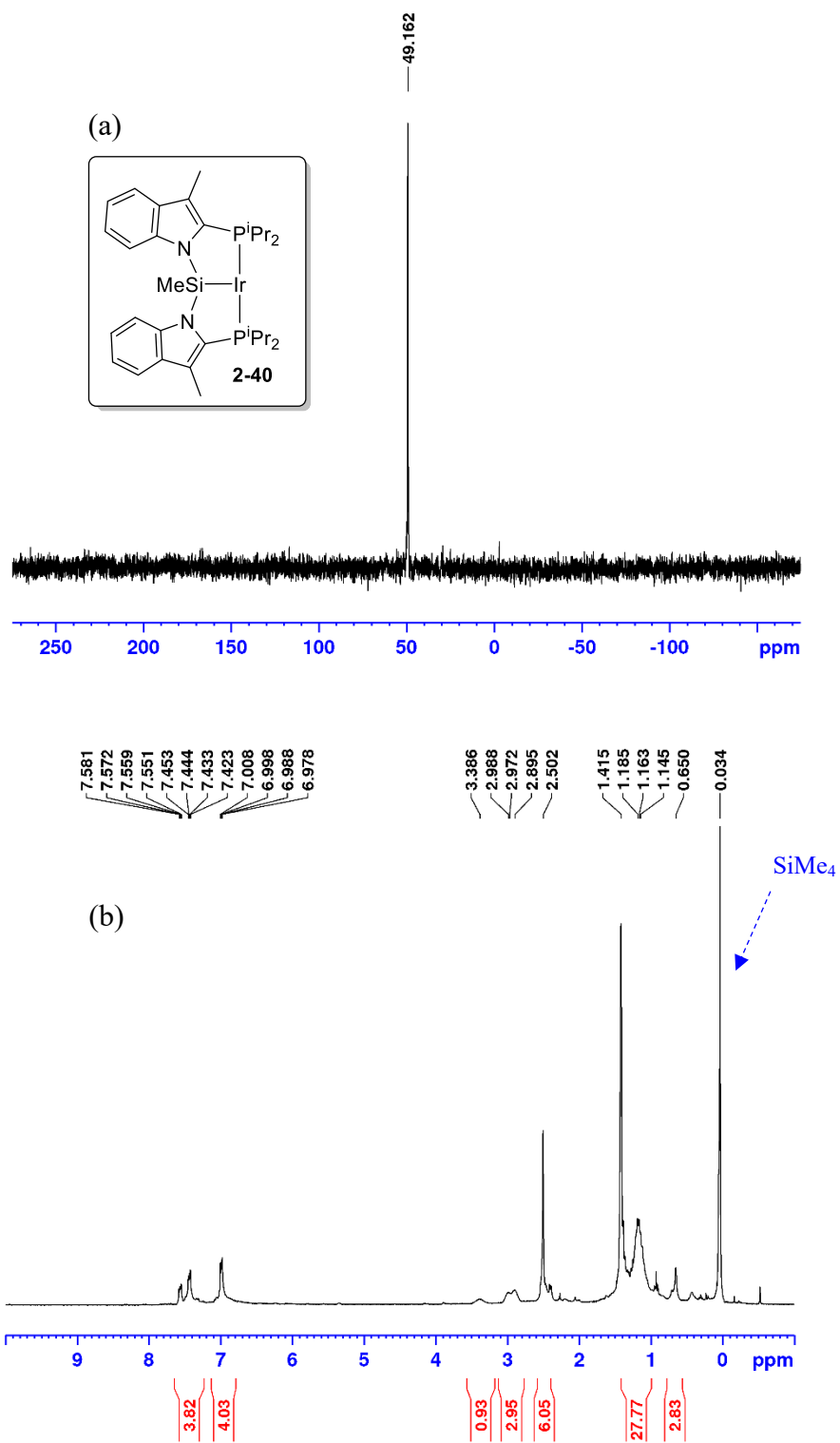
Figure A36. In situ (a) $^{31}P\{^1H\}$ and (b) ^1H NMR spectra (cyclohexane-d_{12}) of (^{i}Pr-PSiP^{Ind})Ir(C$_2$H$_4$) (**2-41a**).
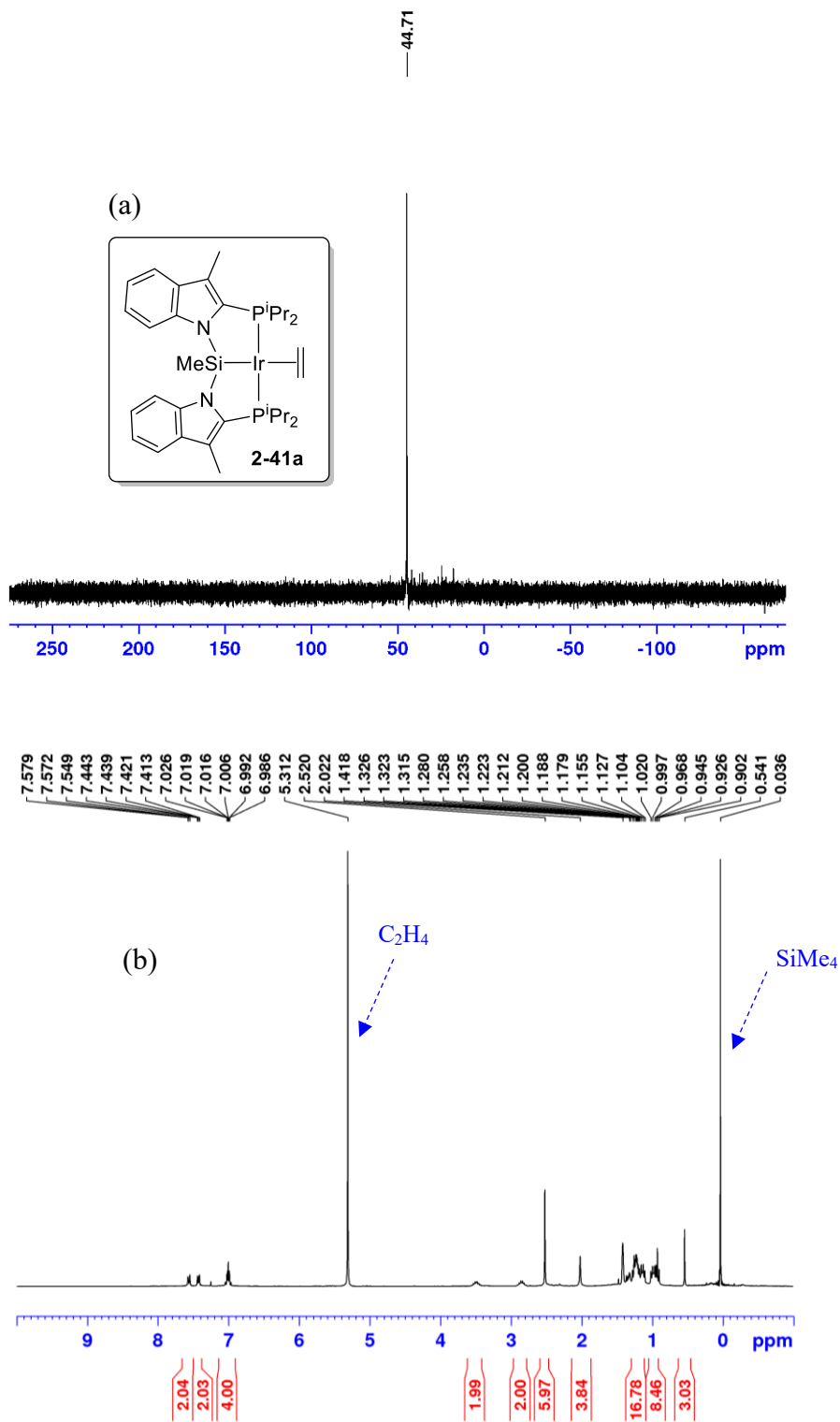
Figure A37. (a) $^{31}P\{^1H\}$, (b) ^1H, and (c) $^{13}C\{^1H\}$ NMR spectra (benzene-d_6) of (fac-κ^3-^{i}Pr-PSiP^{Ind})IrH(κ^2-P,C-o-C$_6$H$_4$PPh$_2$] (**2-43**).
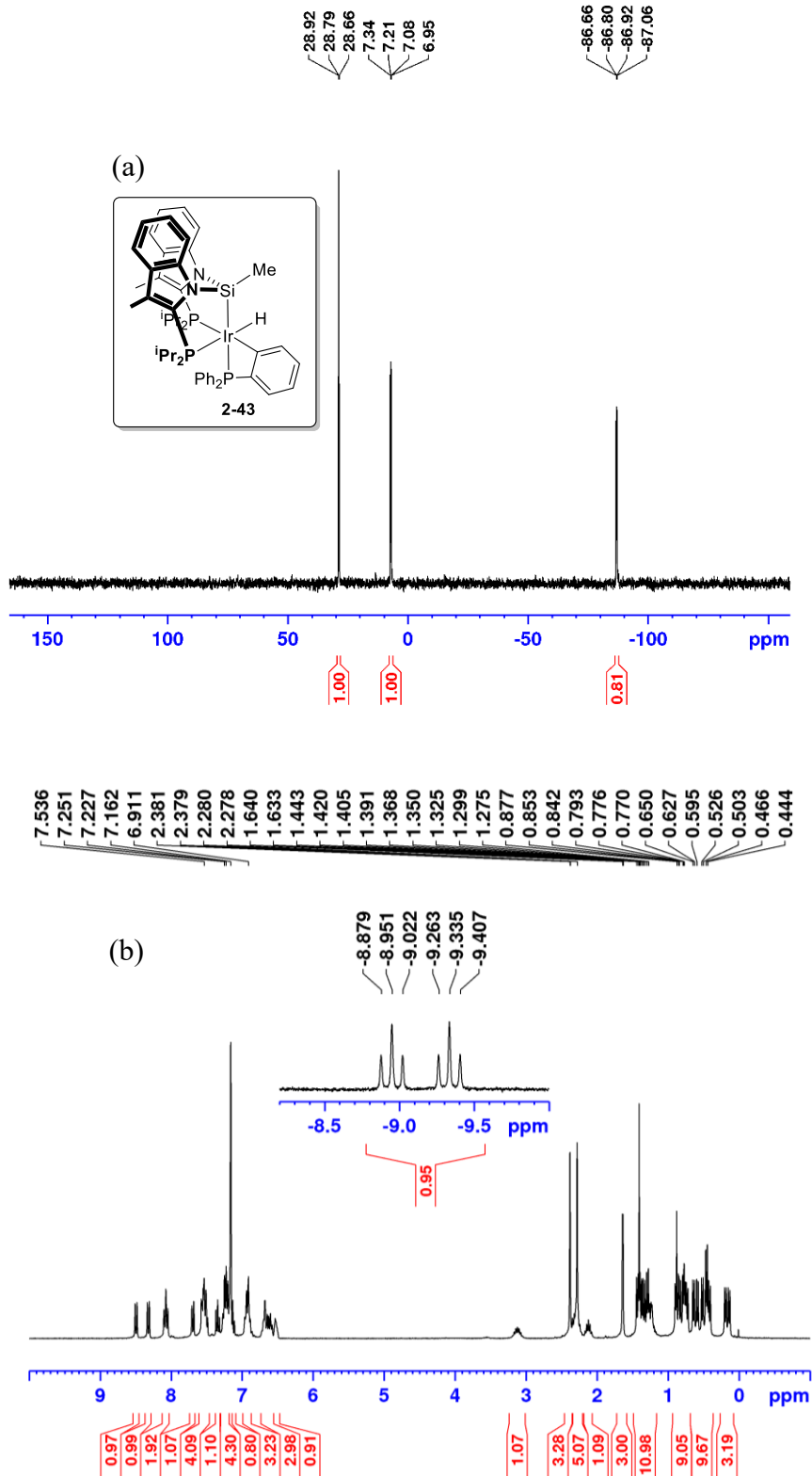
Figure A37. (continued) (a) $^{31}P\{^1H\}$, (b) ^1H, and (c) $^{13}C\{^1H\}$ NMR spectra (benzene-d_6) of (fac-κ^3-^iPr-PSiP^{Ind})IrH(κ^2-P,C-o-C$_6$H$_4$PPh$_2$] (**2-43**).

Figure A38. In situ (a) $^{31}P\{^1H\}$ and (b) ^1H NMR spectra (cyclohexane-d_{12}) of (^iPr-PSiP^{Ind})IrH(Ph) (**2-44**).

(a)

2-44

42.976

250 200 150 100 50 0 -50 -100 ppm

(b)

7.338
7.335
7.332
7.329
7.327
7.324
7.321
7.318
7.316
7.313
7.310
7.215
7.212
7.209
7.128
7.126
7.115
7.109
7.104
2.435
1.468
1.445
1.436
1.415
1.383
1.289
1.265
1.239
1.215
0.994
0.970
0.940
0.924
0.916
0.882
0.853
0.828
0.798
0.036

SiMe$_4$

-10.542
-10.599
-10.657

-10.5 ppm

0.75

9 8 7 6 5 4 3 2 1 0 ppm

1.69
2.53
7.09
1.40
1.07

4.00
6.20

10.65
15.96

277
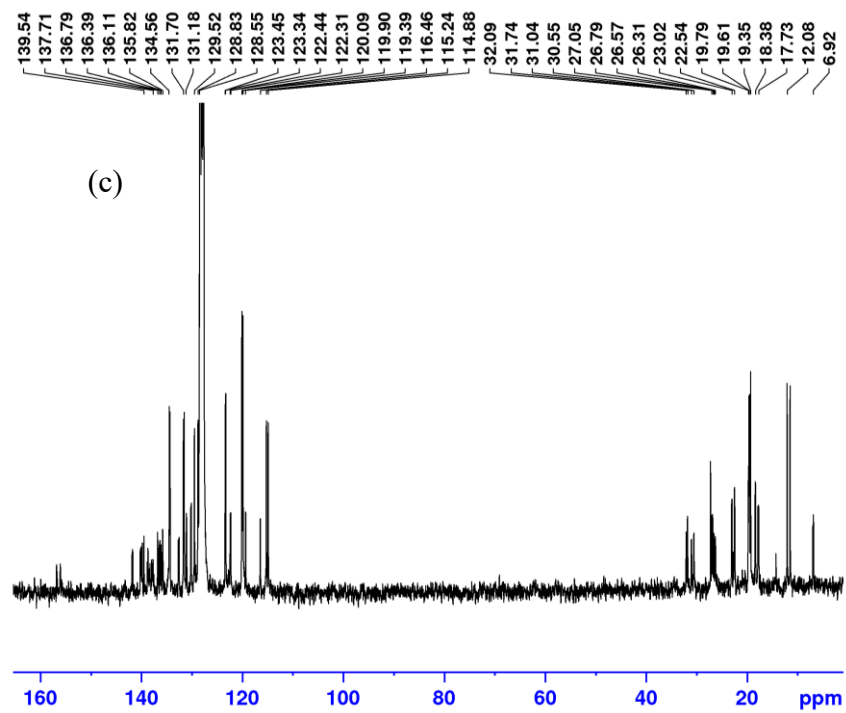
Figure A39. In situ $^{13}C\{^1H\}$ NMR spectrum (benzene-d_6) of (^{i}Pr-PSiP^{Ind})IrH(Ph) (**2-44**).
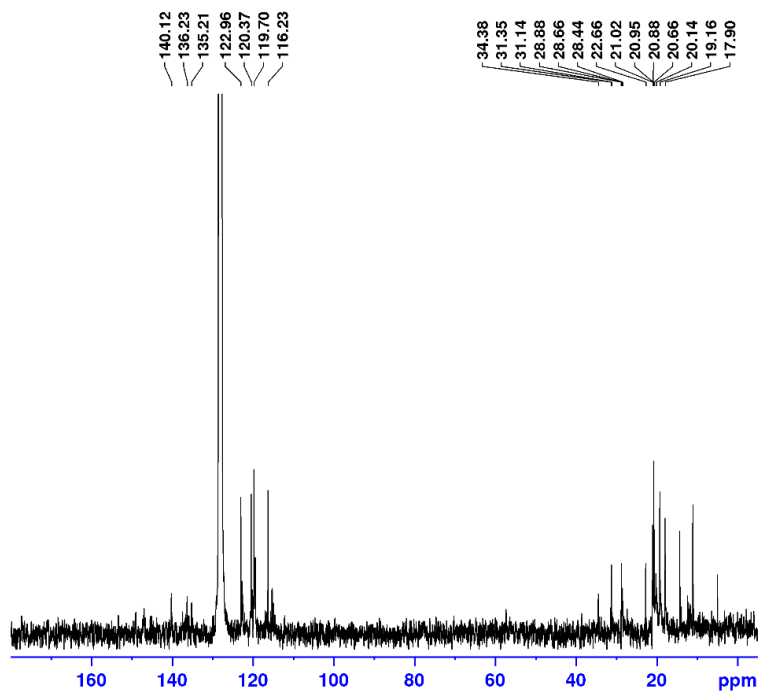
Figure A40. In situ (a) $^{31}P\{^1H\}$ and (b) ^1H NMR spectra (cyclohexane-d_{12}) of the reaction mixture containing (^iPr-PSiP^{Ind})IrH(NHPh) (**2-31a**) and (*fac*-κ^3-^iPr-PSiP^{Ind})IrH(κ^2-N,c-o-C$_6$H$_4$NH$_2$) (**2-31a'**) generated upon treatment of **2-40** with one equiv. of H$_2$NPh.

279
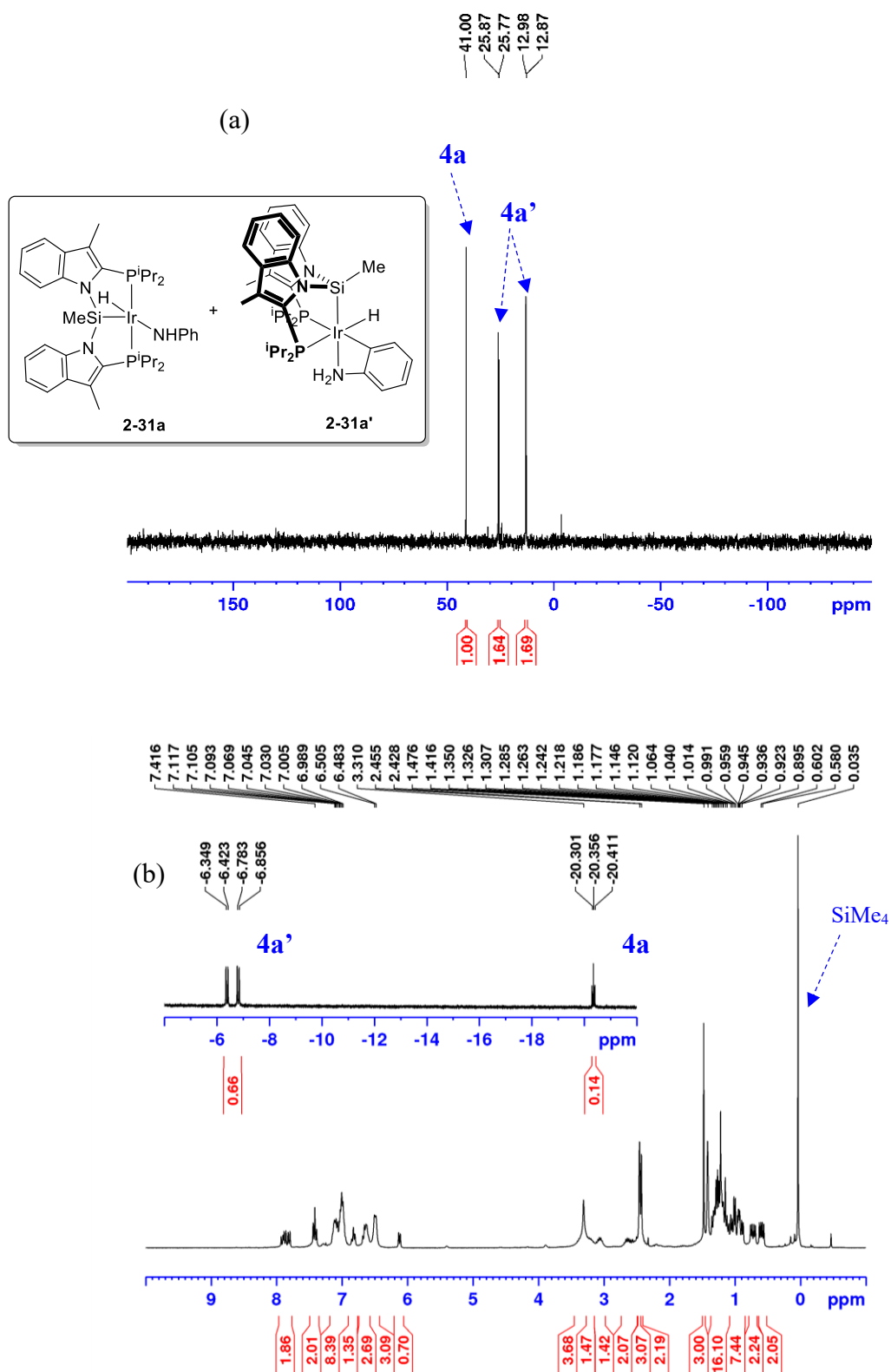
Figure A41. ^{1}H NMR spectra (cyclohexane-d$_{12}$) in the hydride region for product mixtures generated upon treatment of **2-40** with (a) H$_2$NPh-d$_5$ and (b) H$_2$NPh, consistent with ^{2}H incorporation exclusively into the Ir-H of **2-31a'**.
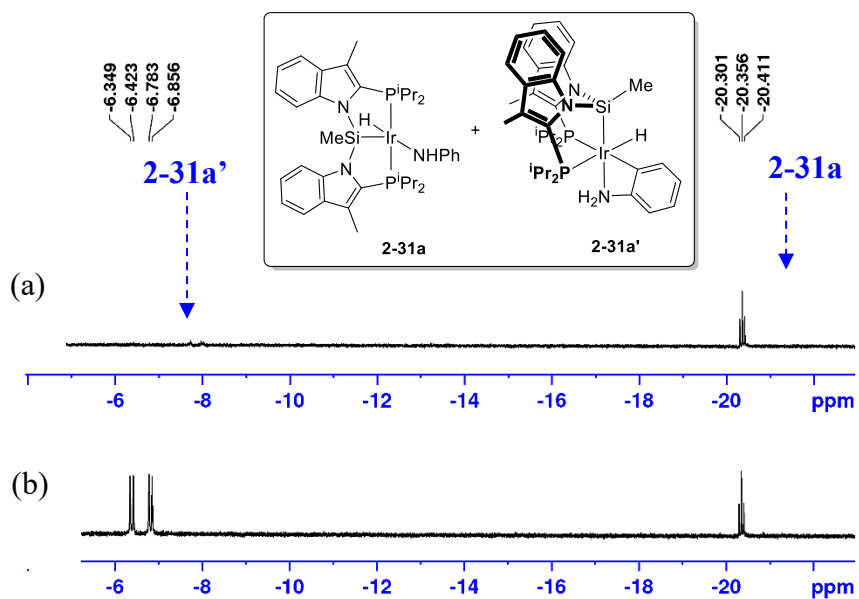
Figure A42. In situ (a) $^{31}P\{^{1}H\}$ and (b) ^{1}H NMR spectra (cyclohexane-d_{12}) of the reaction mixture containing (^{i}Pr-PSiP^{Ind})IrH[NH(2,6-Me$_2$C$_6$H$_3$)] (**2-31b**) and **2-31b'** generated upon treatment of **2-40** with one equiv. of H$_2$N(2,6-Me$_2$C$_6$H$_3$).
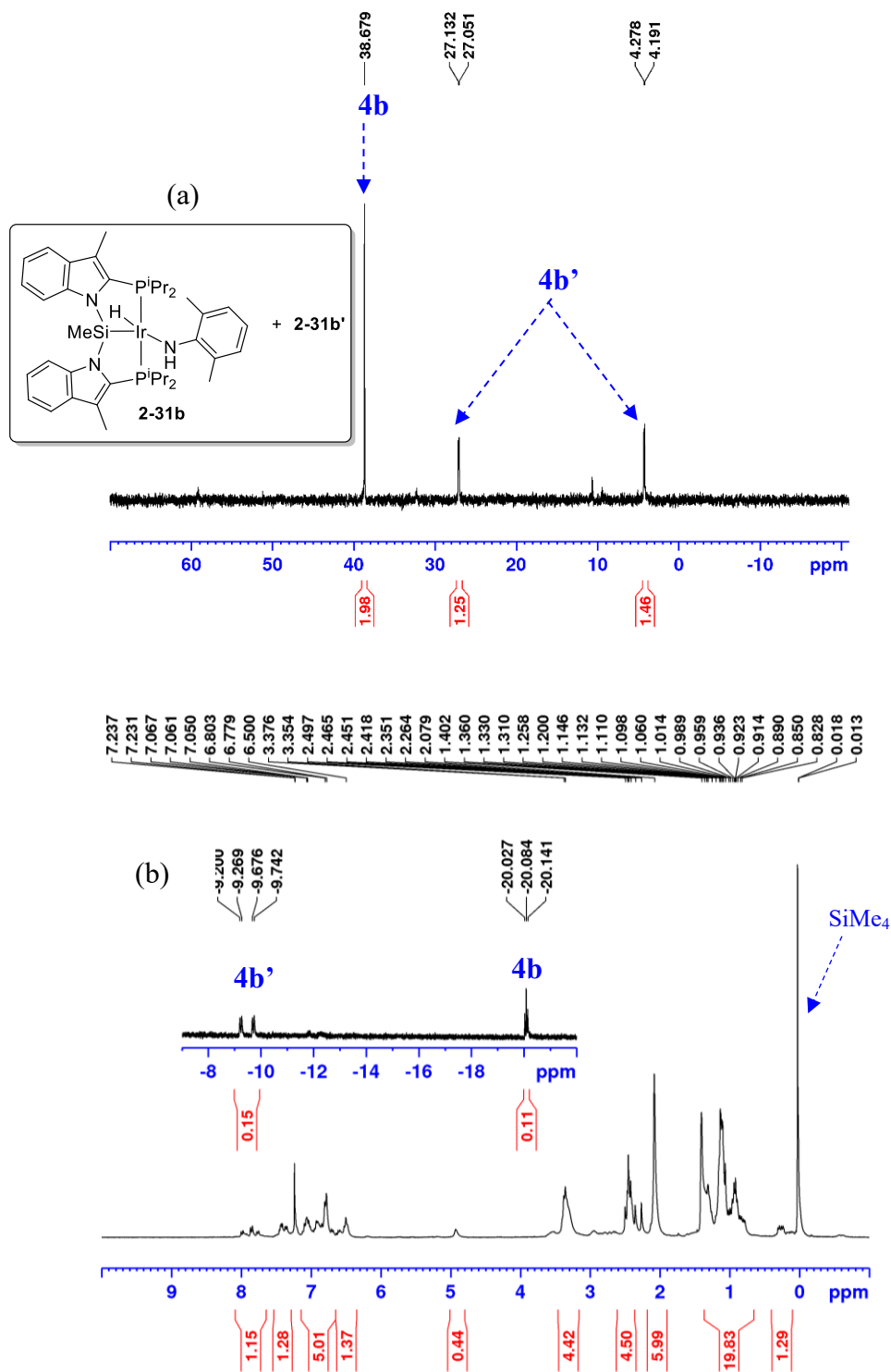
Appendix B: Chapter 3 Supporting Information

B-1: X-ray Crystallographic Data for Chapter 3

Table B1. Crystallographic Experimental Details for (^{i}Pr-PSiP^{Ind})Ir(C≡NAr)$_2$ (**3-1**).

A. Crystal Data

formula	$C_{64}H_{93}IrN_4P_2Si$
formula weight	1200.65
crystal dimensions (mm)	$0.31 \times 0.30 \times 0.04$
crystal system	triclinic
space group	$P\bar{1}$ (No. 2)
unit cell parameters^a	
a (Å)	10.9833 (3)
b (Å)	17.4132 (4)
c (Å)	17.6559 (4)
α (deg)	106.7278 (9)
β (deg)	96.9699 (7)
γ (deg)	106.2916 (8)
V (Å^3)	3028.08 (13)
Z	2
ρ_{calcd} (g cm^{-3})	1.317
μ (mm^{-1})	5.260

B. Data Collection and Refinement Conditions

diffractometer	Bruker D8/APEX II CCD^b
radiation (λ [Å])	Cu Kα (1.54178) (microfocus source)
temperature (°C)	–100
scan type	ω and ϕ scans (1.0°) (5 s exposures)
data collection 2θ limit (deg)	148.00
total data collected	21671 (-13 ≤ h ≤ 13, -21 ≤ k ≤ 21, -21 ≤ l ≤ 21)
independent reflections	11771 (R_{int} = 0.0172)
number of observed reflections (*NO*)	11590 [$F_o^2 \geq 2\sigma(F_o^2)$]
structure solution method	Patterson/structure expansion (*DIRDIF–2008^c*)
refinement method	full-matrix least-squares on F^2 (*SHELXL–2014^d*)
absorption correction method	Gaussian integration (face-indexed)
range of transmission factors	0.9082–0.3468
data/restraints/parameters	11771 / 0 / 656
goodness-of-fit (*S*)^e [all data]	1.054
final *R* indices^f	
R_1 [$F_o^2 \geq 2\sigma(F_o^2)$]	0.0196

Table B1. Crystallographic Experimental Details for (^{i}Pr-PSiP^{Ind})Ir(C≡NAr)$_2$ (**3-1**) (continued).

wR_2 [all data]	0.0503
largest difference peak and hole	0.566 and –1.064 e Å^{-3}

[a]Obtained from least-squares refinement of 9528 reflections with 6.32° < 2θ < 147.14°.

[b]Programs for diffractometer operation, data collection, data reduction and absorption correction were those supplied by Bruker.

[c]Beurskens, P. T.; Beurskens, G.; de Gelder, R.; Smits, J. M. M.; Garcia-Granda, S.; Gould, R. O. (2008). The *DIRDIF-2008* program system. Crystallography Laboratory, Radboud University Nijmegen, The Netherlands.

[d]Sheldrick, G. M. *Acta Crystallogr.* **2015**, *C71*, 3–8.

[e]$S = [\Sigma w(F_o^2 – F_c^2)^2/(n – p)]^{1/2}$ (n = number of data; p = number of parameters varied; $w = [\sigma^2(F_o^2) + (0.0254P)^2 + 1.8513P]^{-1}$ where $P = [Max(F_o^2, 0) + 2F_c^2]/3$).

[f]$R_1 = \Sigma||F_o| – |F_c||/\Sigma|F_o|$; $wR_2 = [\Sigma w(F_o^2 – F_c^2)^2/\Sigma w(F_o^4)]^{1/2}$.
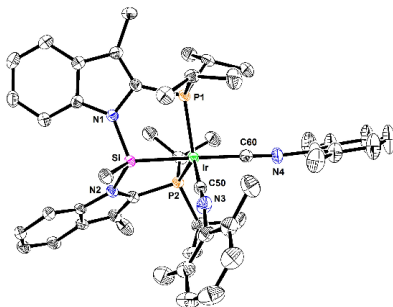
Figure B1. ORTEP diagram of (^{i}Pr-PSiP^{Ind})Ir(C≡NAr)$_2$ (**3-1**).

Table B2. Crystallographic Experimental Details of (^{i}Pr-PSiP^{Ind})Ir(H)(NHPh)(CNAr) (**3-2**).

A. Crystal Data

formula	C$_{52}$H$_{67}$IrN$_4$P$_2$Si
formula weight	1030.32
crystal dimensions (mm)	0.22 × 0.14 × 0.05
crystal system	triclinic
space group	$P\bar{1}$ (No. 2)
unit cell parameters[a]	
a (Å)	13.5359 (3)

Table B2. Crystallographic Experimental Details of (^{i}Pr-PSiP$^{\text{Ind}}$)Ir(H)(NHPh)(CNAr) (**3-2**) (continued)

b (Å)	13.6598 (3)
c (Å)	16.2406 (3)
α (deg)	112.5687 (15)
β (deg)	111.6397 (16)
γ (deg)	92.8589 (16)
V (Å^3)	2512.56 (10)
Z	2
ρ_{calcd} (g cm^{-3})	1.362
μ (mm^{-1})	6.252

B. Data Collection and Refinement Conditions

diffractometer	Bruker D8/APEX II CCD[b]
radiation (λ [Å])	Cu Kα (1.54178) (microfocus source)
temperature (°C)	−100
scan type	ω and ϕ scans (1.0°) (5 s exposures)
data collection 2θ limit (deg)	137.29
total data collected	15702 (-16 ≤ h ≤ 16, -16 ≤ k ≤ 16, -19 ≤ l ≤ 19)
independent reflections	8912 (R_{int} = 0.1192)
number of observed reflections (*NO*)	6145 [$F_o^2 \geq 2\sigma(F_o^2)$]
structure solution method	Patterson/structure expansion (*DIRDIF–2008[c]*)
refinement method	full-matrix least-squares on F^2 (*SHELXL–2014[d]*)
absorption correction method	Gaussian integration (face-indexed)
range of transmission factors	0.8745–0.5021
data/restraints/parameters	8912 / 2[e] / 514
goodness-of-fit (*S*)[f] [all data]	1.045
final *R* indices[g]	
R_1 [$F_o^2 \geq 2\sigma(F_o^2)$]	0.0757
wR_2 [all data]	0.2022
largest difference peak and hole	1.987 and −1.888 e Å^{-3}

[a]Obtained from least-squares refinement of 9629 reflections with 6.50° < 2θ < 136.66°.

[b]Programs for diffractometer operation, data collection, data reduction and absorption correction were those supplied by Bruker.

[c]Beurskens, P. T.; Beurskens, G.; de Gelder, R.; Smits, J. M. M.; Garcia-Granda, S.; Gould, R. O. (2008). The *DIRDIF-2008* program system. Crystallography Laboratory, Radboud University Nijmegen, The Netherlands.

Table B2. Crystallographic Experimental Details of (^{i}Pr-PSiP^{Ind})Ir(H)(NHPh)(CNAr) (**3-2**) (continued).

^{d}Sheldrick, G. M. *Acta Crystallogr.* **2015**, *C71*, 3–8.

^{e}The Ir–H1 (1.55(1) Å) and N4–H4N (0.88(1) Å) distances were constrained during refinement. The carbon atoms of the disordered solvent benzene molecule were split into two sets of six atoms, with occupancy factors of 60% and 40%, and were refined as idealized hexagons with C–C bond lengths of 1.390 Å and C–C–C bond angles of 120.0º.

$^{f}S = [\Sigma w(F_o^2 - F_c^2)^2/(n - p)]^{1/2}$ (n = number of data; p = number of parameters varied; $w = [\sigma^2(F_o^2) + (0.0683P)^2 + 23.1135P]^{-1}$ where $P = [\text{Max}(F_o^2, 0) + 2F_c^2]/3$).

$^{g}R_1 = \Sigma||F_o| - |F_c||/\Sigma|F_o|$; $wR_2 = [\Sigma w(F_o^2 - F_c^2)^2/\Sigma w(F_o^4)]^{1/2}$.
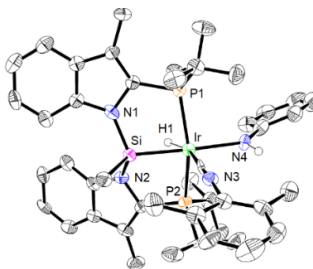

Figure B2. ORTEP diagram for (^{i}Pr-PSiP^{Ind})Ir(H)(NHPh)(CNAr) (**3-2**).

Table B3. Crystallographic Experimental Details for (Cy-PSiP)IrH[O(CO)NHPh] (**3-5a**).

A. Crystal Data

formula	$C_{56}H_{74}IrNO_2P_2Si$
formula weight	1075.39
crystal dimensions (mm)	$0.37 \times 0.17 \times 0.13$
crystal system	monoclinic
space group	$P2_1/n$ (an alternate setting of $P2_1/c$ [No. 14])
unit cell parameters^{a}	
a (Å)	16.6986(3)
b (Å)	14.9712(3)
c (Å)	20.7426(4)
β (deg)	96.6057(7)
V (Å^3)	5151.19(17)
Z	4
ρ_{calcd} (g cm^{-3})	1.387

Table B3. Crystallographic Experimental Details for (Cy-PSiP)IrH[O(CO)NHPh] (**3-5a**) (continued).

μ (mm^{-1})	6.134

B. Data Collection and Refinement Conditions

diffractometer	Bruker D8 /APEX II CCD[b]
radiation (λ [Å])	Cu Kα (1.54178) (microfocus source)
temperature (°C)	–100
scan type	ω and ϕ scans (1.0°) (5 s exposures)
data collection 2θ limit (deg)	148.28
total data collected	213431 ($-20 \leq h \leq 20$, $-18 \leq k \leq 18$, $-25 \leq l \leq 25$)
independent reflections	10460 (R_{int} = 0.0290)
number of observed reflections (*NO*)	9852 [$F_o^2 \geq 2\sigma(F_o^2)$]
structure solution method	intrinsic phasing (*SHELXT-2014*[c])
refinement method	full-matrix least-squares on F^2 (*SHELXL–2017*[d])
absorption correction method	multi-scan (*SADABS*)
range of transmission factors	0.6761–0.3150
data/restraints/parameters	10460 / 0 / 576
goodness-of-fit (*S*)[e] [all data]	1.053
final *R* indices[f]	
R_1 [$F_o^2 \geq 2\sigma(F_o^2)$]	0.0180
wR_2 [all data]	0.0469
largest difference peak and hole	0.745 and –0.770 e Å^{-3}

[a]Obtained from least-squares refinement of 9372 reflections with 6.44° < 2θ < 147.66°.

[b]Programs for diffractometer operation, data collection, data reduction and absorption correction were those supplied by Bruker.

[c]Sheldrick, G. M. *Acta Crystallogr.* **2015**, *A71*, 3–8. (*SHELXT-2014*)

[d]Sheldrick, G. M. *Acta Crystallogr.* **2015**, *C71*, 3–8. (*SHELXL-2017*)

[e]$S = [\Sigma w(F_o^2 - F_c^2)^2/(n - p)]^{1/2}$ (*n* = number of data; *p* = number of parameters varied; *w* = $[\sigma^2(F_o^2) + (0.0237P)^2 + 3.0356P]^{-1}$ where $P = [\text{Max}(F_o^2, 0) + 2F_c^2]/3$).

[f]$R_1 = \Sigma||F_o| - |F_c||/\Sigma|F_o|$; $wR_2 = [\Sigma w(F_o^2 - F_c^2)^2/\Sigma w(F_o^4)]^{1/2}$.
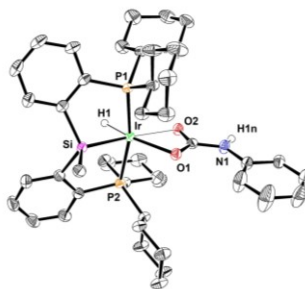
**Figure B3.** ORTEP diagram for (Cy-PSiP)IrH[O(CO)NHPh] (**3-5a**).

Table B4. Crystallographic Experimental Details for (Cy-PSiP)IrH[O(CO)NH^{t}Bu] (**3-5b**).

A. Crystal Data

formula	$C_{42}H_{66}IrNO_2P_2Si$
formula weight	899.18
crystal dimensions (mm)	$0.28 \times 0.04 \times 0.04$
crystal system	monoclinic
space group	$P2_1/c$ (No. 14)
unit cell parameters^a	
a (Å)	10.4039(2)
b (Å)	24.0474(4)
c (Å)	17.7667(3)
β (deg)	102.1178(10)
V (Å^3)	4345.95(13)
Z	4
ρ_{calcd} (g cm^{-3})	1.374
μ (mm^{-1})	7.154

B. Data Collection and Refinement Conditions

diffractometer	Bruker D8/APEX II CCD^b
radiation (λ [Å])	Cu Kα (1.54178) (microfocus source)
temperature (°C)	-100
scan type	ω and ϕ scans (1.0°) (5 s exposures)
data collection 2θ limit (deg)	148.42
total data collected	30655 ($-12 \leq h \leq 12$, $-29 \leq k \leq 29$, $-22 \leq l \leq 21$)
independent reflections	8733 ($R_{int} = 0.0441$)
number of observed reflections (*NO*)	7656 [$F_o^2 \geq 2\sigma(F_o^2)$]
structure solution method	intrinsic phasing (*SHELXT-2014^c*)
refinement method	full-matrix least-squares on F^2 (*SHELXL–*

Table B4. Crystallographic Experimental Details for (Cy-PSiP)IrH[O(CO)NH^{t}Bu] (**3-5b**) (continued).

2017^d)

absorption correction method	Gaussian integration (face-indexed)
range of transmission factors	0.9564–0.3881
data/restraints/parameters	8733 / 0 / 450
goodness-of-fit (*S*)^e [all data]	1.019
final *R* indices^f	
R_1 [$F_o^2 \geq 2\sigma(F_o^2)$]	0.0277
wR_2 [all data]	0.0660
largest difference peak and hole	1.665 and −1.340 e Å^{-3}

^{a}Obtained from least-squares refinement of 9883 reflections with $7.36° < 2\theta < 147.54°$.

^{b}Programs for diffractometer operation, data collection, data reduction and absorption correction were those supplied by Bruker.

^{c}Sheldrick, G. M. *Acta Crystallogr.* **2015**, *A71*, 3–8. (*SHELXT-2014*)

^{d}Sheldrick, G. M. *Acta Crystallogr.* **2015**, *C71*, 3–8. (*SHELXL-2017*)

$^e S = [\Sigma w(F_o^2 - F_c^2)^2/(n - p)]^{1/2}$ (*n* = number of data; *p* = number of parameters varied; *w* = $[\sigma^2(F_o^2) + (0.0156P)^2 + 5.2965P]^{-1}$ where *P* = [Max(F_o^2, 0) + 2F_c^2]/3).

$^f R_1 = \Sigma||F_o| - |F_c||/\Sigma|F_o|$; $wR_2 = [\Sigma w(F_o^2 - F_c^2)^2/\Sigma w(F_o^4)]^{1/2}$.
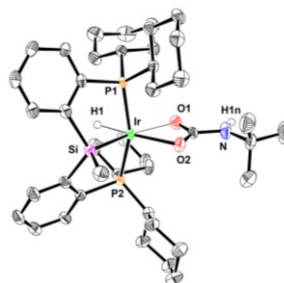
Figure B4. ORTEP diagram of (Cy-PSiP)IrH[O(CO)NH^{t}Bu] (**3-5b**).

B-2: Selected NMR Data for Chapter 3

Figure B5. (a) $^{31}P\{^1H\}$, (b) ^1H, and (c) $^{13}C\{^1H\}$ NMR spectra (benzene-d_6) of (^{i}Pr-PSiP^{Ind})IrH(NHPh)(CNAr) (**3-2**).
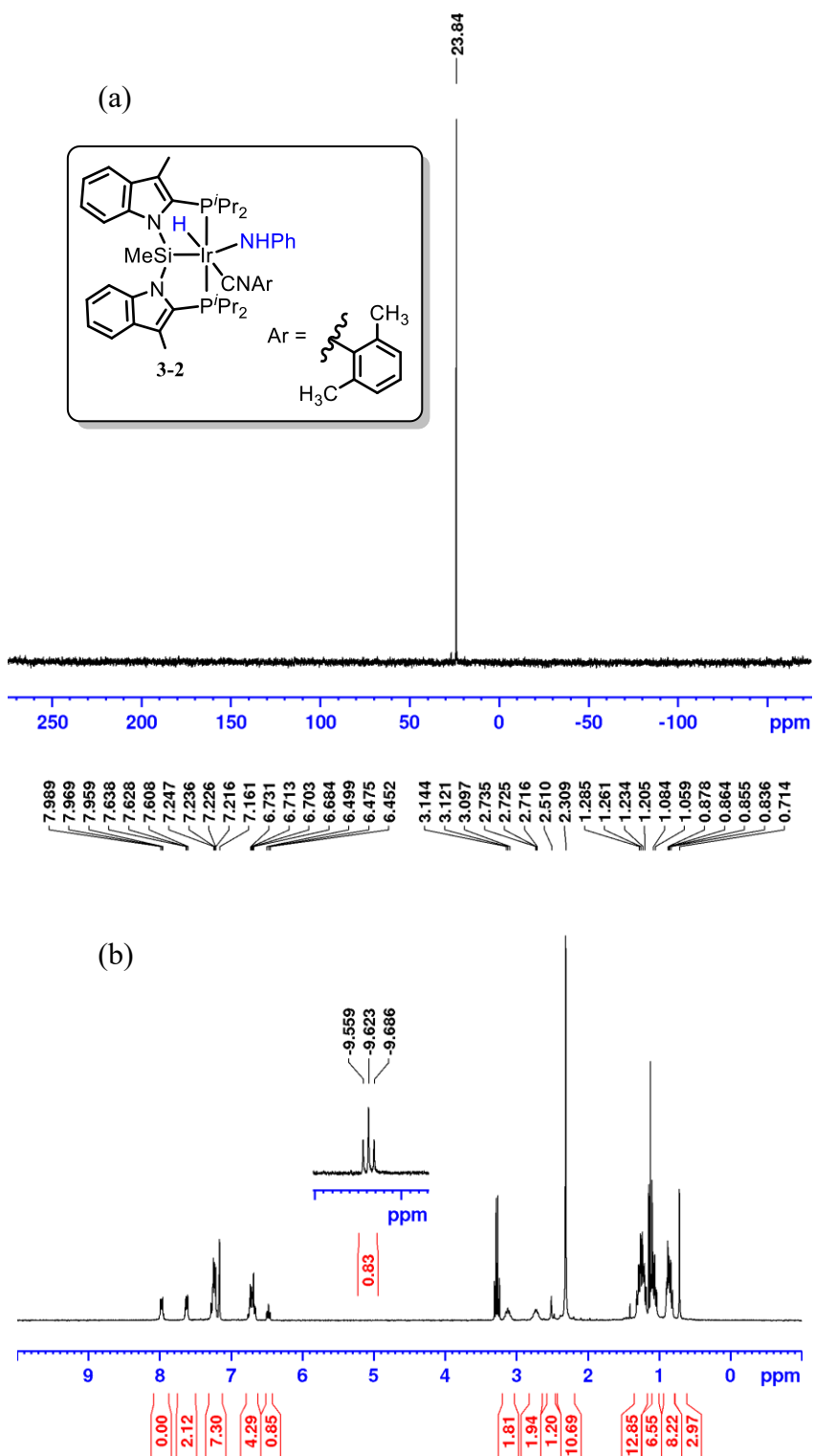
Figure B5. continued. (a) $^{31}P\{^1H\}$, (b) ^1H, and (c) $^{13}C\{^1H\}$ NMR spectra (benzene-d_6) of (^iPr-PSiP^{Ind})IrH(NHPh)(CNAr) (**3-2**).
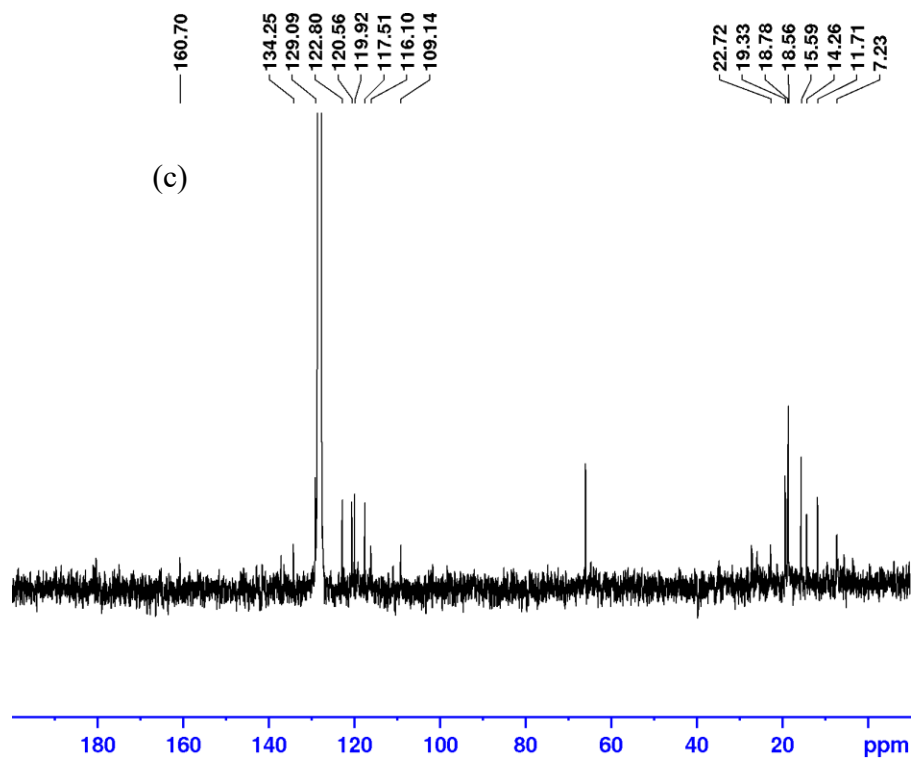
Figure B6. (a) $^{31}P\{^1H\}$, (b) ^1H and (c) $^{13}C\{^1H\}$ NMR (benzene-d_6) of (^{i}Pr-PSiP^{Ind})IrH(O(CO)Ph) (**3-4a**).
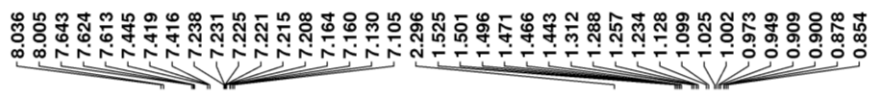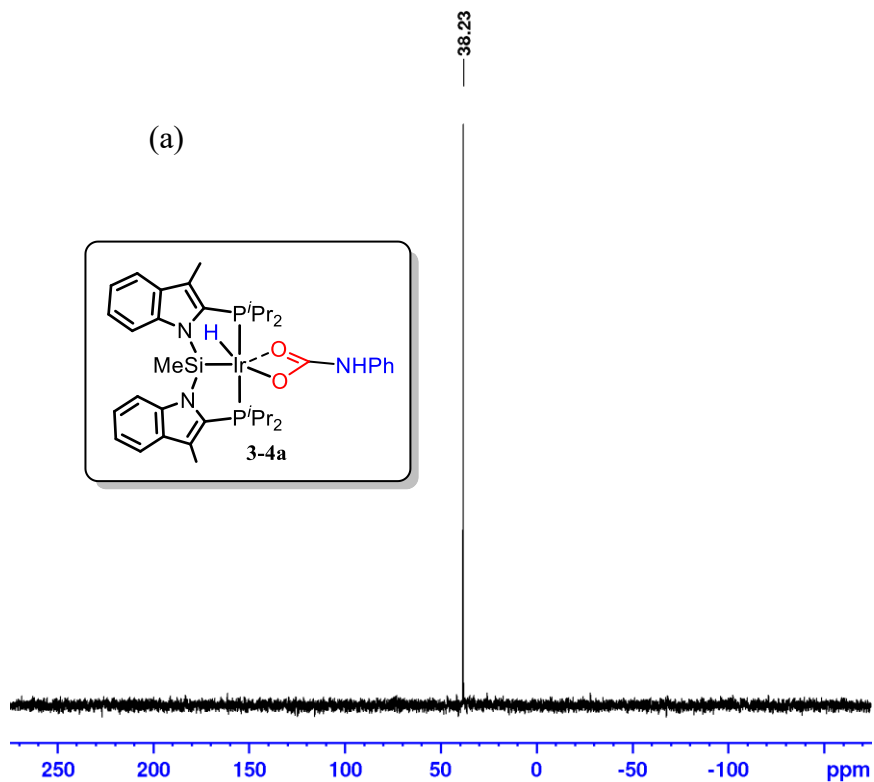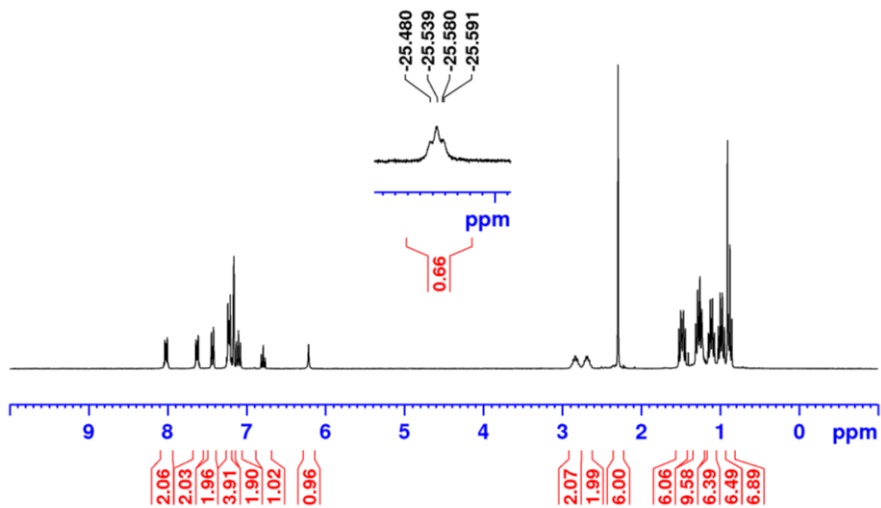
Figure B6. continued. (a) $^{31}P\{^{1}H\}$, (b) ^{1}H and (c) $^{13}C\{^{1}H\}$ NMR (benzene-d_6) of (^{i}Pr-PSiP^{Ind})IrH(O(CO)Ph) (**3-4a**).
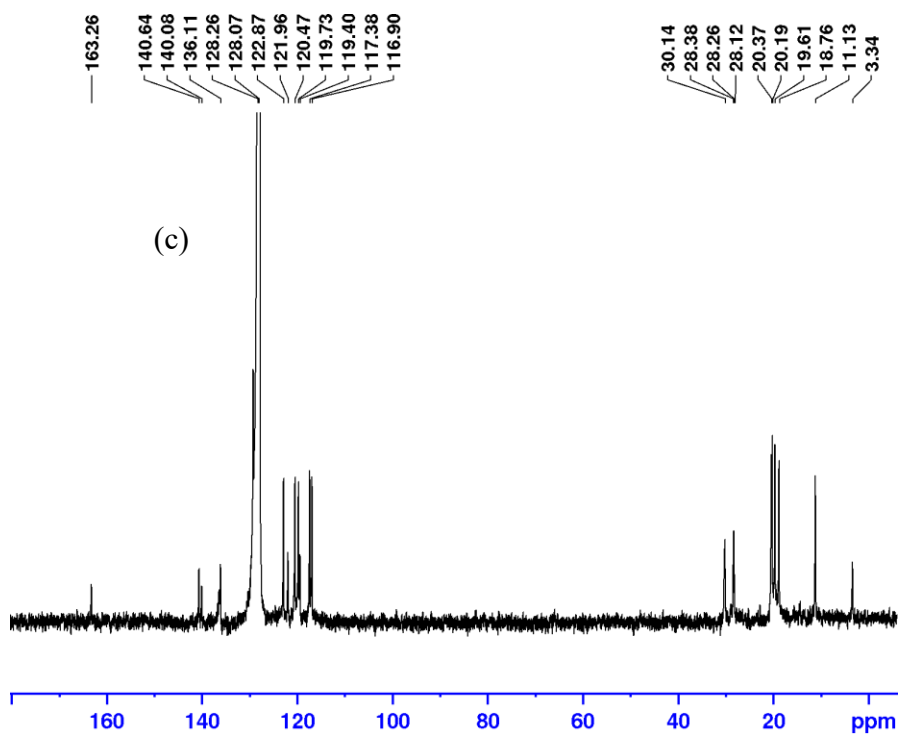
Figure B7. (a) $^{31}P\{^{1}H\}$, (b) ^{1}H and (c) $^{13}C\{^{1}H\}$ NMR (benzene-d_6) of (^{i}Pr-PSiP^{Ind})IrH(O(CO)^{t}Bu) (**3-4b**).

(a)
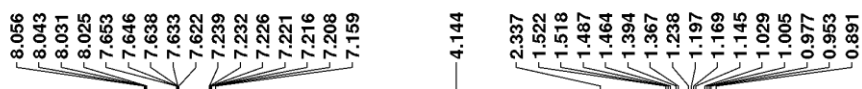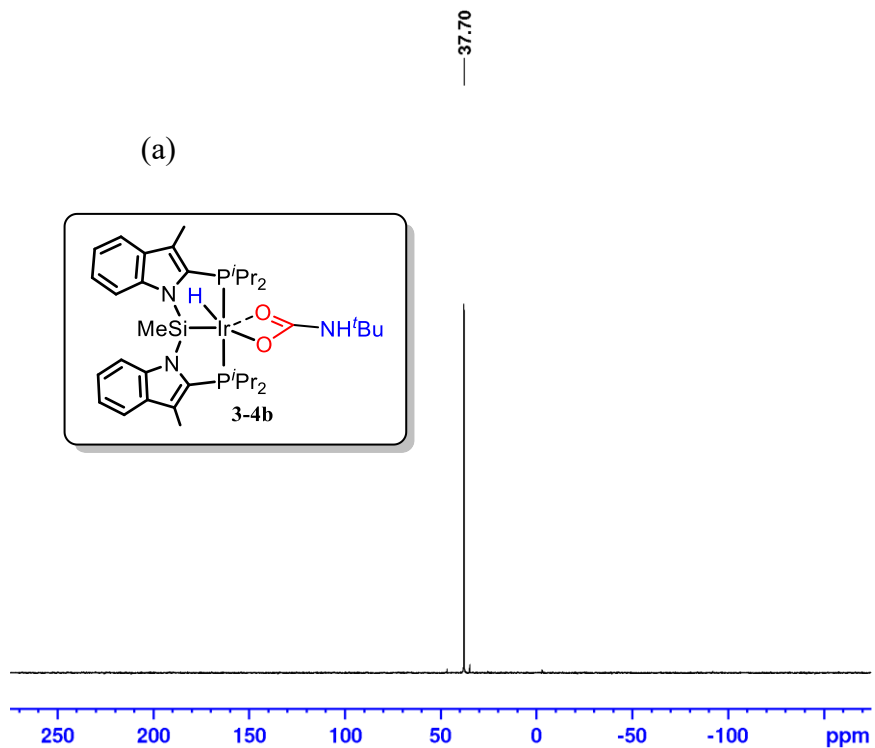
(b)
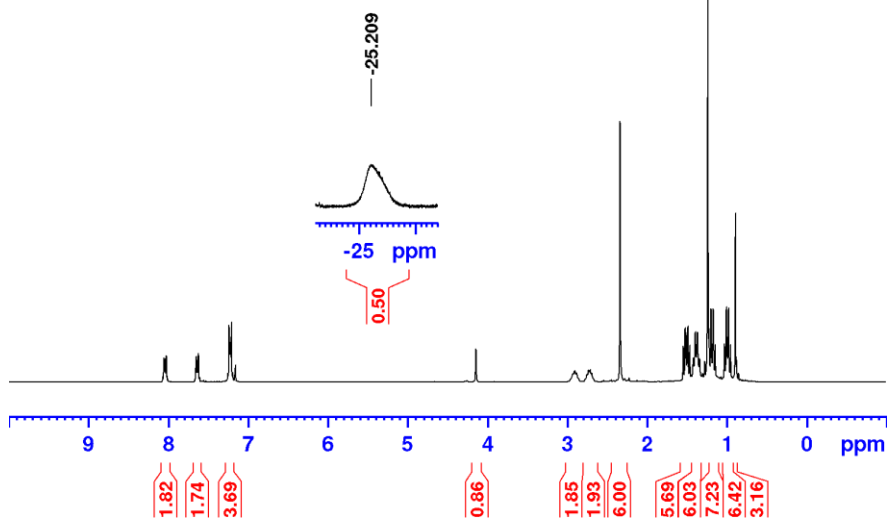
Figure B7. continued. (a) $^{31}P\{^1H\}$, (b) ^1H and (c) $^{13}C\{^1H\}$ NMR (benzene-d_6) of (^{i}Pr-PSiP^{Ind})IrH(O(CO)^{t}Bu) (**3-4b**).
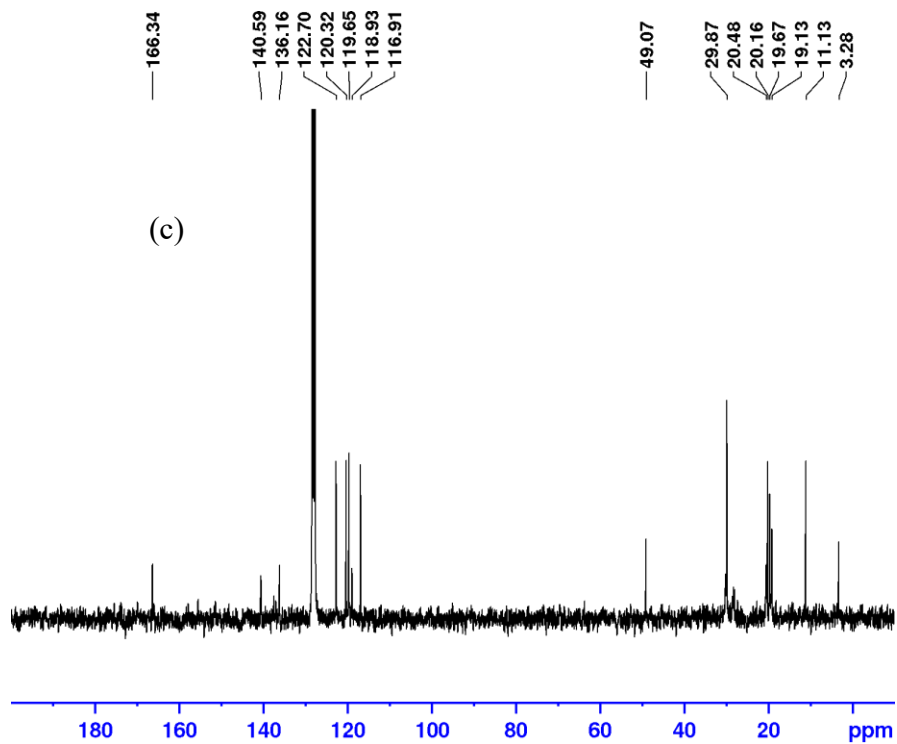
Figure B8. (a) $^{31}P\{^1H\}$, (b) ^1H and (c) $^{13}C\{^1H\}$ NMR (benzene-d_6) of (Cy-PSiP)IrH(O(CO)Ph) (**3-5a**).
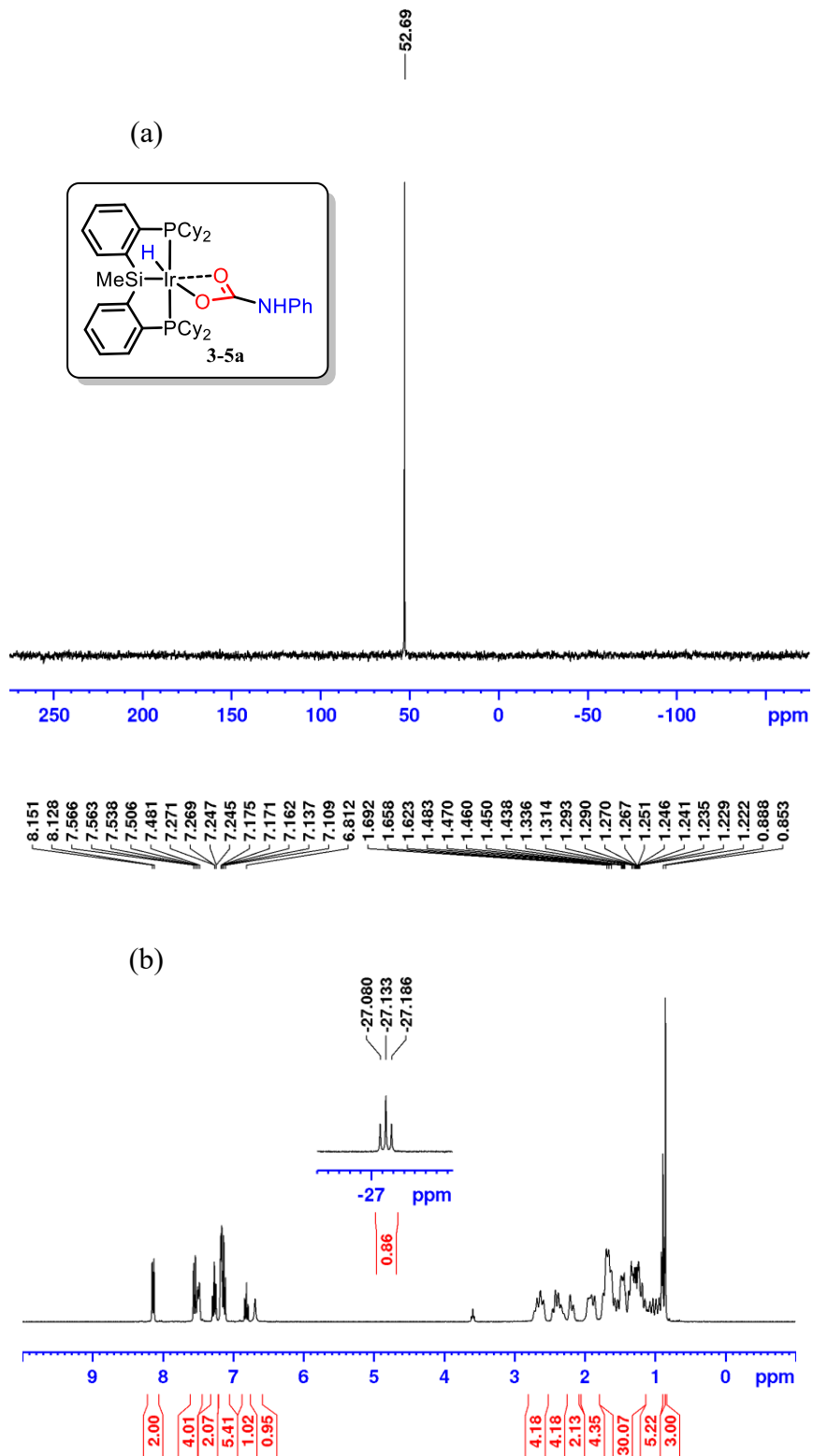
Figure B8. continued. (a) $^{31}P\{^1H\}$, (b) ^1H and (c) $^{13}C\{^1H\}$ NMR (benzene-d_6) of (Cy-PSiP)IrH(O(CO)Ph) (**3-5a**).
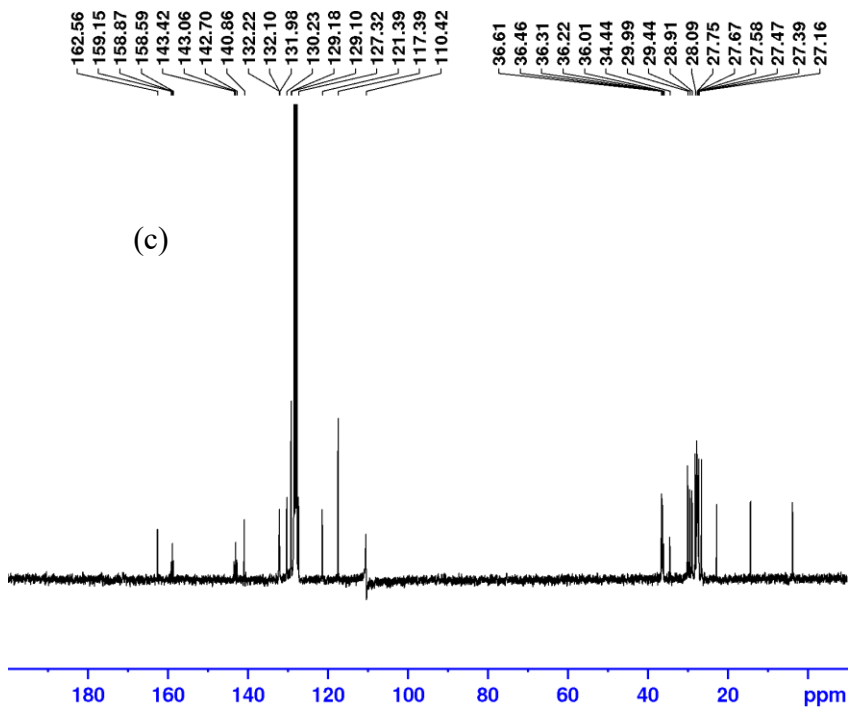
Figure B9. (a) ^{31}P{^{1}H} and (b) ^{1}H (benzene-d_6) of (Cy-PSiP)IrH(O(CO)^{t}Bu) (**3-5b**).
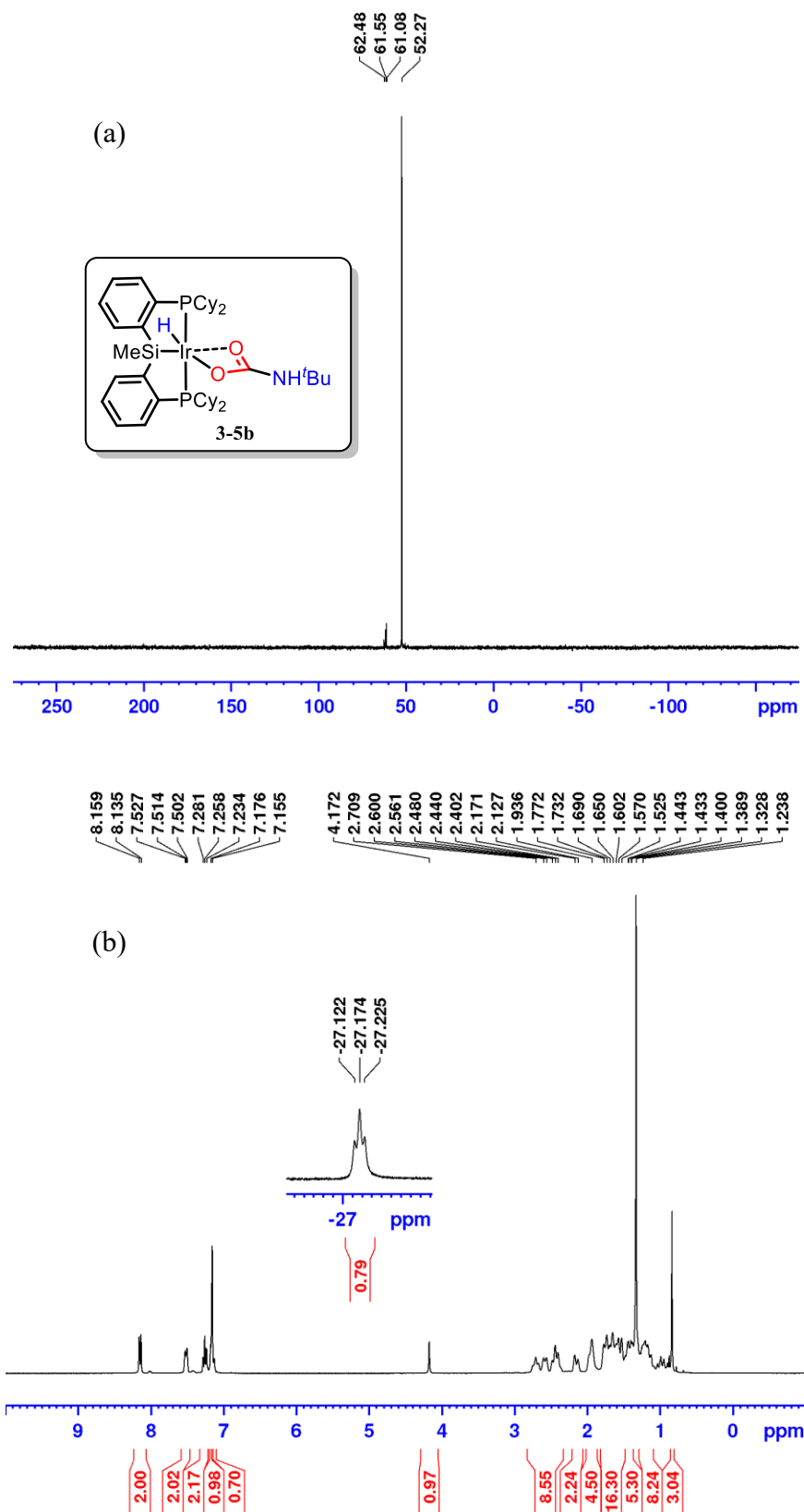
Figure B9. (a) $^{31}P\{^1H\}$ and (b) ^1H (benzene-d_6) of (Cy-PSiP)IrH(O(CO)NH$_2$) (**3-5c**).
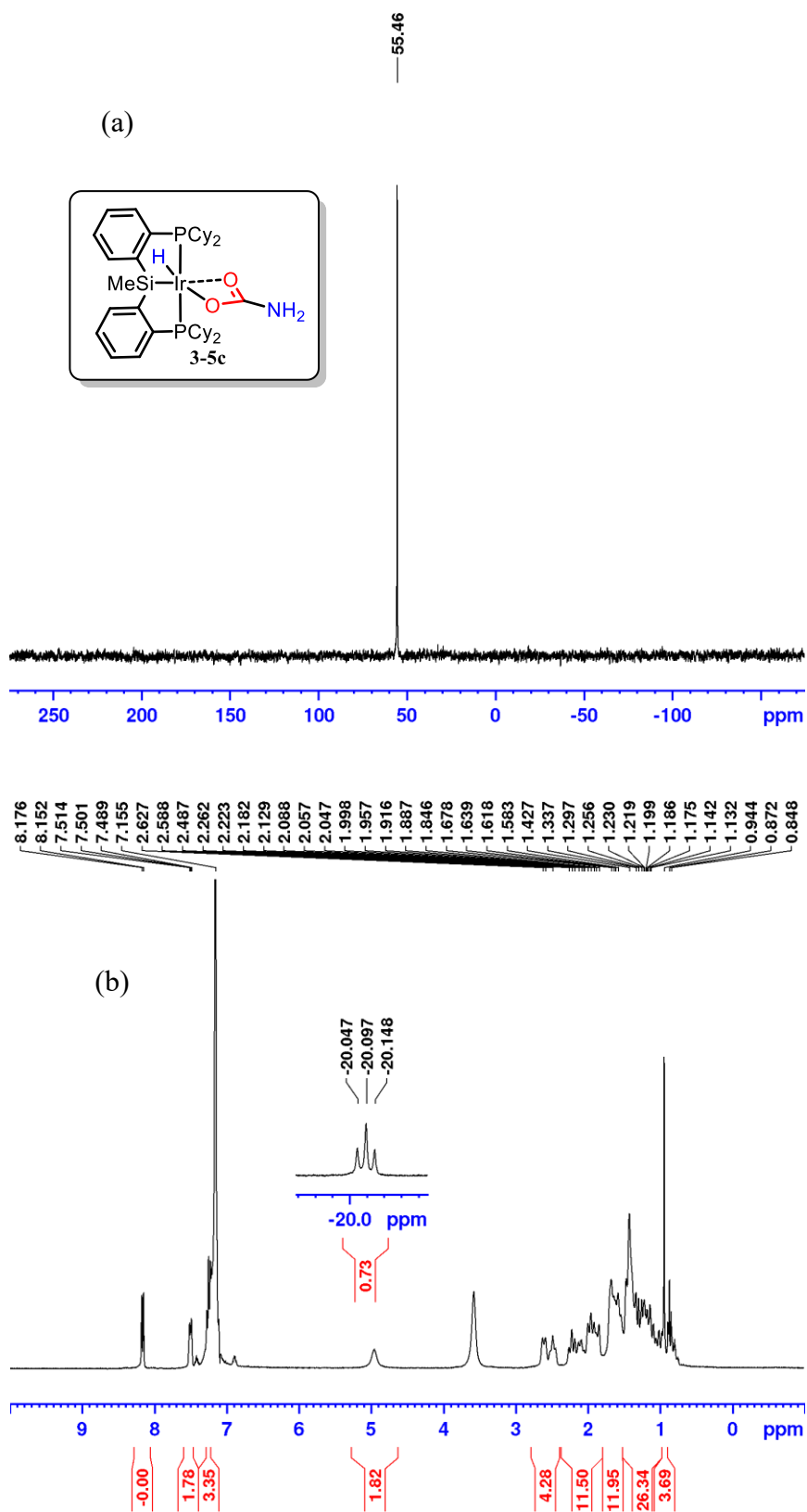
Appendix C: Chapter 4 Supporting Information

C-1: X-ray Crystallographic Data for Chapter 4

Table C1. Crystallographic Experimental Details for [(Cy-PSiP)FeBr]$_2$(MgBr$_2$) (**4-9**).

A. Crystal Data

formula	C$_{80.25}$H$_{125}$Br$_4$Fe$_2$MgP$_4$Si$_2$
formula weight	1725.51
crystal dimensions (mm)	0.14 × 0.09 × 0.03
crystal system	monoclinic
space group	$P2_1/n$ (an alternate setting of $P2_1/c$ [No. 14])
unit cell parameters[a]	
a (Å)	22.0981(6)
b (Å)	12.0324(3)
c (Å)	34.8168(9)
β (deg)	104.5649(18)
V (Å^3)	8960.0(4)
Z	4
ρ_{calcd} (g cm^{-3})	1.279
μ (mm^{-1})	5.963

B. Data Collection and Refinement Conditions

diffractometer	Bruker D8/APEX II CCD[b]
radiation (λ [Å])	Cu Kα (1.54178) (microfocus source)
temperature (°C)	–80
scan type	ω and ϕ scans (1.0°) (5-30-45 s exposures)[c]
data collection 2θ limit (deg)	136.63
total data collected	56817 ($-26 \leq h \leq 26$, $-14 \leq k \leq 14$, $-40 \leq l \leq 35$)
independent reflections	16061 ($R_{int} = 0.1152$)
number of observed reflections (*NO*)	9596 [$F_o^2 \geq 2\sigma(F_o^2)$]
structure solution method	intrinsic phasing (*SHELXT-2014*[d])
refinement method	full-matrix least-squares on F^2 (*SHELXL–2018*[e])
absorption correction method	Gaussian integration (face-indexed)
range of transmission factors	0.9027–0.5687
data/restraints/parameters	16061 / 71[f] / 852
extinction coefficient (*x*)[g]	0.00065(5)
goodness-of-fit (*S*)[h] [all data]	0.997
final *R* indices[i]	

Table C1. Crystallographic Experimental Details for [(Cy-PSiP)FeBr]$_2$(MgBr$_2$) (**4-9**) (continued).

R_1 [$F_o^2 \geq 2\sigma(F_o^2)$]	0.0690
wR_2 [all data]	0.2213
largest difference peak and hole	0.996 and –0.589 e Å^{-3}

[a]Obtained from least-squares refinement of 6111 reflections with $5.24° < 2\theta < 125.06°$.

[b]Programs for diffractometer operation, data collection, data reduction and absorption correction were those supplied by Bruker.

[c]Data were collected with the detector set at three different positions. Low-angle (detector $2\theta = –33°$) data frames were collected using a scan time of 5 s, medium-angle (detector $2\theta = 75°$) frames using a scan time of 30 s, and high-angle (detector $2\theta = 117°$) frames using a scan time of 45 s.

[d]Sheldrick, G. M. *Acta Crystallogr.* **2015**, *A71*, 3–8. (*SHELXT-2014*)

[e]Sheldrick, G. M. *Acta Crystallogr.* **2015**, *C71*, 3–8. (*SHELXL-2018/3*)

[f]The C–C distances within cyclohexyl group (C111 to C116) were restrained to be approximately the same by use of the *SHELXL* **SADI** instruction. The solvent pentane molecules were restrained to have the same refined C–C and C$\cdots$C distances by use of the **DFIX** instruction; further, the ADPs of the pentane molecules were restrained by the rigid bond restraint **RIGU**. Finally, atoms C6S to C10S were constrained to have equivalent ADPs.

[g]$F_c^* = kF_c[1 + x\{0.001F_c^2\lambda^3/\sin(2\theta)\}]^{-1/4}$ where k is the overall scale factor.

[h]$S = [\Sigma w(F_o^2 - F_c^2)^2/(n - p)]^{1/2}$ (n = number of data; p = number of parameters varied; $w = [\sigma^2(F_o^2) + (0.1204P)^2]^{-1}$ where $P = [\text{Max}(F_o^2, 0) + 2F_c^2]/3$).

[i]$R_1 = \Sigma||F_o| - |F_c||/\Sigma|F_o|$; $wR_2 = [\Sigma w(F_o^2 - F_c^2)^2/\Sigma w(F_o^4)]^{1/2}$.
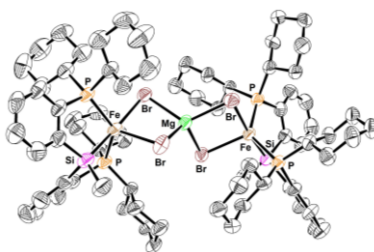
Figure C1. ORTEP diagram for [(Cy-PSiP)FeBr]$_2$(MgBr$_2$) (**4-9**).

Table C2. Crystallographic Experimental Details for (Cy-PSiP)FeBr[CN(2,6-Me$_2$C$_6$H$_3$)$_2$] (**4-10**).

A. Crystal Data

formula	C$_{60}$H$_{85}$BrFeN$_2$P$_2$Si
formula weight	1060.08
crystal dimensions (mm)	0.25 × 0.15 × 0.11
crystal system	monoclinic
space group	$P2_1/c$ (No. 14)
unit cell parameters^a	
a (Å)	11.3247(2)
b (Å)	20.6801(3)
c (Å)	23.7672(4)
β (deg)	92.9336(11)
V (Å^3)	5558.89(16)
Z	4
ρ_{calcd} (g cm^{-3})	1.267
μ (mm^{-1})	4.053

B. Data Collection and Refinement Conditions

diffractometer	Bruker D8/APEX II CCD^b
radiation (λ [Å])	Cu Kα (1.54178) (microfocus source)
temperature (°C)	–100
scan type	ω and ϕ scans (1.0°) (5 s exposures)
data collection 2θ limit (deg)	140.54
total data collected	37628 (-13 ≤ h ≤ 13, -25 ≤ k ≤ 25, -29 ≤ l ≤ 29)
independent reflections	10566 (R_{int} = 0.0694)
number of observed reflections (*NO*)	8996 [$F_o^2 \geq 2\sigma(F_o^2)$]
structure solution method	intrinsic phasing (*SHELXT-2014^c*)
refinement method	full-matrix least-squares on F^2 (*SHELXL–2017^d*)
absorption correction method	Gaussian integration (face-indexed)
range of transmission factors	0.8578–0.5187
data/restraints/parameters	10566 / 28^e / 630
goodness-of-fit (*S*)^f [all data]	1.022
final *R* indices^g	
R_1 [$F_o^2 \geq 2\sigma(F_o^2)$]	0.0441
wR_2 [all data]	0.1201
largest difference peak and hole	0.892 and –0.900 e Å^{-3}

^{a}Obtained from least-squares refinement of 9985 reflections with 5.66° < 2θ < 140.26°.

Table C2. Crystallographic Experimental Details for (Cy-PSiP)FeBr[CN(2,6-Me$_2$C$_6$H$_3$)]$_2$ (**4-10**) (continued).

[b]Programs for diffractometer operation, data collection, data reduction and absorption correction were those supplied by Bruker.

[c]Sheldrick, G. M. *Acta Crystallogr.* **2015**, *A71*, 3–8. (*SHELXT-2014*)

[d]Sheldrick, G. M. *Acta Crystallogr.* **2015**, *C71*, 3–8. (*SHELXL-2017*)

[e]The C–C distance within the disordered solvent pentane molecules were restrained to be approximately the same by the *SHELXL* **SADI** instruction.

[f]$S = [\Sigma w(F_o^2 - F_c^2)^2/(n - p)]^{1/2}$ (n = number of data; p = number of parameters varied; $w = [\sigma^2(F_o^2) + (0.0503P)^2 + 2.1270P]^{-1}$ where $P = [\text{Max}(F_o^2, 0) + 2F_c^2]/3$).

[g]$R_1 = \Sigma||F_o| - |F_c||/\Sigma|F_o|$; $wR_2 = [\Sigma w(F_o^2 - F_c^2)^2/\Sigma w(F_o^4)]^{1/2}$.
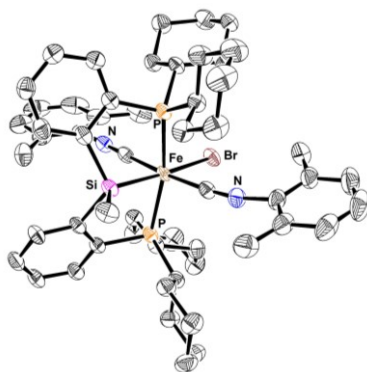
Figure C2. ORTEP diagram for (Cy-PSiP)FeBr[CN(2,6-Me$_2$C$_6$H$_3$)]$_2$ (**4-10**).

C-2: Selected NMR data for Chapter 4

Figure C3. ^{1}H NMR spectrum (benzene-d_6) of [(Cy-PSiP)FeBr]$_2$(MgBr$_2$) (**4-9**).
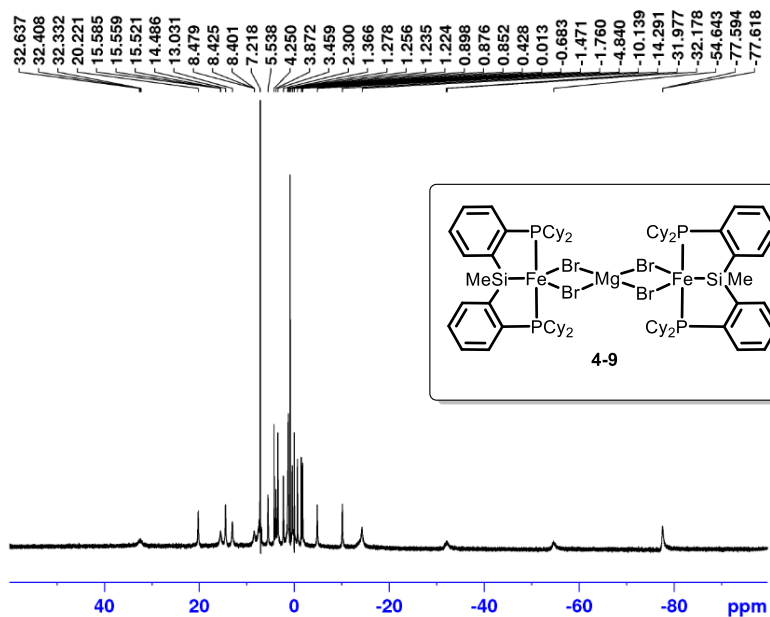
Figure C4. (a) ^{31}P{^{1}H} and (b) ^{1}H NMR spectrum (benzene-d_6) of (Cy-PSiP)FeBr[CN(2,6-Me$_2$C$_6$H$_3$)]$_2$ (**4-10**).
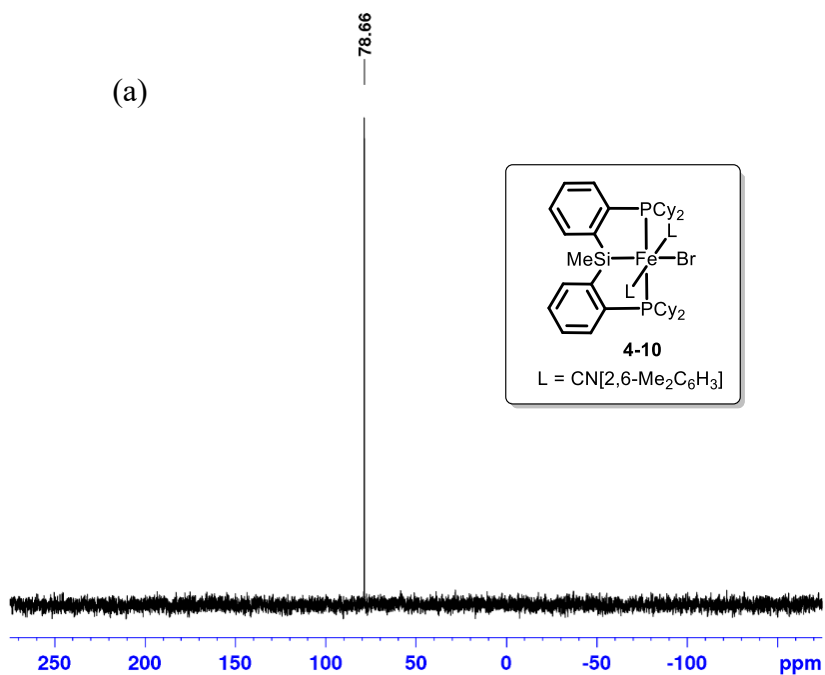
Figure C4. continued. (a) $^{31}P\{^1H\}$ and (b) ^1H NMR spectrum (benzene-d_6) of (Cy-PSiP)FeBr[CN(2,6-Me$_2$C$_6$H$_3$)]$_2$ (**4-10**).

(b)
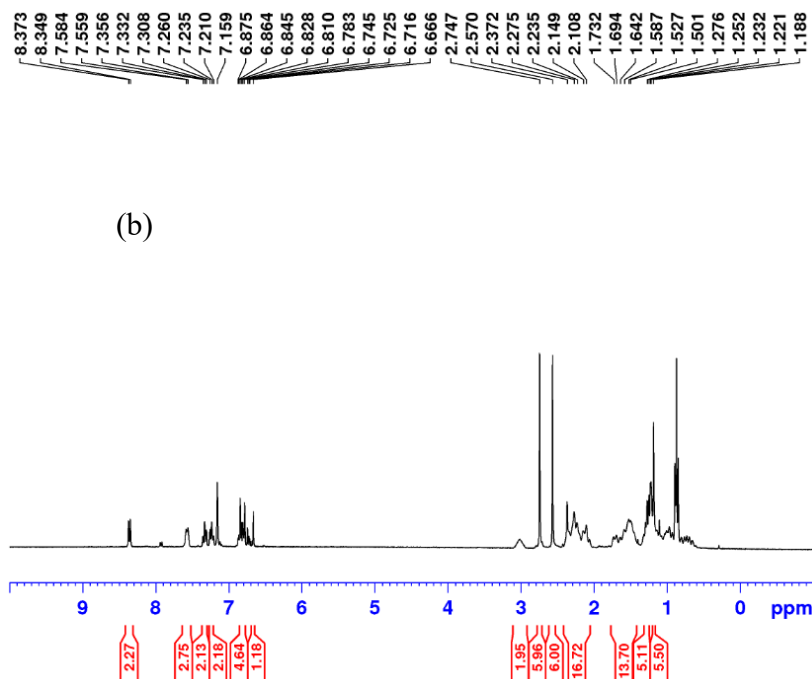
C-3: Selected NMR Spectra of Alkyne Starting Materials

Figure C5. (a) ^{1}H and (b) ^{13}C{^{1}H} NMR spectrum (benzene-d_6) of diphenylacetylene.
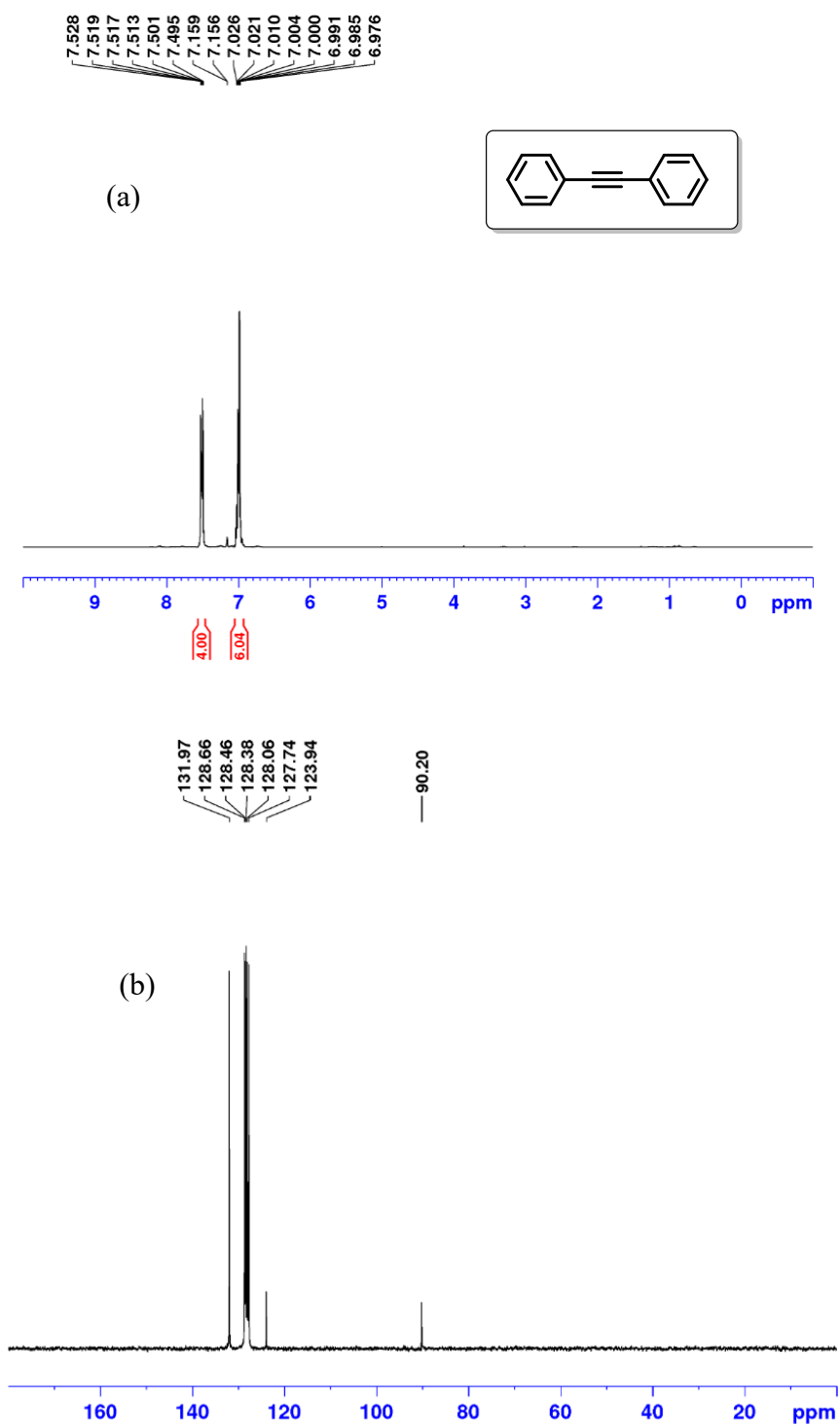
Figure C6. (a) ^{1}H and (b) ^{13}C{^{1}H} NMR spectrum (benzene-d_6) of 2-(2-phenylethynyl)naphthalene.

(a)

(b)
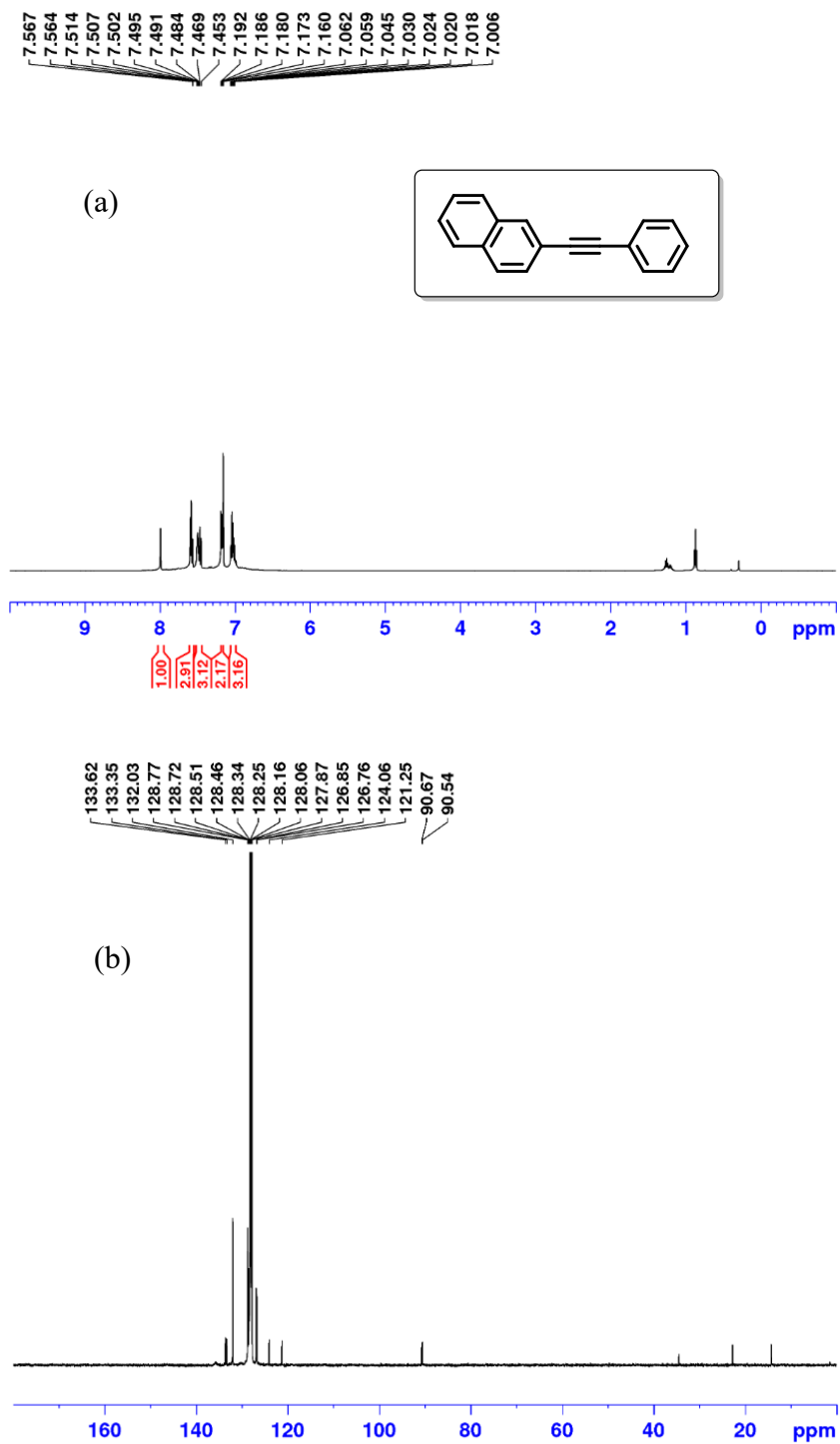
Figure C7. (a) ^{1}H and (b) ^{13}C{^{1}H} NMR spectrum (benzene-d_6) of 1-(2-phenylethynyl)naphthalene.

(a)
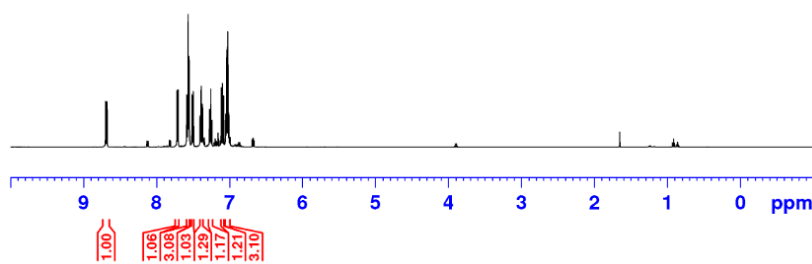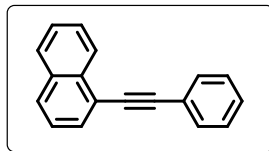
(b)
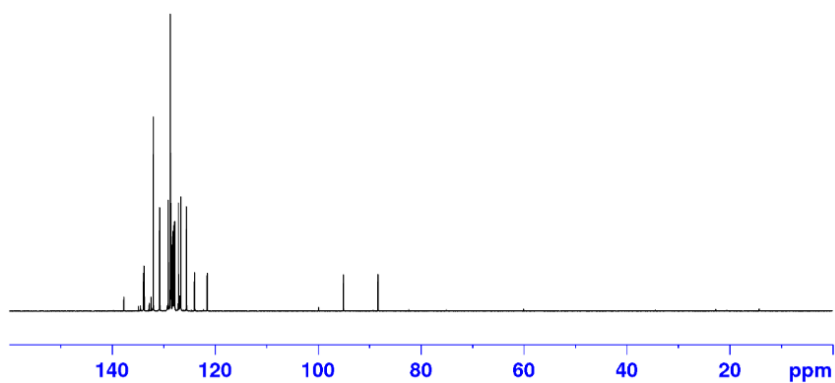
Figure C8. (a) ^{1}H and (b) ^{13}C{^{1}H} NMR spectrum (benzene-d_6) of (4-trimethylsilylphenyl)phenylacetylene.
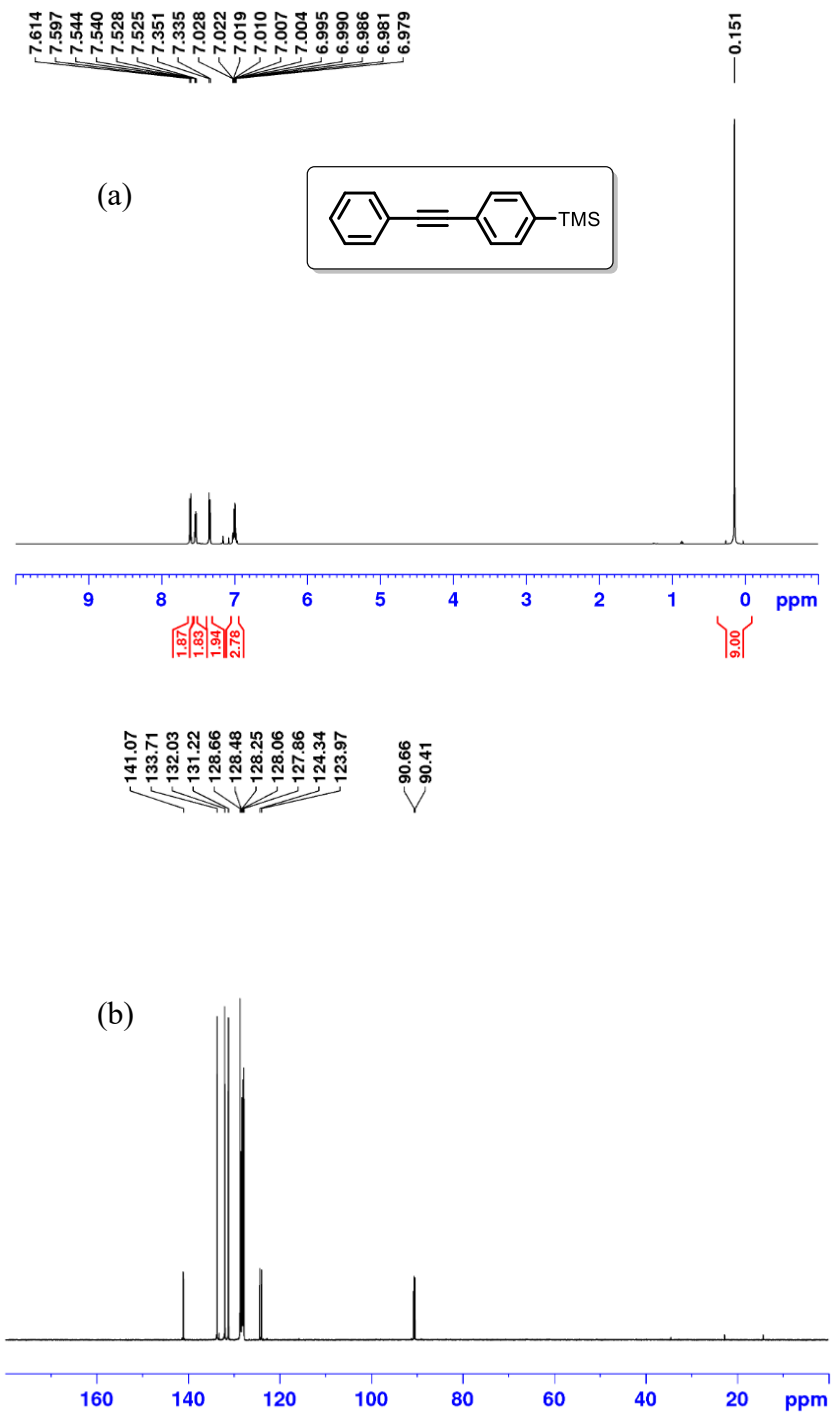
Figure C9. (a) ^{1}H and (b) ^{13}C{^{1}H} NMR spectrum (benzene-d_6) of phenylacetylene.
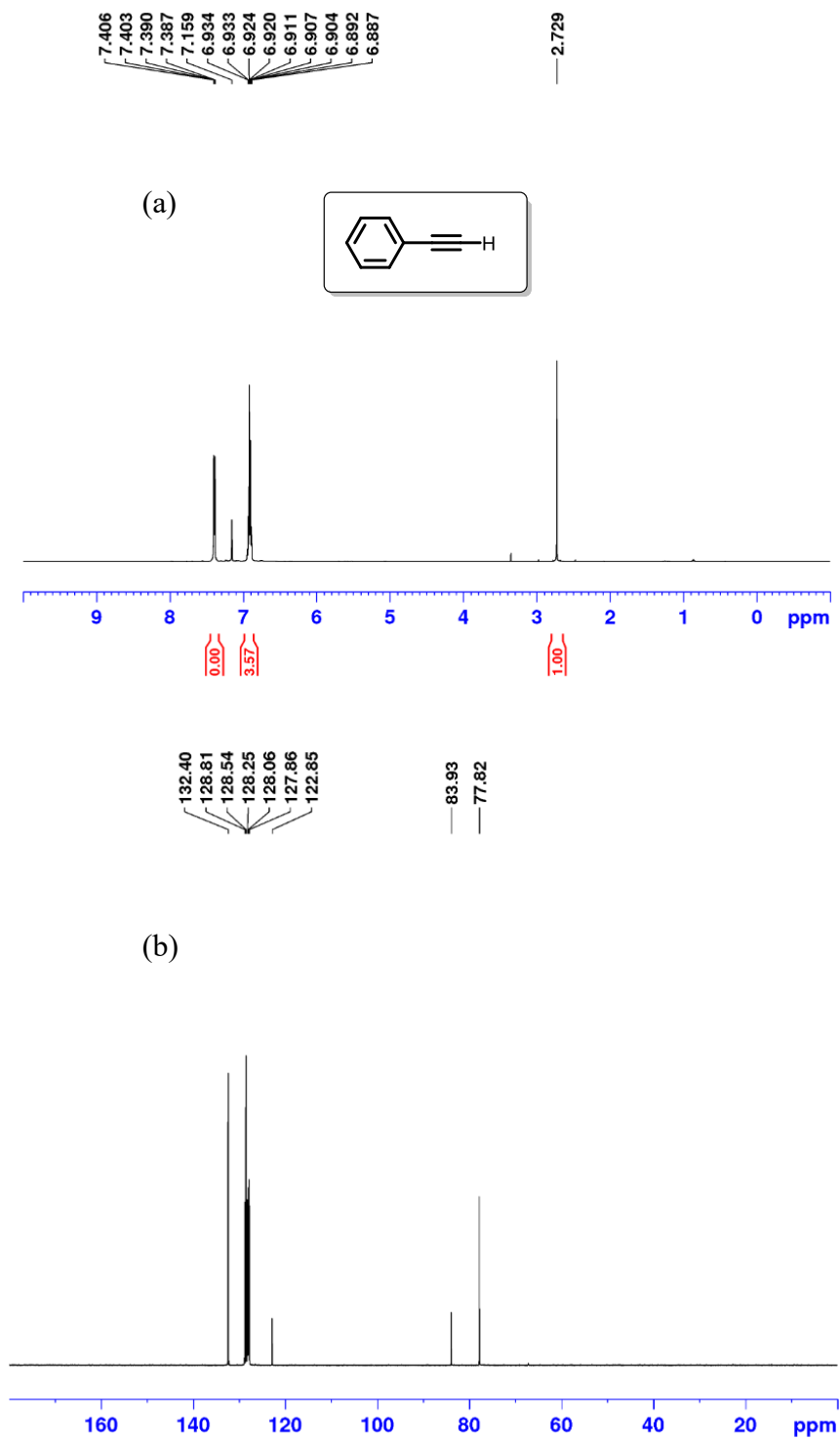
Figure C10. (a) ^{1}H and (b) ^{13}C{^{1}H} NMR spectrum (benzene-d_6) of 1-phenyl-1-propyne.
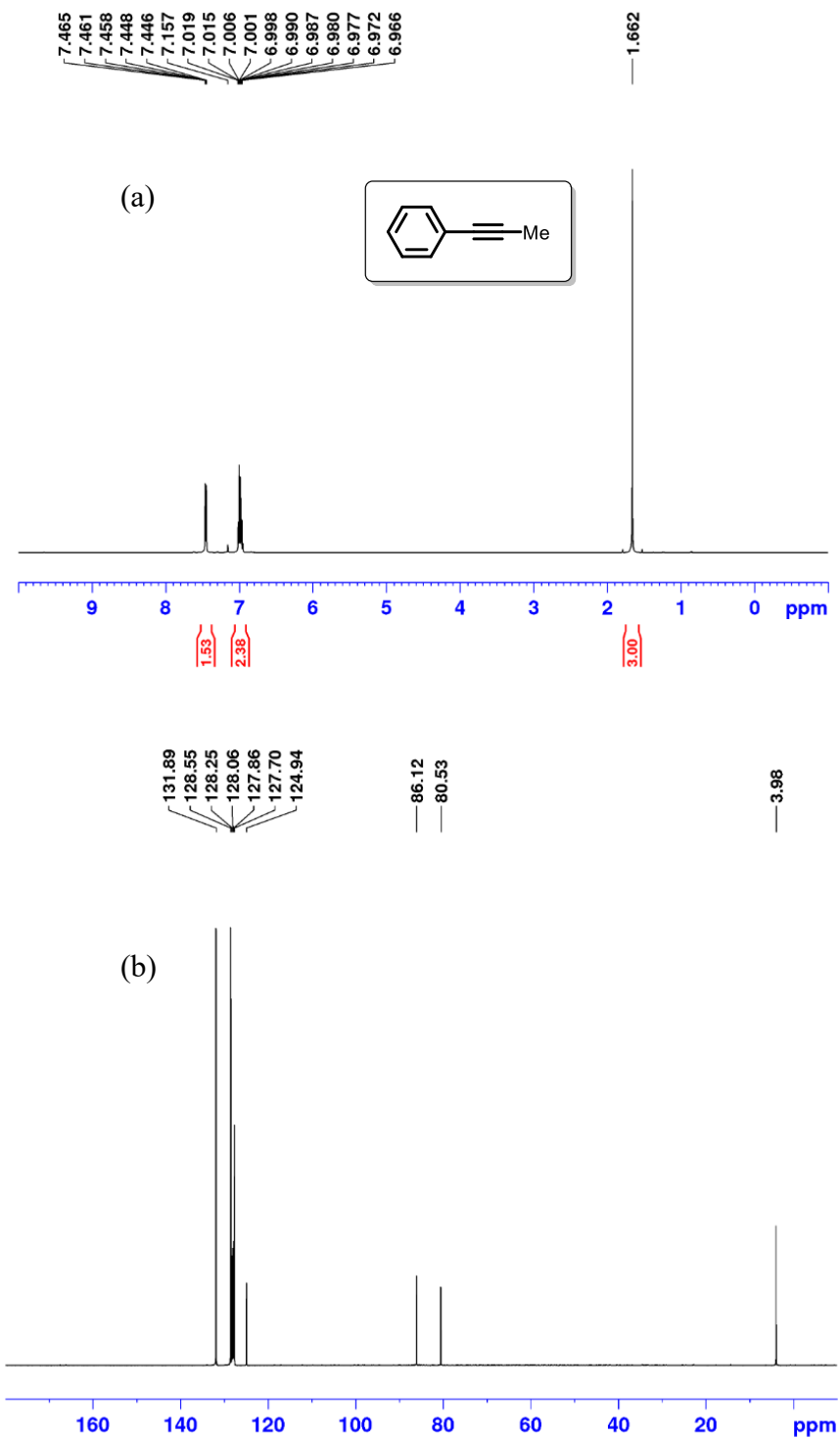
Figure C11. (a) ^{1}H and (b) ^{13}C{^{1}H} NMR spectrum (benzene-d_6) of 1-phenyl-1-butyne.
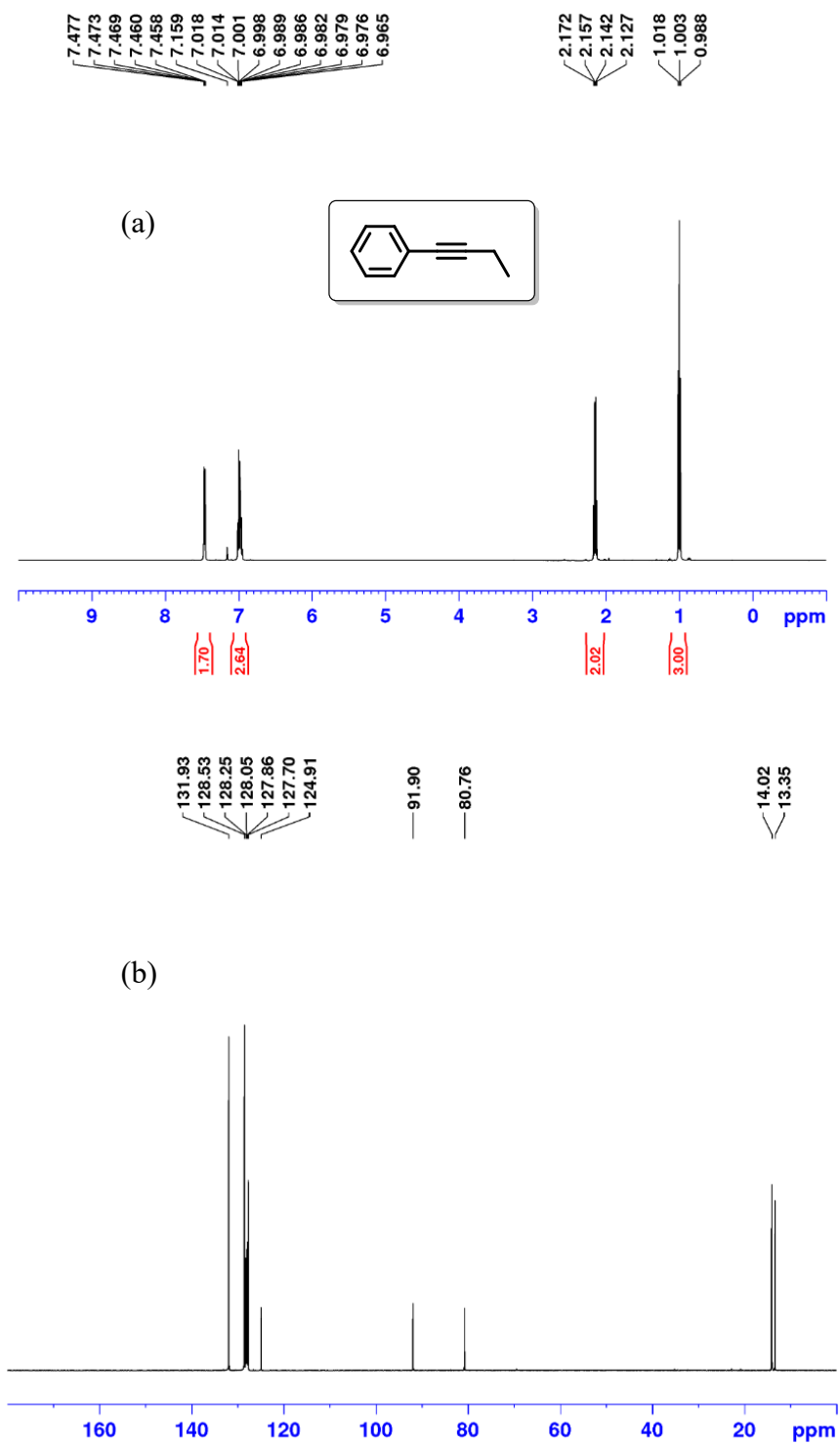
Figure C12. (a) ^{1}H and (b) ^{13}C{^{1}H} NMR spectrum (benzene-d_6) of 1-methoxy-4-(2-phenylethynyl)-benzene.
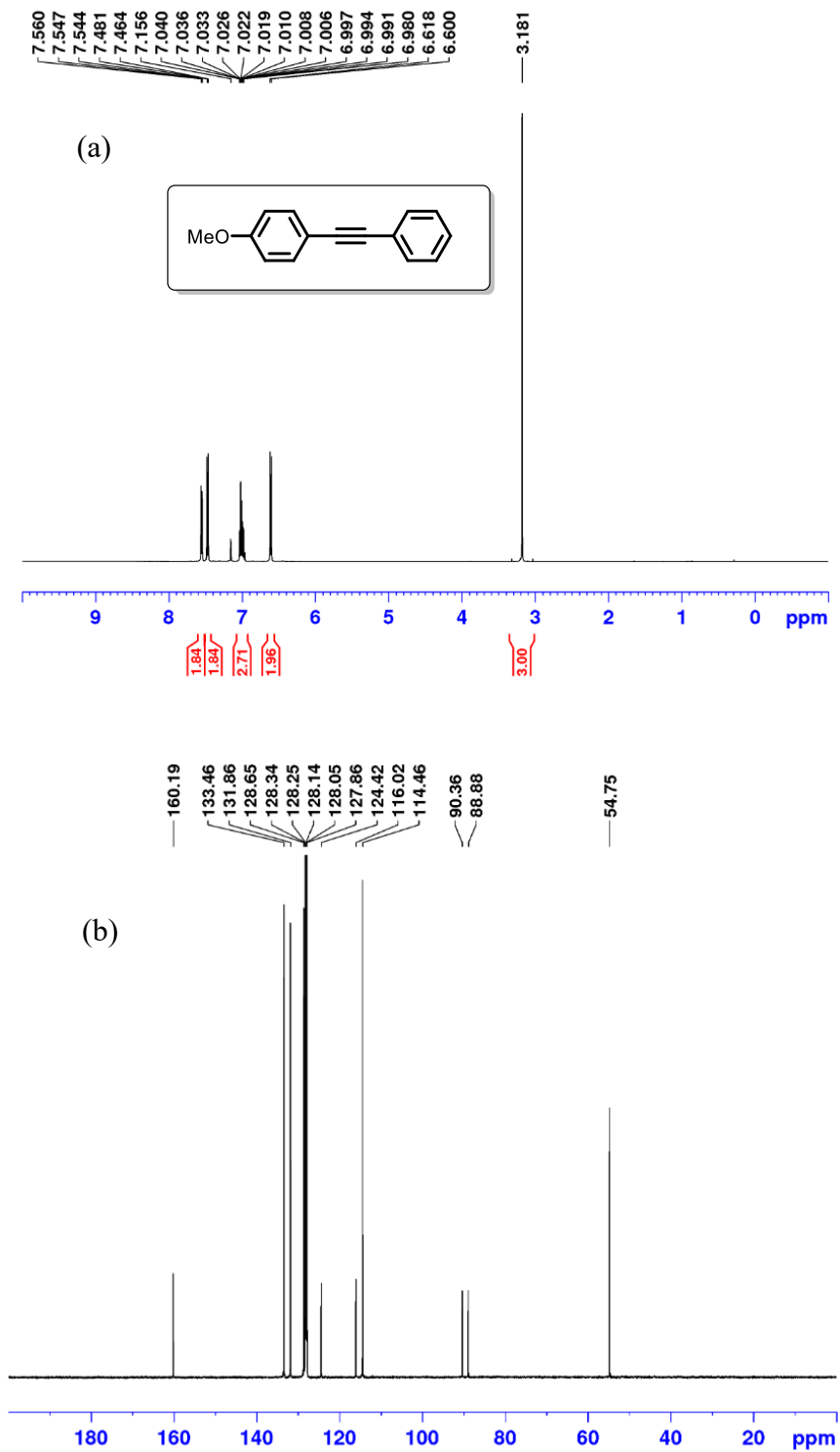
Figure C13. (a) ^{1}H and (b) ^{13}C{^{1}H} NMR spectrum (benzene-d_6) of 1-methoxy-3-(2-phenylethynyl)-benzene.
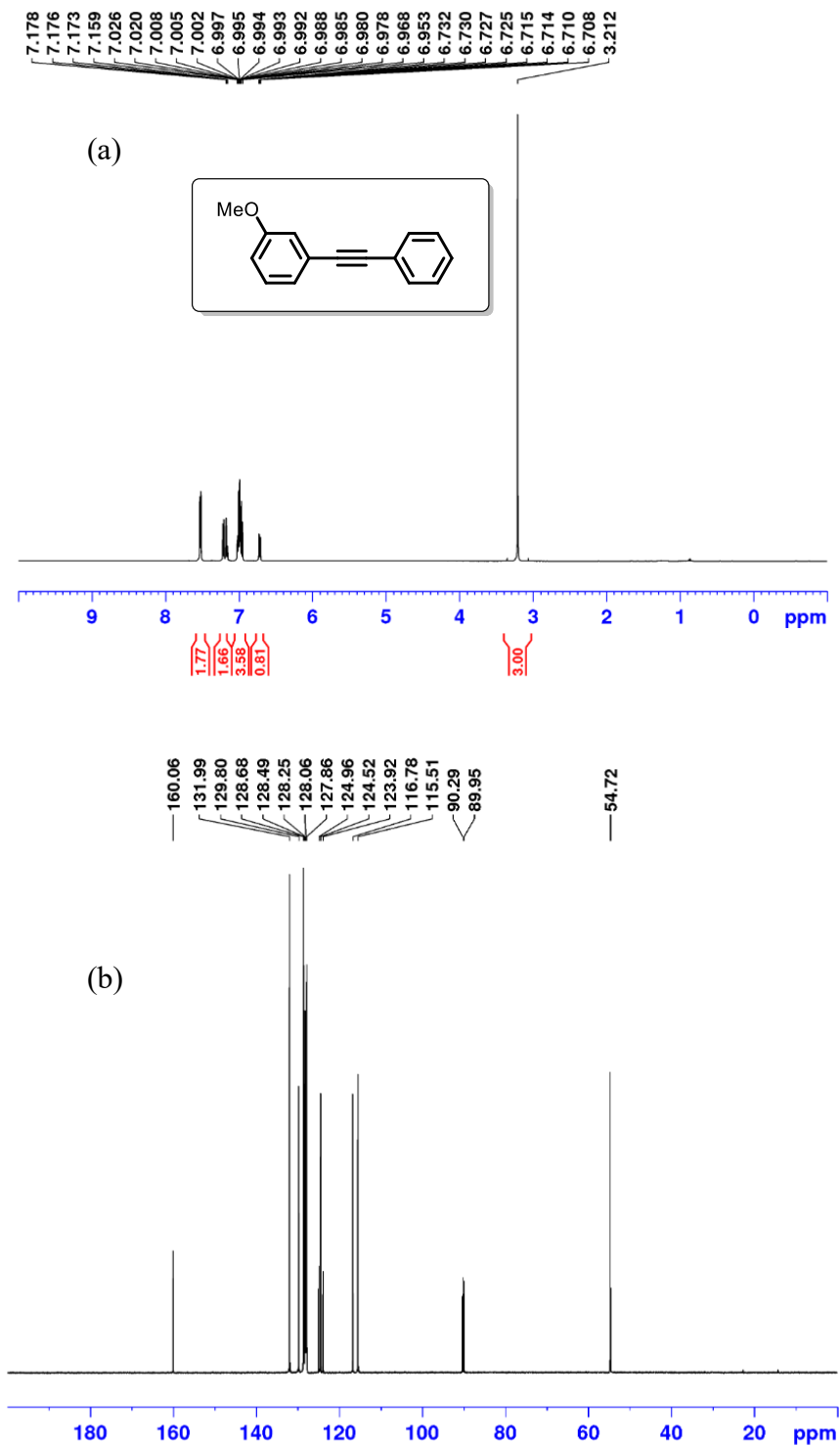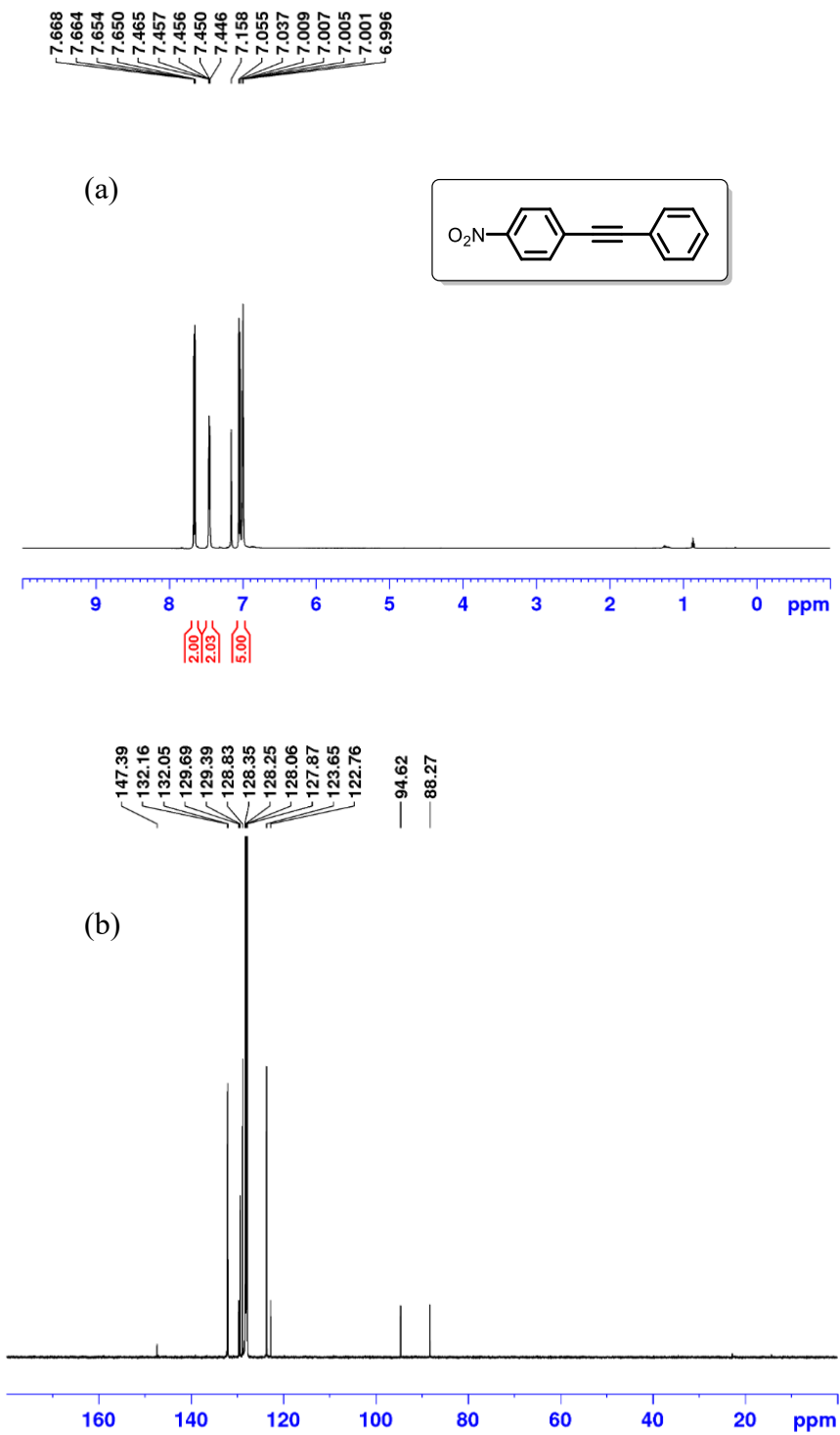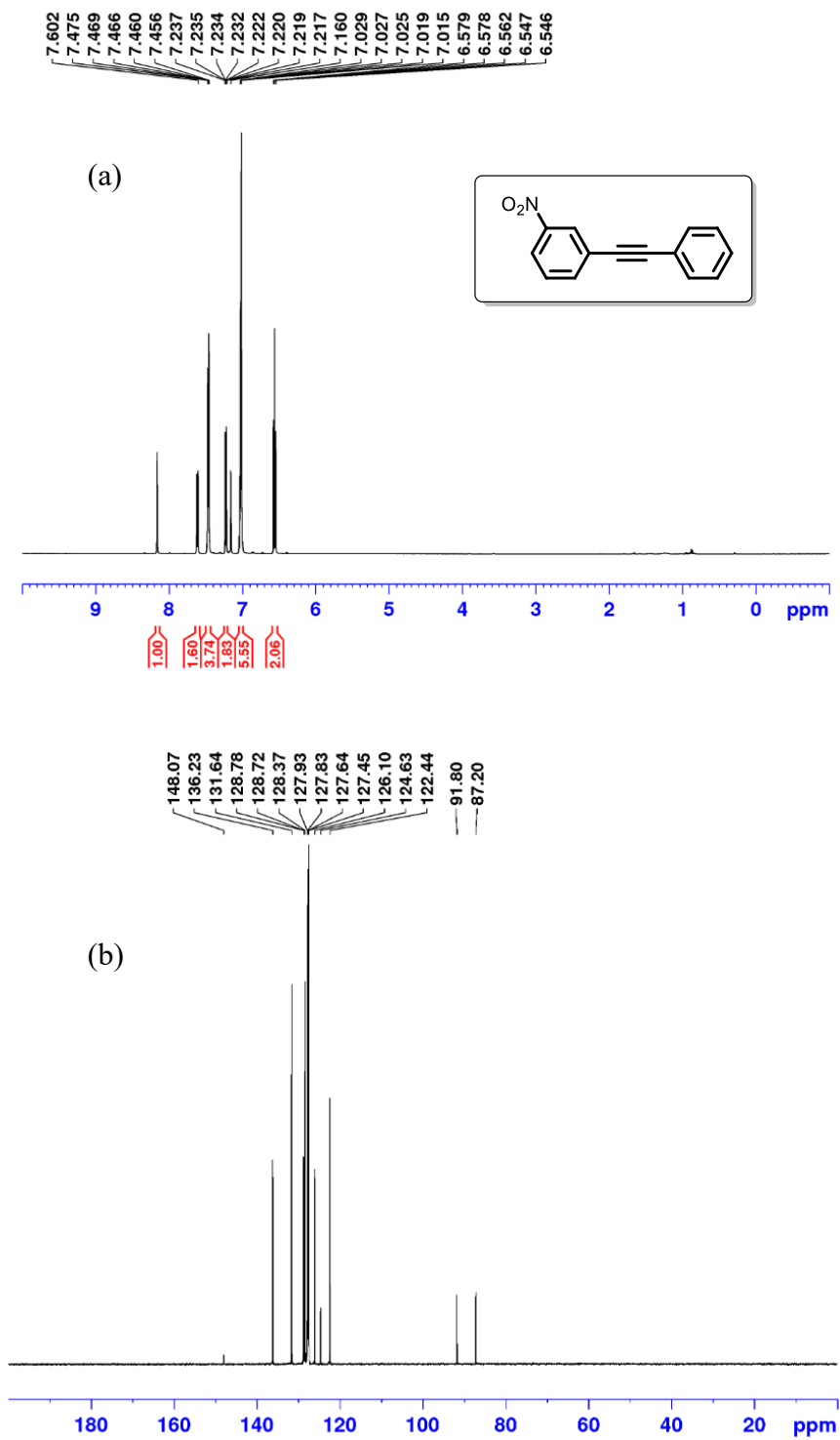
Figure C14. (a) ^{1}H and (b) ^{13}C{^{1}H} NMR spectrum (benzene-d_6) of 1-methoxy-2-(2-phenylethynyl)-benzene.
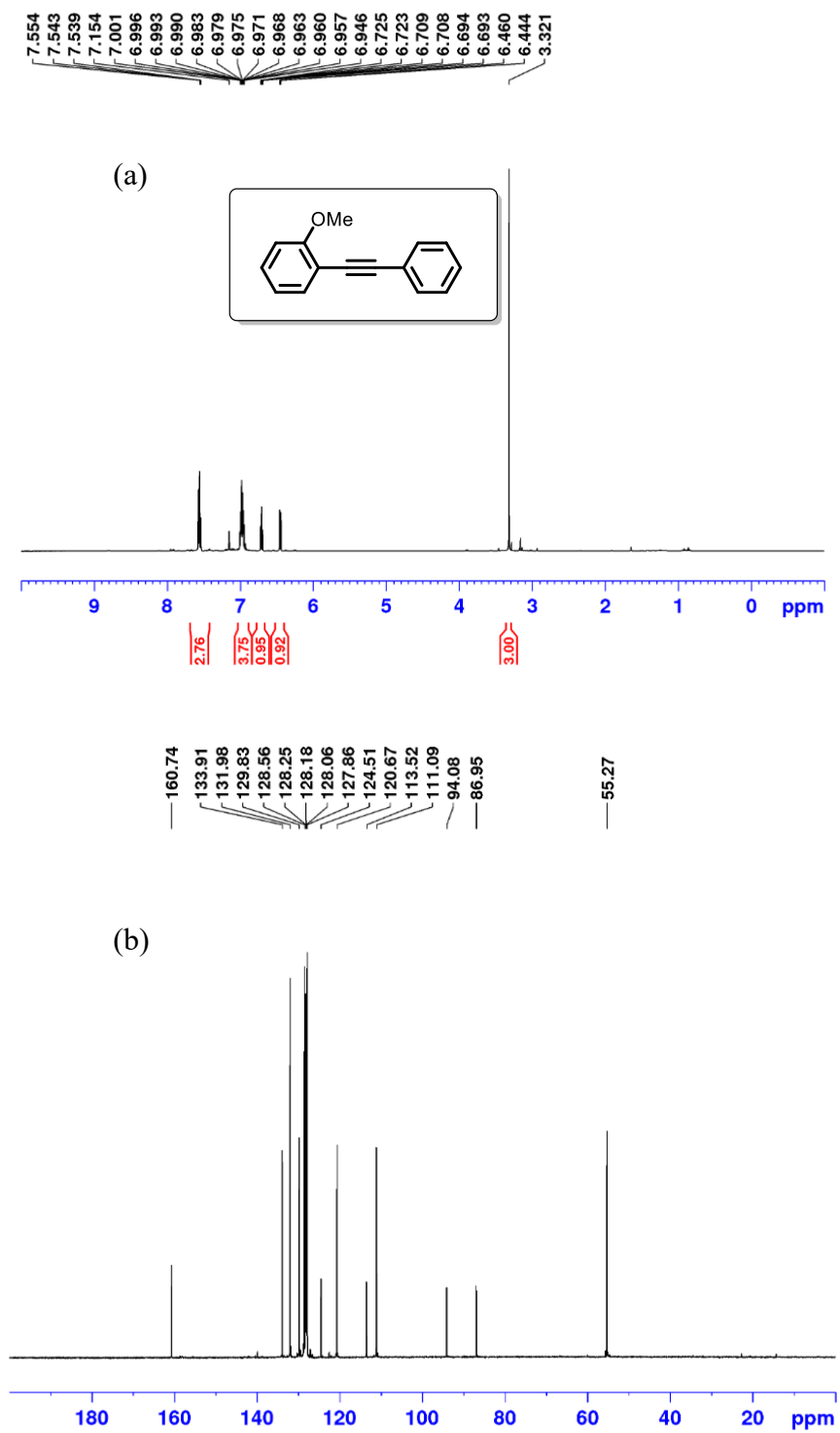
Figure C15. (a) ^{1}H and (b) ^{13}C{^{1}H} NMR spectrum (benzene-d_6) of 1-ethyl-4-[2-(4-methoxyohenyl)ethynyl]-benzene.
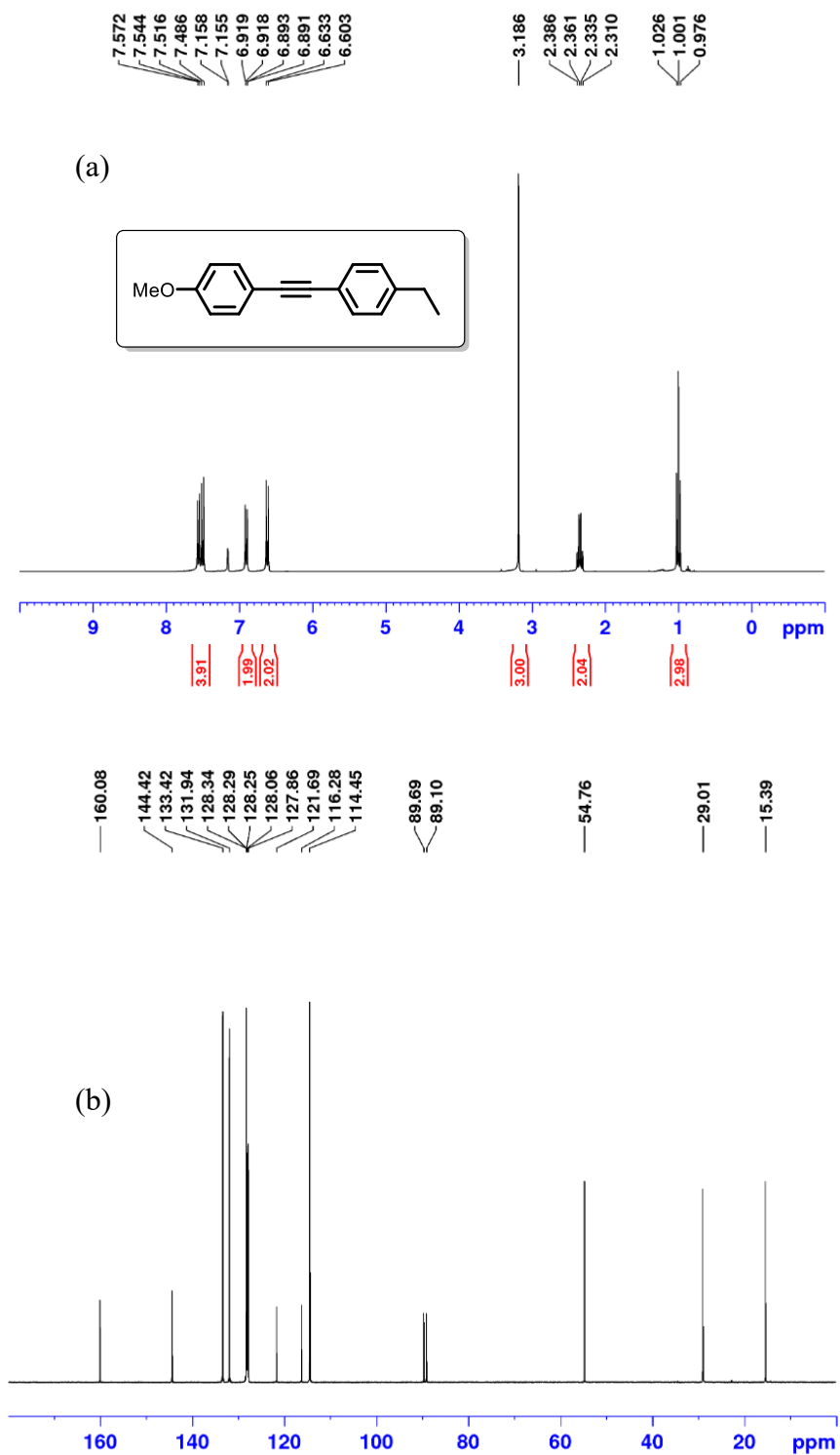
Figure C16. (a) ^{1}H and (b) ^{13}C{^{1}H} NMR spectrum (benzene-d_6) of 2-[4-[2-(4-methoxyphenyl)ethynyl]phenyl]-4,4,5,5-tetramethyl-1,3,2-dioxaborolane.
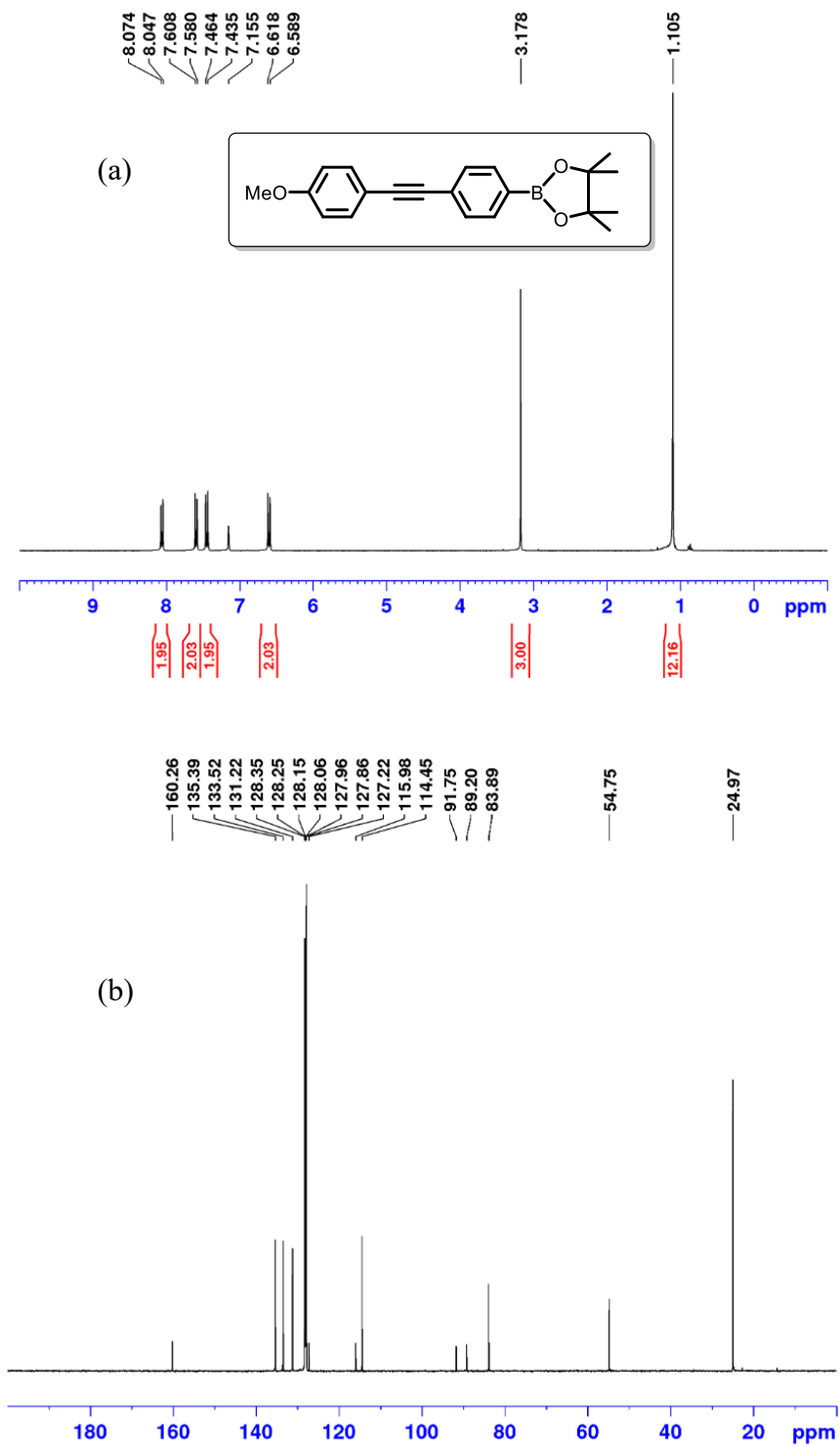
Figure C17. (a) ^{1}H and (b) ^{13}C{^{1}H} NMR spectrum (benzene-d_6) of 1-methyl-4-(2-phenylethynyl)-benzene.
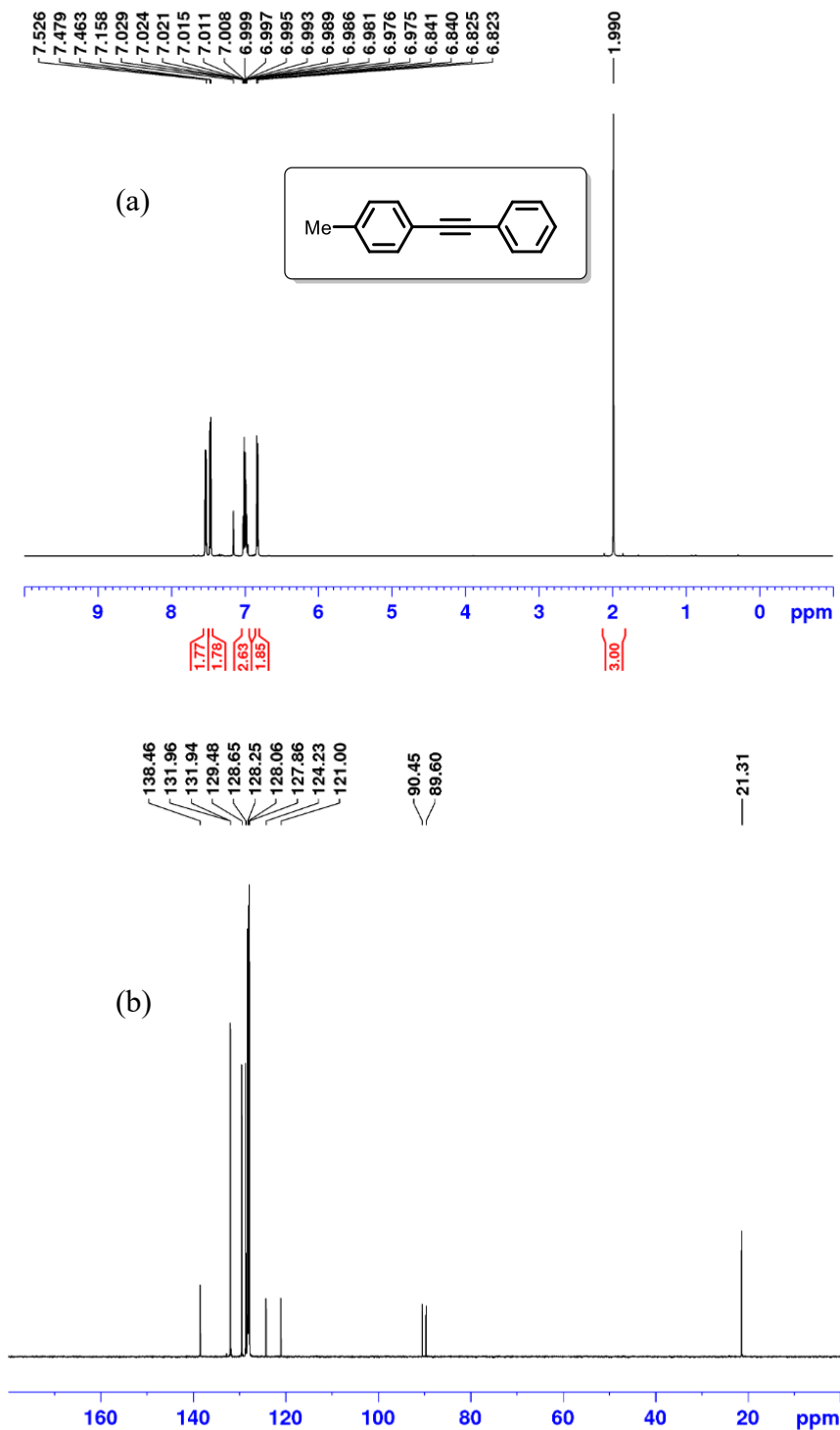
Figure C18. (a) ^{1}H and (b) ^{13}C{^{1}H} NMR spectrum (benzene-d_6) of 1-methyl-3-(2-phenylethynyl)-benzene.

Figure C18. (a) ^{1}H and (b) ^{13}C{^{1}H} NMR spectrum (benzene-d_6) of 1-methyl-3-(2-phenylethynyl)-benzene.
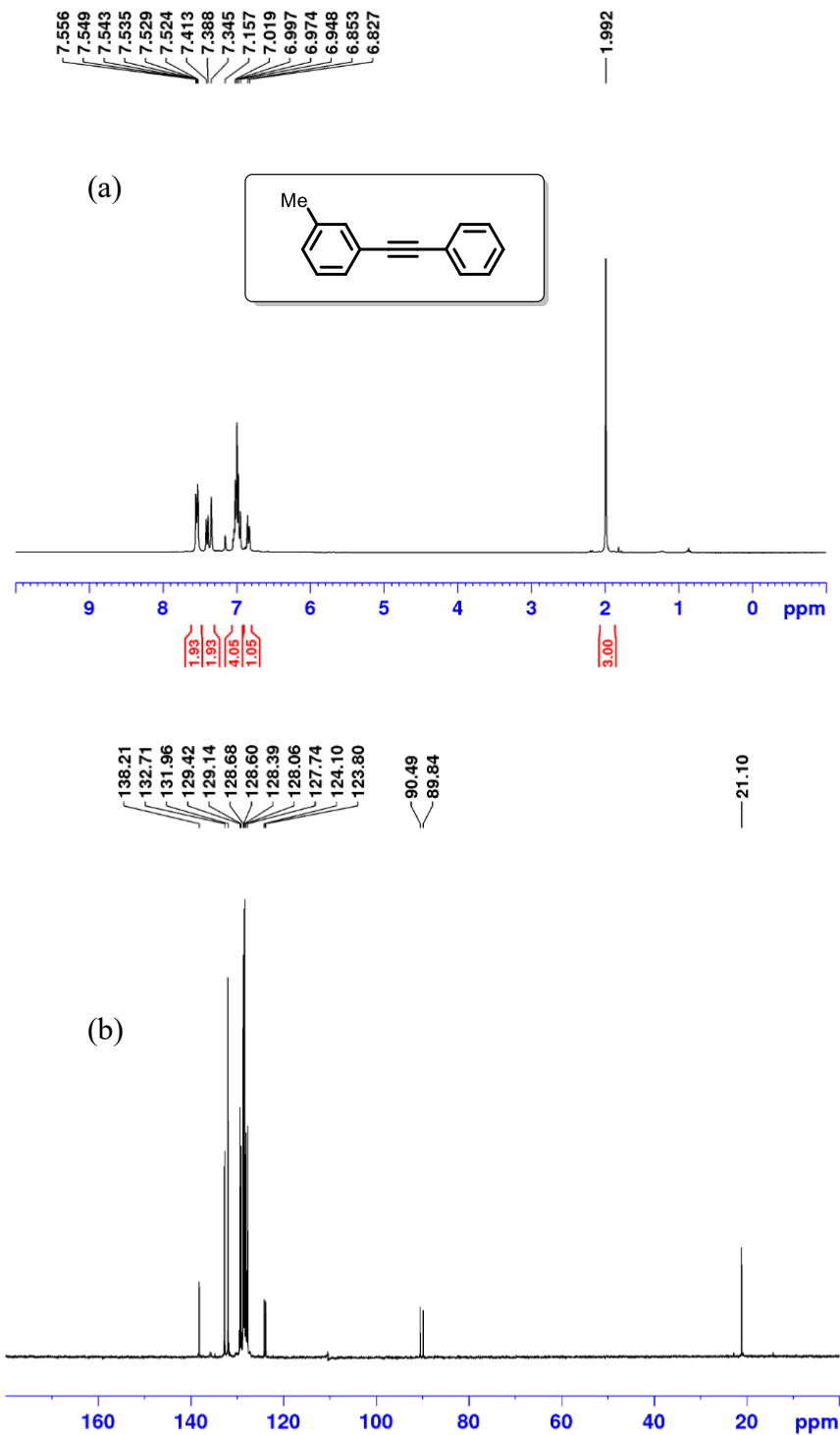
Figure C19. (a) ^{1}H and (b) ^{13}C{^{1}H} NMR spectrum (benzene-d_6) of 1,3-dimethyl-5-(2-phenylethynyl)-benzene.
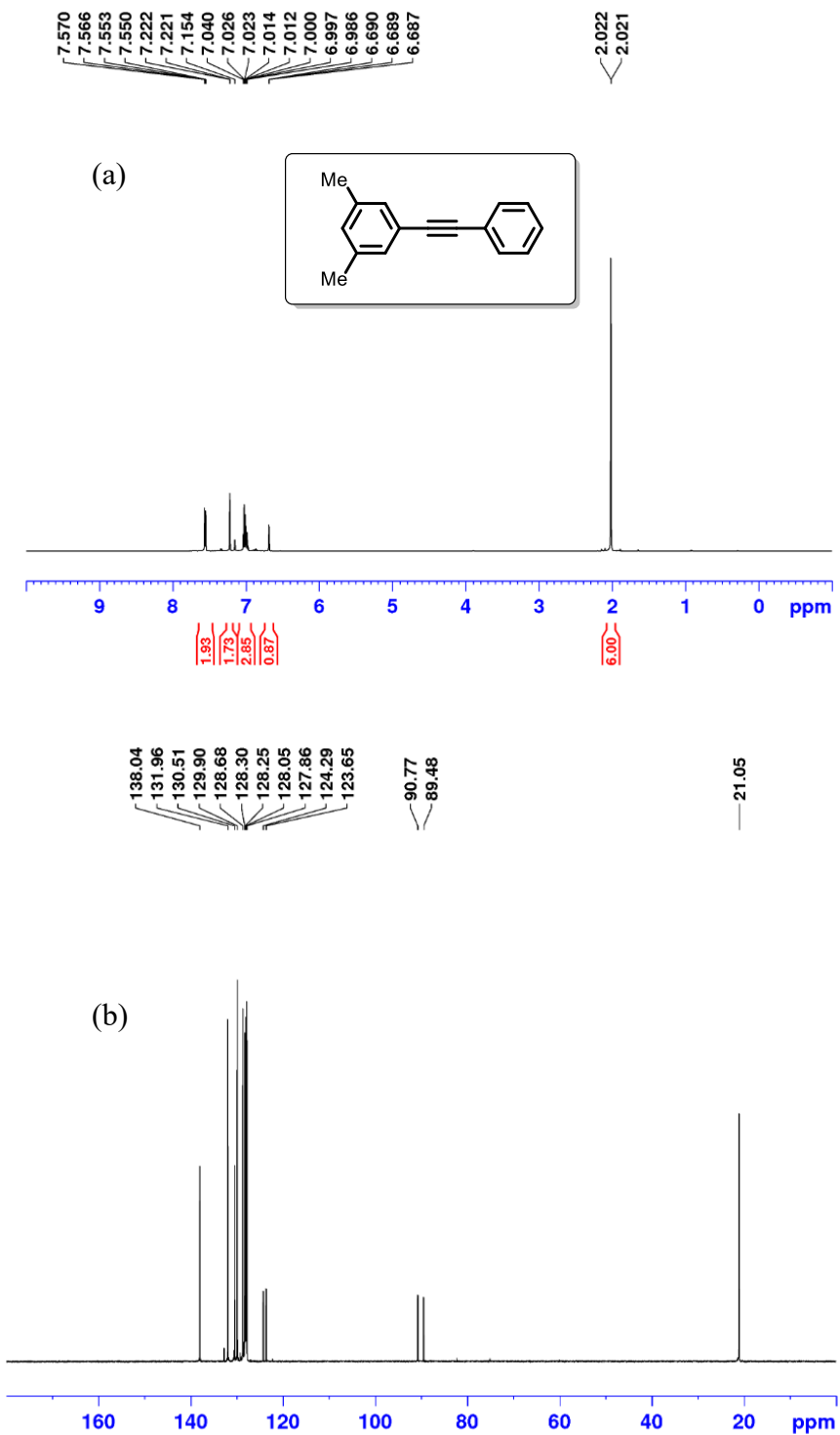
Figure C20. (a) ^{1}H and (b) ^{13}C{^{1}H} NMR spectrum (benzene-d_6) of 1-(1-methylethyl)-3-(2-phenylethynyl)-benzene.
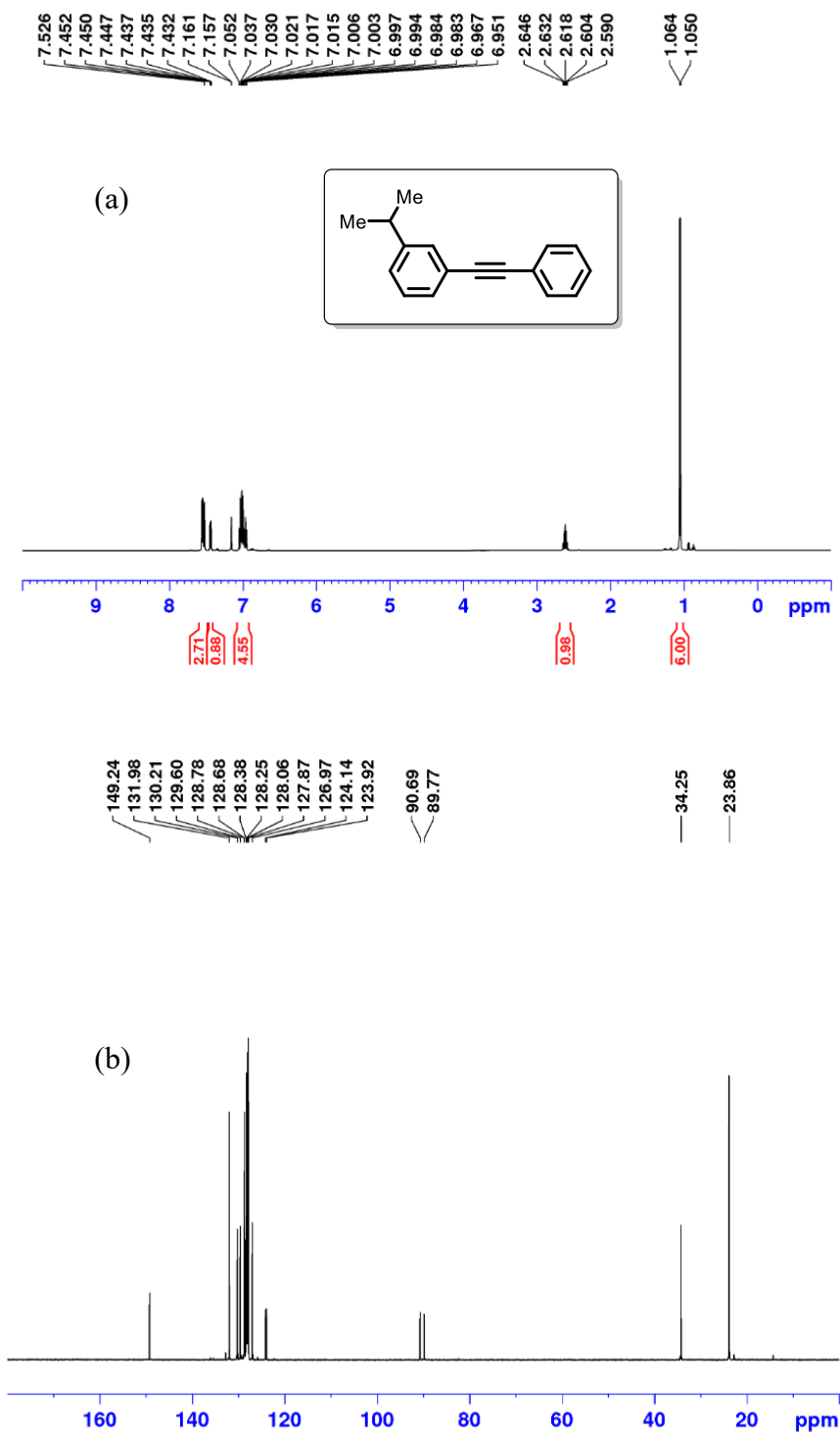
Figure C21. (a) ^{1}H and (b) ^{13}C{^{1}H} NMR spectrum (benzene-d_6) of 1-(1,1-dimethylethyl)-4-(2-phenylethynyl)-benzene.
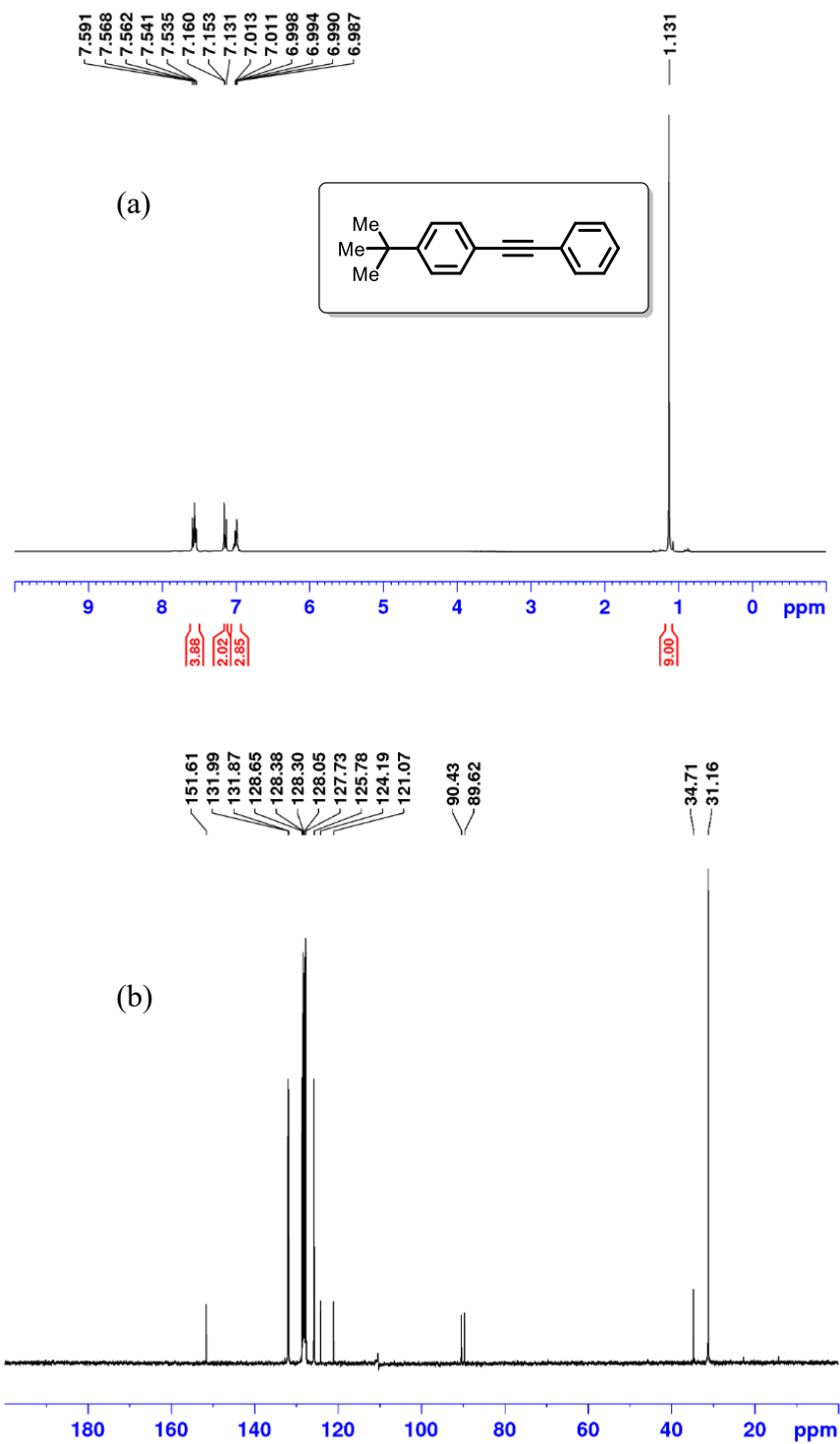
Figure C22. (a) ^{1}H and (b) ^{13}C{^{1}H} NMR spectrum (benzene-d_6) of 1,4-dimethyl-2-(2-phenylethynyl)-benzene.
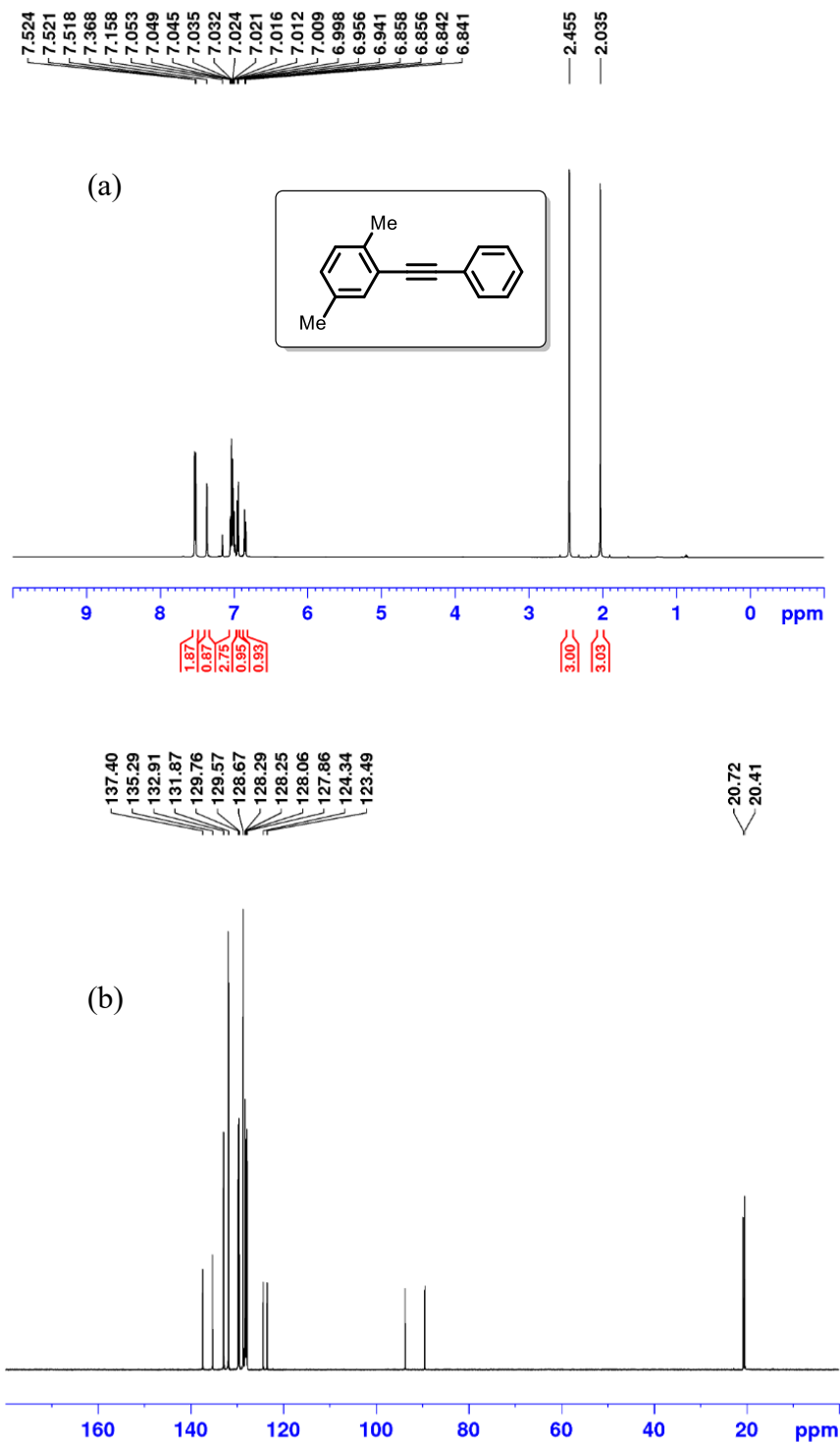
Figure C23. (a) ^{1}H, (b) ^{19}F{^{1}H} and (c) ^{13}C{^{1}H} NMR spectrum (benzene-d_6) of 1-(2-phenylethynyl)-4-(trifluoromethyl)-benzene.
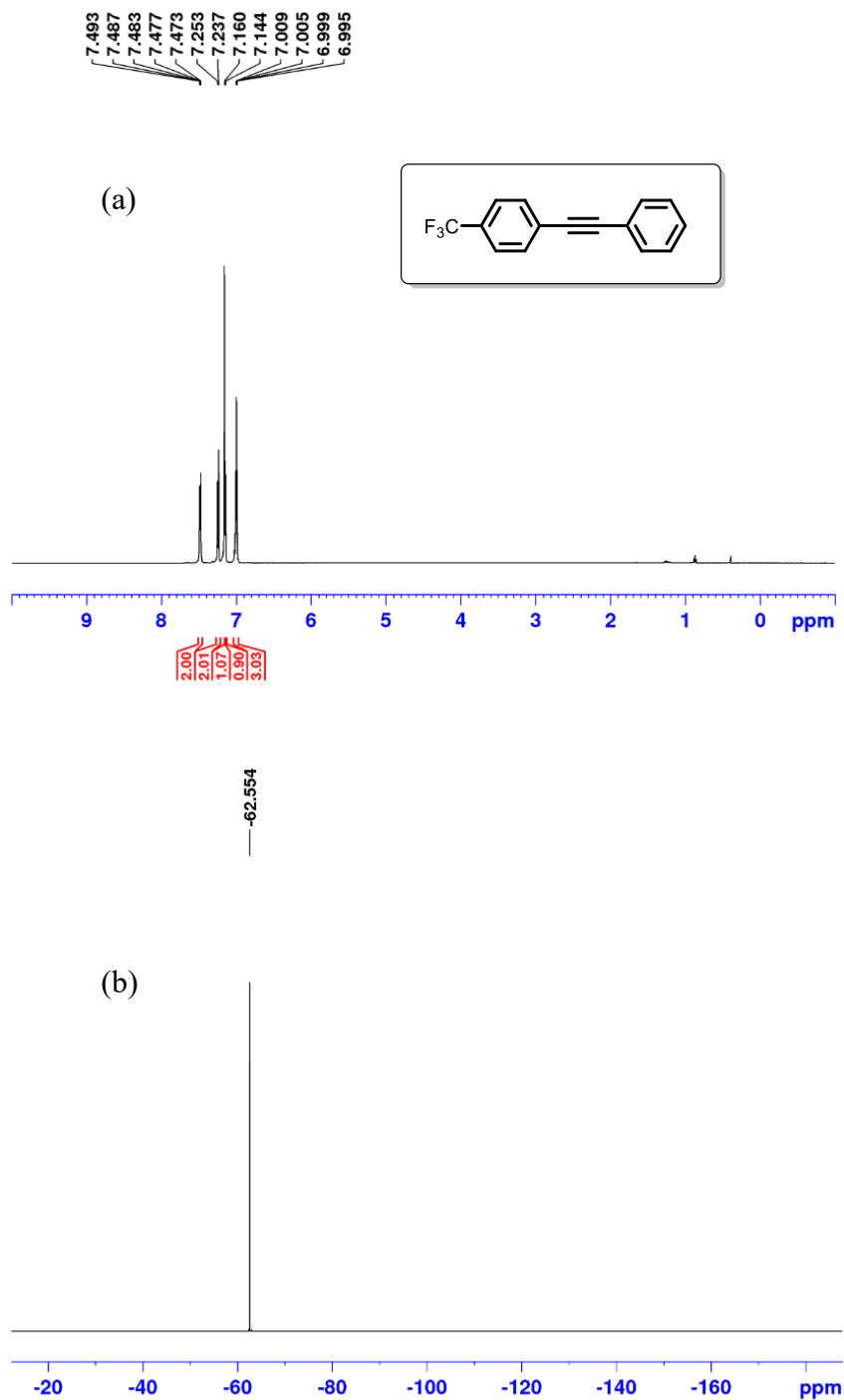
Figure C23. continued. (a) ^{1}H, (b) ^{19}F{^{1}H} and (c) ^{13}C{^{1}H} NMR spectrum (benzene-d_6) of 1-(2-phenylethynyl)-4-(trifluoromethyl)-benzene.
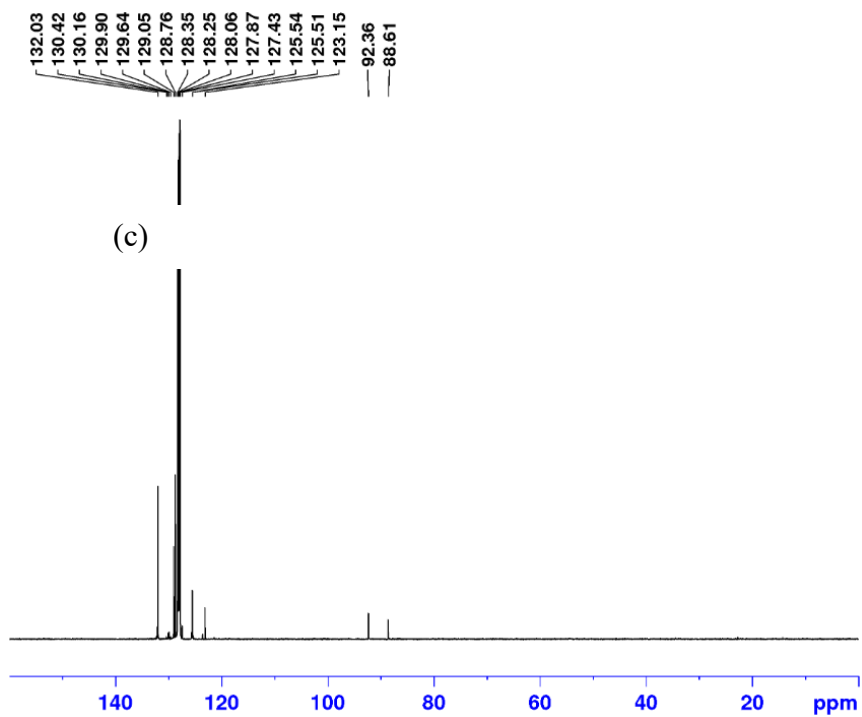
Figure C24. (a) ^{1}H, (b) ^{19}F{^{1}H} and (c) ^{13}C{^{1}H} NMR spectrum (benzene-d_6) of 1-(2-phenylethynyl)-3-(trifluoromethyl)-benzene.
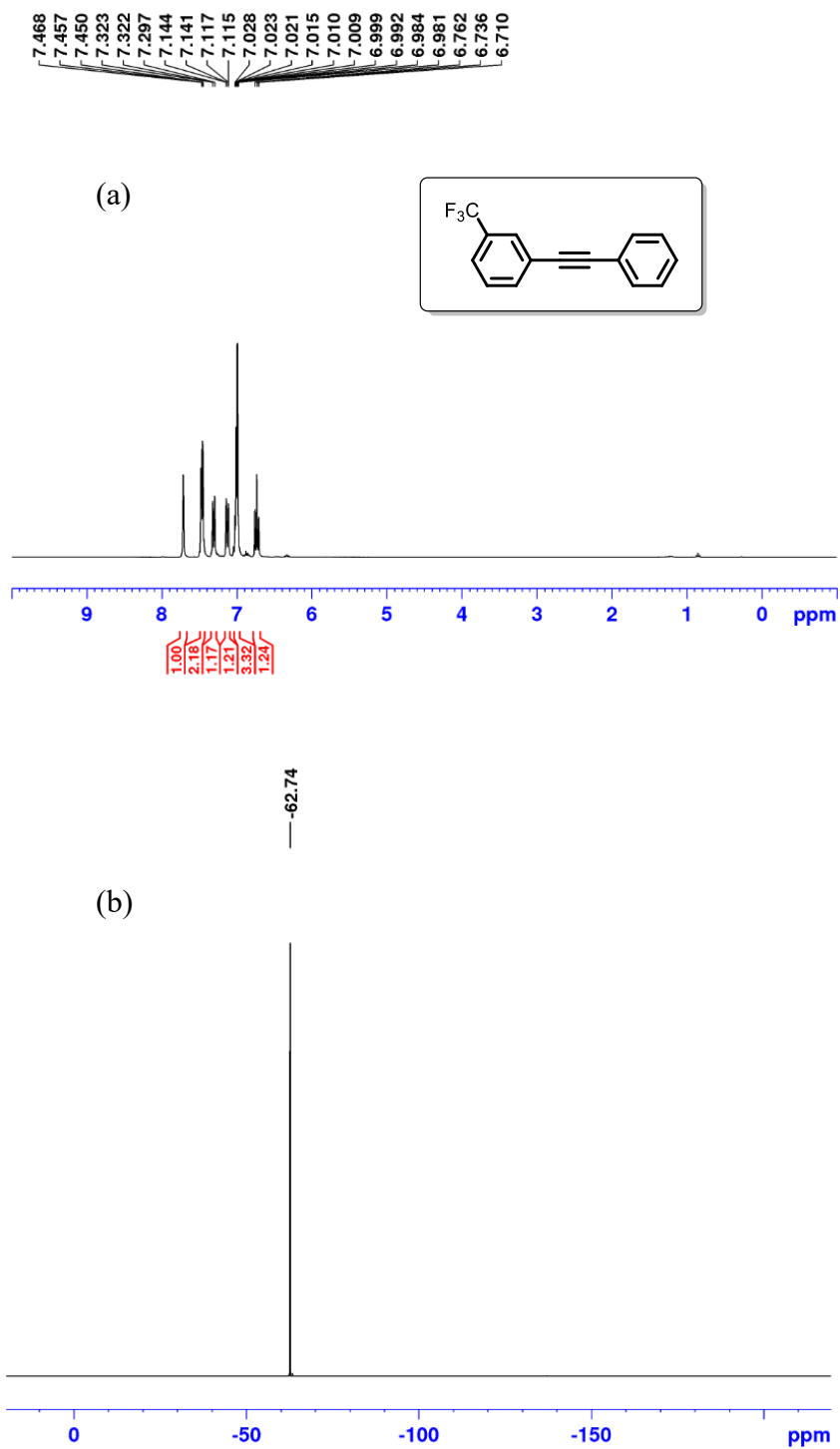
Figure C24. continued. (a) ^{1}H, (b) ^{19}F{^{1}H} and (c) ^{13}C{^{1}H} NMR spectrum (benzene-d_6) of 1-(2-phenylethynyl)-3-(trifluoromethyl)-benzene.

(c)
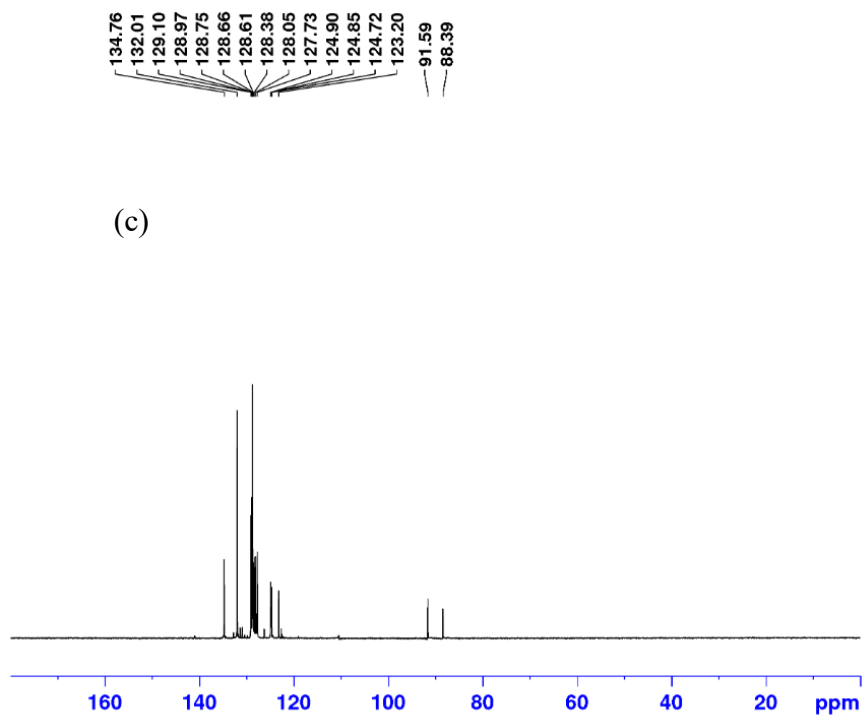
Figure C25. (a) ^1H, (b) $^{19}F\{^1H\}$ and (c) $^{13}C\{^1H\}$ NMR spectrum (benzene-d_6) of 1-(2-phenylethynyl)-3,5-bis(trifluoromethyl)-benzene.
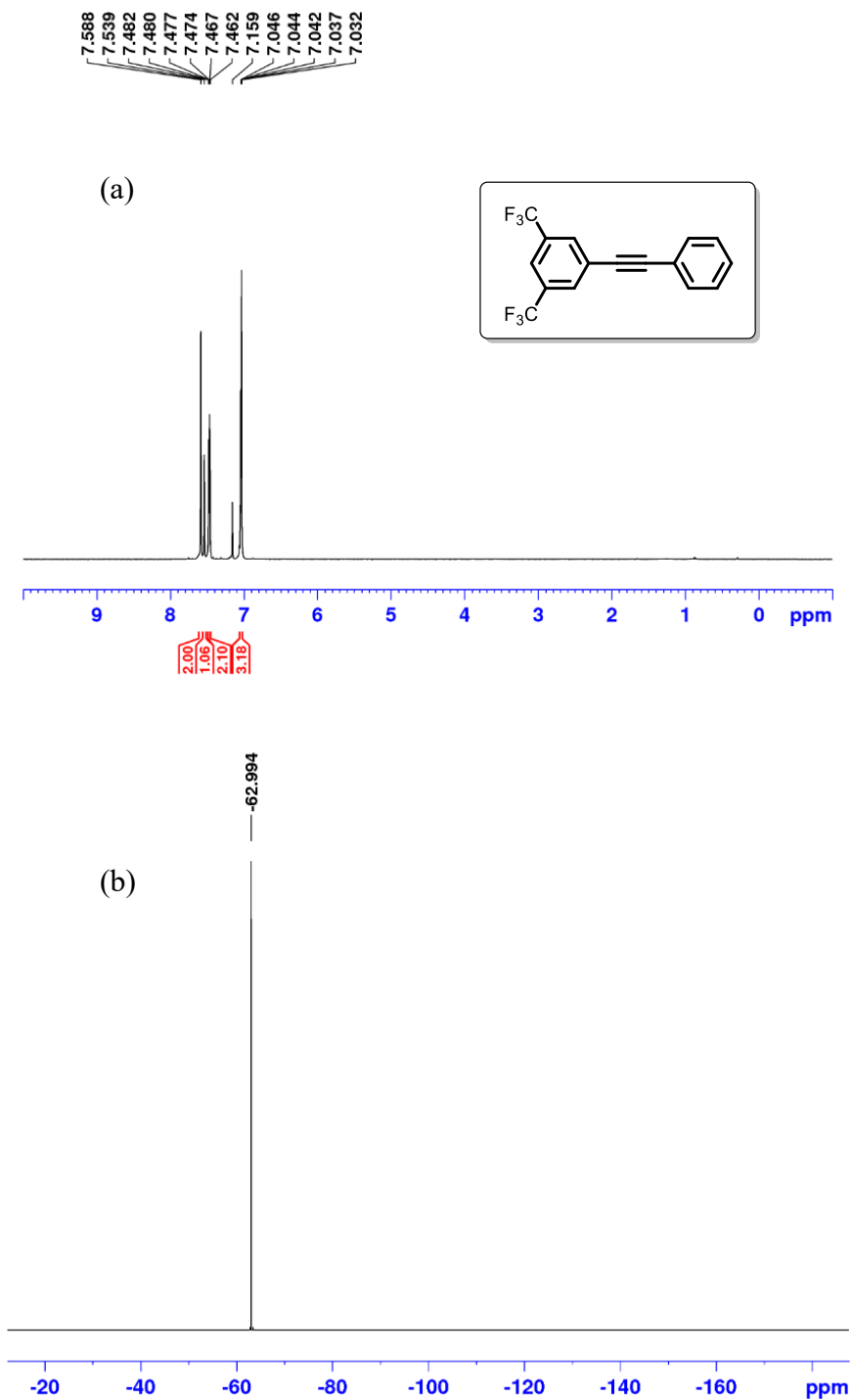
Figure C25. continued. (a) ^{1}H, (b) ^{19}F{^{1}H} and (c) ^{13}C{^{1}H} NMR spectrum (benzene-d_6) of 1-(2-phenylethynyl)-3,5-bis(trifluoromethyl)-benzene.
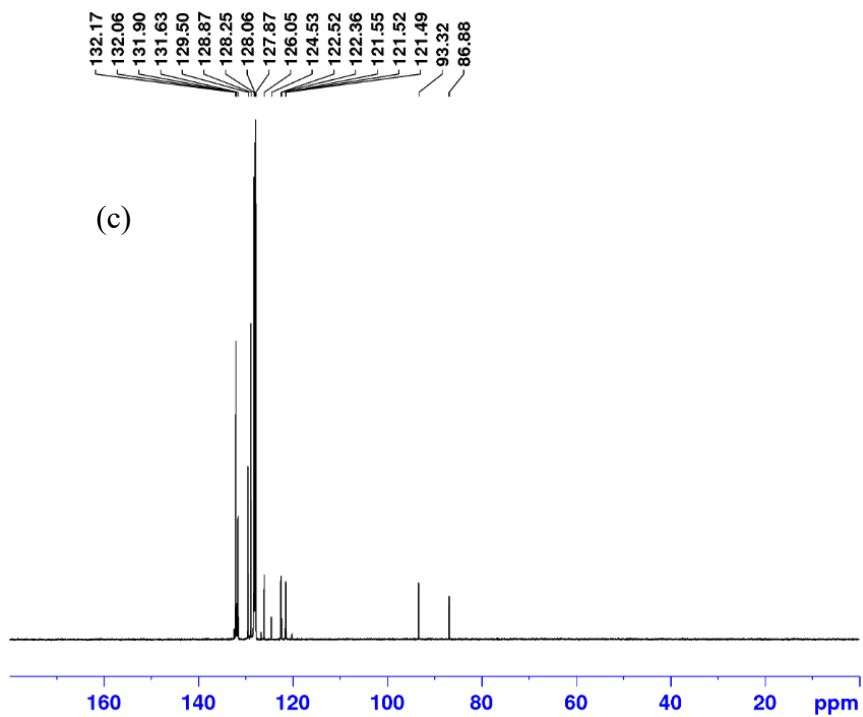
Figure C26. (a) ^1H, (b) $^{19}F\{^1H\}$ and (c) $^{13}C\{^1H\}$ NMR spectrum (benzene-d_6) of 1,2,3,4,5-pentafluoro-6-(2-phenylethynyl)-benzene.
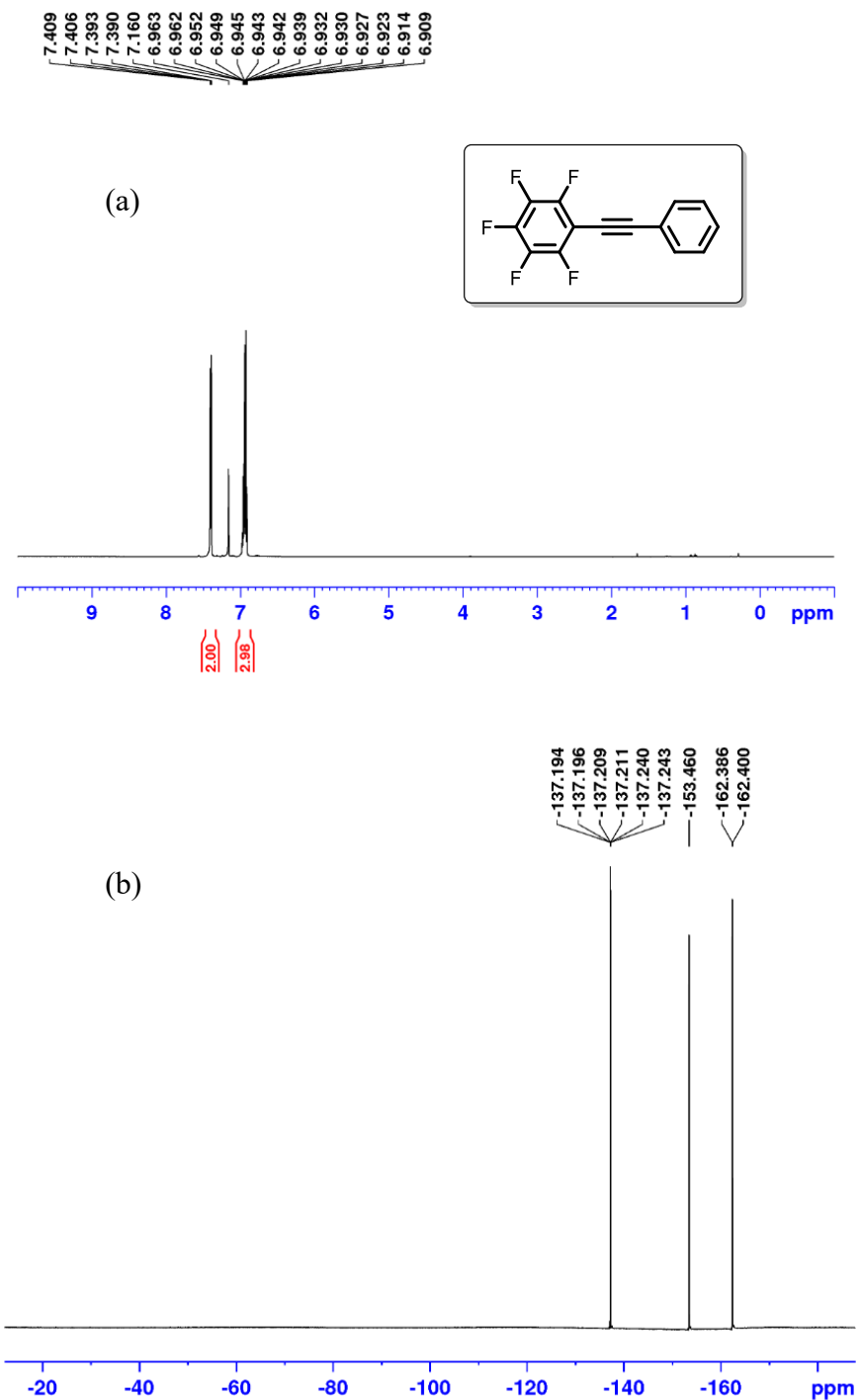
Figure C26. continued. (a) ^{1}H, (b) ^{19}F{^{1}H} and (c) ^{13}C{^{1}H} NMR spectrum (benzene-d_6) of 1,2,3,4,5-pentafluoro-6-(2-phenylethynyl)-benzene.
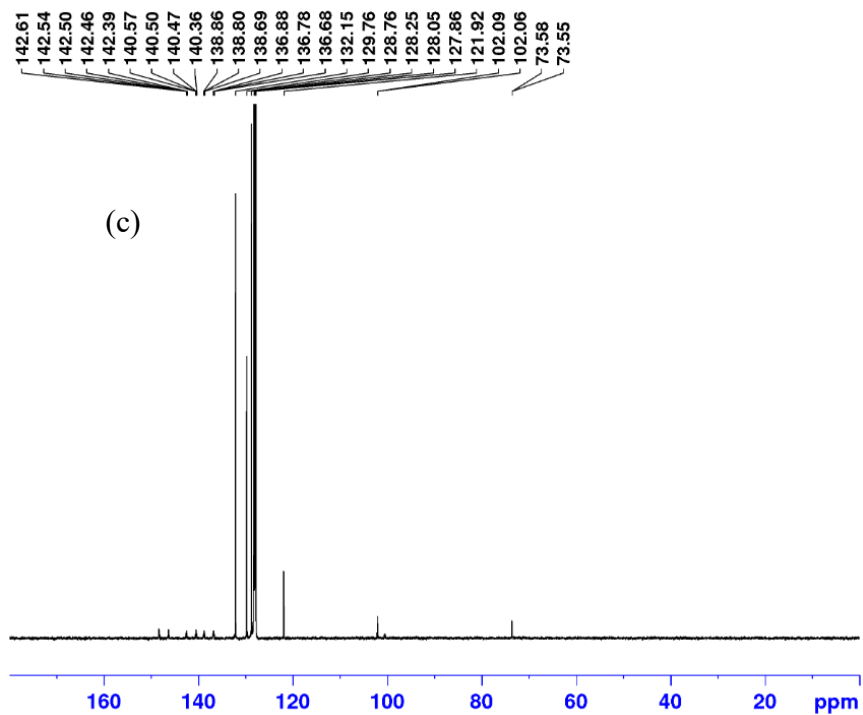
Figure C27. (a) ^{1}H, (b) ^{19}F{^{1}H} and (c) ^{13}C{^{1}H} NMR spectrum (benzene-d_6) of 1-fluoro-4-(2-phenylethynyl)-benzene.
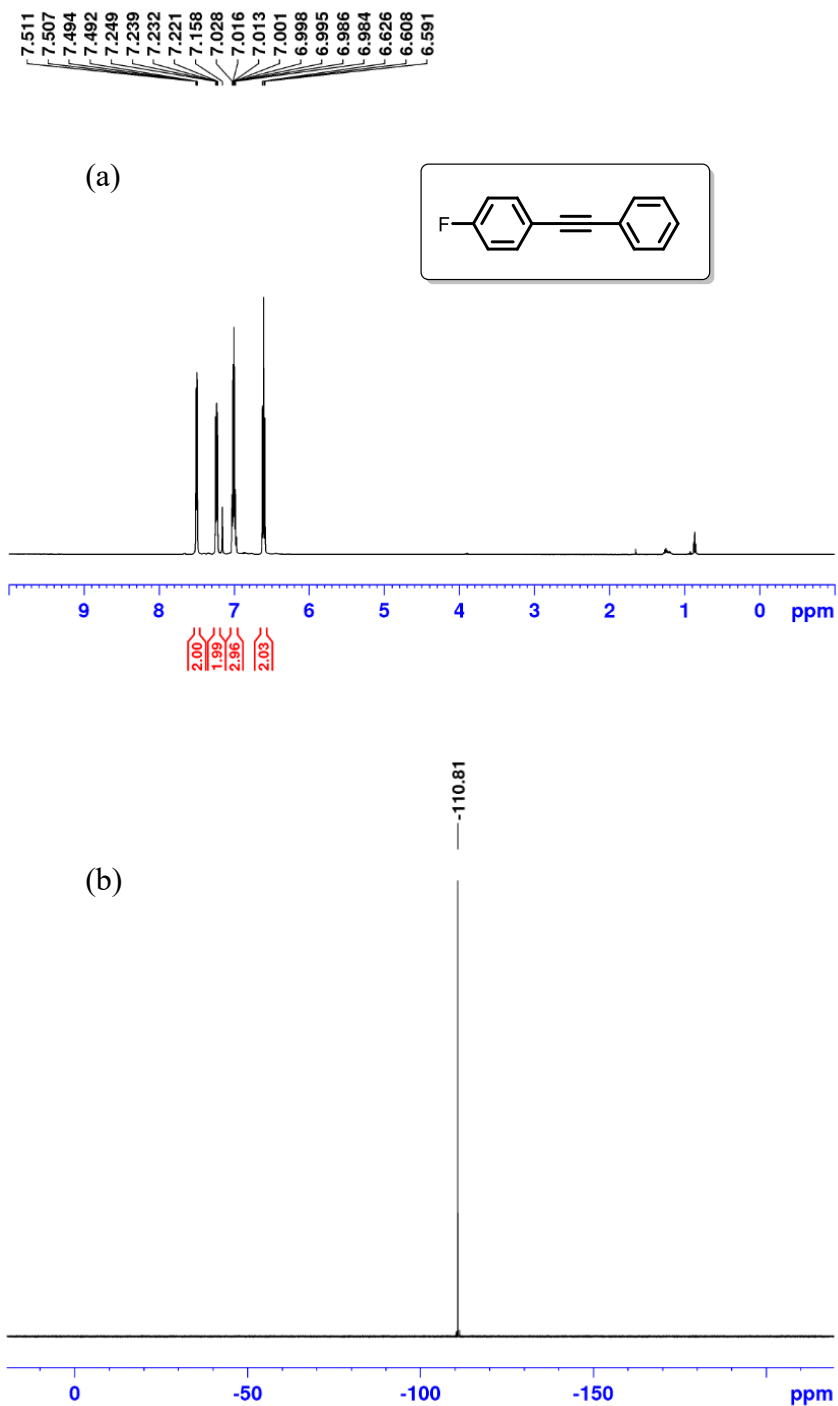
Figure C27. continued. (a) ^{1}H, (b) ^{19}F{^{1}H} and (c) ^{13}C{^{1}H} NMR spectrum (benzene-d_6) of 1-fluoro-4-(2-phenylethynyl)-benzene.
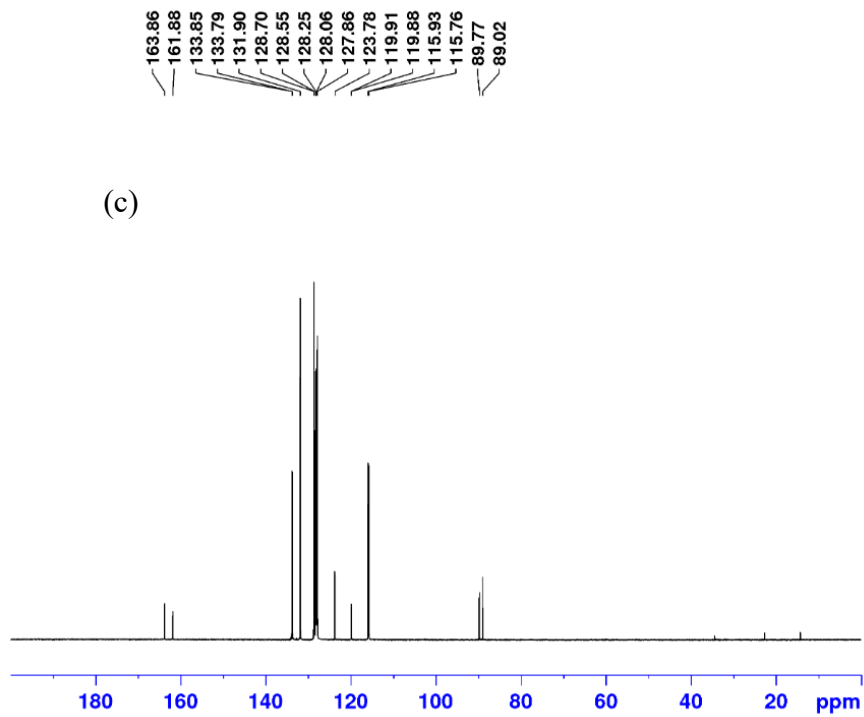
Figure C28. (a) ^{1}H, (b) ^{19}F{^{1}H} and (c) ^{13}C{^{1}H} NMR spectrum (benzene-d_6) of 1-fluoro-2-(2-phenylethynyl)-benzene.
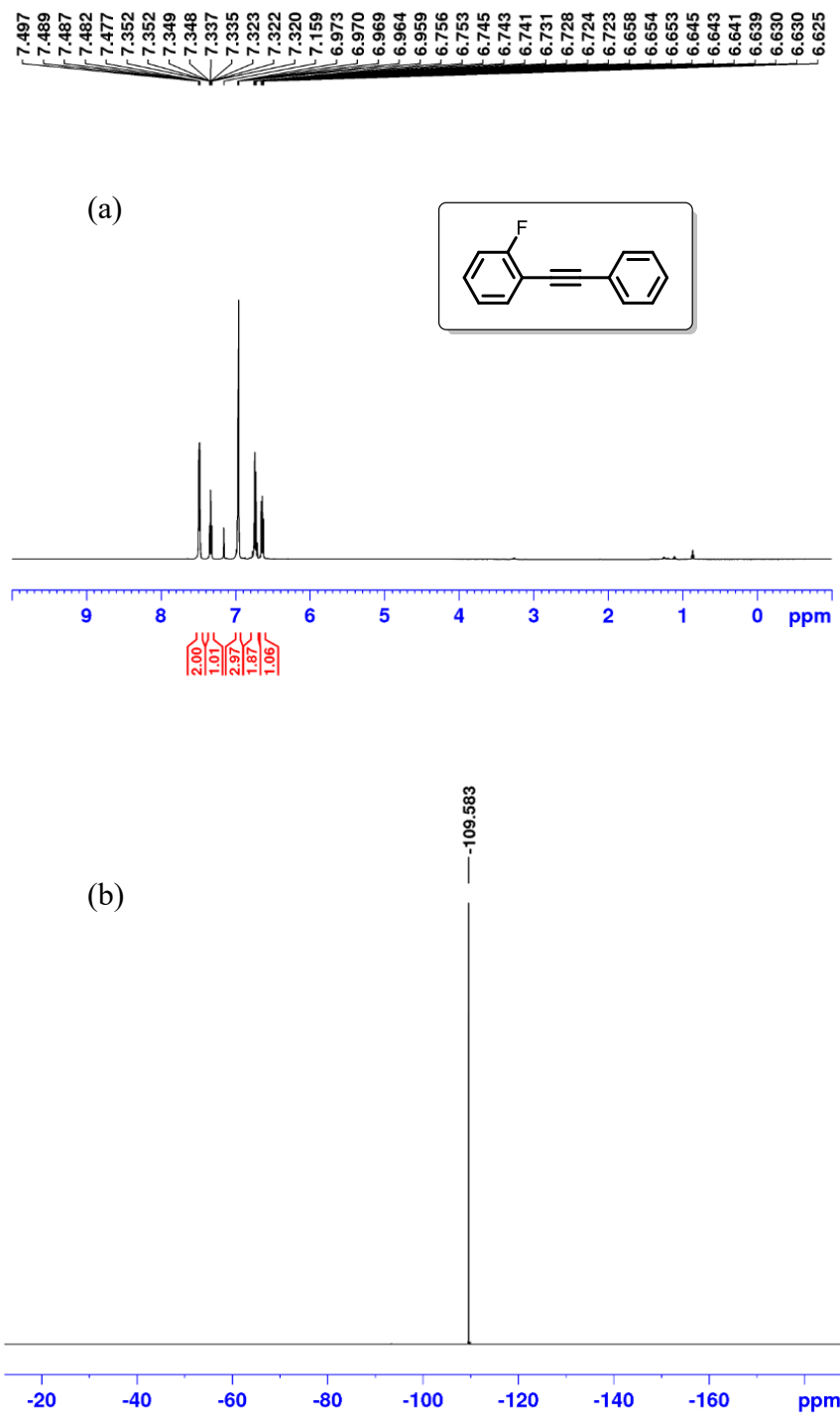
Figure C28. continued. (a) ^{1}H, (b) ^{19}F{^{1}H} and (c) ^{13}C{^{1}H} NMR spectrum (benzene-d_6) of 1-fluoro-2-(2-phenylethynyl)-benzene.
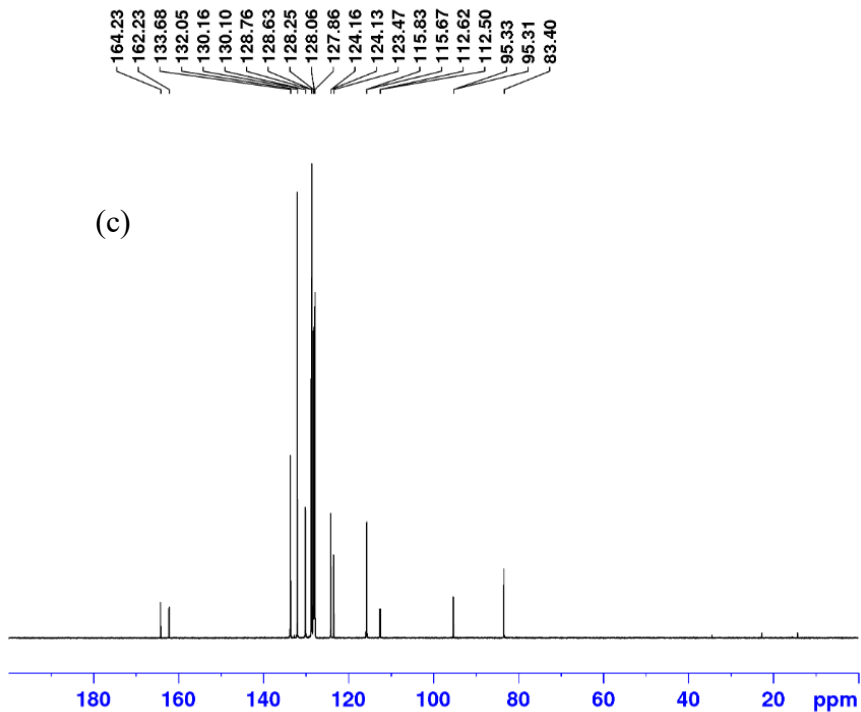
Figure C-29. (a) ^{1}H and (b) ^{13}C{^{1}H} NMR spectrum (benzene-d_6) of 1-chloro-4-(2-phenylethynyl)-benzene.

(a)

(b)
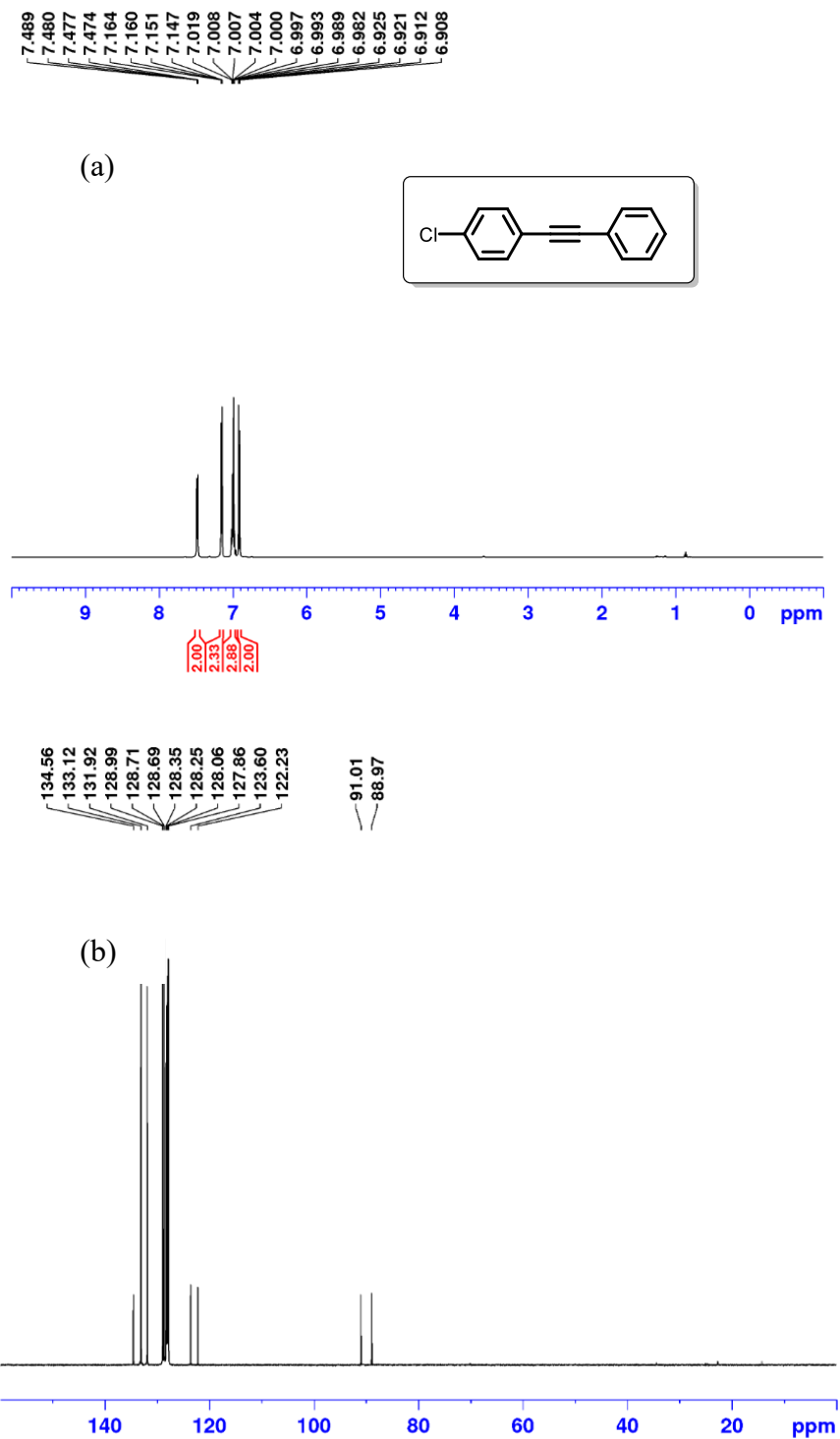
Figure C30. (a) ^{1}H and (b) ^{13}C{^{1}H} NMR spectrum (benzene-d_6) of 1-chloro-3-(2-phenylethynyl)-benzene.

(a)

(b)
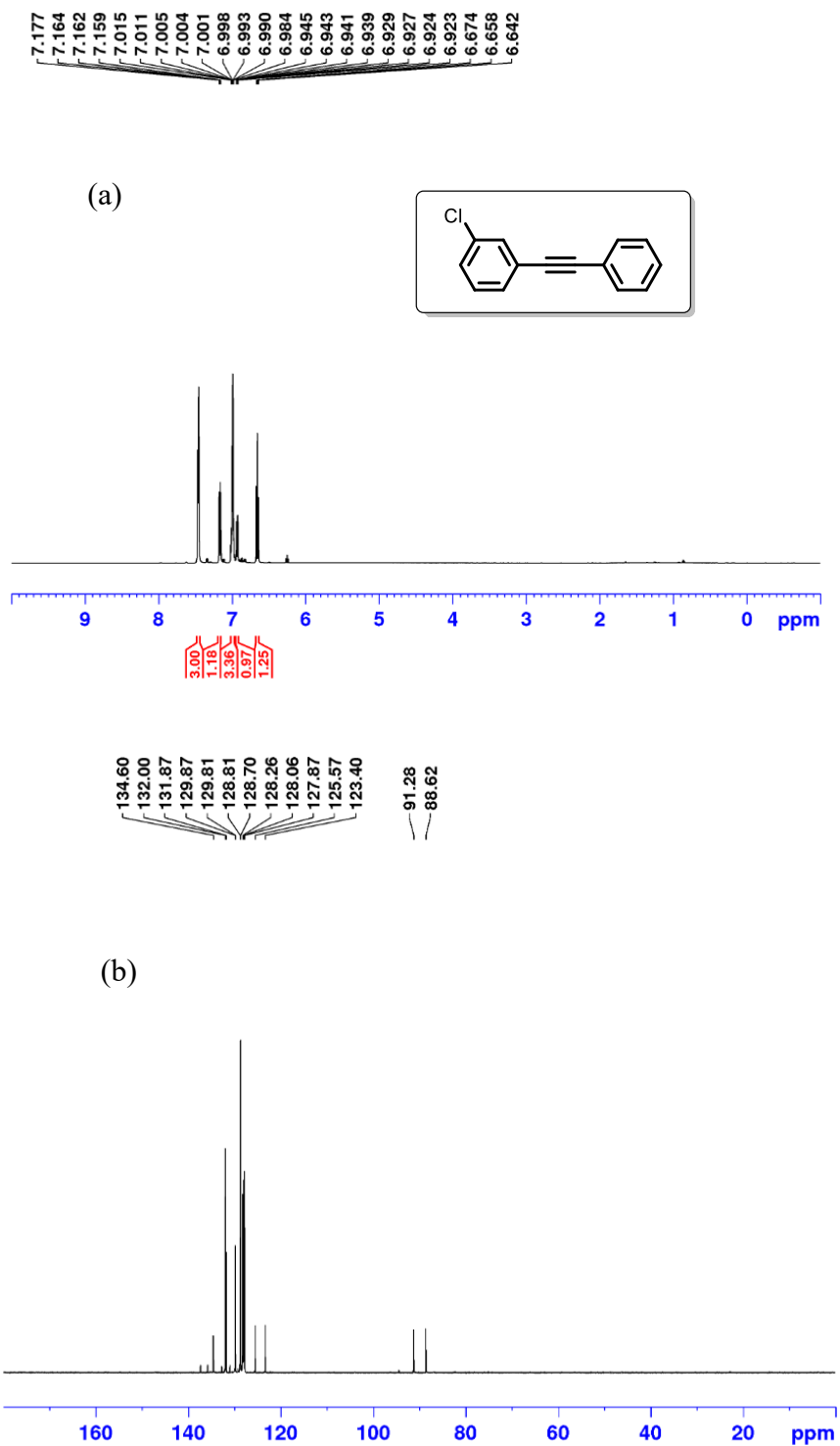
Figure C31. (a) ^{1}H and (b) ^{13}C{^{1}H} NMR spectrum (benzene-d_6) of 1-chloro-2-(2-phenylethynyl)-benzene.
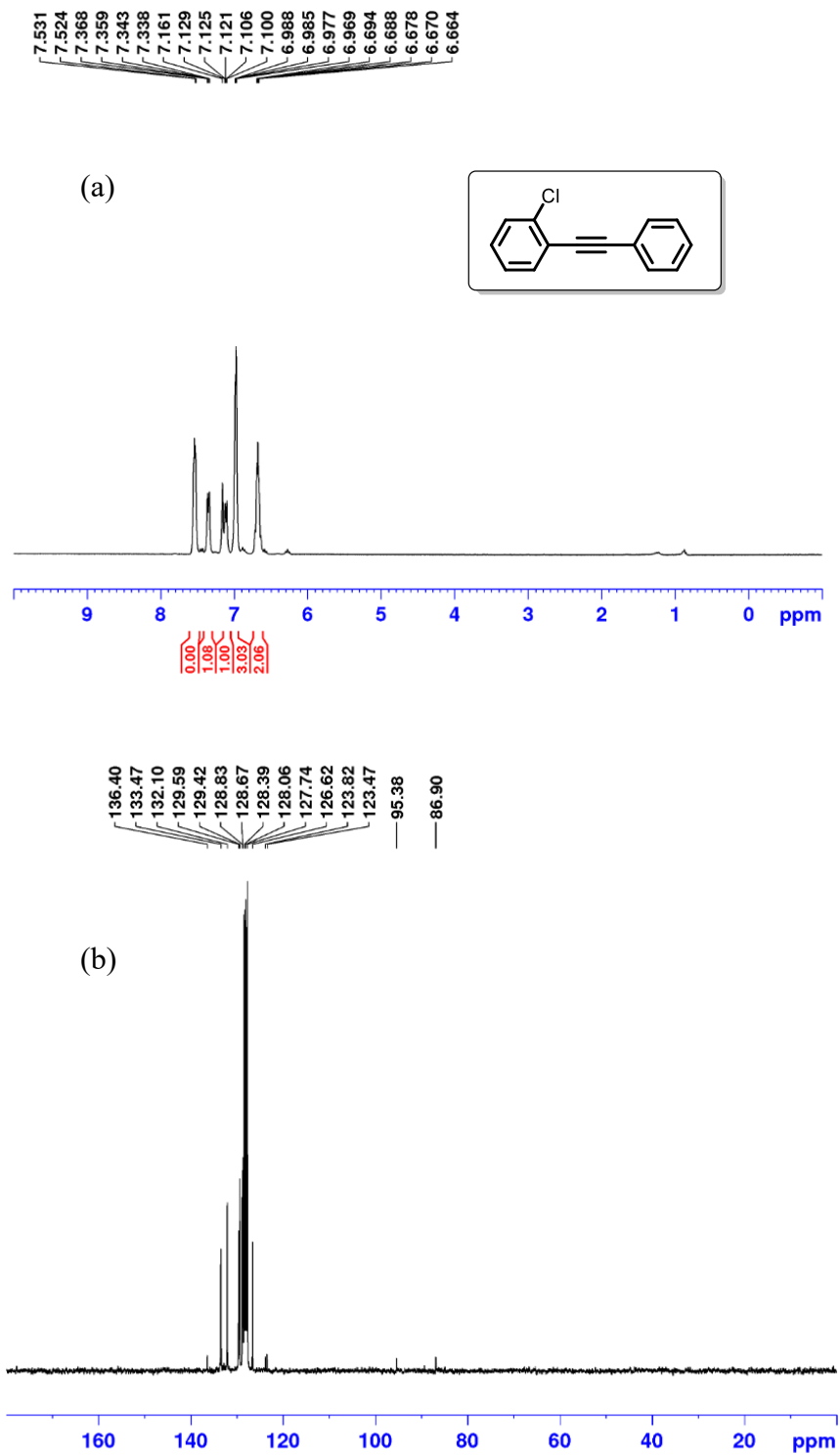
Figure C32. (a) ^{1}H and (b) ^{13}C{^{1}H} NMR spectrum (benzene-d_6) of 1-bromo-2-(2-phenylethynyl)-benzene.
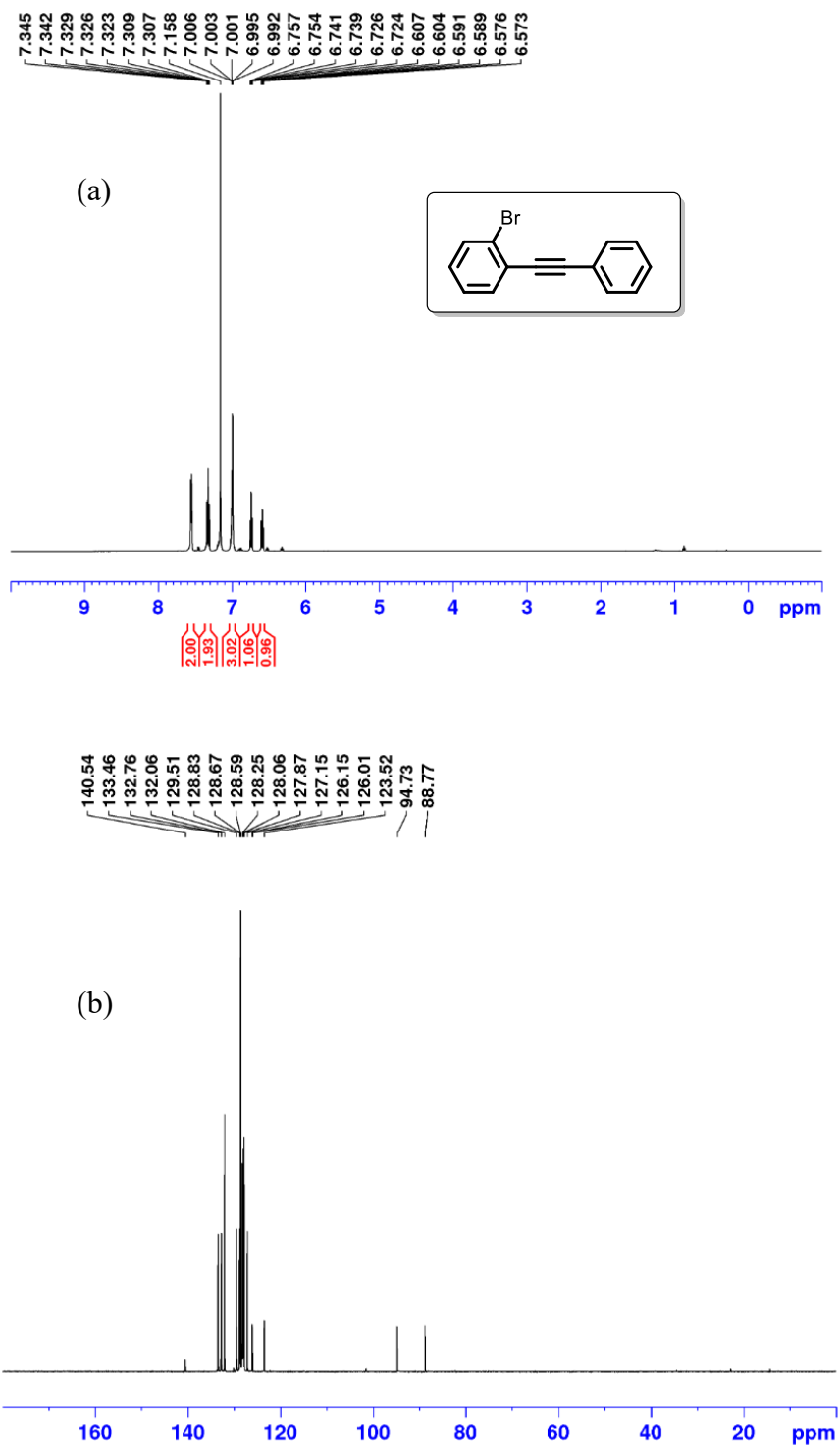
Figure C33. (a) ^{1}H and (b) ^{13}C{^{1}H} NMR spectrum (benzene-d_6) of 1-nitro-4-(2-phenylethynyl)-benzene.

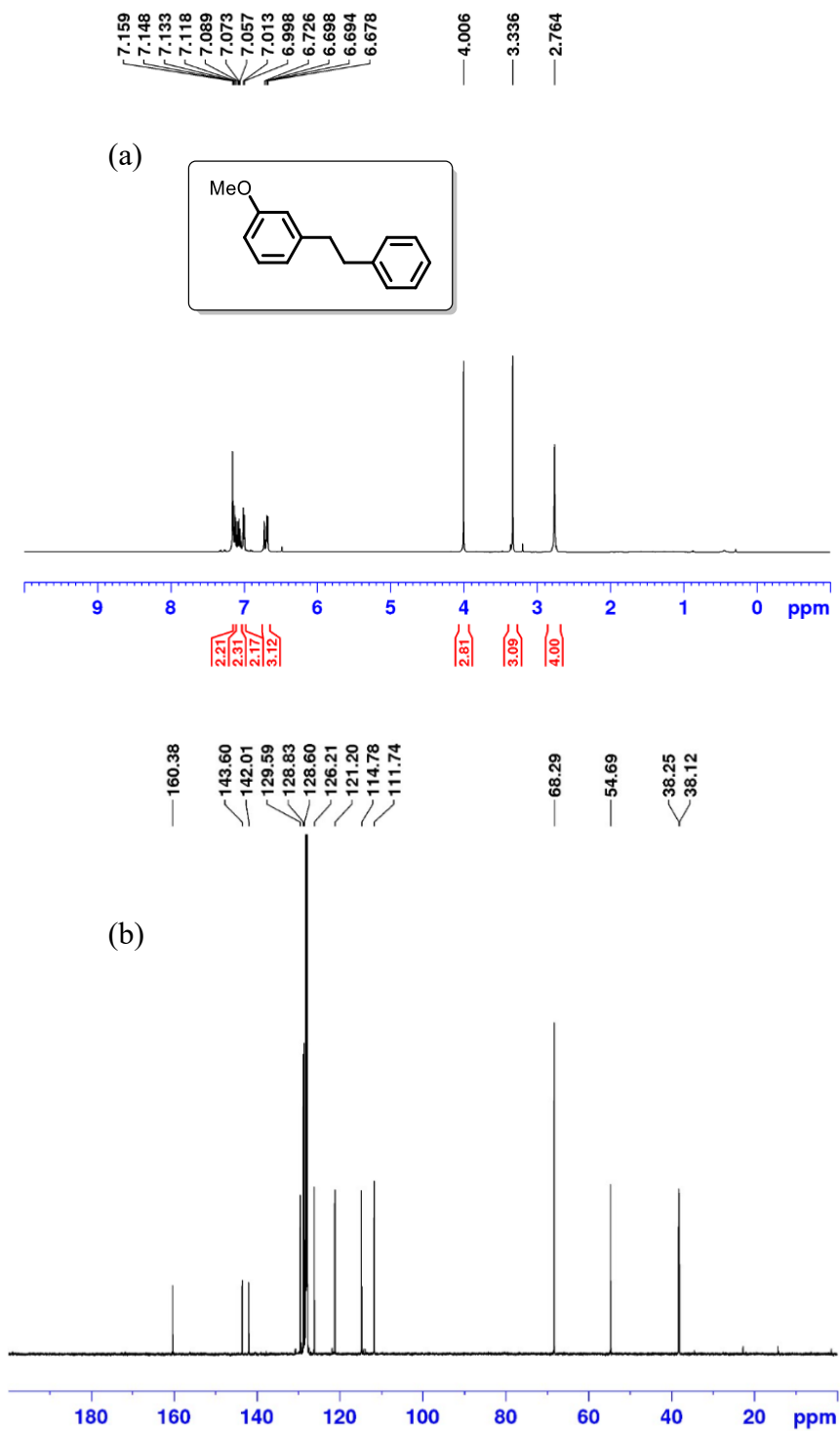**Figure C34.** (a) ^{1}H and (b) ^{13}C{^{1}H} NMR spectrum (benzene-d_6) of 1-nitro-3-(2-phenylethynyl)-benzene.

Figure C35. (a) ^{1}H and (b) ^{13}C{^{1}H} NMR spectrum (benzene-d_6) of 4-(2-phenylethynyl)-benzonitrile.
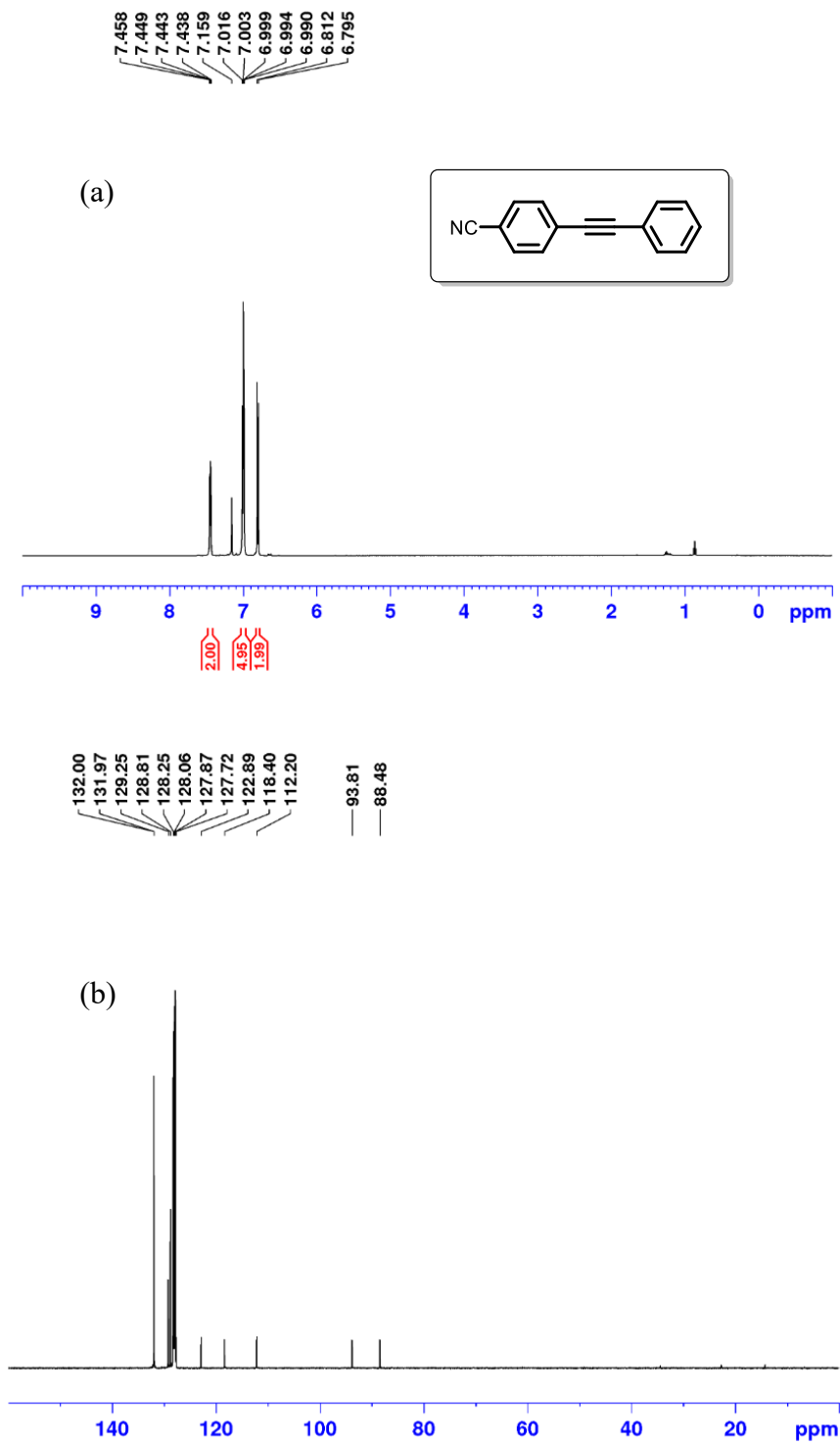
Figure C36. (a) ^{1}H and (b) ^{13}C{^{1}H} NMR spectrum (benzene-d_6) of 3-(2-phenylethynyl)-pyridine.
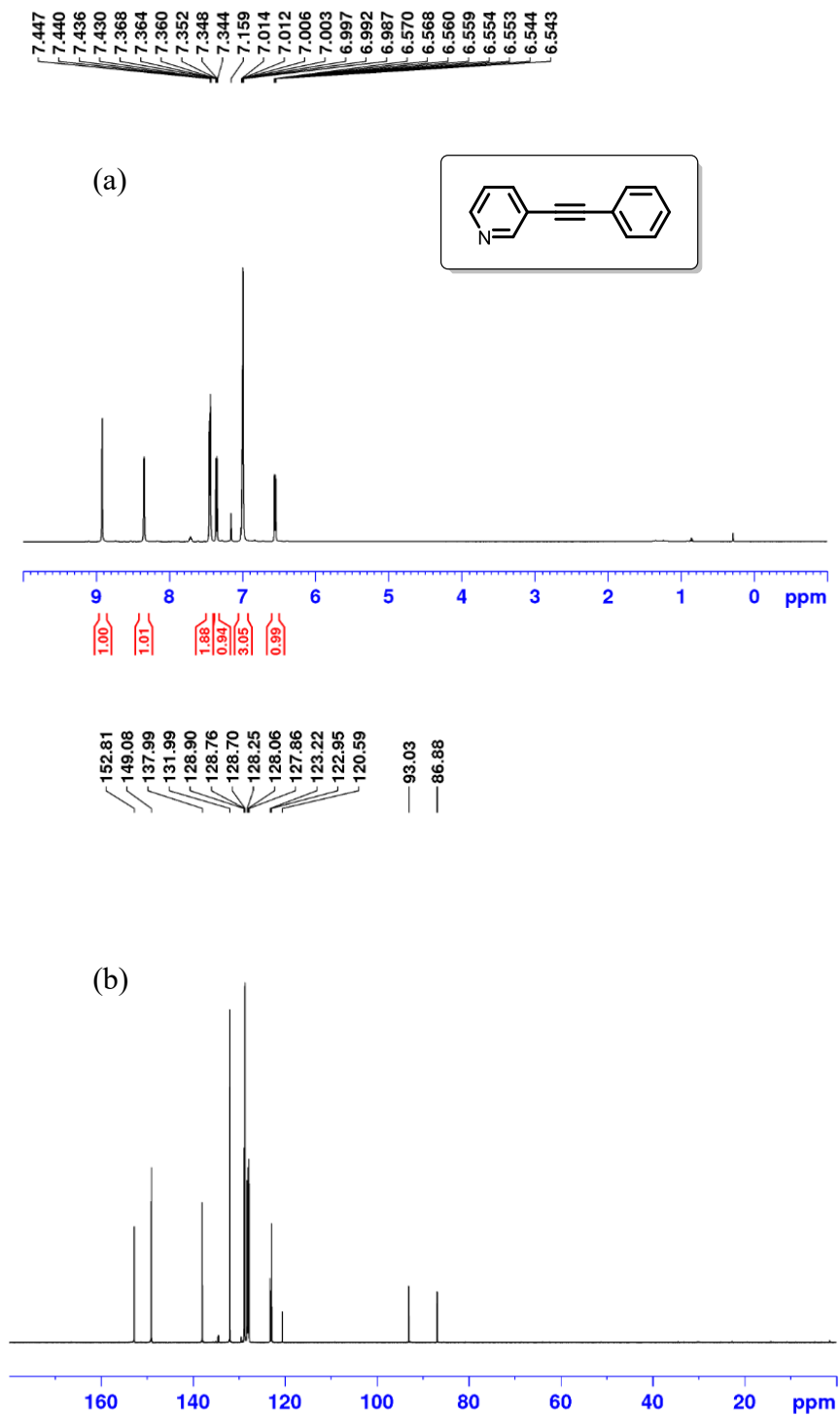
Figure C37. (a) ^{1}H and (b) ^{13}C{^{1}H} NMR spectrum (benzene-d_6) of 3-(2-phenylethynyl)-thiophene.
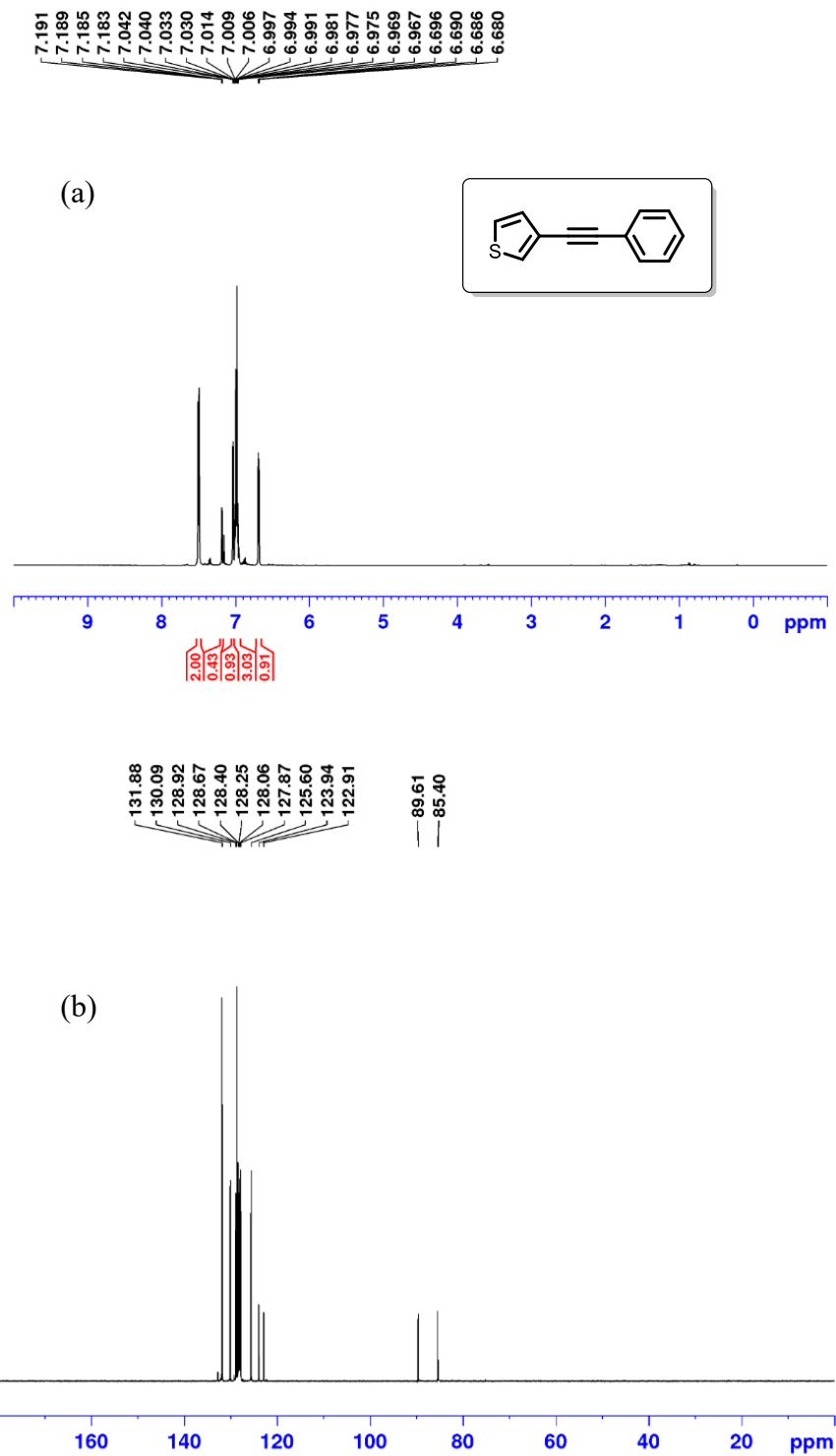
C-4: Selected NMR Spectra of Alkane Products

Figure C38. (a) ^{1}H and (b) ^{1}H (isolated) and (c) ^{13}C{^{1}H} NMR spectrum (benzene-d_6) of 1,1'-(1,2-ethanediyl)bis-benzene.
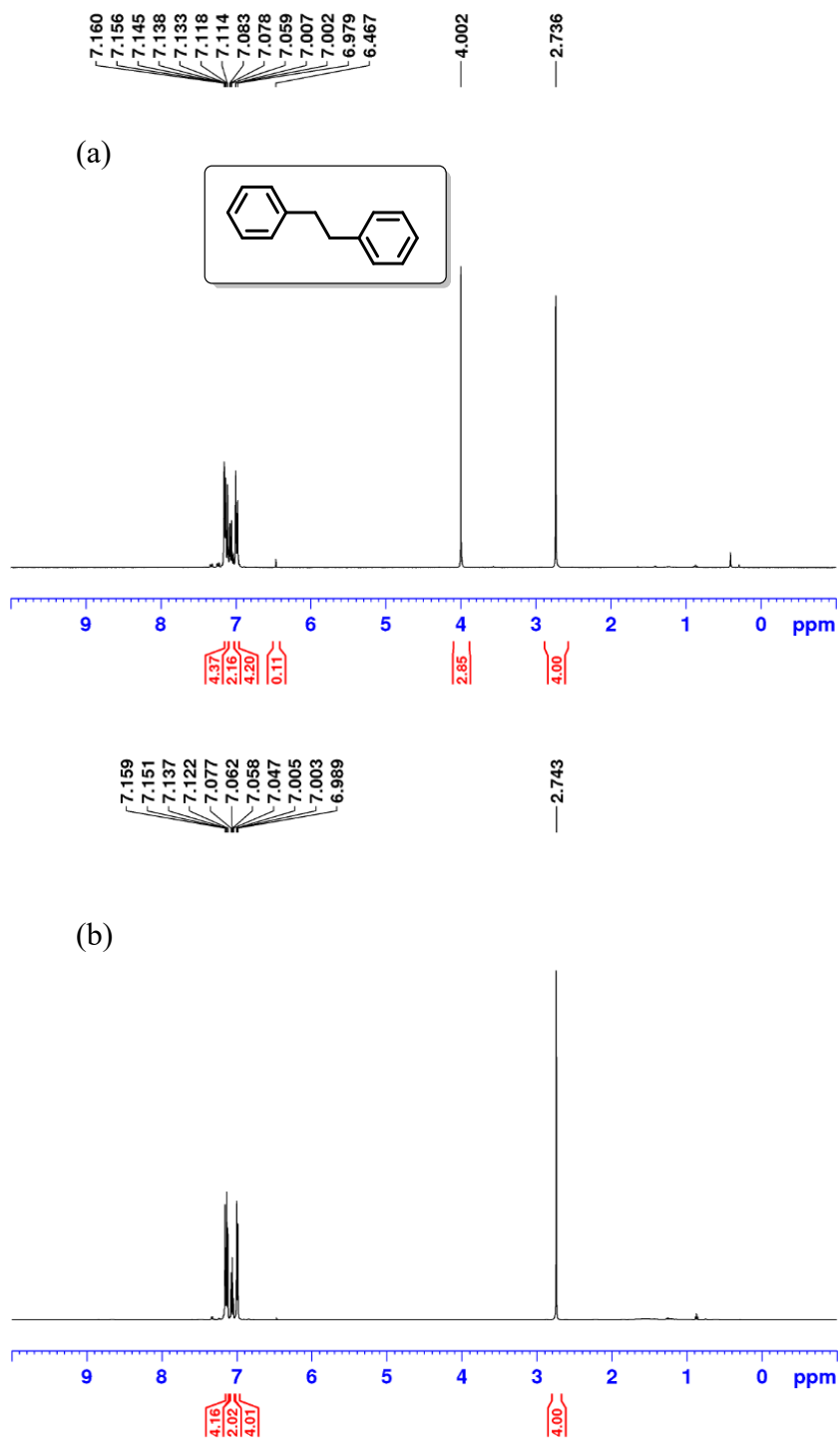
Figure C38. continued. (a) ^{1}H and (b) ^{1}H (isolated) and (c) ^{13}C{^{1}H} NMR spectrum (benzene-d_6) of 1,1'-(1,2-ethanediyl)bis-benzene.
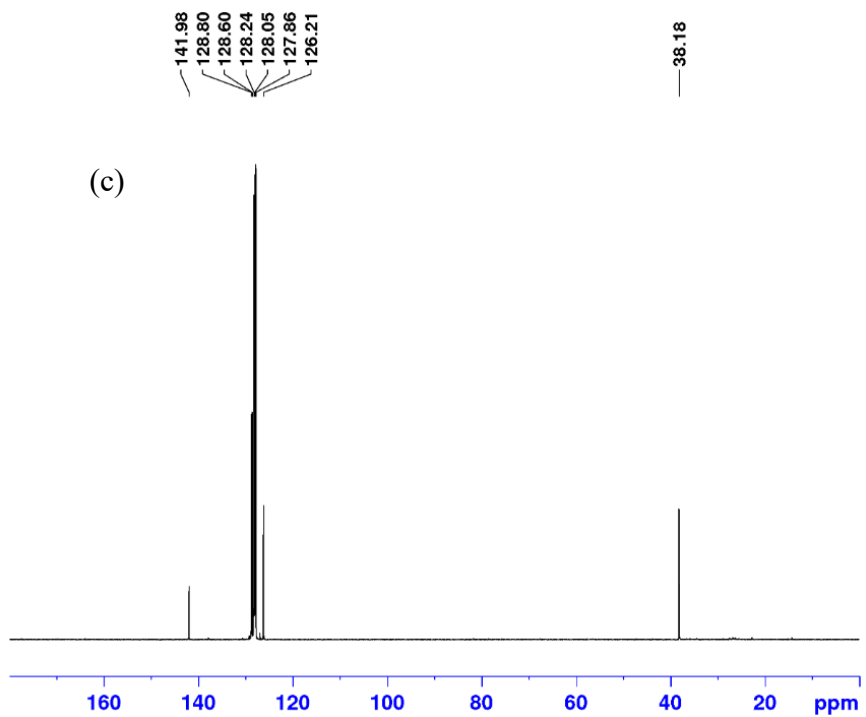
Figure C39. (a) ^{1}H and (b) ^{13}C{^{1}H} NMR spectrum (benzene-d_6) of 2-(2-phenylethyl)-naphthalene.
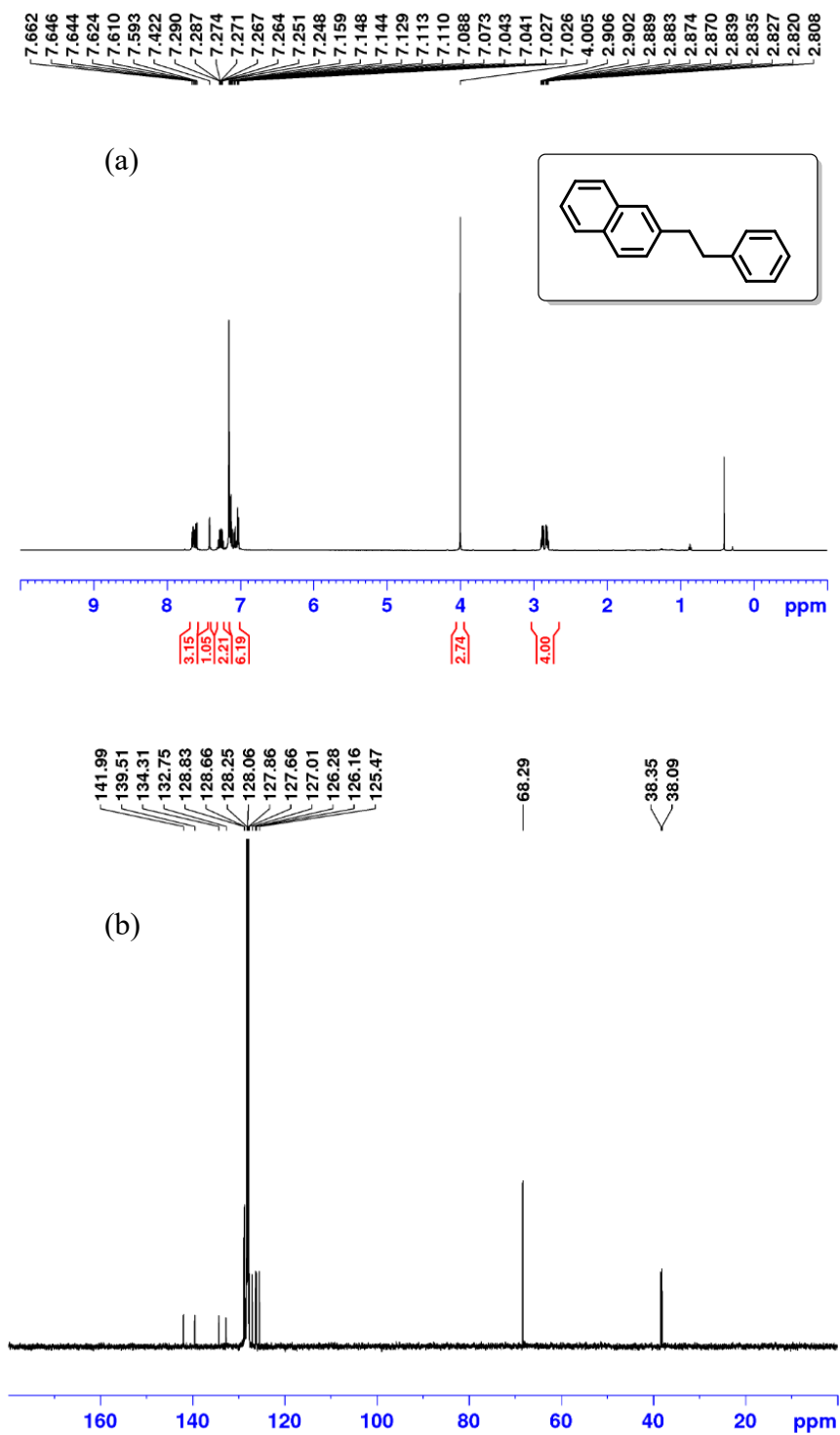
Figure C40. ^{1}H NMR spectrum (benzene-d_6) of 1-(2-phenylethyl)-naphthalene.
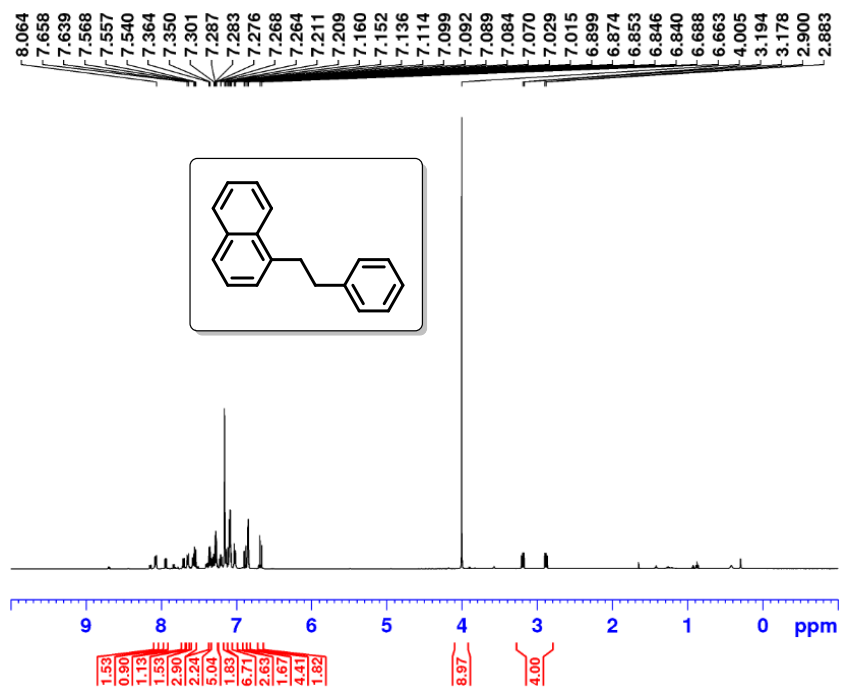
Figure C41. (a) ^{1}H and (b) ^{13}C{^{1}H} NMR spectrum (benzene-d_6) of 1-(2-phenylethyl)-4-(trimethylsilyl)-benzene.
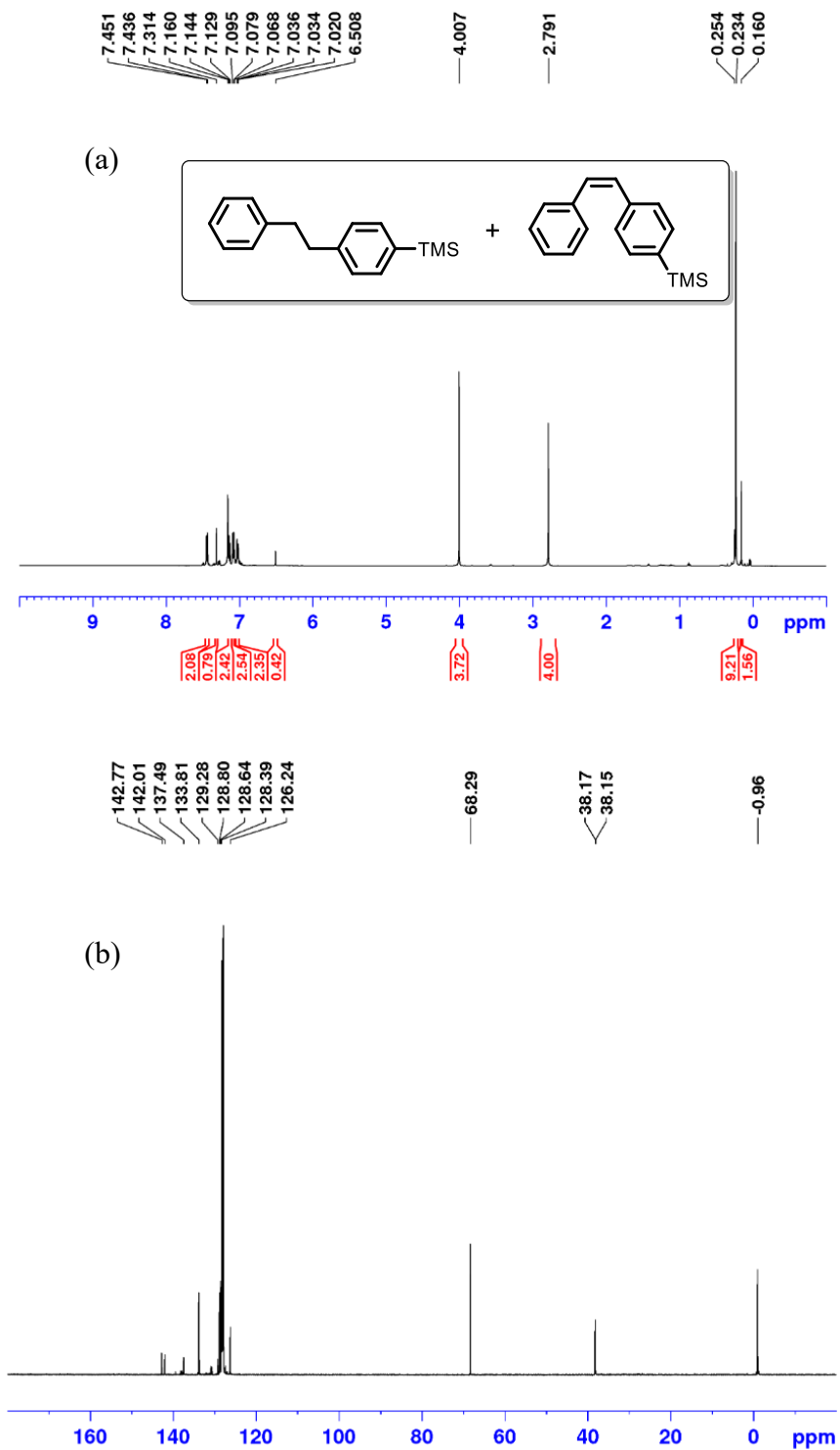
Figure C42. ^{1}H NMR spectrum (benzene-d_6) of propyl-benzene.
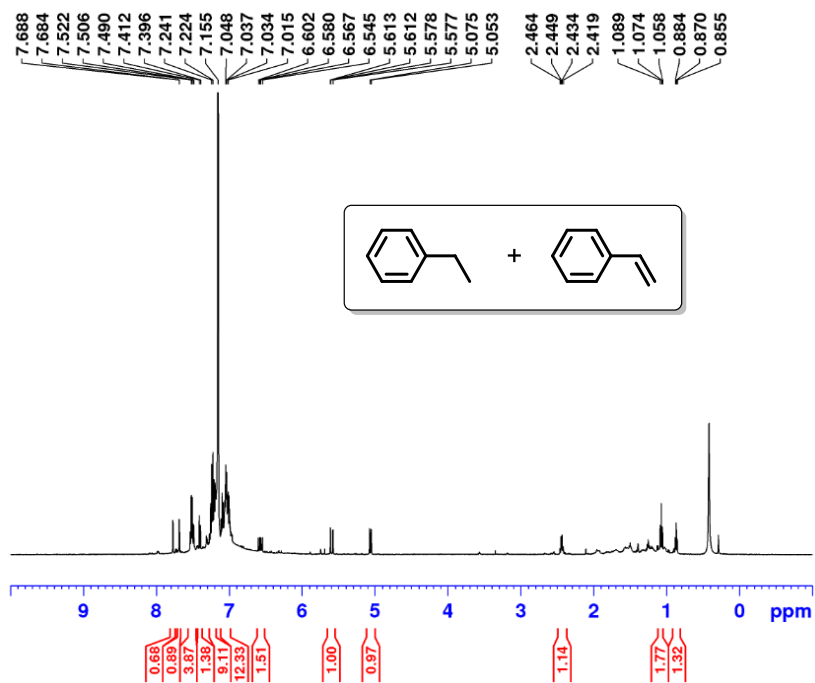
Conditions: 2.5 mol % dimer, 10 atm H_2, 65 °C, 4 hours, 0.228 M, benzene-d_6.

Figure C43. (a) ^{1}H and (b) ^{13}C{^{1}H} NMR spectrum (benzene-d_6) of propyl-benzene.

(a)

(b)
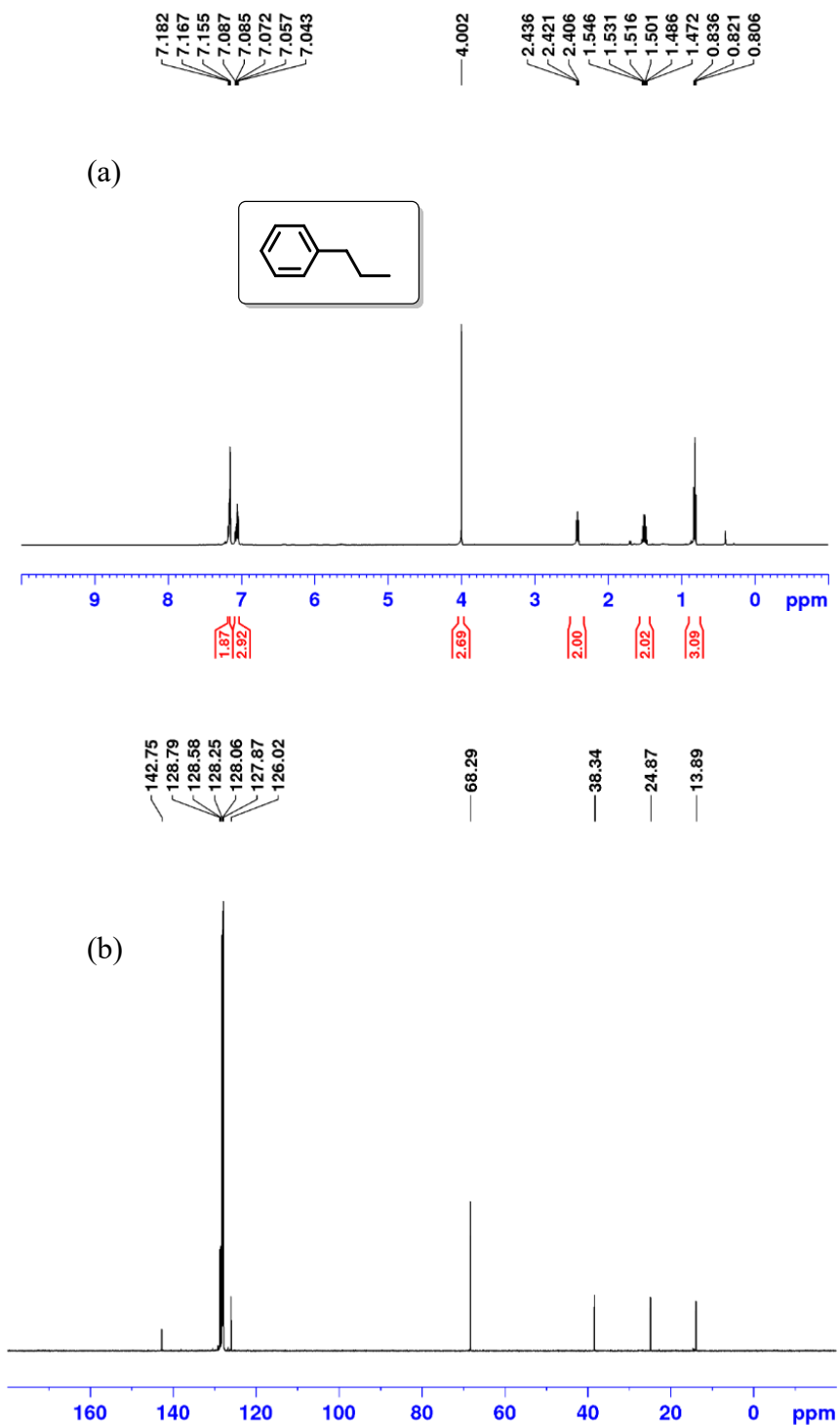
Figure C44. (a) ^{1}H and (b) ^{13}C{^{1}H} NMR spectrum (benzene-d_6) of butyl-benzene.
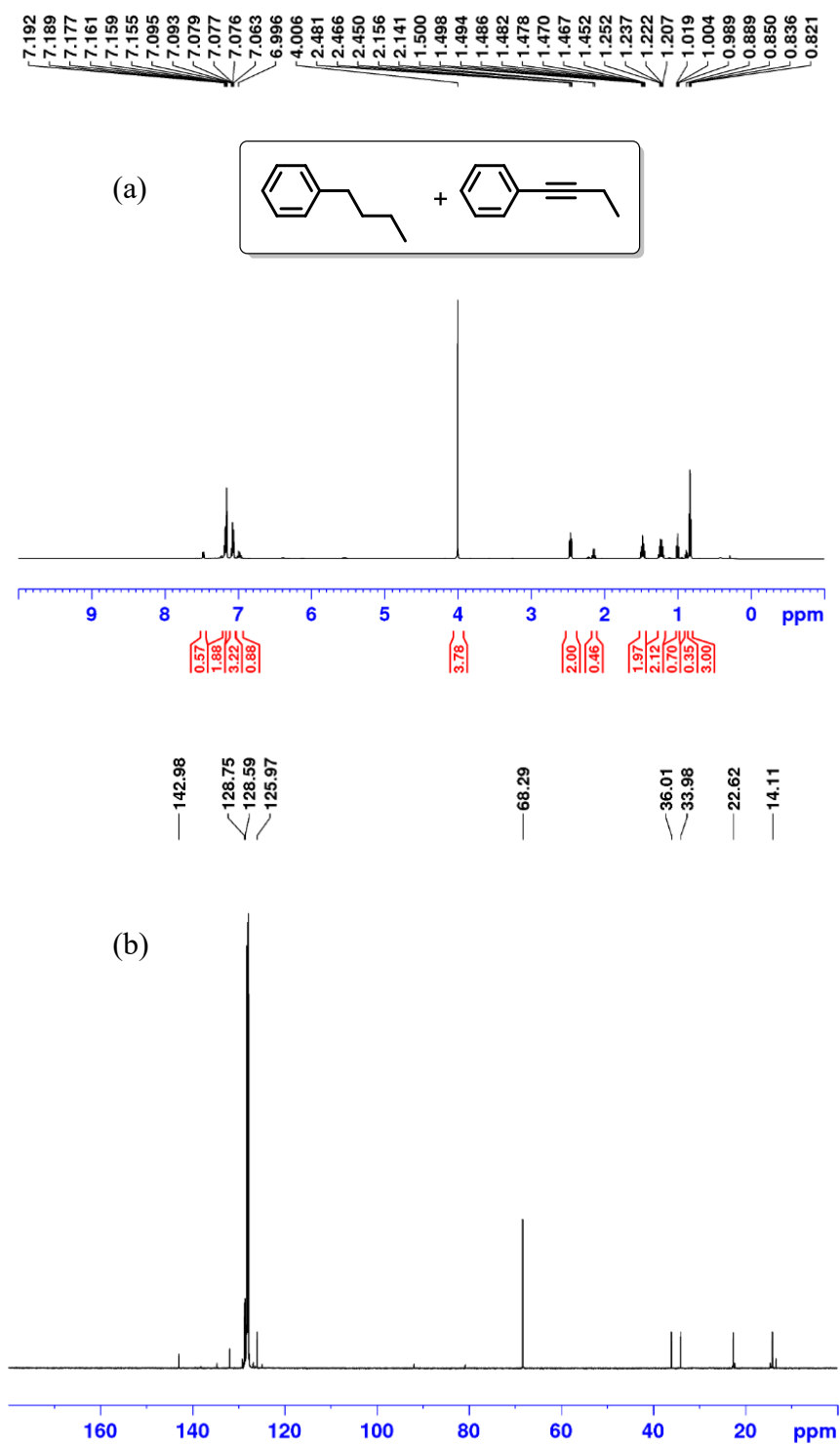
Figure C45. (a) ^{1}H, (b) ^{1}H (isolated) and (c) ^{13}C{^{1}H} NMR spectrum (benzene-d_6) of 1-methoxy-4-(2-phenylethyl)-benzene.
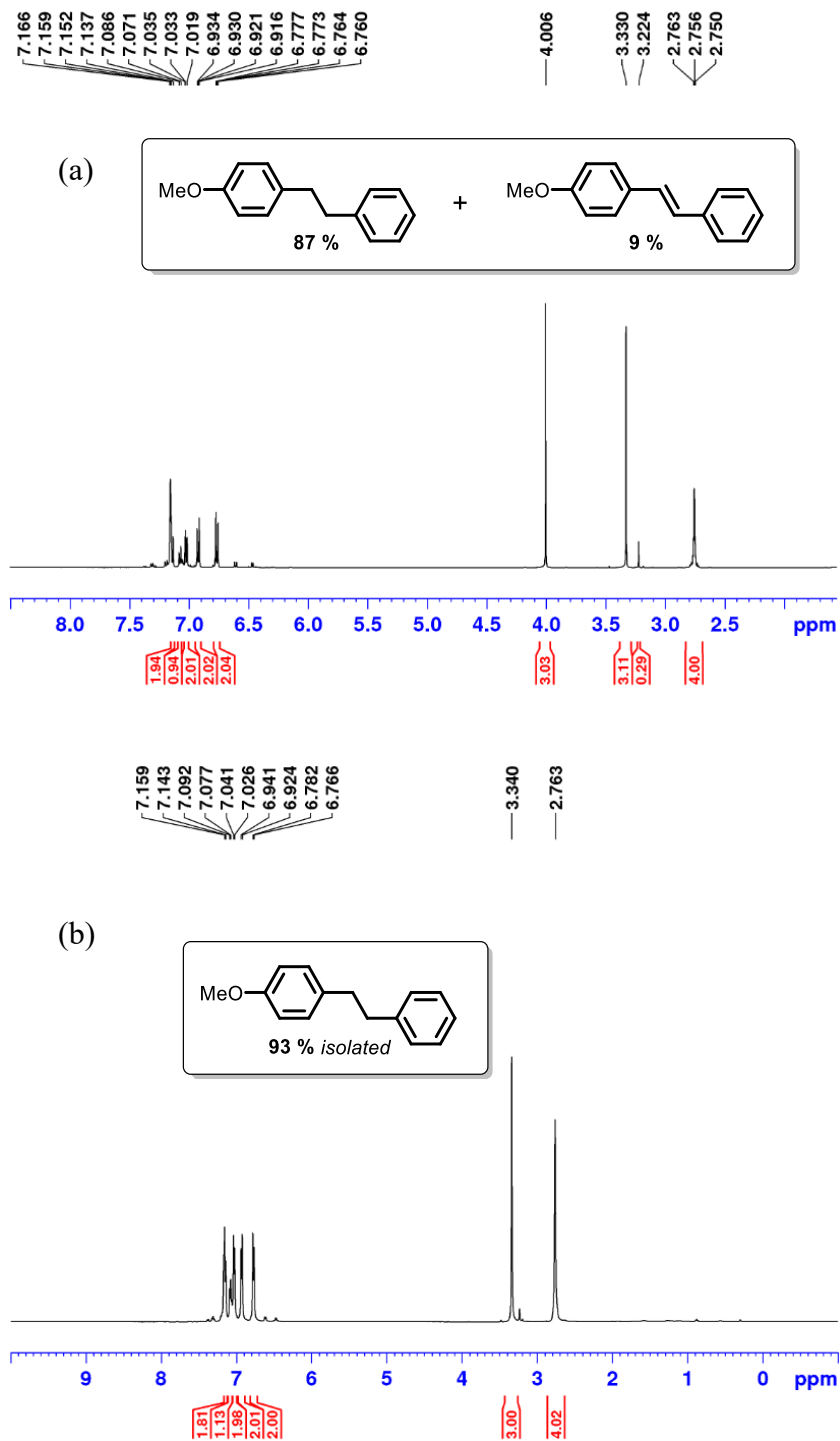
Figure C45. continued. (a) ^{1}H, (b) ^{1}H (isolated) and (c) ^{13}C{^{1}H} NMR spectrum (benzene-d_6) of 1-methoxy-4-(2-phenylethyl)-benzene.

(c)
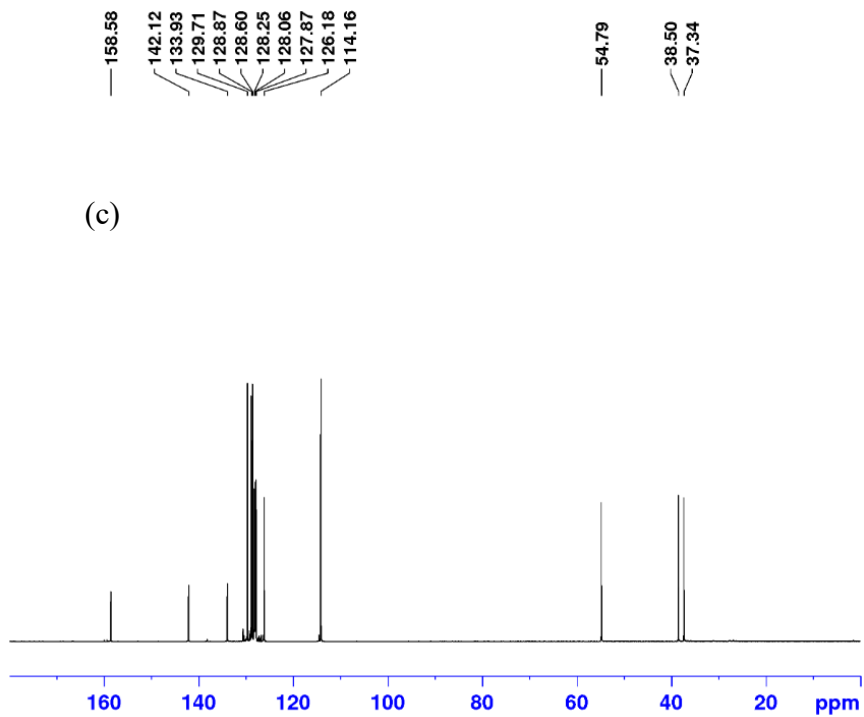
Figure C46. (a) ^{1}H and (b) ^{13}C{^{1}H} NMR spectrum (benzene-d_6) of 1-methoxy-3-(2-phenylethyl)-benzene.

Figure C47. (a) ^{1}H and (b) ^{13}C{^{1}H} NMR spectrum (benzene-d_6) of 1-methoxy-2-(2-phenylethyl)-benzene.
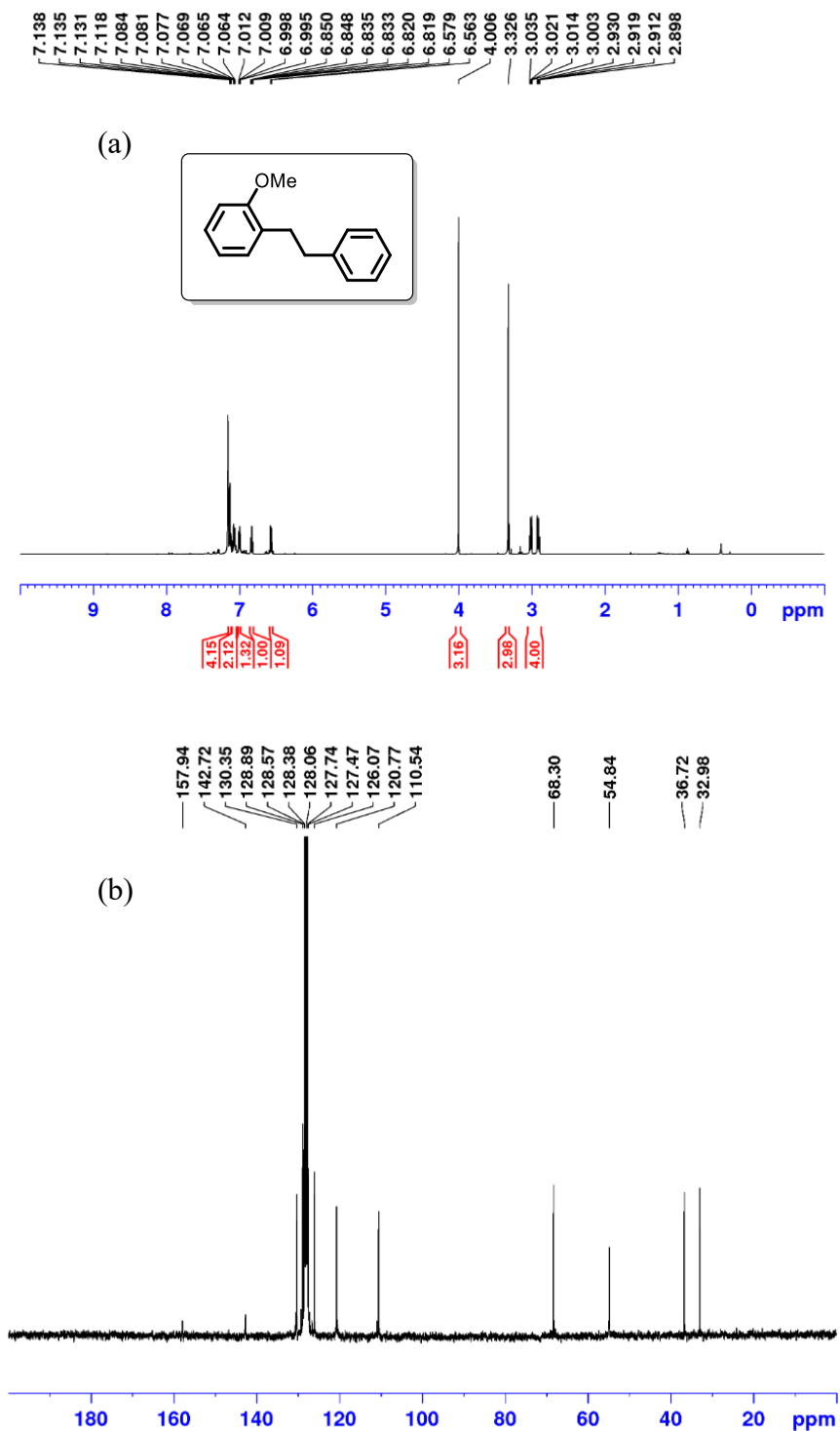
Figure C48. (a) ^{1}H and (b) ^{13}C{^{1}H} NMR spectrum (benzene-d_6) of 1-ethyl-4-[2-(4-methoxyphenyl)ethyl]-benzene.
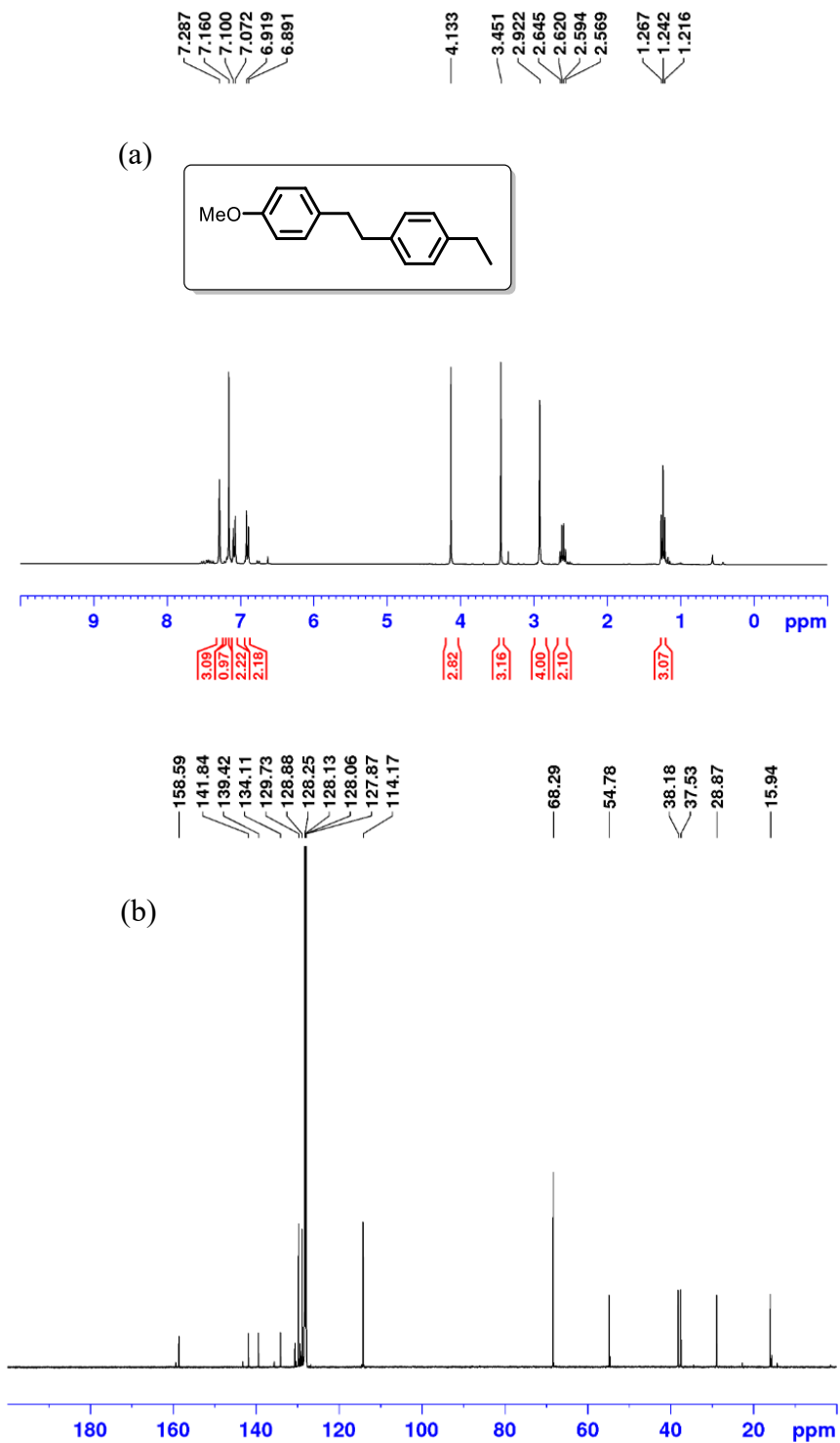
Figure C49. (a) ^{1}H and (b) ^{13}C{^{1}H} NMR spectrum (benzene-d_6) of 2-[4-[2-(4-methoxyphenyl)ethyl]phenyl]-4,4,5,5-tetramethyl-1,3,2-dioxaborolane.
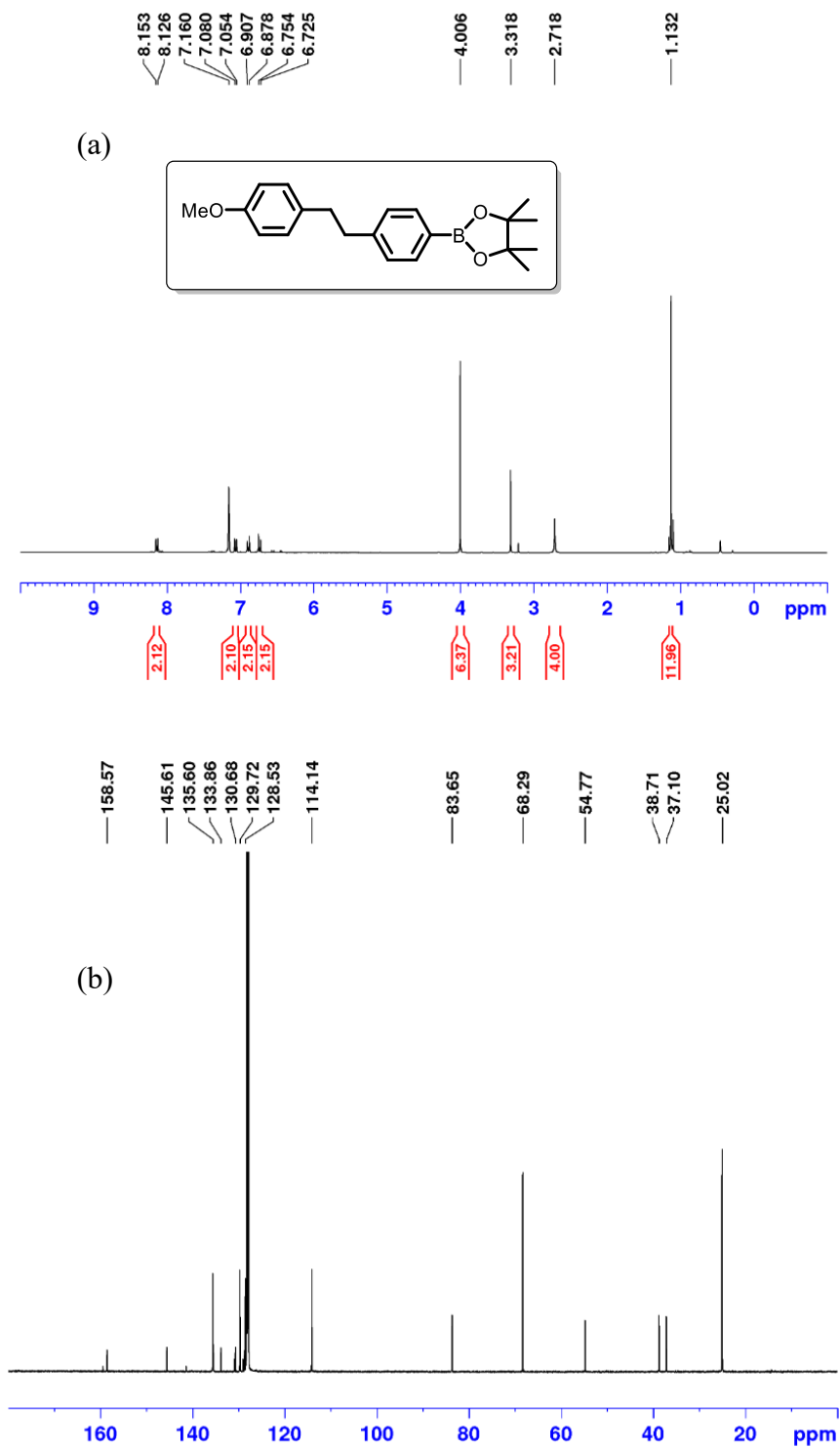
Figure C50. (a) ^{1}H and (b) ^{13}C{^{1}H} NMR spectrum (benzene-d_6) of 1-methyl-4-(2-phenylethyl)-benzene.
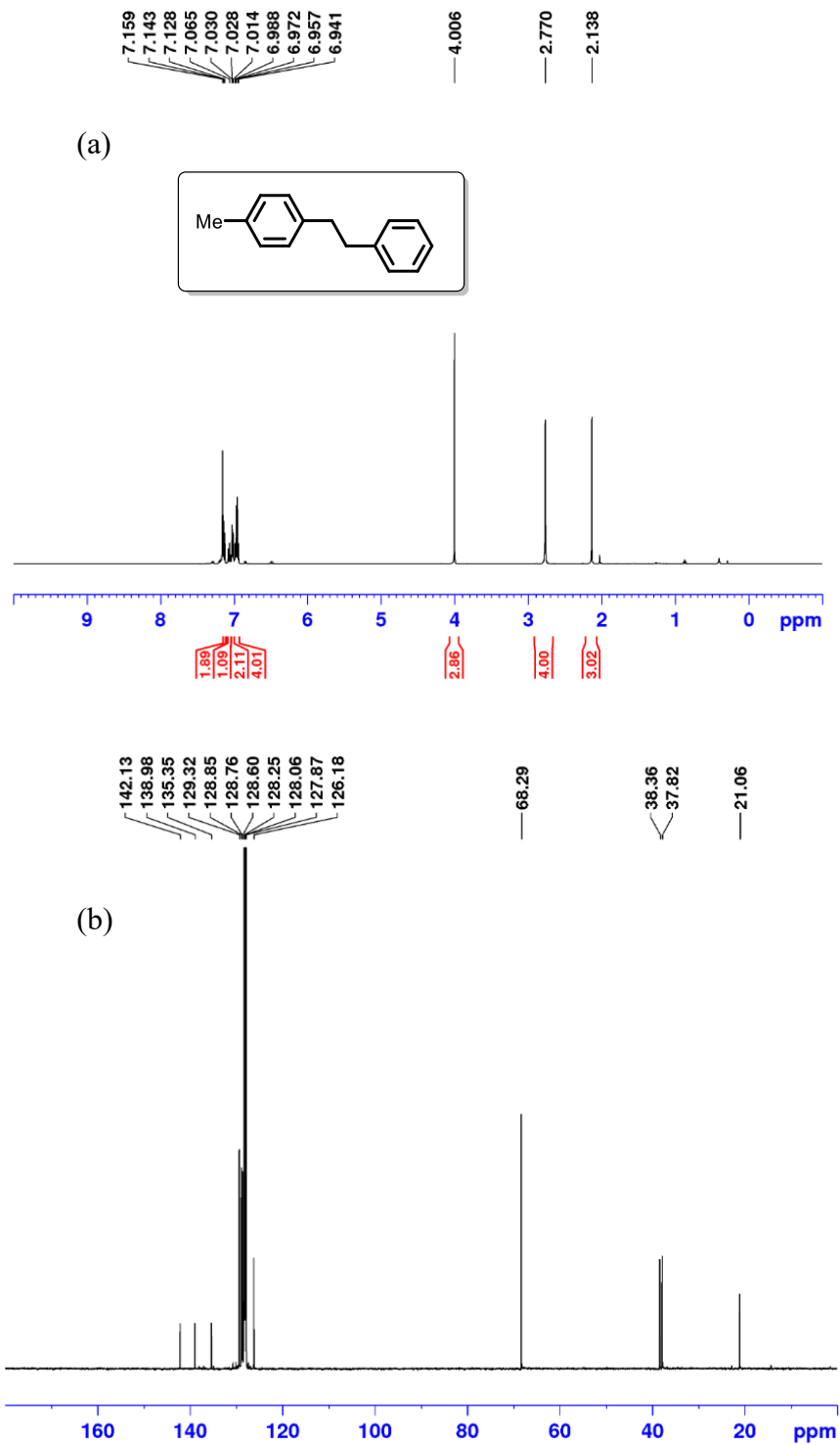
Figure C51. (a) ^{1}H and (b) ^{13}C{^{1}H} NMR spectrum (benzene-d_6) of 1-methyl-3-(2-phenylethyl)-benzene.
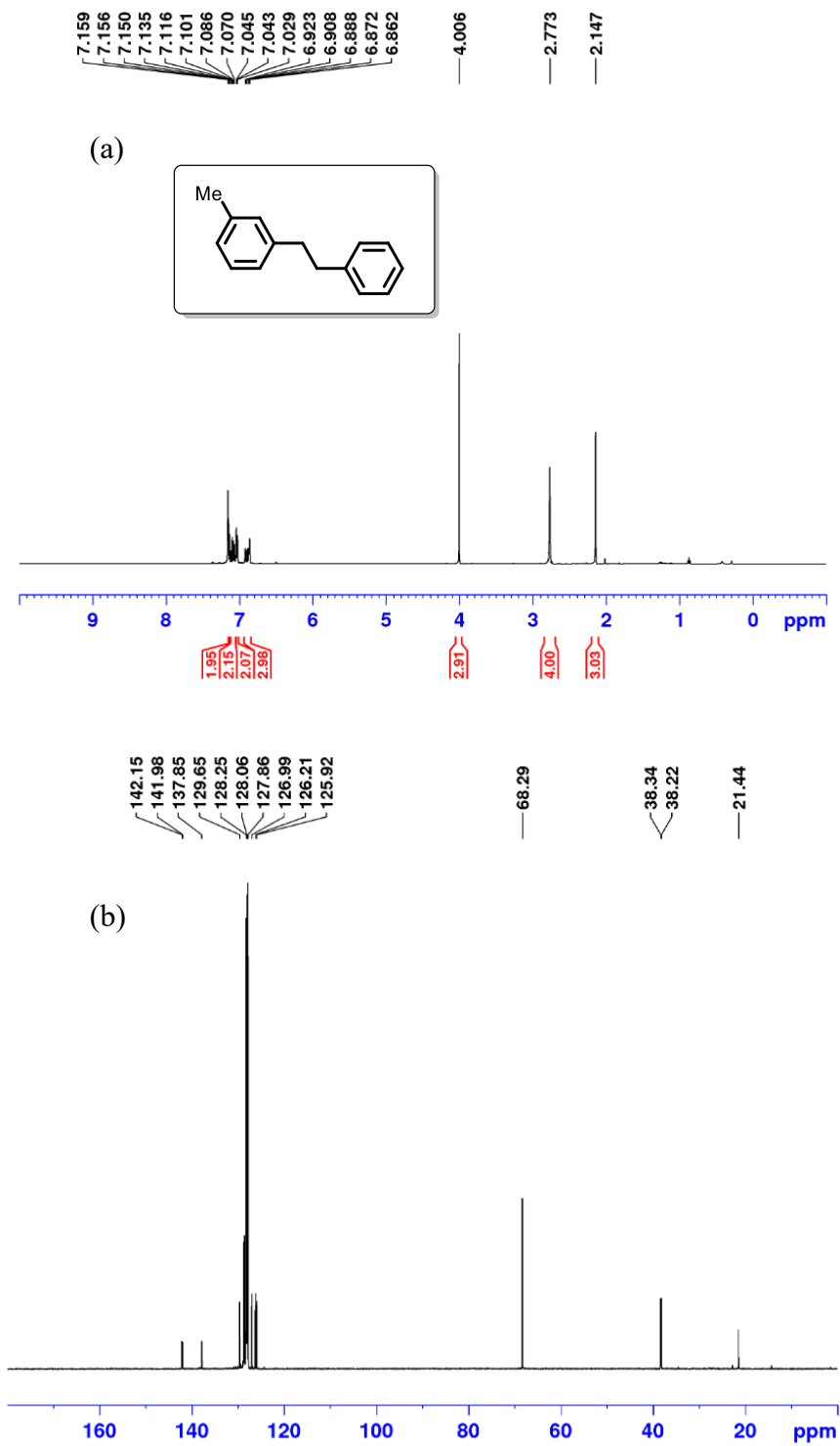
Figure C52. (a) ^{1}H and (b) ^{13}C{^{1}H} NMR spectrum (benzene-d_6) of 1,3-dimethyl-5-(2-phenylethyl)-benzene.
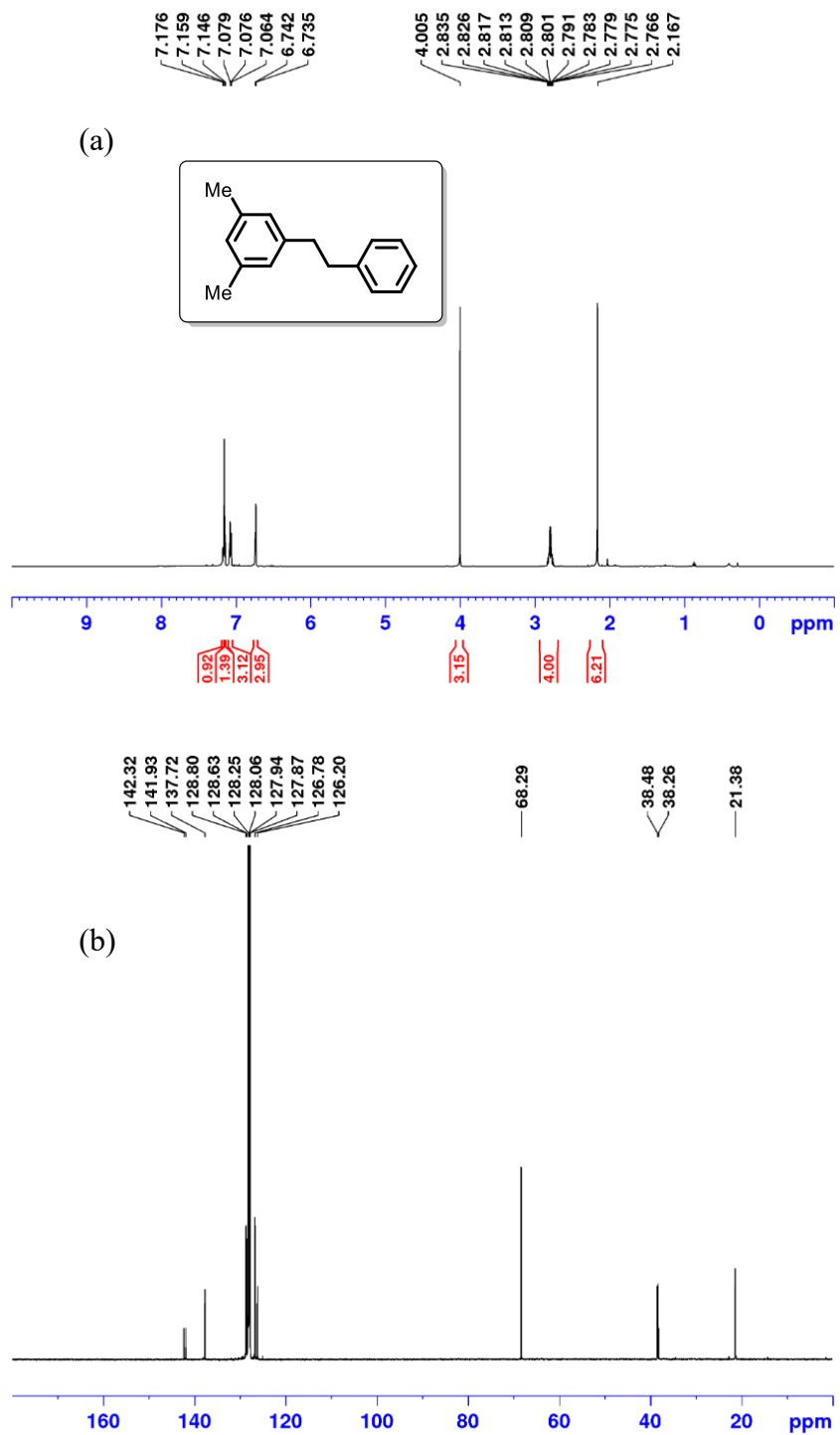
Figure C53. (a) ^{1}H and (b) ^{13}C{^{1}H} NMR spectrum (benzene-d_6) of 1-(1-methylethyl)-3-(2-phenylethyl)-benzene.
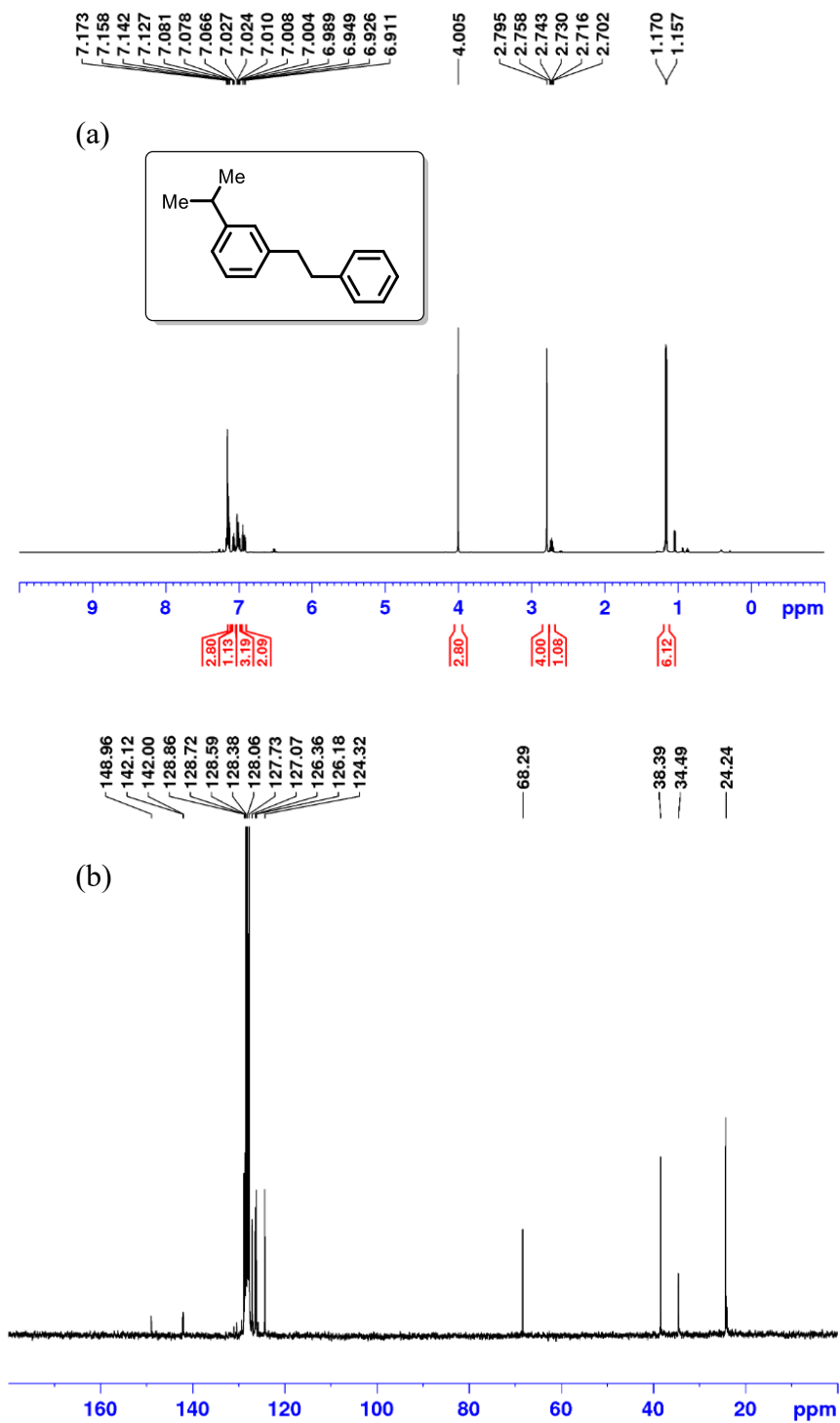
Figure C54. (a) ^{1}H and (b) ^{13}C{^{1}H} NMR spectrum (benzene-d_6) of 1-(1,1-dimethylethyl)-4-(2-phenylethyl)-benzene.
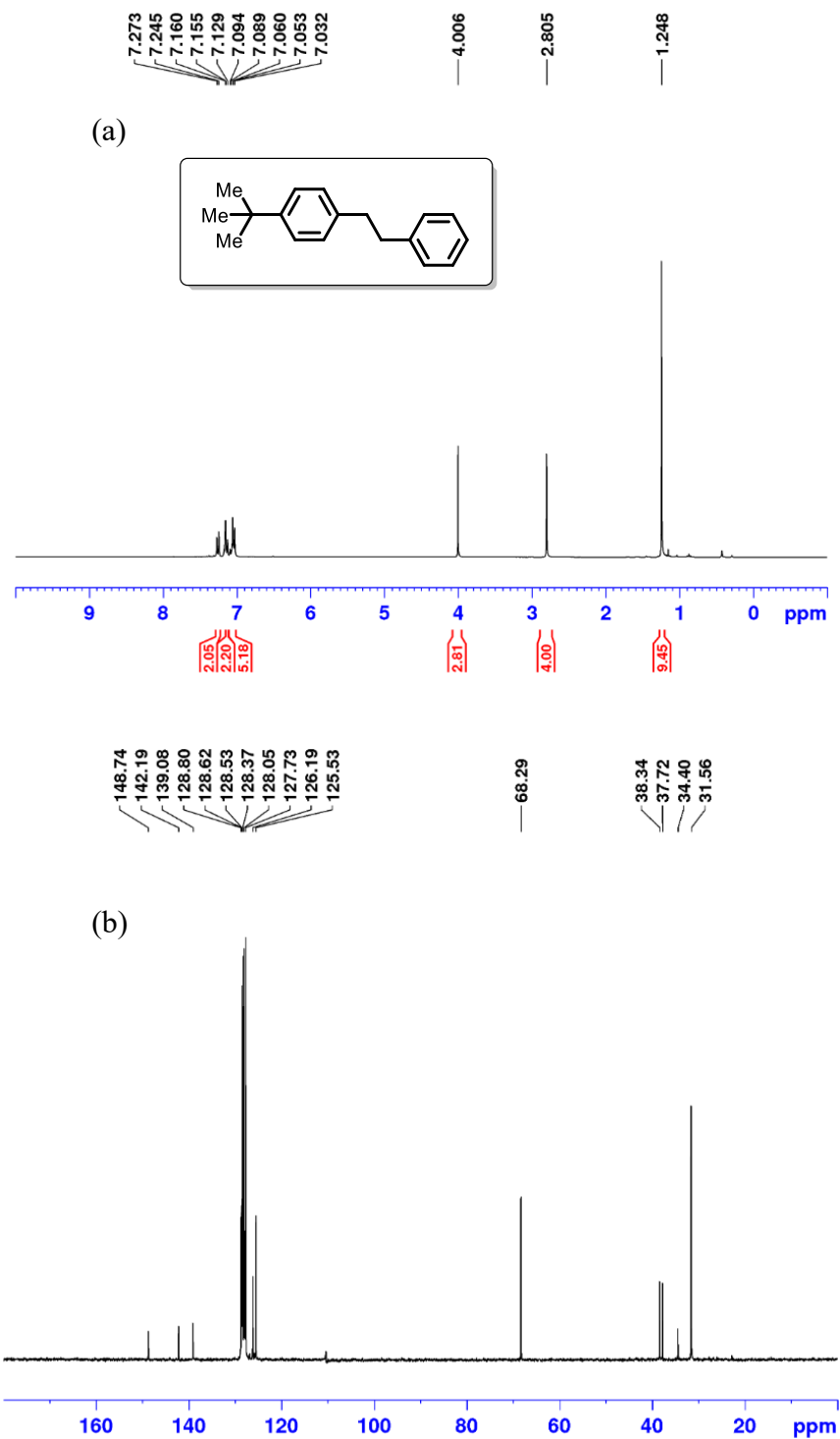
Figure C55. (a) ^{1}H, (b) ^{19}F{^{1}H} and (c) ^{13}C{^{1}H} NMR spectrum (benzene-d_6) of 1-(2-phenylethyl)-4-(trifluoromethyl)-benzene.
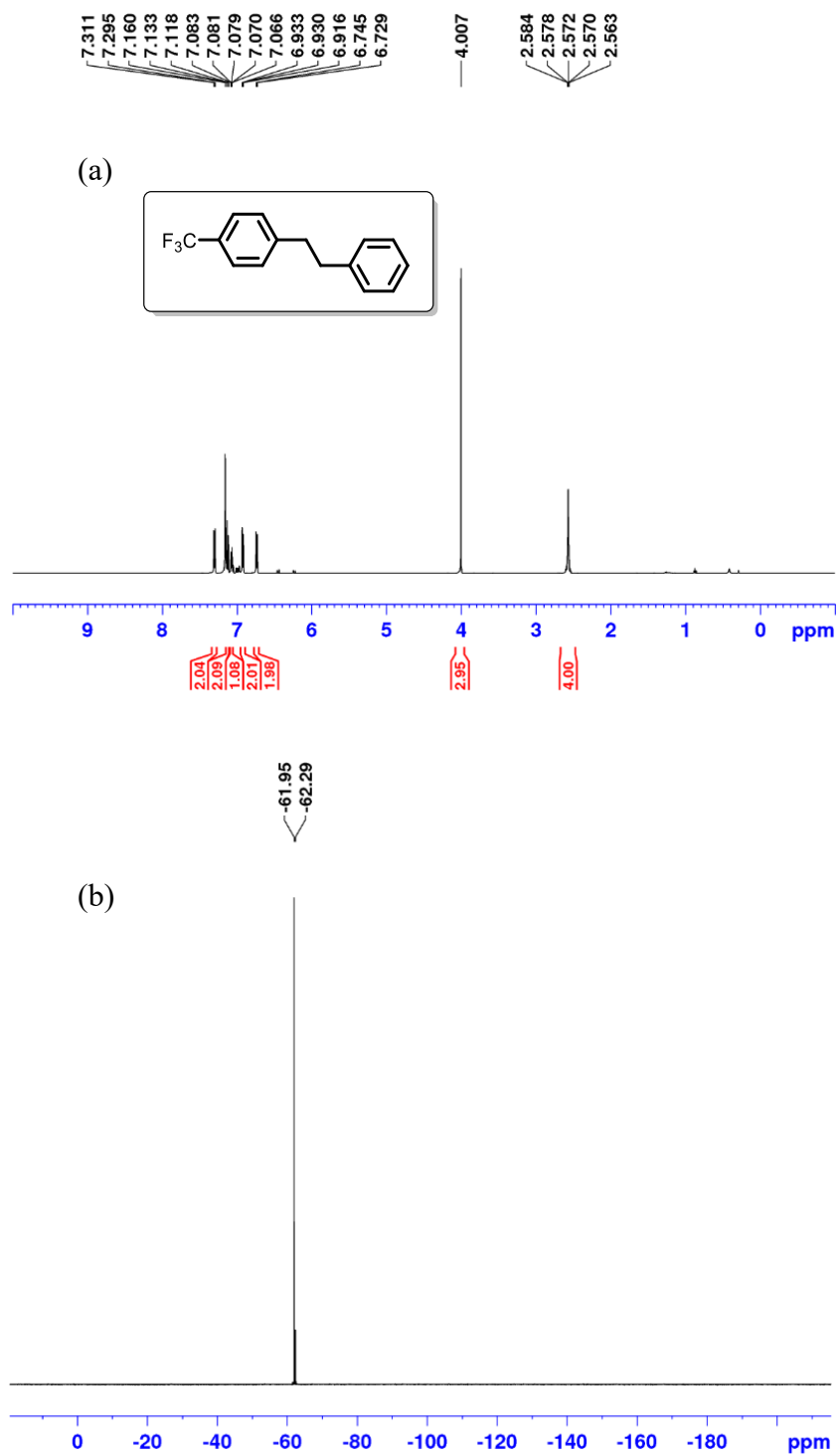
Figure C55. continued. (a) ^{1}H, (b) ^{19}F{^{1}H} and (c) ^{13}C{^{1}H} NMR spectrum (benzene-d_6) of 1-(2-phenylethyl)-4-(trifluoromethyl)-benzene.
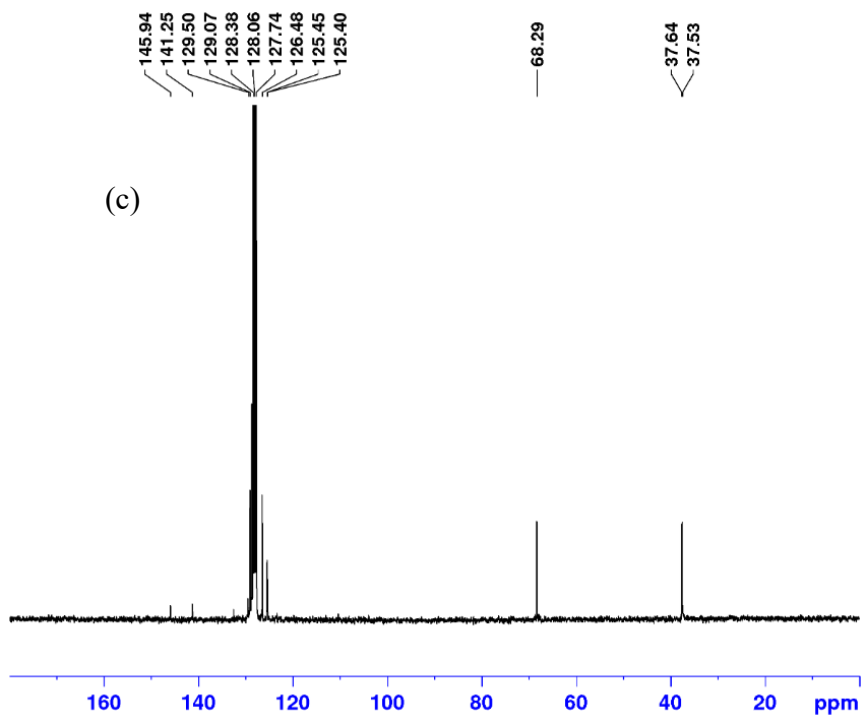
Figure C56. (a) ^{1}H, (b) ^{19}F{^{1}H} and (c) ^{13}C{^{1}H} NMR spectrum (benzene-d_6) of 1-(2-phenylethyl)-3-(trifluoromethyl)-benzene.
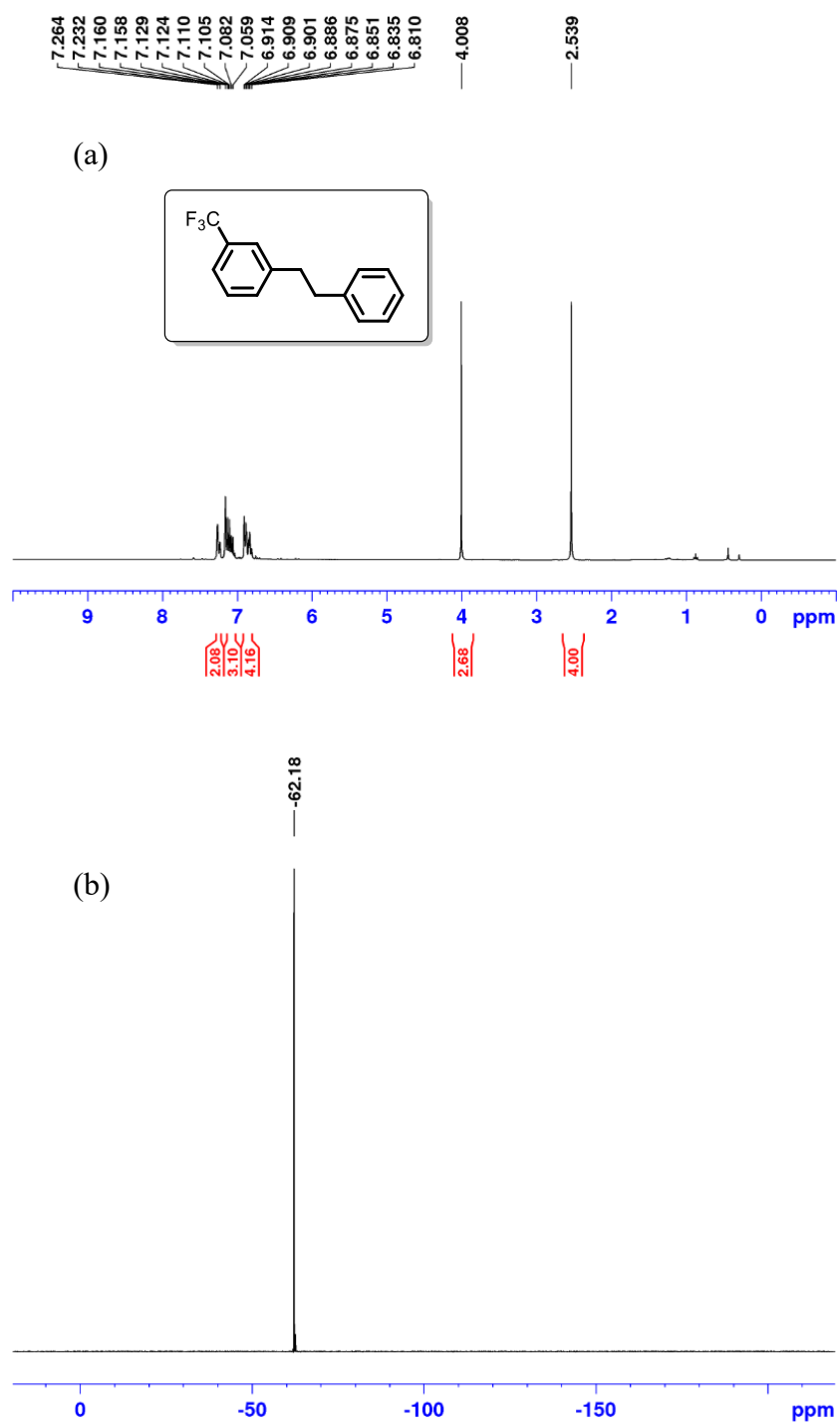
Figure C56. continued. (a) ^{1}H, (b) ^{19}F{^{1}H} and (c) ^{13}C{^{1}H} NMR spectrum (benzene-d_6) of 1-(2-phenylethyl)-3-(trifluoromethyl)-benzene.
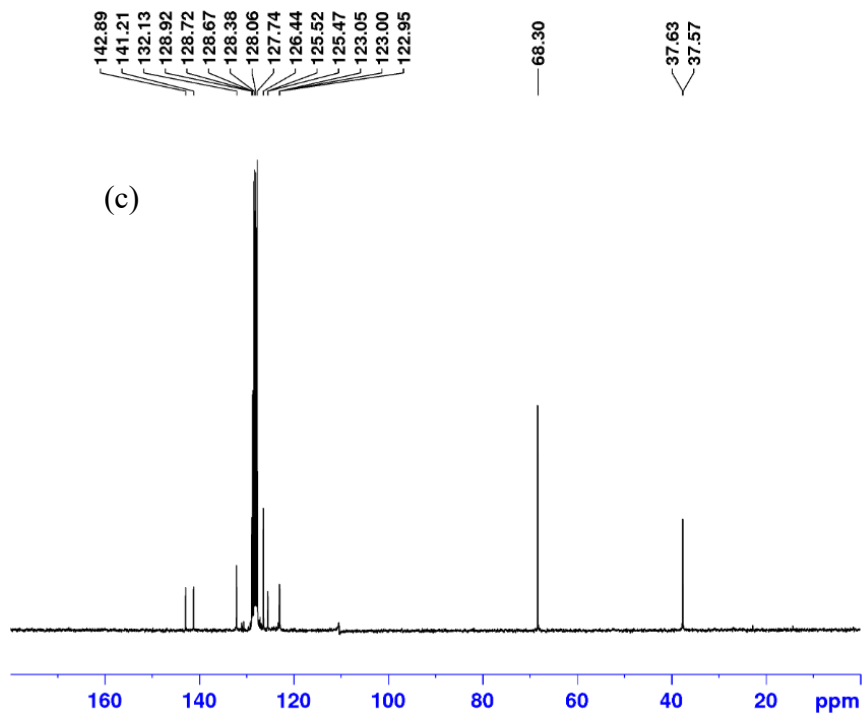
Figure C57. (a) ^{1}H, (b) ^{19}F{^{1}H} and (c) ^{13}C{^{1}H} NMR spectrum (benzene-d_6) of 1-(2-phenylethyl)-3,5-bis(trifluoromethyl)-benzene.
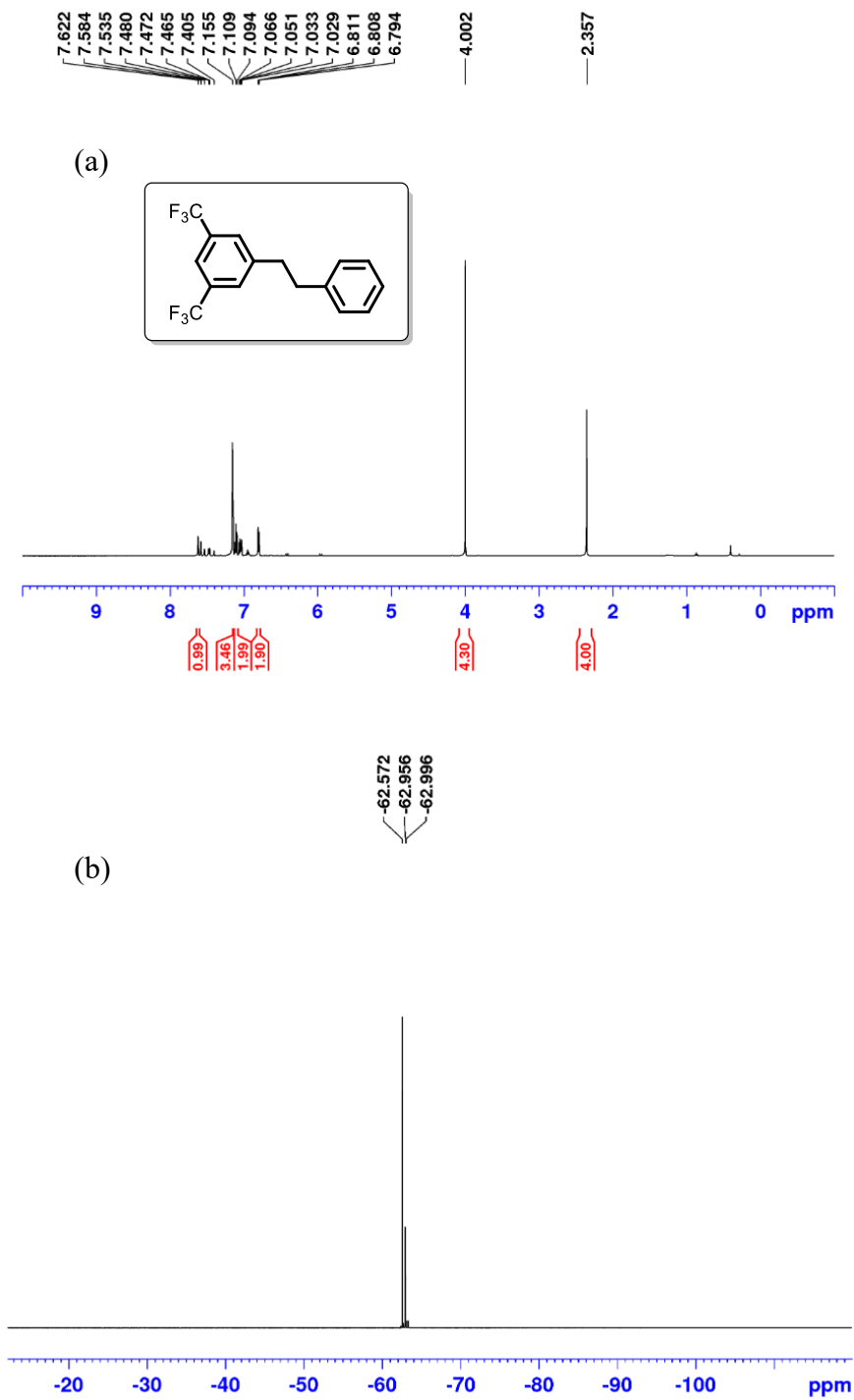
Figure C57. continued. (a) ^{1}H, (b) ^{19}F{^{1}H} and (c) ^{13}C{^{1}H} NMR spectrum (benzene-d_6) of 1-(2-phenylethyl)-3,5-bis(trifluoromethyl)-benzene.
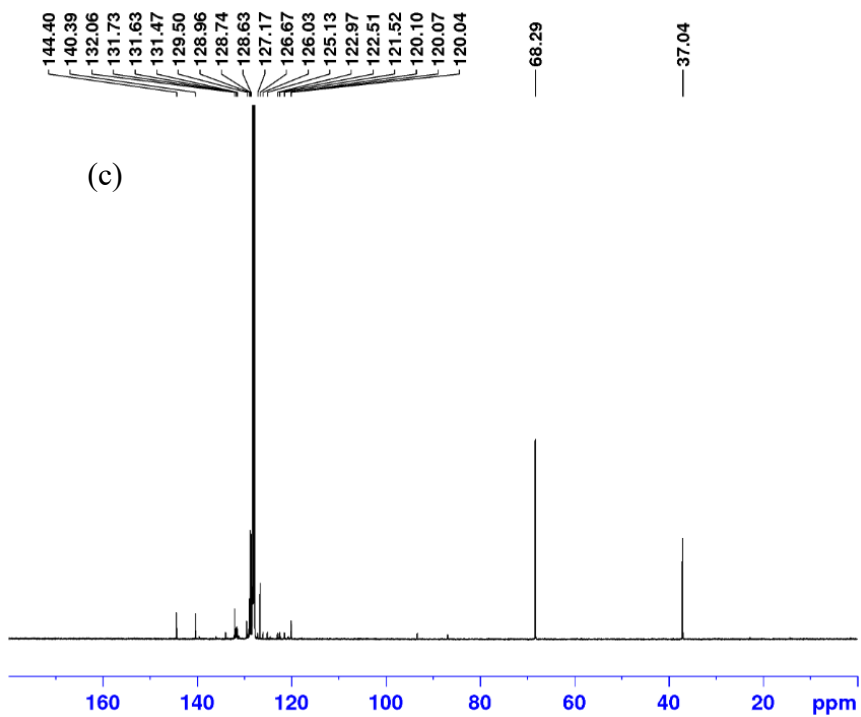
Figure C58. (a) ^{1}H, (b) ^{1}H (isolated), (c) ^{19}F{^{1}H} and (d) ^{13}C{^{1}H} NMR spectrum (benzene-d_6) of 1-fluoro-4-(2-phenylethyl)-benzene.
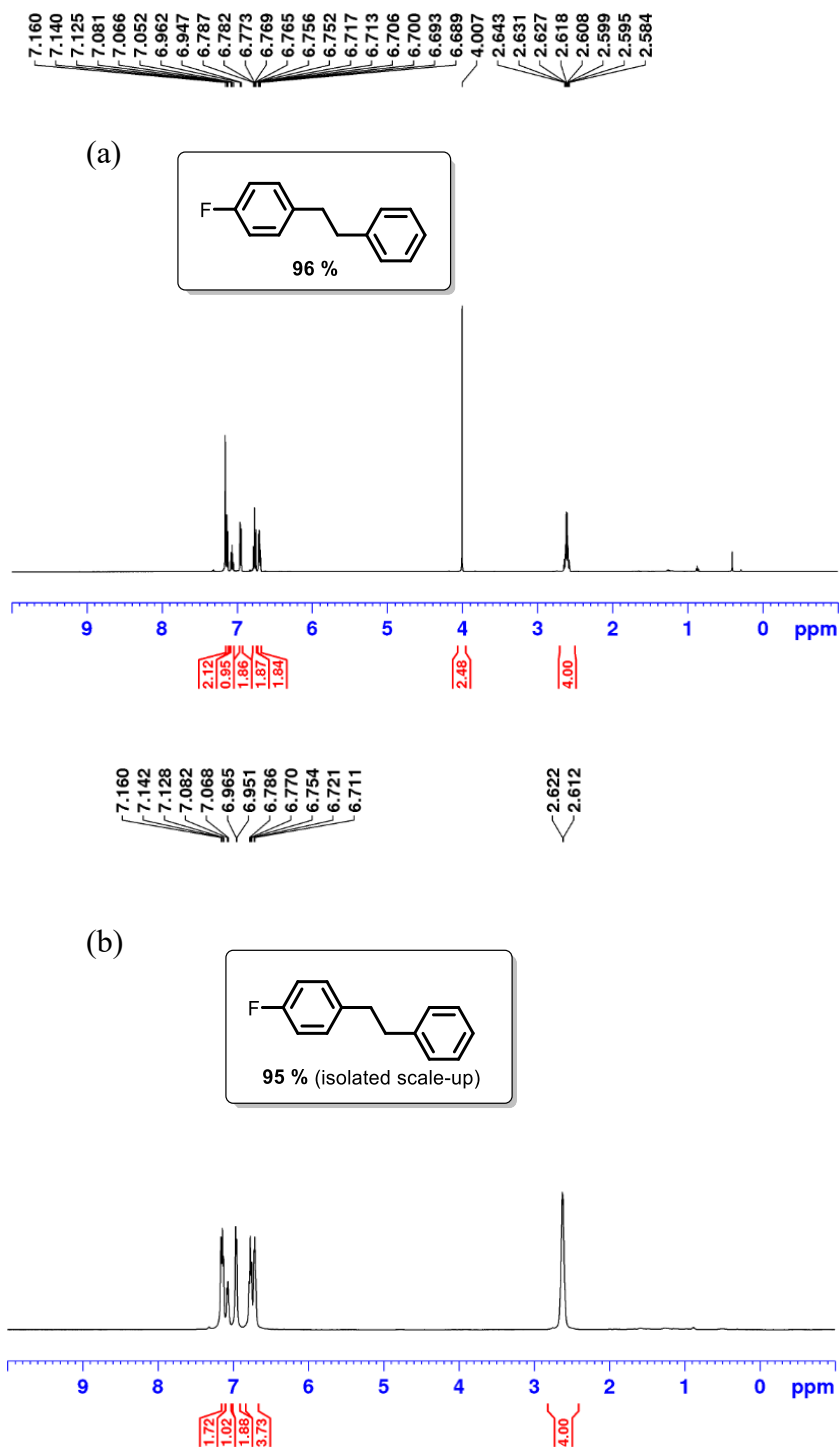
Figure C58. continued. (a) ¹H, (b) ¹H (isolated), (c) ¹⁹F{¹H} and (d) ¹³C{¹H} NMR spectrum (benzene-*d₆*) of 1-fluoro-4-(2-phenylethyl)-benzene.
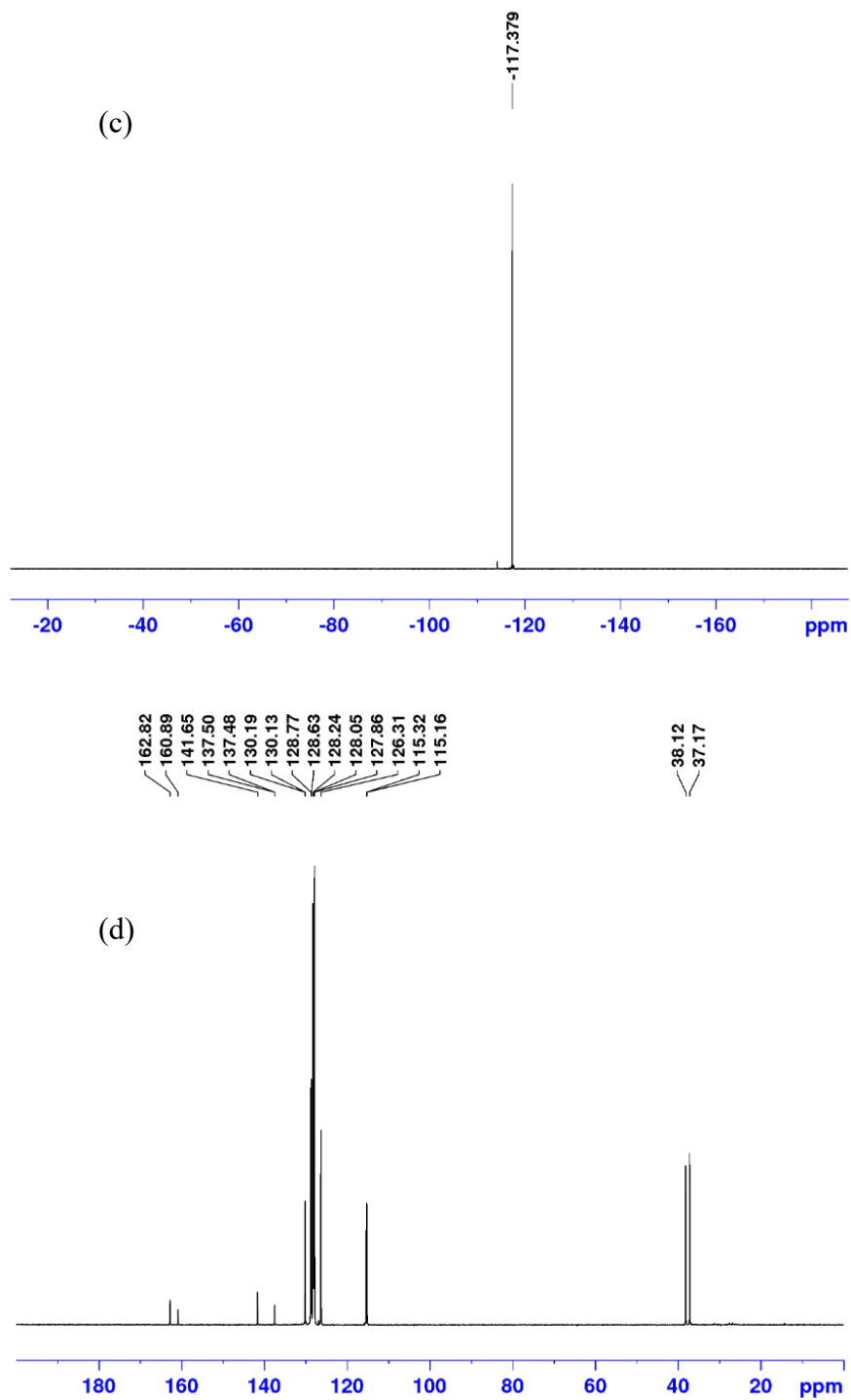
Figure C59. (a) ^{1}H, (b) ^{19}F{^{1}H} and (c) ^{13}C{^{1}H} NMR spectrum (benzene-d_6) of 1-fluoro-3-(2-phenylethyl)-benzene.

(a)

(b)
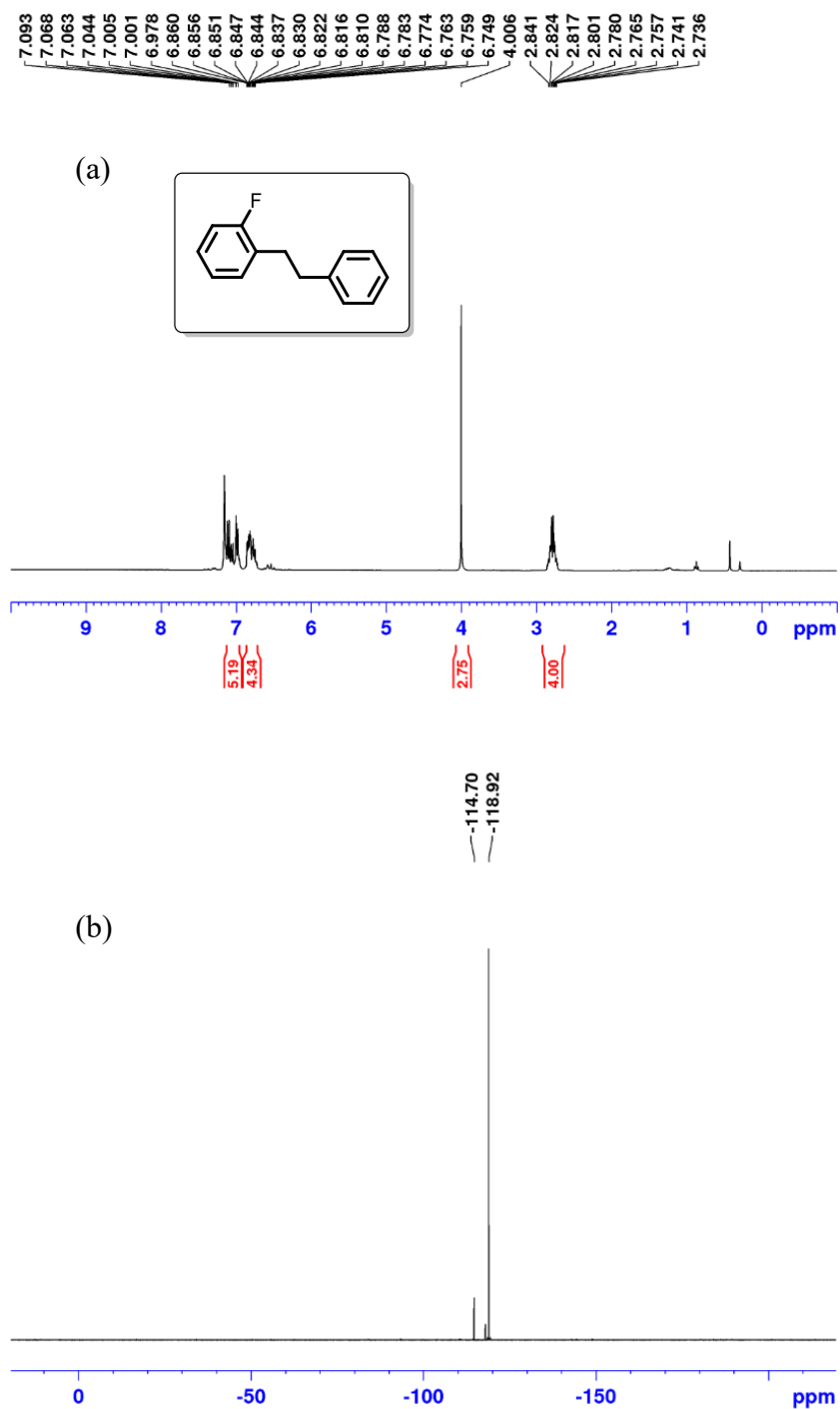
Figure C59. (a) ^{1}H, (b) ^{19}F{^{1}H} and (c) ^{13}C{^{1}H} NMR spectrum (benzene-d_6) of 1-fluoro-3-(2-phenylethyl)-benzene.

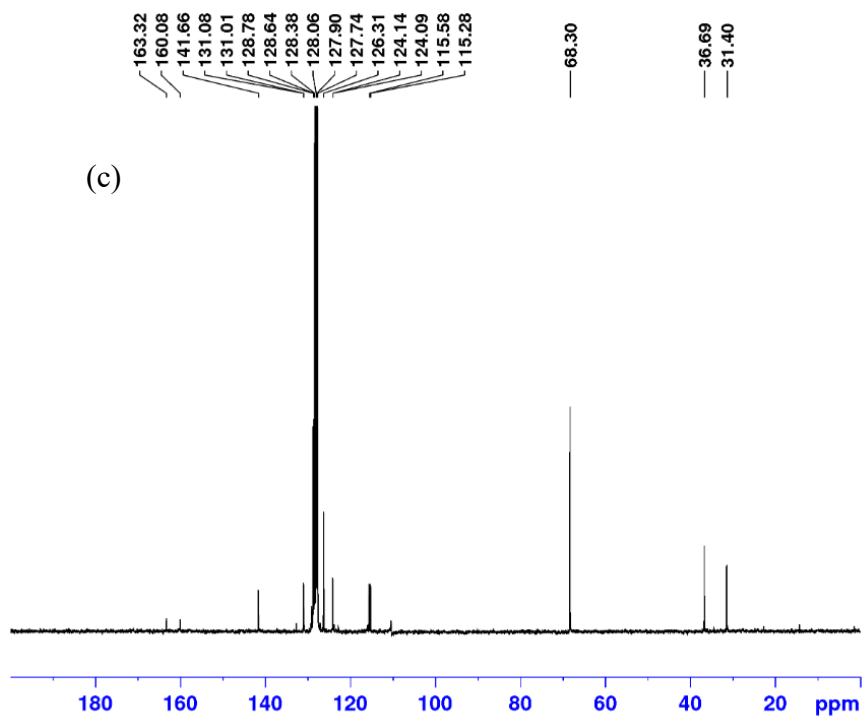**Figure C60.** (a) ^{1}H NMR spectrum (benzene-d_6). Conditions: 2.5 mol % dimer, 1 atm H$_2$, 30 °C, 4 hours, 0.0285 M, benzene-d_6.
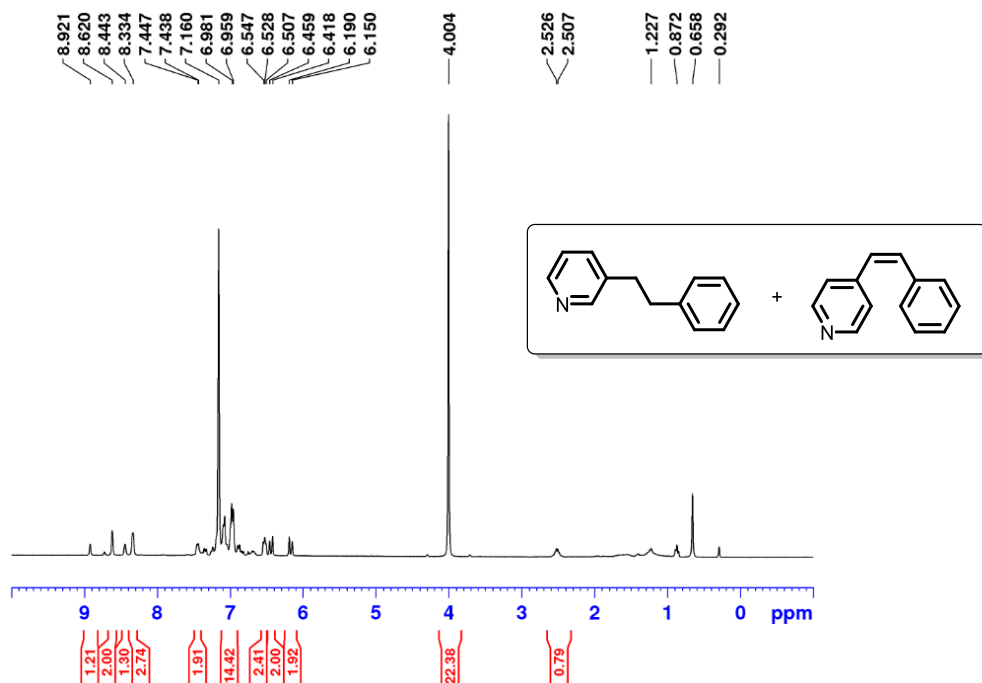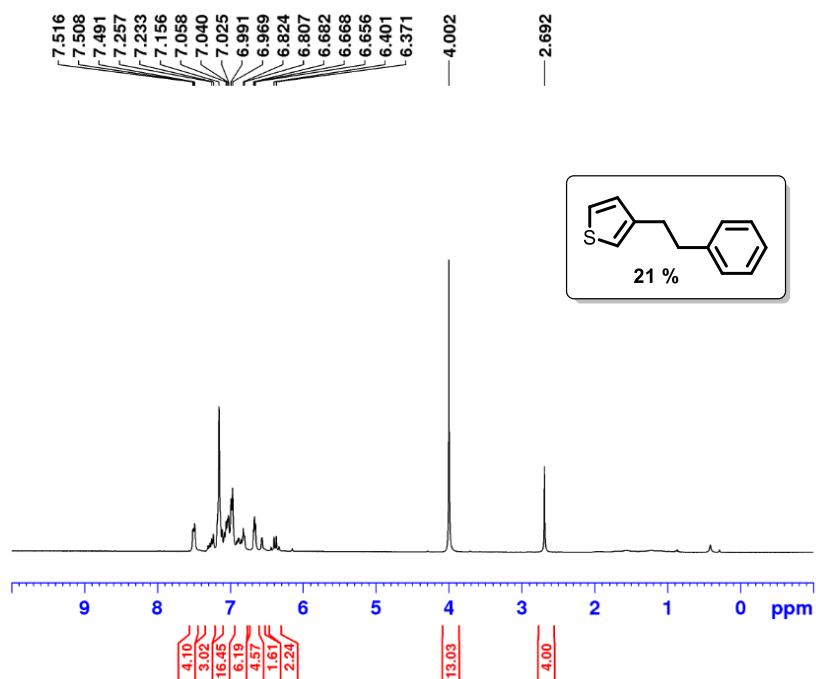

Figure C61. (a) ^{1}H NMR spectrum (benzene-d_6). Conditions: 2.5 mol % dimer, 10 atm H$_2$, 65 °C, 4 hrs, 0.57 M, benzene-d_6.

Appendix D: Chapter 5 Supporting Information

D-1: X-ray Crystallographic Data for Chapter 5

Table D1. Crystallographic Experimental Details for (^{i}Pr-PSiP^{Ind})FeCl(py) (**5-1**).

A. Crystal Data

formula	$C_{36}H_{50}ClFeN_3P_2Si$
formula weight	706.12
crystal dimensions (mm)	$0.31 \times 0.26 \times 0.03$
crystal system	monoclinic
space group	$P2_1/n$ (an alternate setting of $P2_1/c$ [No. 14])
unit cell parameters^a	
a (Å)	9.5653(9)
b (Å)	35.081(3)
c (Å)	10.7547(10)
β (deg)	97.3207(18)
V (Å^3)	3579.5(6)
Z	4
ρ_{calcd} (g cm^{-3})	1.310
μ (mm^{-1})	0.648

B. Data Collection and Refinement Conditions

diffractometer	Bruker PLATFORM/APEX II CCD^b
radiation (λ [Å])	graphite-monochromated Mo Kα (0.71073)
temperature (°C)	–80
scan type	ω scans (0.3°) (30 s exposures)
data collection 2θ limit (deg)	51.36
total data collected	24456 (-11 $\leq h \leq$ 11, -42 $\leq k \leq$ 42, -13 $\leq l \leq$ 13)
independent reflections	6788 (R_{int} = 0.0803)
number of observed reflections (*NO*)	4683 [$F_o^2 \geq 2\sigma(F_o^2)$]
structure solution method	intrinsic phasing (*SHELXT-2014^c*)
refinement method	full-matrix least-squares on F^2 (*SHELXL–2017^d*)
absorption correction method	Gaussian integration (face-indexed)
range of transmission factors	1.0000–0.8310
data/restraints/parameters	6788 / 0 / 400
goodness-of-fit (*S*)^e [all data]	1.020
final *R* indices^f	
R_1 [$F_o^2 \geq 2\sigma(F_o^2)$]	0.0498
wR_2 [all data]	0.1298

Table D1. Crystallographic Experimental Details for (^{i}Pr-PSiP^{Ind})FeCl(py) (**5-1**) (continued).

largest difference peak and hole   0.611 and –0.338 e Å^{-3}

[a]Obtained from least-squares refinement of 3150 reflections with $4.44° < 2\theta < 43.86°$.

[b]Programs for diffractometer operation, data collection, data reduction and absorption correction were those supplied by Bruker. (continued)

[c]Sheldrick, G. M. *Acta Crystallogr.* **2015**, *A71*, 3–8. (*SHELXT-2014*)

[d]Sheldrick, G. M. *Acta Crystallogr.* **2015**, *C71*, 3–8. (*SHELXL-2017*)

[e]$S = [\Sigma w(F_o^2 – F_c^2)^2/(n – p)]^{1/2}$ (n = number of data; p = number of parameters varied; $w = [\sigma^2(F_o^2) + (0.0512P)^2 + 2.3393P]^{-1}$ where $P = [\text{Max}(F_o^2, 0) + 2F_c^2]/3$).

[f]$R_1 = \Sigma||F_o| – |F_c||/\Sigma|F_o|$; $wR_2 = [\Sigma w(F_o^2 – F_c^2)^2/\Sigma w(F_o^4)]^{1/2}$.

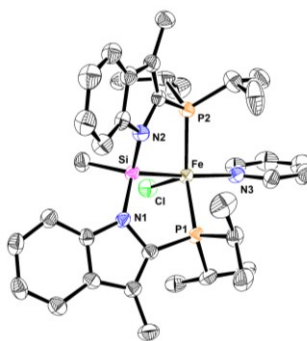**Figure D1.** ORTEP diagram of (^{i}Pr-PSiP^{Ind})FeCl(py) (**5-1**).

Table D2. Crystallographic Experimental Details for (^{i}Pr-PSiP^{Ind})FeH(N$_2$)$_2$ (**5-2**).

A. Crystal Data

formula	C$_{31}$H$_{46}$FeN$_6$P$_2$Si
formula weight	648.62
crystal dimensions (mm)	0.27 × 0.24 × 0.11
crystal system	orthorhombic
space group	$P2_12_12_1$ (No. 19)

Table D2. Crystallographic Experimental Details for (^{i}Pr-PSiP^{Ind})FeH(N$_2$)$_2$ (**5-2**) (continued).

unit cell parameters^a

a (Å)	10.7118(5)
b (Å)	16.7593(8)
c (Å)	18.7511(9)
V (Å^3)	3366.2(3)
Z	4
ρ_{calcd} (g cm^{-3})	1.280
μ (mm^{-1})	0.609

B. Data Collection and Refinement Conditions (continued)

diffractometer	Bruker PLATFORM/APEX II CCD^b
radiation (λ [Å])	graphite-monochromated Mo Kα (0.71073)
temperature (°C)	−80
scan type	ω scans (0.3°) (20 s exposures)
data collection 2θ limit (deg)	61.19
total data collected	116263 ($-15 \leq h \leq 15$, $-23 \leq k \leq 23$, $-26 \leq l \leq 26$)
independent reflections	10334 ($R_{int} = 0.0664$)
number of observed reflections (*NO*)	8917 [$F_o^2 \geq 2\sigma(F_o^2)$]
structure solution method	intrinsic phasing (*SHELXT-2014^c*)
refinement method	full-matrix least-squares on F^2 (*SHELXL–2017^d*)
absorption correction method	Gaussian integration (face-indexed)
range of transmission factors	0.9523–0.8689
data/restraints/parameters	10334 / 0 / 383
Flack absolute structure parameter^e	-0.018(5)
goodness-of-fit (*S*)^f [all data]	1.046
final *R* indices^g	
R_1 [$F_o^2 \geq 2\sigma(F_o^2)$]	0.0391
wR_2 [all data]	0.1034
largest difference peak and hole	0.612 and -0.294 e Å^{-3}

^{a}Obtained from least-squares refinement of 9054 reflections with 4.38° < 2θ < 49.56°.

^{b}Programs for diffractometer operation, data collection, data reduction and absorption correction were those supplied by Bruker.

^{c}Sheldrick, G. M. *Acta Crystallogr.* **2015**, *A71*, 3–8. (*SHELXT-2014*)

^{d}Sheldrick, G. M. *Acta Crystallogr.* **2015**, *C71*, 3–8. (*SHELXL-2017*)

Table D2. Crystallographic Experimental Details for (^{i}Pr-PSiP^{Ind})FeH(N$_2$)$_2$ (**5-2**) (continued).

^{e}Flack, H. D. *Acta Crystallogr.* **1983**, *A39*, 876–881; Flack, H. D.; Bernardinelli, G. *Acta Crystallogr.* **1999**, *A55*, 908–915; Flack, H. D.; Bernardinelli, G. *J. Appl. Cryst.* **2000**, *33*, 1143–1148. The Flack parameter will refine to a value near zero if the structure is in the correct configuration and will refine to a value near one for the inverted configuration.

$^f S = [\Sigma w(F_o^2 - F_c^2)^2/(n - p)]^{1/2}$ (n = number of data; p = number of parameters varied; $w = [\sigma^2(F_o^2) + (0.0576P)^2 + 0.4523P]^{-1}$ where $P = [\text{Max}(F_o^2, 0) + 2F_c^2]/3$).

$^g R_1 = \Sigma||F_o| - |F_c||/\Sigma|F_o|$; $wR_2 = [\Sigma w(F_o^2 - F_c^2)^2/\Sigma w(F_o^4)]^{1/2}$.

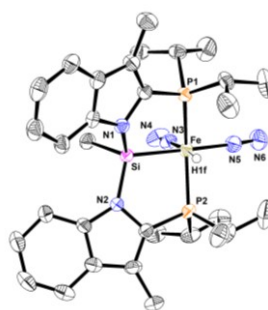**Figure D2.** ORTEP diagram for (^{i}Pr-PSiP^{Ind})FeH(N$_2$)$_2$ (**5-2**).

Table D3. Crystallographic Experimental Details for **5-3**.

A. Crystal Data

formula	$C_{45}H_{63}Fe_2N_3P_3$
formula weight	850.59
crystal dimensions (mm)	$0.19 \times 0.10 \times 0.03$
crystal system	triclinic
space group	$P\bar{1}$ (No. 2)
unit cell parameters^a	
a (Å)	12.9508(6)
b (Å)	18.5784(10)
c (Å)	19.2923(9)
α (deg)	99.533(4)
β (deg)	97.551(4)
γ (deg)	104.765(3)

Table D3. Crystallographic Experimental Details for **5-3** (continued).

V (Å^3)	4352.6(4)
Z	4
ρ_{calcd} (g cm^{-3})	1.298
μ (mm^{-1})	6.639

B. Data Collection and Refinement Conditions

diffractometer	Bruker D8/APEX II CCD[b]
radiation (λ [Å])	Cu Kα (1.54178) (microfocus source)
temperature (°C)	−100
scan type	ω and ϕ scans (1.0°) (5 s exposures)
data collection 2θ limit (deg)	148.53
total data collected	138057 ($-16 \leq h \leq 16$, $-23 \leq k \leq 23$, $-23 \leq l \leq 23$)
independent reflections	17037 (R_{int} = 0.0816)
number of observed reflections (*NO*)	13424 [$F_o^2 \geq 2\sigma(F_o^2)$] (continued)
structure solution method	intrinsic phasing (*SHELXT-2014*[c])
refinement method	full-matrix least-squares on F^2 (*SHELXL–2018*[d])
absorption correction method	multi-scan (*SADABS*)
range of transmission factors	0.7538–0.5037
data/restraints/parameters	17037 / 0 / 959
goodness-of-fit (*S*)[e] [all data]	1.017
final *R* indices[f]	
R_1 [$F_o^2 \geq 2\sigma(F_o^2)$]	0.0404
wR_2 [all data]	0.1014
largest difference peak and hole	0.991 and −0.390 e Å^{-3}

[a]Obtained from least-squares refinement of 3226 reflections with $4.72° < 2\theta < 137.68°$.

[b]Programs for diffractometer operation, data collection, data reduction and absorption correction were those supplied by Bruker.

[c]Sheldrick, G. M. *Acta Crystallogr.* **2015**, *A71*, 3–8. (*SHELXT-2014*)

[d]Sheldrick, G. M. *Acta Crystallogr.* **2015**, *C71*, 3–8. (*SHELXL-2018/3*)

[e]$S = [\Sigma w(F_o^2 - F_c^2)^2/(n - p)]^{1/2}$ (*n* = number of data; *p* = number of parameters varied; *w* = $[\sigma^2(F_o^2) + (0.0236P)^2 + 137.68 P]^{-1}$ where $P = [\text{Max}(F_o^2, 0) + 2F_c^2]/3$).

[f]$R_1 = \Sigma||F_o| - |F_c||/\Sigma|F_o|$; $wR_2 = [\Sigma w(F_o^2 - F_c^2)^2/\Sigma w(F_o^4)]^{1/2}$.
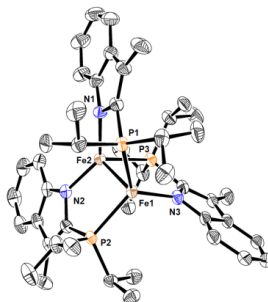
Figure D3. ORTEP diagram of **5-3**.

Table D4. Crystallographic Experimental Details for [(^{i}Pr-PSiP^{Ind})FeBr]$_2$MgBr$_2$(THF) (**5-4**).

A. Crystal Data

formula	$C_{71}H_{110}Br_4Fe_2MgN_4OP_4Si_2$
formula weight	1671.33
crystal dimensions (mm)	$0.15 \times 0.06 \times 0.03$
crystal system	monoclinic
space group	$C2/c$ (No. 15)
unit cell parameters^a	
a (Å)	26.7081(15)
b (Å)	15.3155(9)
c (Å)	20.2305(12)
β (deg)	105.894(5)
V (Å^3)	7958.9(8)
Z	4
ρ_{calcd} (g cm^{-3})	1.395
μ (mm^{-1})	6.721

B. Data Collection and Refinement Conditions

diffractometer	Bruker D8/APEX II CCD^b
radiation (λ [Å])	Cu Kα (1.54178) (microfocus source)
temperature (°C)	–100
scan type	ω and ϕ scans (1.0°) (5-15-30 s exposures)^c

Table D4. Crystallographic Experimental Details for [(^{i}Pr-PSiP^{Ind})FeBr]$_2$MgBr$_2$(THF) (**5-4**) (continued).

data collection 2θ limit (deg)	141.40
total data collected	44311 (-32 $\leq h \leq$ 32, -18 $\leq k \leq$ 18, -24 $\leq l \leq$ 23)
independent reflections	7584 (R_{int} = 0.1418)
number of observed reflections (*NO*)	3952 [$F_o^2 \geq 2\sigma(F_o^2)$]
structure solution method	intrinsic phasing (*SHELXT-2014^d*)
refinement method	full-matrix least-squares on F^2 (*SHELXL–2018^e*)
absorption correction method	Gaussian integration (face-indexed)
range of transmission factors	0.8967--0.4921
data/restraints/parameters	7584 / 74^f / 466
goodness-of-fit (S)^g [all data]	1.103
final R indices^h	
$\quad R_1$ [$F_o^2 \geq 2\sigma(F_o^2)$]	0.0780
$\quad wR_2$ [all data]	0.1826
largest difference peak and hole	0.447 and $-$0.559 e Å^{-3}

^{a}Obtained from least-squares refinement of 2887 reflections with $6.72° < 2\theta < 138.84°$.

^{b}Programs for diffractometer operation, data collection, data reduction and absorption correction were those supplied by Bruker.

^{c}Data were collected with the detector set at three different positions. Low-angle (detector $2\theta = -33°$) data frames were collected using a scan time of 5 s, medium-angle (detector $2\theta = 75°$) frames using a scan time of 15 s, and high-angle (detector $2\theta = 117°$) frames using a scan time of 30 s.

^{d}Sheldrick, G. M. *Acta Crystallogr.* **2015**, *A71*, 3–8. (*SHELXT-2014*)

^{e}Sheldrick, G. M. *Acta Crystallogr.* **2015**, *C71*, 3–8. (*SHELXL-2018/3*)

^{f}The corresponding P–C, C–C, P$\cdots$C, and C$\cdots$C distances within both components of the disordered isopropyl group were restrained to be approximately equal by use of the *SHELXL* **SADI** instruction. Additionally, the rigid-bond restraint (**RIGU**) was applied to improve the quality of the anisotropic displacement parameters of the carbon atoms of the disordered isopropyl group. The rigid-bond restraint was also applied to the carbon atom ADPs of the disordered tetrahydrofuran molecule. Finally, the disordered solvent pentane molecule was restrained by both **SADI** (C–C and C$\cdots$C distances) and **RIGU**.

$^g S = [\Sigma w(F_o^2 - F_c^2)^2/(n - p)]^{1/2}$ (n = number of data; p = number of parameters varied; $w = [\sigma^2(F_o^2) + (0.0001P)^2 + 61.9536P]^{-1}$ where $P = [\text{Max}(F_o^2, 0) + 2F_c^2]/3$).

$^h R_1 = \Sigma||F_o| - |F_c||/\Sigma|F_o|$; $wR_2 = [\Sigma w(F_o^2 - F_c^2)^2/\Sigma w(F_o^4)]^{1/2}$.
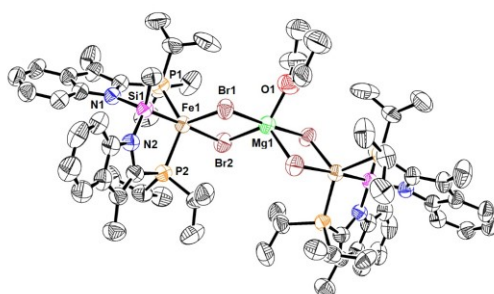
Figure D4. ORTEP diagram for [(^{i}Pr-PSiP^{Ind})FeBr]$_2$MgBr$_2$(THF) (**5-4**).

Table D5. Crystallographic Experimental Details for (^{i}Pr-PSiP^{Ind})FeBr[CN(2,6-Me$_2$C$_6$H$_3$)] (**5-5**).

A. Crystal Data

formula	C$_{49}$H$_{63}$BrFeN$_4$P$_2$Si
formula weight	933.82
crystal dimensions (mm)	0.29 × 0.22 × 0.04
crystal system	monoclinic
space group	$P2_1/c$ (No. 14)
unit cell parameters^a	
a (Å)	14.8841(3)
b (Å)	14.1860(3)
c (Å)	21.9632(4)
β (deg)	93.1192(9)
V (Å^3)	4630.57(16)
Z	4
ρ_{calcd} (g cm^{-3})	1.339
μ (mm^{-1})	4.809

B. Data Collection and Refinement Conditions

diffractometer	Bruker D8/APEX II CCD^b
radiation (λ [Å])	Cu Kα (1.54178) (microfocus source)
temperature (°C)	–100
scan type	ω and ϕ scans (1.0°) (5 s exposures)
data collection 2θ limit (deg)	144.47
total data collected	205005 (-18 ≤ h ≤ 18, -17 ≤ k ≤ 17, -27 ≤ l ≤ 27)
independent reflections	9159 (R_{int} = 0.0629)
number of observed reflections (*NO*)	8522 [$F_o^2 \geq 2\sigma(F_o^2)$]

381

Table D5. Crystallographic Experimental Details for (^{i}Pr-PSiP^{Ind})FeBr[CN(2,6-Me$_2$C$_6$H$_3$)] (**5-5**) (continued).

structure solution method	intrinsic phasing (*SHELXT-2014^c*)
refinement method	full-matrix least-squares on F^2 (*SHELXL–2018^d*)
absorption correction method	Gaussian integration (face-indexed)
range of transmission factors	0.9450–0.3391
data/restraints/parameters	9159 / 314^e / 640
goodness-of-fit (*S*)^f [all data]	1.031
final *R* indices^g	
R_1 [$F_o^2 \geq 2\sigma(F_o^2)$]	0.0305
wR_2 [all data]	0.0816
largest difference peak and hole	0.460 and –0.596 e Å^{-3}

^{a}Obtained from least-squares refinement of 9852 reflections with $5.94° < 2\theta < 144.16°$.

^{b}Programs for diffractometer operation, data collection, data reduction and absorption correction were those supplied by Bruker.

^{c}Sheldrick, G. M. *Acta Crystallogr.* **2015**, *A71*, 3–8. (*SHELXT-2014*)

^{d}Sheldrick, G. M. *Acta Crystallogr.* **2015**, *C71*, 3–8. (*SHELXL-2018/3*)

^{e}All four isopropyl groups were disordered and the following sets of bond length restraints (**SADI**, 182 restraints) were applied: all P–CH(Me$_2$) distances were restrained to be approximately the same; all C–C distances within the isopropyl groups; all P$\cdots$C$_{iPr}$ distances (i.e P–C–(CH$_3$)$_2$; and all C$\cdots$C distances within the isopropyl groups. Additionally, the rigid bond restraint (**RIGU**, 132 restraints) was applied to improve the anisotropic displacement parameters of the carbon atoms of the isopropyl groups.

$^f S = [\Sigma w(F_o^2 - F_c^2)^2/(n - p)]^{1/2}$ (n = number of data; p = number of parameters varied; $w = [\sigma^2(F_o^2) + (0.0391P)^2 + 2.9923P]^{-1}$ where $P = [\text{Max}(F_o^2, 0) + 2F_c^2]/3$).

$^g R_1 = \Sigma||F_o| - |F_c||/\Sigma|F_o|$; $wR_2 = [\Sigma w(F_o^2 - F_c^2)^2/\Sigma w(F_o^4)]^{1/2}$.
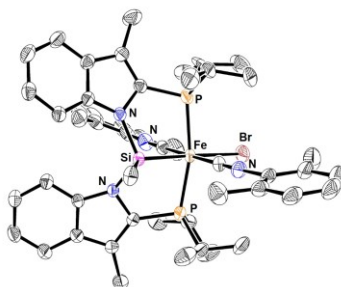

Figure D5. ORTEP diagram for (^{i}Pr-PSiP^{Ind})FeBr[CN(2,6-Me$_2$C$_6$H$_3$)] (**5-5**).

D-2: Selected NMR Data for Chapter 5

Figure D6. ^{1}H NMR spectrum (benzene-d_6) of (^{i}Pr-PSiP^{Ind})FeCl(py) (**5-1**).

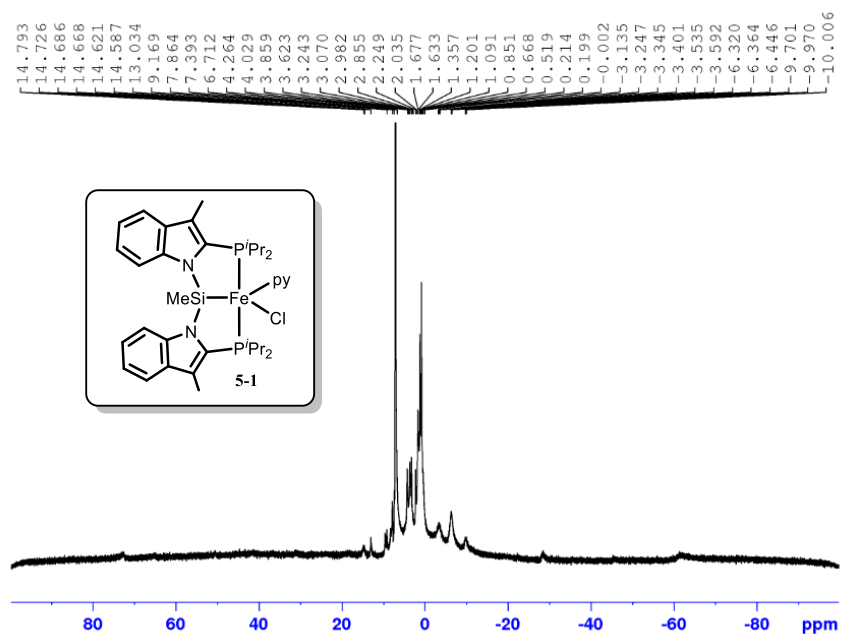**Figure D7.** (a) $^{31}P\{^1H\}$ and (b) ^1H NMR spectrum (benzene-d_6) of (^{i}Pr-PSiP^{Ind})FeH(N$_2$)$_2$ **(5-2)**.
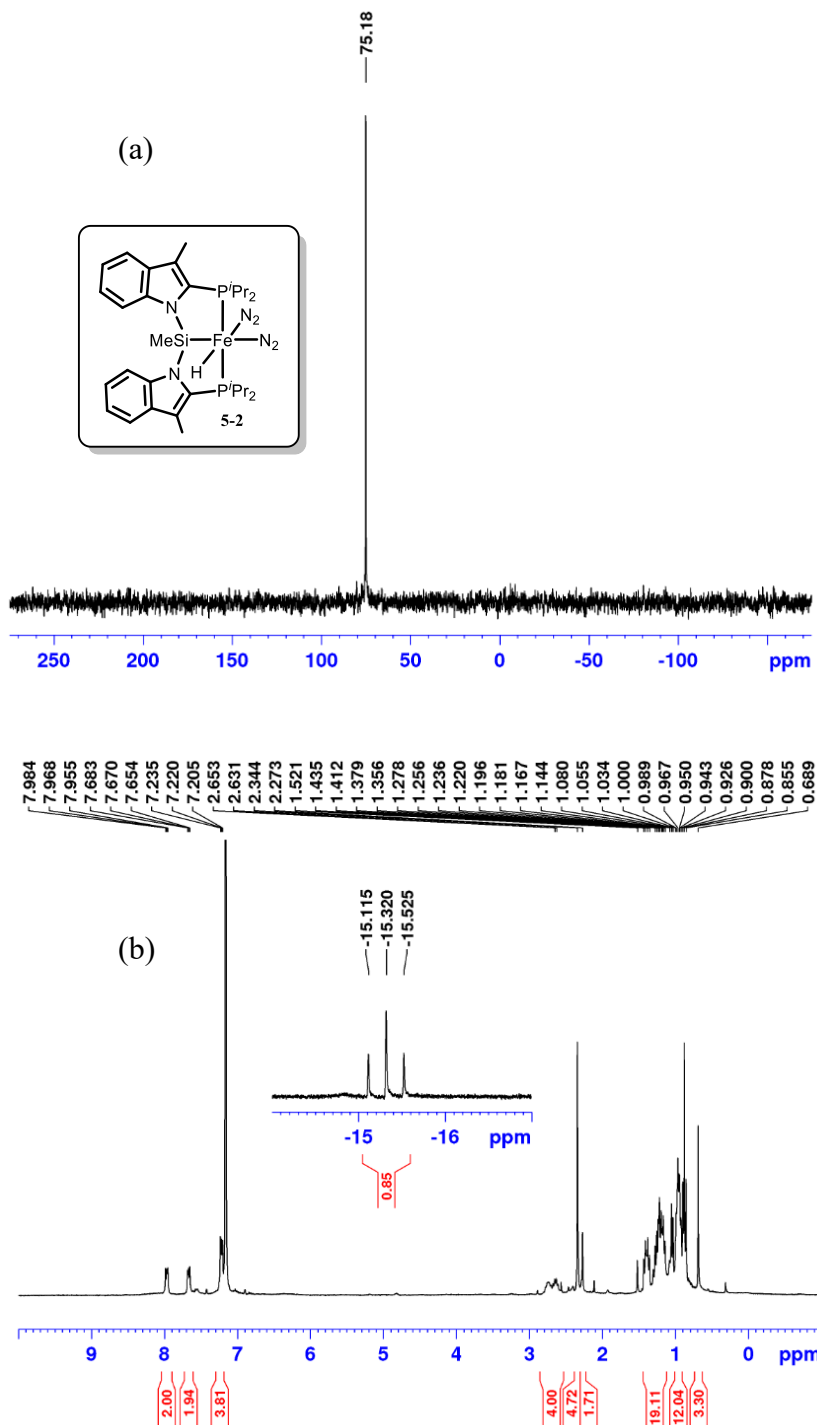
Figure D8. ^{1}H NMR spectrum (benzene-d_6) of [(^{i}Pr-PSiP^{Ind})FeBr]$_2$MgBr$_2$(THF) (**5-4**).
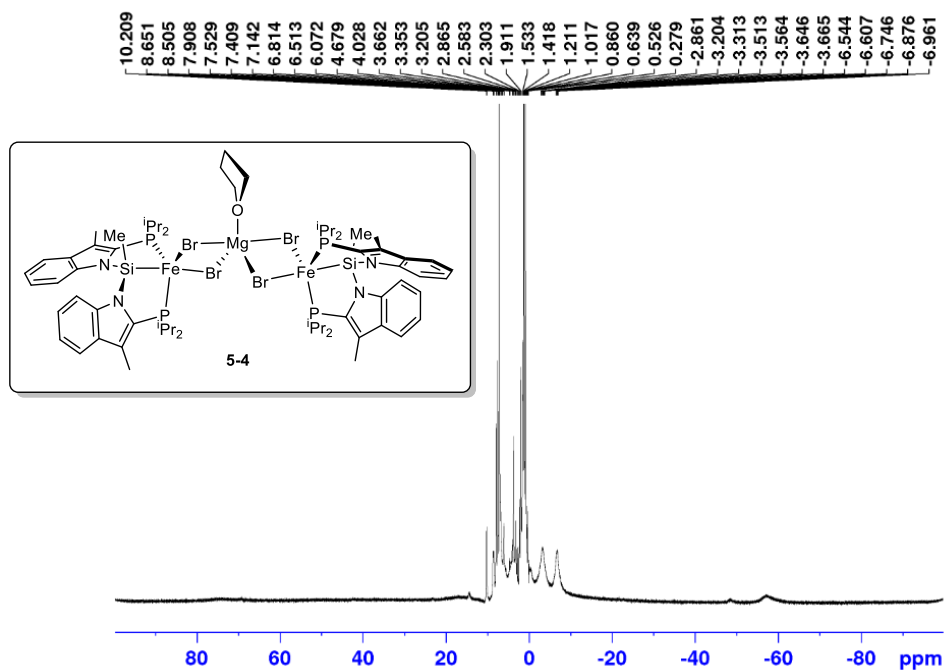
Figure D9. ^{1}H NMR spectrum (benzene-d_6) of (^{i}Pr-PSiP^{Ind})FeBr(CO)$_2$.
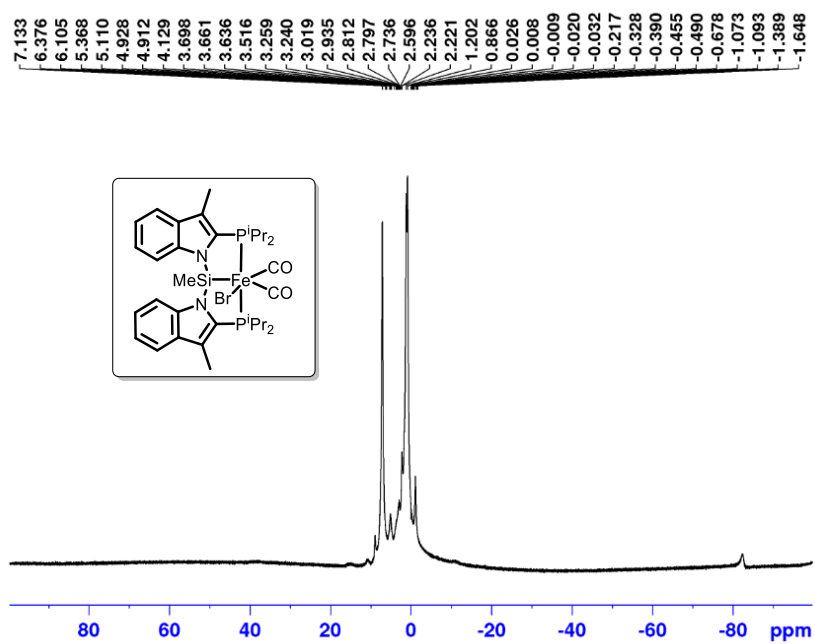
Figure D10. (a) $^{31}P\{^1H\}$ and (b) ^1H NMR spectrum (benzene-d_6) of (^{i}Pr-PSiP^{Ind})FeBr[CN(2,6-Me$_2$C$_6$H$_3$)]$_2$ **(5-5)** .
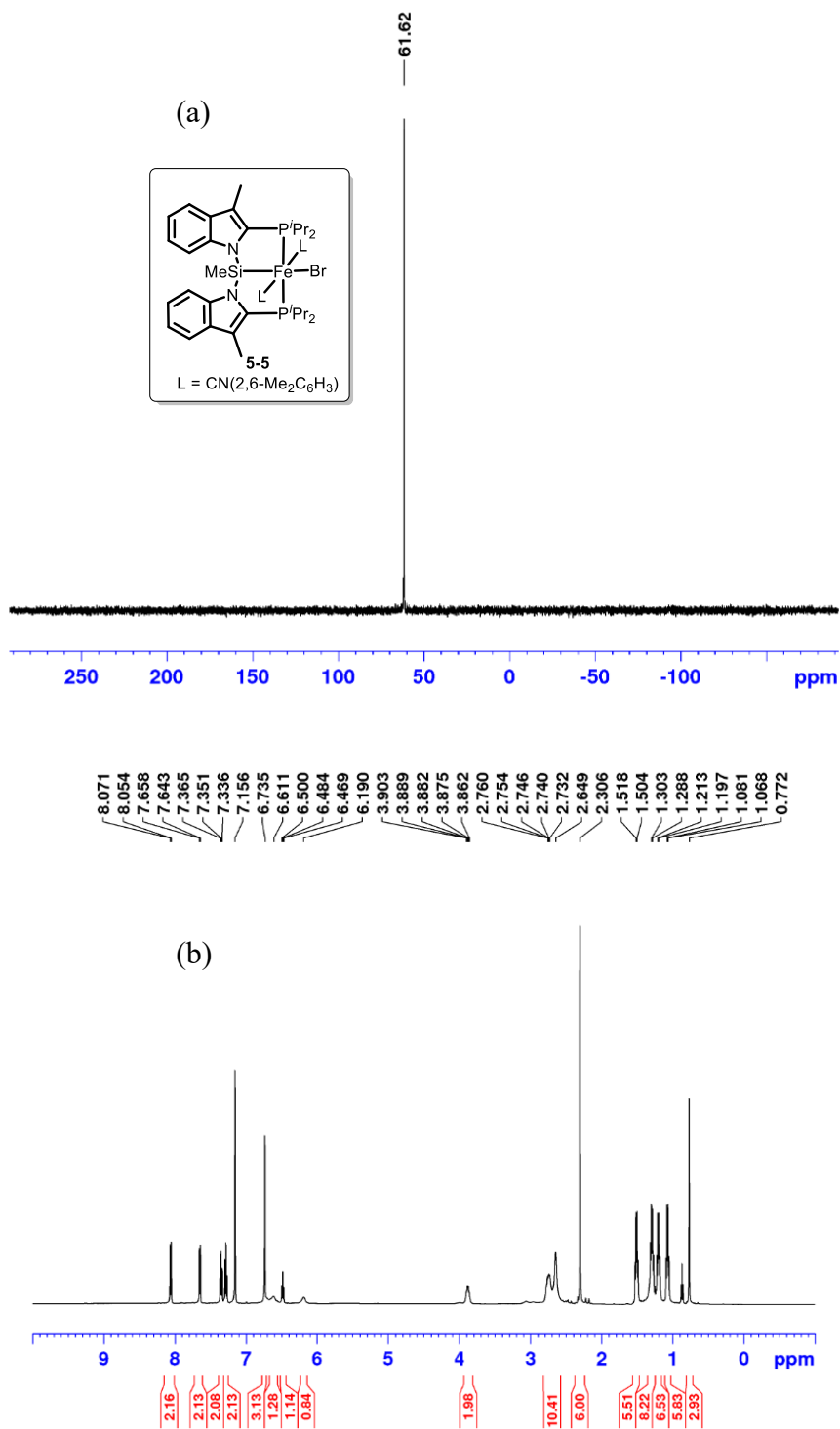
Appendix E: Copyright Agreement

July 8, 2021

Synthesis of Rhodium and Iridium Complexes Supported by Bis(indolylphosphino)silyl Pincer Ligation: Competitive N–H and C–H Bond Activation by an Ir(I) Species

Organometallics, American Chemical Society

I am preparing my PhD thesis for submission to the Faculty of Graduate Studies at Dalhousie University, Halifax, Nova Scotia, Canada. I am seeking your permission to include a manuscript version of the following paper as a chapter in the thesis:

Synthesis of Rhodium and Iridium Complexes Supported by Bis(indolylphosphino)silyl Pincer Ligation: Competitive N–H and C–H Bond Activation by an Ir(I) Species, Helia Hollenhorst, Robert McDonald, Michael Ferguson, Laura Turculet, Organometallics, https://doi.org/10.1021/acs.organomet.1c00114, 2021.

Canadian graduate theses are reproduced by the Library and Archives of Canada (formerly National Library of Canada) through a non-exclusive, world-wide license to reproduce, loan, distribute, or sell theses. I am also seeking your permission for the material described above to be reproduced and distributed by the LAC(NLC). Further details about the LAC(NLC) thesis program are available on the LAC(NLC) website (www.nlc-bnc.ca).

Full publication details and a copy of this permission letter will be included in the thesis.

Yours sincerely,

Helia Hollenhorst

_____

Permission is granted for:

a) the inclusion of the material described above in your thesis.

b) for the material described above to be included in the copy of your thesis that is sent to the Library and Archives of Canada (formerly National Library of Canada) for reproduction and distribution.

Name: __Laurel Schafer_____ Title: __Professor, Associate Editor *Organometallics*_____

Signature:___█████████████_____ Date: ____2021 07 15_____